The University Of Sheffield.

COMBUSTION AND SLOW PYROLYSIS OF OIL PALM STONES AND PALM KERNEL CAKE

A Thesis Submitted to

The University of Sheffield

By

Raja Razuan Raja Deris, BSc, MSc (Eng.), GradEI

For the degree of

Doctor of Philosophy

Project Supervisors:

Professor V.N. Sharifi & Professor J. Swithenbank

Chemical and Biological Engineering Department,
The University of Sheffield
United Kingdom

DECEMBER 2011

ABSTRACT

Biomass is an important new energy source because it is indigenous to every part of the world, inexpensive and renewable. Malaysia's ability to produce and consistently export a large quantity of high quality palm oil has made it one of the major vegetable oil exporters in the world. By-products and waste from the palm oil mills are generated in significant amounts and mainly consist of empty fruit bunches, oil palm stone, oil palm shell, palm kernel cake and palm oil mill effluent. Some of this waste is currently used as fuel for boilers with low energy efficiency, as a soil conditioner, or in furniture making. There is a significant interest in recovering energy from oil palm shells and extensive research has been carried out in this area in other studies. However, research on energy production from oil palm stone (OPS) and palm kernel cake (PKC) is very limited. Waste from the oil palm industry, especially OPS and PKC, is abundant and could help to meet the energy demand if properly managed.

The main objective of this PhD study was to investigate the main characteristics of the thermo-chemical conversion of OPS and PKC. A series of combustion and pyrolysis tests were carried out using OPS and PKC as the raw materials in fixed bed and pilot-scale fluidised bed reactors. In addition, the FLIC modelling code was used to predict key parameters including theoretical solid temperature and gas composition, and to validate the experimental results from fixed bed combustion tests. Pelletisation was also carried out on PKC due to the loose nature and small size of the particles.

In the series of pyrolysis tests using OPS and PKC carried out in a fixed bed reactor, the effects of heating rate at the temperature of 700°C on the yields and properties of the pyrolysis products were investigated. The calorific values of the chars obtained from the OPS and PKC were approximately 28 MJ/kg. The properties of the chars produced were similar to bituminous coal in terms of their calorific value and carbon content. The pyrolysis liquids obtained from the OPS and PKC had calorific values of 21-38 MJ/kg. The pyrolysis liquids obtained from OPS were in the form of a homogeneous liquid, whilst that derived from PKC contained more than half as an aqueous fraction.

The results from the fixed bed combustion tests showed that the burning rates increased with an increase in the air flow rate. In addition, results from the FLIC code used to simulate the fixed bed combustion of the oil palm stone showed good agreement with the experimental data in terms of predicting the dynamic temperature profiles along the bed height and the flue gas composition. The effect of primary air flowrate and initial bed temperature were the main parameters investigated in the pilot-scale fluidised bed combustion tests. Both the internal temperature and the surface temperature were found to decrease as the primary air flowrate increased. In all tests CO emissions were less than 0.2%. The emissions of SO_2 and HCl ranged from 0.02 ppm to 0.05 ppm, significantly below the levels set by legislation. Stable combustion was observed at a bed temperature of 950°C. The most abundant elements found in the ash were Al, Ca, Fe, K, Mg, Mn, P, S and Si.

The variables explored in the pelletisation of PKC were pressure, temperature, fuel moisture content and the effect of binders, which all had significant effects on density and tensile strength. The most favourable conditions for pellet production were found to be a pressure of 9338 psi/64.38 MPa, a temperature of 80-100°C and a fuel moisture content of 7.9%. These pellets had densities of 1184-1226 kg/m^3 and tensile strengths of 930-1007 kPa. Adding small amounts of caustic soda (1.5-2.0wt %) to the PKC under these conditions increased the tensile strength to 3055 kPa, whereas starch additives were not found to be effective binders.

ACKNOWLEDGEMENTS

Table of Contents

List of Tables

List of Figures

Nomenclatures

Symbol	Description	SI Unit
A	Pre-exponent factor	[s^{-1}]
C	Constant, concentration	[-], [kg/m^3]
C_{O_2}	O_2 concentration	[kmol/m^3]
C_{mix}	Mixture-rate constant	[-]
C_p	Specific heat capacity	[J/kgK]
D	Molecular diffusivity, diameter of cylinder	[m^2/s], [m]
Q_1	Bed-to-particle heat transfer rate	[W]
Q_2	Rate of heat conduction through char layer	[W]
q	Specific burning rate of char based on external surface	[kg (C)/m^{2}s]
d	Particle size	[m]
r_c^*	Rate of char combustion	[kg/s]
r_v^*	rate of volatile combustion	[kg/s]
X_{v0}	Weight fraction of initial volatile	[-]
X_{c0}	Weight fraction of initial fixed carbon	[-]
M_c	Molecular weight of carbon	[kg/kmol]
ΔH_v	Heat of volatilization	[J/kg]
ϕ_{s0}	Carman's shape factor (sphericity)	[-]
d_{s0}	Initial diameter of sphere having the same volume as solid	[m]
d_{sc}	Diameter of core where volatile matter remains	[m]
$\bar{k}$	Overall rate coefficient	[m/s]
k_f	Mass transfer coefficient at the surface of char layer	[m/s]
k_c	Chemical reaction rate coefficient at the surface of char layer	[m/s]
k_e	Effective thermal conductivity of the bed	[W/m^{2}K]
t	Time	[s]
t_c	Time for char combustion	[s]

T_{bed}	Bed temperature	[K]
T_{s0}	Surface temperature of solid	[K]
Sh	Sherwood number	[-]
Nu	Nusselt number	[-]
D_{ig}	Diffusion coefficient of gaseous species i	[m²/s]
d_{sc}	Diameter of core where volatile matter remains	[m]
ρ_s	Density of solid	[kg/m³]
ρ_{sc}	Density of char layer	[kg/m³]
d_p	Particle diameter	[m]
E	Activation energy	[J/mol]
E_b	Blackbody radiation intensity	[Wm²/μm]
F	Fractional increase of internal pore space	[-]
H_{evp}	Evaporation heat of solid material	[J/kg]
H	Enthalpy	[J/kg]
h_s	Convective mass transfer coefficient between solid and gas	[W/m²K]
k	Rate constant	[1/s]
K	Constant	[-]
k_a	Radiation absorption coefficient	[1/m]
k_s	Radiation scattering coefficient	[1/m]
k_d	Rate constant of char burning due to diffusion	[kg/atm.m²s]
k_r	Rate constant of char burning due to chemical kinetic	[kg/atm.m²s]
I, I^+, I^-	Radiation intensity	[W/m².μm⁻¹]
P	Mean pressure	[Pa]
p	Pressure	[Pa]
q_r	Radiative heat flux	[W/m²]
$Q_{c,r}$	Heat absorbed by solid	[W/m²]
Q_{sh}	Thermal source term of solid phase	[W/m²]
R	Universal gas constant, Process rate	[J/mol K], [kg/m³s]
R_{mix}	Mixing-rate of gaseous phase in bed	[kg/m³s]

Symbol	Description	SI Unit
S	Source term, stoichiometric coefficient in reactions	[-]
S_a	Particle surface	[m^2]
T	Temperature	[K]
t	Time	[s]
V	Volume	[m^3]
v	Velocity	[m/s]
υ	Remaining volatiles in solid	[kg/m^3]
υ_∞	Ultimate yield of volatiles	[kg/m^3]
y_i	Mass fraction of species i	[-]
z	Distance	[m]

Greek Symbols

σ_b	Boltzmann radiation constant, 5.86×10^8	[W/m^{2}K^4]
σ	Width of distribution in activation energies	[-]
σ_s	Radiation scattering coefficient	[1/m]
ε	Emissivity	[-]
λ	Thermal dispersion coefficient	[W/mK]
ϕ	Void fraction in bed, Equivalence ratio	[-], [W/mK]
ρ	Density	[kg/m^3]
Φ	Parameter to be solved	[-]
ω	Volume fraction	[-]
μ	Viscosity	[Pa]
κ	Permeability	[m^2]

Subscripts

w	Moisture
g	Gas
s	Solid
env	Environment
v	Devolatilasation

sb	Solid bulk
r	Radial
x	Height
vgn	Virgin fuel
i	Component identifiers
A	Initial material
B	Dried material
C	Dried and pyrolysed material
D	Dried, pyrolysed and gasified material

Abbreviations

OPS	Oil Palm Stone
PKC	Palm Kernel Cake
EFB	Empty Fruit Bunches
POME	Palm Oil Mill Effluent
OPSh	Oil Palm Shell
BMT	Biological Mechanical Treatment
BFB	Bubbling Fluidised Bed
CFB	Circulating Fluidised Bed
FLIC	Fluid Dynamic Incinerator Code
FR	Frame retardant
FTIR	Fourier Transform Infrared spectroscopy
GC	Gas Chromatography
GC-MS	Gas Chromatography-Mass Spectrometry
MSW	Municipal Solid Waste
MBT	Mechanical Biological Treatment
MRF	Material Recovery Facility
NOx	Oxides of Nitrogen
RDF	Refuse derived fuel
LLV	Lower Heating Value
HHV	Higher Heating Value

daf	Dry ash free basis
VM	Volatile matter
EU	European Union
RE	Renewable Energy
GDP	Gross Domestic Product
GEF	Global Environmental Facility
UNDP	United Nations Development Programme
GHG	Greenhouse Gases
ktoe	kilo tonne of oil equivalent

1 INTRODUCTION

1.1 Background

1.1.1 Biomass

The term biomass can be defined in many ways. The U.S Department of Energy describes biomass as an organic matter that is available on a renewable or recurring basis which include all plants, plant derived materials such as agricultural crops and trees, wood and wood residues, grasses, aquatic plants, animal manure and municipal residues (Boundy *et al.*, 2010). However, Food and Agriculture Organisation of the United Nation (FAO) has defined biomass as non-fossil material of biological origin, such as energy crops, agricultural, forestry wastes and manure (FAO, 2011). For the purpose of this thesis, biomass is defined as an organic matter from non-geological origin that can be converted into energy (Russell and Jones, 2007).

Biomass has become more important as one of the energy sources to meet the demand of stringent environmental regulations imposed on fossil fuels. It is reasonably affordable, easily available in all parts of the world and, most importantly a renewable. In other words, biomass can be used without fear of depletion. In general, most of the biomass fuels contain significantly low amounts of sulphur that leads to reduced sulphur oxide (SO_x) emissions. With new biomass conversion technologies available nowadays, low emissions of nitrogen oxides (NO_x) and high energy efficiency can be achieved (Vamvuka, 2010). Utilising biomass as fuels can help the farming community particularly in developing countries to increase their income by utilising waste from agricultural residues. The most important biomass fuel available includes oil palm waste, wood waste and municipal solid waste (MSW). Some of the commercially available biomass and its characteristics are shown in Table 1-1.

1

Table 1-1: Typical characteristics of various biomass fuels (Quaak *et al.*, 1999).

Type	LHV$_w$ (MJ/kg)	Moisture (%)	Ash %(dry)	Element	Weight % (daf)
Bagasse	7.7-8.0	40-60	1.7-3.8		
Cocoa husks	13-16	7-9	7-14	Carbon	44-51
Coconut shells	18	8	4		
Coffee husks	16	10	0.6	Hydrogen	5.5-6.7
Cotton residue				Nitrogen	0.12-0.60
Stalks	16	10-20	0.1		
Gin trash	14	9	12	Sulphur	0.0-0.2
Maize				Oxygen	41-50
Cobs	13-15	10-20	2		
Stalks			3-7		
Palm-oil-residue					
Fruit stems	5	63	5		
Fibres	11	40			
Shells	15	15			
Peat	9-15	13-15	1-20		
Rice husks	14	9	19		
Straw	12	10	4.4		
Wood	8.4-17	10-60	0.25-1.7		
Charcoal	25-32	1-10	0.5-6		

1.1.2 Thermal conversion technologies

Conversion of biomass via thermal methods has received a significant attention from researchers (Williams and Besler, 1996, Yang *et al.*, 2006c, Darvell *et al.*, 2010). The three main thermochemical technologies available for biomass conversion for energy purposes as stated below:

i. Direct combustion technology

Direct combustion is the most important thermally treated biomass for energy generation. This technology is commercially available and can be considered technically matured and therefore, present a minimum risk to investors or power generators. Woodchips, pellets, sawdust, bark, bagasse, straw and municipal solid waste are normally used as feedstocks. The main product from direct combustion is heat which can be used to heat water and produce steam for

electricity generation. Biomass fuels undergo series of process during direct combustion including drying, pyrolysis, combustion of volatiles and combustion of char.

ii. Gasification technology

Gasification is a partial oxidation of biomass fuels in the presence of oxygen in the form of air, steam or pure oxygen. The main product from gasification process is gas with high energy content or syngas. The syngas is a mixture of CO, CO_2, H_2 and CH_4. It can be utilised as fuel or chemical feedstocks. Gasification can either be a self-sustaining process due to the exothermic combustion of volatiles or maintained by recycling proportion of the energy from the combustion of the producer gas. Feedstock characteristics play an important role in gasifier design which determines the final syngas compositions. Gasifier can be operated at atmospheric or higher pressure with the temperature at around 800°C.

iii. Pyrolysis technology

Pyrolysis is a thermal degradation of organic matter in the absence of oxygen. The carbonaceous char, liquids and combustible gases are the main products derived from this process. Pyrolysis can be performed at atmospheric, pressurised or vacuum pressure. It also occurs in the first step of the combustion and gasification process, followed by a partial oxidation and complete combustion of the decomposed fuels. In general, pyrolysis process will occur at the temperatures between 400 - 800°C. The products distribution is influenced mainly by process parameters particularly operating temperature and the heating rate. The traditional pyrolysis process is used to make a charcoal, whilst modern fast pyrolysis is for extracting the liquid from biomass. This liquid can be used as fuel or chemical feedstocks. The production of liquid from cellulosic materials via fast and flash pyrolysis is currently receiving a lot of attention from many researchers.

1.2 The current situation

Presently, thermal conversion of biomass for electricity generation is dominated by the combustion or incineration technology. Combustion of biomass is important to reduce the environmental damage due to long standing issues of fossil fuels such as a greenhouse gas (GHG). According to Vamvuka (2010), direct combustion technology has a major contribution to biomass energy conversion.

More advanced technologies such as gasification and pyrolysis still operate in a smaller scale in laboratories or demonstration plants. The tar content in the gas produced by gasification at low temperatures can cause numerous problems in the system. Many researchers have focused their work on reducing or removing tar from gas products (Yu *et al.*, 1997, Henriksen *et al.*, 2006, Li *et al.*, 2008). Current developments in gasification systems are directed towards increasing their performance and reliability. The concept of advanced integrated gasification and combined heat and power is currently being introduced, however it remains at the demonstration stage. At present, there are no available plants operating commercially (Gomez-Barea and Leckner, 2010).

Biomass availability and its ability to serve as an alternative to fossil fuels is a major concern for every head of government in the world. The world's energy demand in 2008 amounted to around 492 EJ (11,749 MToe). About 12.9% of that came from renewable energy. Biomass fuel contributed at around 10.2%, hydropower 2.3%, wind energy 0.2% and geothermal energy 0.1% (IPCC, 2011). The total bioenergy production in 2050 is estimated to be around 1,340 EJ annually. This is more than sufficient to meet the global energy demand at around 1,041 EJ (Ladanai and Vinterbäck, 2009).

The demands for the energy in Southeast Asian countries (Indonesia, Malaysia, the Philippines, Singapore, Thailand, and Vietnam) over the past two decades have increased more than double from 230 to 490 million tonnes of oil equivalent (Mtoe) or about 4% of the world energy demand (ölz and Beerepoot, 2010). The electricity generation also has increased almost fourfold during the same period. The energy supply mix has been

dominated by the following sources: fossil fuels (74%); combustible biomass and waste (22%), geothermal (3%) and hydro (1%) (ölz and Beerepoot, 2010).

More than 130 million tonnes of waste and over 600 waste-to-energy plants that produce heat and electricity have been reported worldwide (ERC, 2011). For example, in the United States, there are about 86 waste-to-energy plants which are currently in operation. Most of these plants use biomass from municipal waste to generate heat and electricity. More than 97,000 tonnes per day of biomass are burnt to produce electricity equivalent of 2,790 MWh (Michaels, 2010). In Europe, about 400 waste-to-energy plants are currently in operation to provide electricity for 27 million populations and district heating for approximately 13 million people across the Europe (Phan, 2007).

By-products from Malaysia's palm oil industry mainly consists of empty fruit bunches (EFB), oil palm stones (OPS), oil palm shell (OPSh), palm kernel cakes (PKC) and palm oil mill effluent (POME). These waste products particularly empty fruit bunches, fibre and shell have recently been studied for their energy or energy related potentials (Guo and Lua, 2002, Abdullah and Gerhauser, 2008, Sukiran *et al.*, 2009). However, none of these biomass materials is successfully utilised as a source of energy in the commercial scale. These waste materials are currently used as fuel for boilers with low energy efficiency, soil conditioners or in furniture making. The Malaysian government has introduced several incentives including financial and fiscal incentives as well as declared biomass as a fifth fuel in the new Five Fuel Strategy during 8th Malaysian Plan (2001-2005) to promote untapped biomass. Due to the failure to achieve the target, the government has announced that this policy is to be continued in the 9th Malaysian Plan (2006-2010) with the new target for grid-connected from renewable-electricity generation is 350 MW by the end of 2010 (ölz and Beerepoot, 2010).

1.3   Objectives and scope of research

The aim of this research is to investigate the thermal behaviour from the combustion and pyrolysis of the oil palm stone (OPS) and palm kernel cake (PKC) materials in fixed and pilot-scale fluidised bed reactors. The mathematical modelling code FLIC was used to model the processes in the reacting bed and validate the experimental results obtained from fixed bed combustion. The combustion characteristics of OPS and PKC were studied experimentally in two different combustion systems; fixed and pilot-scale fluidised bed reactors. Various air flow rates were used to evaluate the key combustion characteristics, as well as the ignition, initial bed temperature and burning rates. These key parameters are of practical interest for the design and operation of industrial scale moving beds. The effect of the final temperature (500 and 700°C) and the heating rates on the yields and properties of slow pyrolysis products was also investigated. The role of pyrolysis is important in the thermal processing of biomass, since it decomposes biomass into three types of intermediate products (char/tar, liquids and gas), to be either collected as fuel feedstock or combusted in the combustion chamber. The properties of these pyrolysis products can be used to design a pyrolyser. Pelletisation of PKC was also conducted in this study. PKC in powder form is not suitable for direct use as a fuel. Extensive analytical and pelletisation studies were also performed to evaluate the physical properties of the PKC pellets. The variables explored included the pelletisation pressure, temperature, fuel moisture content and the effect of binders on density, tensile strength and durability of the pellets.

1.4   Layout of thesis

This thesis consists of nine chapters:

   i.   Chapter 1: an introduction to the research presented in this thesis; outlining the source of biomass waste, thermal conversion technologies and the latest developments in biomass fuels management and policies.

   ii.   Chapter 2: a literature review examining the variety of biomass wastes with a specific focus on palm oil wastes and thermal conversion technologies. The review covers a wide range of issues including palm oil waste properties,

policies and the technologies used to convert and utilise palm oil waste as a fuel to generate heat and electricity. In addition, pelletisation principles and techniques are also reviewed.

iii. Chapter 3: a review of the theoretical aspects of biomass thermal conversion technologies which focuses on the mathematical modelling of the main reactions taking place within the burning bed using the FLIC modelling code.

iv. Chapter 4: a detailed description of the experimental programme and techniques used in pyrolysis, combustion and pelletisation experiments.

v. Chapter 5: a report of the results and discussion of pelletisation of the PKC tests. Physical properties including the effects of temperature, pressure, moisture content and binders on tensile strength and density are examined and discussed.

vi. Chapter 6: a presentation of the results and discussion of the combustion tests in fixed bed and pilot-scale fluidised bed reactors. Comparisons between the results of fixed bed combustion tests and FLIC modelling calculations are also presented.

vii. Chapter 7: a presentation of the results and discussion of the slow pyrolysis tests. The discussion covers the effect of pyrolysis parameters and also the characteristics of pyrolysis products.

viii. Chapter 8: an overall discussion on combustion and slow pyrolysis of oil palm stone. This section covers the general issues pertaining to the technologies, usage, economic, industrial applications and the environmental aspect of the fuel.

ix. Chapter 9: the conclusion drawn and suggestions for future work.

2 LITERATURE REVIEW

2.1 Introduction to Biomass

2.1.1 Biomass feedstock

Biomass covers varieties of fuels including land-based and aquatic-based biomasses. Land-based biomasses include all wood-based biomass, agricultural crops, agricultural wastes or residues and municipal solid waste. Aquatic-based biomass consists mainly of marine plants such as algae or seaweed. Biomass is a renewable fuel if grown sustainably and considered to be a carbon neutral material. Most woods and other plant biomass are constructed from oxygen-containing organic polymers. Carbohydrate polymers and oligomers (cellulose and polyose) are the major constituents (Figure 2-1) of biomass plant followed by lignin and organic extractives (Mohan *et al.*, 2006). At present, biomass fuels contribute to around 10% of the world's energy supplies mix (Suri and Horio, 2010). From that, 20-30% comes from developing countries such as Malaysia, Thailand, Indonesia and Nepal and only 10% contribution comes from developed nations (Suri and Horio, 2010).

Biomass has a high volatile, low sulphur content, significant amount of oxygen and low calorific value compared to a fossil fuel such as coal and petroleum products. Land-based biomass such as wood, rice husk and bagasse is also known as lignocellulosic biomass. It consists of cellulose, hemicelluloses and lignin. Among them, lignin is the major contributor to the releases of aromatic compound and thus, the carbon content. The content of cellulose, hemicelluloses and lignin in the biomass materials varies depending on the biomass types and their origin. Cellulose contains about 40-50 wt% of dry wood and mainly a linear polysaccharide of D-glucose. Hemicelluloses which comprises of about 20-30 wt% of dry wood are branch of polysaccharides which are formed by several monomeric components. Lignin is a crosslinked polymer of phenylpropane units, consists of the remaining dry weight of biomass materials (Mohan *et al.*, 2006). It is important to note that biomass also contains a small amount of water or organic soluble compounds (<10%) known as extractives such as fats, waxes, terpenoids, steroids, and phenolic constituents (Suri and Horio, 2010). Table 2-1 shows the composition of cellulose, hemicelluloses and lignin contents of various biomasses. The chemical structure of

cellulose, hemicelluloses and lignin are shown in Figure 2-2, Figure 2-3 and Figure 2-4 respectively.
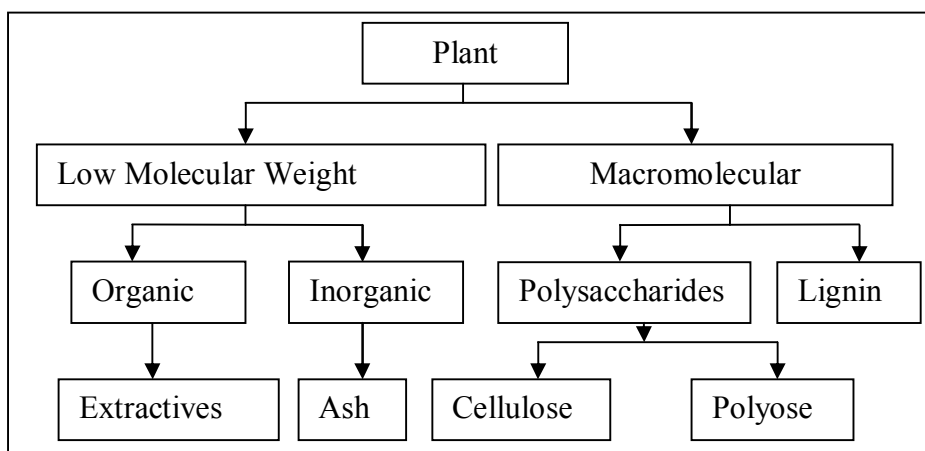
Figure 2-1: General components in plant biomass (Mohan *et al.*, 2006).

Table 2-1: Biochemical composition of various biomass fuels (Bridgeman *et al.*, 2010).

Biomass	Hemicelluloses %(daf)	Celluloses %(daf)	Lignin %(daf)	Extractives %(daf)
Hazelnut shell	30.4	26.8	42.9	3-3
Wheat straw	39.4	26.8	18.6	-
Olive husk	23.6	24.0	48.4	9.4
Beech wood	31.2	45.3	21.9	1.6
Spruce wood	20.7	49.8	27.0	2.5
Corncob	31.0	50.5	15.0	3.5
Tea waste	19.9	30.2	40.0	9.9
Walnut shell	22.7	25.6	52.3	2.8
Almond shell	28.9	50.7	20.4	2.5
Sunflower shell	34.6	48.4	17.0	2.7
Softwood	25-30	35-40	27-30	-
Hardwood	20-25	45-50	20-25	-
Wheat straw	20-25	33-40	15-20	-
Switchgrass	10-40	30-50	5-20	-
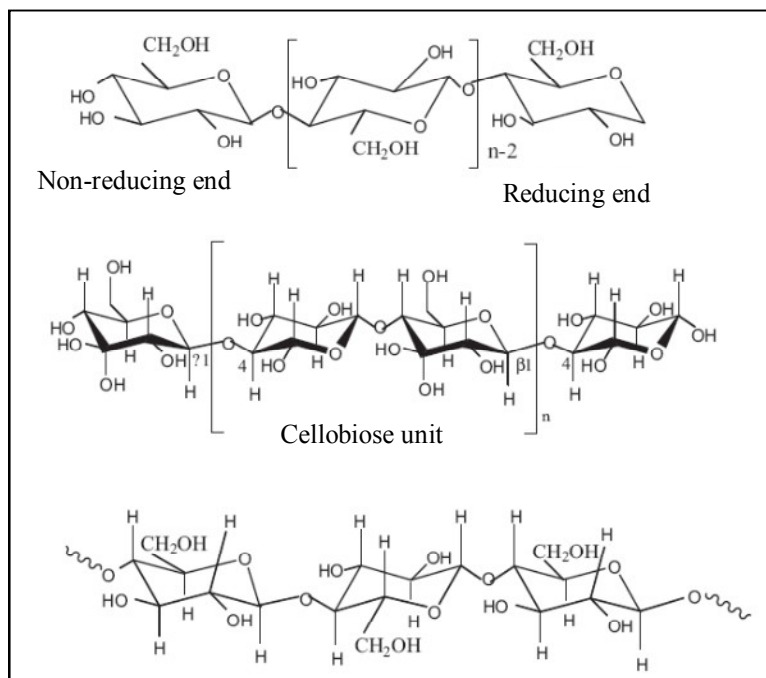
Figure 2-2: Cellulose (Mohammed *et al.*, 2011).
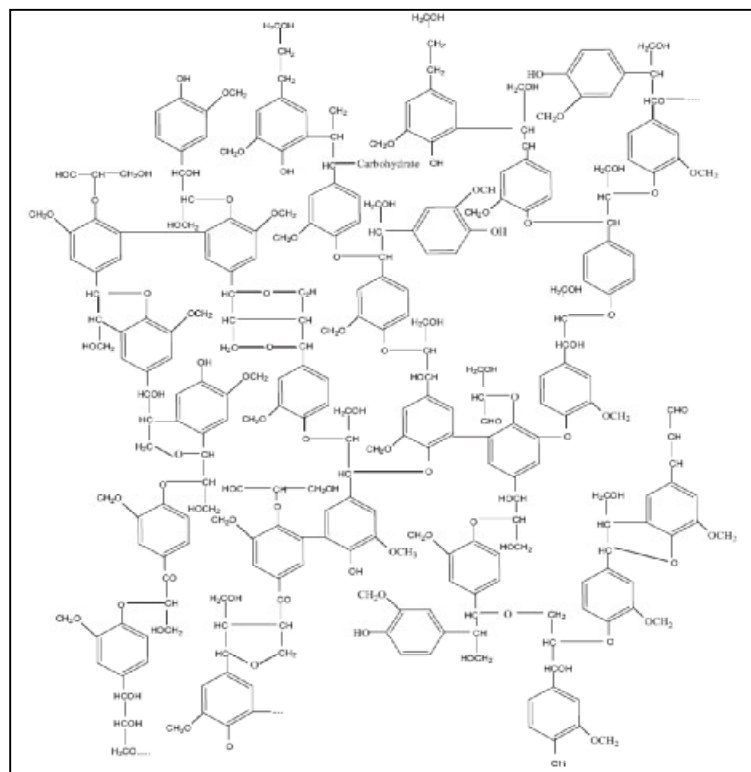
Figure 2-3: Hemicelluloses (Mohammed *et al.*, 2011).
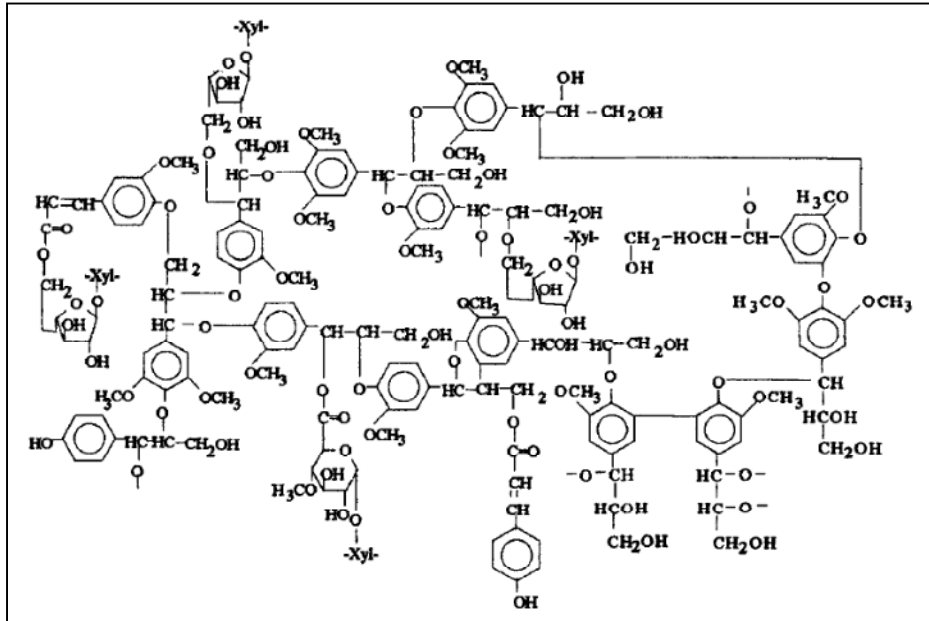
Figure 2-4: Lignin (Sun *et al.*, 1997).

Each biomass type has specific properties that determine its performance as a fuel. The most important properties relating to the thermal conversion of biomass are:

i. Moisture content – the water content in biomass material, expressed as a percentage of the material's weight. Biomass contains water in two forms; 1) free water- The amount of water contained in the cell lumina, is not bound chemically and only held by capillary forces. 2) Bound or hygroscopic water- water that is readily bound in biomass materials via hydrogen bonds. Free hydroxyl (OH) groups in the cellulose, hemicelluloses and lignin molecules in the cell wall react and hold water by hydrogen bonding.

ii. Ash content – the inorganic component of the material. At high temperatures ash can cause problems known as slagging and fouling to combustion systems.

iii. Volatile matter content – heavy molecules fragment to smaller species when biomass is heated up to around 400-500°C. Biomass decomposes into volatile gases, liquids and solid char.

iv. Elemental composition – the composition of an ash-free organic component such as carbon, oxygen, nitrogen, hydrogen and a trace of sulphur in biomass.

v. Calorific value (CV) –is an indication of an energy that is chemically-bound in the fuel with reference to a standard environment i.e. the temperature, state of water and combustion products. The CV is presented in Joules per amount of matter (kJ/kg). This energy is measured based on a reference state, normally water. A lower heating value (LHV) uses water in a gaseous state as a reference; a higher heating value (HHV) uses water in a liquid state as a reference.

vi. Bulk density – the weight of material per unit volume. Biomass varies in bulk density from 150 to 200 kg/m^3 for cereal grain straws to 600-900 kg/m^3 for solid wood.

2.1.2 Global potential of biomass for energy

Sustainable energy supplies, environmental pollution and additional costs of carbon imposed through carbon trading impose pressures on fossil fuels operators to find alternative fuels. At present, renewable energy, particularly biomass offers the best options to overcome all these issues. Biomass has increasingly been utilised across the globe. For example, in the United States, renewable energy contributed to about 11.73% (6.579 trillion kWh) of the total energy production during the first quarter of 2011 (Bossong, 2011). According to Mengjie and Suzhen (2011) China produces about five billion tonnes of biomass every year, of which, approximately 700 million tonnes are harvested from the agriculture sector and provide about 70 % of the energy consumption in the rural areas. In Europe, about 1,000 TWh of primary energy for heat and power is supplied by biomass fuels every year (Hogan *et al.*, 2010). The total energy demand for six countries within the Association of Southeast Asian Nations (ASEAN-6) which include Malaysia, Indonesia, the Philippines, Singapore, Thailand and Vietnam is around 5699 TWh, of which about 22% or 1256 TWh is supplied by biomass (ölz and Beerepoot, 2010).

Many countries have already established the goals of enhancing the roles of renewable sources in their energy supplies mix. For example, the European Commission has established a target to use 20 % of its renewable energy sources to produce heat and power by the year 2020 (Hogan *et al.*, 2010). According to the Directive 2009/28/EC (Directive, 2009), every member states are obliged to reach 10 % of its transport energy consumption from renewable sources by the year 2020. Europe has announced that it will increase the biomass energy share by 44 % between 2010 and 2020 to meet the demand from energy sector (RISI, 2011).

As the fourth largest energy resource after coal, oil and natural gas, biomass contributes to about 470 EJ of global energy use (Ladanai and Vinterbäck, 2009). The potential of biomass production for energy is equivalent to the 4,500 EJ of solar energy captured annually. This is equivalent to 10.5 % of the available energy from biomass (Ladanai and Vinterbäck, 2009). Land availability is one of the factors that affect the biomass potential as an energy source. At present, the amount of land used to cultivate energy crops is only 0.19 % of the world's total land area or 0.5 % of the global agricultural land (Ladanai and Vinterbäck, 2009).

In spite of huge potential being realised from biomass fuels, their growth is still comparatively low compared to fossil fuels. This is due to several factors such as social, political, economical and technological barriers.

2.1.3   Biomass in Malaysia

The world oil crisis in the 1970s illustrated that concerns over resource scarcity were justified. The vulnerability of the energy supply was due to the over-dependence on oil as a fuel which led to the necessity for the diversification of energy fuel resources (Abdullah *et al.*, 1999). This era triggered the development of energy-related legislation and policies to address energy shortage.

Malaysia's Energy Policy has three principal objectives that guide future energy sector developments based on supply, utilisation and the environment.

i. Supply: the main aim is to extend the life of domestic resources and promote other energy forms rather than oil.

ii. Utilisation: it depends heavily on industry and consumers in order to integrate energy efficiency programmes and develop demand-side initiatives to curb the consumption.

iii. Environment: it is linked at every level, thus there is requirement for mandatory assessments to address negative impacts.

The National Energy Balance (NEB) is designed to present basic supply and demand data for all fuels expressed in common energy unit. It serves as an important reference in formulating new policies for energy sectors in Malaysia. Key energy data and indicators allow policy makers to implement programmes to address the future energy demand and supplies (PTM, 2007).

Malaysia is well-positioned to take advantage of its enormous output of biomass from oil palm residues and wood wastes. Biomass power potentials from wood processing and palm oil have been estimated at 280 TJ and 250 TJ, respectively. The fibres, shells, empty fruit bunch and wood wastes are the greatest potential for commercial operations (Yusoff, 2006).

Biomass utilisation leads to substantial economical and environmental gains. For businesses, exploiting renewable resources enhances profit margins and eliminates waste disposal costs. The potential to utilise huge biomass reserves and solar resources allows progressive companies to generate electricity exports, seek regional markets and expand opportunities from lower manufacturing costs. Biomass fuels account for about 16% of Malaysia's energy consumption, of which 51% is from palm oil biomass and 22% from wood waste. Biomass-based power generation capacity stands at 138 MW, of which 100 MW is used in the palm oil industry (Hashim and Ludin, 2008).

Attempts have been made to promote biomass from the oil palm industry to be used as alternative fuels in industrial sectors (Evald and Majidi, 2004, Chuah *et al.*, 2006, Shuit *et al.*, 2009). Evald and Majidi (2004) investigated the feasibility of using biomass fuels as a substitute for fossil fuels in four different industrial sectors in Malaysia, namely paper, cement, rubber and food. They found that replacing fossil fuels with biomass in paper and cement industries were very good in terms of economic feasibility with the financial internal rate of return (FIRR) 67 % and 263 % respectively.

2.2 Oil Palm Waste

Palm oil is the world's most widely traded edible oil. At present, Indonesia is the biggest palm oil producer in the world. It produced about 23.6 million tonnes of palm oil in the year 2010, a 7 % increase from 2009 (agricommodityprices.com). Malaysia is the second largest producer with the planted area of approximately 4.85 million hectares. It has exported about 23.06 million tonnes of oil palm products, consisting of palm oil, palm kernel oil, palm kernel cake, oleochemicals, biodiesel and finished products in 2010 (May, 2011).

In Malaysia, around 60% of the planted area is privately owned of plantation by companies, 30.5 % is under government land schemes and the remaining 9.5 % is owned by individual smallholders (Anis, 2007). Government affiliated company, Federal Land Development Authority (FELDA), is the largest upstream player. The company was established in 1956 and owns 17.7 % of the total planted area (Anis, 2007).

Malaysian Palm Oil Board (MPOB) is the public sector which is responsible for undertaking research and development (R&D) and regulates the industry. Its upstream and downstream R&D is built on three main strategies; 1) to raise income through higher oil palm productivity, 2) to target for zero waste by maximising the utilisation of biomass and 3) to increase the value chain of palm based products for various uses. The R&D activities of MPOB are supported by research levied collected for every tonne of palm oil

or palm kernel produced. Another organisation which directly involved with the Malaysia's palm oil industry is the Malaysian Palm Oil Promotion Council (MPOPC). Its role is to promote the Malaysian palm oil through marketing communications, technical marketing and market promotion to local and international consumers (MPOB, 2011).

2.2.1 The oil palm tree

Elaeis guineensis Jacq., which is commonly known as the oil palm tree, Figure 2-5, is the most important species in the genus *Elaeis* which belongs to the family Arecaceae or Palmae. The second species is *Elaeis oleifera* (H.B.K) Cortes which is found in South and Central America and known as the American oil palm. Figures 2–6 and 2–7 show a fresh fruit bunches (FFB) and cross-sectional of the fruitlet respectively. Although significantly lower in oil-to-bunch content than its African counterpart, *E. oleifera* has a higher level of unsaturated fatty acids and been used for production of inter-specific hybrids with *E.guineensis*.

Figure 2-5: Palm oil tree (Green, 2011).
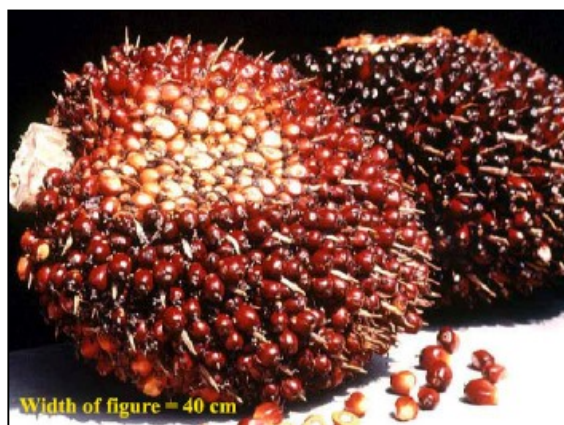
Figure 2-6: Fresh fruit bunches (Hai, 2002).

Harvesting of fruits commence about 24 to 30 months after planting and each palm can produce between 8 to 15 fresh fruit bunches (FFB) per year weighing about 15 to 25 kg each, depending on the planting material and the age of palm. Each FFB contains about 1,000 to 1,300 fruitlets; each fruitlet consists of a fibrous mesocarp layer, the endocarp (shell) which contains the kernel (Figure 2-7). Better quality seeds of palm tree are capable of producing more than 10 tonnes of oil or 50 tonnes of FFB per hectare compared to other oilseed crops such as soybean which can only produce about 0.4 tonnes per hectare per year (Basiron, 2007). However, at present, the production of FFB and oil in Malaysia are 18.03 and 3.69 tonnes per hectares respectively (MPOB, 2011).

Figure 2-7: Cross sectional of fruitlet (PalmOilWorld, 2011).

In 1939, Beirnaert of Belgian Congo discovered the single gene inheritance of shell thickness. This discovery led to the *Dura* x *Pesifera* or DxP crosses. The DxP hybrid is called *Tenera* and this species is the most common species grown in Malaysia.

17

Latif (2000) studied the biology of the *E. guineensis* and revealed that it could be differentiated by fruit pigmentation and characteristics; the most common cultivars being the *Dura*, *Tenera* and *Pesifera* which are classified according to endocarp or shell thickness and mesocarp content. Figure 2-8 shows the morphology of oil palm shell of three different species. *Dura* palms have 2-8 mm thick endocarp and medium mesocarp content (35-55 % of fruit weight), the *Tenera* species has 0.5-3 mm thick endocarp and high mesocarp content of 60-95 % and the *Pesifera* palms have no endocarp and about 95 % mesocarp.
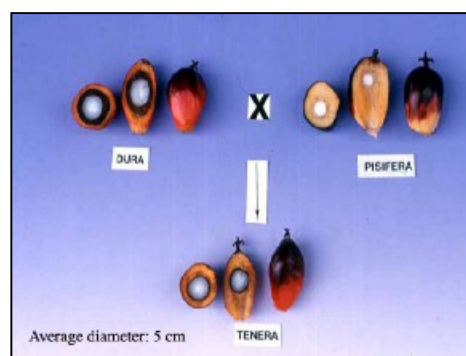
Figure 2-8: Morphology of oil palm shell (Hamid, 1999).

2.2.2   Characteristics of palm oil

The oil palm can produce two types of oils: The first type is extracted from the fibrous mesocarp, and the second is known as lauric oil which is produced from the palm kernel. In the conventional milling process, the fresh fruit bunches are sterilised and stripped of the fruitlets, which are then digested and pressed to extract the crude palm oil (CPO). The nuts are separated from fibre in the press cake and cracked to obtain palm kernels that are crushed in another plant to obtain crude palm kernel oil (CPKO) and a by-product, palm kernel cake. The fractionation of CPO and CPKO in the refinery produces the liquid stearin fraction and a solid stearin component. Figure 2-9 shows the process that produces the by-products of palm oil industry, while Figure 2-10 illustrates the detail output of FFB.
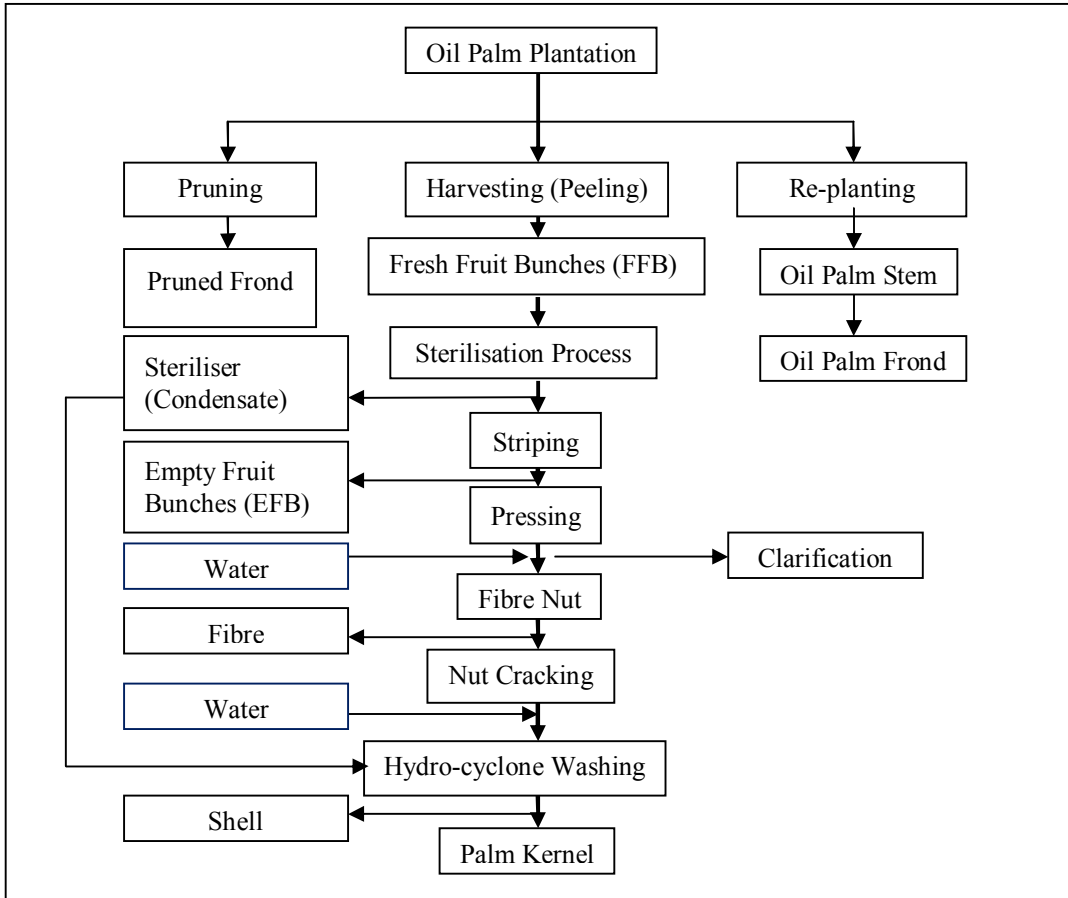
Figure 2-9: Type of oil palm by-products produced by the palm oil industry (After Hamid, 1999).
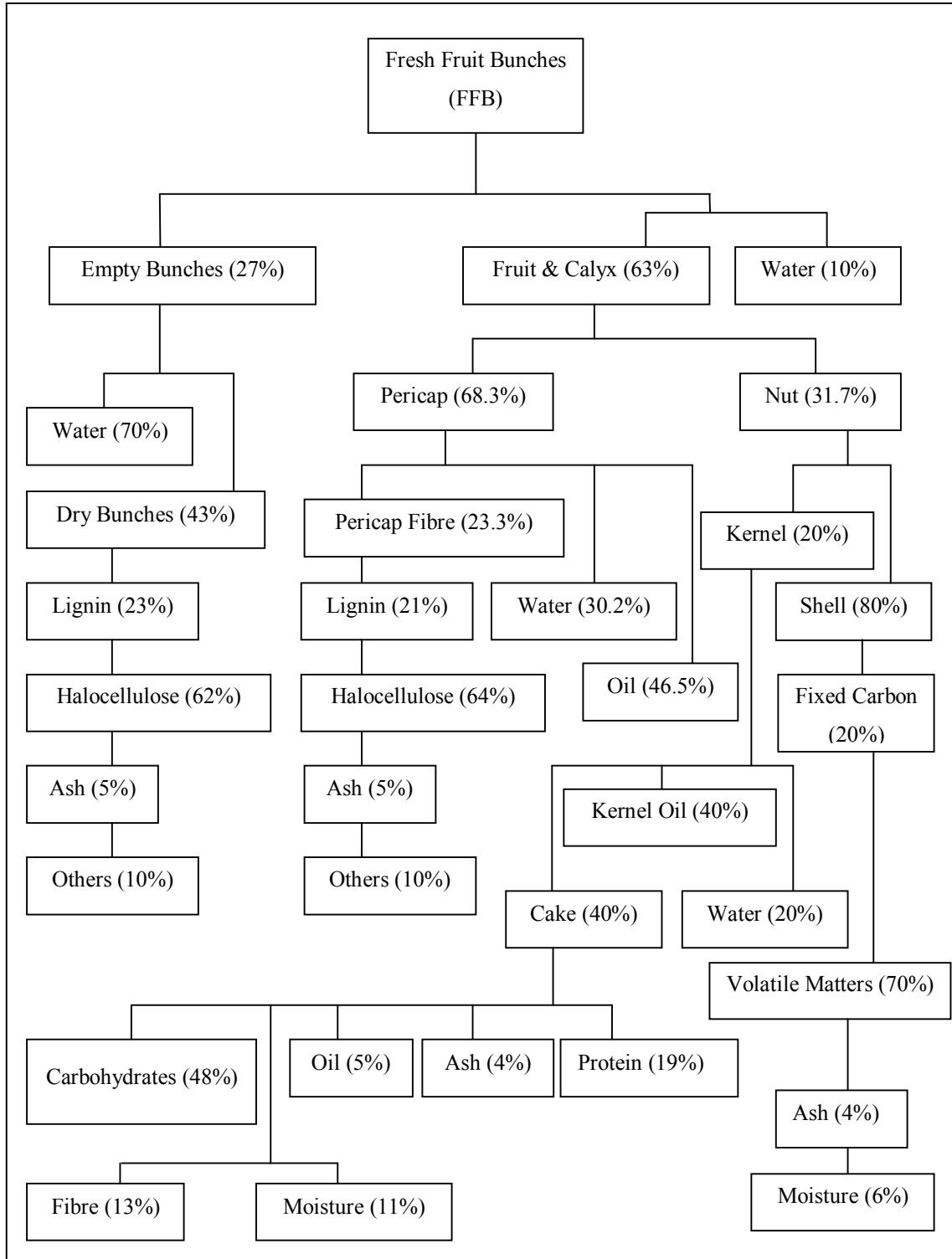
Figure 2-10: A diagramatic representation of output of a palm fruit (After Hamid, 1999).

2.2.3 Key processes in the production of palm oil

The key sub-process involved in the development of plantations for the production of fresh fruit bunches (FFB) is shown in Figure 2-11.
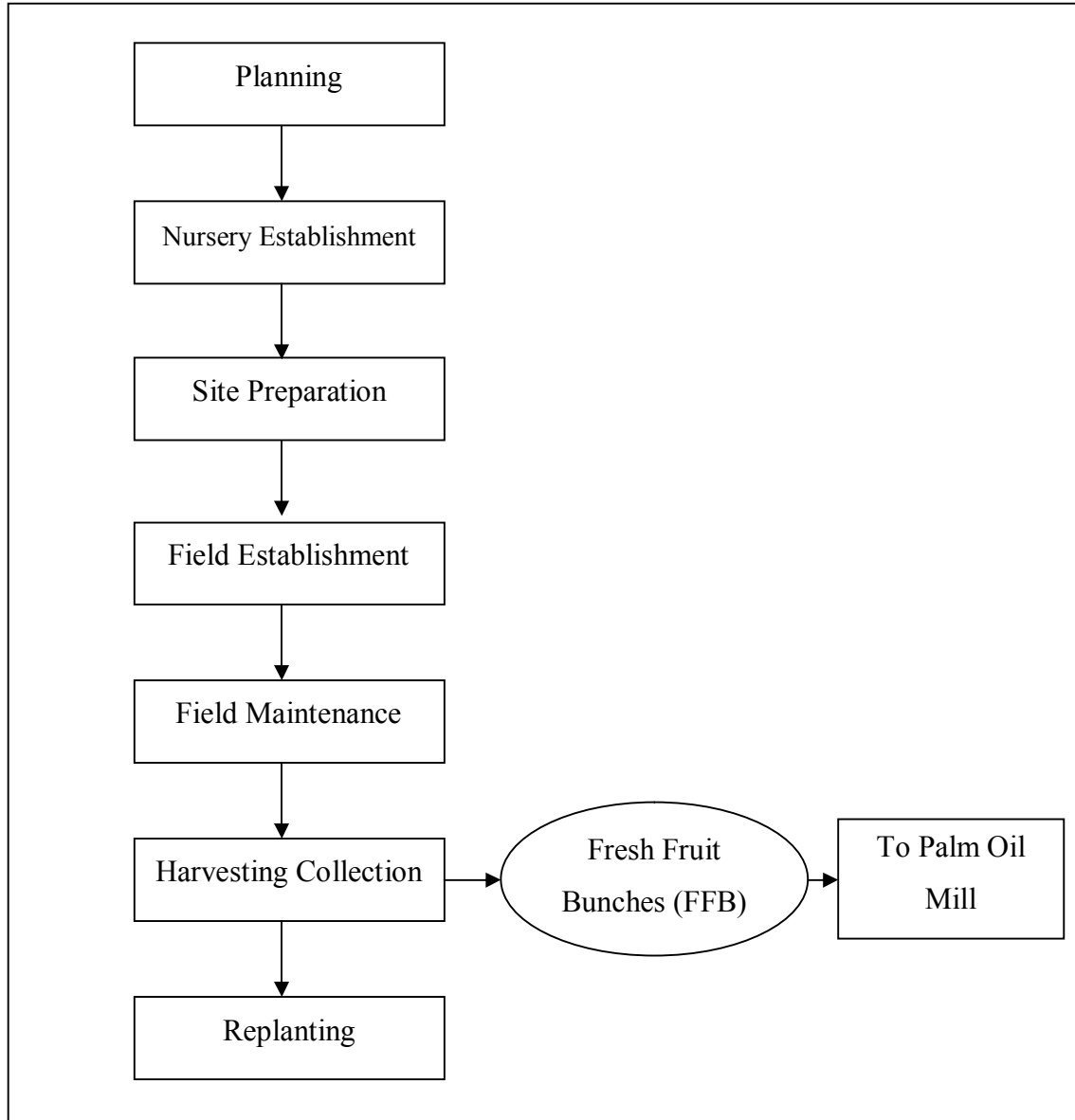
Figure 2-11: Process in the production of fresh fruit bunches (After Hamid, 1999).

All planters have to follow the rules set by the Malaysian government for the development of new plantations which involve the conduct for feasibility studies and an environment impact assessment (EIA) if the area to be developed is primary or secondary

forest in excess of 500 hectares. An EIA is also required if the development involves changes in the types of agricultural use of land in excess of 500 hectares (Hai, 2002). Figure 2-12 shows the process for the approval of EIA reports. The main objective of the EIA study is to facilitate the identification of potential environmental and social impacts and development of management plans to mitigate the adverse effects.
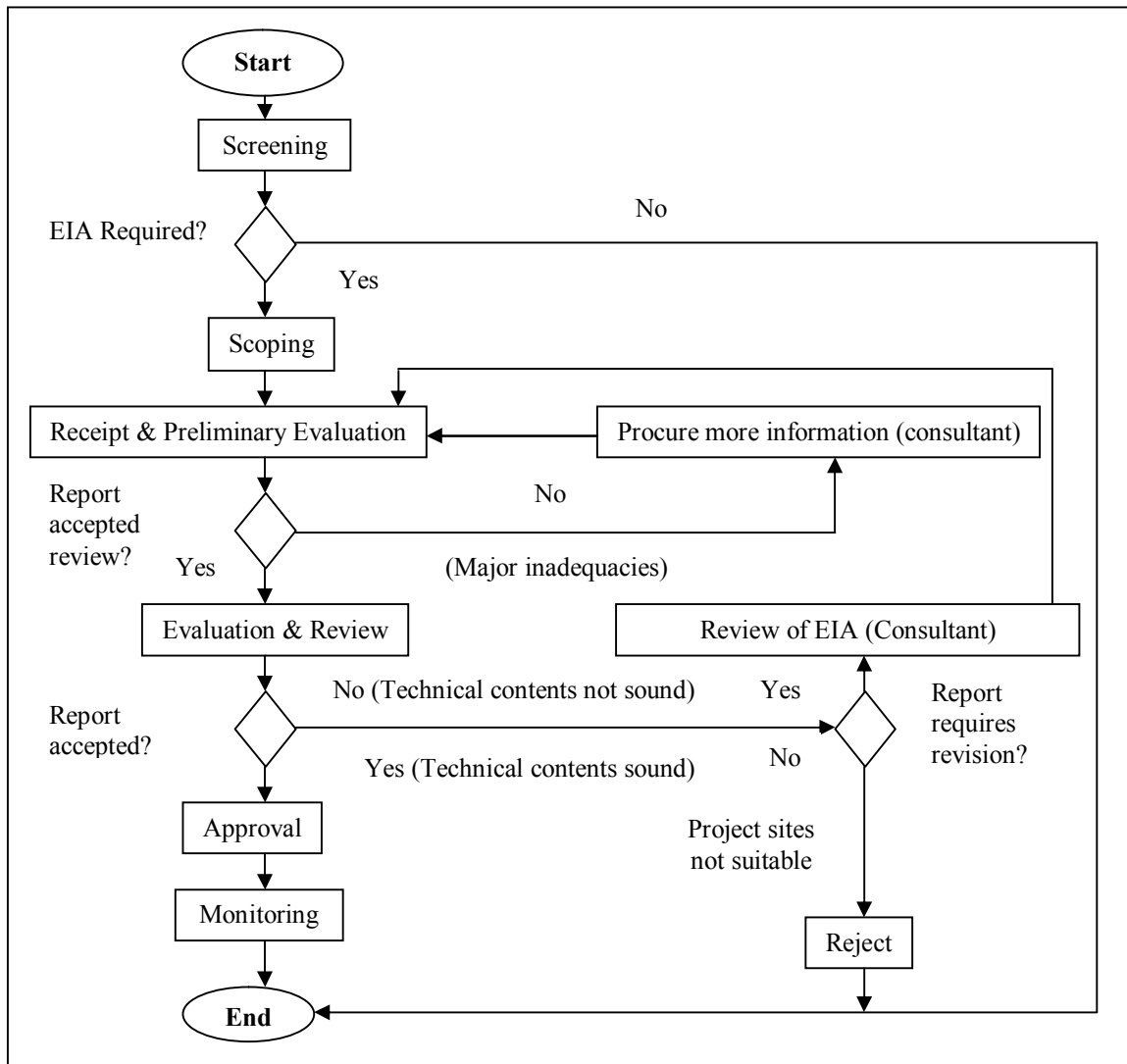
Figure 2-12: Natural resources and environment board EIA process (Hai, 2002).

2.2.4   Harvesting and collection

Harvesting of fresh fruit bunches commence between 24 to 30 months after field planting, depending on the soil type, agronomic and management inputs. Harvesting is done manually, using a chisel in young palms and a sickle mounted on a bamboo or aluminium pole in taller palms. The economic cycle of the oil palm is about 25 years, after which the old palm tree is replanted. The zero burning technique of replanting is now commercially practised. In some situations, plantations use under-planting where new seedlings are planted under the old palms which are progressively removed to allow the development of the new stand. Fresh fruit bunches is processed immediately after harvesting to uphold the quality of palm oil due to the accumulation of free fatty acids (FFA) (Basiron, 2007).

Palm oil mills are generally located in the plantations area to facilitate transportation and effective processing of fresh fruit bunches. In 2001, there were 352 palm oil mills in Malaysia (Hai, 2002). Table 2-2 shows number of oil mills, refineries and palm kernel crushing factories throughout Malaysia, with 70% located in Peninsular Malaysia (Hai, 2002).

Table 2-2: Number of oil mills, refineries and palm kernel crushing factories in operation in Malaysia in 2001.

Region	Oil mills		Refineries		Crushing factories	
	No	Capacity of fresh fruit bunches (tonnes/year)	No	Capacity of crude palm oil (tonnes/year)	No	Capacity of palm kernel (tonnes/year)
Peninsular Malaysia	244	45,373,720	38	10,952,900	30	3,254,600
Sabah	89	18,750,600	9	4,596,500	8	1,057,500
Sarawak	19	3,620,400				
Malaysia	352	67,744,720	47	15,549,400	38	4,312,100

(Source: Malaysian Palm Oil Board, 2001.)

The palm oil milling process involves the physical extraction of palm products as summarised in Figure 2-13.
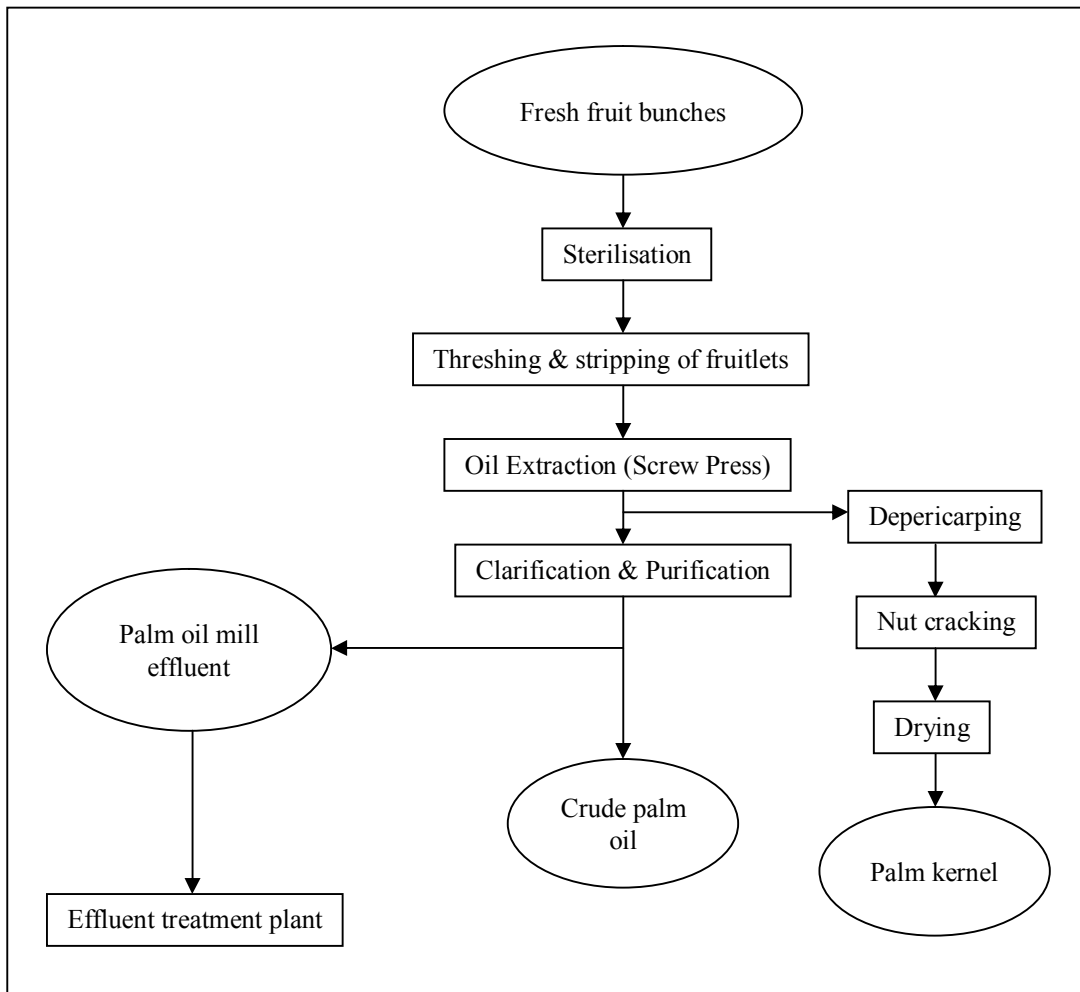
Figure 2-13: Flow chart of palm oil milling process (After Hamid, 1999).

2.2.5   Malaysian palm oil wastes

By-products of oil palm consist of the vegetative mass of the palms which ranges from the palm trunks and fronds in the field, to shells, empty fruit bunches, pressed fruit fibres and palm oil mill effluents at the oil palm mill. Currently, these by-products of oil palm are not effectively utilised and in many instances, they have caused severe pollution problems such as green house gas emission. Attempts have been made to convert these waste materials into chemicals and other value added products such as pulp and papers,

particle boards, pelletised fuels, cement tiles, activated carbon and house hold products. However, little research has been carried out so far on the utilisation of these wastes for energy purposes. The potential of these materials as an energy precursor can be seen by evaluating their proximate and ultimate analyses (Nasrin *et al.*, 2008, Shuit *et al.*, 2009, Idris *et al.*, 2010, ölz and Beerepoot, 2010). Table 2-3 shows the proximate and ultimate analyses of various oil palm wastes.

Table 2-3: Proximate and ultimate analyses of various oil palm waste (Yang *et al.*, 2006a).

Proximate analysis (wt% as received)					Ultimate analysis (wt% as received)				
	Shell	Shell*	Fiber	EFB		Shell	Shell*	Fiber	EFB
Volatiles	73.74	68.8	75.99	79.67	Carbon	53.78	55.35	50.27	48.79
Fixed carbon	18.37	20.3	12.39	8.65	Hydrogen	7.20	6.43	7.07	7.33
Moisture	5.73	8.4	6.56	8.75	Nitrogen	0.00	0.37	0.42	0.00
Ash	2.21	2.3	5.33	3.02	Sulfur	0.51	-	0.63	0.68
					Oxygen	36.30	38.01	36.28	40.18

*Results obtained from Ramlan Zailani *et al.,* 1999.

2.2.6   Woody biomass

Woody biomass is essentially a composite material constructed from oxygen containing organic polymers. High molar masses are carbohydrate polymers and oligomers which contribute to about 65% to 75% and lignin 18% to 35%. Less than 10% of the low molar mass extraneous materials, mostly organic extractives and inorganic minerals also present in woody biomass (Mohan *et al.*, 2006). The main components of woody biomass are cellulose, hemicelluloses and lignin. These components vary with different species of woods. Table 2-1 shows the typical ranges of cellulose, hemicelluloses and lignin content in various biomasses. Table 2-13 shows some of the chemical components and its compositions derived from wood at different temperatures.

The increases in oil and natural gas prices have forced the world's energy provider to consider alternative fuels, such as woody biomass. The prices of wood residue and wood pellets are lower and more stable compared to oil and natural gas (Chau *et al.*, 2009). Woody biomass is used traditionally for cooking and heating in certain parts of the world. For example, in large part of the South East Asian region, biomass is still the main source of energy for daily activities such as cooking and heating. It counts towards a large part of total final energy demand (ölz and Beerepoot, 2010). In the UK, around 10 million tonnes of woody biomass is produced every year (DEFRA, 2008). It is estimated that 2,600 GWh of electricity can be produced and 1.15 million tonnes of CO_2 equivalent emissions can be saved from burning just 2 million tonnes of woody biomass (DEFRA, 2008). The potential of woody biomass across Europe is approximately 770 TWh. About half of this energy is from by-products of the industry such as sawdust and bark, approximately 360 TWh is from roundwood and 30 TWh from forest residue (Hogan *et al.*, 2010). Replacing fossil fuel with wood pellets for residential and district heating, can reduce 81% and 97% of greenhouse gas emissions respectively (Richard *et al.*, 2010). According to the U.S. Department of Energy (Perlack and Stokes, 2011), at present, woody biomass in the U.S varies from 30 million to 129 million dry tonnes depends on price range at the farmgate.

2.2.7 Agricultural waste

Agricultural waste is produced from various agricultural activities including manure and other wastes from farms, poultry houses and slaughterhouses(OECD, 2007). Cultivation of biomass specifically for fuel utilisation known as energy cropping may create new incentives for the agricultural sector, particularly in countries that suffer from overproduction of crops. In the future, energy cropping activities may involve cultivation of fast growing wood species such as poplar, willow and miscanthus in moderate climates, and sugar cane or sweet sorghum or other suitable species in tropical areas (Bracmort and Gorte, 2010).

Europe and North America have huge potentials of agricultural waste due to the large agricultural areas in both regions. The potential of energy crops in these regions is estimated to be around 60% of the overall biomass resources (Parikka, 2004). China is the largest generator of agricultural waste in the world. For example, in 2006, it produced more than 630 million tons of agro-residues amounting to about 20 % of total energy consumption in rural areas (Chen *et al.*, 2009). According to Charles (2011), the byproduct from rice industry alone is estimated to be around 700 million tonnes per year and China has now surpassed the United States in terms of international investor in clean energy with a total investment of around 54.4 billion US$ last year.

2.3 Thermal Biomass Treatment Technologies

Thermal treatment technologies are widely used to convert biomass to other valuable products such as heat and electricity. The three most important biomass thermal conversion technologies are pyrolysis, gasification and combustion. These technologies have been studied by many researchers (Bridgwater and Grassi, 1991, van den Broek *et al.*, 1996, Swithenbank *et al.*, 1997, Heschel *et al.*, 1999, Yang *et al.*, 2006a, Abdullah and Gerhauser, 2008, Sancho *et al.*, 2008, Khan *et al.*, 2009, Mediavilla *et al.*, 2009, Sukiran *et al.*, 2009, Razuan *et al.*, 2010, Razuan *et al.*, 2011). The main objectives of using the thermal treatment methods to convert biomass are to: 1) reduce its volume, 2) convert biomass waste into harmless materials, 3) utilise chemical energy hidden within biomass as heat, steam or electrical energy and 4) protect the environment, human health and the resources. Table 2-4 shows the conditions and products derived from the three thermal conversion methods.

Table 2-4: Basic thermal processes, reaction conditions and main products (Seifert and Vehlow, 2010).

	Pyrolysis	**Gasification**	**Combustion**
Temperature (°C)	250-700	800-1600	850-1300
Pressure (Pa)	1×10^5	$1\text{-}45 \times 10^5$	1×10^5
Atmosphere	Inert/N_2	O_2, H_2O, air	Air, O_2
Stoichiometry	0	< 1	≥ 1
Gas products	H_2, CO, Hydrocarbons	H_2,CO, CH_4, CO_2	CO_2, H_2O, (O_2,N_2)
Solid products	Ash, coke	Slag	Ash/slag

Among the three technologies, combustion offers more flexible and reliable thermal conversion method for biomass fuels. In principle, combustion can be used to burn any type of biomass fuel. However, burning biomass with high moisture content (>50%) can cause more problems and may not be economically viable (McKendry, 2002b). The range of combustion plants may vary from 100 to 3000 MW with the combustion efficiency from between 20 to 40% (McKendry, 2002b).

2.3.1 Pyrolysis

Pyrolysis involves thermal degradation of solid fuels in the absence of or in a very limited amount of oxidising agent, such as air or oxygen. This process is always endothermic and requires an energy input. Pyrolysis can be performed either at atmospheric or under vacuum pressure to produce a carbonaceous char, oils, and combustible gases. The main advantage of pyrolysis is that the by-products are reusable and therefore, potentially resaleable. Relatively no waste is generated because the bio-oil and solid char can each be used as a fuel and the gas can be recycled back into the process or further processing for chemical feedstock (Bridgwater and Bridge, 1991, Babu, 2008).

As opposed to the incineration, pyrolysis process parameters are much easier to control. It is difficult and very costly to control the combustion process in order to meet the legislation demands particularly on flue gases emissions such as nitrogen oxides (NO_x) and sulphur oxides (SO_x). If halogens are present, dioxins could possibly be formed.

Because of the absence of oxidising agent such as oxygen, SO_2 and NOx are not formed during the pyrolysis process (Bridgwater and Boocock, 2006).

2.3.1.1   Types of pyrolysis

Modern pyrolysis methods have been used to derive three primary products such as char, bio-oil, and gas from biomass. There are three modes of pyrolysis process; slow, medium and fast pyrolysis. These modes are characterised by two main parameters, namely reaction temperature and the heating rate. Higher heat transfer rates and temperature maximise the production of bio-oil and/or gases, while low heat transfer rates and temperature produce mainly carbon or charcoal (Bridgwater and Boocock, 2006). The purified carbon has wide applications as additives, adsorbents to rubber and plastic products. Carbon obtained from pyrolysis can be upgraded to activated carbon. Activated carbon has various applications in the filtering processes, gas purification, and water purification in chemical industry (Hamid, 1999). Furthermore, bio-oil and gas from pyrolysis can be used as fuels and help reduce the dependency on fossil fuels. They can also be used in diesel engines and gas turbines (Zailani *et al.*, 1999). Table 2-5 shows typical pyrolysis process conditions and their products.

Table 2-5: Typical characteristics of different types of pyrolysis (Zailani *et al.*, 1999).

Pyrolysis		Residence time	Heating rate (°C/s)	Pressure (bar)	Temperature (°C)	Major product
Slow	Carbonisation	Hours or days	0.01-2.0	1	400	Charcoal
	Conventional	10s to 10 min	2.0-10.0	1	< 600	Gas, Char and Liquid
Fast	Flash-liquid[a]	< 1s	10-1000	1	< 600	Liquid
	Flash-gas[b]	< 1s	100-1,000	1	> 700	Gas
	Ultra[c]	< 0.5s	>1,000	1	1,000	Gas, chemicals
Vacuum		2-30s	2.0 – 10.0	< 0.1	400	Liquid
Hydropyrolysis[d]		< 10s		~ 20	< 500	Liquid and Chemicals
Methanopyrolysis[e]		0.5 to 1.5s	100-1,000	~ 3	1,050	Benzene, Toluene, Xylene + Alkenes

[a] Liquid obtained from flash pyrolysis accomplished in a time of < 1s
[b] Gaseous material obtained from flash pyrolysis within a time of < 1s
[c] Pyrolysis with very high degradation rate
[d] Pyrolysis with water
[e] Pyrolysis with methanol

2.3.1.1.1 Slow pyrolysis

Slow pyrolysis has been studied by many researchers to maximise the yields of char (Antal and Varhegyi, 1995, Williams and Besler, 1996, Williams and Nazzal, 1998, Williams and Williams, 1998b, Yorgun *et al.*, 2001, Antal *et al.*, 2003, Ryu *et al.*, 2007b, Vamvuka, 2010, Brown *et al.*, 2011). Pyrolysis temperature and heating rate are the most influential parameters in determining the final products (Williams and Williams, 1998b). Very slow heating rate (0.1-2.0°C/s) coupled with a low final maximum temperature (400-600°C) maximise the yield of char (Williams and Nazzal, 1998). The process of carbonisation of waste results in reduced concentrations of oil/tar and gas product and are regarded as by-products of the main charcoal-forming process.

In general, the range of heating rate for slow pyrolysis is about 10°C/min to 100°C/min and its temperature is about 300°C to 900°C (Bridgwater and Bridge, 1991). Oil palm wastes, particularly oil palm shell has been investigated under slow pyrolysis conditions by many researchers to produce activated carbon (Mohd Noor, 1995, Wan Mohd Asri, 1996, Lua and Guo, 1998, Hamid, 1999). Williams and Besler (1996) have shown that

pyrolysis of biomass at moderate heating rate 20°C/min to 100°C/min and maximum temperatures of 600°C will give an approximately equal distribution of char, oils, and gases.

2.3.1.1.2 Fast pyrolysis

Fast pyrolysis is characterised by high heating rate and temperature. Some researchers have reported that fast pyrolysis involves heating rates up to 1,000°C/s to 10,000°C/s and final temperature to 650°C (Bridgwater and Grassi, 1991, Zailani *et al.*, 1999). This method used to maximise the production of liquid or bio-oil and gas. Bridgwater and Grassi (1991) have shown that dry feed biomass in using fast pyrolysis mode can produce up to 70 wt% of bio-oil. These products can be used as an energy source or further processing for a chemical feedstock. Mohan *et al.*, (2006) have reviewed fast pyrolysis of wood-based biomass and found that about 60-75 wt% of liquid bio-oil and 10-20 wt% of non-condensable gases are produced via fast pyrolysis process. More than hundred biomass species have been tested using fast pyrolysis methods with the aims to produce liquid fuels and chemicals feedstock (Bridgwater, 1999, Di Blasi *et al.*, 1999a, Zanzi *et al.*, 2002, Putun *et al.*, 2004, Mohan *et al.*, 2006).

2.3.1.2 Pyrolysis of biomass

Varieties of biomasses have been studied by many researchers (Williams and Besler, 1993, Zailani *et al.*, 1999, McKendry, 2002a, McKendry, 2002b, McKendry, 2002c, Mohan *et al.*, 2006, Abdullah and Gerhauser, 2008, Razuan *et al.*, 2010). Among others, biomass from oil palm industry such as oil palm shell, oil palm fibre, empty fruit bunches and oil palm stone. Table 2-6 shows the properties of some oil palm wastes. In general, oil palm wastes contain a high volatile content which is suitable for pyrolysis process. Palm fibre and empty fruit bunches have high ash content (3-5%) and low calorific value (19-21 MJ/kg).

Table 2-6: Proximate and ultimate analysis of oil palm waste.

Properties	Types of biomass			
	Oil Palm Shell[*1]	Oil Palm Stone[2]	Fibre[#3]	Empty Fruit Bunches[#3]
Proximate (wt %)				
Volatiles	68.8	76.5	75.99	79.67
Fixed carbon	20.3	16.4	12.39	8.65
Moisture	8.4	5.3	6.56	8.75
Ash	2.3	1.8	5.33	3.02
Ultimate (wt %)				
Carbon	55.35	NG	50.27	48.79
Hydrogen	6.43	NG	7.07	7.33
Nitrogen	0.37	NG	0.42	0.00
Oxygen	38.01	NG	36.28	40.18
Sulfur	NG	NG	0.63	0.68
Calorific Value (MJ/kg)	22.14[3]	NG	20.64	18.96

[*] as received, [#] air-dried basis, NG = not given

Source: [1](Zailani *et al.*, 1999), [2](Guo and Lua, 1998), [3](Yang *et al.*, 2006a).

Table 2-7 shows the pyrolysis of various materials and their primary products distributions. Product yields from pyrolysis of oil palm shell in fixed bed reactor at various temperatures are shown in Table 2-8.

Table 2-7: Product yields from the pyrolysis of waste (Williams and Besler, 1996).

Waste	Pyrolysis Process	Temperature (°C)	Heating rate	Char	Liquid (%)	Gas
RDF	Fluidised bed moderate (batch)	600	20°C/min	35.2	49.2	18.8
RDF	Fluidised bed moderate (batch)	700	-	30	49	22
Plastic (mixed)	Moderate	700	25°C/min	2.9	75.1	9.6
Wood	Moderate (batch)	600	20°C/min	22.6	50.4	27.0
Wood	Fluidised bed (Fast)	550	~300°C/s	17.3	67.0	14.9
Tyre	Moderate (batch)	600	20°C/min	39.2	54.0	6.8
Tyre	Slow (batch)	850	~5°C/min	49.5	32.5	18
Tyre	Fast (batch)	640	-	38	40	18

Table 2-8: Product yield from pyrolysis of Malaysian oil palm shell (Zailani *et al.*, 1999).

Temperature (°C)	wt % of dry biomass feed		
	Liquid	**Char**	**Gases**
400	42	35	23
450	50	29	21
500	58	26	16
550	53	21	26
600	41	15	34

2.3.1.3   Pyrolysis of plastic materials

There are six main plastics in municipal solid waste namely high-density polyethylene (HDPE), low density polyethylene (LDPE), polypropylene (PP), polystyrene (PS), polyvinyl chloride (PVC) and polyethylene terephthalate (PET). The later are the common forms of plastic waste found in municipal solid waste (Williams and Williams, 1998b). Product distribution from pyrolysis of individual plastics in a fixed-bed reactor at 25°C/min to a final temperature of 700°C is summarised in Table 2-9. According to Williams (1998a), yield and composition of the products from pyrolysis of plastic are significantly influenced by plastic type and process conditions. For example, pyrolysis of the polyalkene plastics, LDPE, HDPE, and PP give oil/wax products that are dominated by alkenes, alkanes, and alkadienes.

Koo and Kim (1991) characterised the yield and composition of simple mixtures of polyethylene with polystyrene. The results showed that polystyrene played an important role to maximised oil production in short period of time during pyrolysis process. Williams and Nazzal (1998) investigated the pyrolysis of polycyclic aromatic compounds in shale oils and their results showed that by increasing the final pyrolysis temperature it increased the yield of gas and char products. However, the yield of oil/wax decreased significantly. Ryu *et al.*, (2005) pyrolysed mixed-plastic waste and found that the product

yield was in the range 30-50 wt % gases, 40-55 wt % oil/wax, and 5-15 wt % char depending on the composition of the plastic mixture and the pyrolysis temperature.

Table 2-9: Product yield from fixed-bed pyrolysis of individual plastics (Williams and Williams, 1998b).

Plastic	HDPE	LDPE	PP	PS	PVC	PET
	(wt %)					
Gases	18.0	15.1	15.3	3.4	2.5	38.7
Oil/wax	79.7	84.3	84.4	83.8	31.7	41.3
Char	0.0	0.0	0.2	3.5	13.8	15.6
HCl	0.0	0.0	0.0	0.0	52.9	0.0
Total	97.7	99.4	99.9	90.7	100.9	95.6

(Heating rate at 25°C/min and final temperature at 700°C)

2.3.1.4 Pyrolysis of refuse derived fuel

Pre-treatment of wood, rubber and plastics can constitute a valid alternative to incineration of the fraction of municipal solid wastes (MSW), which can be utilised as a fuel, known as refuse derived fuel (RDF). In fact, these processes allow the recycling of valuable materials, help to produce fuel products and at the same time reduce the total volume of emissions. Rovatti *et al*., (1994) studied the composition of RDF and the effect of temperature on pyrolysis products. Their results are shown in Table 2-10 and 2–11 respectively.

Table 2-10: Composition of the RDF materials (Rovatti *et al*., 1994).

Composition of RDF materials	
Component	Percentage (wt %)
Paper and cardboard	64
Plastics	26
Textile fibres	4
Natural fibres	6
Carbon	44-48
Hydrogen	5.0-6.6
Oxygen	7-36
Nitrogen	0.6-0.7
Sulphur	0.2-0.3
Chlorine	0.10-0.18

Table 2-11: Product distribution from pyrolysis of RDF at different temperatures (Rovatti et al., 1994).

Temperature (°C)	Solid residue (g)	Liquid residue (g)	Gas (g)	Tar (g)	Total (g)
400	14.36	5.30	0.63	3.72	24
500	13.95	5.90	1.53	2.72	24
600	12.00	6.50	2.71	2.79	24
700	9.15	8.00	4.20	2.66	24
800	8.90	8.60	4.10	2.40	24
900	8.00	9.29	5.55	1.16	24

2.3.1.5 Influence of pyrolysis parameters

2.3.1.5.1 Effect of pyrolysis temperature on products distribution

The mechanism and kinetics from biomass pyrolysis particularly from oil palm wastes in various reactors have extensively been studied by many researchers (Mackay and Roberts, 1982b, Williams and Besler, 1996, Di Blasi *et al.*, 1999b, Zailani *et al.*, 1999, Guo and Lua, 2000, Demirbas, 2001, Yan *et al.*, 2005, Yang *et al.*, 2006a). They found that pyrolysis temperature was the most important parameter, which determined the final pyrolysis products.

Yang *et al.*, (2004) studied the individual components of xylan, cellulose and lignin using TGA. They also compared the pyrolysis curves of the three palm oil wastes including shell, fibre and empty fruit bunches. Their results showed that all samples started to degrade at approximately 220°C and the weight loss began promptly after that temperature as shown in Figure 2-14. Most of the weight loss occurred between temperatures of 220°C to 340°C. Shell and fibre contain high volatile and carbon content, which result in DTG plot having two separated peaks as shown in Figures 2–15 and 2-16 respectively. This was shown to be due to the release of volatiles and slow degradation of carbon content. However, empty fruit bunches showed a single peak (Figure 2-17) due to fast degradation of carbon and release of volatile content (Yang *et al.*, 2004).
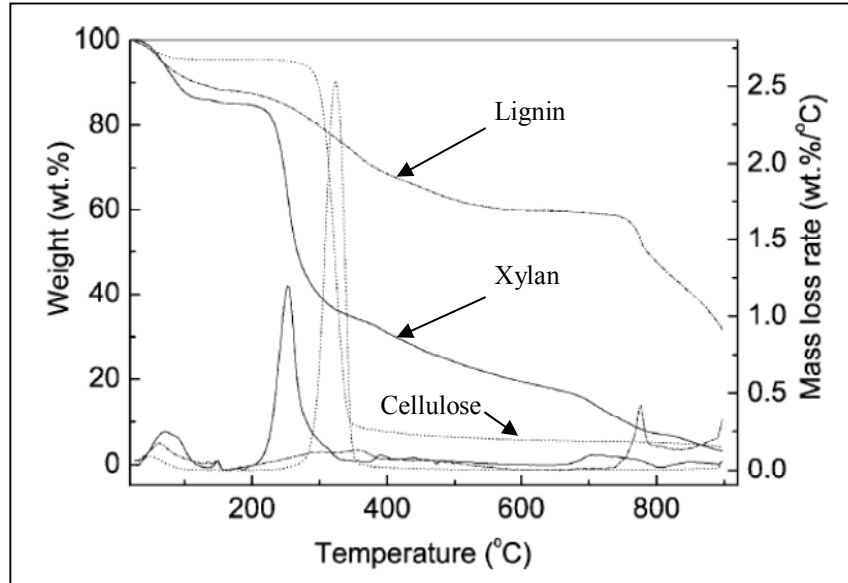
Figure 2-14: Comparison of pyrolysis of xylan, cellulose and lignin (Yang *et al.*, 2004).
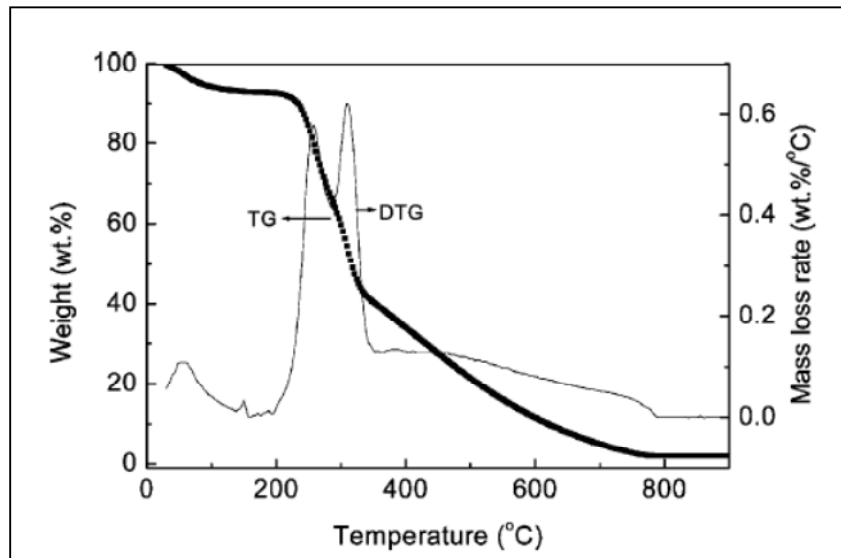
Figure 2-15: Pyrolysis curves of oil palm shell (Yang *et al.*, 2004).
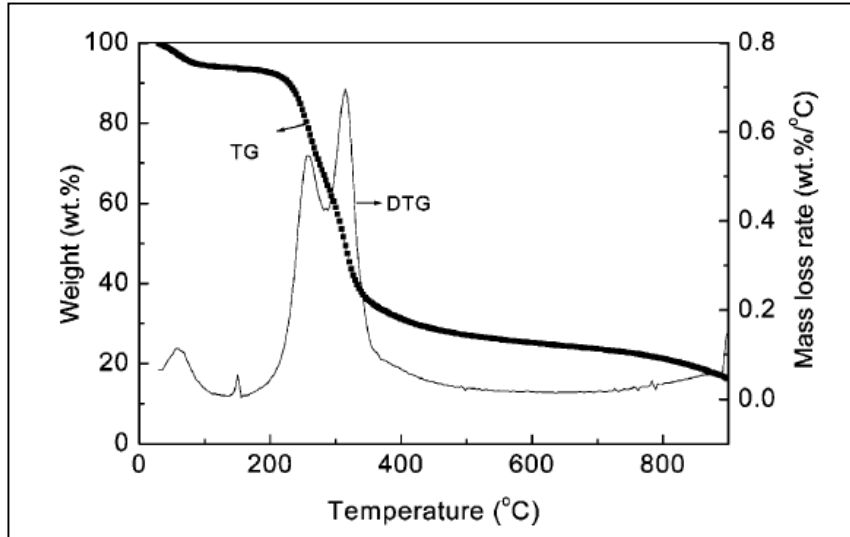
Figure 2-16: Pyrolysis curves of oil palm fibre (Yang *et al.*, 2004).
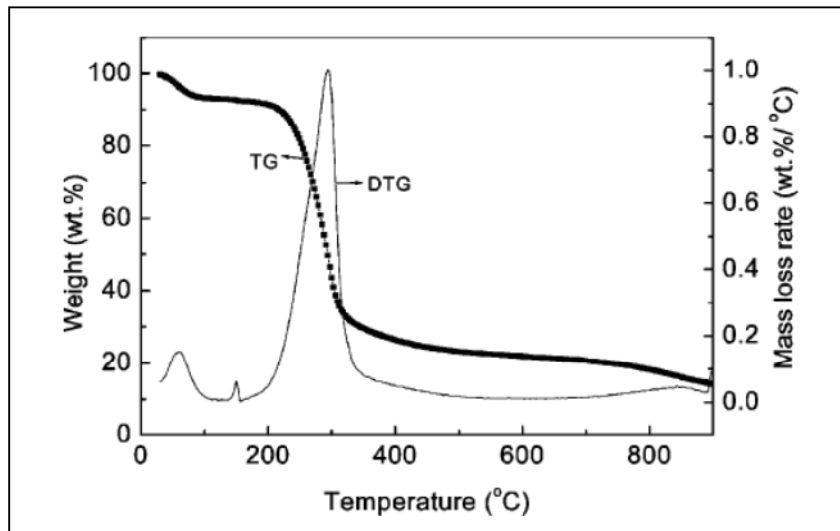
Figure 2-17: Pyrolysis curves of empty fruit bunches (Yang *et al.*, 2004).

Williams and Besler (1993) investigated the thermal behavior of rice husks in a static batch reactor at a heating rate of 5–80°C/min to a maximum temperature of 720°C. Their results showed that most of the volatile compounds, CO, CO_2 and H_2O evolved at low pyrolysis temperatures. Higher molecular weight compounds such as CH_4 and C_2H_6 and oil evolved at higher temperatures. Williams and Besler (1996) also studied the influence of temperature on the pyrolysis of pine wood using static batch reactor at a pyrolysis

temperature from 300°C to 720°C and heating rates from 5 to 80°C/min. They discovered that the amount of char produced decreased, while gas and oil products increased as pyrolysis temperature rose.

Zailani *et al*., (1999) studied the effect of temperature on the pyrolysis of oil palm shell in a fluidised bed reactor at a temperature ranging from 400°C to 600°C with feed particles of sizes between 212 - 425µm. Their results revealed that the maximum liquid yield was obtained at 500°C. Char yields decreased with the increasing final temperature. Demirbas (2004) pyrolysed agricultural residues (olive husk, corncob and tea waste) in a cylindrical reactor with externally heated electrical furnace at high temperature (600-1,000°C). His results showed that char yield decreased with increasing pyrolysis temperature (Figure 2-18). Elemental analysis of the char showed that carbon contents (Figure 2-19) increased while oxygen (Figure 2-20) and hydrogen (Figure 2-21) decreased corresponding to the temperature.
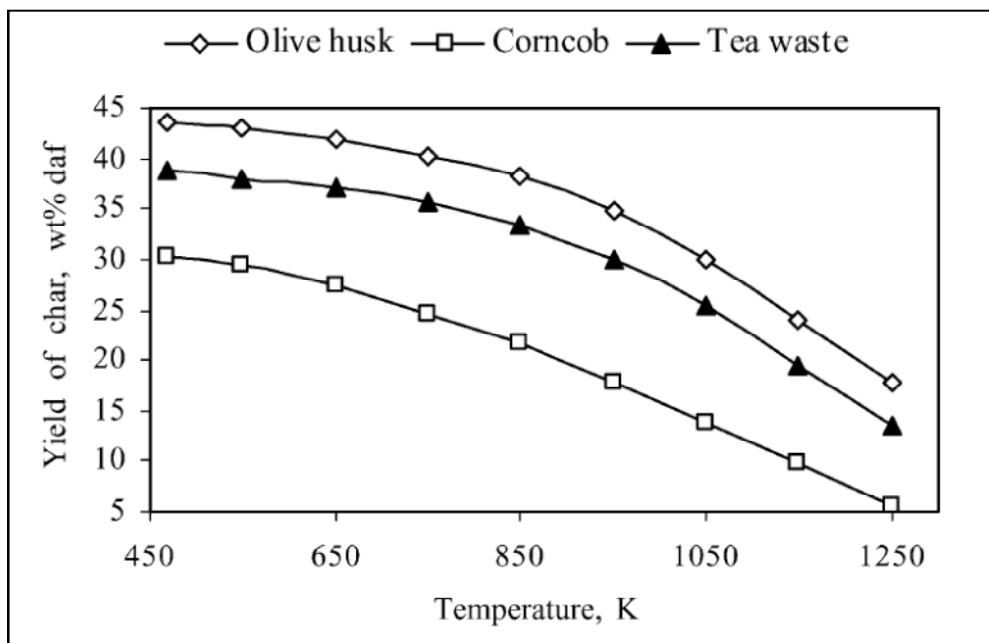
Figure 2-18: Effect of temperature on char yield (Demirbas, 2004).
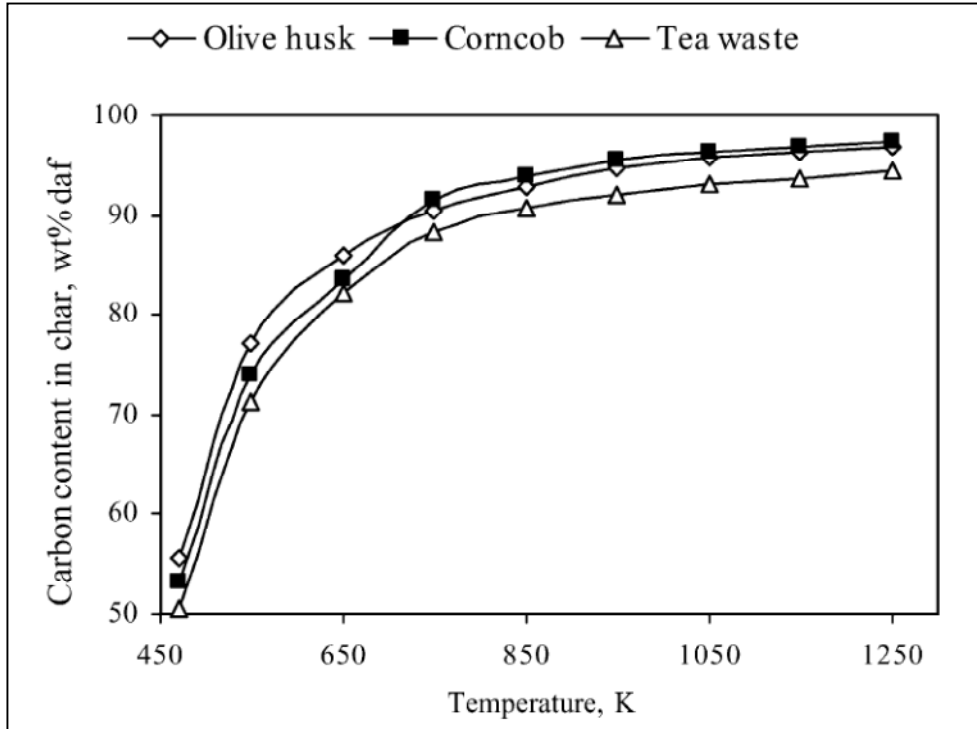
Figure 2-19: Effect of temperature on carbon content in char (Demirbas, 2004).
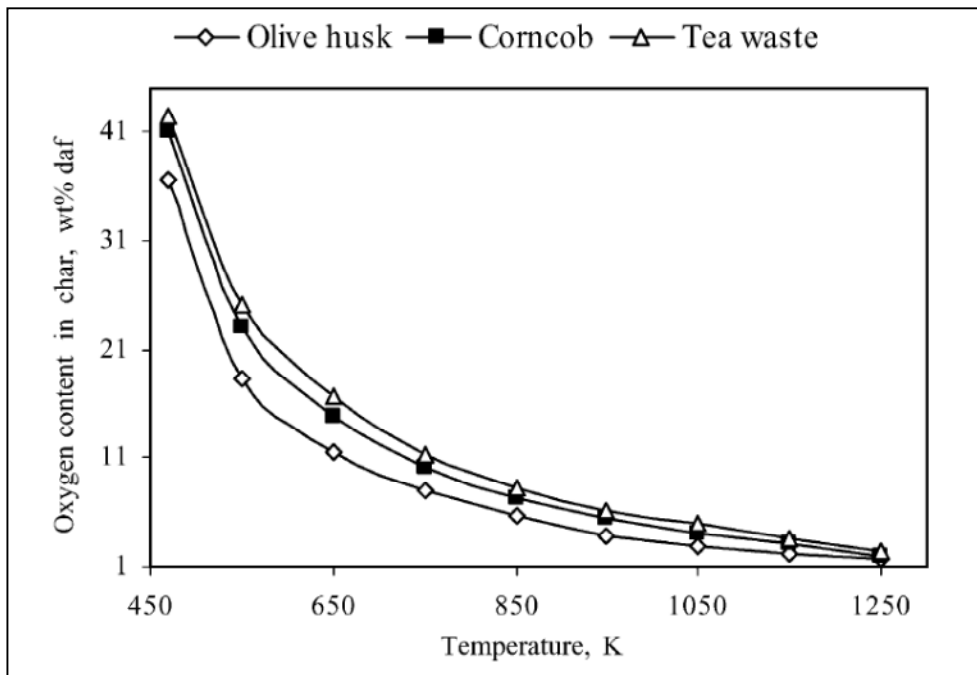
Figure 2-20: Effect of temperature on oxygen content in char (Demirbas, 2004).
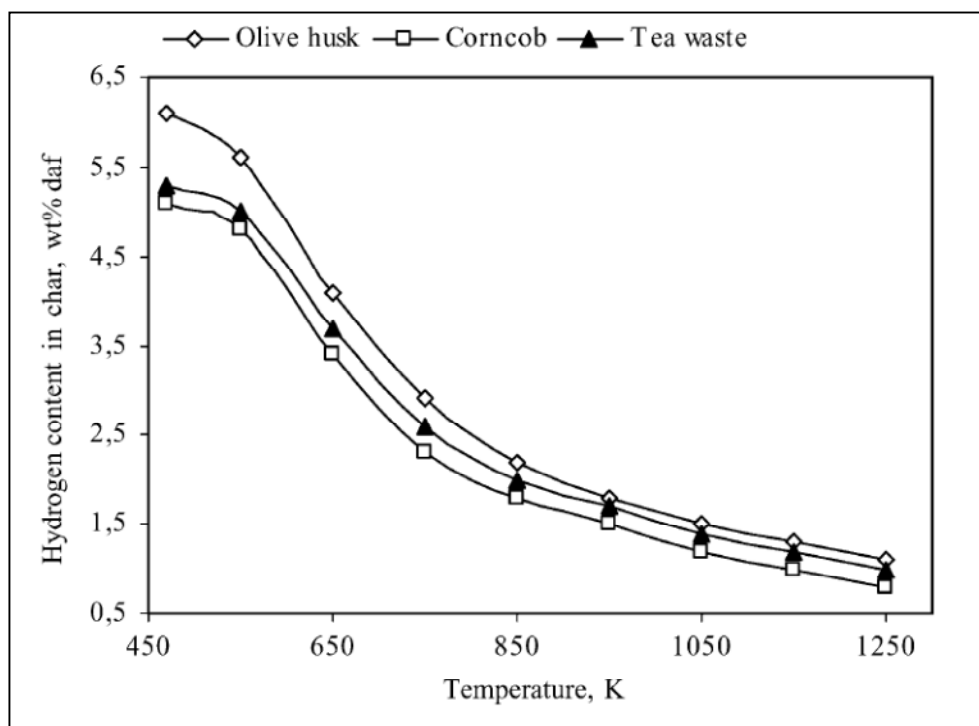
Figure 2-21: Effect of temperature on hydrogen content in char (Demirbas, 2004).

2.3.1.5.2 Effect of heating rate on pyrolysis products distribution

The effect of heating rate on the distribution of pyrolysis products has widely been studied (Horne and Williams, 1996, Williams and Besler, 1996, Demirbas, 2004, Yan *et al.*, 2005, Li *et al.*, 2007, Salehi *et al.*, 2009, Pütün, 2010). Salehi *et al.*, (2009) investigated the pyrolysis of sawdust mixture of waste wood in fixed-bed tubular reactor at four different heating rates: 100, 500, 700 and 1,000°C/min. They found that the primary products were affected by the pyrolysis temperature. Increasing the heating rate also increased the oil yield (Figure 2-22). Debdoubi *et al.*, (2006) conducted pyrolysis experiments on esparto in a fixed bed reactor under argon atmosphere at different heating rates: 50, 150 and 250°C/min. They found that liquid yield increased by the increasing of heating rate and char yield decreased as the heating rate increased.
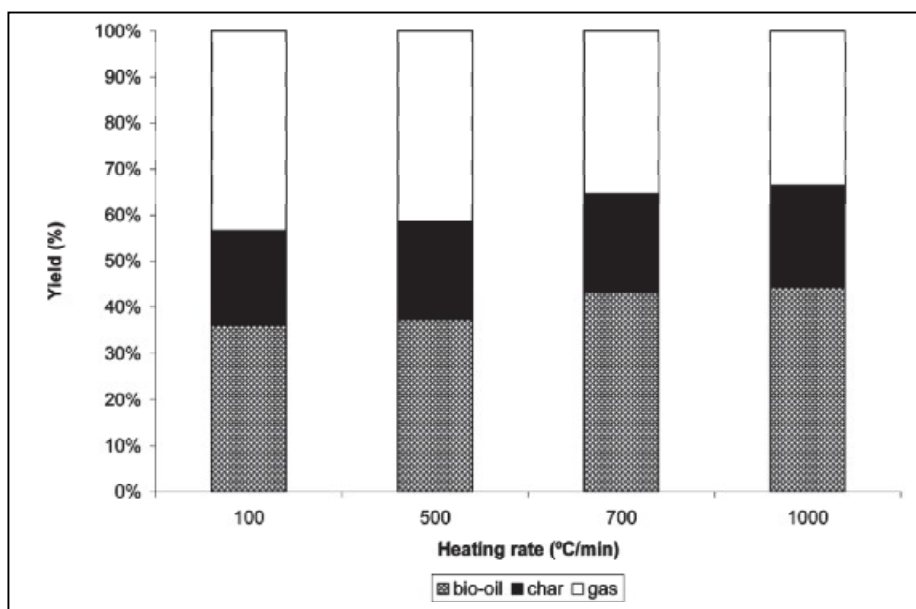
Figure 2-22: Effect of heating rate on pyrolysis products distribution (Salehi *et al.*, 2009).

2.3.1.5.3 Effect of pyrolysis temperature on product gas properties

Yang *et.al* (2006a) investigated the behavior of oil palm waste in the packed-bed reactor on the gas-release profile at room temperature up to 1,000°C. The main gas component consisted of CO_2, CO, and CH_4 together with traces of C_2H_4 and C_2H_6 were released at the temperature below 450°C. Most of the H_2 gas was released at a higher temperature ranging between 600°C to 700°C (Figure 2-23). CO and CO_2 were released at low temperature (<300°C) due to the breaking of carbonyl and carboxyl functional groups. High concentration of H_2 at higher temperature region (>400°C) was due to the breaking-up of the aromatic rings and had released significant amount hydrogen gas.

Phan (2007) studied the pyrolysis of waste wood in a fixed bed reactor at a temperature ranging from 300°C to 700°C. Two distinct stages of gas evolution were observed. At lower temperatures (< 500°C), the most abundant species were CO and CO_2. H_2 and other hydrocarbon species were released at higher temperature region.

Fassinou (2009) investigated the pyrolysis of pine wood chips in a two-stage fixed-bed reactor at a temperature from 450°C to 750°C. The feed rate of 10-20kg/h and residence time of 15-60 min were used. The results showed that the main components released during the pyrolysis process were H_2, CO, CH_4, CO_2, C_2H_6 and C_2H_4. The concentration of the gas rose with increases of pyrolysis temperature.
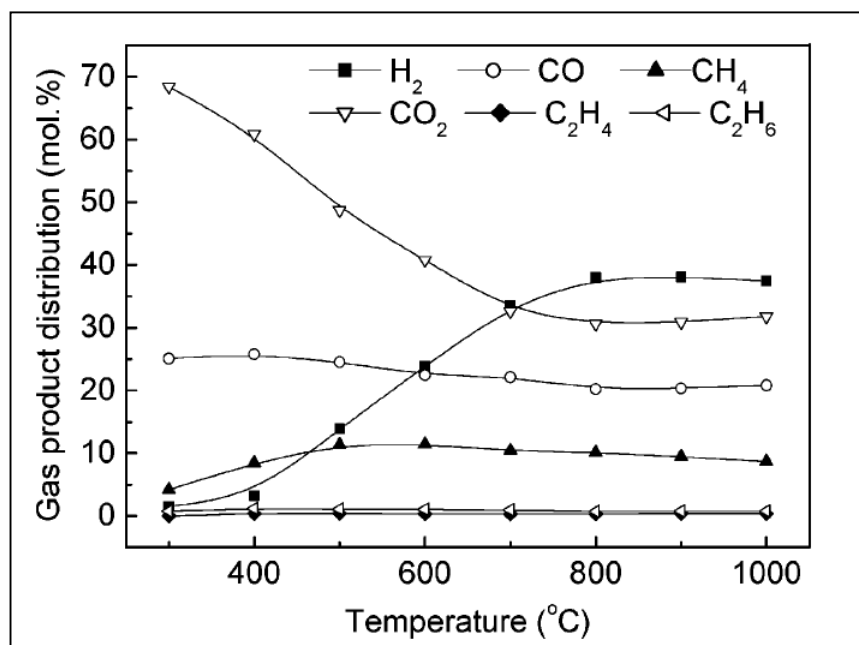
Figure 2-23: Gas product profile from oil palm shell pyrolysis (Yang *et al.*, 2006a).

2.3.1.5.4 Effect of pyrolysis temperature on char properties

The effect of pyrolysis temperature and heating rate on char properties have been published by many researchers (Roberts *et al.*, 1978, Brunner and Roberts, 1980, Suri and Horio, 2010). Brunner and Roberts (1980) investigated the carbonisation of powdered cellulose in the temperature range of 200-950°C. They measured the weight loss, carbon and hydrogen content, BET-adsorption isotherm of nitrogen and carbon dioxide, mercury penetration and particle-size distribution. Their results showed that cellulose decomposition was controlled by dehydration at a low temperature and by cleavage at a higher temperature. The char yield increased by decreasing the heating rate. Slow carbonised cellulose was yield in micropore volume and surface area increased by four

fold compared to rapid heated cellulose. Wereko-Brobby and Hagan (1996) studied the properties of char residue at different temperatures. Their results showed that carbon content increased with an increase in the pyrolysis temperature (Table 2-12).

Table 2-12: Properties of char produced at various temperatures (Wereko-Brobby and Hagan, 1996).

Temperature (°C)	Carbon (%)	Moisture (%)	Volatiles (%)	Gross carbon (%)	Calorific value (MJ/kg)	Char yield (%)	Energy yield (%)
300	30.2	1.9	70.8	28.8	22.40	56.27	65.92
400	71.5	2.8	30.9	66.7	29.88	28.03	43.80
500	87.0	2.8	17.7	80.9	32.14	22.65	38.07
600	87.5	1.0	7.1	90.0	33.20	21.63	37.56
700	92.4	1.8	3.9	94.1	33.40	20.22	34.22
800	93.4	2.2	2.4	95.6	33.90	19.54	34.64

Fassinou (2009) studied the influence of pyrolysis temperature of pine wood chip in fixed-bed reactor. The wood chip was pyrolysed at a temperature ranging from 450°C to 750°C and with the feed rate of 15-20 kg/h with residence times of 15-60 min. Their results showed that the increase in pyrolysis temperature led to a decrease in volatile matter and an increase in char rate. Furthermore, an increase in temperature also promoted the ash formation. This was due to the break up of molecules (particularly molecules with low molecular weight) that constituted biomass when they were exposed to the thermal effect. Increasing the temperature would cause this phenomenon to become stronger and could also explain the behaviour of volatile matter. The decrease of volatile matter with temperature led to an increased of char rate and thus, the production of charcoal.

Yang *et al.*, (2006a) investigated the effect of pyrolysis temperature on char produced from the oil palm shell using fixed bed reactor. They found that most of the pyrolysis reactions occurred between 300°C to 800°C. Devolatilisation of organic components rigorously occurred at temperatures between 400°C to 600°C. As the final temperature approached 800-1,000°C, almost no organic functional groups were left in the solid charcoal residue.

2.3.1.5.5 Effect of pyrolysis temperature on liquid products

The effect of temperature on the liquid products from pyrolysis has been widely studied (Sensöz, 2003, Acikgoz *et al.*, 2004, Uzun *et al.*, 2007, Garcia-Perez *et al.*, 2008, Sensoz and Angin, 2008, Fassinou *et al.*, 2009, Demiral and Ayan, 2011). Fassinou *et al.*, (2009) investigated the effect of pyrolysis temperature on the liquid product obtained from pyrolysis of pine wood in fixed-bed reactor. The main constituents found in liquid products are water, acetic acid, methanol, acetaldehyde, pentane, furfural, phenol, benzene, toluene, naphthalene, and catechol. The species that were found in small quantities included levoglucosan, acenaphthene, fluoren, maltol, butandione, 2-methylcyclopenten-1-one, 2-hydroxy-1-methyl-1-cyclopenten-3-one. The concentration of these species is shown in Table **2-13**. Levoglucosan, acetic acid, methanol, pentanal, furfural, and catechol were among the species that were released between the temperatures of 450°C to 550°C. However, at the higher temperature of 650°C and 750°C, the most abundant species were acetone, 2-3 butandion, pentanal, methanol, phenol, benzene, toluene, and indene. The more stable and heavy compounds such as benzene, toluene, naphthalene and indene were observed at the highest temperature of 750°C (Table **2-13)**.

Table 2-13: Pyrolysis liquid composition of pine wood in fixed-bed reactor (Fassinou *et al.*, 2009).

Compound	450°C	550°C	650°C	750°C
	(mg/g)			
Acetic acid	16.72	15.71	6.78	
Acetol			8.03	
Acetaldehyde	2.21	7.12	16.77	
Methanol	12.44	11.30		13.27
Pentanal	9.03	12.65	12.31	
2-3-Butandion			13.17	15.75
Acetone	2.51	6.54	19.49	45.21
Furfural	7.96	6.40	4.95	
2-Methylcyclopenten-1-one	1.20	1.33	1.41	
2-Hydroxy-1-methyl-1-cyclopenten-3-one	3.00	1.19		
3-Methyl-2-cyclopentenone	0.66	0.64		
Furfurylic alcohol		0.56	2.34	
5-Methyl-2-furfuraldehyde	2.03	1.39		
2-Acethylfuran	0.75	0.76	0.40	
Levoglucosan	33.57	34.46		
Guaiacol	4.35			
Eugenol	0.89			
4-Methyl Guaiacol	6.74			
Isoeugenol trans	2.78			
Vaniline	2.00			
Phenol	0.75	2.51	8.12	12.81
P-Cresol	0.71	1.19	2.38	0.75
M-Cresol	0.64	1.89	3.46	3.41
O-Cresol	1.00	2.26	4.56	2.58
2-4 Dimethylphenol	0.87	2.25	3.04	
3,4-Dimethylphenol	0.67	1.00	0.87	
Maltol	1.24	2.12	1.49	
3-Picolin			1.76	1.44
O-Xylen	0.27			
Benzene		0.80	7.67	52.67
Toluene		2.10	7.58	25.10
Indene	1.05	0.79	1.55	7.24
Catechol	3.79	6.15	3.23	
Fluoren				1.02
Phenantren				1.83
Acenaphthene				0.38
Naphthalene			0.90	9.37
Total organics (mg/g)	119.82	123.10	132.25	192.82
Total organics (%)	11.98	12.31	13.22	19.28
Water (%)	51.00	51.83	65.14	86.90
Total (%)	62.98	64.14	78.36	106.18

Sensöz (2003) studied the effect of temperature on liquid products from slow pyrolysis of pine bark in an externally heated fixed-bed reactor. It was found that the oxygen content of liquid was 28.36%. The main chemical functional groups discovered were alkenes, carboxylic acid and their derivatives, ketones and/or aldehydes as confirmed by FTIR analysis. Sukiran *et al*., (2009) investigated the effect of temperature on liquid obtained from the pyrolysis of oil palm empty fruit bunches in a fluidised bed reactor at temperatures of 400-600°C. They found that the oil consisted of a range of functional groups of chemical species such as phenol, alcohols, ketones, aldehydes and carboxylic acid (Figure 2-24). Yang *et al*.,(2006a) studied the effect of temperature on the liquid obtained from the pyrolysis of oil palm shell in a fixed-bed reactor at a temperature ranging from the room temperature up to 1,000°C. They suggested that the liquid consisted of a mixture of alcohols, phenols, acids, aldehydes, alkanes, ethers, ketones, and esters as revealed by the IR data in Table 2-14. More than ten separated peaks were also discovered by GC-MS analysis and among them are (1) m/z =146, 2-pentanone-4-hydroxy-4-methyl; (2) m/z =137, phthalic acid diisooctyl ester; (3) m/z =154, phenol, 2,6-dimethoxy; and (4) m/z =158, nonanoil acid, $CH_3(CH_2)_7COOH$ (Figure 2-25).
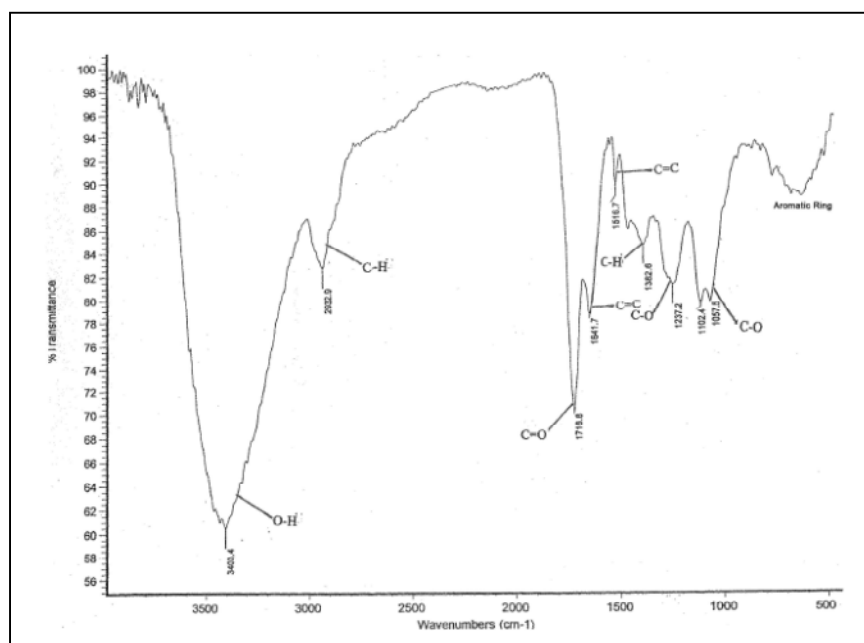
Figure 2-24: FTIR spectra of liquid obtained from the pyrolysis of oil palm empty fruit bunches (Sukiran *et al.*, 2009).

Table 2-14: FTIR functional group composition of oil obtained from pyrolysis of oil palm shell (Yang *et al.*, 2006a).

Frequency (cm^{-1})	Mode	Functional group
3300-3600	O-H stretching	Polymeric O-H, water impurities
3050-2800	C-H stretching	Alkanes
1750-1650	C=O stretching	Ketones, aldehydes, carboxylic acids
1650-1580	C=C stretching	Alkenes
1470-1350	C-H bending	Alkenes
1300-950	C-O stretching	Primary, secondary and tertiary alcohol
915-650	O-H bending	Phenol, esters, ethers and aromatic compounds
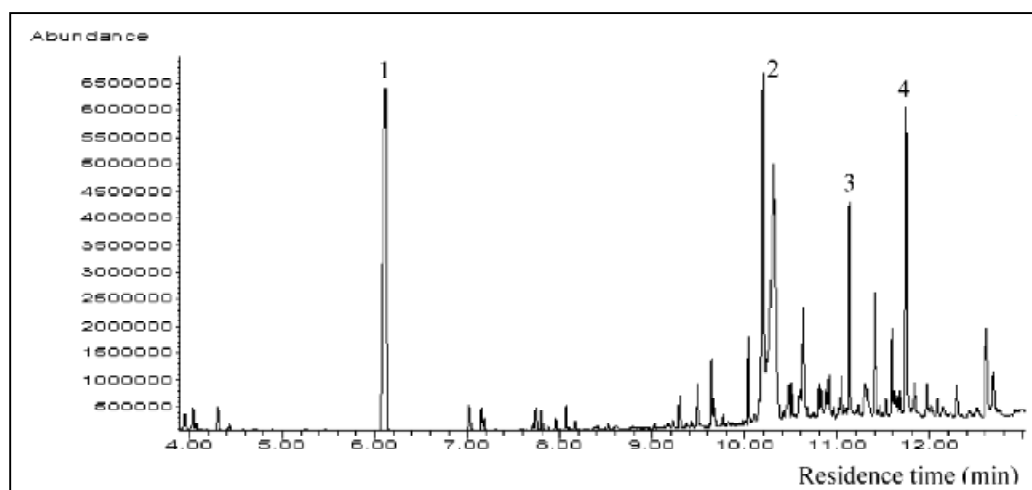
Figure 2-25: Typical total ion chromatogram of liquid oil from oil palm shell pyrolysis (Yang *et al.*, 2006a).

2.3.1.5.6 Effect of biomass feedstock particle size

Biomass particle size plays an important role in determining the pyrolysis products distribution. This is due to its ability to be heated quickly in a heat flux environment (Abdullah, 2005). Heat is transferred from the hot surfaces to biomass particles in three ways, conduction, convection and radiation. A heated biomass particle decomposes into vapor fragments (volatiles matter) and char. Upon heating a biomass particle, a pressure

is built-up inside a biomass particle due to the volumetric vapor production, which maximises at the centre and decreases towards the outer layer of the particle (see Figure 2-26). Further cracking of the produced vapor inside the particle leads to the formation of char, gases and tars.

Zailani *et al*., (1999) studied the pyrolysis of oil palm shell in an externally heated 4 cm diameter, 30 cm high fluidised bed pyrolysis reactor with nitrogen as the fluidising gas and silica sand as the bed material. The particle size ranges from 0-150, 150-300, 200-300, 300-500µm and 500µm-1mm were used in the study. They found that the maximum liquid yields were obtained with the middle size range 212-425µm. The smaller particles were either overheated or escaped from the reactor before the pyrolysis could take place. The larger size particles were not adequately heated up causing incomplete pyrolysis.

Sensöz *et al*., (2000) investigated the influence of particle size on the pyrolysis of rapeseed in a Heinze reactor. The Heinze reactor was made up of 316 stainless-steel tubular retort with 104mm length and 70mm (i.d) diameter. Reactor was heated externally by an electrical furnace in which temperature was controlled by a thermocouple inside the bed. The trapping system was heated to 400°C to avoid condensation of tar vapour. The particle size of rapeseed varied in the range of 0.224-1.8 mm. They found that the pyrolysis product distribution was independent of particle size in this experimental condition. The maximum oil yield 46 wt% was found at a particle size range of 0.85-1.8 mm.

Babu and Chaurasia (2003) studied the pyrolysis on single solid particle for a wide range of temperature from 30–2400°C and of particle diameter from 0.5–26.0 mm. It is found that as the particle size increases, the time required for completion of pyrolysis at a certain pyrolysis temperature and the effect of secondary reactions increases. For particle sizes below 1 mm, the process is controlled by the primary pyrolysis reactions and, possibly, by the external heat transfer. For particles greater than 1 mm, heat transfer, primary pyrolysis and secondary pyrolysis control the pyrolysis process.
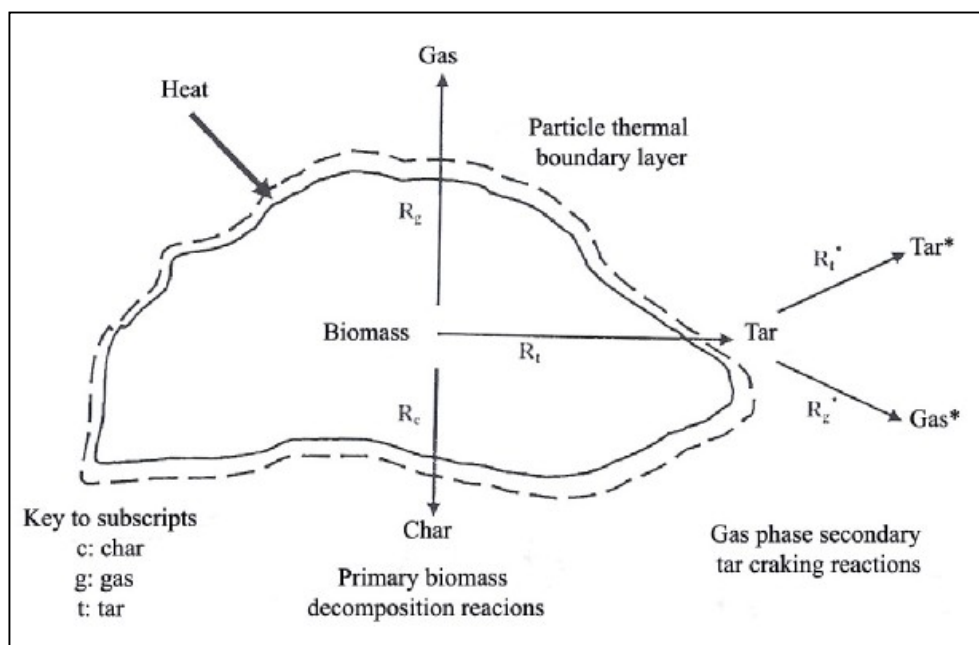
Figure 2-26: Biomass thermal decomposition model (After Abdullah, 2005).

2.3.1.5.7 Summary

In summary, pyrolysis technology and factors that affect the primary products distribution have been reviewed and discussed. The main parameters discussed are the influence of temperature, heating rate and particle size on liquid, char and gas production. Reactor temperature is the most influential factor in determining the primary products output; char, liquid and gas. Many researchers have agreed that the optimum liquid products of biomass pyrolysis are achieved at the temperatures between 400°C and 600°C. Pyrolysis of oil palm shell, fibre and empty fruit bunches have show that all samples begin to degrade at approximately 220°C and the weight loss starts promptly after that temperature. Most of the weight loss occurred between temperatures of 220°C to 340°C. Heating rate has a significant effect on pyrolysis products distribution. Increasing heating rate increases liquid yield. The char yield decreases as the heating rate increases. The smaller particles are either overheats or escaped from the reactor before the pyrolysis process can happen. On the other hand, the larger size particles are not adequately heated up causing incomplete pyrolysis. For particle sizes below 1 mm, the process is controlled by the primary pyrolysis reactions and, possibly, by the external

heat transfer, while for the particles with sizes greater than 1 mm, heat transfer, primary pyrolysis and secondary pyrolysis control the pyrolysis process.

2.3.2 Gasification

2.3.2.1 Gasification of biomass

Gasification occurs in the third stage of the combustion process after drying and pyrolysis during thermal treatment methods. It involves a process of conversion of solid or liquid fuels into a clean combustible gas or syngas. The syngas consists mainly of carbon monoxide, hydrogen, methane and carbon dioxide which can be produced from biomass. There are three different modes of thermal gasification process; partial oxidation with air, partial oxidation with oxygen and steam gasification. Detail modes and products derived from these are shown in Table 2-15 (Bridgwater, 2003).

Gasification offers an efficient method for extracting energy from many different types of organic materials. It has several advantages over direct combustion: i) As gasification converts solid fuel into gas, more energy contained in the original fuel can be extracted; ii) Syngas can be burnt directly in internal combustion engines, or used as a raw material to produce methanol and hydrogen fuels, or convert into synthetic fuel; iii) Gasification can operate at high-temperature and pressure to produces syngas, which allows for easier treatment of SOx and NOx and refines corrosive ash elements such as chloride and potassium, allowing clean gas production from problematic fuels (Gomez-Barea and Leckner, 2010).

Table 2-15: Modes of thermal gasification and gaseous products (Bridgwater, 2003).

Modes of thermal gasification	Products
Partial oxidation with air	• Main products are CO, CO_2, H_2, CH_4, N_2 and tar. • Heating value of gas produced ~5 MJ/m^3.
Partial oxidation with oxygen	• The main products are CO, CO_2, H_2, and CH_4, tar without N_2. • Heating value ~10-12 MJ/m^3.
Steam (pyrolytic) gasification	• The main products are CO, CO_2, H_2, CH_4, tar. • Heating value ~15-20 MJ/m^3.

Even though gasification technology offers several advantages for biomass thermal treatments, there are factors that limit this technology, for example: i) low carbon conversion efficiency, particularly in fluidised beds; ii) when this technology is used in cold gas applications such as engines, syngas could potentially lose their sensible heat; iii) gasifier needs to be at high temperature to avoid formation of tar, which could damage the systems.

2.3.2.2 Thermochemical conversion of biomass gasification

The thermal conversion of biomass in gasification processes is simplified in Figure 2-27. Thermochemical biomass gasification involves a series of processes: drying and devolatilisation, volatile and char combustion, gasification and tar reforming with steam and carbon dioxide. Drying is a process of removal moisture contents from fuel and it occurs at lower temperatures (< 200°C). Pyrolysis or devolatilisation process is thermally decomposed fuel in oxygen free or very limited oxygen environment. Its occurs at temperature around 300-500°C (Bridgwater, 2003). The fuel is converted into a carbonaceous solid or chars, during which, volatiles such as non-condensable gases (CO_2, H_2, CO, CH_4), condensable gases or tar and water vapour are released. Detail thermochemical reactions of biomass gasification are shown in Table 2-16.
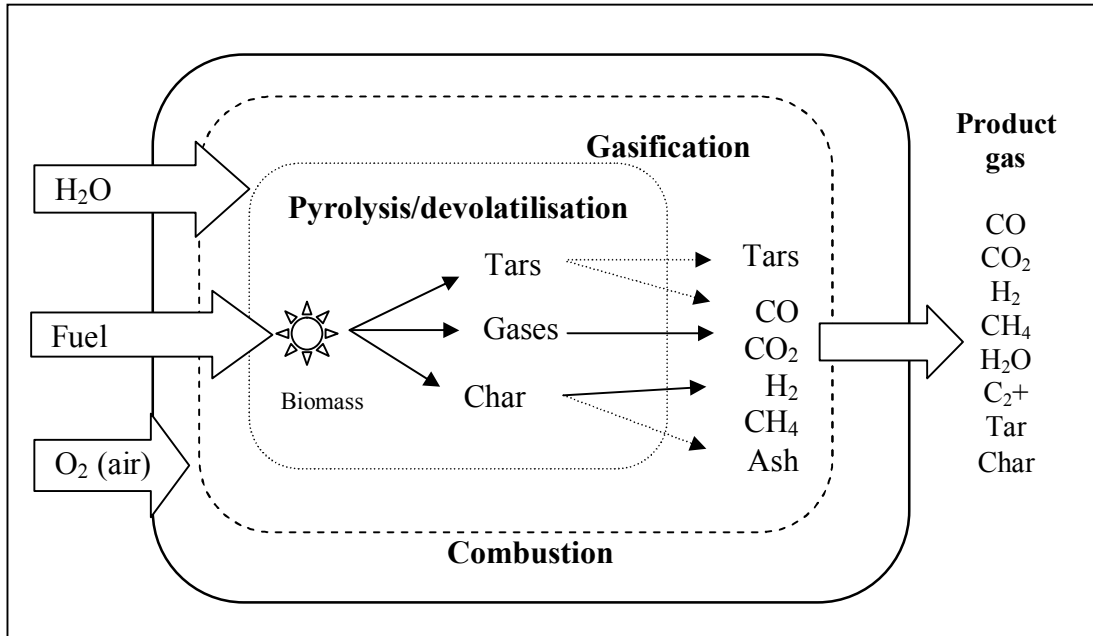
Figure 2-27: Main processes during biomass conversion in gasifier (After Gomez-Barea and Leckner, 2010).

Table 2-16: Main chemical reactions in biomass gasification (Gomez-Barea and Leckner, 2010).

Stoichiometry reaction	Heat of reaction (kJ/mol)	Process
Biomass → char + light gas ($CO+CO_2+H_2+CH_4+C_2+N_2+...$)+$H_2O$+tar	Endothermic	Biomass devolatilasation
$C + \frac{1}{2}O_2 \rightarrow CO$	-111	Partial combustion
$C + O_2 \rightarrow CO_2$	-394	Complete combustion
$C + CO_2 \rightarrow 2CO$	+173	Boudouard reaction
$C + H_2O \rightarrow CO + H_2$	+131	Steam gasification
$C + 2H_2 \rightarrow CH_4$	-75	Hydrogen gasification
$CO + \frac{1}{2}O_2 \rightarrow CO_2$	-283	Carbon monoxide oxidation
$H_2 + \frac{1}{2}O_2 \rightarrow H_2O$	-242	Hydrogen oxidation
$CH_4 + O_2 \rightarrow CO_2 + 2H_2O$	-283	Methane oxidation
$CO + HO_2 \leftrightarrows CO_2 + H_2$	-41	Water gas-shift reaction
$C_nH_m + (n/2)O_2 \rightarrow nCO_2 + (m/2)H_2$	Highly endothermic (200-300)	Partial oxidation
$C_nH_m + nCO_2 \rightarrow (m/2)H_2 + (2n)CO$		Dry reforming
$C_nH_m + nH_2O \rightarrow (m/2 + n)H_2 + nCO$		Steam reforming
$C_nH_m + (2n\text{-}m/2)H_2 \rightarrow nCH_4$		Hydrogen reforming
$C_nH_m \rightarrow (m/4)CH_4 + (n\text{-}m/4)C$		Thermal cracking

2.3.2.3 Types of gasifiers

There are four types of gasifier currently available in the market for research and commercial use: counter-current fixed beds or updraft (Figure 2-28), co-current fixed beds or downdraft (Figure 2-28), fluidised beds (Figure 2-29-2-30) and entrained-flow

gasifiers. The counter-current fixed bed gasifier consists of fixed bed of carbonaceous fuel through which the "gasification agent" (steam, oxygen and/or air) flows in counter-current configuration. The ash is either removed dry or as a slag. The slagging gasifiers require a higher ratio of steam and oxygen to carbon in order to reach temperatures higher than the ash fusion temperature. The throughput for this type of gasifier is relatively low. Thermal efficiency is high as the gas exit temperatures are relatively low. However, this means that tar and methane productions are significant at the typical operation temperatures, so product gas must be extensively cleaned before it can be used or recycled.

The co-current fixed bed gasifier (Figure 2-28) is similar to the counter-current type gasifier, except that the gasification agent flows in co-current configuration. Heat is required for this type of gasifier, particularly at the upper part of the bed, either by combusting small amounts of the fuel or supplying from external heat sources. The gas produced leaves the gasifier at a high temperature. Excess heat is transferred to the gasification agent at the top of the bed, resulting in an increase in energy efficiency. Since all tars must pass through a hot bed of char in this configuration, tar levels are much lower than the counter-current type.
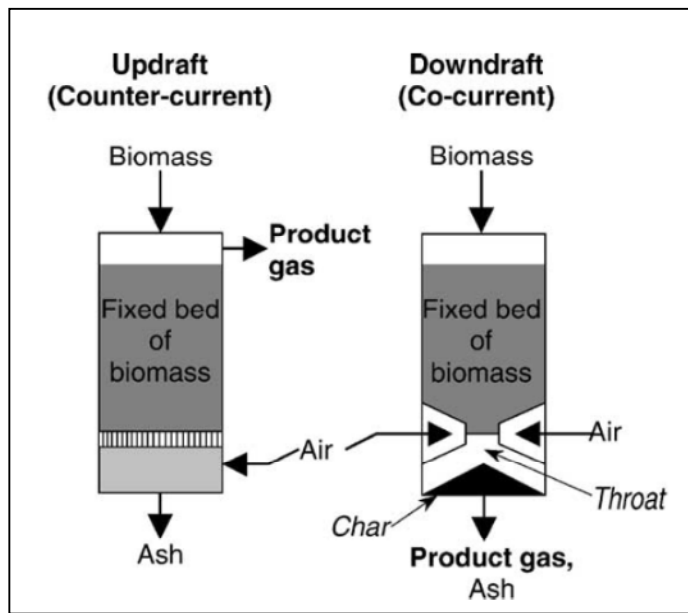
Figure 2-28: Fixed bed gasifiers (Bridgwater, 2003).

Oxygen and steam or air is used as a fluidising agent in fluidised bed gasifiers (bubbling or circulating fluidised bed). The ash is either removed dry or as heavy agglomerates. The temperatures are relatively low in dry ash gasifier, therefore, the fuel must be highly reactive; low-grade fuels such as biomasses are particularly suitable. The agglomerating gasifiers have slightly higher temperatures, therefore it suitable for higher rank fuel such as coal. Fuel throughput is higher than for the fixed bed, but not as high as for the entrained flow gasifier. The conversion efficiency is low due to elutriation of carbonaceous material. Recycling or subsequent combustion of solids can be used to increase conversion efficiency. Fluidised bed gasifiers are most useful for fuels that form highly corrosive ash that would damage the walls of slagging gasifiers.

Entrained flow gasifiers are used for fine, dry, or pulverised fuel, slurry or atomised liquid fuels. The gasification reactions take place in a dense cloud of very fine particles or droplets. Most coals are suitable for this type of gasifier because of the high operating temperatures (around 1,200-1,500°C) and because the pulverised coal particles are well-separated from one another. The high temperatures and pressures also mean that a higher throughput can be achieved. However, thermal efficiency is somewhat lower as the gas must be cooled before it can be cleaned. Due to the high temperatures, tar and methane are not present in the product gas. However, the oxygen requirement is higher compared to other types of gasifiers. All entrained flow gasifiers remove the major part of the ash as a slag since the operating temperature is well above the ash fusion temperature. A smaller fraction of the ash is produced either as a very fine dry fly ash or fly ash slurry (Beychok, 1974a, Beychok, 1974b, Beychok, 1975). Due to economic of scale effects, the development of these types of gasifier has been abandoned (Gomez-Barea and Leckner, 2010). Development of medium and large scale biomass gasification are currently based on fluidised bed technology (Gomez-Barea and Leckner, 2010).
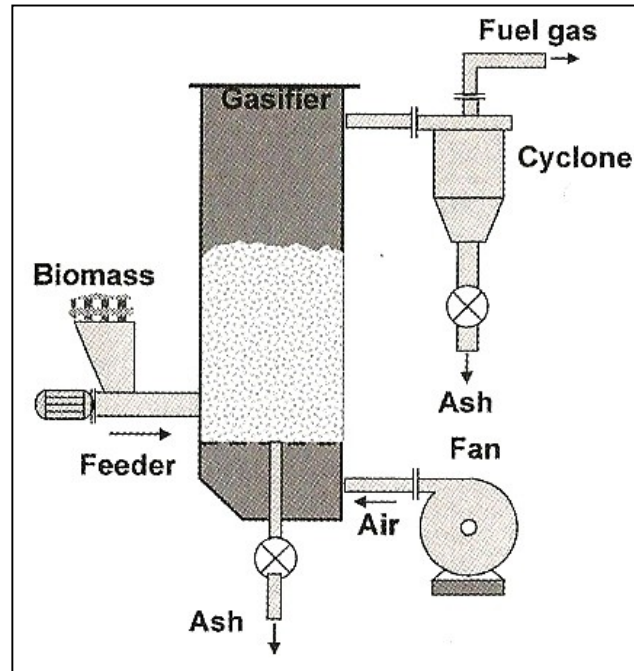
Figure 2-29: Bubbling fluidised bed gasifier (Gomez-Barea and Leckner, 2010).
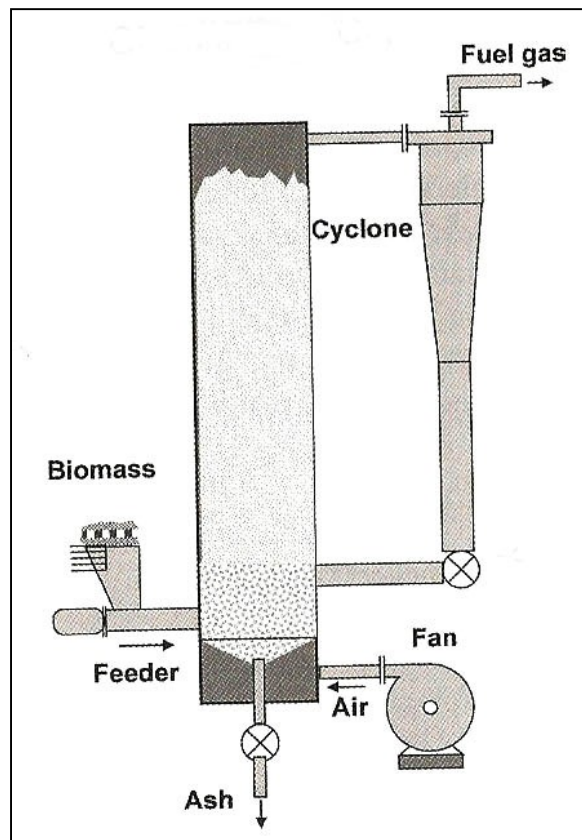
Figure 2-30: Circulating fluidised bed gasifier (Gomez-Barea and Leckner, 2010).

2.3.2.4   Effect of operating conditions on properties of syngas

Gasification of biomass and waste technology have been developed across Europe and North America in both single-stage and multi-stage processes (Na *et al.*, 2003). Syngas properties produced via gasification technology have extensively been studied over the past three decades (Na *et al.*, 2003, Aguiar and Garcia, 2006, Sheth and Babu, 2009). Safi *et al.* (2004) studied the global degradation kinetics of pine needles at different heating rate. The air flow rate of 50 ml/min was used in their study. They found that the char obtained at different heating rates were less than the available fixed carbon, due to the presence of reactive medium such as air. This may result in complete gasification of the biomass. However, to date, there has been no attempt reported on the effect of static inert or static reactive medium on the gasification of biomass.

Sharma (2009) examined the temperature profile, gas composition, calorific value and trends for pressure drop across the porous gasifier bed, cooling–cleaning train and across the 75 kWth, downdraft (biomass) gasifier system. The study was conducted for both non-firing and firing mode. The results showed that non-firing gasifier, the extinguished bed (progressively decreasing particle size distribution) gave much higher pressure drop as compared to a freshly charged gasifier bed (uniformly distributed particle size). The pressure drop across the porous bed, cooling–cleaning train and across the spray cooler was found to be sensitive to the increase in the flow rate. However, the sand bed filters had a strong function of quartz particle size in addition to the flow rate through them. A higher pressure drop across the filter bed was due to the tar or particulate deposited over the quartz particles. Decreased particles size caused an increase in pressure drop through both gasifier bed and the entire system.

On the other hand, in the firing mode, the higher temperature in bed tended to improve the conversion of non-combustibles component (such as CO_2, H_2O) into combustible component (such as CO, H_2) in the resulting gas and, thus, improve the calorific value of product gas. Any increase in temperature in bed either due to energetic of reactions or any other reason such as an increase in gas flow rates tended to have higher resistance to flow through the porous bed and, thus higher pressure drops.

According to Na *et al.*, (2003), the concentration of H_2 and CO gases were dependent on the oxygen/fuel ratio. The formation of H_2 and CO increased with bed height due to the char-CO_2 reaction. The oxygen/waste ratio of 0.35 to 0.45 gave maximum CO concentration. The heating value of produced gas was around 11.7 to 13.4 MJ/Nm^3.

Aguiar and Garcia (2006) studied the gasification of orange peel in three different temperatures; 750, 800 and 850°C and the ratio of air used in gasification to the air for stoichiometric combustion was 30%. Three different air ratios 26, 30 and 35 were used at the temperature of 850°C. Their results showed that an increasing air ratio led to an increased in the gas concentration. Any increase in temperature caused the decrease in tar and char production.

Di Blasi *et al.*,(1999b) studied several biomass gasification including beech woods, nutshell, olive husks and grape residue in a counter-current fixed bed reactor. Their results showed that the gas produced had a heating value around 5.0 to 5.5 MJ/Nm^3. The main gases released were CO, CO_2, H_2 and CH_4. Small amount of higher hydrocarbons gas was also reported. They also concluded that the air-to-fuel ratio was inversely proportional to the heating value of the gas in all biomass cases.

2.3.2.5 Tar in pyrolysis and gasification of biomass

The production of low-heating-value gaseous fuels by thermal decomposition pyrolysis and gasification of biomass such as wood and agricultural waste provides a renewable source of heat and electric power generation (Brage *et al.*, 1996a). One of the main problems is the presence of tars in product gaseous. Tars can cause damages to internal combustion engines (IC), gas turbines and other machinery. Many papers have been published in relation to tar problems (Brage *et al.*, 1996b, Yu *et al.*, 1997, Henriksen *et al.*, 2006). The main pyrolysis and gasification products are permanent gases such as CO, CO_2, H_2 and CH_4. Small amount of condensable tar by-products are also formed and likely to induce operating problems (condensation) in piping system and link gas turbines (Brage *et al.*, 1996a). Since tar composition supplies quantitative and qualitative chemical

information about pyrolysis and gasification conditions, tar analysis is complementary to gas analysis in monitoring and controlling the process and catalyst performance.

Tar derived from the lignin part of biomass, is normally very complex heterogeneous aqueous mixtures of organic molecules such as aromatics, phenols, bases, asphaltenes, preasphaltenes, and particulate matter. Its concentration may vary depending on the formation conditions such as temperature, residence time, pressure, feedstock and reactor design (Brage *et al.*, 1996a). Sampling techniques for tar analysis have been widely discussed (Brage *et al.*, 1996a, Brage *et al.*, 1996b, Yu *et al.*, 1997). A highly efficient method based on solid-phase adsorption (s.p.a) on amino phase was designed. This method is suitable for intermittent trapping of tar compounds ranging from benzene to coronene prevailing in product gases from thermal decomposition of biomass at 700-1,000°C. The advantage of this technique is the sampling step allows the collection of one of three samples per minute compared to one or two sample per hour using conventional cold trapping.

Henriksen *et al* (2006) studied a two-stage gasifier known as "Viking" gasifier (Figure 2-31) which was operated for more than 200 hours. The gas produced by gasification was used to fuel engine (75 kW thermal). The pyrolysis products were partially oxidised by means of air addition and the tar content in the volatiles was reduced by a factor of 100. In the second stage gasifier the tar was further reduced by a factor of 100 as partially oxidised pyrolysis products passed through the char bed. They also revealed that small amounts of deposits consisting of salts and carbonates were observed in the hot gas heat exchanger.
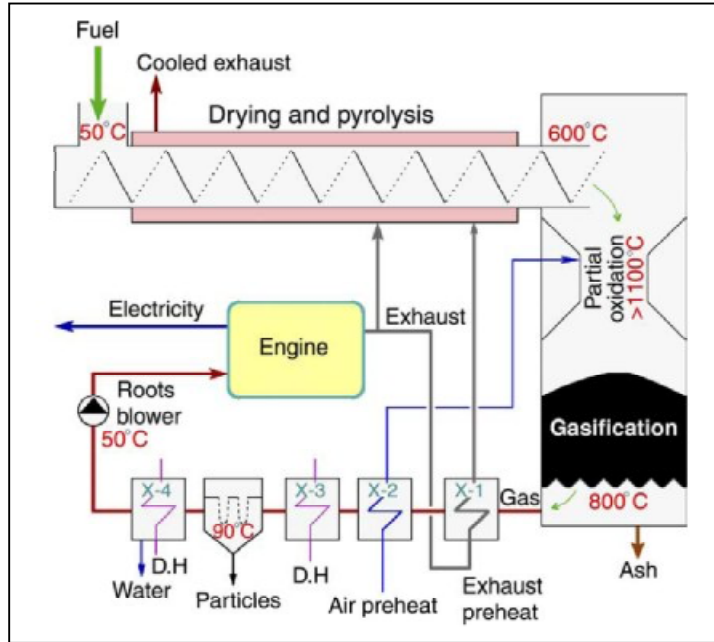
Figure 2-31: The Viking gasifier (Henriksen *et al.*, 2006).

2.3.3 Combustion

Thermochemical conversion technologies, namely combustion, gasification and pyrolysis, are widely used to convert biomass fuel for heat and power generation. Combustion is a proven technology for heat and power production (Nussbaumer, 2003). It involves a series of exothermic chemical reactions between a fuel (solid, liquid or gas) and an oxidising agent such as air or oxygen to complete the oxidation process.

The important steps involved during combustion processes are drying, devolatilisation, gasification, char combustion and gas-phase oxidation. The time spent in each reaction of biomass combustion is influenced by solid fuel particle size and properties, temperature and combustion conditions. Nussbaumer (2003) studied the influence of time and temperature over mass loss of wood particles by thermogravimetric analysis. It was found that there exists a distinct separation between volatile and char combustion phases in the combustion of a small biomass size particle as shown in Figure 2-32(A). Combustion of biomass with a large particle size showed the phases overlapped to a certain degree. High

volatiles content released during the combustion of a large particle size biomass was also observed (Figure 2-32(B)). The high volatile content is an important issue to consider during the design of a suitable combustion chamber.
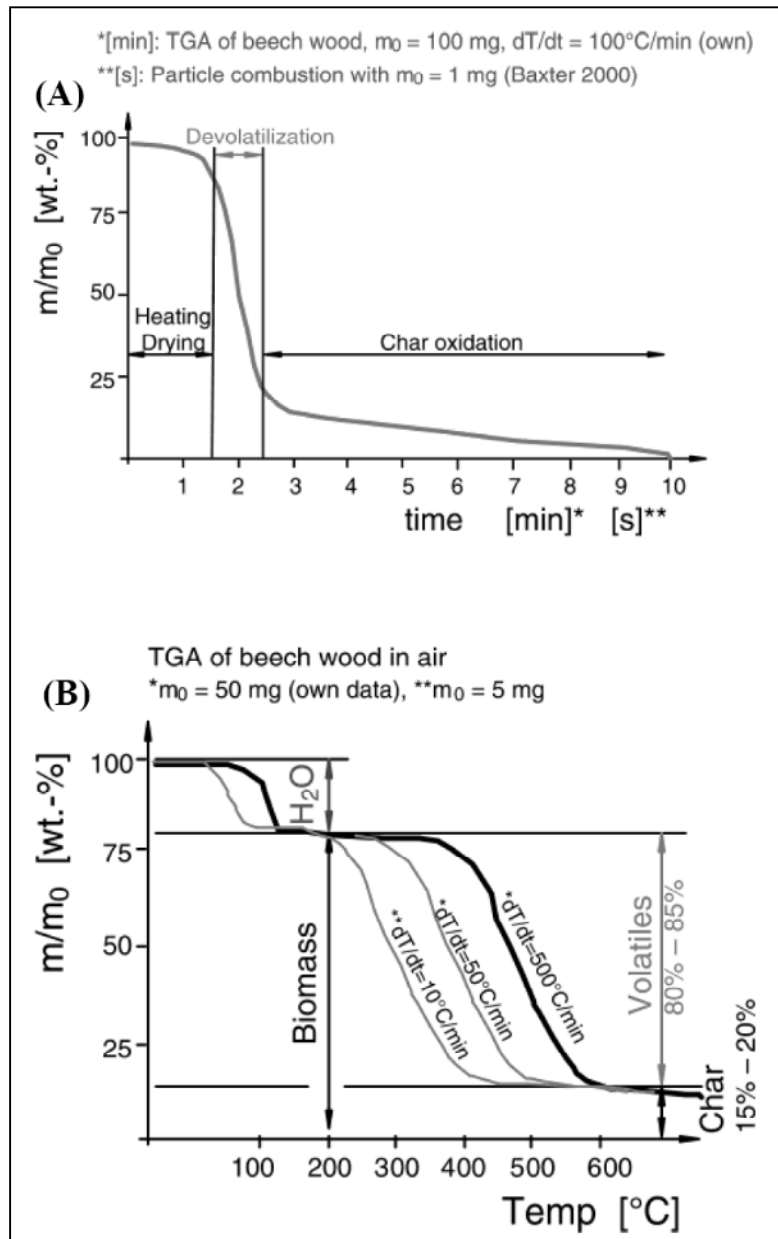
Figure 2-32: Mass loss as a function of time (A) and temperature (B) during combustion of biomass (Nussbaumer, 2003).

2.3.3.1 Combustion principle

Biomass combustion normally takes place at temperatures between 850°C and 1,100°C with a large excess of air or oxygen (Suri and Horio, 2010). The process involves both organic and the mineral parts which undergo decomposition process. The process starts with the desorption of gases stored in biomass and occurs at a temperature around 100°C. The release of gaseous hydrocarbons, tar, carbon dioxide, carbon monoxide and steam take place at temperatures above 300°C. For the combustion of coal, below 400°C the coal particles remain intact. At temperature above 400°C coal particle undergoes a plastic state during which the shape and the size of the particle changes. The plastic state normally ends when the combustion temperatures are above 550°C and the particle becomes a hard substance, also known as char. Further heating stabilised the char due to the releases of hydrogen and carbon monoxide from the particle (Tomeczek, 1994). Tomeczeck (1994) outlined the general chemical processes involved during the combustion of coal as follows:

➢ Coal or biomass → Metaplast   Eq: 2-1

➢ Metaplast → Primary char + Primary volatiles   Eq: 2-2

➢ Primary char → Char + Secondary gas   Eq: 2-3
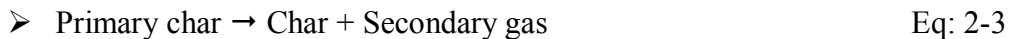
Metaplast is a nonstable temporary state of coal or biomass that occurs at temperatures above 300°C.

The formation of lower molecular tar and gases within the pores of particle occurs according to reactions:

➢ Liquid → Liquid + Gas   Eq: 2-4

➢ Liquid → Solid + Liquid   Eq: 2-5

➢ Liquid → Solid + Gas   Eq: 2-6
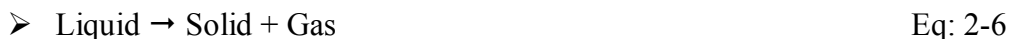
During the devolatilisation process, the reactions that could take place are as follows:

➢ $CO + 3H_2 \rightarrow CH_4 + H_2O$ (Methanation)   Eq: 2-7

➢ $C + 2H_2 \rightarrow CH_4$ (Hydrogasification)   Eq: 2-8

➢ $CO + H_2O \rightarrow CO_2 + H_2$ (Water gas)   Eq: 2-9

➢ $C + CO_2 \rightarrow 2CO$ (Boudouard)   Eq: 2-10
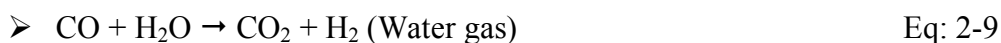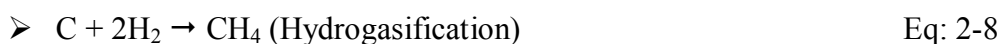
Excess air ratio (λ) is the most important parameter in any combustion process. This property describes the ratio between the locally available and the stoichiometric amount of combustion air (Nussbaumer, 2003). The combustion process takes place in a furnace, where chemical-bond energy in the fuel is converted into a thermal energy, which becomes available in the form of hot flue gas. This hot flue gas is an important output of the furnace. It is used to measure the efficiency of the combustion process. Not all the chemical energy from the fuel is converted into thermal energy. This is due to the energy losses during the combustion process. These losses come from several factors such as heat losses to the environment through furnace wall, release of hot ash, unburnt particles in the ash and unburnt pyrolysis gases and carbon monoxide (CO) in the flue gas. In general, the combustion reaction of biomass (without N, K, Cl) can be described as follows:

$CH_{1.44}O_{0.66} + \lambda 1.03(O_2 + 3.76\ N_2) \rightarrow$ intermediates (C, CO, H_2, CO_2, C_mH_n, etc.) $\rightarrow CO_2$, $+ 0.72H_2O + (\lambda-1)O_2 + \lambda 3.87N_2$ (-439kJ/kmol).   Eq: 2-11

Where,

        $CH_{1.44}O_{0.66}$ is an average composition of typical biomass such as wood, straw, or similar material.

Combustion is normally conducted in stages with the excess air varies in various sections of the combustion chamber. Figure 2-33 shows the main reactions involved during the two-stage combustion of biomass.
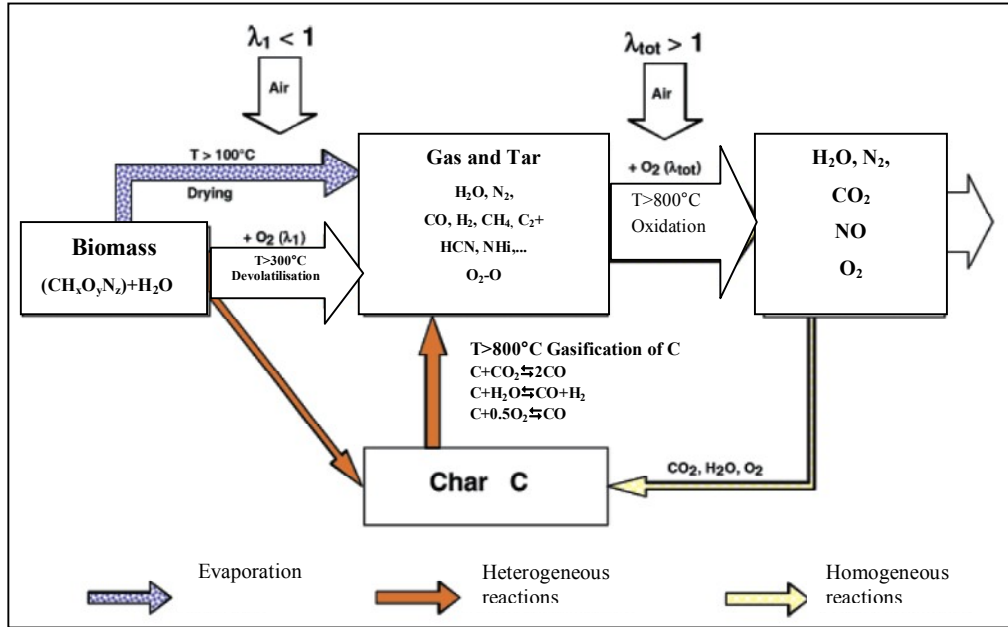
Figure 2-33: Main reactions during two-stage combustion of biomass with primary and secondary air (Nussbaumer, 2003).

According to van den Broek *et al*., (1996), commercial biomass power plants (> 10MW$_e$) have overall efficiencies around 30% at low heating value. Vibrating grates and circulating fluidised bed technologies which are solely fired by biomass have the highest efficiency around 33%. Co-firing biomass with pulverised coal could achieve efficiency around 37% at low heating value. The efficiency of the furnace or the combustion process can be defined as follows:

$$\eta_{comb.} = \frac{Thermal\ energy\ available\ in\ the\ flue\ gas}{Chemical\ energy\ in\ the\ supplied\ fuel} \qquad \text{Eq: 2-12}$$

The efficiency of the boiler can be express as follows:

$$\eta_{boiler.} = \frac{Thermal\ energy\ available\ in\ the\ water\ or\ steam}{Thermal\ energy\ in\ the\ flue\ gas} \qquad \text{Eq: 2-13}$$

2.3.3.2 Emission from biomass combustion

The most important parameter in combustion is the ratio between air supply and the theoretically minimal amount of air calculated based on stoichiometric combustion reaction. The optimal value for λ depends on the furnace, the type of fuel and the applied firing system. Typical values for biomass (wood) in well-designed systems range from 1.6 to 2.5. In poor designs, values may be as high as 4 to 5. According to Nussbaumer (2003), it is possible to operates a combustion systems at low excess air ($\lambda < 1.5$) provided that the mixing of combustion air and the combustible gases is good e.g. fluidised bed combustion. It is important to keep the λ value as low as possible as it determines the efficiency of the combustion process.

Theoretically, the highest flue-gas temperatures will be reached using $\lambda = 1$ in which, the supplied air is sufficient to burn all combustible materials or in other words, the combustion reaction reaches the stoichiometric reaction. However, in reality λ is always greater than 1. Figure 2-34 shows the effect of λ on flame temperature. Moisture content and ash content also have a significant effect on the flame temperature. According to Quaak *et al*., (1999), the influence of moisture content is by factor of four in the considered ranges of both moisture content and λ, but in the case of ash, it can be neglected as shown in Figure 2-35.
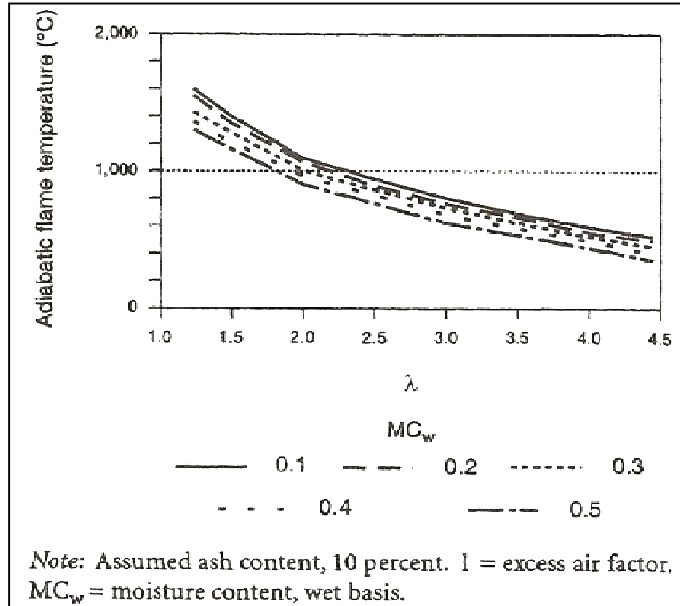
Figure 2-34: Adiabatic flame temperature as a function of biomass moisture content and excess air, λ. (Quaak *et al.*, 1999).
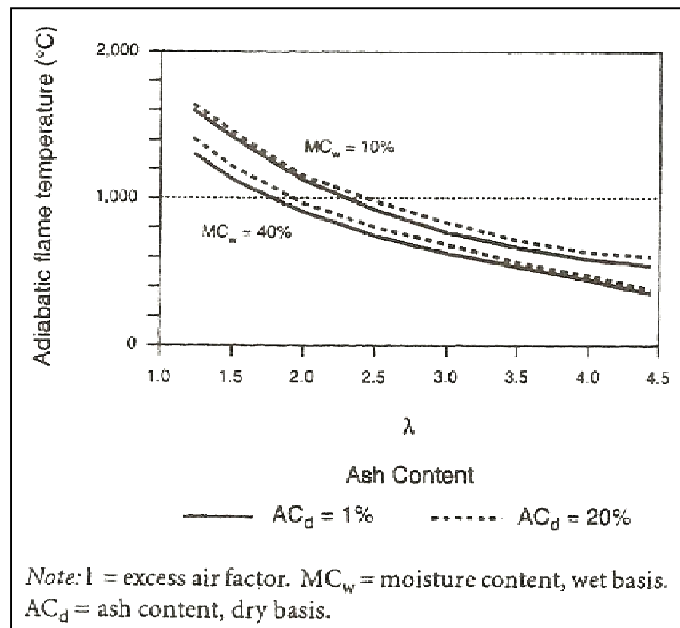
Figure 2-35: Adiabatic flame temperature as a function of biomass ash, moisture content and excess air, λ. (Quaak *et al.*, 1999).

Nussbaumer (2003) studied the effect of adiabatic flame temperature on the combustion of wood with different humidity and excess air ratio, λ. He also compared the CO emission over excess air ratio with different furnace types. It was found that combustion of wood could operate at low excess air ($\lambda < 1.5$) with high efficiency, high temperature (Figure 2-36) and achieved complete burnout (Figure 2-37). The concentrations of unburnt pollutants could be reduced to almost a zero if good mixing process was achieved, CO < 50 mg/m^3 and C_xH_y < 5 mg/m^3 at 11 vol% O_2 (Nussbaumer, 2003).
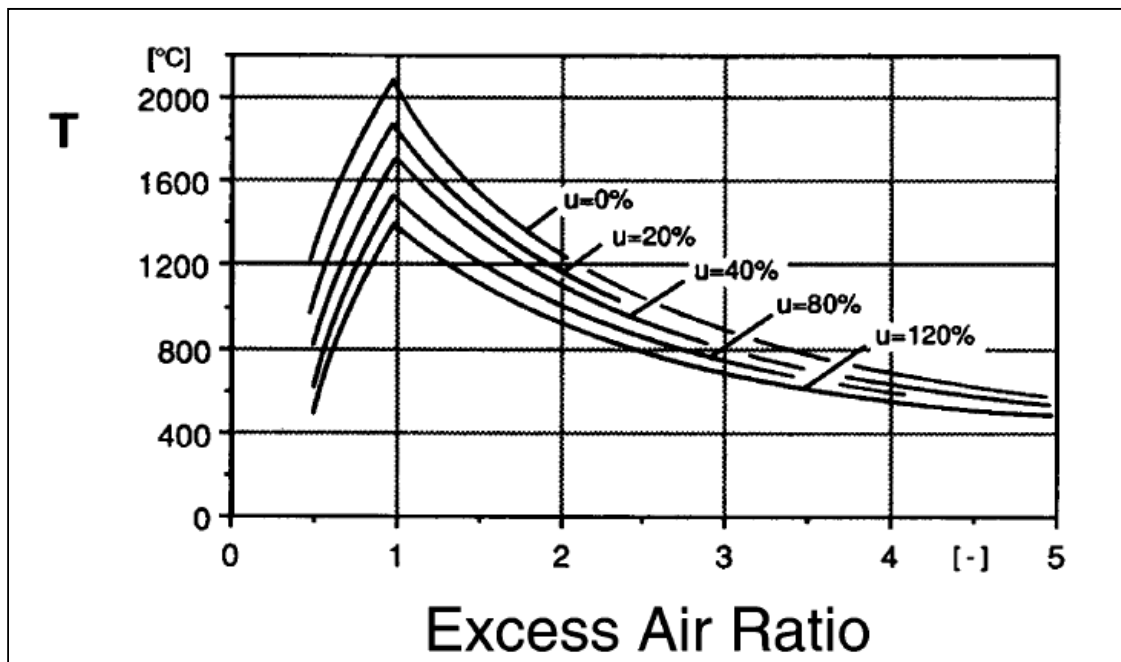
Figure 2-36: Adiabatic flame temperature for the combustion of wood with different humidity, u. (u is based on dry fuel, u = 100% corresponds to a moisture content, w = 50%) (Nussbaumer, 2003).
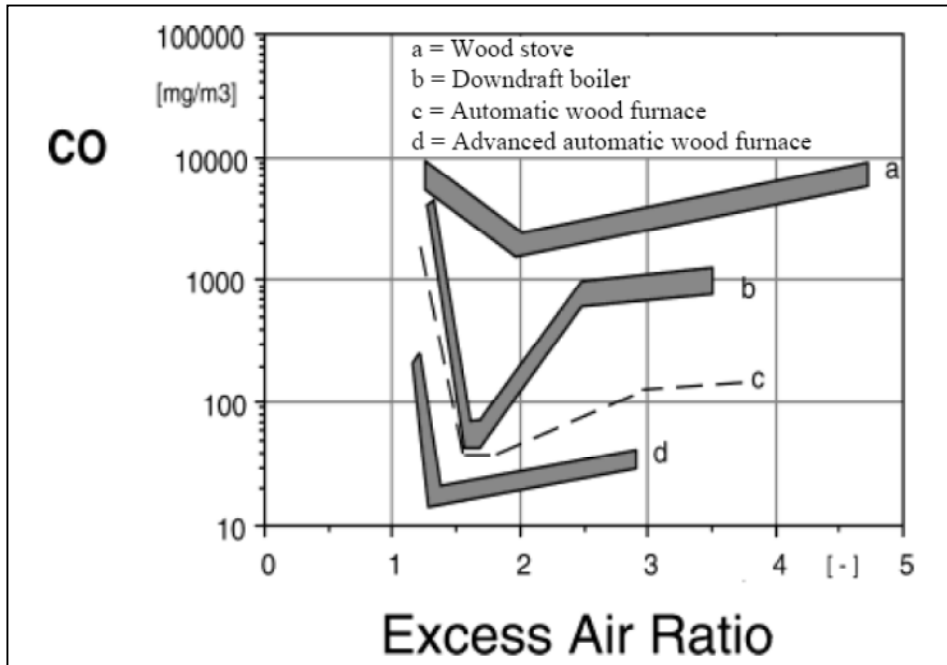
Figure 2-37: Carbon monoxide emissions as a function of excess air ratio (λ) for different furnace types (Nussbaumer, 2003).

There are two common approaches to control emissions from combustion of biomass: air staging and fuel staging, both are used in biomass combustion to control emissions particularly NOx. Air staging applies air injection at two levels with primary air normally supplies understoichiometric ($\lambda < 1$) conditions. Longer residence time is needed between the fuel bed and the secondary air inlet to allow more reduction reactions to occur in the furnace. In fuel staging condition, fuel is fed into the reactor at two different levels with the primary fuel is combusted in excess air or superstoichiometric ($\lambda > 1$). A consecutive reduction reactions are achieved by feeding the secondary fuel and delaying the final combustion air for the secondary fuel (Nussbaumer, 2003).

➢ Unburnt pollutants - temperature, residence time and turbulence (mixing) are the main parameters required for complete burnout. A good mixing between combustible gases and combustion air at the temperature around 850°C and residence time around 0.5s is a basic requirement for the burnout quality. Sufficient mixing quality can be achieved in fixed bed reactor with two-stage

combustion systems. Excellent mixing process in the fuel bed, freeboard and dust combustion can be achieved by fluidised bed reactor (Nussbaumer, 2003).

➢ Nitrogen oxides (NOx) - NOx emissions is the combination of NO and NO_2 species. It can be formed in three different reactions; thermal and Prompt NOx which are formed due to the oxidation of nitrogen in the air at high temperatures and the presence of hydrocarbons (in the case of prompt NOx). Another route of NOx formation is via oxidation of nitrogen-containing fuels, the most relevant source of NOx emissions in biomass combustion. Thermal and prompt NOx are not important due to relatively low temperatures (Nussbaumer, 2003, Suri and Horio, 2010). Figure 2-38 shows the routes of NOx conversion during biomass combustion.
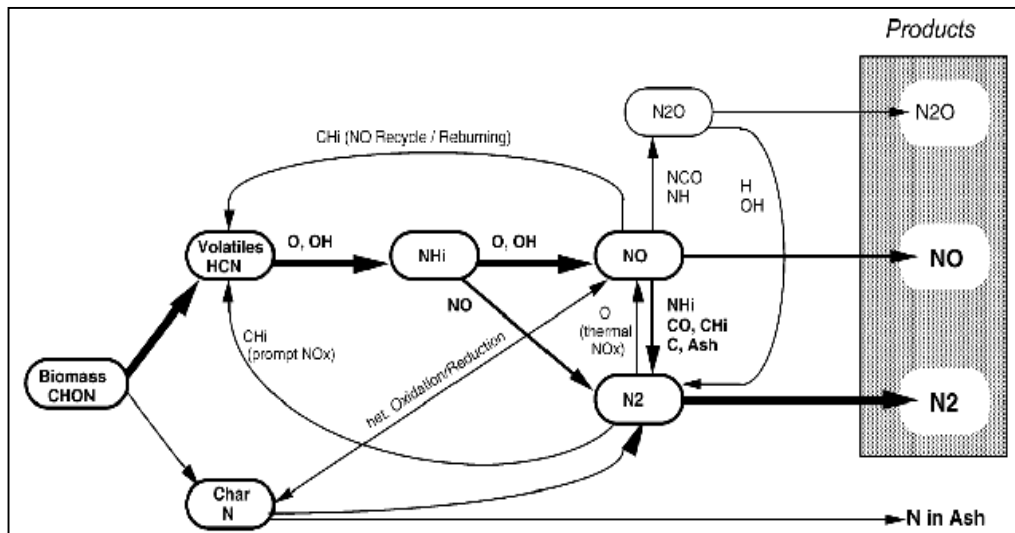
Figure 2-38: Mechanism of NOx formation (Nussbaumer, 2003).

Nitrogen species bound in biomass fuels is converted to intermediate components such as HCN and NHi where i=0, 1, 2, 3. In excess of oxygen, these compounds can be oxidised to NOx. Without oxygen, these intermediate compounds can react in the reduction zone to form N_2 by the following reaction:
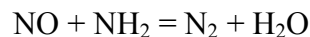
$$NO + NH_2 = N_2 + H_2O$$ Eq: 2-14

Secondary measures can also be implemented in order to reduce impact on NOx emission. The techniques are selective noncatalytic reduction (SNCR) and selective catalytic reduction (SCR). The working principles in both techniques are based on the reaction in Eq: 2-14. Urea or ammonia is used as a reducing agent and source of NH_2. Even though, SNCR and SCR are capable to reduce NOx emissions up to 90% and 95% respectively at optimum conditions, these techniques also produce unwanted chemical compounds such as HNCO, N_2O, NH_3, HCN and other by products (Nussbaumer, 2003). Thus, primary measures are important to achieve sufficient emission reduction.

➢ Sulfur oxides (SOx) - Fuel sulfur is oxidised at lower temperatures to form mainly SO_2 (> 95%) and SO_3 (< 5%) (Suri and Horio, 2010). In the combustion processes, both products are summarised as SOx. Not all fuel sulfur is converted to SOx during this process. A portion of fuel sulfur will remain in the ashes and some are emitted as a salt (K_2SO_4) or (H_2S). According to Suri and Horio (2010), about 57-65% of the sulfur is released into the flue gas and the remainder is bound in the ashes during the combustion of straw. Primary measures such as injection of lime or limestone during the biomass combustion could reduce the SOx emission.

➢ Hydrogen chloride (HCl) - The chlorine content in biomass fuels such as miscanthus, grass, straw and municipal wastes is a major contribution to the formation of corrosion in biomass combustion systems. Most of the chlorine bound in fuel is retained in salt in the form of KCl and NaCl. A fraction of it is converted into HCl and its traces are emitted as dioxin and organic chlorine compounds (Suri and Horio, 2010). Chlorine-containing ash caused the corrosion to occur when deposited on the furnace or boiler tube. Kobyashi *et al*., (2005) studied the effect temperature and calcium on HCl formation during the combustion of refuse derived fuel in a fluidised bed reactor. They found that the HCl removal ratio in the flue gas decreased with the increasing bed temperature, with 80% of HCl was removed at the temperatures above 800°C. The HCl

concentration decreased with the increasing calcium component ratio. However, HCl emission could be reduced by washing the fuels and implementing secondary emission reduction measures (Suri and Horio, 2010).

> Particulate emissions – Another important issue in biomass combustion is emissions of submicron particles (PM1). According to Nussbaumer (2003), particles found in fluidised bed combustor with submicron size particles consisted mainly of K, Cl, S, Na and Ca, while coarse particles composed of Ca, Si, K, S, Na, Al, P and Fe. In fixed bed reactor, K, S, Cl and Zn were found mainly in the submicron fraction.

2.3.3.3   Types of combustion

In general, there are two types of combustion systems commercially available; fixed-bed and fludised-bed. The fixed-bed system is the oldest technology dating from the first steam systems, whereas fluidised-bed technology has became available for the last 25 years (Quaak *et al.*, 1999, Bridgwater *et al.*, 2002). The difference between fixed-bed and fluidised-bed combustion systems are the grates and the way the fuel is transported through the furnace. Fixed-bed systems characterised by manual-fed systems, spreader-stoker systems, underscrew systems, through-screw systems, static grates and inclined grates. On the other hand, fluidised-bed systems are based on the bubbling or circulating varieties.

2.3.3.4   Fixed-bed system

Combustion of biomass in fixed-bed systems has been used for many years. The simplest systems are fixed-grate systems which consist of a grate in a furnace. Primary air for the combustion of the char is supplied under the grate, while secondary air, for the volatile gases is supplied above it. The combustion of the char provides heat for the continuing pyrolysis of newly added fuel above the char. The temperatures of the typical fixed-bed systems are in the ranges of 850°C to 1,400°C, and normally ash is removed manually

from the systems (Quaak *et al.*, 1999). The fixed-bed biomass combustion systems is similar to fixed-bed combustion systems for coal, except for the furnace designs. This is due to high volatile content in biomass fuels, which requires large combustion rooms above the grate and the furnaces require a higher proportion of secondary to primary air for the same reasons. Figure 2-39 shows a simple fixed-bed combustion system.
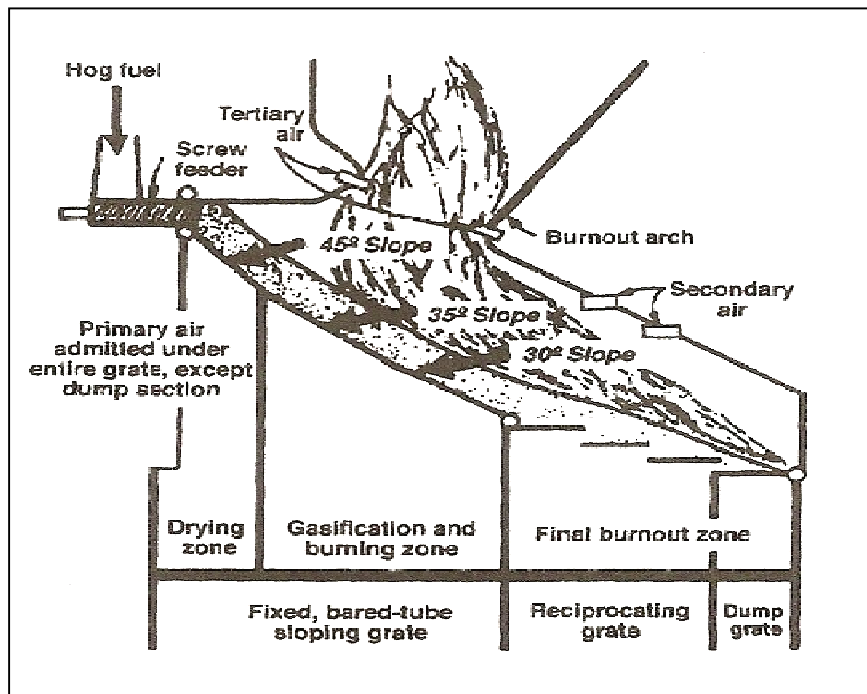
Figure 2-39: A simple sloping-grate combustion system (Quaak *et al.*, 1999).

2.3.3.5 Fluidised bed system

Fluidised bed technology is widely used than any other types of combustion systems and it is very important for waste or biomass applications due to its advantages over the conventional systems. Thus, it has become an attractive choice for industry. The important feature of the fluidised bed technology is the use of solid turbulence as a mixing medium which has a great impact on heat and mass transfer (Quaak *et al.*, 1999, Suri and Horio, 2010).

Fluidised bed combustion (FBC) technology is commercially available for a wide range of fuels including wood-based fuels and residues such as wood chips, sludge from paper mills, municipal solid waste and refuse derived fuel. Two types of fluidised bed combustion methods that are mostly used in industry: a) bubbling fluidised bed combustors (BFBC), Figure 2-40, in which the solid material is stationary in the bed b) circulating fluidised bed (CFBC), in which the solid material circulates through the bed to a cyclone, then back to the bed as shown in Figure 2-41.
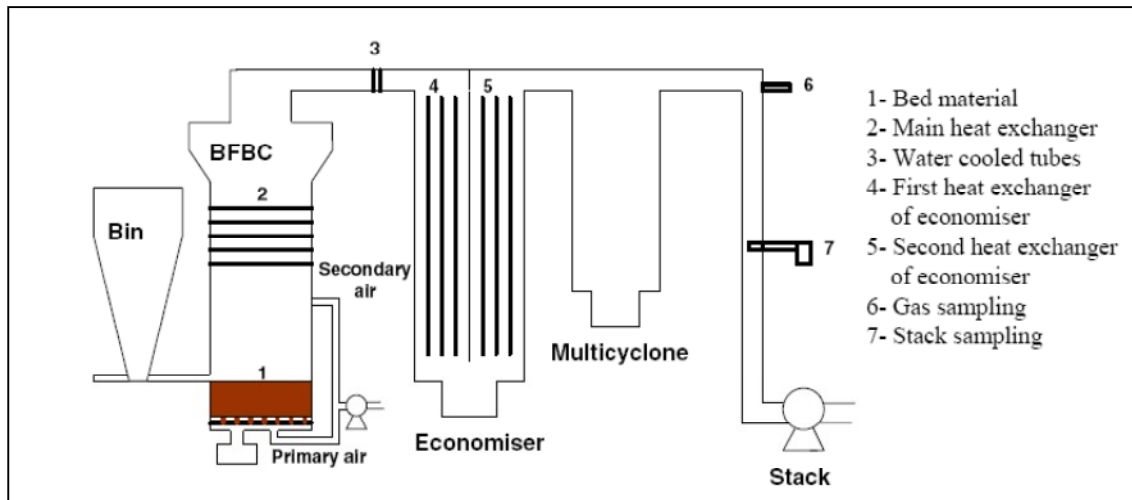
Figure 2-40: Schematic diagram of bubbling fluidised bed combustion (Llorente and Cuadrado, 2007).
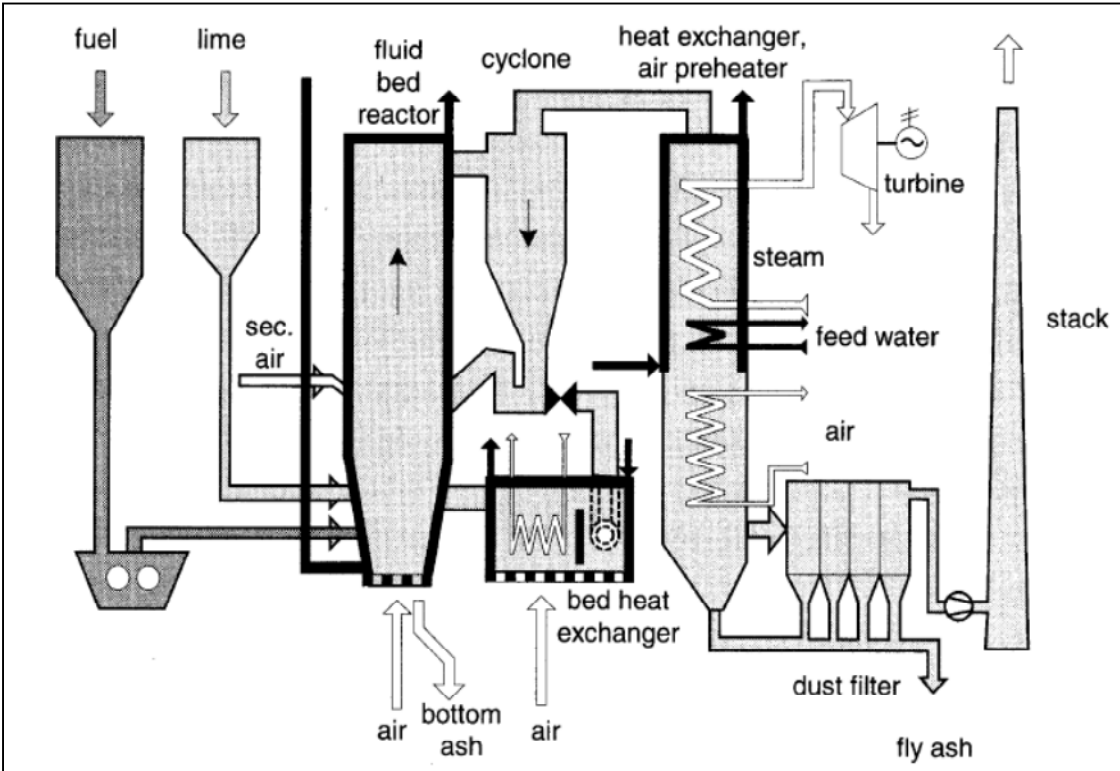
Figure 2-41: Schematic diagram of circulating fluidised bed combustion (Nussbaumer, 2003).

The most important features of fluidised bed combustion are:

- Flexibility to change in fuel properties sizes and shapes;
- Acceptance of high fuel moisture content
- Acceptance of high fuel ash content.

These features make FBC technology more attractive for biomass combustion and superior to fixed-bed combustion. Other advantages of fluidised bed technology over fixed bed systems are: a) Compact construction that causes high heat exchange and reaction rates because of intensive mixing in the bed, and b) Low excess-air factor (approximately 1.2 to 1.4), implying low heat losses from flue gases leaving the stack. Turbulent mixing in CFBC systems is even more intensive than in BFBC systems due to the high air velocities. For heat exchange, CFBC systems have all the advantages. The

circulating bed system is also more flexible than the bubbling bed, since the circulation rate of the bed material can be used as an additional control (Quaak *et al.*, 1999).

In FBC, fuel is burnt within an inert bed of sand or ash. This bed is maintained in a fluidised state by the upward passage of air. The resulting turbulent conditions cause excellent gas-solids mixing, and therefore, result in high combustion efficiency of the fuel. A wide range of fuels and wastes can be utilised, as fuels with high ash and water contents can be burnt in FBCs. As an additional benefit, most of the sulphur in the fuel can be removed in-situ by the addition of limestone. The high degree of mixing, and the ability to control the bed temperature accurately at the required set-point, make fluidised bed technology ideal for biomass.

The choice between BFB and CFB technology is largely linked to the choice of fuels. BFB is favoured for the plants exclusively fuelled with biomass or similar low-grade fuels, containing high volatile content. This is because the technology is considerably cheaper and easier to handle. Enhanced CFB designs, on the other hand, may be more competitive even in smaller biomass-fired plants. At present, there are more than 600 large (20+ MWth) FBC boilers with a total installed thermal capacity of more than 70,000 MWth have been built. Around 75% of this capacity is CFB technology, the rest is mostly BFB (Hupa, 2007).

In either case, the low operating temperature of fludised-bed boilers means that effectively no thermal nitrogen oxides are formed. Due to their relatively large mass of solids stored in the expanded bed, fluidised bed systems exhibit high ignition stability; therefore, fuels of high ash content and low calorific value, even with low content of volatiles can be burned steadily with good results (Poersch, 1987). Furthermore, sulphur emissions control is not required due to the low sulphur content of biomass. The benefits from fludised-bed-combustion technology have attracted a considerable interest in biomass heat and power generation.

2.3.3.5.1 Furnace design

Several issues need to be addressed when designing fluidized beds; such as the particle size and gas velocity in order to comply with the gas and solids residence time requirements. The important parameters that need to be considered when designing a reactor are:

i. Operating Temperature

The regular operating temperature in an AFBC is within the limits of 775 - 950°C. It is important to keep the temperature below 950°C to avoid any problems related to ash agglomeration and sintering. However, it is convenient to keep temperatures as close as possible to the upper limit in order to increase the combustion efficiency and to ensure a complete oxidation of the char.

Armesto *et al.*, (2002) studied the effect of combustion temperature on a bed height of rice husk in a bubbling fluidised bed reactor. The results showed that a peak of maximum temperature corresponding to the zone at 40 cm from the distribution plate and they recommended that the combustion process is produced mainly between 40 and 60 cm from the distribution plate due to the combustion of volatile matter in the rice husk. Figure 2-42 shows the bed temperature profile along the height of the combustor with three different fuidisation velocities. The low fuidising velocity promotes a poor mixing of the bed. If the fuidisation velocity grows further, the strong combustion zone will move to the top of the freeboard.
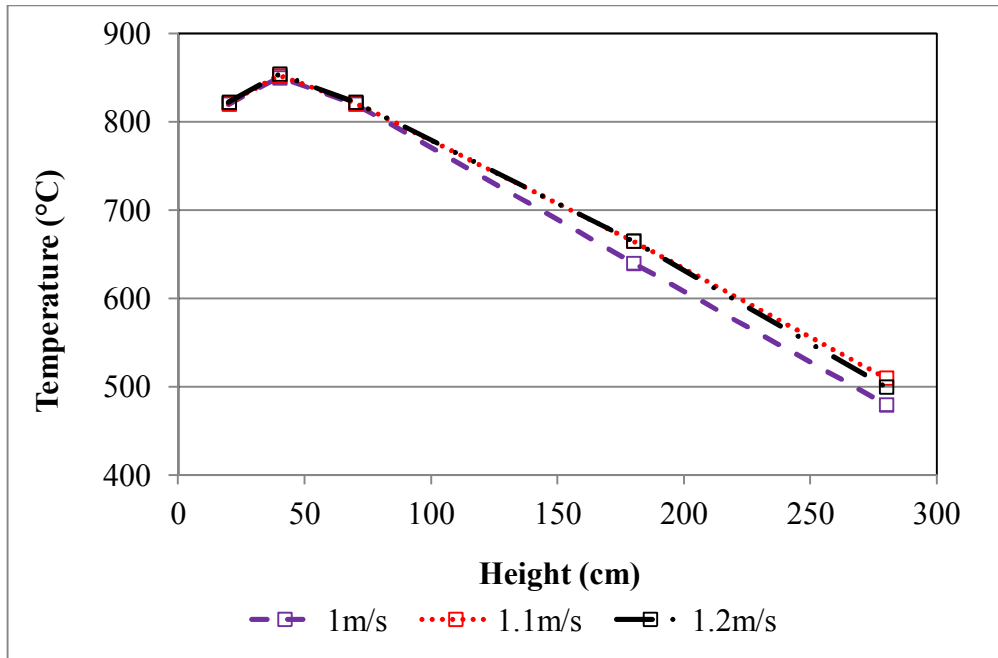
Figure 2-42: Temperature profiles in the combustor with different gas (Armesto *et al.*, 2002).

ii. Excess Air

The main problem of using excess air is the impact on the heat recovery. The higher the amount of air use, the higher the sensible heat will be removed with the combustion gases. Hernandez-Antonal (2007) pointed out that around 150% excess of air is enough to remove all the heat in the bed. At 30% of excess air, approximately half of the heat released from combustion is removed by the combustion gases and the rest by the heat recovery tubes.

Gungor and Eskin (2008) studied the effects of operational parameters on emission performance and combustion efficiency of coal in small-scale CFBCs. Their results showed that increased excess air ratio would decrease the bed temperature and increased the CO emission. The positive effect of increasing excess air is the decrease of SO_2 and NOx emissions. In general, increased excess air has a negative effect on combustor efficiency in small-scale CFBCs.

iii. Bed Particle Size

The bed particles size (d_p) is an important parameter in fluidised bed reactor as this size has been related to the particle size of the ash residue. According to Rozainee *et al.*, (2008), sand particle sizes between 351 and 420 µm were the best for combustion of rice husk with the velocity of air at 0.185-0.37 m/s at room temperature and pressure in a fluidised bed reactor. They concluded that the sand size (351-420 µm) was deemed to be the most suitable as there was considerable sand entrainment with sand size much smaller than 351 µm. On the other hand, sand particles that are too large would not mix well with rice husk, resulting in poor combustion behaviour. Other literature (Bhattacharya *et al.*, 1984, Armesto *et al.*, 2002) have consistently been reported of using sand size of less than 830 µm, mostly in the range of 300-500 µm.

Lin *et al.*, (2004) studied the effect of concentration of bed materials on combustion efficiency during waste incineration. They found that the heat transfer efficiency increases with the fluidisation velocity. However, if the bed is largely expanded, the heat transfer efficiency is reduced. Therefore, it is essential to consider the elements that promote a good transfer of heat as well as an adequate residence time in the bed in order to maintain a high combustion efficiency of the system.

iv. Fluidising Velocity

The minimum fluidisation velocity (U_{mf}) of a material is the superficial air velocity (defined as volume flowrate divided by bed area) at which material bed starts to fluidise. The choice of material size to be used for the operation of fluidised bed combustor affects the amount of air input required in order to maintain a certain fluidising condition. The Ergun equation (Eq. 2-15) is the widely accepted model to determine the minimum fluidisation velocity of a fluid to fluidise the particle. The values for velocity obtained by this equation are said to be reliable for spherical and relatively small particles (Senadeera, 2009).

$$\left(1-\varepsilon_{mf}\right)\left(\rho_s - \rho_f\right)g = 150\frac{\left(1-\varepsilon_{mf}\right)^2}{\varepsilon_{mf}^{~3}}\frac{\mu u_{mf}}{\left(\phi d_p\right)^2} + 1.75\frac{\left(1-\varepsilon_{mf}\right)}{\varepsilon_{mf}^{~3}}\frac{\rho_f u_{mf}^{~2}}{\left(\phi d_p\right)} \qquad \text{Eq: 2-15}$$

The Ergun equation consists of viscous and kinetic energy terms. In the case of larger particles at higher Reynolds numbers (Re > 1000) the fluidisation behaviour is mainly governed by the kinetic energy term. Hence, this equation can be simplified to suit a wide variety of systems and a generalised equation can be applied to predict the minimum fludisation velocity for larger particles when Reynolds number > 1000 by using some of the following modifications (Senadeera, 2009):

$$U_{mf} = \left(\frac{\phi d_p (\rho_p - \rho_f)}{1.75 \rho_f} g \varepsilon_{mf}^{3} \right)^{1/2}$$

Eq: 2-16

For a wide variety of systems, it is found that value $\left(\dfrac{1}{\phi \varepsilon_{mf}^{3}} \cong 14 \right)$ and a generalised equation can be applied to predict (U_{mf}) for larger particles when Re > 1000.

$$U_{mf} = \left(\frac{dp(\rho_p - \rho_f)g'}{24.5 \rho_f} \right)^{1/2}$$

Eq: 2-17

The bubbling action causes the particles to mix continuously and thereby, promotes uniformity of the bed temperature and composition. However, the bubbling phenomena can also lead to an excessive by-pass of un-reacted fluidising gas. At sufficiently high fluidising velocity, some of the particles will be entrained in the gas leaving the bed. A further increase in fluidising velocity more particles will be escaped and the bed pressure drop is reduced until all particles are completely blown out of the vessel.

The pressure drop over the incipiently fluidised bed is explained by the following equation:

$$\frac{\Delta P_b}{L} = 150 \frac{(1-\varepsilon)^2}{\varepsilon^3} \frac{\mu_f U}{(\phi_s d_m)^2} + 1.75 \frac{(1-\varepsilon)}{\varepsilon^3} \frac{\rho_f U^2}{\phi_s d_m}$$

Eq: 2-18

From the definition of (U_{mf}), the minimum fluidisation occurs when the drag force by upward moving gas is equal to the weight of particles. This can be written in mathematical equation as:

$$\Delta P_b A_t = A_t L_{mf} \left(1 - \varepsilon_{mf}\right)\left[\left(\rho_p - \rho_f\right)\frac{g}{g_c}\right]$$

Eq: 2-19

By re-arranging,

$$\frac{\Delta P_b}{L} = \left(1 - \varepsilon_{mf}\right)\left(\rho_p - \rho_f\right)\frac{g}{g_c}$$

Eq: 2-20

The combination of Eq: 2-18 and Eq: 2-20 will result in:

$$\frac{\rho_f\left(\rho_p - \rho_f\right)gd_m^3}{\mu_f^2} = 150\frac{\left(1 - \varepsilon_{mf}\right)}{\phi_s^2\varepsilon_{mf}^3}\frac{\rho_f U_{mf} d_m}{\mu_f} + \frac{1.75}{\phi_s^2\varepsilon_{mf}^3}\frac{\rho_f^2 U_{mf}^2 d_m^2}{\mu_f^2}$$

Eq: 2-21

The left hand side of the Eq: 2-21 is the dimensionless group known as the Archimedes Number, *Ar*:

$$Ar = \frac{\rho_f\left(\rho_p - \rho_f\right)gd_m^3}{\mu_f^2}$$

Eq: 2-22

Reynolds number at incipient fluidisation is defined as:

$$\text{Re}_{mf} = \frac{\rho_f U_{mf} d_m}{\mu_f}$$

Eq: 2-23

Thus, at a minimum fluidising velocity:

$$Ar = 150\frac{\left(1 - \varepsilon_{mf}\right)}{\phi_s^2\varepsilon_{mf}^3}\text{Re}_{mf} + \frac{1.75}{\phi_s^2\varepsilon_{mf}^3}\text{Re}_{mf}^2$$

Eq: 2-24

However, at a particular range of materials;

$$\frac{\left(1 - \varepsilon_{mf}\right)}{\phi_s^2\varepsilon_{mf}^3} \approx 11.0 \text{ and } \frac{1}{\phi_s\varepsilon_{mf}^3} \approx 14$$

Therefore, by inserting these values into an Ergun equation and then solving the positive root for Re_{mf};

$$\text{Re}_{mf} = \left(33.7^2 + 0.0408 Ar\right)^{1/2} - 33.7 \qquad \text{Eq: 2-25}$$

Theoretically, if accurate values for ε_{mf} and the mean diameter of a particle d_m can be obtained, then Eq: 2-24 can be used to calculate the minimum fluidising velocity U_{mf}, expressed in terms of Ar and Re_{mf}. However, predicting the fluidising velocity can be difficult due to the problem in determining the properties of particles. The ε_{mf} varies with bed temperature in a complex manner and is not easily predicted when particles size ranges of 40-500μm and density of 1400-4000 kg/m³. Denser and larger particles ($Ar \geq 26000$ and $\text{Re}_{mf} \geq 12.5$) do not seem to show an increase in ε_{mf} with bed temperature (Botterill *et al.*, 1982).

2.3.3.5.2 Combustion of solid in a fluidised bed

The temperature of a fluidised bed reactor is usually maintained at approximately 850°C. When the fuel particle is introduced into the bed, the fuel particle is heated by the hot inert particles and gas in the bed. Heat transfer within bed is very high since the boundary layers are comparable in thickness to the diameter of the particles. Initially, moisture will be driven off. Then, the devolatilisation or pyrolysis process starts when the temperature of the reaction front reaches approximately 450°C. The devolatilisation process leaves a porous residual char with some ash content. The combustion process will then continue with the oxidation of char (Quaak *et al.*, 1999).

The fuel particle is usually fed over the surface of the bed. The process of drying starts instantaneously. Particles may remain on the bed surface due to the buoyancy caused by the evolving steam. The process is dependent on the specific gravity, mass to surface area ratio of the particle and the superficial velocity of the gas. The devolatilisation process involves evolution of volatile matter which reduces the specific gravity of the particle and

impacts buoyancy force on the particle. Therefore, the fuel particle may continue to float on the bed surface during the devolatilisation process in a fluidised bed combustion (Andrei *et al.*, 1985).

According to Andrei *et al*., (1985), the evolution of volatiles was accompanied by the ignition of a laminar diffusion flame close to the particle. The particles did not glow during the devolatilisation process. After the evolution of volatile matter died out, and oxygen was able to reach the surface of the residual char, the particle began to glow or commenced char combustion process. Therefore, it can be assumed that solid fuels with high volatiles/fixed carbon ratio that are fed onto the surface of the bed are likely to burn on surface rather than within the bed.

According to van den Broek *et.al* (1996), fluidised beds, particularly circulating systems, are able to combust a range of fuels, often at high efficiency, with good carbon burn-out and low NOx emissions from thermal sources, due to the lower combustion temperatures. In addition, SOx concentrations may also be minimal and acid gas retention in the bed can be increased with lime. Various aspects of biomass combustion in fluidised bed systems have been investigated (Kuo *et al.*, 2008, Khan *et al.*, 2009, Youssef *et al.*, 2009). Over the recent years, studies have also been focused on the gasification reactions of biomass in fluidised beds. A range of papers have been published for a variety of biomass such as waste from the olive oil industry (García-Ibañez *et al.*, 2004, André *et al.*, 2005), eucalyptus red gum wood chips and commercial wood pellets (Ross *et al.*, 2007), and plastic waste (Sancho *et al.*, 2008).

2.3.3.5.3 Environmental, economic and technical issues

The main purpose for investigating the fluidised bed combustion of biomass is to analyse the effect of fuel and technology on the environment, the costs efficacy and technical feasibility. McIlveen-Wright *et al.*, (2001) studied the factors influencing the suitability of wood combustion for power generation. Ranges of factors such as fuel moisture content, plant sizes, feedstock requirements (afforestation level) and transportation costs

were investigated. Their results showed that the discount cash flow rate and the level of afforestation mainly affected the former, whereas the moisture content of the fuel and the conditions of the steam cycle were found to have the largest influence on the latter. The effect of economy of scale and of steam cycle conditions on the technical and economic performance of a wood-fired power generation plant is summarised in Table 2-17 and Table 2-18 respectively. Medium-sized plants (500 dry tonnes/day) would be economically viable, whereas large plants (capacity > 1000 dry tonnes/day) would be more competitive with coal-fired power stations. However, the economics of scale achieved by building a larger power station are offset by the increased transportation costs for the wood fuel.

Table 2-17: The effect of economies of scale and of steam cycle conditions on the technical performance of a wood-fired power generation plant (McIlveen-Wright *et al.*, 2001).

Plant size(DTE*/day)	10	100	500	1,000	2,000	5,000	10,000
Steam pressure (bar)	23	60	80	80	80	160	160
Steam temperature (°C)	350	480	520	520	520	538	538
Heat input (MW, LHV)	2.0	20.1	100.5	201.1	402.1	1005.3	2010.6
Gross electrical output (MW	0.43	5.3	28.1	56.2	112.3	338.6	676.5
Ancillary electrical consumption							
Receipt/storage/dryer/solids	0.04	0.2	0.5	0.8	1.4	3.3	5.9
removal (MW)	0.03	0.3	1.3	2.6	5.2	11.3	22.5
Fans/compressors (MW)	0.00	0.0	0.4	0.8	1.6	7.5	15.2
Condensate pumps (MW)	0.01	0.1	0.4	0.8	1.6	3.7	7.4
Cooling water (MW)	0.08	0.6	2.6	5.0	9.8	25.8	51.0
Total ancillary (MW)							
Overall results							
Net electrical output (MW)	0.35	4.7	25.5	51.2	102.5	312.8	625.5
Overall efficiency (%)	17.5	23.1	25.4	25.4	25.5	31.1	31.1
Gaseous emissions							
CO_2 (g/kWh)	2190	1650	1500	1500	1490	1220	1220
SO_2 (g/kWh)	0	0	0	0	0	0	0
NOx (g/kWh)	3.1	2.6	2.4	2.4	2.4	2.0	2.0

*Dry tonne equivalent

Table 2-18: The effect of economies of scale and of steam cycle conditions on the economic performance of a wood-fired power generation plant (McIlveen-Wright *et al.*, 2001).

Power station size (DTE*/day)	10	100	500	1,000	2,000	5,000	10,000
Wood reception/storage	0.3	1.4	4.7	7.6	18.5	35.1	57.1
CFBC and steam generator	0.8	3.7	13.3	22.9	42.3	106.8	224.2
Steam turbines	1.1	2.8	9.0	10.5	13.5	55.5	111.0
Condenser/condensate system	0.1	0.4	1.1	1.9	3.3	14.5	27.9
Utilities systems	0	0.2	0.6	1.3	2.4	5.4	10.7
Miscellaneous items	0	0.1	0.3	0.6	1.3	4.0	7.0
Total capital cost	2.3	8.6	29.0	44.8	81.3	221.3	437.9
Specific investment (£/kW)**	6680	1850	1130	880	790	710	700

*Dry tonne equivalent
** The cost is £Million

Armesto *et al.*, (2002) and Rozainee *et al.*, (2008) have studied the combustion characteristics of rice husks in the atmospheric bubbling fluidised bed reactor. The temperature profile in the furnace has a strong influence on both CO emissions and combustion efficiency. As the temperatures increased, the combustion efficiency also increased. Increases in the U_{mf} resulted in reduced combustion efficiency, and higher CO concentration. The CO concentration peaked at 860°C. X-ray analysis of the bottom ash revealed that it contained mainly quartz (SiO_2) and hematite (Fe_2O_3) (see Figure 2-43). Moreover, fly ash contained corrosive KCl, Figure 2-44.

Rozainee *et al.*, (2008) investigated the optimum fluidising velocity during the combustion of rice husk in a bench-scale fluidised bed combustor (ID 210 mm) to obtain low carbon ash in the amorphous form. It was found that the optimum fluidising velocity was approximately 3.3 U_{mf} as the mixing of rice husk with the bed was good with a high degree of penetration into the sand bed. The ash retained its amorphous form with low residual carbon content (at 2.88 wt %).
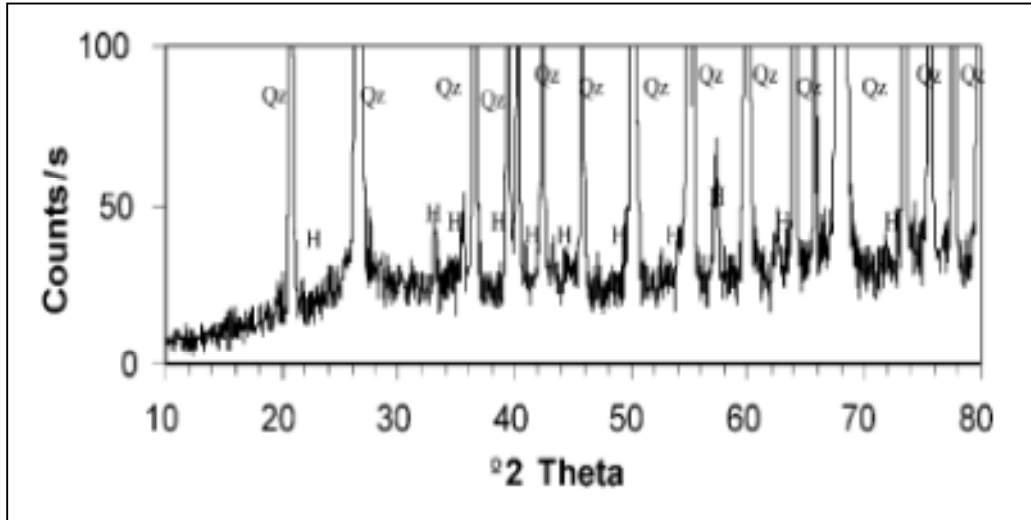
Figure 2-43: X-ray diffraction analysis of the ashes from the bed (quartz (Qz): SiO_2, hematite (H): Fe_2O_3). (Armesto *et al*., 2002).
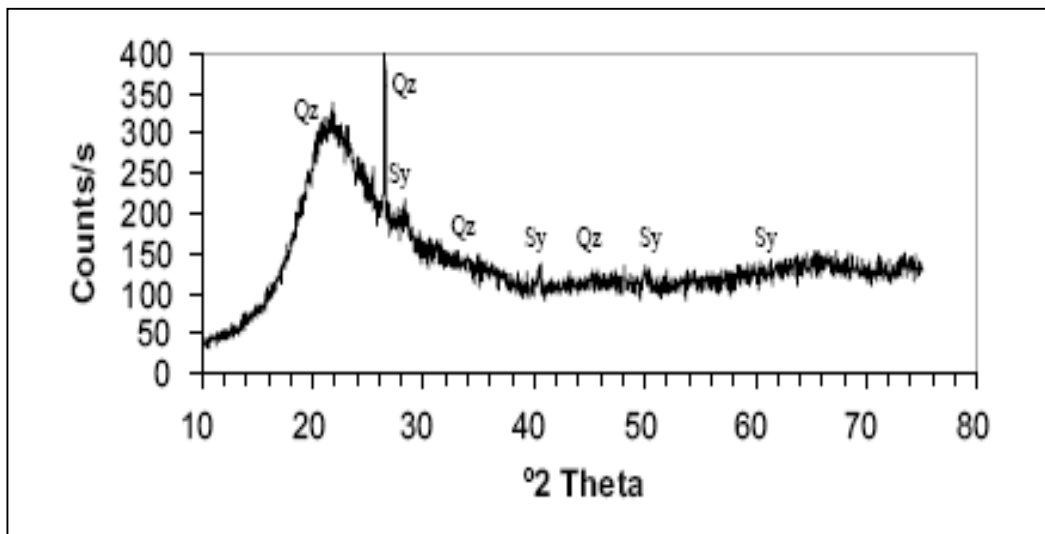
Figure 2-44: X-ray diffraction analysis of the ashes from the cyclones (quartz (Qz): SiO_2, sylvinite (Sy): KCl). (Armesto *et al*., 2002).

2.3.4 Combustion of char

Char combustion is very important for both pulverised coal boilers and fludised bed boilers. The heat transfer coefficient at the particle surface and the oxygen diffusion from the bulk flow to the particle surface are usually dependent on the particle diameters. For the particle under 100 microns, the char reaction is chemically controlled. The burning time of the particle above 100 microns is proportional to the square of the diameter, and for particles under 100 microns, it is proportional to the 0.4 power of the diameter (He *et al.*, 2003). In pulverised coal combustion at high temperatures, the combustion of small char particles is mainly under the chemical control and partly is affected by the diffusion control. In fluidised beds, the environmental temperature is relatively low and the particle size is relatively large. Char combustion is under diffusion control for these large particles. In the char combustion, the particle sizes also affect mass transfer, heat transfers and combustion rates. In general, the combustion rate is inversely proportional with particle size of the char. However, it is difficult to investigate the effects of single char particle size on the combustion rate if it is too small.

Figure 2-45 shows the schematic diagram of shrinking core of char particle during thermal treatment process. The shrinking core without ash layer diffusion and the kinetic expression for the reaction rate of char combustion can be expressed as follows:
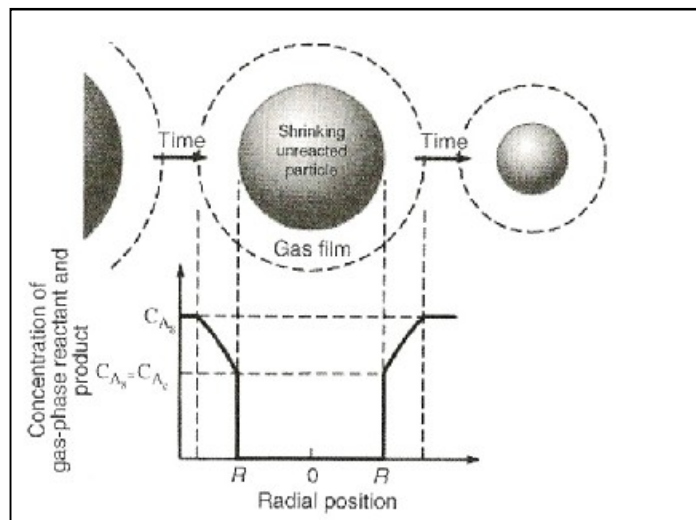
Figure 2-45: Schematic diagram for char combustion (Suri and Horio, 2010).

$$Combustion\ rate\ (r_c^*) = \frac{\pi \rho_{sXv0}}{6} \frac{d(d_{sc}^3)}{dt}$$

Eq: 2-26

The combustion rate is proportional to concentration of O_2 in the bulk and can be written as:

$$r_c^* = \frac{1}{\phi_{s0}} M_c \pi d_s^2 \bar{k} C_{O_2}$$

Eq: 2-27

Where $\bar{k}$ is the overall reaction rate and defined as:

$$\bar{k} = \frac{1}{(1/k_f + 1/k_c)}$$

Eq: 2-28

Since the particle is moving slow relative to the gas flow, as normally the case in fluidised beds, the Sherwood number is equal to 2 and the expression for k_f can be written as:

$$k_f = \frac{ShD}{d_{sc}} = \frac{2D}{d_{sc}}$$

Eq: 2-29

Equating Eq: 2-26 and Eq: 2-27 and integrating from the outer char layer, that is, $d_{sc} = d_{s0}$ at $t = 0$, obtain:

$$\left(\frac{1}{k_c} + \frac{d_{sc}}{4D} \right) d_{sc} - \left(\frac{1}{k_c} + \frac{d_{s0}}{4D} \right) d_{s0} = -\frac{2M_c C_{O_2} t}{\rho_s X_{c0} \phi_{s0}}$$

Eq: 2-30

Thus, the burnout time for char can be calculated by substituting $d_{sc} = d_{s0}/2$ at $t = t_c$:

$$t_c = \frac{\rho_s X_{c0} \phi_{s0} d_{s0}}{2M_c C_{O_2}} \left(\frac{1}{k_{sc}} + \frac{d_{s0}}{4D} \right)$$

Eq: 2-31

The dependency of t_c on initial particle size is different for the two extreme cases:

➢ For chemical reaction control:

$$t_c = \frac{\rho_s X_{c0} \phi_{s0} d_{s0}}{2M_c k_c C_{O_2}}$$

Eq: 2-32

➢ For film diffusion control:

$$t_c = \frac{\rho_s X_{c0} \phi_{s0} d_{s0}^2}{8M_c D C_{O_2}}$$

Eq: 2-33

2.3.5 Combustion of volatiles

The possibilities for a biomass particles either for thermal treatment in a fluidized bed or in a grate furnace are (1) the particles decompose to form volatiles which combust to form gaseous products or (2) the particles decompose to form a char layer and volatiles which then combust to produce gaseous products (Suri and Horio, 2010). Figure 2-46 shows the schematic model for the volatile combustion for the both cases.
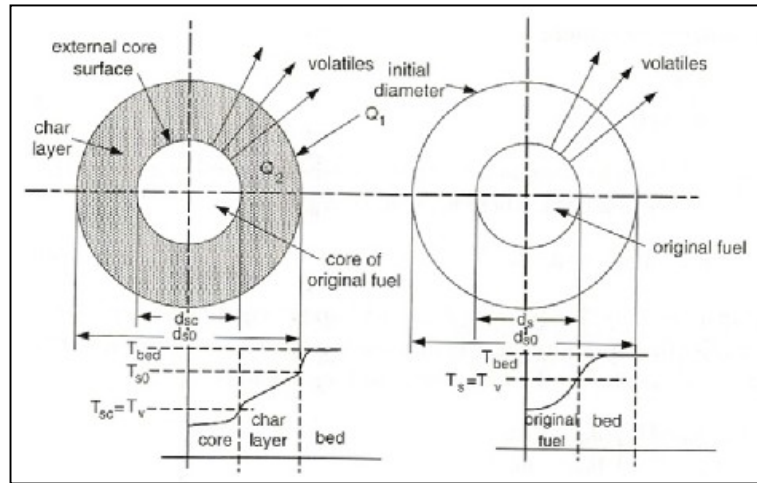
Figure 2-46: Schematic diagram for the volatile combustion (Suri and Horio, 2010).

According to Suri and Horio (2010), the rate of volatile combustion in both cases is controlled by heat transfer rate between the bed and thermal conductivity of char or biomass particles. Thus, the heat transfer for the combusting particles and the bed and the rate of heat transfer within the particle during the steady state can be expressed as follows:

$$Heat\,transfer\,from\,the\,bed\,(Q_1) = \frac{\pi d_{s0}^2}{\phi_{s0}} q_1 = \frac{\pi d_{s0}^2}{\phi_{s0}} h_{s0} \left(T_{bed} - T_{s0} \right)$$ Eq: 2-34

$$The\,rate\,of\,heat\,transfer\,within\,the\,particle\,(Q_2) = \frac{\pi d_{sc}^2}{\phi_{s0}} q_2 = \frac{\pi d_{sc}^2}{\phi_{s0}} k_s \frac{\partial T}{\partial r}$$ Eq: 2-35

Integrating Eq: 2-34 from $r = d_{s0}/2$ to $r = d_{sc}/2$ to obtain:

$$Q_2 = \frac{\pi k_s}{\phi_{s0}} \left(\frac{T_{s0} - T_v}{\dfrac{1}{d_{sc}} - \dfrac{1}{d_{s0}}} \right)$$

Eq: 2-36

Since $r = d_{s0}/2, T = T_{s0}$ and $r = d_{sc}/2, T = T_v$. During the steady state condition, $Q_1 = Q_2$ and Q_2 is equal to the heat released due to the volatile combustion, $\Delta H_v r_v^*$ where r_v^* is the rate of decomposition of volatiles, which is given by:

$$r_v^* = \frac{\pi \rho_s X_{v0}}{6} \frac{d(d_{sc}^3)}{dt}$$

Eq: 2-37

Thus, for the case with char layer formation:

$$r_v^* = \frac{\pi (T_{bed} - T_v)}{\phi_{s0} \Delta H_v \left[\dfrac{1}{h_{s0} d_{s0}^2} + \dfrac{1}{k_s} \left(\dfrac{1}{d_{sc}} - \dfrac{1}{d_{s0}} \right) \right]}$$

Eq: 2-38

➤ For no char layer formation:

$$r_v^* = \frac{\pi h_s d_s^2 (T_{bed} - T_v)}{\phi_{s0} \Delta H_v}$$

Eq: 2-39

Integrating Eq: 2-38 and Eq: 2-39 to obtain the time for volatile combustion, t_v. For the case of fluidised bed combustion, $h_{s0} = h_s = h_{s,max}$:

$$Nu_{max} \equiv h_{s,max} d_s / k_e = (d_s / d_p)^{0.8}$$

Eq: 2-40

Equating Eq: 2-37 with Eq: 2-38 and Eq: 2-39 and integrating from $t = 0$ to $t = t_v$ for $d_{sc} = d_{s0}$ to 0 for the case with char layer formation, and $d_s = d_{s0}$ to 0 for no char layer formation to obtain:

➤ For the case with char layer formation:

$$t_v = \frac{\rho_s X_{v0} \phi_{s0} \Delta H_v}{2(T_{bed} - T_v)} \left(\frac{d_{s0}}{3 h_{s0}} + \frac{d_{s0}^2}{6 k_s} \right)$$

Eq: 2-41

➤ For the case without char layer formation:

$$t_v = \frac{\rho_s \Delta H_v d_p^{0.8}}{2.4 k_e (T_{bed} - T_v)} \phi_{s0} d_{s0}^{1.2}$$

Eq: 2-42

2.3.6   The combustion scheme

Optimal operation is important in the combustion process in order to obtain the full benefits from the products released and it is important to avoid the release of any toxic gas into the environment. Shin and Choi (2000) investigated the combustion of simulated waste particles in a fixed bed and proposed the schematic of the ignition propagation front for fixed bed combustion. It consists of three successive regimes known as oxygen-limited, reaction-limited and convective cooling as shown in Figure 2-47.
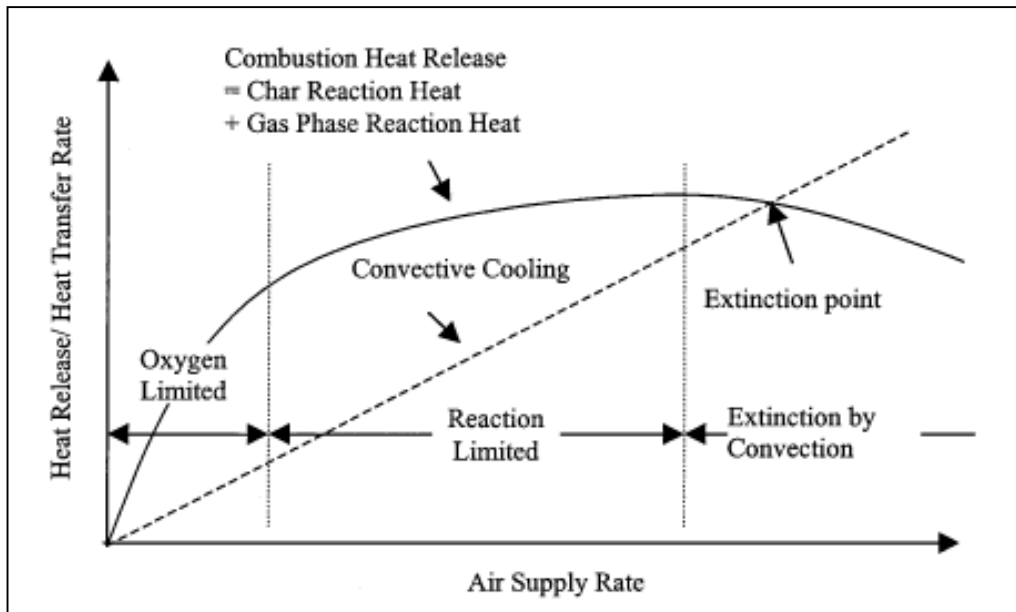
Figure 2-47: Effect of air supply rate on the combustion of a fuel bed (Shin and Choi, 2000).

2.3.6.1   Oxygen limited regime

In the oxygen limited region, the air supply is very low. The oxygen completely reacts with volatile compounds and char accumulates as the ignition front propagates. The reaction rate in this regime depends on the air or oxygen supply. Increasing the air supply causes a higher burning rate, accompanied by a higher temperature and larger extent of solid conversion.

2.3.6.2   Reaction limited regime

The burning rate increases with the increase air supply. Beyond the critical point corresponding to the stoichiometric burning, the total amount of solid consumed and an excess of oxygen remains. Furthermore, convective cooling – in this region, the air or oxygen supply is sufficiently high to sweep the gas phase during combustion. Also, the char combustion zone experiences high convective cooling and causes extinction of the flame.

2.3.7   Effect of operating parameters on fixed bed combustion characteristics

2.3.7.1   Moisture content

Horttanainen *et al*., (2002) studied the effect of the flow rate of air, moisture content, particle size and density of wood against the velocity of the ignition front and the maximum temperature in the bed. Their results showed that if the moisture content is more than 30%, it will significantly lower the propagation of the ignition front due to the reduction of bed temperature. According to Klass and Donald (1998), high moisture content and excess air significantly reduce the theoretical flame temperature as shown in Figure **2-48**. Yang *et al*., (2003b) studied the effect of moisture content on pinewood and simulated waste on a fixed bed combustion. The finding showed that the moisture content caused a reduction of the burning rate. The drier fuel underwent two distinctive combustion stages and the burning rate was inversely proportional to the moisture content. On the other hand, wetter fuels had a thinner flame front and the combustion stoichiometry shifted from sub-stoichiometric (fuel rich) to super-stoichiometric (fuel lean) as the moisture content increased.
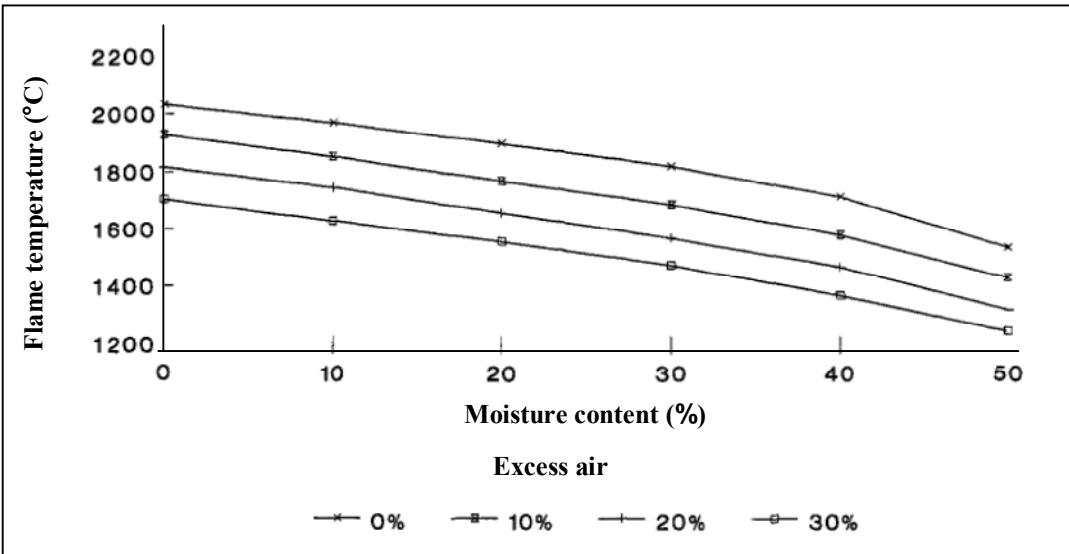
Figure 2-48: Theoretical flame temperature vs. wood moisture content and excess air (Klass and Donald, 1998).

Saatamoinen *et al* (2000b) investigated the propagation of the ignition front in fixed beds of wood chips. They discovered that the moisture content significantly lowered the speed of the ignition front. However, fuel with 30% or less did not have any obvious effects on the maximum temperature in the bed. The size, shape, and orientation of a particle affected the local turbulence, the mixing of fuel volatile with oxygen, and the combustion in the bed, all of which are important factors affecting ignition.

2.3.7.2 Air flow rate

According to Horttanainen *et al*., (2002), the significant point of air velocity over air flow rate is varied in relation to biomass types and particle size. At very low of air flow rates, the flame temperature remains excessively low, due to lack of oxygen, hence, extinction takes place. On the other hand, as the flow rates of air is increased, the conditions close to the ignition front transforms from fuel-rich to oxygen-rich. Zakaria (2000) studied the simulated municipal solid waste and found that the ignition front speed is directly proportional to primary air flow rate. Primary air below 100°C shows no significant effect on the combustion process. However, the effects are more apparent at higher

temperature (above 100°C). The results are strongly supported by van der Lans *et al.*, (2000).

2.3.7.3   Particle size

There was no effect of particle size on the ignition front's speed, but it is strongly influenced the bed temperature. The ignition speed was directly proportional to the ratio of the surface area of particles over volume and inversely proportional to the density of fuel (Saastamoinen *et al.*, 2000b). Yang *et al.* (2005), studied the effect of pinewood combustion in a stationary packed bed. They found that smaller particles are quicker to ignite than larger particles and have distinctive combustion stages. Furthermore, burning rate is higher with smaller fuel size; and smaller fuels have a thinner reaction zone and result in both higher CO and CH_4 concentrations in the out-of-bed flue gases. In contrast larger particles produced a higher flame temperature and result in higher H_2 concentration in the flue gases. Shin and Choi (2000) studied the effect of particles size and superficial air velocity on flame propagation of simulated waste particles in fixed bed. They found that when the particle size increases, the maximum air supply rate for stable combustion also increases (Figure 2-49). This is due to the fact that larger particles have a smaller surface area per unit mass, therefore, the cooling effect of the air supply is diminished (Shin and Choi, 2000).
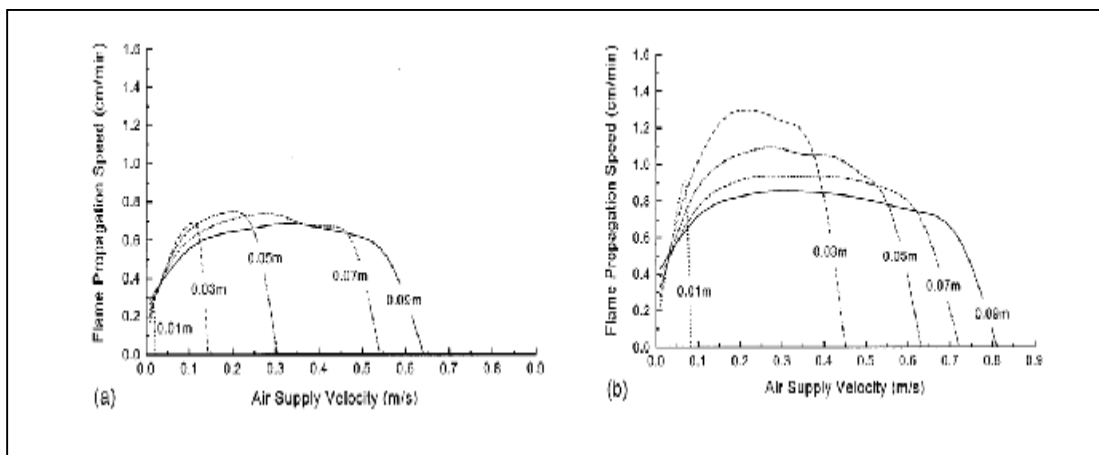
Figure 2-49: Effect of particle size and superficial air velocity on flame propagation (a) LHV=1380 kcal/kg, (b) LHV=2010 kcal/kg (Shin and Choi, 2000).

According to Thunman and Leckner (2005), particle size has significant effects on air distribution and the stages of the combustion process of a packed bed. However, particle density has a very small effect on the conversion rate. Large particles showed an overlap on the stages of drying, devolatilisation and char burning. The model calculation confirmed that an increase of fuel density does not have any significant effect on the conversion rate if the conversion rate is related to the mass loss per unit time and cross-sectional area of the bed.

Ryu *et al.*, (2006) revealed that fuels with small particle sizes have a higher burning rate compared to larger ones. Large particles are thermally thick having slow devolatilisation rate and distribute more heat transfer to the nearby particles, rates and ignition front speeds. Figure 2-50 shows the relationship between fuel particle sizes and the ignition front speed, burning rate and mass loss.
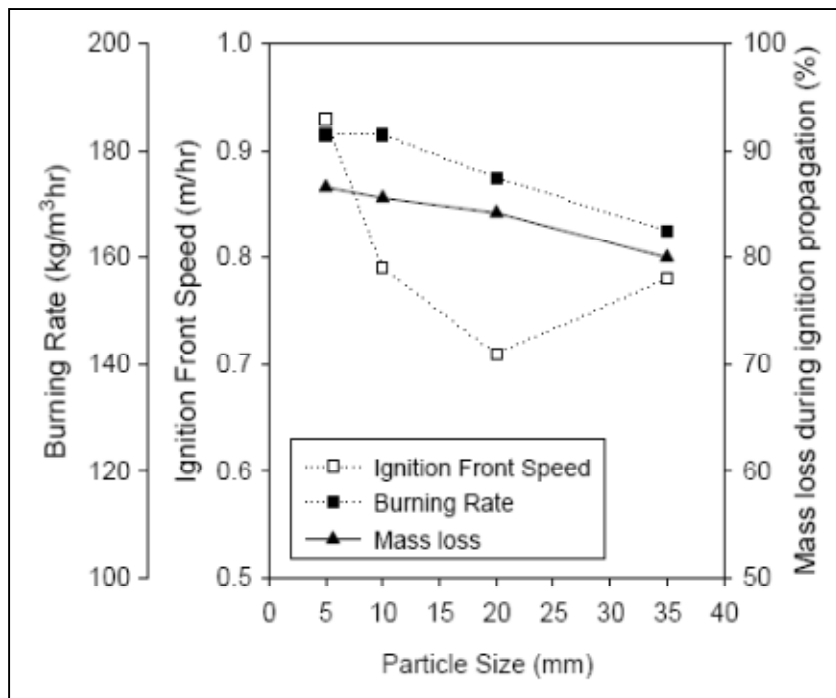
Figure 2-50: Effect of particle size on ignition front speed, burning rate and mass loss during the ignition propagation period (Ryu *et al.*, 2006).

2.3.7.4 Temperature, gas composition and mass loss

Ryu *et al*., (2006) carried out combustion experiments on pine wood with a particle size of 20mm. Their results showed that the combustion propagated continuously into the bed by transfering of the heat released from the gaseous reactions and char oxidation. The temperature reached 1100°C after the ignition front passes and remained stable at 1000°C (see Figure 2-51). The gas at the bed top was 15% of CO_2, had slightly higher CO and zero O_2 was measured (see Figure 2-52). They also discovered that the effect of channeling on the burning rate of small miscanthus pellets and larger pinewood particles (35 mm cubes) was not significant.
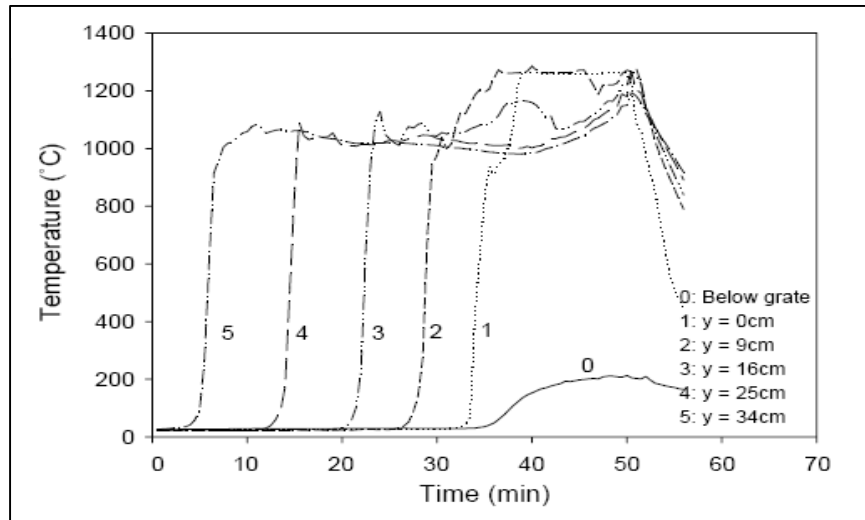
Figure 2-51: Temperature profile of pine wood, 20mm (Ryu *et al*., 2006).
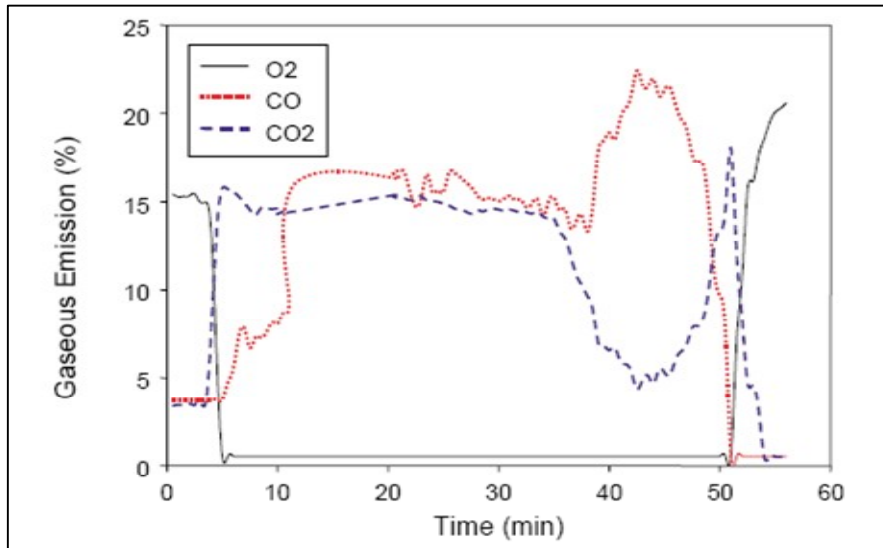
Figure 2-52: Gas composition at the bed top of pine wood, 20mm (Ryu *et al.*, 2006).

During the ignition propagation period, the mass left on the bed decreased with a uniform slope. The mass loss slowed down as the char oxidation period commenced and accelerated as the air flow rate increased. Figure 2-53 shows that mass loss during the ignition propagation period of miscanthus.
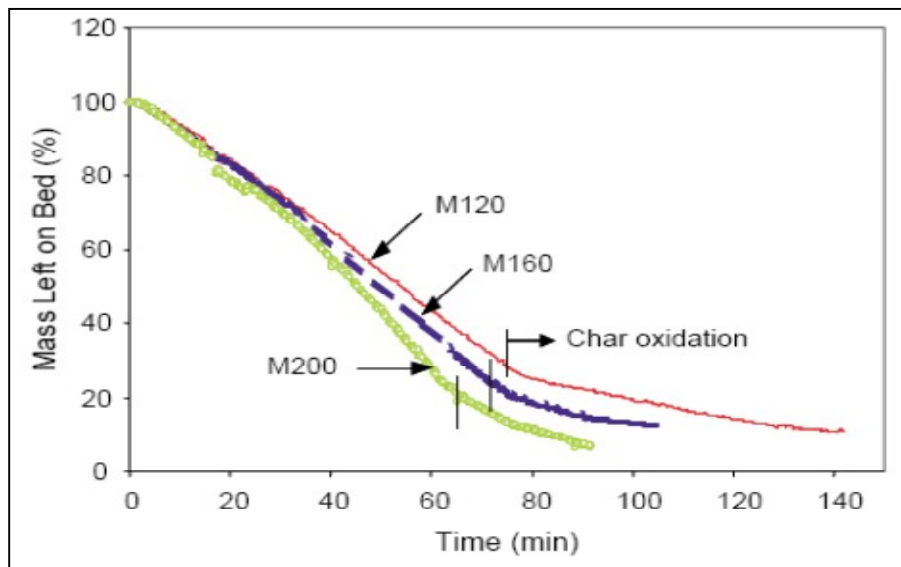
Figure 2-53: Mass loss during ignition propagation period of miscanthus (Ryu *et al.*, 2006).

2.3.7.5 Channeling

Void spaces between particles in the bed are interconnected. Channeling causes most of the air or gas flow pass through passages with higher local void fraction inside the bed. The ignition front propagates much faster around the channel. It also causes large transient or spatial fluctuations of temperature and chaotic burning patterns. Large voids between particles create several shortcuts for air. Once the channels have collapsed by volumetric shrinkage of the nearby particles, new channels appear with different number and location. The effect of channeling on the burning rate was not significant (Yang *et al.*, 2006b).

2.3.7.6 Combustion gases

The effects of combustion parameters on combustion gases particularly toxic gas such as CO, NOx and SOx have been studied by a lot of researchers (Friberg and Blasiak, 2002, Rogaume *et al.*, 2002, Johansson *et al.*, 2003, Yan *et al.*, 2005). At low primary air flow rates or sub-stoichiometric conditions, increasing air flow rate decreases the CO concentration as shown in Figure 2-54. In contrast, the concentration of NO (see Figure 2-55) depends on the total air available independent of the source where the contribution is made whether primary or secondary air (Rogaume *et al.*, 2002). Johansson *et al.*, (2003) claim that increasing the excess of air or super-stoichiometric regime causes an increase in the CO yield and the particle emission in the flue gas.
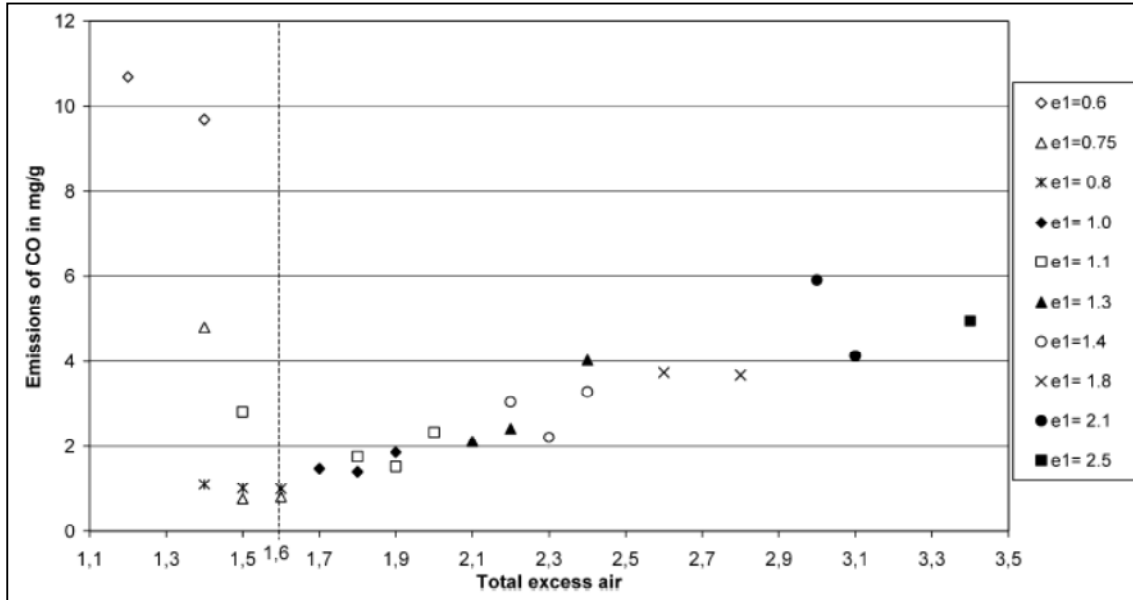
Figure 2-54: CO emissions as a function of the total excess air. Different symbols indicate different primary excess air flows (Rogaume *et al.*, 2002).
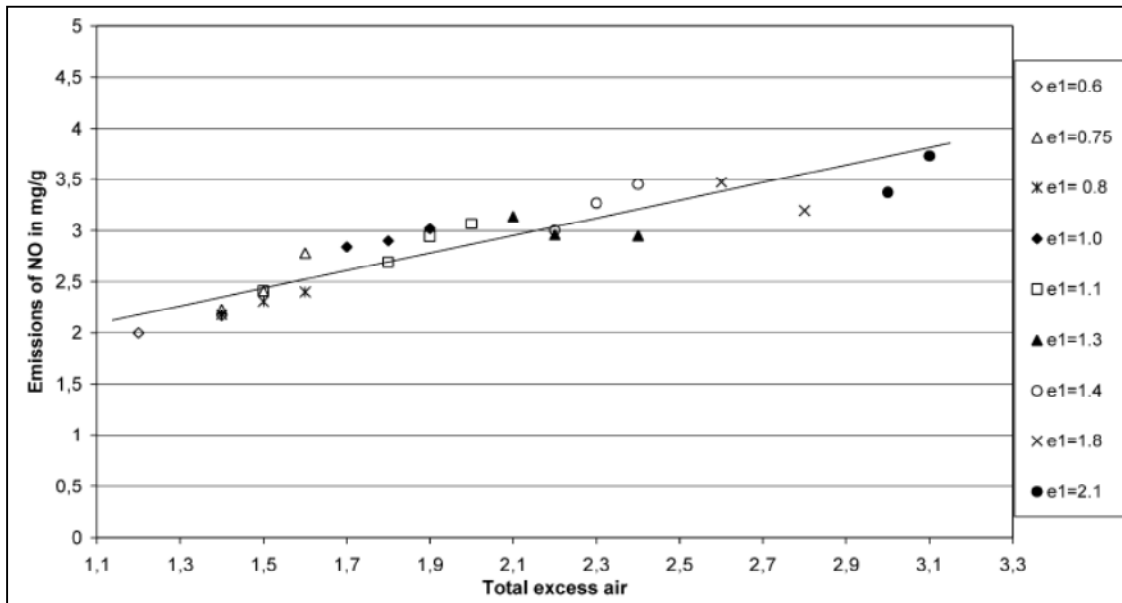
Figure 2-55: NO emissions as a function of the total excess air. Different symbols indicate different primary excess airflows (Rogaume *et al.*, 2002).

An Ellingham diagram (see Figure 2-56) is used to 1) determine the relative ease of reducing a given metallic oxides to metal, 2) determine the partial pressure of oxygen that

is equilibrium with a metal oxide at a given temperature, and 3) determine the ratio of carbon monoxide to carbon dioxide that will be able to reduce the oxide to metal at a given temperature. The Gibbs free energy(ΔG) of a reaction is a measure of the thermodynamic driving force that makes a reaction occurs. A spontaneous reaction (without external inputs) occurs when the Gibbs free energy is negative. A positive value indicates that a reaction will not occur without external inputs. The Gibbs free energy is defined as follows:

$$\Delta G = \Delta H - T\Delta S$$
<div align="right">Eq: 2-43</div>

Where;

ΔH is the enthalpy change

T is absolute temperature

ΔS is entropy change

An Ellingham diagram is a plot of ΔG versus temperature. The diagram can also be used for metals reacting with sulphur and chlorine. However, it is commonly used for metals reacting to form oxides (Russell, 1998, Gaskell, 2001). The reaction of carbon species with oxygen to form products such as CO_2 or CO can also be obtained from this diagram. The standard Ellingham line for $C + O_2 \rightarrow CO_2$ is almost horizontal (AB line in Figure 2-56) at $\Delta G \approx -400\,kJ$ because a solid (C) reacting with a mole of gas (O_2) to produce a mole of gas(CO_2) has little change in entropy. However, for the reaction of $2C + O_2 \rightarrow 2CO$, there is a substantial increase in entropy, therefore the line (CD line in Figure 2-56) slopes sharply downward. The two lines cross at about 700°C in which the gas in equilibrium with carbon and $p(CO) = p(CO_2) = 0.5\,atm$, at the point marked E in Figure 2-56. The thermodynamic stability of CO-CO_2 gas at 1 atm pressure in equilibrium with carbon varies with temperature along line AED (red line) in Figure 2-56. This line is also known as a carbon line. At a temperature below 700°C, CO_2 formation is thermodynamically more stable than CO. However, above 700°C, CO is thermodynamically more stable than CO_2, thus the gas in equilibrium with carbon is mostly CO.
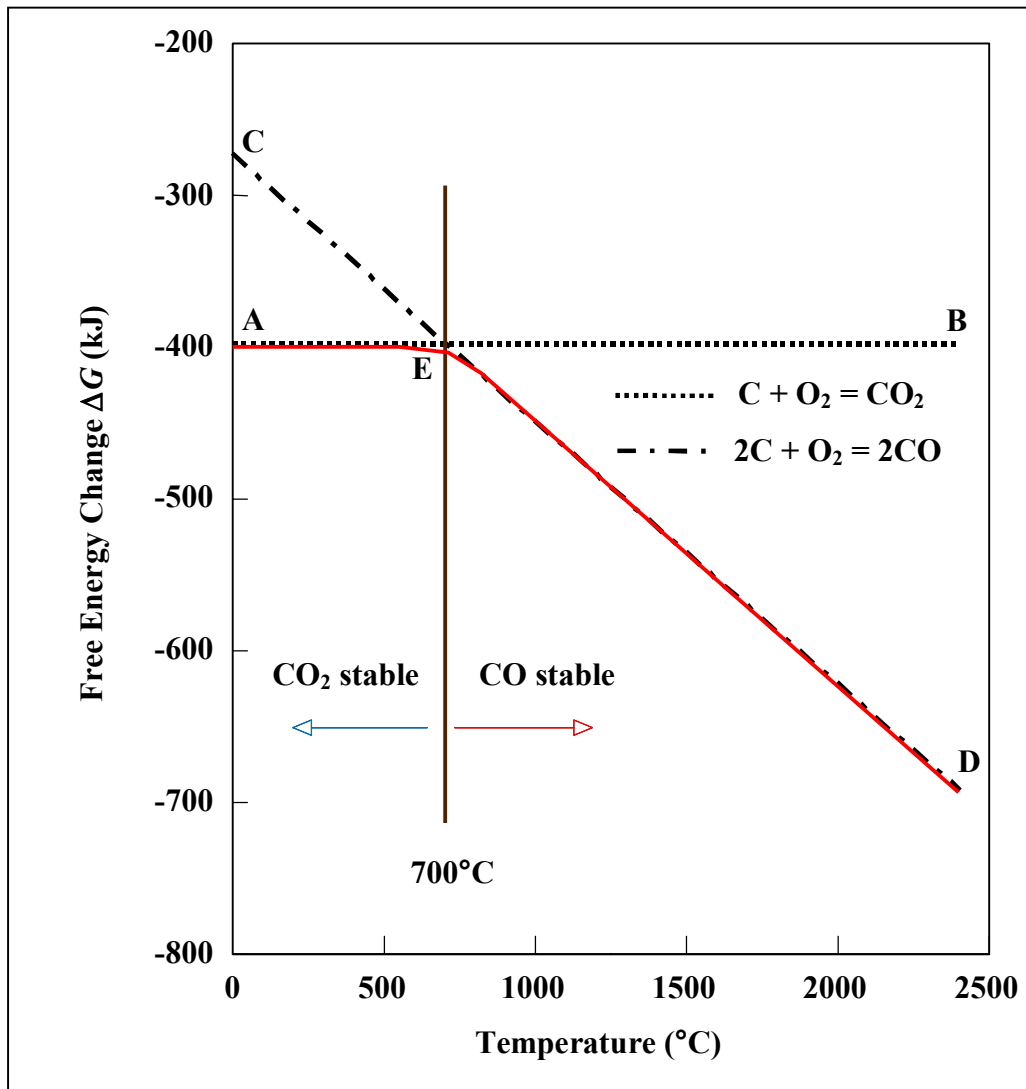
Figure 2-56: Ellingham diagram (after Russell, 1998).

2.4 Pelletisation

2.4.1 Introduction to pelletisation

An agglomeration or size enlargement is an important step to improve fuel properties. There are many ways to enlarge the size of fine particulate fuel; one is through pelletisation process. This section reviews the pelletisation theory, which focuses on the purpose of making and classifying of pellets, and discusses the treatment, storage and transport of pellets. Pelletisation technologies, particularly on compaction and extrusion methods are also reviewed. Pellet quality assessment techniques such as the effect of particle size, feed moisture content, temperature, binders and oil/fat in the feed material are also discussed.

2.4.2 Pelletisation theory

2.4.2.1 Reasons for pelletisation

Pelletisation or briquetting is a process of consolidation of loose material in a mould to form a densified material. Pellets and briquettes are quite similar apart from their shapes. Pellets comprise of cylindrical pieces of compressed material. Similarly, briquettes is also a compressed material, but it can be cylindrical or take any other shape (Rosilli-Calle *et al.*, 2007). Both usually have a maximum diameter of 25 mm. The size of pellets and briquettes depends on their end user requirements. In general, pellets and briquettes are produced with sizes ranging from 10-30 mm, having moisture content and densities of around 7-15 % and 1300 kg/m^3 respectively (Rosilli-Calle *et al.*, 2007).

According to Messman (1977), the following terms are used to describe the consolidation of loose materials:

a) Agglomeration – is a process of consolidation of particles into larger shapes by means of agitation alone without any application of mechanical pressure in mould, or between rolls, or through dies.

b) Briquetting – is any little brick of particles formed by mechanical pressure in a mould, a roll briquet machine, an extruder or some other device in any shape that is larger than a pellet.

c) Pelletising – is a process to consolidate loose particles to form larger products of a stable nature by the application of heat, moisture and mechanical pressure, where the primary purpose is to form solid materials of uniform properties and size.

d) Granulation – is a consolidation of particulate solids into grains or granules which typical size range between 2 to 4 mm.

e) Compaction – indicates a mechanical consolidation of solid particles between rolls, or by piston, screw or other means.

f) Nodulising – is a simultaneous sintering and drum balling, usually in a rotary kiln.

g) Sintering – is heat bonding in which a relatively small portion of a particulate solid fuses and forms a tacky binder at elevated temperature.

h) Extrusion – means forcing a material through an aperture or mould.

The aim of these processes is to produce a similar size and shape of solid fuel. The process can be divided into two main categories; with binder, and without binder. Some loose materials can be pelletised without any binder due to the Van der Waals' forces effect that interacts between individual particles to form a pellet (Rieschel, 1963). However, in the case of binder pelletising, cohesion of the pellets is particularly due to admixture or binding agent. There are two functions of adding admixture; 1) to coat the surface of individual grain in order to form a film of individual particle, and 2) to penetrate the larger particle by capillary action. Because of these actions, less force is required to consolidate loose material to form pellets or briquettes (Rieschel, 1963).

In general, converting loose biomass into a densified fuel such as pellets and briquettes can improve their quality in terms of density, strength, transportation cost and durability. The main reason for pelletising biomass for fuel application is to increase its bulk and energy content per unit volume, making it easier to burn or co-fired with coal in power plants (Li and Liu, 2000). Lyne and Johnston (1981) identify five key parameters of pelletisation and briquetting:

i) To improve the quality of finished products. Pelletisation is a tool to blend all required ingredient in the form of fine particles to produce good quality products.

ii) In some cases, bigger particle size material is much easier to handle. Therefore, pelletisation can help in terms of handling and marketing of the material without compromising their functional properties and characteristics.

iii) To improve handling properties of very fine particles. Pelletisation can increase the density of very fine particles, making it easier to transport, store and feed them.

iv) Some processes such as bag filter and electric precipitators produce very tiny particles. It is difficult to handle or dispose them. Pelletisation can help to dispose such material safer and environmentally cleaner.

v) By products from processing materials are always in fine particles. Therefore, it is not suitable to directly re-use or recycle them. Pelletisation may help fine particle to be returned to the process.

Nasrin *et al*., (2008) investigated the physical and chemical properties of the mixture of empty fruit bunches (EFB) and palm kernel cake (PKC) briquettes. It was found that the conversion of oil palm biomass, particularly EFB and PKC into a uniform fuel such as pellets or briquettes can improve its properties. The energy content of the briquettes was increased by 5% and moisture content was reduced to 38% compared to the original materials.

According to Grover and Mishra (1996), the most influential parameters in the selection of raw material are moisture content, ash content, flow characteristics and particle size. Moisture content in the range 10-15% is preferred due to the high energy required for drying. The granular (6-8 mm in size) homogeneous materials which can flow easily in conveyors, bunkers and storage silos are suitable for briquetting. The most common used materials for pelletising and briquetting are sawdust, groundnut shells, cotton stalks, maize stalks, rice husk, tamarind shells, coir pith, coffee husk, mustard stalks, sunflower stalks, mustard husk, bagasse, wood chips and forest residues. A combination of raw materials could also be used (Grover and Mishra, 1996).

2.4.2.2 The fundamental consideration

The press tools designed for the production of briquettes and pellets are generally based on three pressing methods outlined in Table 2-19. Method 1 - the pressing process is a continuous stroke or constant volume. The pressure (P) is a function of the amount of material (Q_m). The pressing process is limited to the minimum amount of material filled into the mould. If the material filled is below the minimum required amount no pressing will occur. This is because the stamp will not reach and compress the material. Mechanical table press is one example of the commercially available pelletiser that is based on this principle. This technology is widely applied in the brick industry along with fixed roll presses. Method 2 - the stroke and volume are variable. The products are almost of similar quality because of the consistency in the pressure. This principle is employed mostly on the presses operating with hydraulic pressure such as column-type presses and ring roller presses. Method 3 - constant stroke, produces pellets are almost similar quality. However, the volume varies depending on the material fed into the mould. The operations of extrusion presses pelletiser are based on this principle (Rieschel, 1963, Finney, 2009).

Table 2-19: The variable adjusted for the three different types of pressing methods (after Finney, 2009).

Variable	Method 1	Method 2	Method 3
Stoke (S)	Constant	Variable	Constant
Volume (V)	Constant	Variable	Variable
Pressure (P)	$f(Q_m)$	Constant	Constant

The Production of hard-type pellets is not an easy task. Hard-type pellets are normally produced using equipment based on a die and roll principle. A combination of rolls and dies for pressure, extrusion and forming are used to produce hard-type pellets (Robinson, 1971). Figure 2-57 shows the first steel dies and rollers equipment for pellets making and was developed by E.T Meakin of the California Pellet Mill Co. This design of the equipment is based on four rollers operating on a flat steel surface or mould. Particles are poured and distributed evenly on to the mould face, then forced though the mould by

rollers. Multiple knives are used to cut off pellets extrusions according to the required size. Another unit using the same principle is ring-type die pellet mill (Figure 2-58). This unit is designed based on the following working principle: 1) the fed material is introduced and distributed by three main forces, gravity, centrifugal force and mechanical deflectors; 2) Rotating die and rollers build up pressure that causes the material to compact and forces it to pass through the mould to form pellets; and 3) Pellets are cut using adjustable knives according to the desired length (Robinson, 1971). The pellets making process via ring-type die and roller is shown in Figure 2-59.
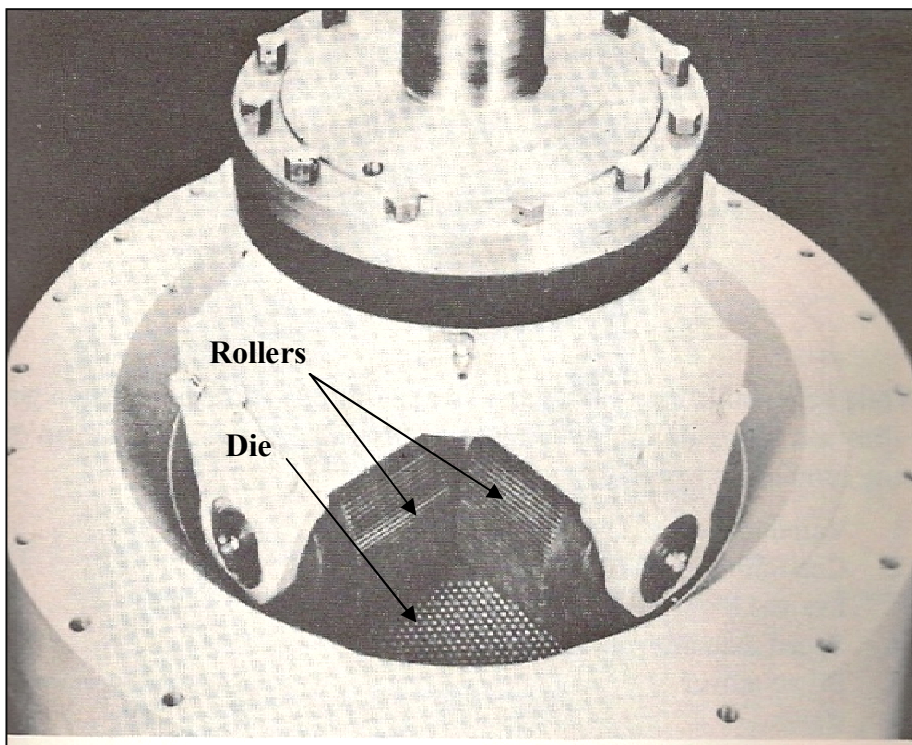
Figure 2-57: Die and roller pelletiser (Robinson, 1971).
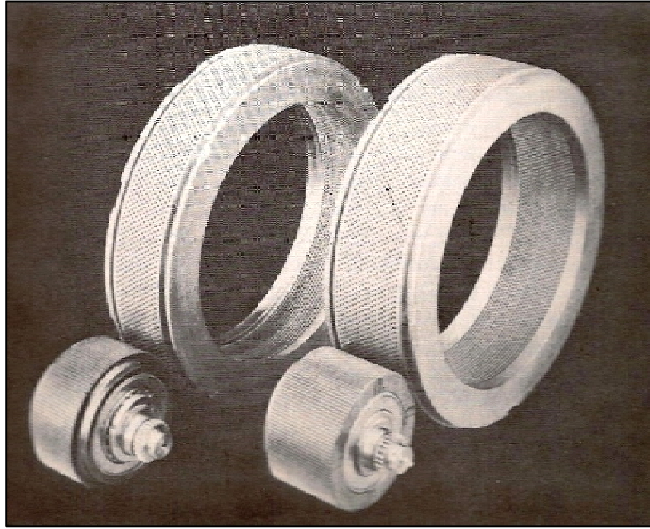
Figure 2-58: Dies and rolls for ring-type die pellet mill (Robinson, 1971).

1. Feed material
2. Compaction and extruded feed
3. Knives
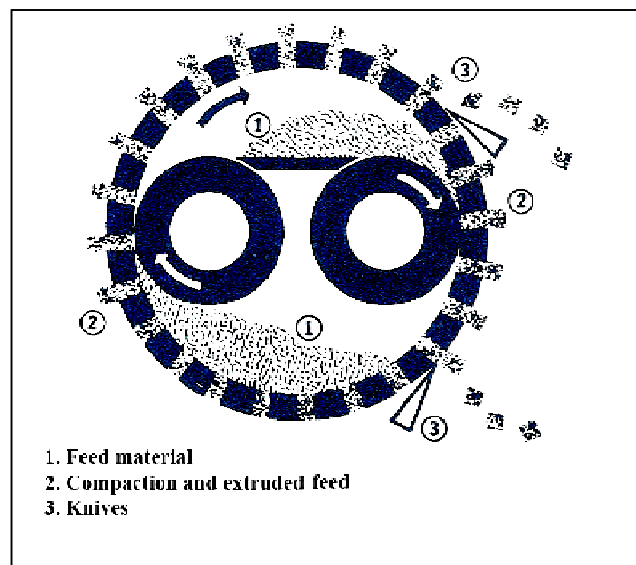
Figure 2-59: Schematic of operation of ring-type die and roller (Robinson, 1971).

2.4.3   The selection of pelletisers

Table 2-20 illustrates the wide range of equipment used for size enlargement, which classifies them according to the principle employed, namely compaction, extrusion, tumbling, mixing, drying, and sintering. However, despite this apparent diversity, the action of each machine involves one of the three principles or a combination of them: application of pressure, agitation and heat (Lyne and Johnston, 1981). The pelletiser

chosen for a particular function is largely determined by the material properties (Rieschel, 1963).

Table 2-20: Size enlargement equipment (Lyne and Johnston, 1981).

Operating principle	Typical equipment
Compaction	• Tableting machine • Briquetting rolls • Ring roller press
Extrusion	• Pellet mill • Screw extruder
Tumbling	• Drum granulator • Inclined disc or drum • Pelletiser
Mixing	• Spiral path granulator • Ribbon blender • Granulating mixers
Drying	• Spray dryer • Band dryer for preformed pastes • Instantiser • Fluidised bed granulator
Sintering	• Rotary kiln • Shaft kiln

Lyne and Johnston (1981) reviewed the various types of pelletisers and their features are summarised in Table 2-21. One can select the most appropriate type or at least specify the choice by considering the main product requirement; 1) the uniform of pellet size, high bulk density or elimination of dust. 2) the nature of the feed material e.g. dustiness and flow properties, and 3) any other limitations e.g. space and capital. All the pelletisers rely on the same mechanism for size enlargement, for there to be a single candidate of every application.

Table 2-21: Comparison of pelletisers (Lyne and Johnston, 1981).

	Horizontal drum	**Inclined drum**	**Inclined disc**
Production rate	10-80 t/h	0.8-100 t/h	0.8-140 t/h
Pelletiser diameter	1.5-4.6 m	0.6-4.3 m	1.0-7.6 m
Space requirements	Large	Least of the three types	Moderate
Capital cost	High	Medium	Medium
Pellet target size	3-20 mm; up to 50 mm	3-20 mm; up to 50 mm	3-20 mm
Uniformity of pellet size	Screening necessary	Good	Good
Production of hard pellets	Yes	Yes	May need re-roll ring
Increase in bulk density	Very good	Good	Good
Suitability for dusty materials	Very suitable	Very suitable	Suitable with dust hood
Other features	Less sensitive to fluctuation because of re-circulating load	Good for pelletising multi-component feed	Good visibility of tumbling charge

In general, there are essentially two mechanisms involved in the pellet making industry; compression and extrusion. The briquetting technologies based on compaction can be classified as follows:

i. High pressure compaction

ii. Medium pressure compaction with a heating device

iii. Low pressure compaction with a binder

In all these compaction techniques, solid particles are the starting materials. The individual particles are still identifiable to some extent in the final product. Briquetting and extrusion both represent compaction (Grover and Mishra, 1996). Fine particles which deform under high pressure without a binder gained this strength caused by Van der Waals' forces, valence forces or interlocking. Natural components of the material may be activated by the prevailing high pressure forces to become binders. Figure 2-60 shows some of the binding mechanisms.
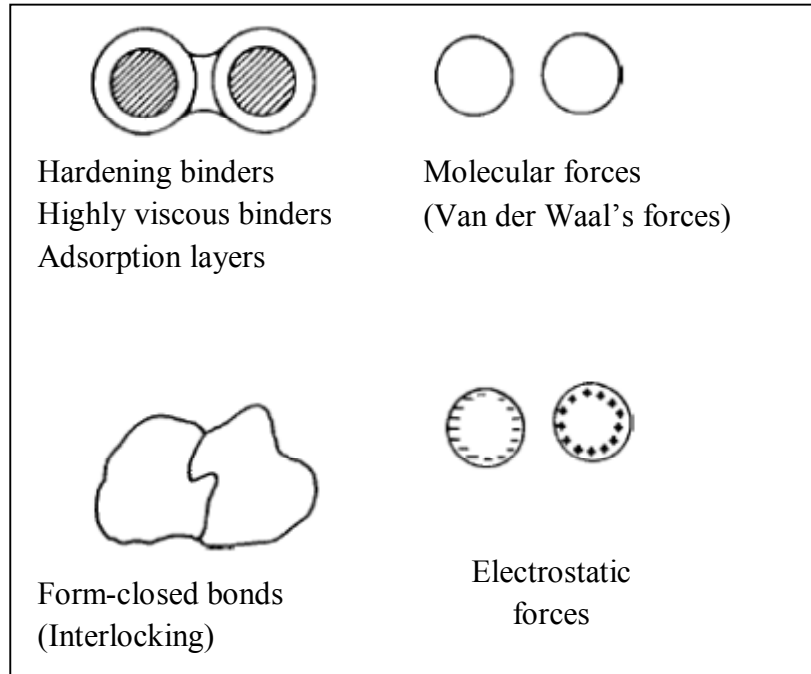
Figure 2-60: Binding mechanisms (Grover and Mishra, 1996).

2.4.3.1 Compression methods

The compaction mechanism of different materials will be different from one another. In general, during the first stage of compression process, particles rearrange themselves to form a closely packed mass as shown in the schematic representation in Figure 2-61. In this phase, the original particles retain most of their properties, although energy is dissipated due to friction. At high pressures, the particles are forced against each other, undergone elastic and plastic deformation, which increases inter-particle contact. Therefore, short range bonding forces like Van der Waal's forces, electrostatic forces and sorption layers become effective (Mani, 2005).
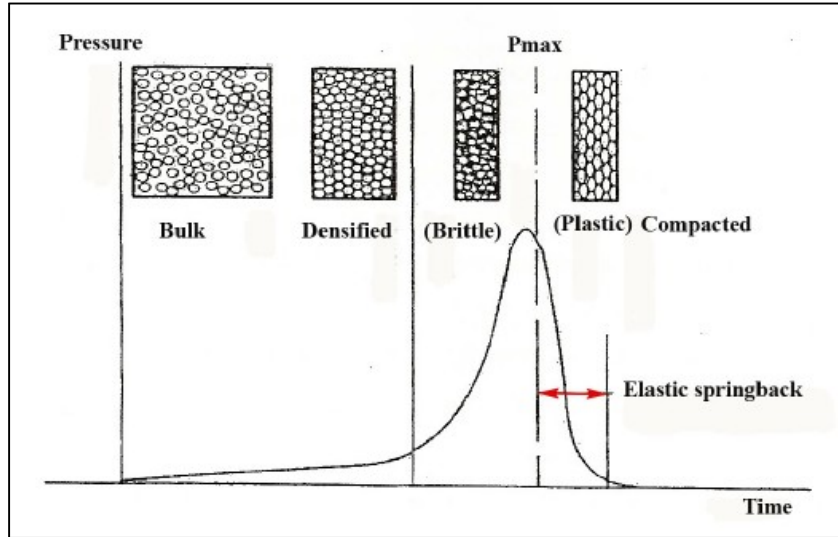
Figure 2-61: Typical compaction process (Mani, 2005).

Rieschel (1963) and Deaubert (1973) point out that the basic concept of compacting loose materials are as follows: sealing the bottom by a lower punch, charging, pressing and ejecting as illustrated in Figure 2-62. Loose material is fed into the mould while the lower punch stationary is at the bottom. The upper punch is used to compress the material during the pressing stage. When the pellet is formed, the lower punch is used to eject the pellet at the final stage. The lower punch is released to the initial position, and then the process repeats the cycle with new loose materials.
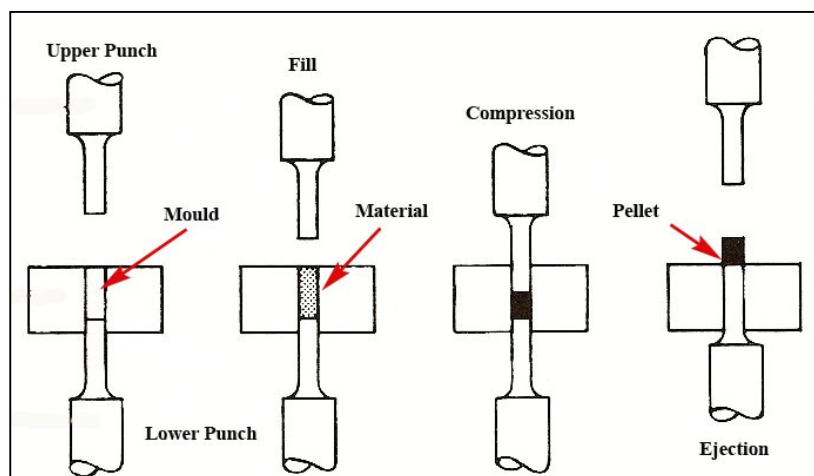
Figure 2-62: Basic compacting sequence (Daubert, 1973).

110

Material is fed by gravity into the mould. The weight of the feed is established volumetrically. When the feed source moves away, the volume of material is measured from the top of the lower punch to the top of the mould or die. As the upper knock enters the die, the bulk volume of the material in the mould is reduced until the knock reaches its lowest point. According to Daubert (1973), this point is known as 'green density'. The part is then expelled from the mould, removed from the press, and sometimes subjected to another processing step such as heat treatment. Almost all compacting presses are based on mechanical, hydraulic or a combination of both techniques.

Due to the compaction process, the occluded air is pushed back to the feed zone and improved thermal conductivity. The biomass absorbs energy from friction; therefore, it heated and mixed uniformly through its mass. Some of the important parameters for pellets produced using this technique are brittleness, plasticity and abrasivity. The properties of the solids that are important to pelletisation or densification are flow ability and cohesiveness, particle size, surface forces, adhesiveness, hardness and particle size distribution.

2.4.3.2 Extrusion methods

Two widely used types of extrusion technology are a screw-type extrusion and piston extrusion. A screw-type extrusion machine is one of the older pelletising equipments available. It is used to pelletised a truly plastic material (Schweizer, 1963). Brittle and under stress particles may fracture leading to mechanical interlocking. This bonding is the only bonding mechanism that does not involve atomic forces and contributes very little to the overall strength of pellet (Gray, 1968). If the melting point of the ingredients in a powder mix that forms a eutectic mixture is favourable, the heat generated at a point of contact can lead to a local melting of materials. Once cooled, the molten material forms very strong solid bridges (Ghebre-Sellassie, 1989).

According to Grover and Mishra (1996), a simple extruder features three distinct zones: feed, transport, and extrusion zones. The important forces that influence the compaction

of biomass play their role mostly in the compression zone. When the biomass is fed into a screw extruder and force is applied due to the restriction in the form of a die, compaction occurs due to the following mechanisms: 1) before reaching the compression zone (a zone usually formed by tapering of the barrel) the biomass is partially compressed. This leads to closer packing and increased density. Energy is dissipated to overcome the particle friction. 2) At the compression zone, the biomass material becomes relatively soft due to high temperature. Due to loss of elasticity, it is pressed into void spaces and as a result, the area of inter-particle contact increases. When the particles bind together they form local bridges which selectively support and dissipate the applied pressure. Interlocking of particles may also occur. Moisture is evaporated to steam at this stage and helps in moistening the biomass. 3) The biomass is further compressed in the tapering die to form the pellet. In this section, the removal of steam and compaction take place simultaneously; the pressure exerted transmits throughout the material giving uniform pressure, and therefore, uniform density throughout the pellet.

In a screw extruder press (Figure 2-63), the biomass is extruded continuously by a screw through a heated taper die. In a piston press, the wear of the contact parts for example, the ram and die is less compared to the wear of the screw and die in a screw extruder press. Furthermore, the energy consumption in piston press is less than in screw extruder press. However, in terms of the pellets quality and production procedures screw press has a better quality than the piston press. Table 2-22 shows a comparison between a screw extruder and piston press (Grover and Mishra, 1996).
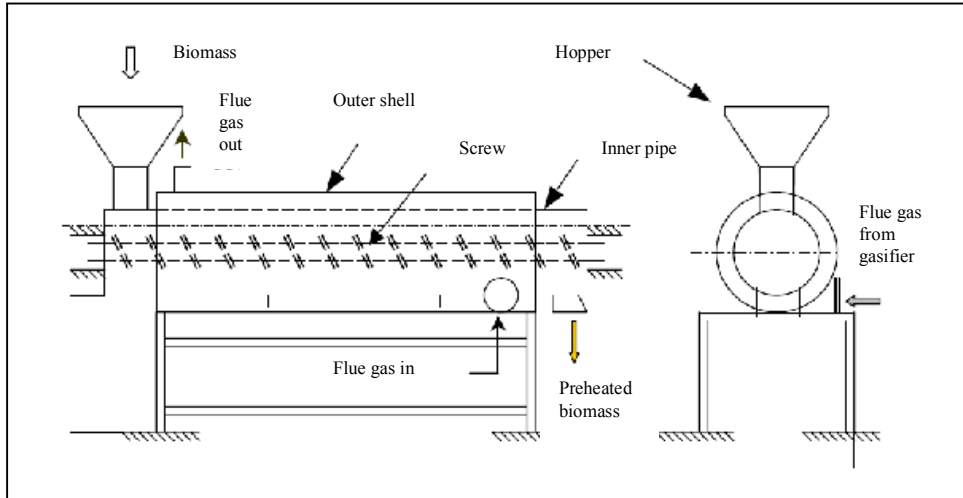
Figure 2-63: Screw extruder (Bhattacharya *et al.*, 2002).

Table 2-22: Comparison of a screw extruder and a piston press (Grover and Mishra, 1996).

	Piston press	**Screw extruder**
Optimum moisture content of raw material	10-15%	8-9%
Wear of contact parts	Low	High
Output from the machine	In strokes	Continuous
Power consumption	50 kWh/ton	60 kWh/ton
Density of product	1-1.2 g/cm^3	1-1.4 g/cm^3
Maintenance	High	Low
Combustion performance	Not good	Very good
Carbonisation of charcoal	Not possible	Makes good charcoal
Suitability in gasifiers	Not suitable	Suitable
Homogeneity of pellets	Non-homogeneous	Homogeneous

2.4.4 Press technologies

Various types of press have been developed depending on the requirements of the pelletising process and the properties of the raw materials. According to Rieschel (1963), there are four main types of presses commercially available in the market:

113

2.4.4.1 Table presses

There are two types of table presses; rotating and sliding. The difference between them is the output. The rotating table presses can produce about 6000 bricks per hour at 20 strokes per min, while sliding can fabricate only 4200 bricks per hour at 7-9 strokes per min. The reason for the difference is the rotating table press works with different working cycles in which the processes such as charging, pressing and ejecting can be done simultaneously. However, the sliding table press requires the processes to be performed in an order. Both types of presses required about 25-35 kW (33-47 HP) of driving power to achieve pressures of up to 400 kp/cm^2 (5700 psi) or equivalent to 350-400 tons load. These types of presses are considered one of the oldest types of pelletising press available in the market. They are exclusively used for making building and refractory bricks.

2.4.4.2 Roll presses

Roll presses (Figure 2-64) consist of two rolls with similar diameter, operating at synchronous speed in opposite path. Several rows of moulding cups attached to the rims of the rolls that are driven by gear wheels. The synchronism is generally controlled by the gearing and gear wheels. The raw material is fed between the rolls (Figure 2-65) by a distributer pan and a feeding hopper or screw feeder. Snow *et al.*, (1997) stated that the most difficult problem in the briquetting operation using roll presses is to choose an appropriate amount of material to be introduced into rotating moulding cups in the rolls. The material is drawn into the moulding cups by the rotation of the rolls and formed a pellet. The shape and size of the products are determined by the roll diameter or feed angle (Snow *et al.*, 1997). The frictions between rolls are the major contribution to the amount of material drawn to the moulding system and the properties of the raw material. The quality of the pellets depends on material charge, since the moulds always provide a constant volume and the moulding pressure is a function of the charge. However, in modern presses design, a sliding displacement unit is fixed in one of the rolls to avoid excessive filling of the material.
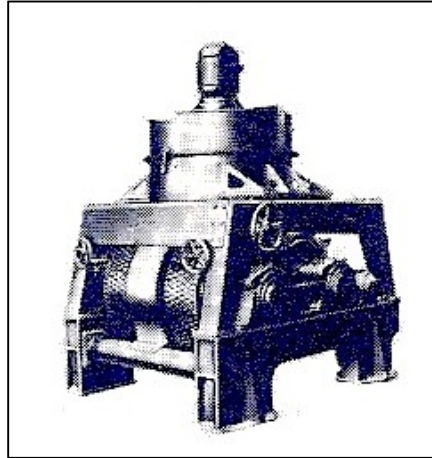
Figure 2-64: Roller press (Rieschel, 1963).
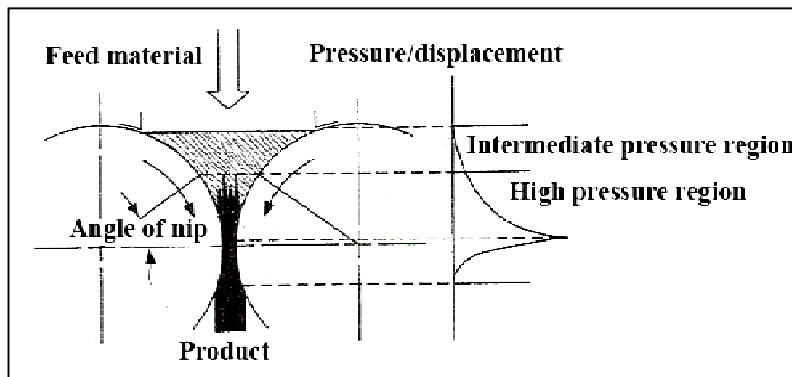
Figure 2-65: Regions of compression in roll presses (Snow *et al.*, 1997).

In general, the pressure at the central of the rows is greater than the outer one. It is because the central rows receive a greater charge and determine the roll spacing. Most of the pressure is developed at the centre of the material as shown in Figure 2-66. Less pressure experienced by the material at the top and the bottom may result in both the formation of non-uniform consolidation of pellet and non-uniform expansion of individual section of the pellet. Limited forces are achieved on roll presses, within the range of 2.5 to 15 ton per linear inch. Limited contact of the convex roll surfaces and the mould cups causes the hard and elastic materials to spread out immediately. These phenomena may lead to the formation of cracks or even cause the pellet to break-up. For

115

these reasons, roll presses are suitable for pelletising soft material with sufficient plasticity (or using a binder) but not apt for hard and brittle materials. According to Snow *et al*.,(1997), roller presses can produce large quantities of pellets at low cost. However, it is less uniformed compared to the pellets produced with table presses.
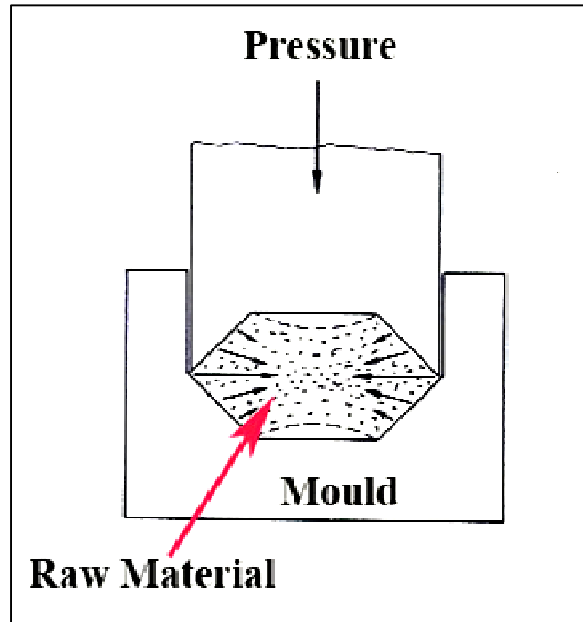
Figure 2-66: Distribution of pressure in a round shaped mould (Rieschel, 1963).

2.4.4.3   Extrusion press

The press works on a similar principle of a piston-type steam engine. It consists of two main components; the driving mechanism (crankshaft) and the press head. Figure 2-67 shows the schematic representation of the operations of the extrusion press. The driving mechanism is made up of the crankshaft that is attached to the two adjustable slide bearings. A rod or piston is used as the press rams and it connect to the centre bearing of crankshaft.
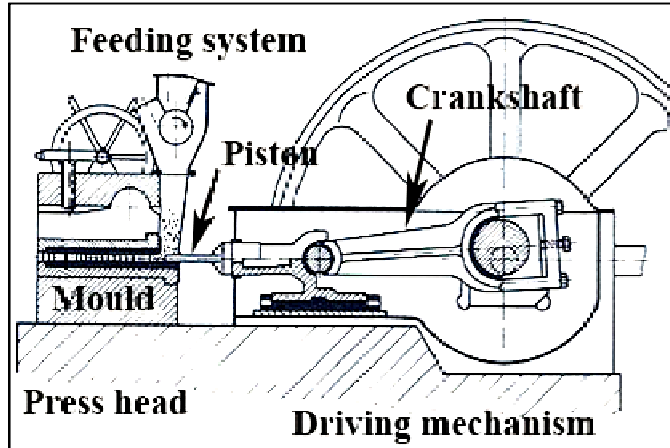
Figure 2-67: The schematic diagram of extrusion press (Rieschel, 1963).

In general, the mould channel consists of a cylinder with approximate length of 3 feet (0.91 m). This size of mould can produce about 15-20 pellets. The quality of the pellets produced by this press does not depend on material charge since the material is continuously compressed until the maximum pressure. The amount of pelletising pressure mainly depends on the friction force between pellet strand and mould wall. The friction force depends on the material properties of pelletising material such as hardness, plasticity, elasticity, and their change during compression (Rieschel, 1963).

There are two parts of the mould channel; convergent and divergent. The convergent section is used to direct and partly compress the raw material. The divergent part is set to control the pellets expansion to avoid cracking. A gradual drop in pressure at the end of the mould channel is very important to maintain the quality of the pellets. This phenomenon also prevents pellets cracks during compression process particularly if the raw material is hard and elastic such as plastic. However, hard material such as older lignite cannot be pelletised using extrusion presses due to the limitation on pressure in the mould (Rieschel, 1963).

2.4.4.4 Ring roller press

The ring roller presses are developed for pelletising hard material. Figure 2-68 shows the schematic representation of a pelletising process of ring-roller press. The ring roller press

consists of a press wheel, a ring carrying moulding channel and two supporting rollers attached from the outside of the ring. A press wheel runs on the surface of material in the moulding channel and acts as a pressing tool. The press wheel releases an average pressure of 30,000 to 70,000 psi (206.8 to 482.6 MPa). Sometime closed and split moulding systems are used to pelletise hard, brittle and elastic materials. The split moulding systems are used because elastic materials interlock more after pressure release due to an expansion. The main problem with the ring roller press is wear and tear on mould channel and press wheel. It varies depending on the type of material used. Most of the designs carry wearing parts that can be reground. The press wheel requires more frequent grinding due to heavier stress which is based on the fraction of the wheel and ring diameter (Rieschel, 1963).
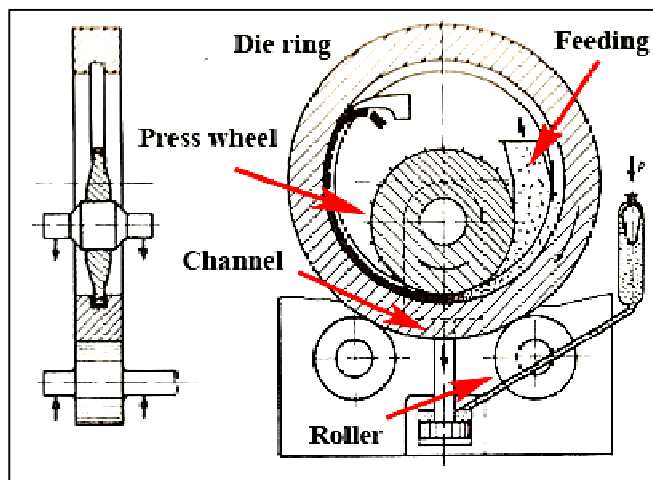
Figure 2-68: Ring-roller press (Rieschel, 1963).

A very fine-grained material causes more problems, mainly in the feeding systems. Charging of the mould channel can also be affected by the air which blows out material from the channel. This may cause formation of the non-uniform size of pellets due to insufficient compressed pellets. These problems can be trounced by exhausting the air out of the mould channel or by enlarging the ring and wheel to increase the feeding angle. Modification on the pressing orientation from vertical to horizontal (Figure 2-69) may help to overcome these problems.
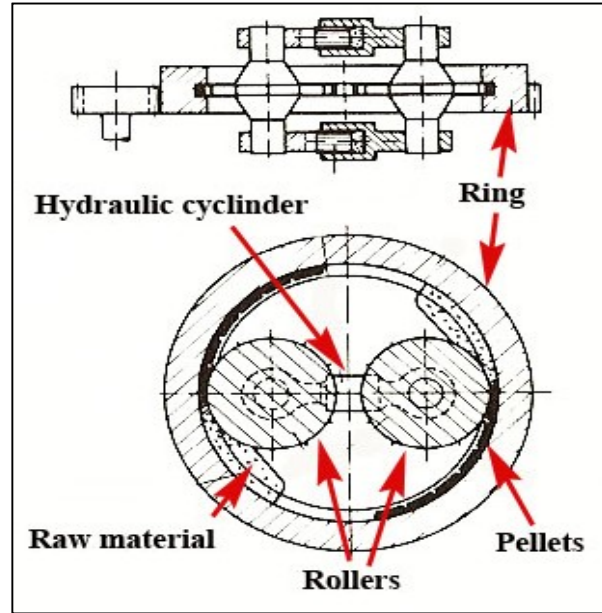
Figure 2-69: Horizontal ring-roller press (Rieschel, 1963).

Rieschel (1963) also categories pelletisation press based on applied pressure as shown in Table 2-23. The first group of pressure (below 7,000 psi) is considered as low pressure press. These ranges of pressures may be suitable for table and roller presses which are used for pelletising with binders. Medium group of pressure (8500 – 17000 psi) is used for pelletising of lignite, peat, wood, bagasse and fruit waste as well as soft metals, such as lead and copper. High pressures (2300 – 35500 psi) pelletising are generally used for binderless pelletisation or in case of the substance is particularly hard or brittle, such as sponge metal, soda ash and lignite.

Table 2-23: The pressure variations for pressing processes (Rieschel, 1963).

Pressure level	Pressure range	
	psi	**MPa**
Low	<7000	<48
Medium	8500-17000	58.5-117
High	23000-35500	158.5-245

2.4.5   Compaction characteristics and their significance

In order to produce good quality pellets, feed preparation is very important. Feed properties are discussed in this section, as they play a significant role in pelletising or briquetting technology. The most important properties are particle size, moisture content and temperature. The effects of these properties are discussed in the following sub-sections.

2.4.5.1   Specific energy requirement

The quality of biomass pellets depends greatly on energy consumption during the pelletisation processes. Most of this process involves compression and extrusion techniques, which requires more energy due to friction and it narrows the cross sectional area of the pressing channel. The contribution of energy due to friction during pelletisation of straw and hay is about 37-40 %, the rest 60-63 % of the energy is required to overcome the friction (Mani, 2005). Figure 2-70 shows the energy consumption to compress a straw with two different pelletisation techniques. Extrusion method consumed more energy than compression technique due to the friction between surface channel and the material.
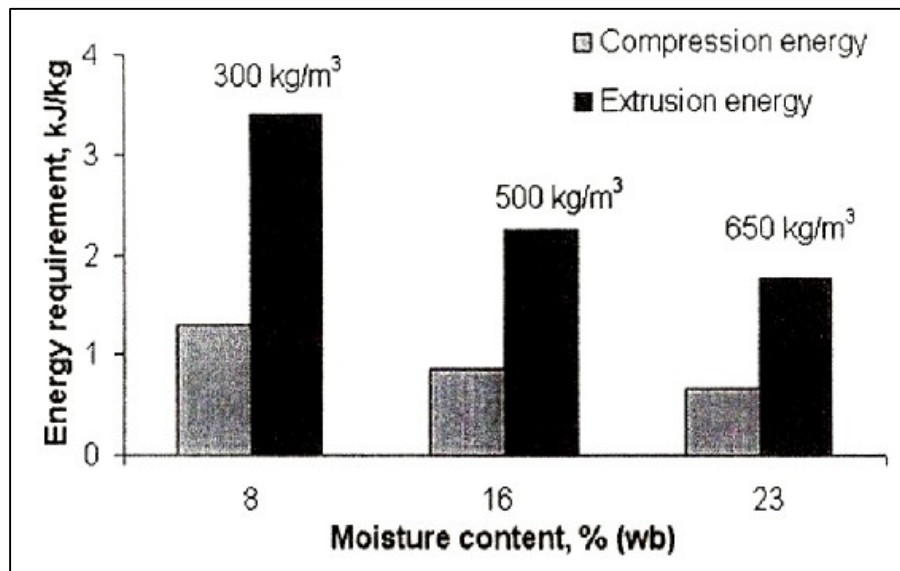
Figure 2-70: Energy requirements for densification of straw and hay biomass (Mani, 2005).

Mani *et al*., (2006) studied the specific energy requirement for briquetting corn stover at different pressure and moisture content. They revealed that the specific energy consumption was in the range of 12-30 MJ/t and it depended on briquette density. Almost half of the total energy required in the compaction of corn stoves was used to overcome the skin friction.

2.4.5.2   Effect of particle size

Pellet durability is highly influenced by the particle size of a raw material. In general, the finer the grind, the higher the durability. Fine particles usually accept more moisture than large particles and, therefore, undergo a higher degree of conditioning. In addition, large particles are fissure points that cause cracks and fractures in pellets (Kaliyan and Morey, 2009) who also pointed out that particle size for good pellet quality is between 0.6-0.8 mm. However, Grover and Mishra (1996), suggested that biomass material of 6-8 mm size with 10-20% powdery component (< 4 mesh) gives the best results when produced using screw extruder technology. Fine and powdered particles of size less than 1 mm are not suitable for a screw extruder because they are less dense, more cohesive, non-free flowing entities.

Although the screw extruder which employs high pressure (100 - 150 MPa) is capable of pelletising material of oversized particles, the pelletising will not be smooth and clogging may take place at the entrance of the die resulting in the jamming of the machine. The larger particles, which are not conveyed through the screw, start accumulating at the entry point. The steam produced due to high temperature (due to rotation of screw, heat conducted from the die and also if the material is preheated) inside the barrel of the machine starts condensing on fresh cold feed resulting in the formation of lumps and leads to jamming.

Due to the problems outlined above, the processing conditions should be changed to suit the requirements of each particular biomass. Therefore, it is important to crush larger particles to achieve a random distribution of particle size. Hence, an adequate amount of

small particles is present to be embedded into the larger particles. The presence of different size particles improves the packing dynamics and contributes to high static strength.

2.4.5.3   Effect of feed moisture content

The percentage of moisture in the feed biomass is a critical factor. In general, it has been found that when the feed moisture content is 8-10 %, the pellets or briquettes will have 6-8% moisture (Grover and Mishra, 1996). At this moisture content, the pellets are strong and free of cracks and the pelletising process is smooth. However, when the moisture content is more than 10%, the pellets are poor and weak and the pelletising operation is erratic. Excess steam is produced at higher moisture content leading to the blockage of incoming feed from the hopper, and sometimes it shoots out the briquettes from the die. Hence, it is crucial to maintain an optimum moisture content. According to Ryu *et al.*, (2008), excessive moisture content increases the gap between particles and wastes the compression energy, while too low moisture content reduces the plasticity of the particles and increases the friction during pelletisation. They studied the effect of moisture content and pellet drying on coal tailing pellets. Their results showed that the moisture content greatly affected the strength of the pellet. Optimum moisture content that gave the highest tensile strength (120-128 kPa) was 10-12%.

However, water also can act as a film type binder by strengthening the bonding in pellets. In the case of organic and cellular products, water helps in promoting bonding by Ven der Waals' forces by increasing the true area of contact of the particles (Grover and Mishra, 1996). Grover and Mishra (1996) claimed that the surface effects of water are so pronounced that the success or failure of the compaction process solely depends upon the moisture content of the material. The right amount of moisture develops self bonding properties in lignocellulosic substances at elevated temperatures and pressures prevalent in briquetting machines. It is important to establish the initial moisture content of the biomass feed so that the pellets produced have moisture content greater than the

equilibrium value. Otherwise, the pellets may swell during storage and transportation and disintegrate when exposed to humid atmospheric conditions.

2.4.5.4 Effect of temperature of biomass

Internal and external friction causes local heating and the material develops self-bonding properties at elevated temperatures. It can also be assumed that the moisture present in the material forms steam under high pressure conditions which then hydrolyses the hemicelluloses and lignin portions of biomass into lower molecular carbohydrates, lignin products, sugar polymers and other derivatives. These products, when subjected to heat and pressure in the die, act as adhesive binders and provide a bonding effect "in situ". The addition of heat also relax the inherent fibres in the biomass and apparently softens its structure, thereby reducing its resistance to briquetting which in turn results in a decreased specific power consumption and a corresponding increase in production rate and reduction in wear of the contact parts. However, the temperature should not be increased beyond the decomposition temperature of biomass which is around 300°C (Grover and Mishra, 1996).

2.4.5.5 Effect of temperature of the die

The distinctive feature of a screw type briquetting machine is that heat is applied to the die 'bush' section of the cylinder. This brings about two important operational advantages. The machine can be operated with less power and the life of the die is prolonged. Further, the surface of the pellet is partially carbonised/torrified to a dark brown colour making the pellet resistant to atmospheric moisture during storage. The temperature of the die should be kept at about 280-290°C (Grover and Mishra, 1996). If the die temperature is higher than required, the friction between the raw material and the die wall decrease and cause the compaction to occur at lower pressure which results in poor densification and inferior strength. On the other hand, low temperature will result in higher pressure, and power consumption as well as lower production rate.

2.4.5.6 Effect of external binders or additives

A binder (or additive) can be liquid or solid that forms a bridge, film, matrix, or cause a chemical reaction that create strong inter-particle bonding (Kaliyan and Morey, 2009). Some materials require steam conditioning or preheating in order to provide heat and moisture to activate the inherent or added binders. The selection of binders mainly depends on costs and environmental friendliness of the binders. More than fifty organic and inorganic binders have been employed for densification. Commonly used binders in the animal feed industry are lignosulfonate (a byproduct from pulp and paper industries), bentonite (a clay mineral), modified cellulose binders (e.g., sodium carboxymethylcellulose), molasses, starches, and proteins. In some European countries, addition of binders is prohibited. For example, in Austria, biological additives rich in starch content (e.g., maize and rye flour) of only 2% (by weight) are allowed for wood pellet production (Kaliyan and Morey, 2009).

The pelletising process does not add to the calorific value of the base biomass. In order to upgrade the specific heating value and combustibility of the pellet, additives such as charcoal and coal in very fine form can be added. About 10-20% char fines can be employed in pelletising without impairing their quality (Kaliyan and Morey, 2009).

2.4.5.7 Effect of fat/oil in feed material

Addition of fat/oil (animal or vegetable based) in feed results in lower pellet durability due to the fact that fat acts as a lubricant between the feed particles, and between the feed and the pellet mill die-wall. Due to low friction in the die, pressure in the die is decreased which will result in lower durability pellets. The hydrophobic nature of the fat causes it to inhibit the binding properties of the water-soluble components in the feed such as starch, protein, and fibre (Thomas *et al.*, 1998). To obtain maximum pellet quality, fat and oil content should not exceed 1.5% and 5.6% respectively. Fat inclusion levels beyond 6.5% are deleterious to pellet durability. Moreover, high levels of fat (>6.5%) affected the binding functionality of starch and protein, and the fat content was the dominant factor determining the pellet durability (Kaliyan and Morey, 2009).

2.4.6   Economic Aspects

Concerns about climate change and renewable energy targets are predominant drivers for the growth of biomass pellets, particularly wood (Richard *et al.*, 2010). Figure 2-71 shows the price of densified biomass pellets and their raw materials from 1993 to 2001. Hirsmark (2002) reviewed international pellet production costs in Austria, North America, Sweden and the Baltic States. The costs are categorised in four groups; 1) Capital costs (capital and maintenance), 2) Usage-based costs, 3) Operational costs, and 4) Other costs. The raw saw dust with a moisture content of 57% and a bulk density of 350 kg/m^3 were used. The overall production was €4,909,000 corresponding to €61 per tonne of produced pellets. The energy costs was dominated by the overall production expenses. The stages that consume a lot of energy are the drying and compaction processes. The breakdown costs for each step of the pelletisation process are given in Table 2-24. Uslu *et al.*, (2008) revealed that a total of 2 to 2.6 million Euros of investment costs are required for the production of 24,000 tonne of pellets per year or 0.15 - 0.25 million €/MW$_{th (input)}$ of the specific investment costs.
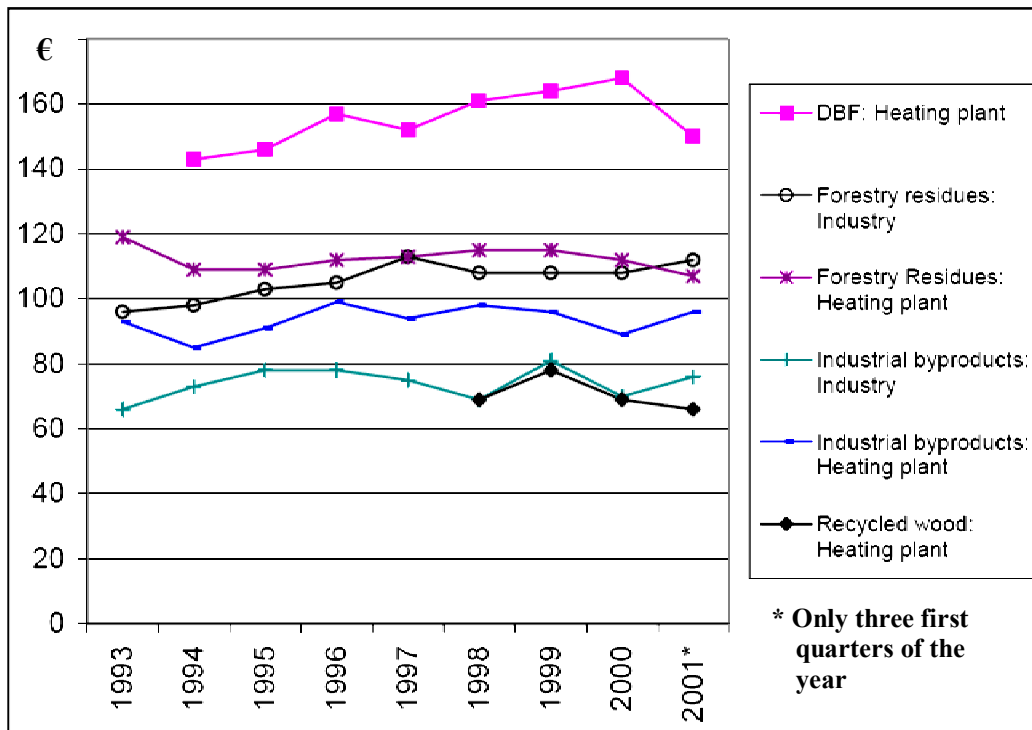
Figure 2-71: Biomass fuel prices 1993-2001 (Hirsmark, 2002).

Table 2-24: Details costs for each step of the pelletising process (Hirsmark, 2002).

Production step/cost unit	Total costs (€)	€/tonne
Raw material	2 494 000	31.3
Drying	1 033 000	13.0
Comminution	164 000	2.1
Pelletisation	280 000	3.6
Cooling	41 000	0.5
Storage	233 000	3.0
Peripheral equipment	68 000	0.9
Personnel	440 000	5.5
Construction	111 000	1.4
Overall costs	**4 909 000**	**61.0**

Richard (2010) reviewed the international logistics of wood pellets for heating and power production in Europe. Three different cases have been evaluated: 1) Pellets for district heating in Sweden to replace heavy fuel oil, 2) Bagged pellets for residential heating in Italy to replace natural gas, 3) Canadian pellets for electricity production in the Netherland to replace coal. The main cost factors are feedstock collection, drying and transportation. A total of €110 - €170 per tonne is required to transport pellets from Canada to the Netherlands. Wood pellets are relatively expensive compared to coal. Using wood pellets to substitute heating oil for district heating is not commercially viable, except in the case of high oil prices. However, substitution can be made possible with the financial support from the national government in term of feed-in tariffs or carbon taxes credit (Richard *et al.*, 2010).

Uslu *et al.*, (2008) point out that torrefaction in combination with pelletisation (TOP) can offer significant advantages when the biomass logistics are considered. It can be delivered to Europe at the costs of 74€/tonne (3.3€/GJ) and produced electricity as cheap as 4.4€cent/kWh$_e$ from an existing co-firing plant. Furthermore, conventional pelletisation and TOP is comparable to the gasoline production costs ranging from 3-7€/GJ$_{HHV}$ and diesel from 2-7€/GJ$_{HHV}$ depending on the oil market.

According to Thek and Obernberger (2004), the main contribution to the production costs of wood pellets are raw material and drying costs. These two parameters can contribute up to one-third of the total pellets production costs. A minimum of three shifts, 5 day per

week operations is required for an economic production of wood pellets. However, 7 days per week operation is needed for the optimum wood pellets production. Plant capacity does not affect the pellets production, however it might jeopardise non-economic pellets production.

2.5 Costs and economic overview

The major concern of any investments on any new technologies is the costs and profits. The important part in implementation of pyrolysis technologies, as with gasification technologies, is the economics of production. Many researchers have been working on the issues of biomass conversion costs as compared to conventional fossil fuel. Ramlan Zailani *et al*., (1999) studied the production costs of conversion of oil palm shell to liquid oil with the yield of 58 wt% of dry feed and 25 wt% of char products. Biomass feed costs of Malaysian Ringgit (RM) RM40/t, labour costs of RM3/h, plant life span 10 years with capacity of 1.5t/y and total annual operating hours of 3,000. They found that the costs were higher than the conventional petroleum derived fuel price at that time. However, it may be competitive with conventional fossil fuel for scale-up large unit along with the other incentive policies for renewable sources of energy.

Bridgwater (1990), revealed the costs of liquid fuels derived from biomass. Table 2-25 and Table 2-26 are the summaries of production and capital costs for various biomasses. The production costs show the significant potential of utilising biomass as energy feedstock. However, there are many issues that need to be addressed in making biomass successful as an energy feedstock. They include technological barriers, economy, environment, politics and social attitudes. Today, although the price of petroleum derived fuel is significantly low, the issue of environmental problem still remain unresolved. Hence, this will give the biomass energy or bio-energy a great potential to develop and utilise in the near future.

Table 2-25: Typical economic and financial parameters for pyrolysis base cases (Bridgwater, 1990).

Typical economic and financial parameters for pyrolysis bases case	
Pyrolysis technology	Entrained flow or fluid bed
Pyrolyser efficiency	58 to 93%
Feed stocks	Refuse, Straw and Wood
Feedstock heating value	20.00 GJ/t daf
Number of shifts (for 8000 h/y operation)	4
Project life	10 y
Scheduled operating hours per year	8000
Availability (Actual operating hours/Schedule operating hours)	80%
Actual operating hours	6400
Throughput	5 te/h, daf basis
Utility costs	£ 0.24/GJ produced
Yearly maintenance costs, fraction of capital costs	0.025
Yearly overheads, fraction of capital costs	0.080
Total costs of labour per shift	£25,000/y
Nominal costs of capital	10%
Inflation rate	5%

Table 2-26: Capital costs of pyrolysis processes for bio-oil, char-water slurry and char-oil slurry production (Bridgwater, 1990).

Capital cost of pyrolysis processes	1t/h	2.5t/h	5t/h	10t/h
			(£)	
Basic pyrolysis process				
Lower	213000	412000	678600	1117800
Average	370000	715700	1178900	1941800
Higher	735000	1421700	2341800	3857300
Target capital cost (*mean of average and lower cost*)	291500	563800	928700	1529800
Pyrolysis for bio-oil *(Target capital + 50% for feed preparation: drying and oil recovery)*	437250	845700	1393000	2294700
Pyrolysis for char-water slurry *(Target capital + 10% for slurry preparation)*	320650	620200	1021600	1682800
Pyrolysis for char-oil slurry *(Target + 60% for feed preparation: drying, oil recovery and slurry preparation)*	466400	902100	1485900	2447700

2.6 Malaysian policies on renewable energy from biomass

The first National Energy policy was introduced in 1979 and its three main objectives were outlined as follows:

➢ To warrant adequate, secure and cost-effective energy supply from indigenous resources.

➢ To promote the efficiency and conservation measures to eliminate wasteful and non-productive patterns of energy consumption.

➢ To protect the environment that caused by the supply and utilisation of energy.

At present, most of the energy sources in Malaysia are derived from fossil fuel. Due to the increasing demand for energy, the Malaysian government has taken several actions to explore and promote the use of renewable energy. Among others, the introduction of Fifth-Fuel Policy under the eighth (2001-2005) and ninth (2006-2010) Malaysia Plan, Biomass fuels, Energy Efficiency in Commercial Building, the Kyoto Protocol, the Malaysian Building Integrated Photovoltaic Programme (Haw *et al.*, 2006).

Under the Fifth-Fuel Policy, the Malaysian government has launched the Small Renewable Energy Power (SREP) programme to encourage and intensify the utilisation of renewable energy. This programme allowed the independent power providers (IPP) to sell electricity produced to national grid. However, the first phase of this programme (under eight Malaysia Plan, 2001-2005) was not successful. Only 105 MW was delivered from 14 projects approved under the SREP programme which targeted for 500 MW of electricity generated from renewable sources to the national grid (Haw *et al.*, 2006).

In order to fulfill the target, the Government has decided to continue the Fifth-Fuel Policy into the nine Malaysia Plan from 2006 to 2010. By the end of the nine Malaysia Plan, renewable energy contribution towards the country's total energy mix through grid connected power generation from the SREP programme only achieved 56.7 MW (Hashim and Ho, 2011). Due to this scenario, Malaysia aggressively continues its goal to promote and increase the share of renewable energy in the country's energy mix under the ten Malaysia Plan from 2011 to 2015. The new energy target from renewable energy sector is of 985 MW by 2015 contributing to 5.5% of Malaysia's total electricity

generation mix (Hashim and Ho, 2011). Several new incentives launched, among others are the introduction of a Feed-in Tariff (FiT) and establishment of a renewable energy fund from the FiT.

Malaysia has also identified biomass as one of the potential renewable energies particularly biomass from oil palm industry such as empty fruit bunches, shells and palm kernel cake. More than 300 palm oil mills operate across the country. It is estimated that Malaysia could possibly generate electricity power from biomass fuels approximately 2,400 MW (Hashim and Ludin, 2008).

To encourage more participation and promote biomass energy in Malaysia, the Malaysia's cabinet approved the Renewable Energy Act for a Feed-in Tariff in April, 2011. In June, 2010 the government announced the National Renewable Energy Policy and Action Plan with a goal of increasing renewable energy from 1 to 5.5% of electricity supply by 2015 (Gipe, 2011).

2.7   UK Directives

2.7.1   Incineration Directives

In the UK, the directive on the incineration of waste (WID) for the environmental permitting (England and Wales) regulations 2007, updated 2009, is used in line with the European Community (EC) Directive 2000/76/EC on the incineration of waste ("the Waste Incineration Directive") to control emission from power plants. The directive imposes stringent requirements on incineration and co-incineration plants within its scope. These requirements cover the types of wastes permitted at the plant, their delivery and reception, combustion furnaces, abatement plant, residue handling, monitoring equipment and emission limit values. It aims to reduce as far as possible the negative effects on the air, soil, surface and groundwater caused by emissions from waste-to-energy plants. Table 2-27 shows the emission limits for energy-from-waste plants in the UK and Europe as stated in article 7 of the WID.

Table 2-27: Emission limit values for incinerators (WID, 2009).

Component	Daily average values(mg/m^3)	Half-hourly average values (mg/m^3)	
		(100%) A	(97%) B
Total dust	10	30	10
Gaseous and vaporous organic substances, expressed as total organic carbon.	10	20	10
Hydrogen Chloride (HCl)	10	60	10
Hydrogen Fluoride (HF)	1	4	2
Sulphur Oxides (SO$_2$)	50	200	50
Nitrogen monoxide (NO) and nitrogen dioxide (NO$_2$), expressed as nitrogen dioxide for existing incineration plants with a nominal capacity exceeding 6 tonnes per hour or new incineration plants.	200	400	200
Nitric oxide (NO) and nitrogen dioxide (NO$_2$), expressed as nitrogen dioxide for existing incineration plants with a nominal capacity of 6 tonnes per hour or less.	400		

Note:

1. Reference conditions are: Temperature 273 K, pressure 101.3 kPa, 11% oxygen (3% oxygen if burning waste oils), and dry gas.

2. Exemption for NOx may be granted before January 2010 for the existing incineration plants with a nominal capacity between 6 and 16 tonnes per hour provided the half-hourly average value does not exceed 600mg/m^3 (A) or 400 mg/m^3 (B).

Table 2-28 shows the average values of heavy metal and its compounds emissions over the sample period of a minimum of 30 minutes and a maximum of 8 hours. These average values cover also gaseous and the vapour forms of the relevant heavy metal emissions as well as their compounds.

Table 2-28: Average values for heavy metal emissions of a minimum of 30 minutes and a maximum of 8 hours (WID, 2009).

Heavy metal	Average values (mg/m^3)
Cadmium and its compounds, expressed as cadmium (Cd)	Total 0.05
Thallium and its compounds, expressed as thallium (TI)	
Mercury and its compounds, expressed as mercury (Hg)	0.05
Antimony and its compounds, expressed as antimony (Sb)	
Arsenic and its compounds, expressed as arsenic (As)	
Lead and its compounds, expressed as lead (Pb)	
Chromium and its compounds, expressed as chromium (Cr)	
Cobalt and its compounds, expressed as cobalt (Co)	Total 0.5
Copper and its compounds, expressed as copper (Cu)	
Manganese and its compounds, expressed as manganese (Mn)	
Nickel and its compounds, expressed as nickel (Ni)	
Vanadium and its compounds, expressed as vanadium (V)	

The average values permitted for the dioxins and furans emissions measured over a period of a minimum of 6 hours and a maximum of 8 hours is 0.1 ng I-TEQ/Nm^3. This value refers to the total concentration of dioxins and furans calculated using the concept of toxicity equivalence factors (TEF). In the UK, the independent health advisory committee known as Committee on Toxicity of Chemicals in Food, Consumer Products and the Environment (COT) is responsible for dioxins and furans released to the environment. The COT committee has adopted TEF for both dioxins and furans.

2.8 European Commission Legislation

Waste Incineration Directive (2000/76/EC) aims to bring closer the requirements for incineration and co-incineration. This is going in the right direction to address the concern of environmentalists that industrial plants co-incinerating waste derived fuels are

not as strictly controlled as waste incinerators. The implementation of the EC Landfill Directive (1999/31/EC) has an indirect impact on production in EU. The strategies chosen by Member States to divert biodegradable fraction of MSW and used tyres from landfill as required under this Directive are likely to encourage refuse derived fuel production. In addition, several countries are implementing similar policies in respect of climate change and control of greenhouse gas emissions, which will also have an impact on the use of refuse derived fuel in co-incineration facilities.

The overlapping concerns regarding waste management, greenhouse gas control and energy need thoughtful integration, which takes into account of the broader environmental implications. In addition, flexibility is needed to accommodate continuing progress in minimisation, re-use and source separation for recycling/composting/anaerobic digestion. As there are some variations in the interpretation of the European Directives, it is difficult to make clear predictions as to what is likely to happen in future. What does seem clear, however, is that the policies being put in place are accelerating the overlapping of energy and waste policies. The legislative changes, which are in the pipeline are helpful (i.e. new Waste Incineration Directive) and they appear to move matters in the right direction in seeking to harmonise the standards as far as possible across co-incineration facilities and incinerators (European Commission – directorate general environment, 2000).

3   THEORETICAL BACKGROUND

3.1   Modelling of combustion process

Research on modelling of the combustion process has been carried out for many years. Some studies evaluated the combustion of municipal solid waste or biomass in full-scale grate furnace (Frey *et al.*, 2003, Yang *et al.*, 2007). However, most of the studies were carried out in laboratory scale fixed-bed units to simulate operation on grate furnaces (Saastamoinen *et al.*, 2000a, Shin and Choi, 2000, van der Lans *et al.*, 2000). The modelling work is important because it is difficult and expensive to acquire detailed in-bed data from full scale furnaces. Moreover, data from experiments and simulated results showed that an analogy exists between combustion in a fixed bed and on a grate.

Due to the relatively small horizontal gradients as compared to the vertical orientation in industrial facilities, the analogy shows that the results from fixed bed combustion can be used as a good approximation of moving-bed combustion (Zhou *et al.*, 2005). Combustion characteristics such as the bed temperature profile, combustion rates and efficiency, as well as gas emissions from bed surface are the similarities that can be used to assess the moving bed combustion process.

Thunman and Leckner (2005) studied a one dimensional model of the combustion of mono-sized wood particles and wood pellets with similar moisture content, burning under sub-stoichiometric conditions to establish the influence of size and density of fuel on combustion in a packed bed environment. Solid fuel conversion in a grate furnace occurs in a fixed fuel bed, interacting with the freeboard and the grate. The main features of this model are as follows; firstly, the fuel bed consists of gaseous and solid phases. Secondly, two fictitious boundary surfaces, representing the grate and the freeboard, limit the bed. Thirdly, the solid phase consists of equal sized particles of optional shape. This model can be used to monitor the combustion process in co-current or counter-current combustors and moving grates. The conversion system is modelled by conservation of mass, momentum, energy, and species in the gaseous and solid phases, regarded as one-dimensional continua.

Shin and Choi (2000) studied one-dimensional experiments using wooden cubes to simulate the complex process in moving bed (Figure 3-1). The schematic model of the fixed bed used in their study is shown in Figure 3-2.
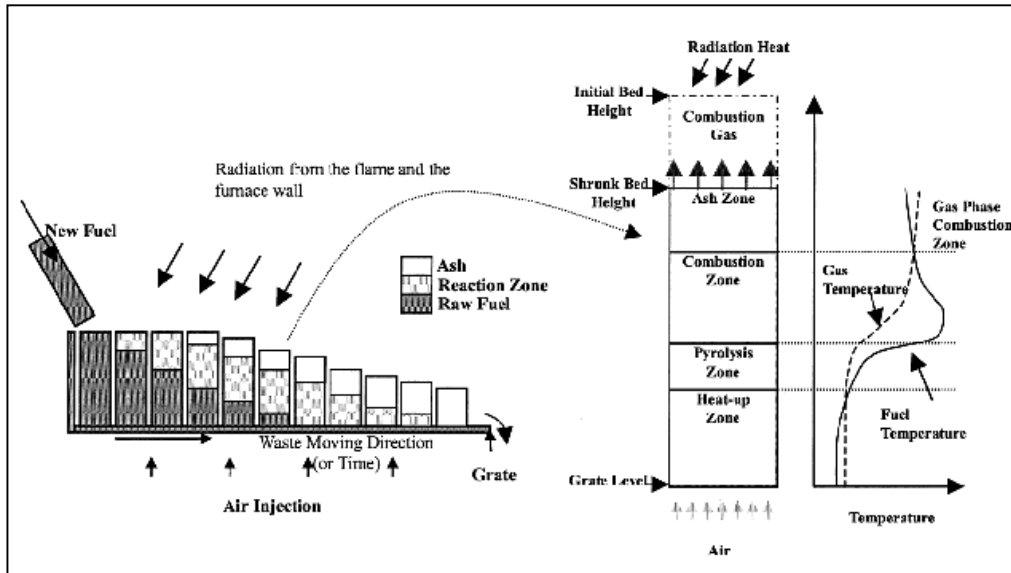
Figure 3-1: Schematic view of solid waste combustion in fixed bed reactor (Shin and Choi, 2000).
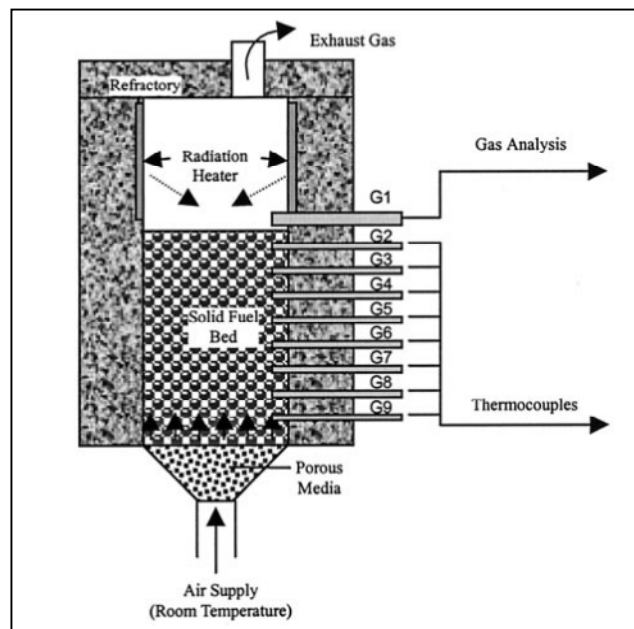
Figure 3-2: One dimensional combustor for fixed bed of solid fuel (Shin and Choi, 2000).

The combustion of solid fuels in a bed is modelled mathematically by a model based on a finite volume method. The model incorporates various sub-models for moisture evaporation, devolatilisation and char burn-out for the solid phase. The process occurs based on the concept proposed shown in Figure 3-3. The mass of the bed in a given volume exchanged heat with the upper layer and lower layer fuel through conduction and radiation heat transfer, which governed the propagation of the ignition front. Their results showed that there was a similarity between predicted and experimental data in terms of bed temperature and the transient oxygen yield above the bed. However, the ignition front speed shows over-predicted due to the limitation of the simplified model which neglected the effect of the side wall of the bed and the homogeneous packing of fuel particles with a void fraction at 0.3.
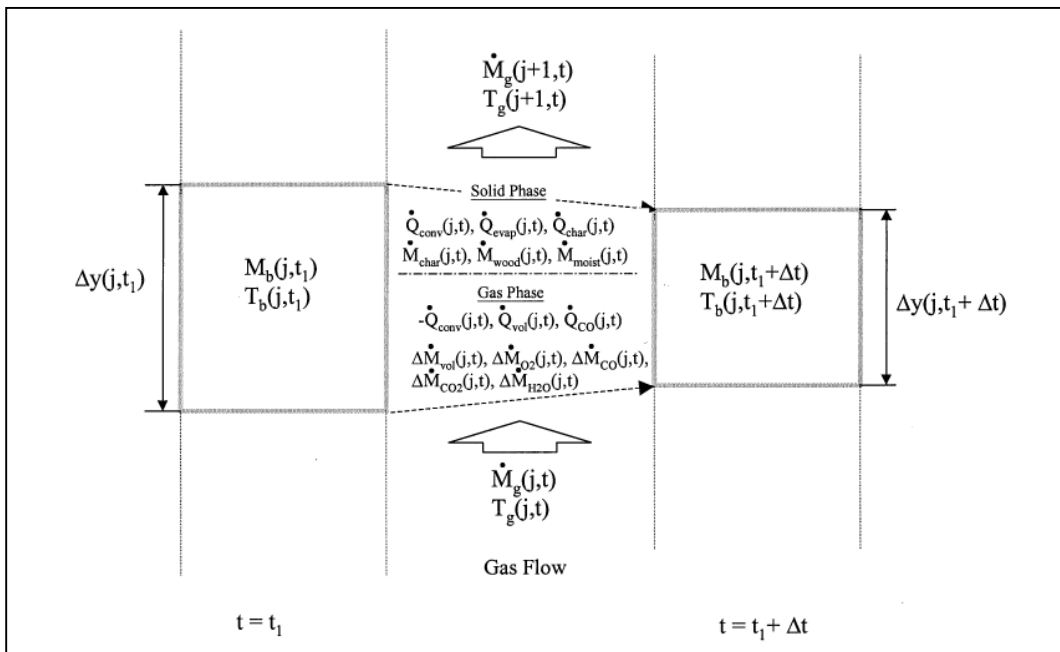
Figure 3-3: Concept of numerical modelling of the solid and gas phases (Shin and Choi, 2000).

Yang *et al.*, (2005) carried out mathematical modelling to evaluate the effect of fuel properties on biomass combustion in fixed bed system. The two dimensional models consisted of equations for mass reduction, momentum, species, energy conservation for

both solid and gas phases as well as the equation for radiation heat transfer. The model was based on the ideal conditions of three reacting waves traveling down the bed as visualised in the schematic diagram in Figure 3-4.
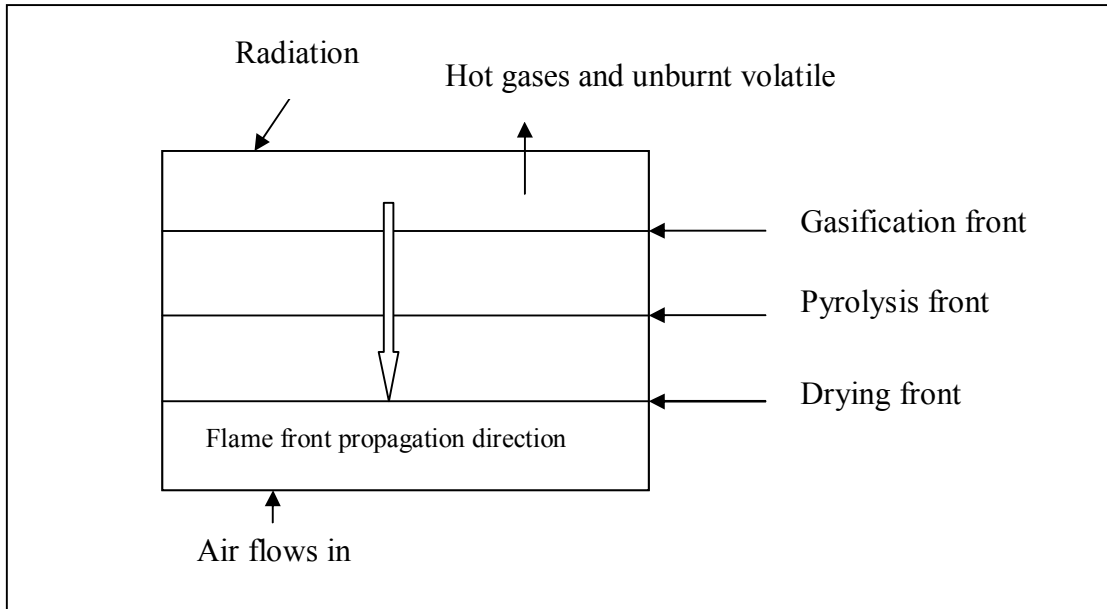
Figure 3-4: Propagation of flame front in a packed bed (Yang *et al*., 2005).

Sub-models included combustion of volatile matter, evaporation, pyrolysis and char gasification. The governing equations were solved using the Fluid Dynamic Incinerator Code (FLIC code). To validate the simulation work, experimental works were also carried out by using small-scale fixed bed reactor as shown in Figure 3-5.
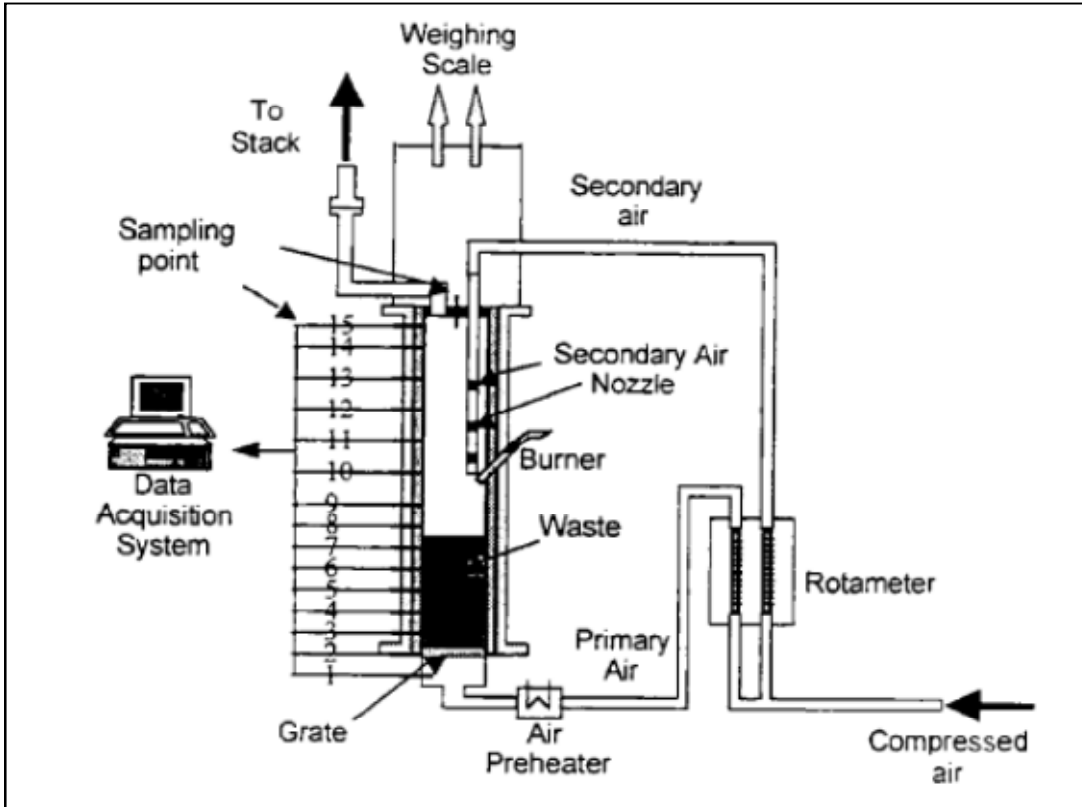
Figure 3-5: Schematic diagram of fixed bed reactor (Yang *et al*., 2002).

Their results showed an agreement between the modelling results and experimental data with reference to mass loss and O_2 concentration. Channelling phenomena in the bed had been pointed out as one of the setbacks that inhibited the mixing between combustible gases and air and caused a lower combustion efficiency of hydrocarbons as well as increased the hydrocarbon gases emission in the flue gas (Yang *et al.*, 2002).

3.2   Mathematical modelling using FLIC Code

The processes that occur within a burning biomass bed include drying, pyrolysis, solid and gas phase combustion, conductive, convective and radiative heat transfer, mass transfer and gas flowing through a randomly packed bed of material whose size, shape, orientation and composition are continuously changing. According to Goh *et al*. (2001), solid fuel particles can be assumed to consist of four main components namely moisture, volatile, fixed carbon and ash. During the combustion process, moisture, volatile matter

and fixed carbon are removed by the evaporation, devolatilisation, and gasification processes as shown in Figure 3-6.
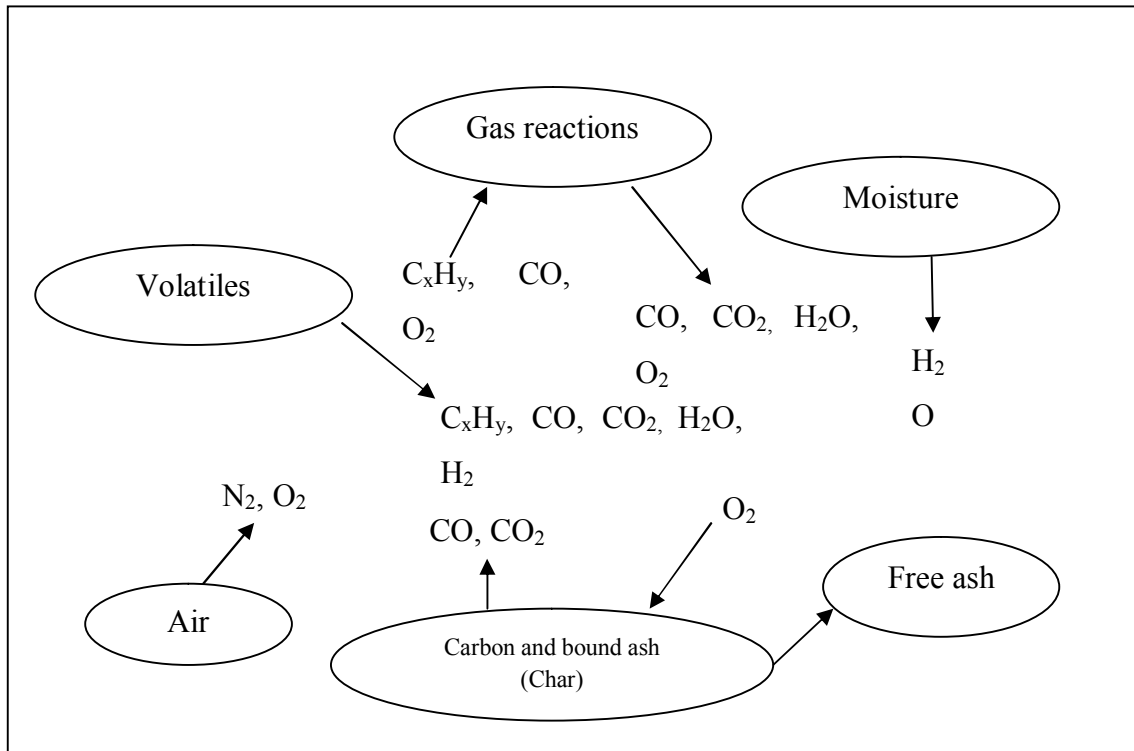
Figure 3-6: Overall combustion process (Goh *et al.*, 1998).

As the solid waste is heated, the moisture is removed by vaporisation at 100°C. The drying period can be calculated from the amount of heat transferred to the solid to supply the heat required for the change of phase from liquid to vapour under the assumption that the regressing drying surface remains at the temperature of 100°C until all moisture has evaporated. The volatiles consisting of carbon, hydrogen and oxygen are released during the pyrolysis process at about 260°C. In an oxygen limited condition, the gaseous volatiles released are assumed to consist of hydrocarbons and CO. The pyrolysis front is assumed to remain at the pyrolysis temperature until all volatiles are driven out. After the moisture and volatiles have been driven off, the remaining solid consists mainly of carbon char and bound ash. According to Goh *et al* (1998), any carbon in the solid surface is assumed to be oxidised by any available O_2 to form CO and CO_2.

These processes lead to a significant change in the volume of the bed. Therefore, a physical representation of the bed volume change which is mathematically linked to these three processes is required. The removal of moisture and volatiles has left void spaces within the particles, which in turn leads to the particles becoming more porous. Goh *et al* (1998) also suggested that in order to represent the void space within the solids left by the drying and pyrolysis processes, a component known as the internal pore space is introduced in to the model. This additional component helps to differentiate the internal pore space within the solid particles from the space which is normally occupied by the gas phase (Yang *et al.*, 1999). The internal pore is assumed to increase during the evaporation and pyrolysis processes, compensating fully or partially for the volumes of water and volatile matter removed. This internal pore space may be fully removed during the char gasification or oxidation process, causing a significant reduction of the bulk volume of the bed as illustrated in Figure 3-7.

The volume distribution of the various defined components in the bed and the change in the bed bulk volume over time due to drying, pyrolysis and gasification. The first vertical column in Figure 3-7 shows the initial volume distribution of the five main components in the bed (gas space); void fraction in the bed, carbon, volatile matter, moisture and bound ash. During the drying and pyrolysis processes, the reduction in the volume of moisture and volatile content in the solid is partially compensated by an increase in the internal pore space.

During the gasification process, fixed carbon is removed. The removal of carbon from the char converts the bound ash to free ash. Thus, the bulk volume reduces while maintaining a constant volume ratio of the ash and the internal pore space. Hence, the net change in the internal pore space is given by the internal pore space formed during drying and pyrolysis minus the space removed during gasification. If the rate of formation of the internal pore space is greater than the rate of the removal of the pore space, then the volume of the internal pore space will continue to increase until drying and pyrolysis cease. It is assumed that no internal pore remains in the free ash at the end of the gasification process (Goh *et al.*, 2001).
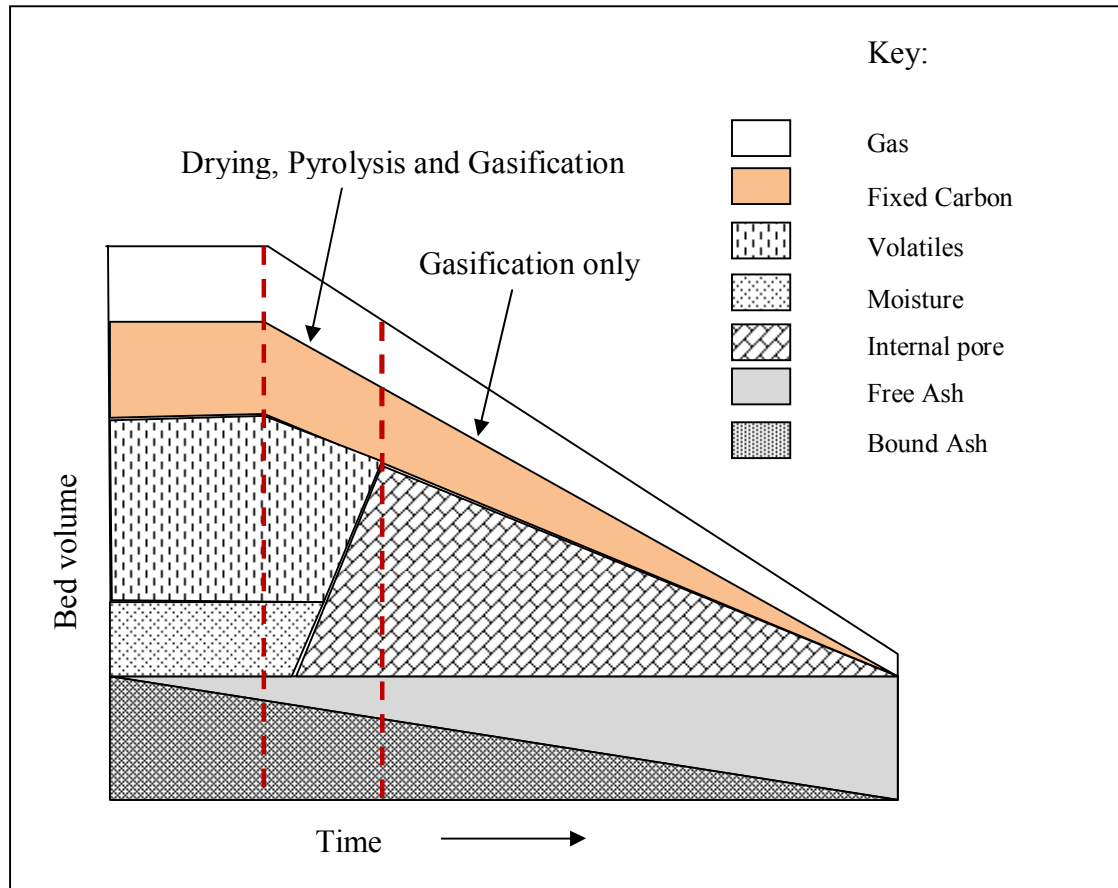
Figure 3-7: Variation in bed volume due to incineration (Goh *et al.*, 2001).

3.2.1 Mathematical model of biomass bed combustion

The moving grate type systems that used in many waste incinerators can be treated as cross-flow reactors, in which solid fuel in the reactor is initially ignited at the top of the fuel bed with combustion air entering from below the bed (Zakaria, 2000). The combustion process on a moving grate type is therefore, governed by the reaction front propagating from the top of the fuel bed against the opposing air flow. A direct simulation of the process in such a system can be modelled by an unsteady-state batch type combustion system since predicted variations with respect to time (t), can be related to variations with distance (z) from the point of waste input using the equation ($z = v_z t$), where v_z is the velocity of the bed. The calculation is based on the assumptions below:

  i.   there is a uniform solid movement parallel to the grate,

  ii. the waste is fed at a constant rate,

iii. heat is transferred in the direction normal to the grate.

Therefore, any variations in the conditions above the bed and the rate of underfeed air input with respect to (z) for the steady-state moving bed can be modelled as variations with respect to time in the unsteady-state static bed using ($t = z/v_z$). Figure 3-8 shows a simplified model of the unsteady-state static bed model which illustrated the four main combustion processes: drying, pyrolysis or devolatilisation, char oxidation and gas phase combustion. These four parameters form the basis of the present theoretical study of the biomass bed modelling.
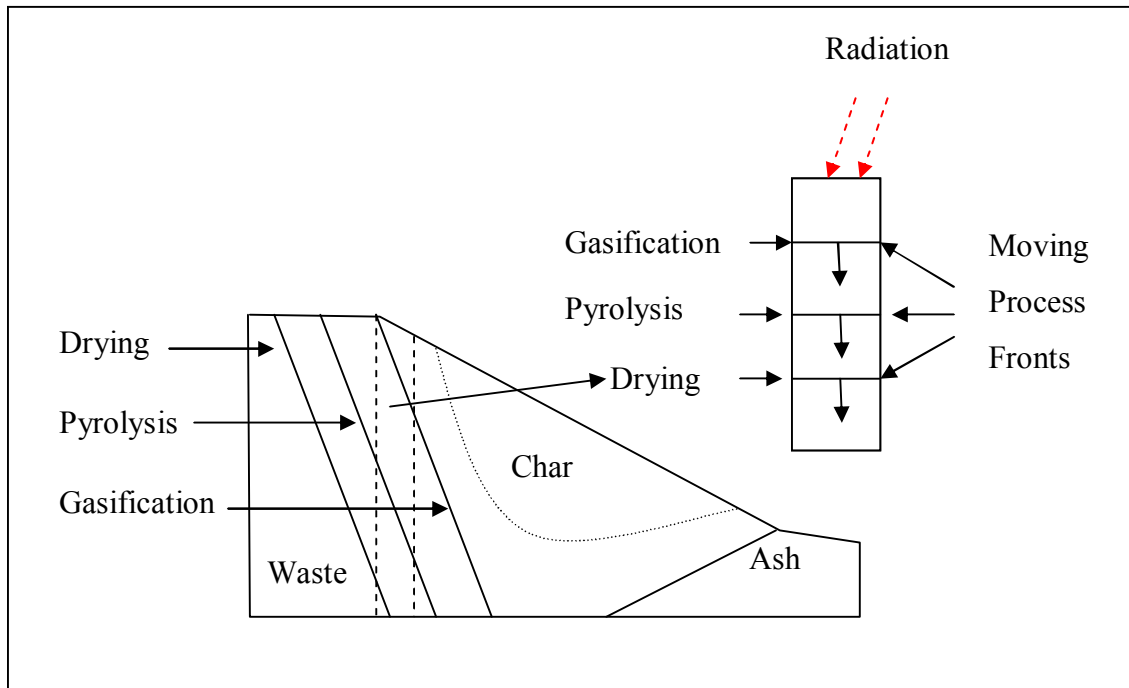
Figure 3-8: A Fixed bed model for the waste bed (Goh *et al.*, 1998).

3.2.1.1 Physical sub-processes

Yang *et al.*, (2003a) proposed that the combustion of solid fuel can be divided into four main successive stages; drying, pyrolysis (devolatilisation), combustion of volatiles and the gasification of char particles.

The mathematical models used for each sub-process are as follows:

i. Drying

The first development that occurs in waste combustion is the drying process. There are two mechanisms that cause the drying process to occur: convective diffusion below the boiling temperature and boiling at a bed temperature close to 100°C. In the convective diffusion phase, moisture is driven out by the mass exchange between the wet solids and the drier air supply from under the grate. The rate of moisture released from the solids can be expressed as follows:

$$R_2 \begin{cases} S_a h_s \left(C_{w,s} - C_{w,g} \right) \text{When } T_s < 100° C \\ \dfrac{Q_{cr}}{H_{evp}} \qquad\qquad \text{When } T_s = 100° C \end{cases}$$
Eq. 3-1

Where, h_s is the convective mass transfer coefficient between solid and gas, which is given by the following equation:

$$h_s = \frac{D_{ig} \left(2 + 1.1 S_c^{1/3} \, \mathrm{Re}^{0.6} \right)}{d_p}$$
Eq. 3-2

$Q_{c,r}$ is heat absorbed by the solids, including convection and radiation heat transfer and can be calculated as follow:

$$Q_{c,r} = S_a \left\{ h_s \left(T_g - T_s \right) + \varepsilon \sigma_b \left(T_{env}^4 - T_s^4 \right) \right\}$$
Eq. 3-3

h'_s is the convective heat transfer coefficient between solid and gas, which is given by the following equation:

$$h_s = \frac{0.1 \lambda_g \left(2 + 1.1 \mathrm{Pr}^{1/3} \, \mathrm{Re}^{0.6} \right)}{d_p}$$
Eq. 3-4

The Nusselt number for heat transfer and Sherwood number for mass between the solid and gas phases are calculated as $Nu = 2 + 1.1 \Pr^{1/3} \mathrm{Re}^{0.6}$ and $Sh = 2 + 1.1 S_c^{1/3} \mathrm{Re}^{0.6}$ respectively.

ii. Pyrolysis

Pyrolysis process occurs in the second stage of the combustion process. As a solid fuel particle reaches the reaction temperature around 350°C to 500°C, pyrolysis commences vigorously to convert solid fuel into volatiles and char or tar products. Many researchers agreed that for biomass, devolatilisation starts at a temperature of 200°C to 300°C (Horne and Williams, 1996, Williams and Besler, 1996). Volatiles are driven out of the particle through its pore structure when the internal pressure of the particle is sufficient or by rupturing its internal structure. The volatiles produced include both non-condensable gases and condensable gases or tar. The conversion of tars into gases and char occur during secondary reactions. These reactions can occur homogenously in the gas phase or heterogeneously at the surface of the biomass or char particles (Wurzenberger *et al.*, 2002). Yang *et al.*,(2002) proposed the one-step reaction as follows:

$$Waste \rightarrow Volatile\left(C_m H_n, CO, CO_2, H_2, etc\right) + Char \qquad \text{Eq. 3-5}$$

According to Smoot and Smith (1985), the release rate of volatiles R_3 from the solid is proportional to the amount of volatiles remaining in the solid.

$$R_3 = k_v\left(v_\infty - v\right) \qquad \text{Eq. 3-6}$$

And

$$k_v = A_v \exp\left(-\frac{E_v}{RT_s}\right) \qquad \text{Eq. 3-7}$$

Where;

v is the remaining volatile yield at time t

v_∞ is the ultimate volatile yield

k_v is the rate constant of devolatilisation

A_v is the pre-exponential factor in the devolatilisation rate equation

Thurner and Mann (1981) and Rovatti *et al*., (1994) used the model proposed in Shafizadeh and Chin (1977) assuming that the pyrolysis reaction follows the first order reaction and the products can be subdivided in char, tar and gases as shown in Figure 3-9. Barooah and Long (1976) used two stages model as illustrated in Figure 3-10 to investigate the two-stage parallel reaction model to predict the yields of pyrolysis products. Bramer (2006) used the same model to investigate the primary product from the pyrolysis of beech wood.
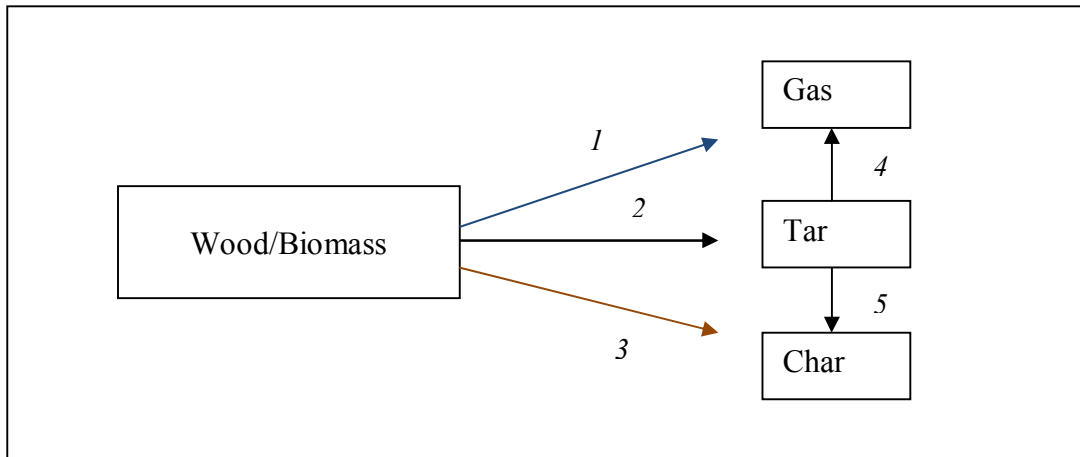
Figure 3-9: Mechanism of wood biomass pyrolysis (Thurner and Mann, 1981).
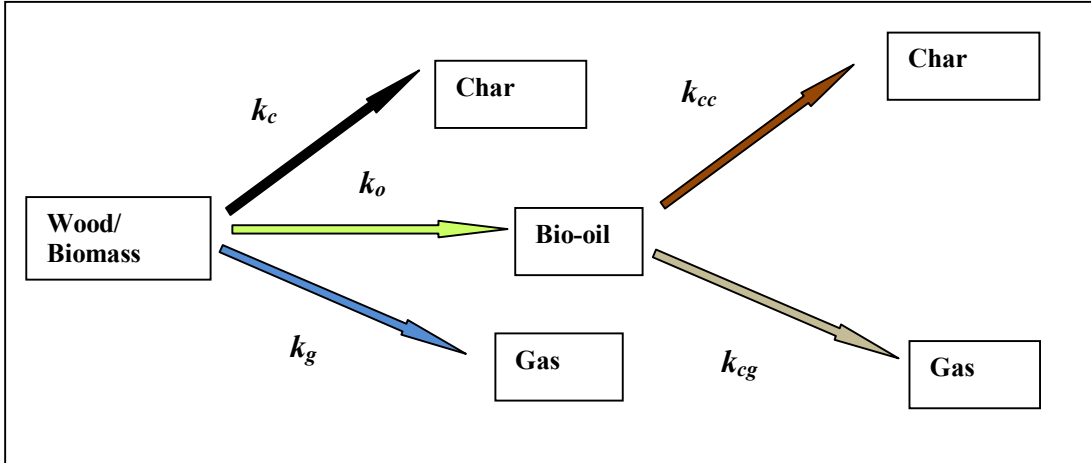
Figure 3-10: Wood decomposition pathway (Barooah and Long, 1976).

According to Bramer *et al.*, (2006), by assuming the decomposition of a biomass particle to be a single order reaction in the weight of the unconverted biomass $m - m_c$

$$\frac{d_m}{d_t} = k_1(m - m_c)$$
Eq. 3-8

Where;

m = mass (kg)

m_c = mass of remaining char after complete conversion   (kg)

k_1 = first order reaction rate constant   (s^{-1})

the reaction rate k_1 constant is described by the well-known Arrhenius equation.

$$k_1 = k_o \exp\left(\frac{-E_a}{RT}\right)$$
Eq. 3-9

Where;

k_o = Pre exponential constant   (s^{-1})

R = Gas constant   (J/mole.K)

E_a = Activation energy   (J/mole)

T = Reaction temperature   (K)

By measuring the weight change over time, the conversion (ξ) a biomass sample can be calculated as follows:

$$\xi = \left(\frac{(m_o - m)}{(m_o - m_c)} \right)$$
Eq. 3-10

Where;

$$M_o = \text{initial mass of biomass sample (kg)}$$

Solving equation Eq. 3-8 with Eq. 3-10 gives;

$$\xi = 1 - \exp\left(-k_1^* t\right)$$
Eq. 3-11

Assuming that all the primary cracking reactions as given in the reaction scheme are first order reaction on the remaining biomass, the biomass decomposition rate constant k_1 is a summation of each individual primary cracking rate constant k_o, k_c and k_g. Therefore, decomposition rate constant $(k_1) = k_o + k_c + k_g$.

The formation rate of char (R_{char}), tar (R_{tar}) and gas (R_{gas}) as well as the conversion of solid fuel R_{vgn} can be written as follows:

$$R_{char} = \rho_{sb} Y_{vgn} k_1 + \phi \rho_g Y_{tar} k_4 = \rho_{sb} Y_{vgn} A_1 \exp\left(-\frac{E_1}{RT_s}\right) + \phi \rho_g Y_{tar} A_4 \exp\left(-\frac{E_4}{RT_s}\right)$$
Eq. 3-12

$$R_{tar} = \rho_{sb} Y_{vgn} A_2 \exp\left(-\frac{E_2}{RT_s}\right) - \phi \rho_g Y_{tar}\left[A_{4\exp}\left(-\frac{E_4}{RT_s}\right) + A_5 \exp\left(-\frac{E_5}{RT_s}\right)\right]$$
Eq. 3-13

$$R_{gas} = \rho_{sb} Y_{vgn} A_3 \exp\left(-\frac{E_3}{RT_s}\right) + \phi \rho_g Y_{tar} A_5 \exp\left(-\frac{E_5}{RT_s}\right)$$
Eq. 3-14

$$R_{vgn} = \rho_{sb} Y_{vgn} \left(k_1 + k_2 + k_3 \right)$$

Eq. 3-15

iii. Combustion of Volatiles

Volatile matter consist of gases such as CO, CO_2, H_2, light hydrocarbon gases (C_1-C_4) and tar or high molecular weight compounds. Yang *et al.*, (2002) assumed that the volatile hydrocarbon is a single product in the tar fraction with the general formula ($C_m H_n$). There are two-step of chemical reaction involving hydrocarbons gases and oxygen; firstly, hydrocarbons are oxidised to CO and H_2O and secondly, CO further reacts with oxygen to form CO_2. The kinetic rates involving of these reactions are listed in Table 3-1.

Table 3-1: Reactions in the gas phase and their kinetic parameters (Phan, 2007).

Reactions	Kinetic rate
$C_m H_n + \left(\dfrac{m - \dfrac{n}{2}}{2} \right) O_2 \rightarrow$ $mCO + \dfrac{n}{2} H_2 O$	$R_{C_m H_n} = 59.8 T_g P^{0.3} \exp\left(\dfrac{-12,200}{T_g} \right) C_{C_m H_n}^{0.5} C_{O_2}$
$CO + \dfrac{1}{2} O_2 \rightarrow CO_2$	$R_{CO} = 1.3x10^{11} \exp\left(\dfrac{-62,700}{T_g} \right) C_{CO_2} C_{H_2 O}^{0.5} C_{O_2}^{0.5}$
$H_2 + \dfrac{1}{2} O_2 \rightarrow H_2 O$	$R_{H_2} = 3.9x10^{17} \exp\left(\dfrac{-20,500}{T_g} \right) C_{H_2}^{0.85} C_{O_2}^{1.42} C_{C_m H_n}^{-0.56}$

Where;

$C_{CO}, C_{H_2O}, C_{O_2}, C_{C_m H_n}$ represent the species concentrations, and P is the pressure, which is atmospheric pressure for the packed-bed combustion.

The loss of energy through the bed is assumed to be proportional to the mixing rate inside the bed. The Ergun equation was correlated as follows (Yang *et al.*, 2002).

$$R_{mix} = C_{mix}\rho_{gas}\left\{150\frac{D_g(1-\phi)^{\frac{2}{3}}}{d_p^2\phi} + 1.75\frac{V_g(1-\phi)^{\frac{1}{3}}}{d_p\phi}\right\} \times \min\left\{\frac{C_{fuel}}{S_{fuel}}, \frac{C_{O_2}}{S_{O_2}}\right\} \qquad \text{Eq. 3-16}$$

The actual reaction rates of volatile species are taken as the minimum of the temperature-dependent kinetic rates and their mixing rates with oxygen (Yang *et al.*, 2003a).

$$R = \min\left[R_{kinetic}, R_{min}\right] \qquad \text{Eq. 3-17}$$

iv. Char Combustion

Char is a primary product from pyrolysis reaction. It formed when volatiles escape from particles. The main components of char combustion are CO and CO_2 (Yang *et al.*, 2003b).

$$C(s) + \alpha O_2 \rightarrow 2(1-\alpha)CO + (2\alpha - 1)CO_2 \qquad \text{Eq. 3-18}$$

With the ratio $\dfrac{CO}{CO_2} = 2500\exp\left(\dfrac{-6420}{T}\right)$ $\qquad \text{Eq. 3-19}$

Smoot and Smith, (1985) proposed the char combustion rate can be calculated as follows:

$$R_4 = \frac{dC_{C(s)}}{dt} = \frac{C_{O_2}}{\dfrac{1}{kr} + \dfrac{1}{kd}} \qquad \text{Eq. 3-20}$$

Where;

k_r and k_d are rate constants of chemical kinetics and diffusion respectively.

3.2.1.2 Step change model

The mathematical model used to physically represent the change in the burning fixed bed volume occurring during incineration is the step change method (see Figure 3-11).

149
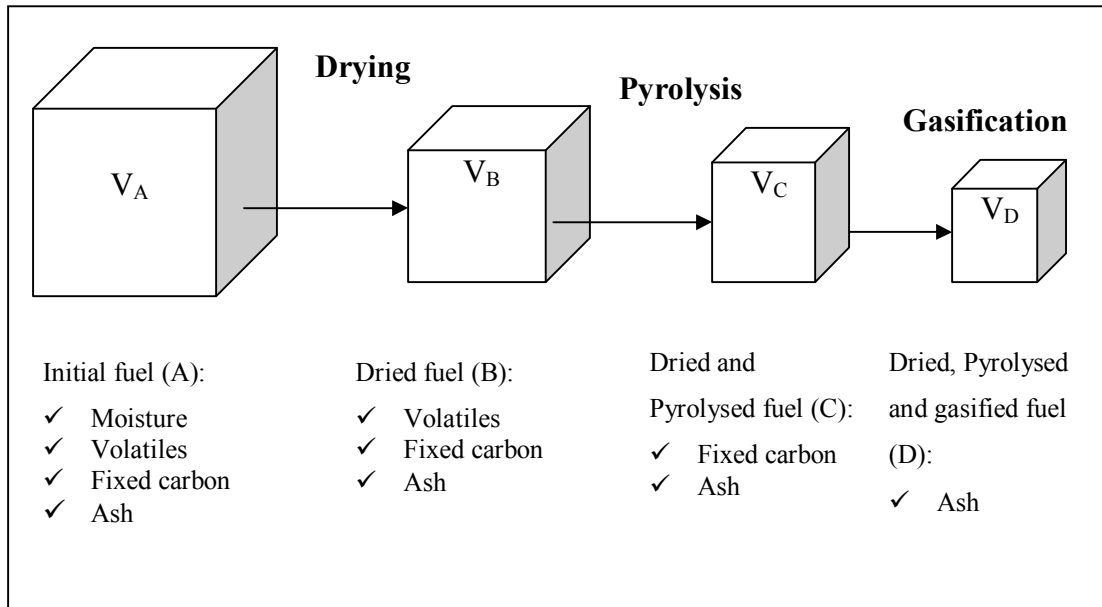
Figure 3-11: Step change model for solid waste volume during combustion (Goh *et al.*, 2001).

Each unit goes through the consecutive biomass combustion stages. Stage A represents the layer of the bed at the initial stage with initial volume of waste V_A. Stage B consists of the dried waste after moisture content has evaporated, and the volume of the waste is reduced to V_B. As the combustion process proceeds, the waste starts to pyrolysed at stage C. At this stage, the waste is completely dried and the volume is further reduced to V_C. Finally, the combustion process proceeds to the last stage, D, where the process proceeds by gasification and only ash (V_D) is left in stage D.

The initial volume of a fuel A is given by:

$$Initial\ volume\ of\ fuel\ A = (1 - \phi_A)V_A \qquad \text{Eq. 3-21}$$

The volume of moisture in fuel A is given by:

$$Volume\ of\ moisture\ in\ fuel\ A = (1 - \phi_A)V_A\omega_{2,A} \qquad \text{Eq. 3-22}$$

When an initial volume of fuel A is fully dried, the remaining fuel has a volume of V_B. For each unit volume of moisture removed from V_A, it is assumed that the interior pore space is increased by F_2. Thus, the solid volume would decrease by $(1 - F_2)$. F_2 would have a value between 0 and 1. In the extreme cases, (i) where $F_2 = 0$, there would be no

increase of pore space during drying process, (ii) where $F_2 = 1$, the increase in pore space is equal to the moisture removed. When the moisture in fuel A is completely evaporated, the volume of the dried fuel B can be calculated as follows:

V_B =Initial volume of fuel A – Volume of moisture in fuel A + Volume of pores formed

$$V_B = (1-\phi_A)V_A - (1-\phi_A)V_A\omega_{2,A} + (1-\phi_A)V_A F_2 \omega_{2,A}$$

$$= (1-\phi_A)V_A \left[(1-F_2)\omega_{2,A}\right]$$

Eq. 3-23

Thus, V_A related to V_B by the following equation:

$$\frac{V_B}{V_A} = \frac{(1-\phi_A)}{(1-\phi_B)}\left[1-(1-F_2)\omega_{2,A}\right]$$

Eq. 3-24

Where, ϕ_A and ϕ_B represent the void fraction in the fuel at state A and B respectively. $\omega_{2,A}$ represents the volume fraction of moisture in fuel A. The volume fraction of moisture, volatile matter, carbon and ash in the initial waste can be denoted as $\omega_{2,A}$, $\omega_{3,A}$, $\omega_{4,A}$ and $\omega_{5,A}$ respectively. Those values can be estimated from proximate and ultimate analysis of the original fuel using the following equation:

$$\omega_{n,A} = \frac{\rho_A X_n}{\rho_n (1-\phi_A)}$$

Eq. 3-25

Where n = 2, 3, 4, 5 represent the moisture, volatile matter, fixed carbon and ash respectively. According to Yang *et al.*, (1999), for each volatile matter removed from the dried fuel B, the interior pore space is increased by F_3 and the solid volume is decreased by $(1-F_3)\omega_{3,B}$. The correlation between V_B and V_C is given by the equation below:

$$\frac{V_C}{V_B} = \frac{(1-\phi_B)}{(1-\phi_C)}\left[1-(1-F_3)\omega_{3,B}\right]$$

Eq. 3-26

The volume of volatile matter in fuel B is equal to that in fuel A by the equation:

$$(1-\phi_A)\omega_{3,A}V_A = (1-\phi_B)\omega_{3,B}V_B$$

Thus,

$$\omega_{3,B} = \frac{\omega_{3,A}(1-\phi_A)V_A}{(1-\phi_B)V_B}$$

Eq. 3-27

Substituting Eq. 3-27 into Eq. 3-26 gives:

$$\frac{V_C}{V_B} = \frac{(1-\phi_B)}{(1-\phi_C)}\left[1-(1-F_3)\frac{\omega_{3,A}(1-\phi_A)V_A}{(1-\phi_B)V_B}\right]$$

Eq. 3-28

From Eq. 3-24 and Eq. 3-28, the ratio of remaining volumes $\frac{V_C}{V_A}$, is described as follows:

$$\frac{V_C}{V_A} = \frac{(1-\phi_A)}{(1-\phi_C)}\left[1-(1-F_2)\omega_{2,A}+(1-F_3)\omega_{3,A}\right]$$

Eq. 3-29

Also, the volume fraction of ash in D is related to that in C as follows:

$$\frac{V_D}{V_C} = \frac{(1-\phi_C)}{(1-\phi_D)}\left(\frac{\omega_{5,C}}{\omega_{5,D}}\right)$$

Eq. 3-30

As $\omega_{5,D}=1$, hence:

$$\frac{V_D}{V_A} = \frac{(1-\phi_A)}{(1-\phi_D)}\left(\omega_{5,A}\right)$$

Eq. 3-31

In actual combustion process, the drying, pyrolysis and char gasification occur between layers shown in Figure 3-12.
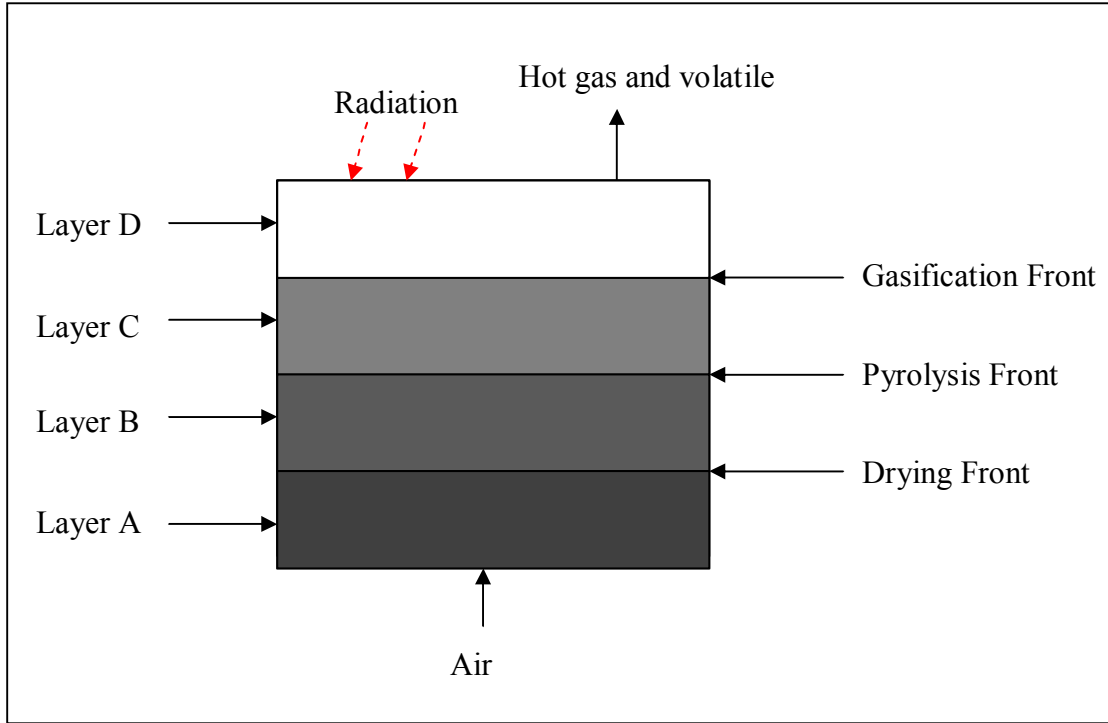
Figure 3-12: Processes in the packed bed combustion chamber (Goh *et al.*, 2001).

The change of volume V_A over time during the drying process can be expressed as follows:

$$\frac{\partial V_A}{\partial t} = -\frac{R_2}{\rho_2 \omega_{2,A}(1-\phi_A)}$$

Eq. 3-32

At the same time, fuel B is formed from each unit of volume of fuel A that has dried. The rise in fuel B volume can be written as follows:

$$\left(\frac{\partial V_B}{\partial t}\right)_{drying} = \frac{R_2}{\rho_2 \omega_{2,A}(1-\phi_A)} \times \frac{V_B}{V_A}$$

Eq. 3-33

Pyrolysis occurs after the drying process, the volume of fuel B reduces can be expressed as follows:

$$\left(\frac{\partial V_B}{\partial t}\right)_{pyrolysis} = \frac{R_3}{\rho_3 \omega_{3,B}(1-\phi_B)}$$

Eq. 3-34

In the actual combustion process, the drying and pyrolysis processes may occur simultaneously. Therefore, the rate of the net change of the fuel B volume can be calculated as:

$$\left(\frac{\partial V_B}{\partial t}\right) = \left(\frac{\partial V_B}{\partial t}\right)_{drying} + \left(\frac{\partial V_B}{\partial t}\right)_{pyrolysis}$$

$$\left(\frac{\partial V_B}{\partial t}\right) = \frac{R_2\left[1-(1-F_2)\omega_{2,A}\right]}{\rho_2 \omega_{2,A}(1-\phi_B)} - \frac{R_3}{\rho_3 \omega_{3,B}(1-\phi_B)}$$

Eq. 3-35

Fuel C is formed during the pyrolysis process of each unit volume of fuel B pyrolysed. Char gasification also occurs at the same time, thus, the net change of volume of fuel C is equal to the rate that fuel C is formed during pyrolysis minus the rate that fuel C is removed during gasification:

$$\frac{\partial V_C}{\partial t} = \frac{R_3\left[1-(1-F_3)\omega_{3,B}\right]}{\rho_3 \omega_{3,B}(1-\phi_C)} - \frac{R_4}{\rho_4 \omega_{4,C}(1-\phi_C)}$$

Eq. 3-36

The volume of fuel D formed during gasification process is related to the volume of fuel C gasified. Thus, the rate of change of volume D is given by the following equation:

$$\frac{\partial V_D}{\partial t} = \frac{R_4 \omega_{5,C}}{\rho_4 \omega_{4,C}(1-\phi_D)}$$

Eq. 3-37

3.2.1.3 Heat and mass transfer in the fixed bed

i. Solid phase

The equations that represent the volume change can be re-written in time differential form that can be solved using numerical methods. The equation of particle transport in a packed bed reactor can be treated as a similar form to that of a fluid. Yang *et al.*, (2003a) used the following equation to investigate the particle phenomena in a packed bed reactor.

a. *Solid continuity:*

$$\frac{\partial\left[(1-\phi)\rho_{sb}Y_{i,s}\right]}{\partial t}+\nabla.\left[(1-\phi)\rho_{sb}v_{s}Y_{i,s}\right]=S_{sg} \qquad \text{Eq. 3-38}$$

Where;

v_s is the solid velocity due to the downward movement of the bed caused by mass loss, which is given by the following equation:

$$\frac{dv_s}{dt}=\frac{\partial V_A}{\partial t}+\frac{\partial V_B}{\partial t}+\frac{\partial V_C}{\partial t}+\frac{\partial V_D}{\partial t} \qquad \text{Eq. 3-39}$$

b. *Conservation of solid phase species:*

$$\frac{\partial\left[(1-\phi)\rho sbY_{i,s}\right]}{\partial t}+\nabla.\left(\rho_{sb}Y_{i,s}v_{s}\right)=S_{Y_{i,s}} \qquad \text{Eq. 3-40}$$

Where;

$Y_{i,s}$ is the mass fractions of moisture, volatile, fixed carbon and ash

$S_{Y_{i,s}}$ takes into account the loss of individual components (moisture, volatile, fixed carbon and ash)

c. The energy equation for the solid:

$$\left(\begin{array}{l} \dfrac{\partial\left[(1-\phi)\rho_{sb}H_s\right]}{\partial t} + \nabla\cdot\left[(1-\phi)\rho_{sb}v_s H_s\right] = \\[4mm] \nabla\cdot\left[\lambda_s\nabla\cdot(T_s - T_g)\right] - S_a h_s(T_s - T_g) + \nabla\cdot q_r + Q_{sh} \end{array} \right)$$

Eq. 3-41

Where;

λ_s is the effective thermal dispersion coefficient of the porous solid phase, depending on particle density and temperature, which is given by:

$$\lambda_s = (1-\phi)\left[\frac{\rho_s}{4511}\right]^{3.5} T_s^{0.5} + 2.27x10^{-7} d_p \left(\frac{\varepsilon}{2-\phi}\right) T_s^3$$

Eq. 3-42

Q_{sh} is the source term, which accounts for the heat effects due to evaporation and heterogeneous combustion.

d. Radiation heat transfer in the bed

The gas phase radiation is an important parameter that governs the rate of heat transfer between solid particles within the bed. Hence, the gas phase flow prediction can also be based on the widely used flux model for gaseous and entrained flow combustion (Smoot and Pratt, 1976).

$$\frac{dI_x^+}{dx} = -(k_a + k_s)I_x^+ + \frac{1}{2}k_a E_b + \frac{1}{2}k_s\left(I_x^+ - I_x^-\right)$$

Eq. 3-43

$$-\frac{dI_x^-}{dx} = -(k_a + k_s)I_x^- + \frac{1}{2}k_a E_b + \frac{1}{2}k_s\left(I_x^+ - I_x^-\right)$$

Eq. 3-44

I_x^+ and I_x^- are radiation intensities in the positive and negative directions respectively.

According to Shin and Choi (2000), k_s is assumed to be zero as the first approximation, and k_a is taken as:

$$k_a = -\frac{1}{d_p}\ln(\phi)$$

Eq. 3-45

ii. Gas phase

The gas phase simulation is based on the hydraulic radius theory of porous media, which allows flows within such a complicated and randomly arranged network to be treated. De Wiest (1969) studied the flows in porous media to the governing pressure gradient through viscosity and porosity as essential parameters of porous media. A system of equations for the gas phase in a packed bed is established based on the following assumptions:

➢ The packed bed consists of solid particles and void spaces,
➢ Void spaces or channels are distributed at random,
➢ No void space is sealed off,
➢ Slip phenomena are absent,
➢ The channels are reasonably uniform in size.

Mass continuity equation:

$$\frac{\partial(\phi\rho_g)}{\partial t} + \nabla.(\phi\rho_g v_g) = -S_g$$

Eq. 3-46

Momentum:

$$\frac{\partial(\phi\rho_g v_g)}{\partial t} + \nabla.(\phi\rho_g v_g) = -\nabla\rho_g + F(v_g)$$

Eq. 3-47

Where;

$F(v_g)$ represents bed resistance to the gas flow, depending on the different flow regimes, which can be defined by the values of Reynolds number as flows:

$$F(v_g) = \begin{cases} -\dfrac{\mu}{k}v_g & if\ \mathrm{Re} < 10 \\ \\ -\dfrac{\mu}{k}v_g - \rho_g v_g|v_g| & if\ \mathrm{Re} \geq 10 \end{cases}$$

Eq. 3-48

Species transport equation:

$$\frac{\partial(\phi\rho_g Y_{ig})}{\partial t} + \nabla.(\phi\rho_g Y_{ig} v_g) = \nabla(D_{ig}\nabla(\phi Y_{ig})) + S_{ig}$$

Eq. 3-49

Where;

The source term S_{ig} is for the mass added to the fluid due to evaporation, devolatilisation and combustion of volatile gasses and char.

The term D_{ig} is fluid dispersion coefficient, including diffusion and turbulent contributions and given by the following equations:

$$D_{igx} = E^o + 0.5 d_p |v_g|$$

Eq. 3-50

$$D_{igr} = E^o + 0.5d_p \left| v_g \right|$$

Eq. 3-51

Energy equation:

$$\frac{\partial\left(\phi\rho_g H_g\right)}{\partial t} + \nabla.\left(\phi\rho_g H_g v_g\right) = \nabla\left(\lambda_g \nabla T_g\right) + S_a h_s^{'}\left(T_{so} - T_g\right) + Q_h$$

Eq. 3-52

Where;

The thermal dispersion coefficient λ_g consists of diffusion and turbulent contributions in a similar way as species dispersion and can be stated as:

$$\lambda_{gx} = \lambda^o + 0.5d_p \left| v_g \right| \rho_g C_{pg}$$

Eq. 3-53

$$\lambda_{gr} = \lambda^o + 0.1d_p \left| v_g \right| \rho_g C_{pg}$$

Eq. 3-54

3.2.1.4   Solution Procedure

The governing equation described in section 3.4.1.3 above can be generalised to a standard form (except for radiation):

$$\frac{\partial\rho\Phi}{\partial t} + \nabla.\left(\rho v\Phi\right) = \nabla.\left(\lambda\nabla.\Phi\right) + S_\Phi$$

Eq. 3-55

Where;

λ is the transport coefficient and S_Φ is the source term. Eq. 3-55 can be solved by using the finite volume method. The whole geometrical domain of the bed is divided into a number of control volumes. Each control volume has a grid point and stores the value of Φ. Eq. 3-55 can be discretised over each control volume to

159

derive a set of algebraic equations using the SIMPLE algorithm (Patankar, 1980). For individual cell, the equation becomes:

$$a_{ij}\Phi_{ij} + a_{i-1,j}\Phi_{i+1,j} + a_{i,j-1}\Phi_{i,j-1} + a_{i,j+1}\Phi_{i,j+1} = S_{i,j}\left(i=1,M; j=1,N\right) \qquad \text{Eq. 3-56}$$

The radiation equations are solved by the fourth-order Runge-Kutta method. The entire mathematical problem and solution procedure can be solved using the Fluid Dynamic Incinerator Code (FLIC).

4   EXPERIMENTAL PROGRAM

The experimental programme reported in this chapter is divided into five sections:

- Experimental setup;

- Operating conditions;

- Measurement and accuracy;

- Procedures; and

- Sample preparation.

The main objectives of the experimental work were to investigate the combustion and pyrolysis characteristics of each material under a wide range of parameters including the effects of reactor temperature, air flow rates and heating rate on the product distribution and properties. The pyrolysis experiments were designed to study the effect of temperature and heating rates on the product yields and their characteristics. Two different temperatures, 500°C and 700°C along with three different heating rates 5°C/min, 10°C/min and 15°C/min were investigated. The combustion experiments were carried out in two different reactor configurations; fixed bed and fluidised bed reactors to investigate the effects of combustion parameters such as air flowrate, air ratio and initial bed temperature on the combustion characteristics. Physical properties of pellets produced from palm kernel cake were also investigated. Process variables including pressure, temperature, fuel moisture content, as well as binders were assessed and quantified based on physical characteristics such as tensile strength and density of the pellets.

4.1   Experimental set up

4.1.1   Fixed Bed Pyrolyser

The Pyrolyser unit consists of two furnaces, temperature controller, reactor, and condenser, Figure **4-1**. The fixed bed pyrolyser was arranged as shown in Figure 4-2.
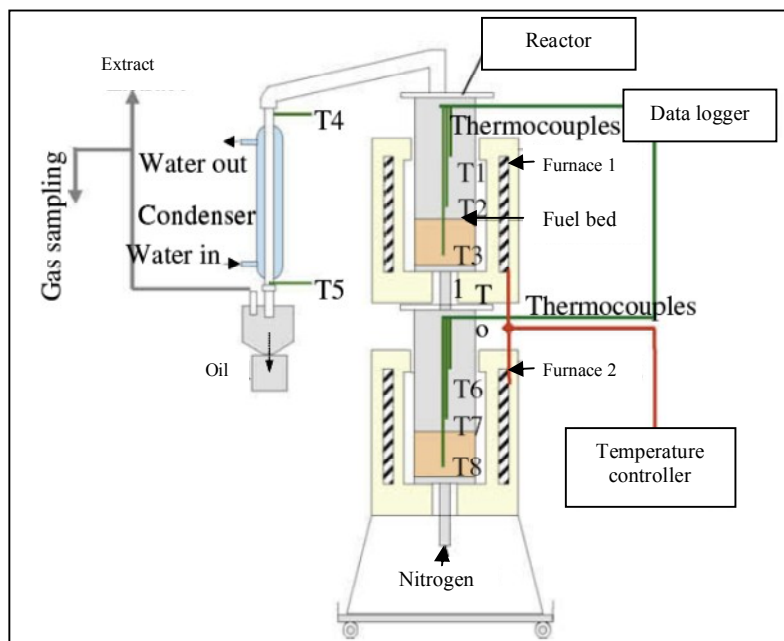
Figure 4-1: Schematic diagram of fixed bed pyrolyser.
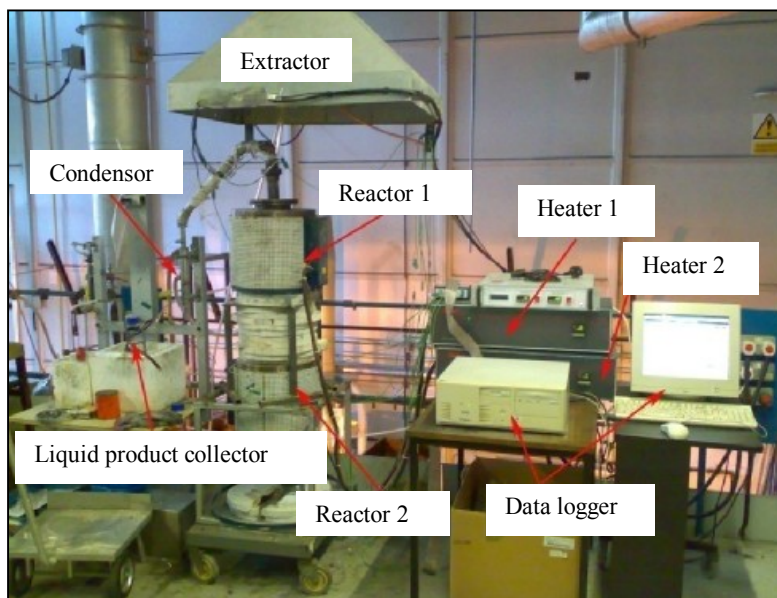
Figure 4-2: Layout of the fixed bed pyrolyser.

4.1.1.1   Reactors

The fixed bed reactors were made from 316 stainless steel vertical cylinder of 125 mm internal diameter and 300 mm height. The flange lid had a gas outlet hole of 36 mm diameter and three holes of 8 mm diameter for thermocouples. The reactors were sealed tightly to avoid any leakage of volatile products and insulated properly in order to prevent heat transfer between reactor and the surrounds.

4.1.1.2   Furnaces

Two Carbolite vertical tubes were used. Each furnace was fitted with a 91e controller system (ε Eurotherm controls) and could be heated up to a maximum temperature 1,050°C with maximum heating rate of 15°C/min.

4.1.1.3   Condenser

One water cooled condenser made from stainless steel was used to cool the pyrolysis gas. A glass bottle was attached at the end of the condenser pipe to collect the condensed liquid.

4.1.1.4   Thermocouples

Eight K-type thermocouples were attached to the system, three were fixed to each reactor and another two were used to measure the temperature of the gaseous product and the condensate. Six thermocouples which were attached to the reactors were placed at three different heights; approximately 50 mm, 100 mm and 200 mm above the grate. The thermocouples were attached from the top of the reactor.

4.1.1.5   Data logger

The sensory 7409TB data acquisition board was used to record and transfer data from the thermocouples to the computer. Azeo Tech, Inc-DAQ Factory Lite Release 5.11 software

was used to store the data from thermocouples. The data was automatically stored to the computer system as a log file.

4.1.1.6   Analysis of pyrolysis gas

Gas samples were collected at different temperatures: 200, 300, 400, 500, 600 and 700°C. A gas sampling bottle was initially filled with 30ml of mixture 60:40 glycerine-water prior to use to collect gas samples. The gas compositions were analysed using a Varian CP-3800 Gas Chromatograph (GC). Capillary column (CP sil 5,5 μm), 60 m length and 0.32 inner diameter with helium as a carrier gas. Hayesep (C 80-100 mesh, porous polymer column 2.0 m length and 0.32 cm inner diameter with 2.0 mm support solid), and A Molecular Sieve (13X, 60-80 mesh, packed column 1.5 m length, 0.32 cm inner diameter with 2.0 mm support solid) with argon as carrier gas. A thermal conductivity detector (TCD) was used to analyse H_2, N_2, CO and CO_2 while Flame Ionisation Detector (FID) was used to analyse light hydrocarbon gases (CH_4, C_2H_4, C_2H_6 and C_3H_8) products.

4.1.2   Fixed Bed Combustor (Pot Burner)

A counter-current fixed bed combustor was used to simulate combustion stages, Figure **4-3**. The experimental rig and data logger were arranged as shown in Figure 4-4. It consisted of three main parts; reactor, grate and gas burner.
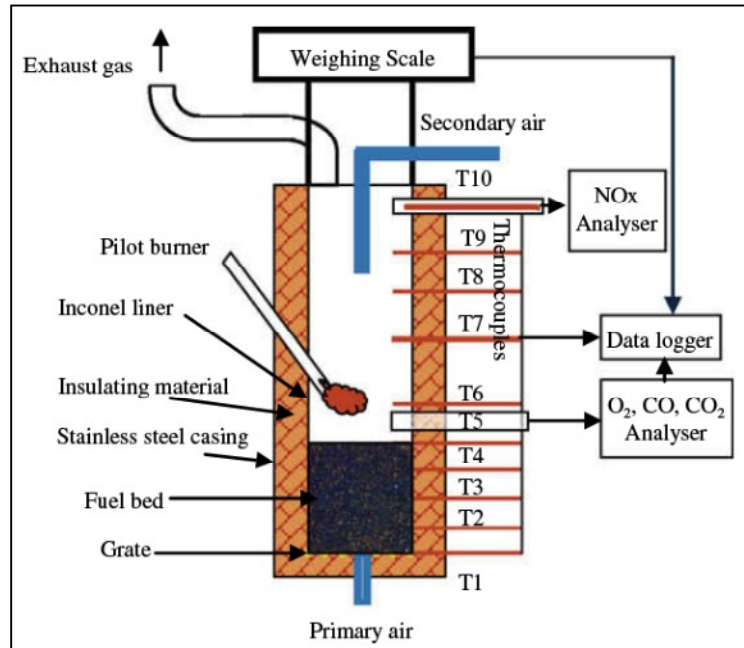
Figure 4-3: Schematic diagram of the fixed bed reactor.
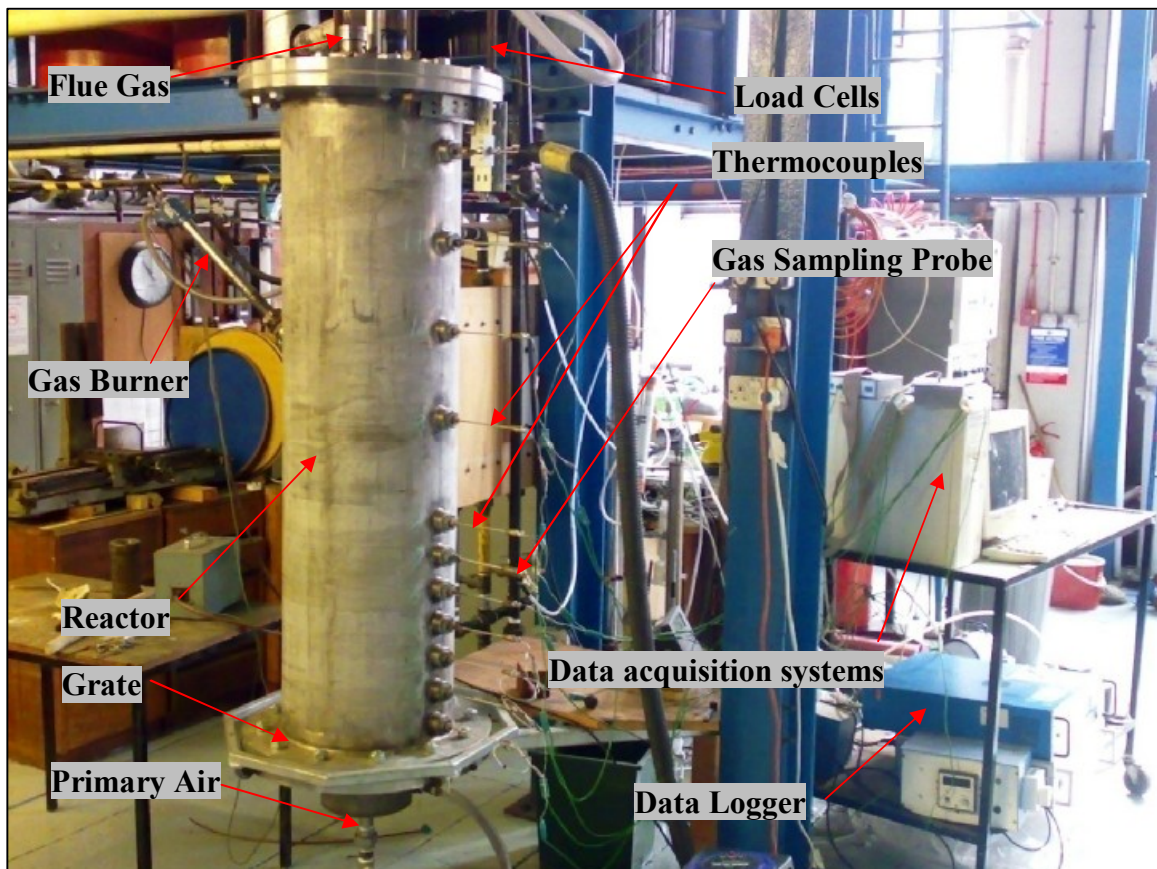
Figure 4-4: Fixed bed reactor.

4.1.2.1 Reactor

The combustion took place in the fixed bed reactor also known as a 'Pot Burner'. The reactor was designed in vertical orientation, cylindrical in shape with 200 mm inner diameter and 1500 mm height. It consisted of an Iconel 600 nickel alloy interior tube of 8 mm thickness and was surrounded by a 72 mm layer of insulating material and confined in an external casing, which could withstand high temperatures up to 1250°C. The insulating material was made of Kaowool Blanket S thermal ceramic and could withstand temperatures up to 1260°C.

4.1.2.2 Perforated grate

The perforated grate used in this study was made from stainless steel in order to withstand a high temperature. It was placed at the bottom of the reactor. It consisted of 700 holes of 2 mm diameter and representing about 7% of open area, Figure 4-5. The series of holes was designed to give a homogeneous distribution of primary air supplied from the bottom of the grate.
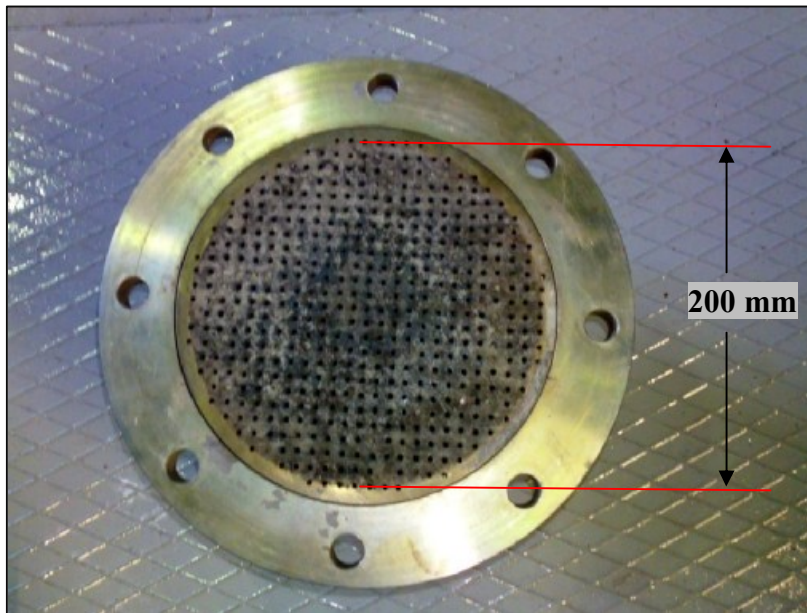
Figure 4-5: Perforated grate.

4.1.2.3   Gas burner

The gas burner was used to initiate the burning process of the sample and to maintain the freeboard combustion temperature during the experiment. It was placed 750 mm above the grate with a 45° angle.

4.1.2.4   Gas analyser

Typical combustion gas CO, CO_2 and O_2 were analysed using MGA 3000 Multi-Gas Analyser. NOx was analysed using SiGnal 4000VM NOx Analyser, Figure 4-6. The combustion gas was continuously purged via a stainless steel probe, which was placed 430 mm above the grate. The gas was passed through a glass wool filter and drying agent (calcium chloride) granules before entering the gas analyser to prevent any particulate matter and water passing through the gas analyser. It is important to make sure that the gas entering the analyser is dry and clean to prevent any damages to the unit. Table 4-1 shows detail of the gas analyser specification.
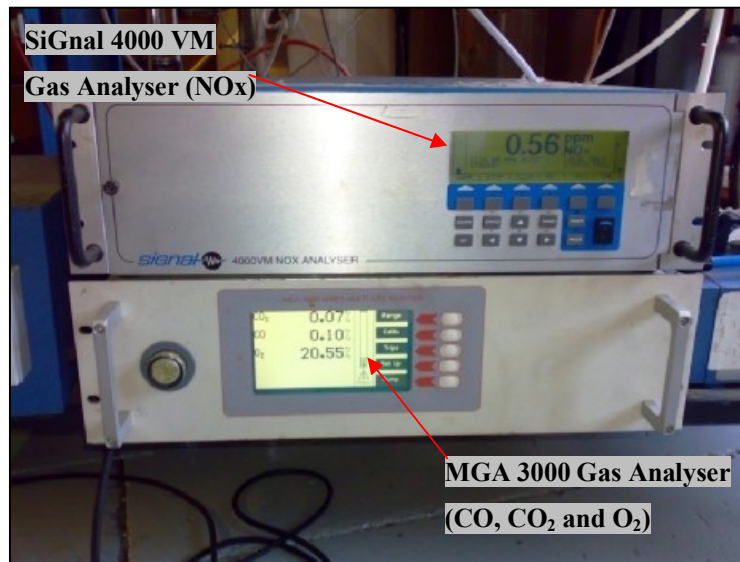
Figure 4-6: Gas analyser.

Table 4-1: Gas analyser specification.

Analyser	Manufacturing	Model	Accuracy
O_2	Analytical Development Co. Ltd.	MGA 3000 Multi-Gas Analyser	$\pm 1.5\%*$
CO			$< 5\%*$
CO_2			$< 5\%*$
NOx	The Signal Instrument Co. Ltd	Series 4000	$\pm 1\%$

*Based on calibrated gas supplied by BOC specialty gases.

4.1.2.5 Thermocouples

Ten K-Type Ni-Cr thermocouples of 0.5 mm diameter were aligned along the reactor at different positions. The thermocouples were arranged based on height above the grate inside the reactor, Table 4-2. Thermocouples no 1 to 7 were designed to measure temperatures inside the fuel bed, while thermocouples no 8 to 10 were used to measure temperatures in the freeboard.

Table 4-2: Positions of thermocouples in the fixed bed combustor.

Thermocouple No.	Position above the grate (mm)
1	96
2	176
3	256
4	336
5	416
6	496
7	576
8	816
9	1016
10	1216

K type, Ni-Cr thermocouples measured continuous temperature in the range from 0°C to a maximum temperature up to 1350°C. The tips of the thermocouples were inserted to the centre of the combustion chamber to reduce error due to channelling effect.

4.1.2.6 Data logging system

Data acquisition software from Azeo Tech, Inc-DAQ Factory Lite Release 5.11 was used to record the continuous data automatically from the analysers and thermocouples. The system has 16 channels, 10 channels which were used for thermocouples and another six channels were used for gas analysers. The data was transferred automatically to a computer under a log file, which can be transferred to an excel file for further analysis.

4.1.2.7 Weighing balance

The fixed bed reactor was suspended from a weighing scale, Figure 4-7 to monitor the weight loss history of the sample during the experiment. It was built-in with four load cells which can take up to a maximum load of 2000 kg. In order to avoid any interference, the pipes connected to the fixed bed combustion chamber were made from flexible hoses.
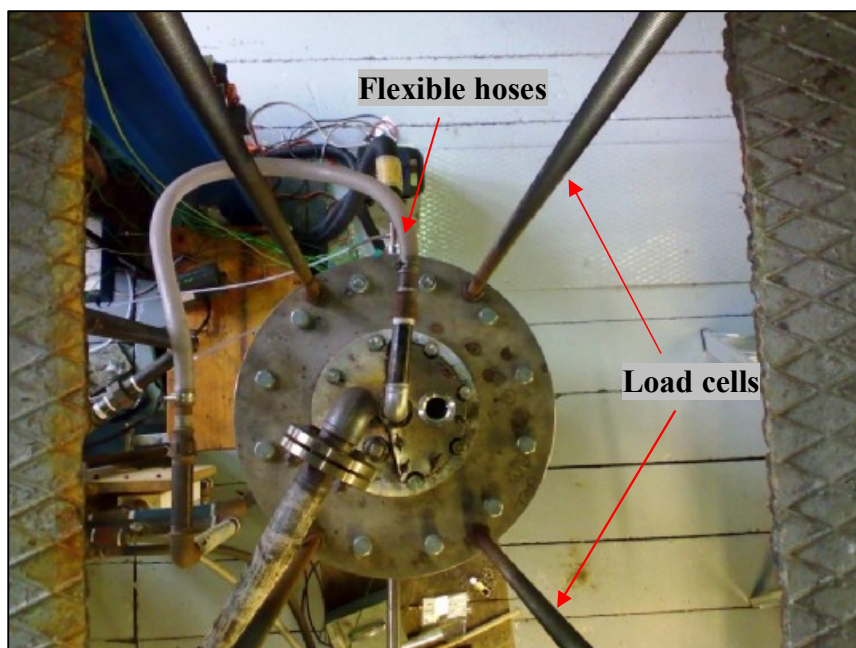
Figure 4-7: Weighing balance.

4.1.2.8 Combustion air

A compressor was used to supply primary and secondary air to the reactor. The primary air was supplied from the bottom part of the bed while secondary air was fed from the top of the bed via a stainless steel tube of 20 mm diameter and 965 mm length having 21 holes at the edge to ensure that air distributed evenly in the combustion chamber. A rotameter series 2000 manufactured by KDG Mobrey Ltd. was used to control the flow rate of both primary and secondary air, Figure 4-8.
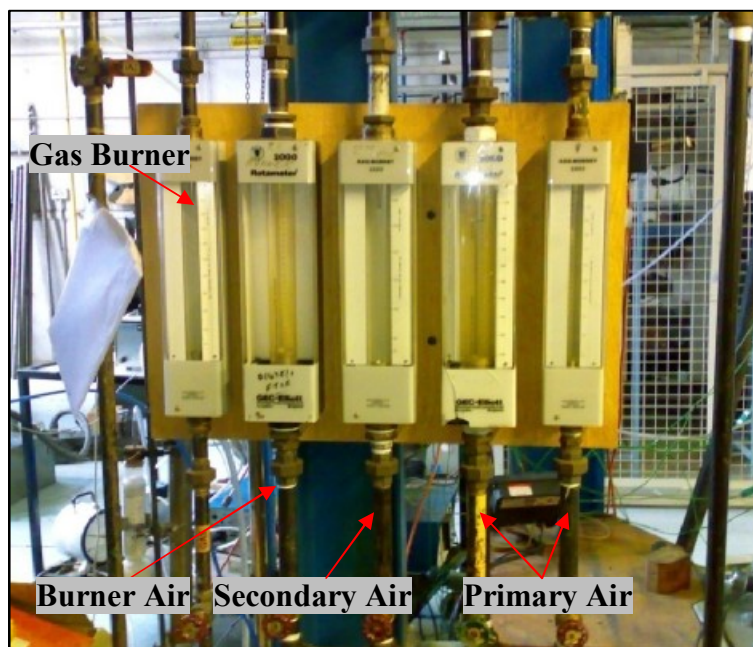
Figure 4-8: Rotameter systems.

4.1.3 Fluidised Bed Combustor

The pilot-scale fluidised bed combustor consists of combustion chamber, distributor plate, pilot burner, pneumatic screw feeding system and cyclone. A schematic and a photograph of the pilot-scale fluidised bed combustor are shown in Figure 4-9 and Figure 4-10 respectively.

4.1.3.1 Combustion chamber

The pilot-scale combustion chamber was built using 1 cm-thick 306 stainless steel. The dimension of the chamber was 2.3 m high and 0.15 m of internal diameter. The 850 μm size of sand with medium sphericity was used as a fluidising agent. The depth of the sand was about 0.3 m. The chamber was surrounded with cold water tubes and insulated with a Kaowool blanket, Figure 4-10.

4.1.3.2 Main air distribution system

The plate was located at 200 mm above the base of the combustion chamber. It consists of nineteen 6cm-high capped standpipes, Figure 4-11. Each unit contain twenty seven 1.5 mm diameter holes incline of 70° from the cylinder axis. It was used to distribute the air evenly through the bed.
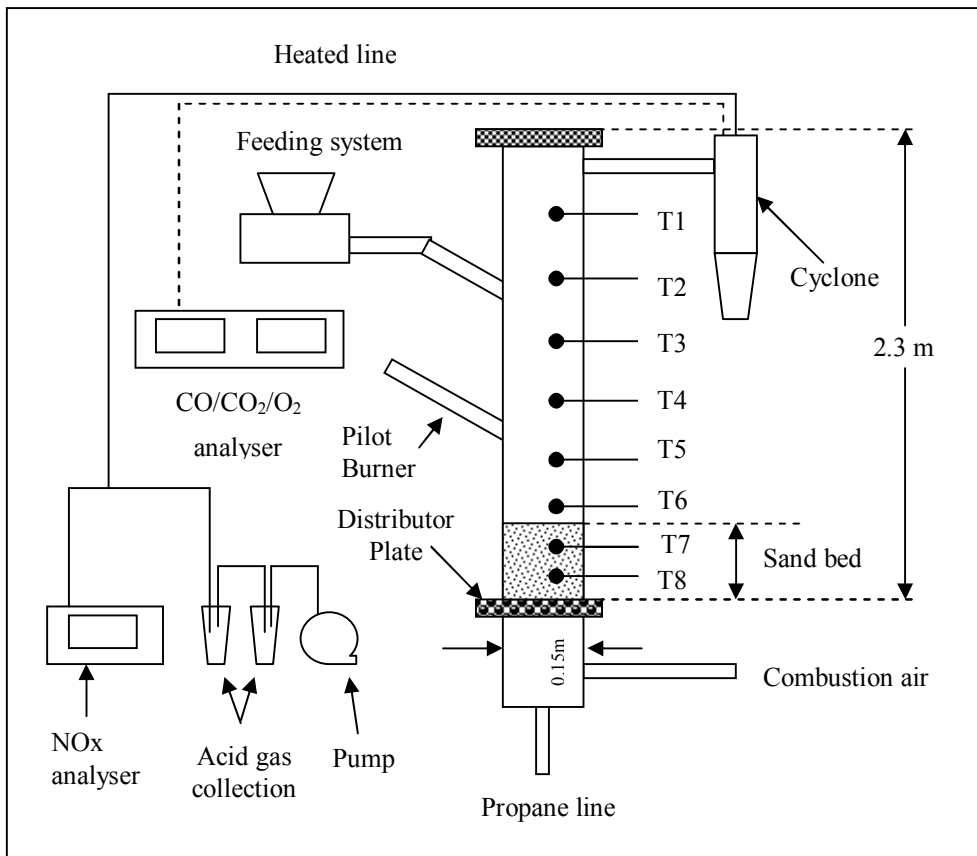
Figure 4-9: Schematic diagram of the pilot-scale fluidised bed.
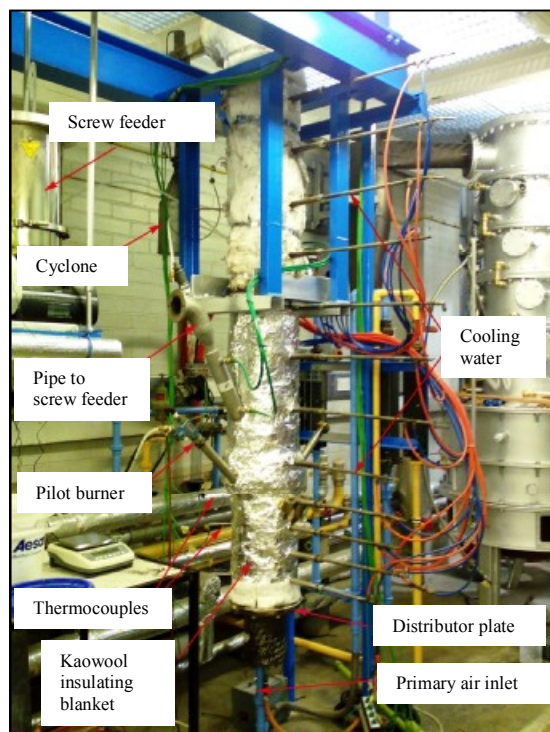
Figure 4-10: Pilot-scale fluidised bed combustor.
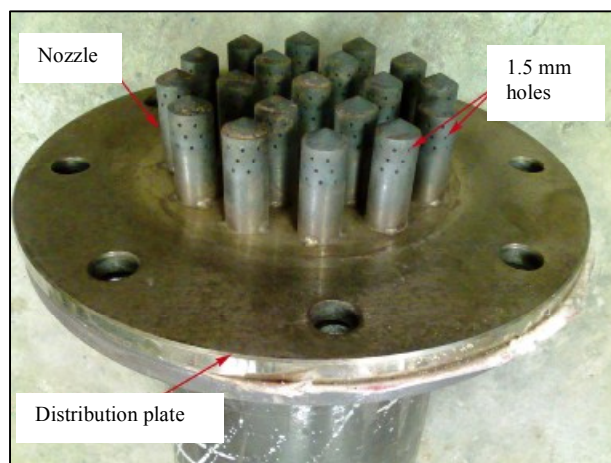
Figure 4-11: Distributor plate.

4.1.3.3   Pilot burner

The pilot burner was used at the start-up stage to ignite the propane to pre-heat the combustion chamber up to a bed temperature of 800°C. The propane was then shut-off

prior to combustion tests. The burner was placed at an angle towards the top of the bed as shown in Figure 4-10 above.

4.1.3.4   Pneumatic screw feeding system

The pneumatic screw feeding system, Figure 4-12, consists of hopper, motor, control panel, screw feeder and feeding pipe connector attached at 45° angle to the combustion chamber. The feeding pipe connector was located at 0.7 m above the distributor. Water jacket was used to regulate the temperature of the pipe to prevent combustion occur before the material reached the combustion chamber. Some of the secondary air was introduced into the hopper to ensure that it operated under slightly positive pressure to prevent combustion gas push back into the feeding system, which may cause fire to the system. The screw feeder was calibrated prior to the combustion tests, by applying a variety of screw speeds over the fuel feedrate, Figure 4-13.
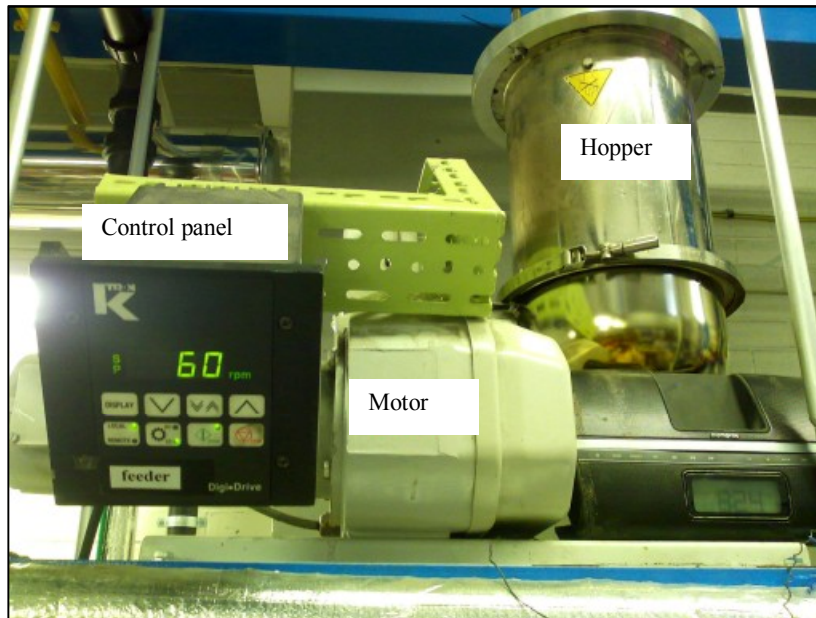
Figure 4-12: Pneumatic screw feeder.
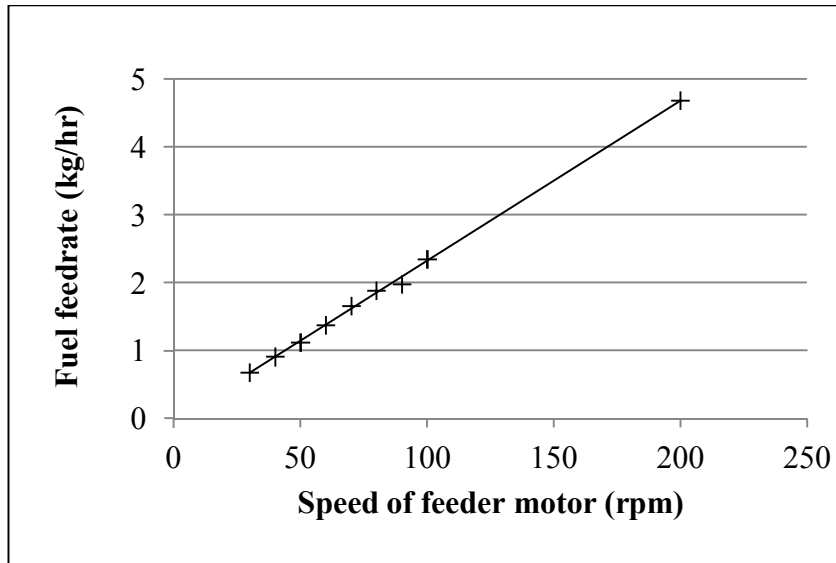
Figure 4-13: Screw feeder calibration.

4.1.3.5 Cyclone

Cyclone was used to trap small particles and fly ash. The unit was attached at the top of the reactor, Figure 4-14.
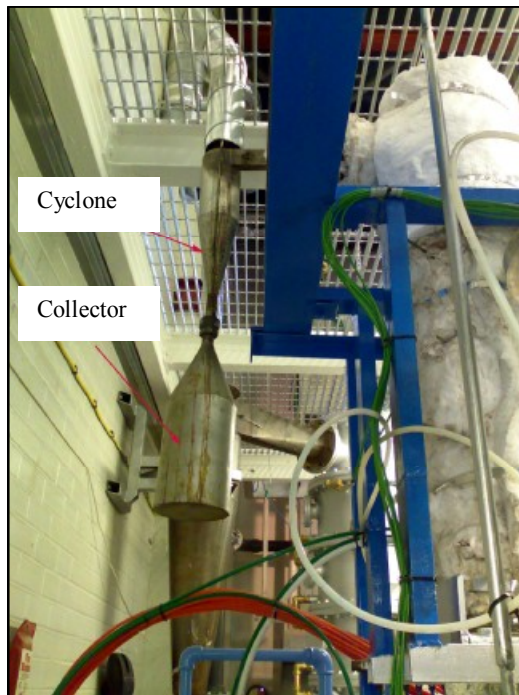
Figure 4-14: Cyclone.

4.1.4 Pelletisation Experiments

Pelletisation experiments focus on a production and evaluation of pellet produced from palm kernel cake. Process variables such as temperature, pressure and fuel moisture content was assessed and evaluated for their effects on pellets quality. In addition, effects of binders were also evaluated. Both organic and inorganic binders are tested. Produced pellets were evaluated based on density and tensile strength. Palm kernel cake pellets were produced using a manual compression technique, Figure 4-15.
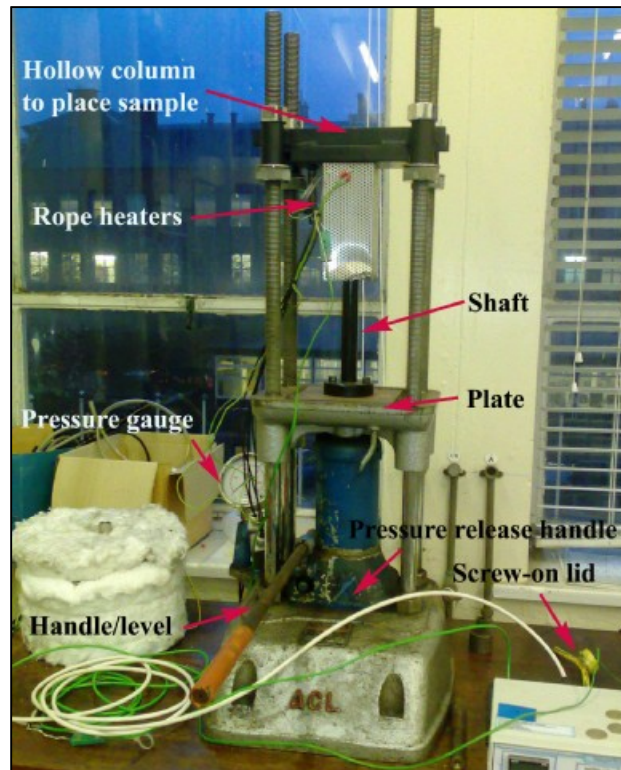
Figure 4-15: The pelletiser.

4.1.4.1 Density and tensile strength

The density of a pellet was computed by a ratio of pellet weight to its volume, in kg/m^3. Tensile strength was assessed using Brazilian test. The Brazilian test is a test used to determine the tensile strength for pellets. In this test compressive stresses are applied to a circular disk pellet or sample. The sample fails due to the formation of the tensile splitting fracture. A Monsanto tensometer, Figure 4-16, was used to measure the force

that the pellet can withstand. This is an indicator of cohesion related to pellet size and shape.
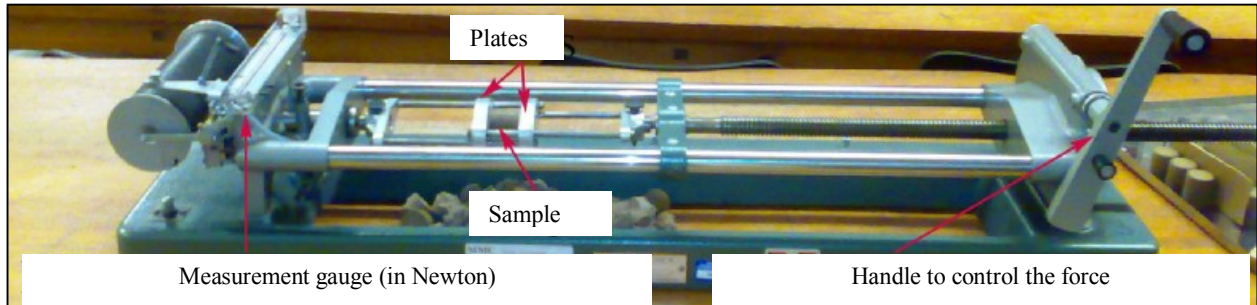
Figure 4-16: Monsanto tensometer.

The tensile strength was computed using the following equation:

$$TS = \frac{2000 \times CS}{\pi \times L \times d}$$

Eq: 4.4

Where;

TS = Tensile strength (kPa)

CS = Compressive strength (N)

L = Pellet length (mm)

d = pellet diameter (mm)

Student's t-tests were carried out to evaluate the statistical significance between results for density and tensile strength.

4.1.4.2   Durability tests

The procedure for durability tests was adopted from Temmerman (2006) and Finney (2009), Figure 4-17. The pellets were assessed based on their ability to absorb mechanical shock and tolerate with the vibrations, frictions and abrasion. These tests could simulate the conditions during handling and transport the pellets. The drum was designed using perspex, size 200 mm (height) x 100 mm (radius) cylinder with small baffle attached to inside wall. The drum was mounted into the lathe which rotated at 40 rounds per minutes. The unbroken pellets were weighted in five intervals during duration

of 20 minutes. The durability of the pellets was calculated and expressed in terms of percentage mass remaining of the total sample weight. The tests were repeated three times for each sample.
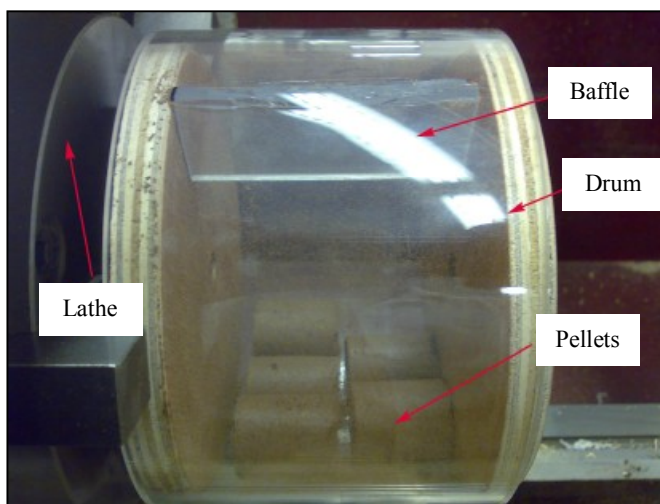
Figure 4-17: The drum for durability test.

4.2 Experimental Operating Conditions

4.2.1 Slow Pyrolysis Experiments

Slow Pyrolysis experiment was conducted in the fixed bed pyrolyser with nitrogen pre-heater. Two important pyrolysis conditions were evaluated during pyrolysis experiments; the effect of final pyrolysis temperature and the heating rate on the pyrolysis product (liquid, char and gas) distributions and its characteristics. The pyrolysis experimental operating conditions are shown in Table 4-3.

4.2.2 Combustion Experiments

4.2.2.1 Fixed bed combustion

The combustion of oil palm stone was conducted in fixed bed reactor or 'pot burner'. The operating parameters for oil palm stones combustion are shown in Table 4-4. The evaluation of the oil palm stone combustion characteristics was based on the effect of

primary air supplied during the combustion process. The primary air flow rate was varied from 250 L/min to 650 L/min.

Table 4-3: Experimental conditions for slow pyrolysis test.

Material	Sample weight (g)	Sample size (mm)	Setting temp. (°C)	Heating rate (°C/min)	N₂ flow rate (l/min)
Oil palm stone (OPS)	250	±10	500 and 700	5, 10 and 15	1.5
Oil palm cake (OPC)	250	±1	500 and 700	5, 10 and 15	1.5

Table 4-4: Fixed bed combustion parameters.

Material	Case	Sample weight (kg)	Sample size (mm)	Bed height (mm)	Air flow rate (l/min)	(λ)	Equivalence ratio (ϕ)
	001	6.00	±10	320	250	0.33	3.0
Oil Palm Stone	002	6.00	±10	350	450	0.60	1.67
	003	4.12	±10	220	600	0.80	0.83
	004	6.00	±10	320	650	0.87	1.16

Detail of combustion calculations is presented in appendix 1.

The superficial mass velocity for minimum fluidisation was calculated based on Eq. 4.5 in order to maintain the fuel bed at fixed bed condition.

$$G_{mf} = \frac{0.005 D_p^2 g_c \rho_f \left(\rho_s - \rho_f \right) \varphi_s^2 \varepsilon_{mf}^3}{\mu \left(1 - \varepsilon_{mf} \right)}$$

Eq: 4.5

$$G_{mf} = 0.874842 \, \frac{\text{kg}}{\text{m}^2.\text{s}}$$

Where;

G_{mf} = fluid superficial mass velocity for minimum fluidisation

D_p = particulate diameter g_c = dimensional constant

ρ_f = fluid density ρ_s = solids density

ϕ = particle shape factor ε_{mf} = voidage at minimum fluidisation

μ = fluid velocity

4.2.2.2   Fluidised bed combustion

The pilot-scale fluidised bed reactor was used to evaluate the combustion characteristics of oil palm stone. The temperature profile, combustion gas, fly ash and acid gases were the main combustion characteristics examined. A series of primary air flowrates and initial temperature of the sand bed were used to investigate the combustion behaviour. The sand bed depth was kept constant in all tests. The operating parameters for both cases are shown in Table 4-5 and Table 4-6.

Table 4-5: Operating conditions used to evaluates the effects of primary air on combustion behaviour of oil palm stone.

Case no.	Primary air (kg/m²hr)	Secondary air (kg/m²hr)	Fuel feedrate (kg/hr)	Excess air (%)	Bed temperature (°C)	Depth of sand bed (m)
001	791	356	1.2	120	900	0.25
002	989	356	1.2	150	800	0.25
003	1187	356	1.2	180	800	0.25

Table 4-6: Experimental setting used to investigate the effects of initial bed temperature on combustion characteristics of oil palm stone.

Case no.	Primary air (kg/m²hr)	Secondary air (kg/m²hr)	Fuel feedrate (kg/hr)	Excess air (%)	Bed temp. (°C)	Depth of sand bed (m)
004	791	356	1.2	120	850	0.25
005	791	356	1.2	120	900	0.25
006	791	356	1.2	120	950	0.25

The temperature of the sand bed and freeboard were monitored using eight K-type thermocouples. The descriptions of the thermocouples can be found in section 4.3.1. The thermocouples were located at the centre of the reactor as shown in Figure 4-9. The position of each thermocouple as measured from the surface of the distributor plate is shown in Table 4-7.

Table 4-7: Location of the eight thermocouples in fluidised bed.

Thermocouple	T1	T2	T3	T4	T5	T6	T7	T8
Height above distributor plate (m)	1.74	1.54	0.76	0.56	0.42	0.31	0.20	0.11

4.3 Experimental Measurement Accuracy

4.3.1 Temperature Measurements

Both slow pyrolysis and combustion temperature were measured using Ni-Cr K-type thermocouples. These thermocouples are made up of a positive Chrome wire and a negative Alumel wire. It offers a wide measurement range of temperature from 0°C to 1350°C continuously. The accuracy of thermocouples used in this study was ± 0.75% of the measured temperature.

4.3.2 Gas Measurements

The accuracy of the gas analyser (MGA 3000 Multi-Gas Analyser) was checked using the 1565 AV span gas supplied by BOC Specialty Gases. The error was less than 5% for the concentration ranges of 20 %vol of CO and 16 %vol of CO_2. However, for the concentration ranges of 30 %vol for CO and 20 %vol for CO_2 give the error reading less than ±4%. Oxygen gas was calibrated using ambient air which consists of 21 %vol and nitrogen gas for zero calibration. The maximum error was less than 2 %vol.

Signal 4000M NOx analyser was used to monitor the NOx gas concentration in the flue gas chamber. The manufacturer quoted accuracy of the analyser within ±1% of the range

or ±0.2 ppm whichever is greater. The analyser was calibrated using a 400 ppm NOx gas. It was supplied by BOC Specialty Gases with the accuracy of ±1.23%.

All gases were measured on a volumetric basis. The data obtained from these measurements can be used to calculated the combustion efficiency as proposed by Burling et.al., (2010) and Llorente and Cuadrado, (2007).

$$\text{The Combustion Efficiency } (\eta_{CE}) = \frac{\%CO_2}{\%CO_2 + \%CO} \times 100 \qquad \text{Eq: 4.6}$$

In order to obtain a better understanding of the combustion gas behaviour, acid gas species were also analysed. Two important species, chloride (Cl^-) and sulphate (SO_4^{2-}) ions were measured, in which to predict the presence of hydrochloric acid (HCl) and sulphur oxide (SOx) releases during the combustion process. The species were collected using a wet chemical method. The flue gases were bubbled through a 3% hydrogen peroxide solution. The liquid mixtures were then analysed using ion gas chromatography.

Varian CP-3800 Gas Chromatograph was used to analyse gas collected from slow pyrolyser. The Gas Chromatograph was calibrated using standard calibration gas supplied by BOC Specialty Gases. Two standard calibration gases were used. Firstly, Carbon Monoxide (16 % CO) and Carbon Dioxide (20 % CO_2) gases were used to calibrate for combustion gases. Secondly, Ethane (1 %mol C_2H_6), Propane (1 %mol C_3H_8), Ethylene (3 %mol C_2H_4), Methane (8 %mol CH_4), Carbon Monoxide (20 %mol CO), Hydrogen (30 %mol H_2) and Nitrogen (N_2 balance) were used to calibrate for hydrocarbon gases. The error for individual gases was less than 0.5 % for every gas species. The calibration process was repeated if the calibration error exceed more than ± 5% deviation from the calibration concentration values quoted by gas supplier.

4.3.3   Air Flow Measurements

The air was supplied through a Rotameter Series 2000 KDG Mobrey Ltd from the bottom of the reactor in both combustion experiments. It was factory calibrated using air at 15°C

and 1013 mbars absolute pressure. The accuracy of the rotameter quoted by the manufacturer was ±2.0%. The influence of air temperature to the combustion temperature was very small. However, correction for temperature difference can be made by multiplying the flow rate by

$$\sqrt{\frac{Tm}{Tc}}$$ Eq: 4-7

Where:

Tm is the temperature of the metered air (average room temperature 19°C)

Tc is the temperature of the calibrated air (15°C)

Thus the error due to the temperature difference was less than 1% which can be neglected.

4.3.4   Weight Measurement

The calibrated scale was used to measure the weight of the sample. The scale could be used to measure accurately to the maximum error ± 40 g. The accuracy of a digital scale used to display the reading of weight loss during experiment was ± 0.1 g. Thus, the accuracy of the burning rate could be quoted as weight loss is ± 0.1 g.

The measurement was affected by the thermal expansion of the reactor due to heat release during the combustion process, which caused the reactor to expand. However, the expansion was restricted due to the bottom of the reactor which was fixed to the primary air pipeline.

4.4   Sample Preparation

4.4.1   Raw materials

Oil palm stones, Figure 4-18 and palm kernel cake, Figure 4-19, were supplied by A.M.E. Teras Marin Services Sdn. Bhd., Malaysia. The oil palm stones were removed from the

shell and air dried at room temperature prior to the experiments. Loose palm kernel cake is obtained from the palm kernel after the oil has been extracted. The palm kernel cake was dried at room temperature prior to the experiments.
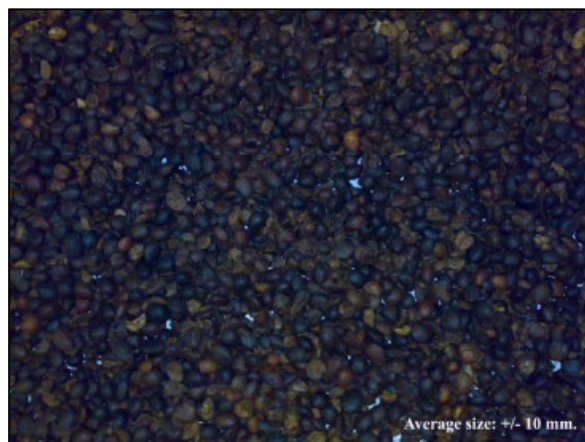
Figure 4-18: Oil palm stones.

Figure 4-19: Palm kernel cake.

4.4.2   Proximate and ultimate analysis

The proximate analysis of both samples and pyrolysis products (char and liquids) were determined according to British Standard 1016-104. Parr 1261 bomb calorimeter was used to analyse calorific value (CV) of the samples and products as stipulated in British

Standard 1016-105. The ultimate analysis of both samples and products were determined using NA 2000 N-Protein Elemental Analyser, Figure 4-20.

Figure 4-20: NA 2000 N-Protein elemental analyser.

4.4.3   Thermogravimetric analysis

The thermal characteristics of dry oil palm stone were also analysed using a computerised Perkin-Elmer Pyris 1 thermogravimetric analyser, Figure 4-21. The experiments were carried out with the following conditions; about 5 mg of sample were heated at a rate of 5°C/min from 50 - 800°C. Oxygen-free nitrogen gas was used as the carrier.

Figure 4-21: Thermogravimetric analyser.

5 RESULTS AND DISCUSSION: PELLETISATION OF PALM KERNEL CAKE

The experiments were designed to investigate the effect of a range of parameters on palm kernel cake (PKC) pellet properties. The main objective of the pelletisation study was to examine the effects of process parameters on the physical properties of palm kernel cake pellets, such as tensile strength, density and durability. The variables investigated included the pelletisation pressure, temperature, fuel moisture content and the effect of binders. An attempt was made to determine the optimum values of these parameters which would result in the best pellet quality. The findings from this research may help promote palm kernel cake as a source of renewable fuel in the future.

5.1 Effect of fuel moisture content

The effect of the moisture content on biomass pellet qualities such as density, strength and durability has been examined by various researchers (O'Dogherty and Wheeler, 1984, Mani *et al.*, 2006, Finney *et al.*, 2009a, Sultana *et al.*, 2010). In this study, however, the relationship between moisture and pellet quality could not be established as viable pellets could not be produced at high or low moisture contents. In the case of high moisture levels (15%) the pellets collapsed immediately upon ejection from the mould, Figure 5-1(a). At low moisture contents (5%) the pellets cracked instantly after being removed from the mould, Figure 5-1(b). Figure 5-1(c) shows a good quality pellet produced at the 'as received' moisture content of 7.9%. As this was the only moisture level to produce coherent pellets all subsequent tests were conducted at this moisture content.
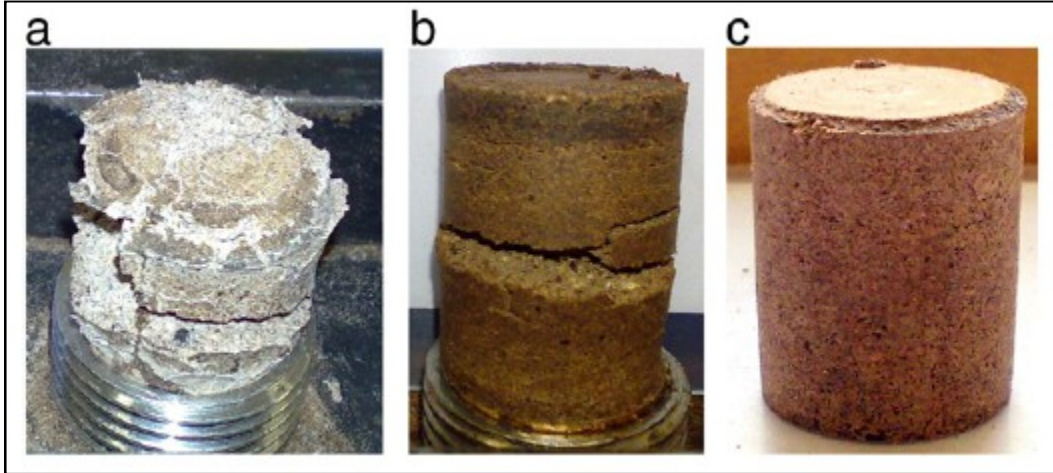
Figure 5-1: Palm kernel cake pellets produced at different moisture contents: (a) at 15%, (b) at 5%, and (c) at 7.9% 'as received' moisture content.

5.2 Effect of pelletisation pressure

Figure 5-2 shows the effect of pelletisation pressure on the tensile strength and density of PKC pellets. Pellets formed at higher pressures were found to be stronger and more uniform in shape over time. As the pressure increased from 4060 to 9338 psi (28.0 to 64.38 MPa), the densities of the PKC pellets increased steadily from 1060 to 1187 kg/m^3. This was due to the low compression energy required to fill the inter-particle spaces during the compression process (Ryu *et al.*, 2008). The density of the PKC pellets was almost comparable with the pellets made from palm fibres and shells, which ranged between 1100 kg/m^3 and 1200 kg/m^3 (Husain *et al.*, 2002). The pellet tensile strengths increased from 72 to 387 kPa as the pressure increased from 4060 to 9338 psi (28.0 to 64.38 MPa). Although only a slight increase in density was observed between pelletisation pressures of 8120 and 9338 psi (55.99 and 64.38 MPa), the tensile strength of the pellets was found to increase quite significantly. As expected, the highest tensile strength (387 kPa) and the greatest pellet density (1187 kg/m^3) were both obtained at a maximum pelletisation pressure of 9338 psi (64.38 MPa).
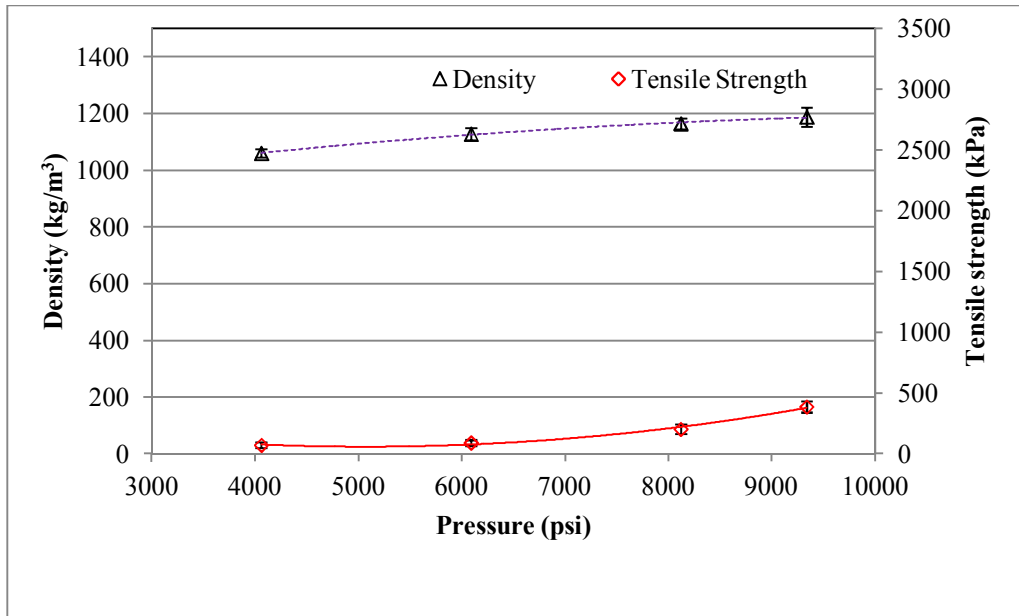
Figure 5-2: Effect of pressure on palm kernel cake pellet density and tensile strength.

5.2.1 Pressure-Density relationships

The association between pressure and density has been reported by many researchers. O'Dogherty, *et al.*(1984) suggested that the association between the density and pressure of high-density straw pellets was a simple power-law at low density due to the immediate elastic recovery of the straw. However, at high-density (relaxed density) straw pellets the relationship was an exponential increase. Husain, *et al*. (2002) established the relationship between the pressure and density of palm fibre and shell briquettes; they found an exponential increase in density with the increase in pressure. Figure 5-3 shows the plot of pressure and density for the PKC pellets. This shows an exponential increase in density with the increase in PKC pelletisation pressure. The relationship is in the form of:

$$P = 3.689e^{0.0066x}$$

Eq. 5-1

Where *P* is mould pressure in psi.
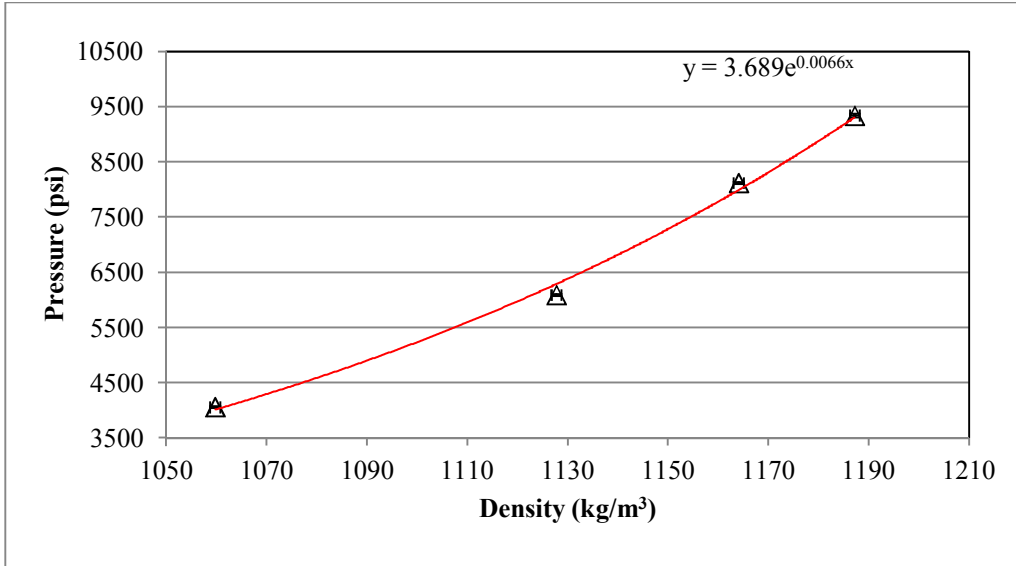
Figure 5-3: Relationship between pelletisation pressure and palm kernel cake pellet density.

5.3   Effect of pelletisation temperature

The tensile strength of the PKC pellets was found to improve significantly at elevated temperatures, Figure 5-4. As the pelletisation temperature increased from 20 to 40°C, the tensile strength increased from 358 kPa to 914 kPa. The density, however, increased from 1157 kg/m^3 to 1200 kg/m^3. For the pellets formed at temperatures above 40°C the tensile strength increased steadily from 914 kPa at 40°C to 989 kPa at 100°C. This has been observed to be due to a natural binding effect where the lignin content of the material was softened and bound the pellets upon compression (Uslu *et al.*, 2008). According to Beker, *et al.* (1959) the protein and long cellulose fibre content of biomass are responsible for the bonding and stabilisation of pellets. In the present study the optimum pelletisation temperature was found to be in the region of 80-100°C. Temperatures above 100°C had negative effects on the pellet tensile strength, due to the evaporation of water which resulted in lower moisture contents.
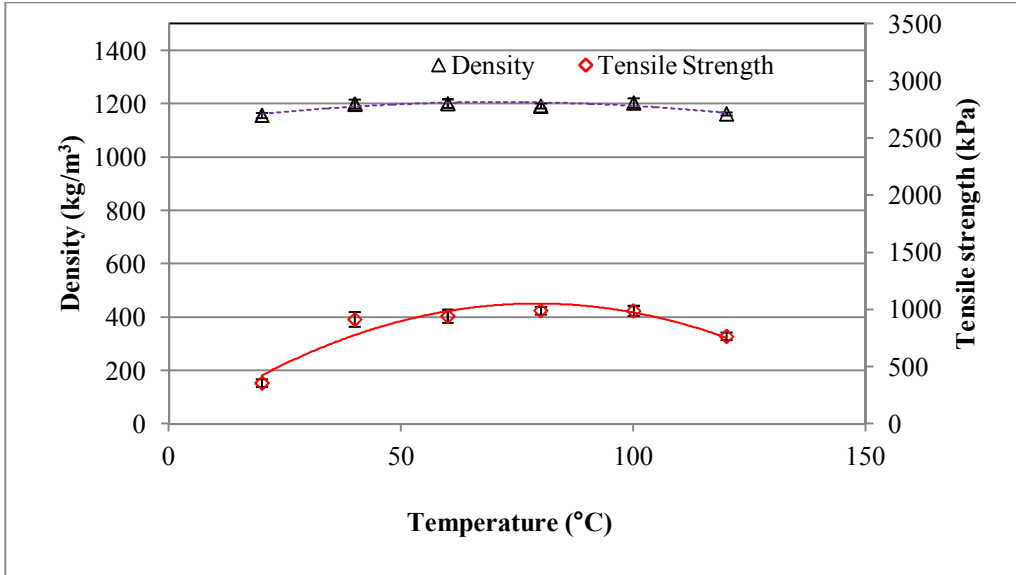
Figure 5-4: Effect of temperature on palm kernel cake pellet density and tensile strength.

5.4 Effect of binders

5.4.1 Inorganic binders

Two inorganic binders were used in this study: sodium hydroxide (NaOH) and calcium carbonate ($CaCO_3$). Figure 5-5 and Figure 5-6 show the effects of these binders on PKC pellets, in terms of density and tensile strength. As the concentration of sodium hydroxide increased from 0.5 wt.% to 2.0 wt.%, the tensile strength increased from 1441 kPa to 3055 kPa (Figure 5-5). However, further additions reduced the tensile strength to 1968 kPa. Sodium hydroxide has the ability to bind loose particles together, thus improving pellet quality. In spite of its ability to produce good quality pellets, sodium hydroxide may cause problems to combustion systems. As reported by Finney *et al*. (2009b) the combustion efficiency of spent mushroom compost-coal tailing pellets was reduced from 95% to 88.7% when a sodium hydroxide binder was used to aid pellet agglomeration. Furthermore, higher concentrations of alkali metals in the ash could promote the formation of fouling (Vamvuka and Zografos, 2004). Therefore, it is important to keep the amount of sodium hydroxide as low as possible without compromising pellet quality. However, Yang *et al*. (2004) claimed that sodium compounds additives including sodium

hydroxide could promote NO reduction efficiency in a tube stove and a drop tube furnace at high temperature (>800°C).

As can be seen in Figure 5-6, the tensile strength of the PKC pellets increased gradually with the increase in calcium carbonate from 0.5 wt.% to 2.0 wt.%. Further increases in calcium carbonate resulted in an increase in tensile strength, over 1450 kPa for 5 wt.%, although the strengths attained were not as high as for the sodium hydroxide binder. The effect on density was less clear. In both cases, the density fluctuated between 1192 kg/m^3 and 1237 kg/m^3.

A student's t-test is a test of the null hypothesis that the difference between two responses measured on the same statistical unit has a mean value of zero. The null hypothesis (H_o) is no significant difference of tensile strength between pelletisation of PKC without binder and PKC with sodium hydroxide or calcium carbonate binder. Student's t-tests were conducted for both inorganic binders. The differences between these and the control (no binder) were assessed. The results for the tensile strength of PKC pellets with these binders are given in Table 5-1 and Table 5-2. Since the critical value p=0.05 (two tail, unpaired and unequal sample variance), both hypothesis were rejected; these show that the effects of both binders on pellet tensile strength were highly significant using a 95% confidence interval (P<0.05).
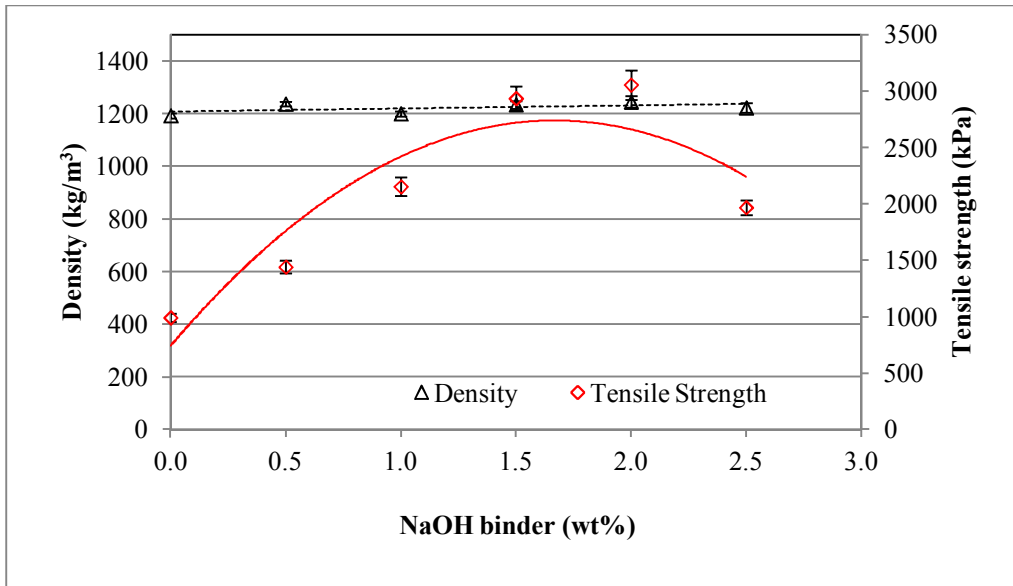
Figure 5-5: Effect of sodium hydroxide on the tensile strength and density of palm kernel cake pellets.
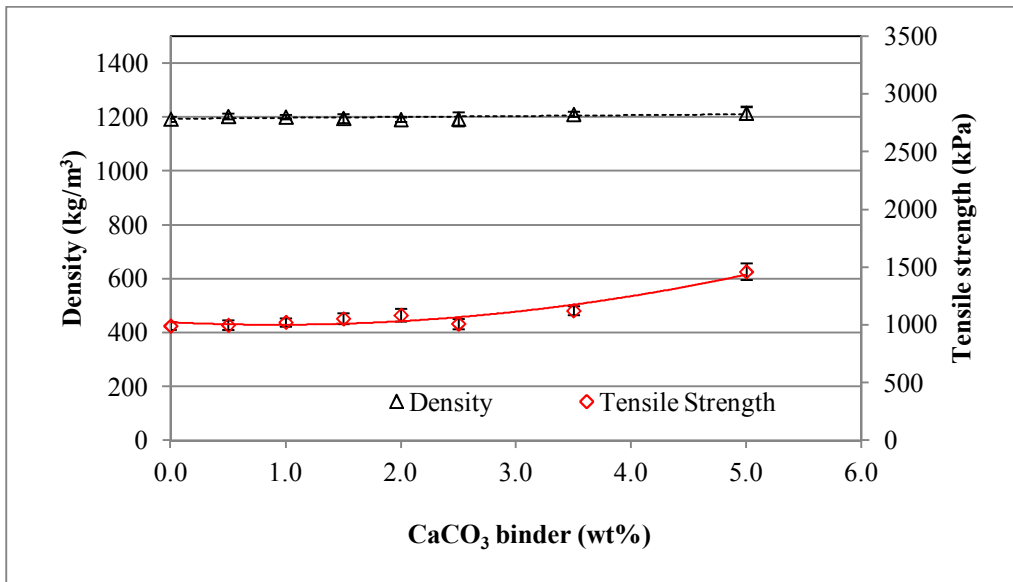
Figure 5-6: Effect of the calcium carbonate binder on the tensile strength and density of palm kernel cake pellets.

Table 5-1: Student's t-test (two-sample assuming unequal variances) for the palm kernel cake pellets with 2 wt.% sodium hydroxide binder.

	Variable 1	**Variable 2**
Mean	991.94	3054.57
Variance	1201.25	17027.45
Observations	5	5
Hypothesized Mean Difference	0	
df	5	
t Stat	-34.16	
P(T<=t) one-tail	2.02E-07	
t Critical one-tail	2.02	
P(T<=t) two-tail	4.04E-07	
t Critical two-tail	2.57	

Variable 1: Tensile strength of PKC pellet without binder (control).
Variable 2: Tensile strength of PKC pellet with 2 wt.% sodium hydroxide.

Table 5-2: Student's t-test (two-sample assuming unequal variances) for the palm kernel cake pellets with 5 wt.% calcium carbonate binder.

	Variable 1	**Variable 2**
Mean	991.94	1460.52
Variance	1201.25	5169.96
Observations	5	5
Hypothesized Mean Difference	0	
df	6	
t Stat	-13.13	
P(T<=t) one-tail	6.03E-06	
t Critical one-tail	1.94	
P(T<=t) two-tail	1.21E-05	
t Critical two-tail	2.45	

Variable 1: Tensile strength of PKC pellet without binder (control).
Variable 2: Tensile strength of PKC pellet with 5 wt.% calcium carbonate.

5.4.2   Organic binders

Three organic binders were chosen for this study: maize starch, tapioca starch and potato starch. Maize starch was the most effective of the starch binders, but was not as successful in aiding agglomeration as either of the inorganic binders considered above

(Section 5.4.1). As shown in Figure 5-7, adding up to 10 wt.% of maize starch improved the tensile strength of PKC pellets, increasing it from 991 kPa to 1361 kPa. The tapioca starch and potato starch had very little effect at low concentrations 5-10 wt.%. Figure 5-8 and Figure 5-9 show that further additions of up to 20 wt.% binders deteriorated the pellets in terms of tensile strength. However, the density almost unchanged in both cases with increasing proportions of these binders.
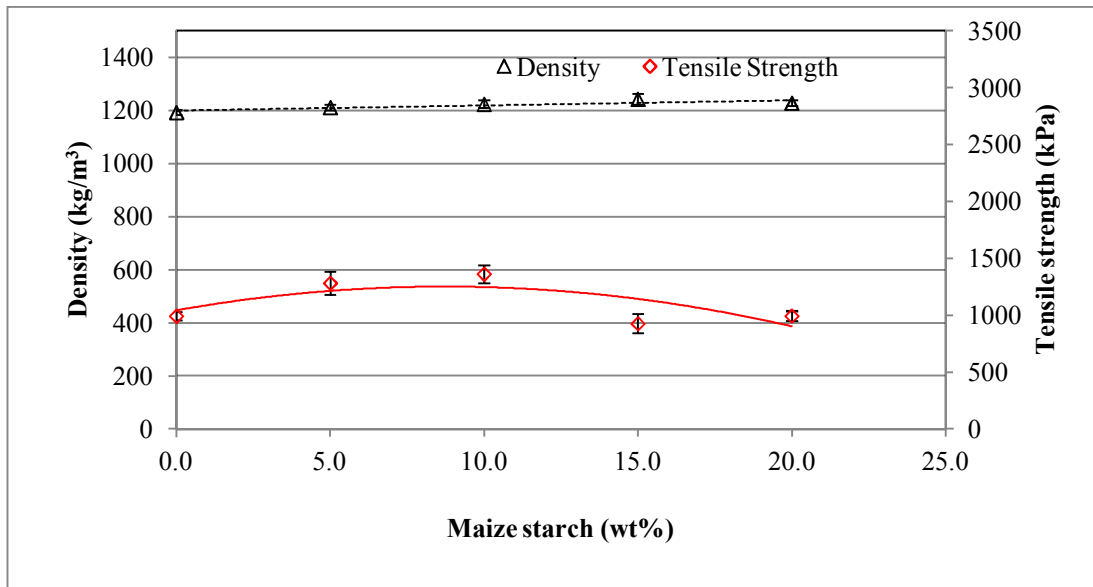
Figure 5-7: Effect of maize starch on the tensile strength and density of palm kernel cake pellets.
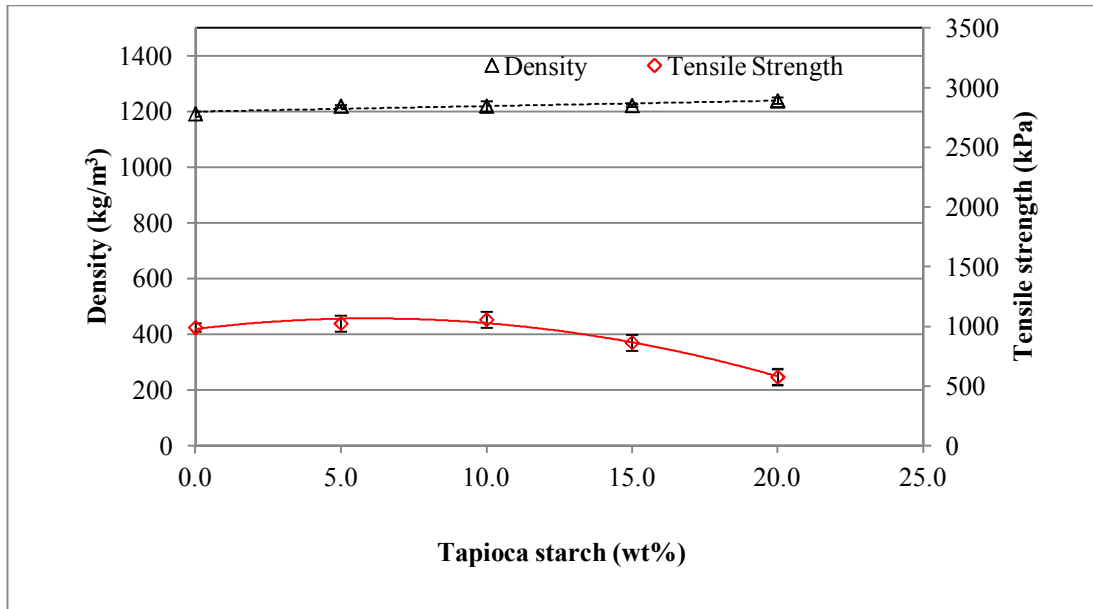
Figure 5-8: Effect of tapioca starch on the tensile strength and density of palm kernel cake pellets.
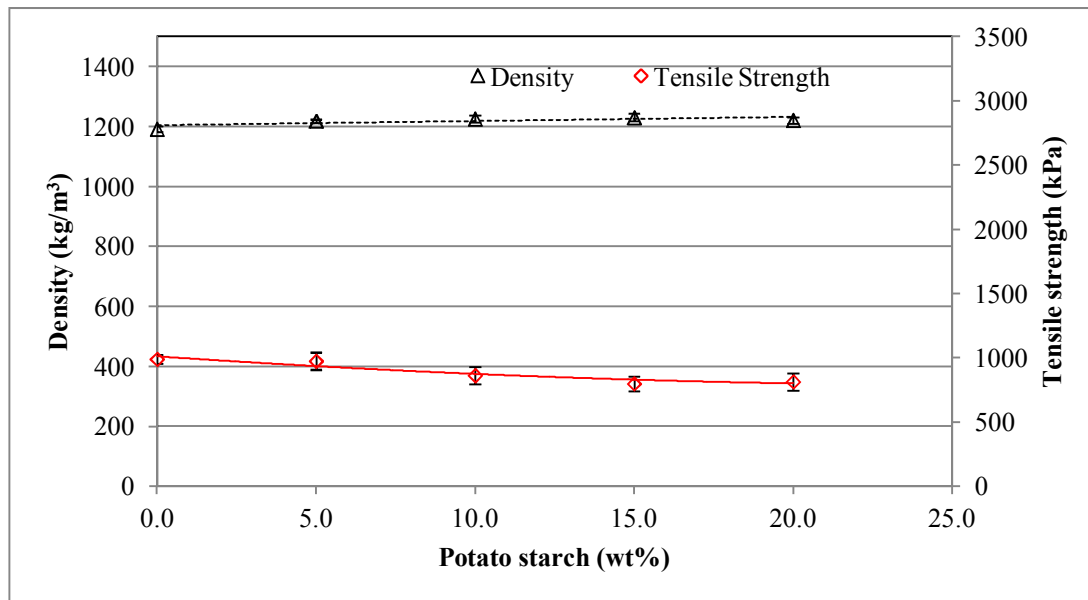
Figure 5-9: Effect of potato starch on the tensile strength and density of palm kernel cake pellets.

5.5 Pellet durability

Pellet durability is one of the important quality assessments for the biomass pellet. The durability of the pellet can be defined as the ability of densified biofuels to remain intact when handled (Temmerman *et al.*, 2006). This property is evaluated by the resistance of densified fuels towards shock or/and friction, normally using a dustproof rotating drum. Details process and procedures is discussed in Chapter 4, Section 4.1.4.3.

Table 5-3 shows the comparison between the durability of PKC pellets and pellets made from wood, straw and spent mushroom compost. The durability of the compressed PKC pellets was almost 50% lower than the other pellets. These low durability results may be due to the fact that PKC contains fat from the palm oil residue. Briggs *et al*. (2009) studied the effect of ingredients and processing parameters on pellets quality made from rations containing varying ratios of corn, high-oil corn, soybean meal, and mechanically expelled soybean meal. They found that increasing the oil content above 7.5% significantly decreased pellet durability. Fat with its hydrophobic nature may interfere with the binding properties of the water-soluble components in the mixture. Furthermore, fat acts as a lubricant between the particles and the wall of the mould which may result in a lower compacting pressure (Finney *et al.*, 2009b). Further investigations into a specific binder are needed to enhance the durability of PKC pellets.

Table 5-3: Durability of palm kernel cake pellets tested using a rotating drum compared to other biomass fuel pellets.

Pellet Type	Pelletisation Conditions	Durability (%) After 10 Minutes
Wood pellet*	extruded	98.8
Straw*	2436 psi	98.8
Coal tailings*	2436 psi, air-dried	79.7
Spent mushroom compost*	2436 psi, air-dried	93.0
PKC pellet	9338 psi, 80°C, 1.5 wt% NaOH binder	48.9
	9338 psi, 80°C, 10 wt% maize binder	47.0

*Data obtained from (Finney *et al.*, 2009a).

5.6   Summary

Pelletisation experiments were conducted to determine the optimum value for various process parameters for the formation of good quality biomass fuel pellets from palm kernel cake - a waste material from the palm oil industry. It was established that palm kernel cake can be pelletised to relatively high densities and tensile strengths at elevated temperature and pressure. The moisture content of the biomass strongly affected pellet quality; increasing the moisture from the 'as received' level of 7.9 % caused pellets to deteriorate, whereas reducing the moisture content resulted in the formation of weak pellets that were prone to cracking. The optimum conditions for the production of these pellets were found to be a moisture content of 7.9 %, a compaction pressure of 9338 psi (64.38 MPa) and a pelletisation temperature of 80-100°C. At these conditions, the pellets formed had a density of 1184-1226 kg/m^3 and a tensile strength of 930-1007 kPa.

Small additions of inorganic binders improved the quality of the palm kernel cake pellets. Sodium hydroxide (<2 wt.%) increased the tensile strength to a maximum of 3055 kPa, where the density fluctuated between 1192 kg/m^3 and 1237 kg/m^3. Improvements were also seen with ~5 wt.% of calcium carbonate, where the tensile strength reached ~1500 kPa. Of the three organic binders tested, only small amounts of maize starch resulted in improved pellet quality, although this was not as effective as the inorganic binders. The addition of the other organic binders (tapioca starch and potato starch) did not result in any improvements in terms of tensile strength or density.

6 RESULTS AND DISCUSSION: COMBUSTION OF OIL PALM STONE

This chapter focuses on the discussion of results obtained from combustion tests of oil palm stone in two different reactor's configurations; fixed bed and fluidized bed reactors. Section 6.1 is dedicated to combustion of oil palm stone in a fixed bed reactor. This section also covers the validation of those results using fluid dynamic incinerator code (FLIC). Section 6.2 concentrates on combustion of oil palm stone in a pilot-scale fluidised bed reactor.

6.1 Fixed bed reactor and FLIC modelling

Travelling-grate combustion systems are commonly used in mass burn technology such as incinerators. The combustion characteristics are difficult to measure in the actual combustion process due to the massive plant area and difficulty of controlling the environment of study (Ryu *et al.*, 2009). A batch type fixed bed with the aid of computer technology enables the moving bed combustion process in a small batch type fixed bed reactor to be simulated. Heat and mass transfer in the transverse direction and additional particle mixing gives a significant impact in the traveling grate system. The heat and mass transfer in the vertical direction were shown to be more dominant. The time elapsed in a fixed bed corresponds to the residence time of fuel in a moving bed (Ryu *et al.*, 2009). Therefore a fixed bed reactor can be used as a simplified system to simulate the moving bed or actual combustion plant. This chapter presents the results and discussion obtained from the combustion of oil palm stone (OPS) in a fixed bed reactor using four different air flow rates and weights: 250 l/min (6.0 kg), 450 l/min (6.0 kg), 600 l/min (4.0 kg) and 650 l/min (6.0 kg). Mathematical modelling (FLIC code) was also applied to predict the reacting bed behaviour and to validate the experimental results.

6.1.1 Temperature profile

The temperature profile obtained during the combustion of OPS in a fixed bed reactor is shown in Figure 6-1. This temperature profile was measured during a combustion test with 6 kg of OPS and 250 l/min of primary air flow rate. Figure 6-2 shows the gas emission and the mass left on the bed.
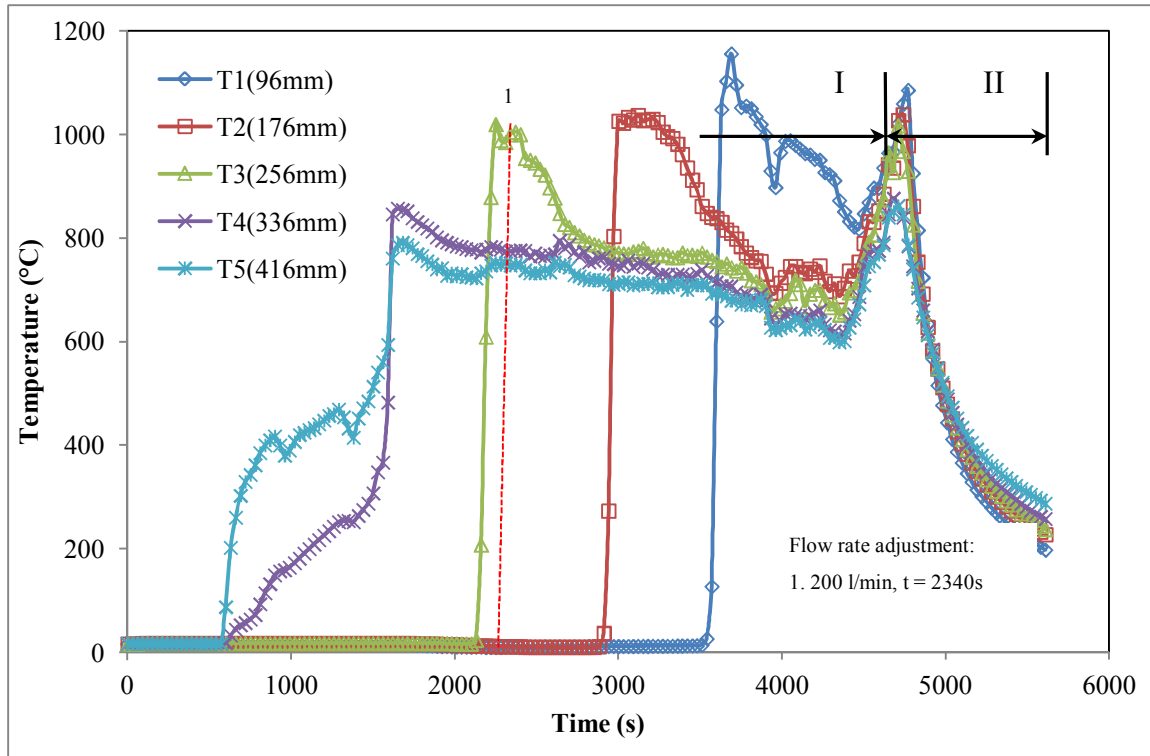
Figure 6-1: Temperature profile of the combustion of the OPS at an air flow rate of 250 l/min.

The initial bed height was approximately 400 mm above the grate. The density of the fuel bed was 459 kg/m^3. The bed temperatures were measured at ten different points inside the reactor. Four thermocouples T1, T2, T3 and T4 were placed inside the sample bed at 96, 176, 256 and 336 mm respectively. Thermocouple T5 was placed just above the surface of the sample bed at 416 mm. Thermocouples T6, T7, T8, T9 and T10 were positioned in the freeboard at 496, 576, 816, 1016 and 1216 mm, respectively. For the purpose of evaluating the combustion characteristics in a fixed bed reactor only five temperature profiles measured by thermocouples T1 to T5 which were fixed inside the fuel bed were plotted versus time. Detailed descriptions of the experimental rigs are described in

199

chapter 4 (Figure 4-3). All of the thermocouples were fixed at the centre of the fuel bed. This ensured that the measured temperature represented closely the weighted mean temperature of the bed in which the thermocouple was in radiative exchange.
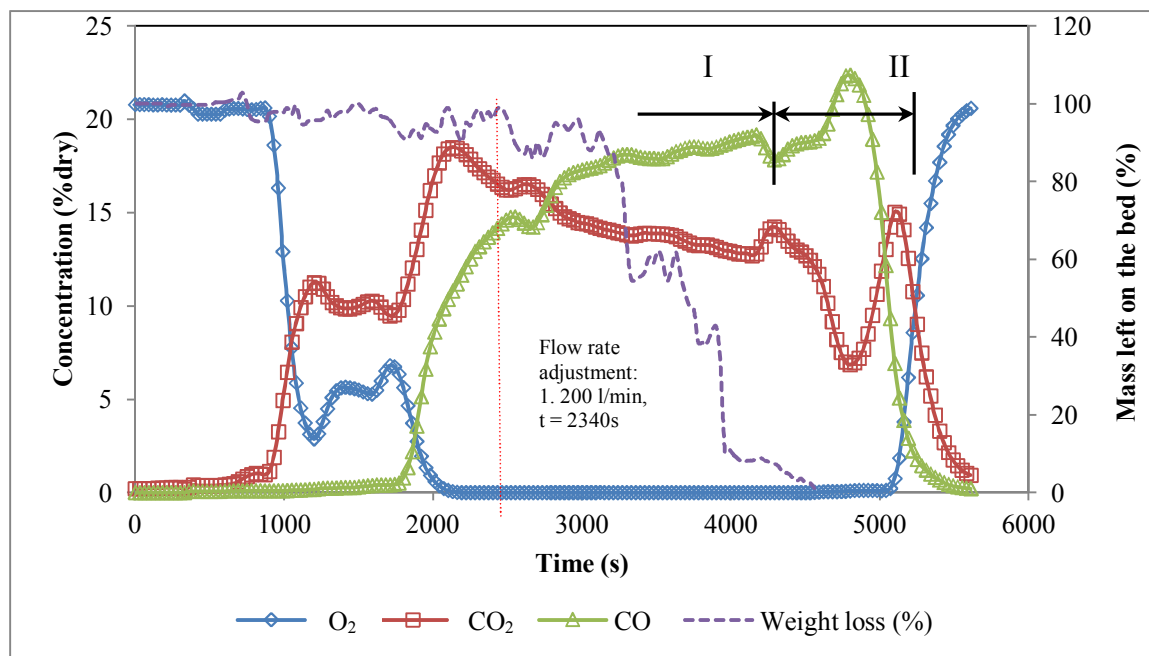
Figure 6-2: Gas emission and mass left on the bed for the combustion of the OPS at an air flow rate of 250 l/min.

The gas burner was used to ignite the fuel bed in order for the material to start the combustion process. Generally, this temperature profile showed two discrete regions, marked 'I' and 'II' (Figure 6-1). Region 'I', characterised by high temperature profiles, was measured by thermocouples T1 to T4 and a strong flame was observed above the burning bed. This was due to the heat generated from the combustion of the volatile gases released from the burning particles as well as the heat radiation from the reactor wall. Region 'II' was recognised as the char combustion stage. Region 'II' can be characterised by a glowing char burning as shown in Figure 6-3, which caused a high temperature after the ignition front reached the grate area.

Due to the heat radiation from the burning material and the reactor wall, the temperature in the freeboard (T5 = 416 mm) rose quickly to about 800°C (Figure 6-1), followed by the ignition propagation, and moved down the fuel bed from T4 to T1. This can be

confirmed by the increase of temperature T5 (416mm) at 1,650s to 787°C. When the ignition propagation moved downwards and passed through each of the thermocouples the volatile gases, that evolved from the burning materials ignited by the local flames, resulted in an increase in temperature to approximately 800°C (from room temperature) in a few minutes. It was observed that, as the combustion proceeded beyond this point, a plateau temperature profile was established for about 60 minutes. During this period, heat generated by the reaction of the volatile gases with air transferred downwards to the fresh particles for further heating up and devolatilisation. This process caused the ignition front to propagate. The ignition propagation process stopped when the ignition front reached the grate area at t = 3450s, and the weight loss fraction was about 60%, as shown in Figure 6-2.

As the ignition propagation front reached thermocouples T3 (t = 2,070s) and T2 (t = 2,880s) and T1 (t = 3,450s) in region I, the temperatures rose to 1016°C, 1051°C and 1157°C, respectively. This was due to the combustion of the volatile gases and char combustion as the thermocouple T1, located just above the glowing char burning area (Figure 6-3). The char layer top was located between the grate area and T1, as can be judged by the highest temperature measured by this thermocouple. In region II (Figure 6-2), the peak of CO concentration increased gradually up to a maximum value of 22.33 %dry at t = 4,770s and a decrease of CO_2 concentration were also observed, due to the gasification of char in the hot gases.

Figure 6-2 shows the combustion gases measured during the test. It was observed that the oxygen (air) supply was insufficient to complete the combustion process. All the oxygen supplied was consumed during the combustion process; as can be observed, from time 2,000s to 5,000s, there was no oxygen left above the bed. The combustion reactions occurred at t = 810s. As the oxygen level dropped, the CO_2 concentration rose in a few seconds, reaching a maximum peak (18.1 %dry) at t = 2,070s, due to the reaction between carbon (C) in fuel and oxygen (O_2), which produced carbon dioxide (CO_2). This was followed by a decrease to a minimum (7.0 %dry) at t = 4,770s due to lack of oxygen. The carbon turned into carbon monoxide (CO); as can be observed from Figure 6-2, the

CO concentration increased steadily during this period. The air flow rate was adjusted during the combustion process to avoid a temperature overshoot beyond the reactor's limits (1,200°C) which might damage the test rig. The adjusted point is indicated by the dotted red line in Figure 6-1 and Figure 6-2 respectively. For example, the air flow rate was reduced to 200 l/min at t = 2,340s (dotted line) as the temperature approached 1,100°C.

The CO concentration was gradually increased during the period t = 2,000s to t = 5,000s, while the oxygen concentration reached a plateau, as shown in Figure 6-2. The highest peak of CO concentration was observed at 22.3 %dry, appearing at t = 4,770s. This was due to the limited amount of oxidising agent (oxygen) left in the reaction chamber during this period, as it had been consumed during the combustion of volatile gases.
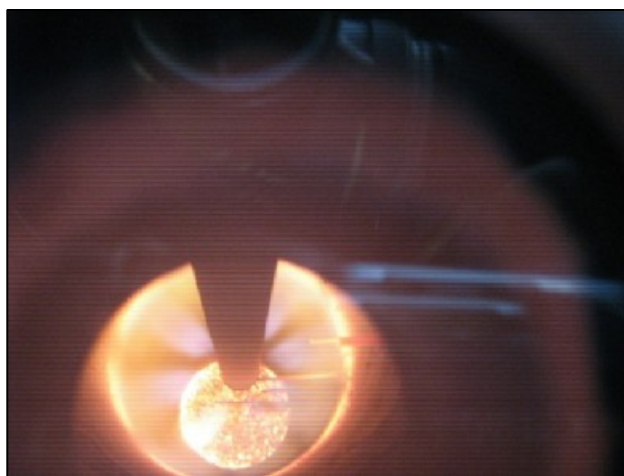
Figure 6-3: Char burning on the grate.

Figure 6-4 shows the temperature profile for the combustion of the OPS at an air flow rate of 450 l/min. In this case, the highest temperature measured for all of the thermocouples was fluctuating around 900°C. The char gasification region did not appear in this case. As soon as the ignition front reached the surface of the grate area, all temperatures began to drop. All char products were oxidised with the fresh fuel during the combustion process in region I. Two adjustments were made to the air flow rates, at t = 2,310s and t =2,820s, to 365 l/min and 330 l/min, respectively (Figure 6-4). However,

these actions did not appear to have a significant effect on the combustion process, apart from causing minor fluctuations in the temperature and gas measurements for a short period of time, as represented by the dotted lines in Figure 6-4 and Figure 6-5 respectively.
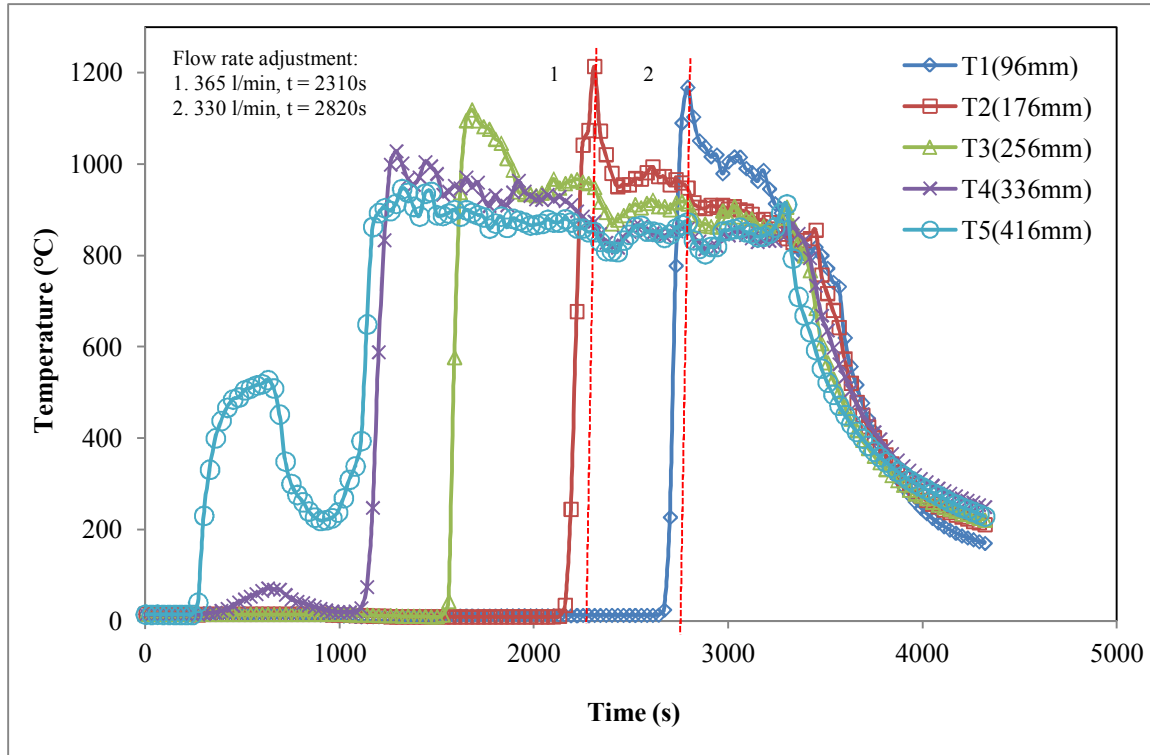
Figure 6-4: Temperature profile of the combustion of OPS at an air flow rate of 450 l/min.

Figure 6-5 shows the gas emission (CO, CO_2 and O_2) and mass losses, whilst Figure 6-6 shows the emission of NO_x during the combustion of the OPS at a flow rate of 450 l/min. In general, the gas emission profiles were similar to those with an air flow rate of 250 l/min, except that, at higher air flow rates (450 l/min), a lower gas concentration and a shorter combustion period were observed. The O_2 concentration dropped to zero after t = 1,740s and continued until t = 3,570s. The CO concentration increased gradually, from t = 1,380s to t = 2,130s, reaching a maximum peak at 14 %dry. A plateau CO concentration was observed afterwards until it dropped down at the end of the combustion process. However, the CO_2 concentration increased to a maximum

concentration of 16 %dry at t = 1,740s, and then remained at the same level for a period of approximately 30 minutes.

The NOx concentration was also measured during the combustion tests. The NOx concentration (Figure 6-6) increased to a maximum value of about 47 ppm at the initial stage (t < 1,000s). This was due to the firing of the gas burner. The NOx concentration was measured at around 5 ppm from t = 1,170s to t = 3,630s, then it increased sharply to a maximum peak value of 46 ppm at t = 3,810s. This low NOx concentration can be attributed to the reduction of NOx in the char layer which had formed on the surface of the bed. As noted by Zakaria (2000), the CO and NOx can react to form CO_2 and N_2 using carbon in char as the reagent. An increase in NOx concentration at t = 3810s was due to the char gasification reaction. Fuel nitrogen is converted into intermediate products, such as HCN and NH_i (i = 0, 1, 2, 3), which can react with oxygen to form NOx (Nussbaumer, 2003).
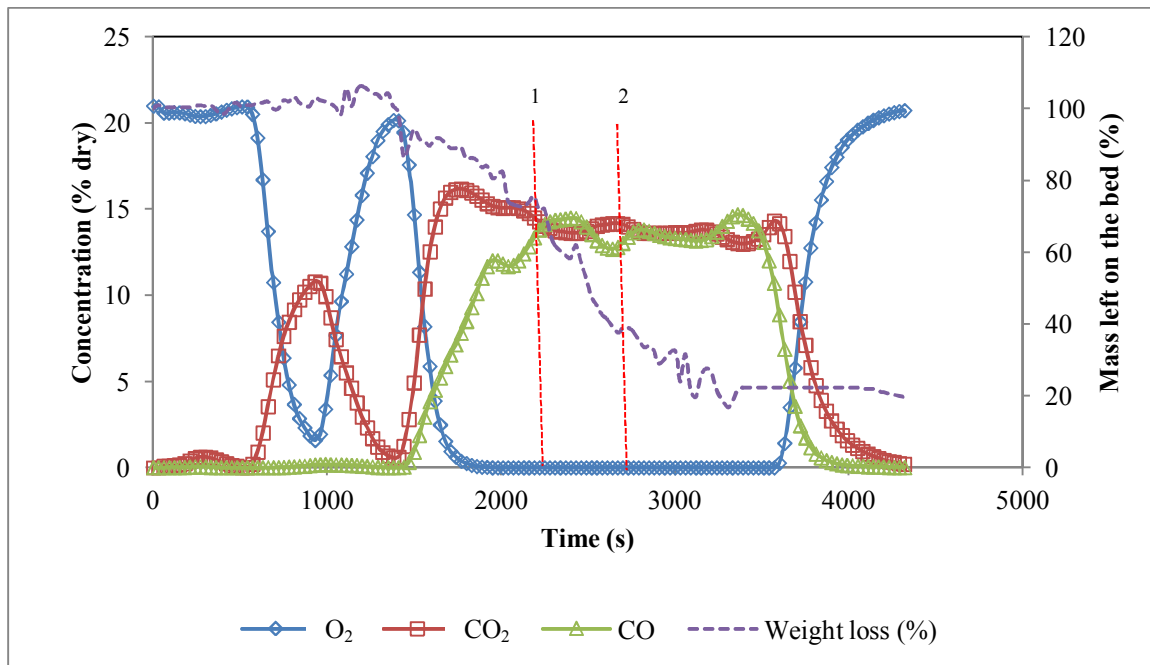
Figure 6-5: Gas emission and mass left on the bed for the combustion of the OPS at an air flow rate of 450 l/min.
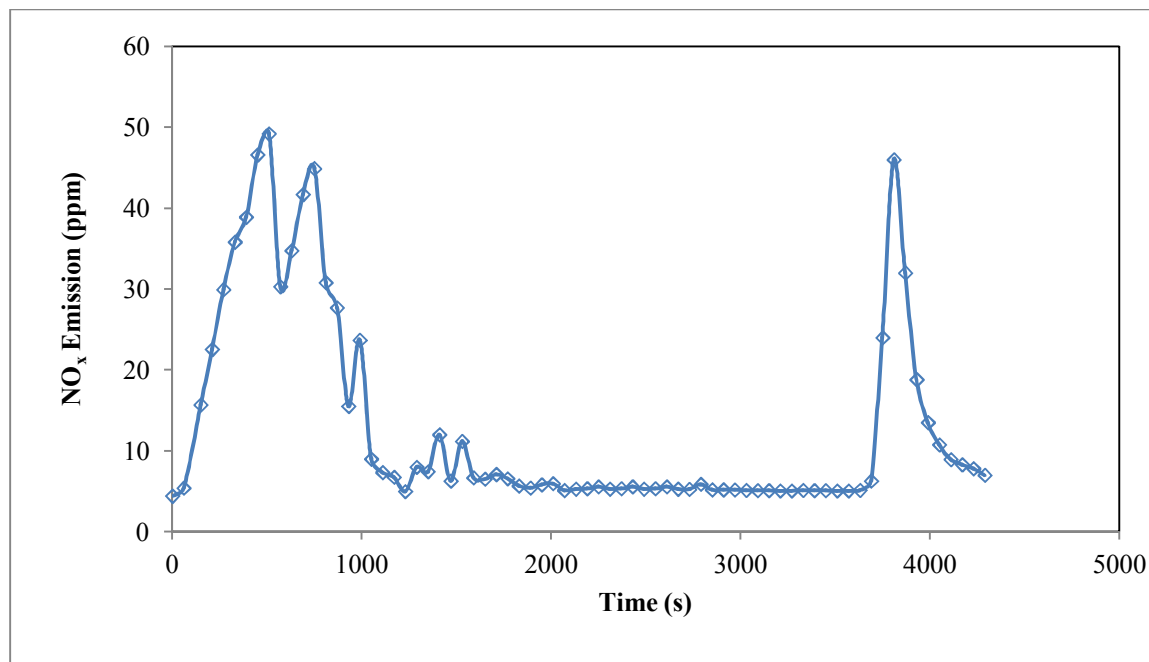
Figure 6-6: Oxides of nitrogen concentration from the combustion of the OPS at an air flow rate of 450 l/min.

Figure 6-7 shows the temperature profiles, and Figure 6-8 illustrates the gas emission and mass left on the bed by the combustion of 4 kg OPS at an air flow rate of 600 l/min. In this case the fuel bed thickness was approximately 200 mm. The ignition front was propagated from the top of the bed at a slower rate compared to previous cases (250 l/min and 450 l/min) with temperatures around 900°C.

The typical compositions of the gases are shown in Figure 6-8. Initially, as the combustion process started at the top of the waste surface, at about 200 mm above the grate area, there was no indication of combustion at the locality of the gas measuring probe. Therefore, no combustion gases (CO and CO_2) were observed, except a high O_2 concentration, indicating that no combustion reaction was occurring in this position (t < 300s).

The ignition front started at approximately t = 350s, the O_2 concentration decreased sharply to a value of about 14.88 % dry at t = 570s, and the CO_2 concentration rose dramatically to a value of around 3.1 % dry at t= 600s. The CO concentration levelled out at zero percent. As the combustion process progressed further, between t = 540s and t = 1,710s, the O_2 concentration showed fluctuating values of between 10 to 16 %dry, and the CO_2 production of between 3 to 7 %dry. The weight loss of the fuel bed showed that the percentage of mass loss during the combustion process was almost constant during the initial period, from t = 300s to t = 1,890s. However, there was a mass loss after combustion reactions occurred between t = 2,250s and t = 3,300s.

At approximately t = 1,710s, it was observed that there was a sharp decrease in O_2 concentration to zero percent, at t = 2,400s. At the same time, the concentration of CO_2 rose steadily, reaching a maximum value of 17 %dry, and then showing fluctuating values of between 15 to 17 %dry until the end of combustion process. A plateau concentration of O_2 at zero percent was established between t = 2,400s and t = 3,300s. The CO concentration increased between t= 2,250s and 2,500s to reach a peak value of 11 %dry, followed by a drop at t = 2,730s to a value of 9 %dry. It then increased to a maximum value of 16 %dry at t = 3,000s, before decreasing until the end of the combustion process.
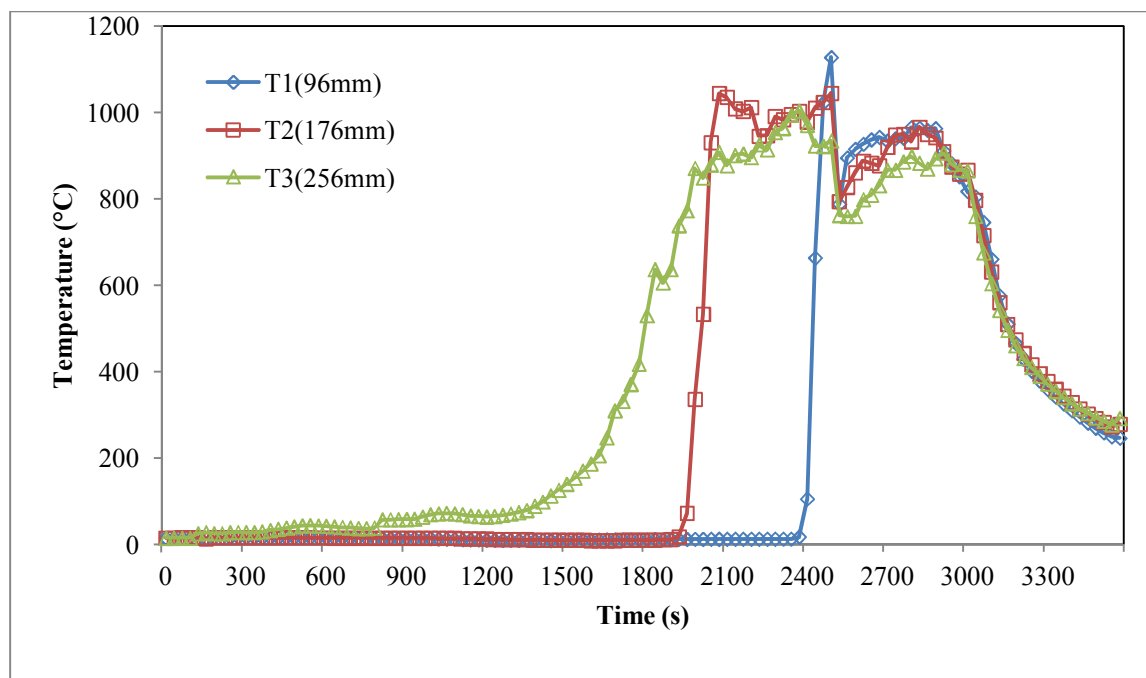
Figure 6-7: Temperature profile of the combustion of the OPS at an air flow rate of 600 l/min.
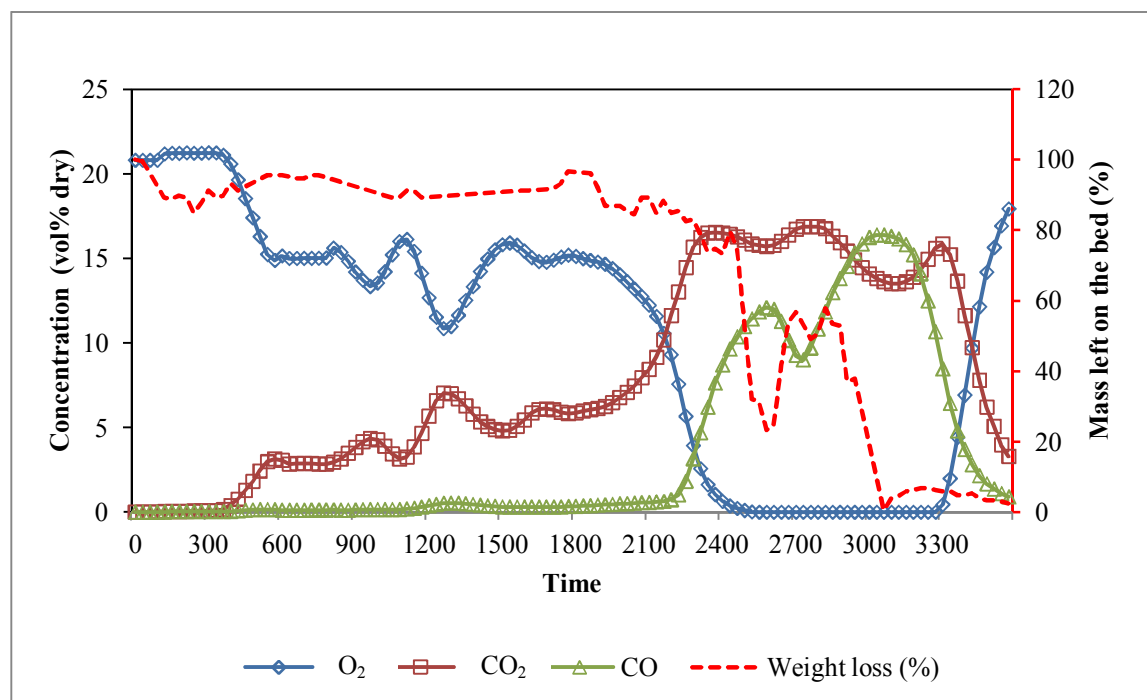
Figure 6-8: Gas emission and mass left on the bed for the combustion of the OPS at an air flow rate of 600 l/min.

The highest air flow rate used in this study was 650 l/min. The temperature profile obtained during the combustion process is shown in Figure 6-9. The weight loss during the combustion process and the gas emissions (CO, CO_2 and O_2) are presented in Figure 6-10. The NOx emissions measured from the combustion of OPS at 650 l/min are shown in Figure 6-11. The temperatures were fluctuating from 700 to 1100°C. Similar to the previous cases, except for the case of 250 l/min, no indication of char gasification took place when the ignition front reached the grate area. This is because the air supply is sufficient to burn the char. Thus the char gasification stage does not occur (Ryu *et al.*, 2009).
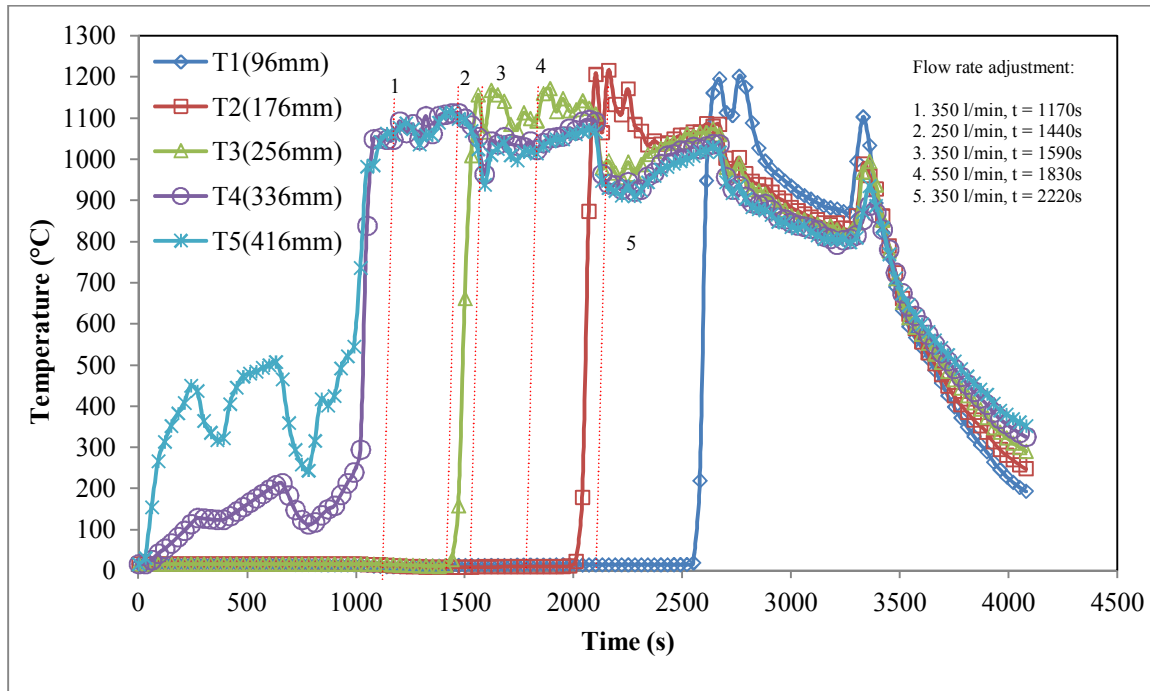
Figure 6-9: Temperature profile of the combustion of the OPS at an air flow rate of 650 l/min.

Figure 6-10 shows the gas emission and mass loss at the flow rate of 650 l/min. The gaseous emission profiles showed the trends which were quite similar to the previous three cases. However, in this case, the concentration of CO_2 was much higher compared to the CO level. This showed that the combustion process was improved even though the oxygen supplied was insufficient to complete the combustion process. The NOx

concentration levelled at approximately 5 ppm from the ignition stage. A plateau concentration was established subsequently up to t = 2,880s. After this point, the NOx increased steadily, to a maximum concentration of 21 ppm at the end of the process, at t = 3,540s. A similar trend for the NOx concentration with the case of an air flow rate of 450 l/min was observed and the reason for the high concentration of NOx at the end of the combustion process was similar to the 450 l/min case.
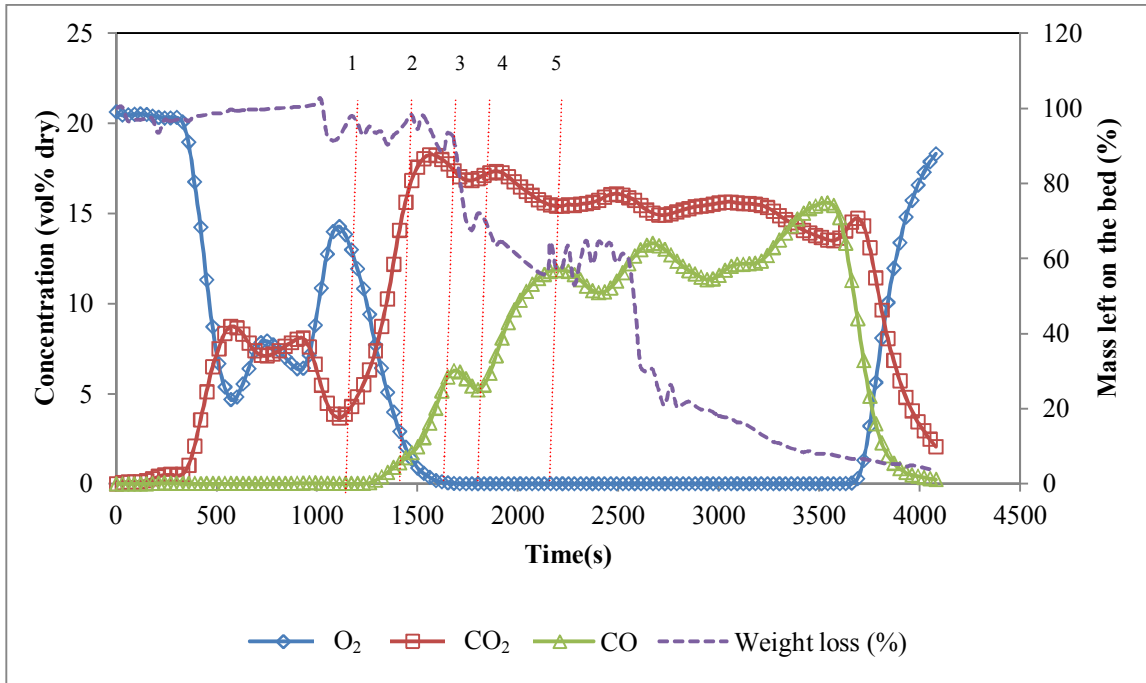
Figure 6-10: Gas emission and mass left on the bed for the combustion of the OPS at an air flow rate of 650 l/min.
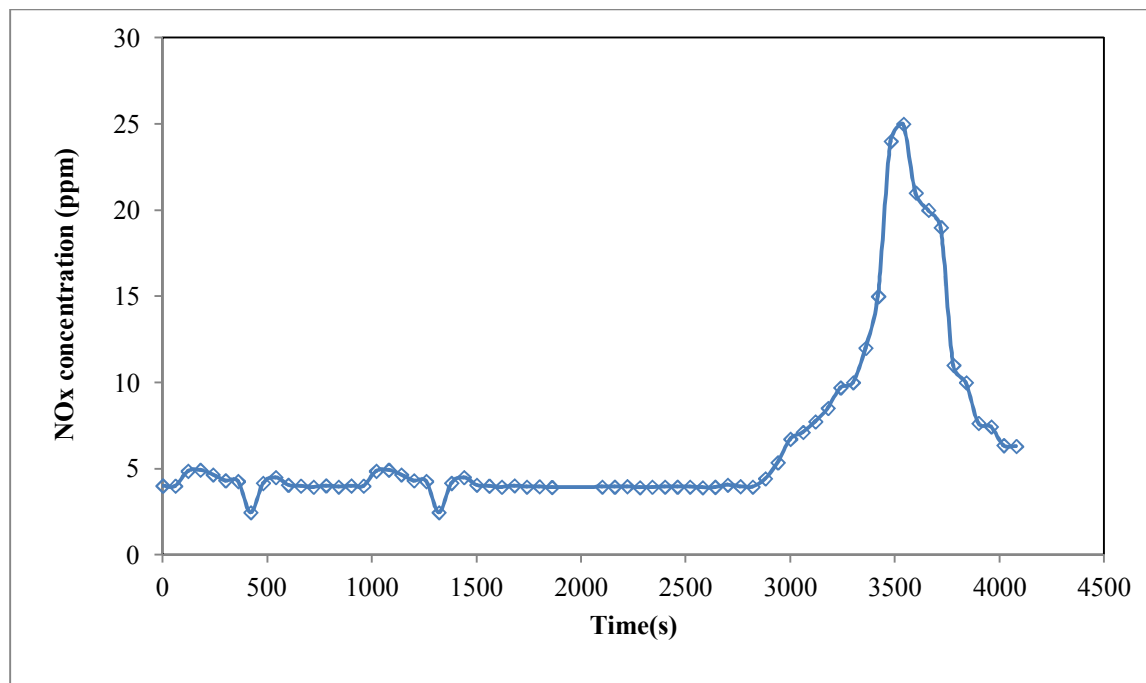
Figure 6-11: Oxides of nitrogen concentration from the combustion of the OPS at an air flow rate of 650 l/min.

6.1.2 Effect of air flow rate on combustion behaviour

The important characteristics of the combustion process in a fixed bed reactor are the ignition rate, burning rate and percentage of mass loss in the ignition stage. Figure 6-12 shows the average ignition and burning rates, and the ignition front speed for the combustion of the OPS at various air flow rates. The results showed that the burning rates increased with an increase in the air flow rate. The ignition rate and ignition front speed were low at the lower air flow rate (250 l/min); however, both properties were almost constant at the air flow rates of 450 and 650 l/min respectively. It was also observed that the burning rate was lower than the ignition rate. This suggested that there was some unburnt fuel left above the ignition front.
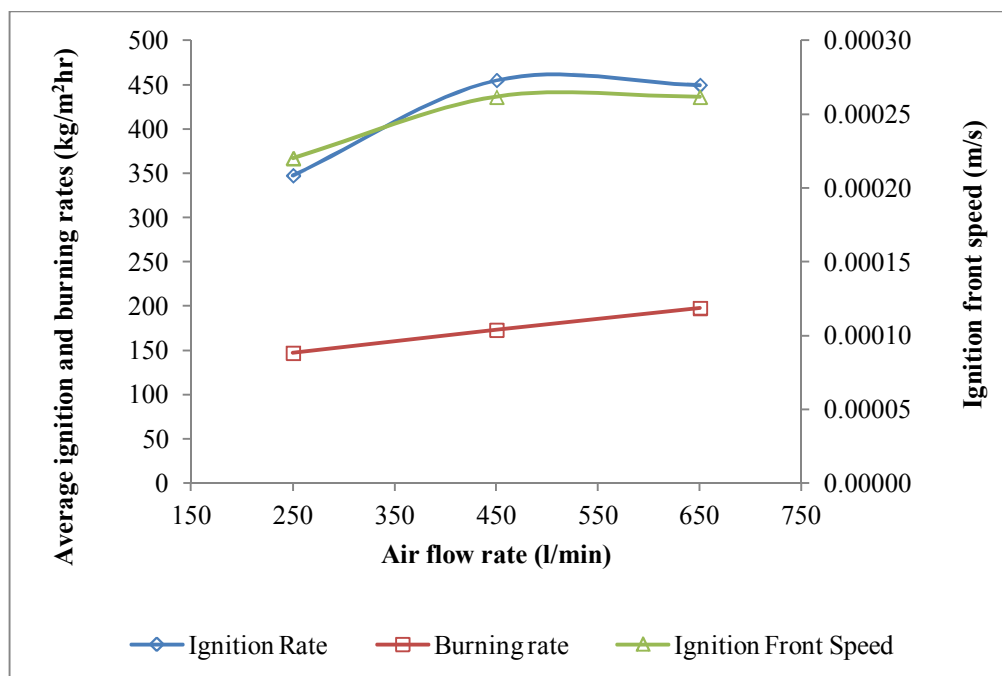
Figure 6-12: The ignition and burning rates of the combustion of OPS at different air flow rates.

The weight loss during the combustion of the OPS at three different air flow rates is shown in Figure 6-13. A higher air flow rate shows a faster weight loss. This finding is in agreement with Ryu et al., (1999) and Zakaria, (2000). However, high air flow rate caused the flame to be extinguished due to the high rate of cooling air in the reaction zone. This resulted in the cooling of the burning bed and a lowering of the reaction rate of the gaseous reactants as well as the char. The air flow rate was not high enough to cool the reaction zone and the flame was observed during the tests.

Figure 6-14 shows the unburnt carbon in ash samples obtained from the combustion of the OPS at three different air flow rates. At the air flow rate of 250 l/min, the unburnt carbon was 3.02 wt%, at the air flowrate of 450 l/min, the unburnt carbon was 3.59 wt% and at the highest air flow rate (650 l/min), the unburnt carbon was observed to be 1.08 wt%. This low percentage of unburnt carbon in ash may be due to the formation of soot during the combustion process at 700-800°C. This soot was easily burnt in the burn-out stage at temperatures higher than 800°C (Phan, 2007).
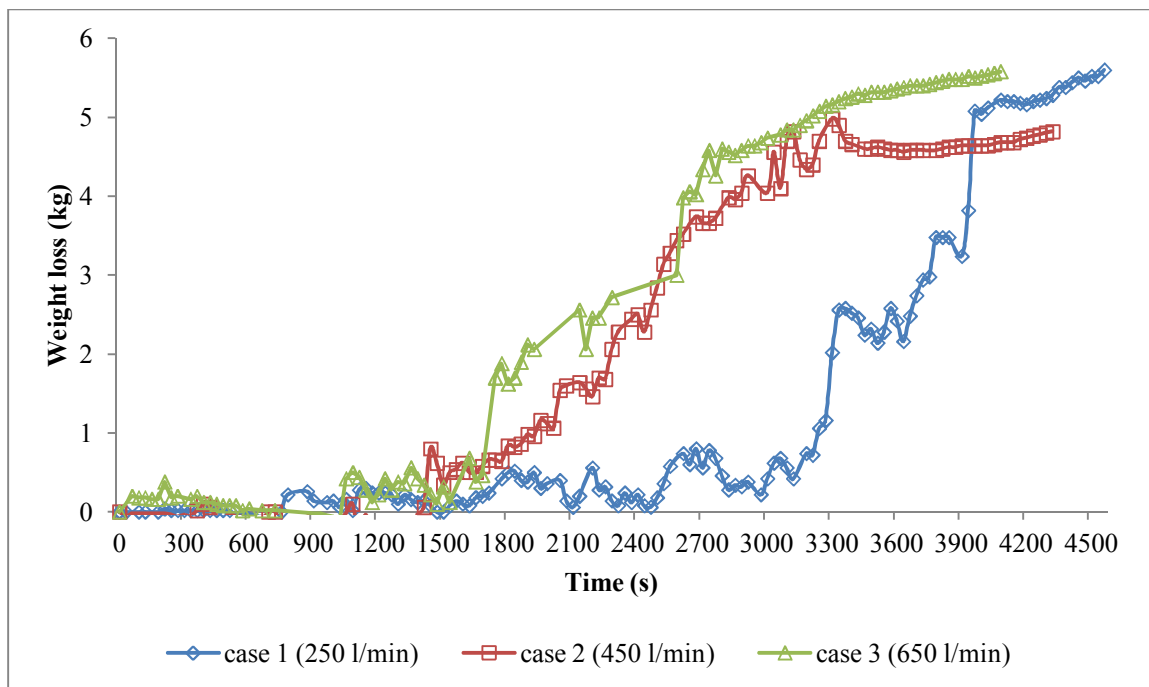
Figure 6-13: Weight loss during the combustion process.
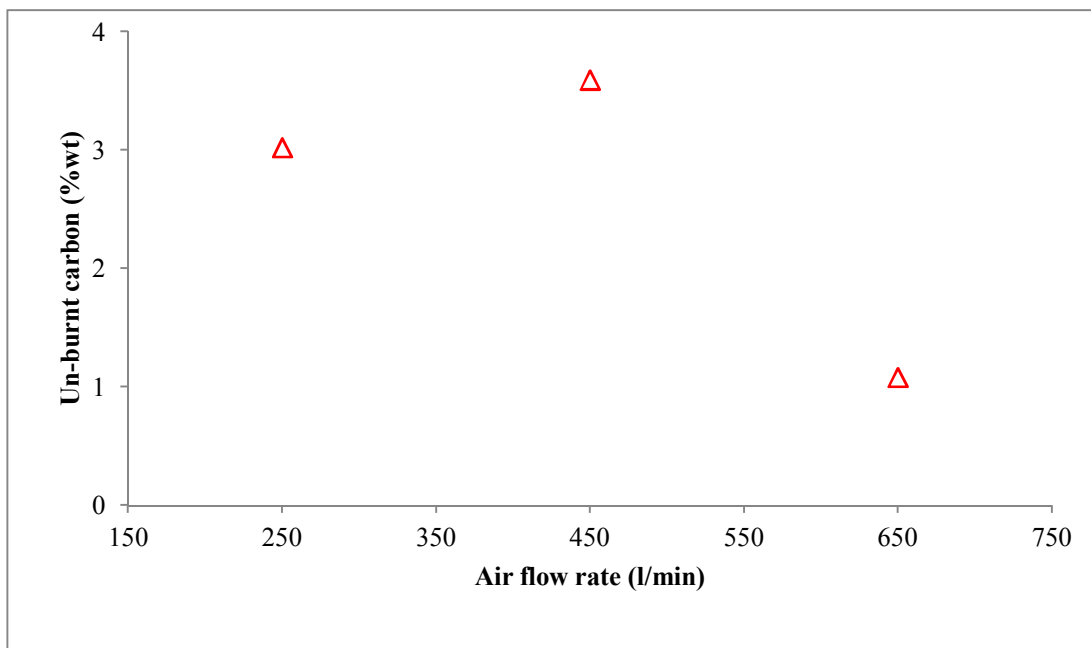
Figure 6-14: Unburnt carbon in bottom ash at various air flow rates.

6.1.3 Comparison between the experimental and FLIC modelling results for fixed bed combustion

The Fluid Dynamics of Incinerator Combustion Code (FLIC), developed at Sheffield University Waste Incineration Centre (SUWIC), was used to model the combustion of a solid fuels bed in a fixed bed reactor. FLIC was designed primarily to model the burning characteristics of a moving waste bed. However, it can also be adapted to deal with a fixed bed reactor. This model assumes the fuel bed to be a one-dimensional fuel bed of uniform fuel particles. Three main combustion stages (moisture evaporation, devolatilisation and the char burn-out of the solid phase), as well as the reaction in the gas phase, are considered by various sub-models, along with various modes of heat transfer. In this study FLIC modelling was used to predict the influence of air flow rates on the combustion of the OPS in a fixed bed reactor.

In order to compare FLIC modelling data with the experimental results some preliminary calculated data was input into the computer programme. The input data for the numerical cases are shown in Table 6-1. The bed height of 240 mm to 416 mm was divided into 300 computational cells. The time step was set at 5 seconds for every test. The particle diameter was assumed to be 10 mm and the ignition temperature was 1373 K. The model assumes the particle shape to be spherical, which is calculated based on a surface-volume average. This is because the rates of moisture evaporation and char burnout, as well as the heat transfer to the particle surface, are derived using the total surface area of the solids.

Table 6-1: Major input conditions and model parameters for fixed bed combustion.

Model parameters	Sample (OPS)		
Bed height (mm)	361	361	240
No of cells	300	300	300
Time step (s)	5	5	5
Fuel:			
Size (mm)	10 (100%)	10 (100%)	10 (100%)
Moisture (%)	4.71	4.71	4.71
Volatile (%)	86.5	86.5	86.5
Char (%)	6.55	6.55	6.55
Ash (%)	2.24	2.24	2.24
Oxidiser:			
Type	Air	Air	Air
T (K)	298	298	298
N (Nm^3/min)	0.241	0.434	0.579
Bed voidage fraction- ε	0.65	0.65	0.65
Pyrolysis:			
A (1/s)	5160000	5160000	5160000
E/R (K)	10700	10700	10700
Char Gasification:			
A (kg/m^2/s/kP(n)/K(m)	2.3	2.3	2.3
E/R (K)	11100	11100	11100

6.1.4   Numerical Model Prediction

6.1.4.1   Temperature Profile

The solid temperature profile obtained from the FLIC computational modelling for the fixed bed combustion of the OPS at an air flow rate of 250 l/min is shown in Figure 6-15. The temperature was predicted as fuels gradually burnt down towards the grate. The top fuel bed burnt at around t = 600s due to the over-bed radiation. The temperature was approximately 600 K. The fuel bed started to decrease from the initial bed height of 361 mm at t = 600s. During this combustion period, the moisture bound in the fuel started to evaporate. As combustion progressed further, the fuel bed decreased steeply, until it reached the grate area at t = 3,900s. The highest temperature measured during this period was around 800-1,000 K, due to the combustion of volatile gases. The maximum

temperature obtained from this modelling work was approximately 1,500 K at t = 4,000s. The high temperature measured at this point was due to the combustion of volatile gases and radiation heat transfer from the reactor wall, as well as the heat released from the char combustion reaction.
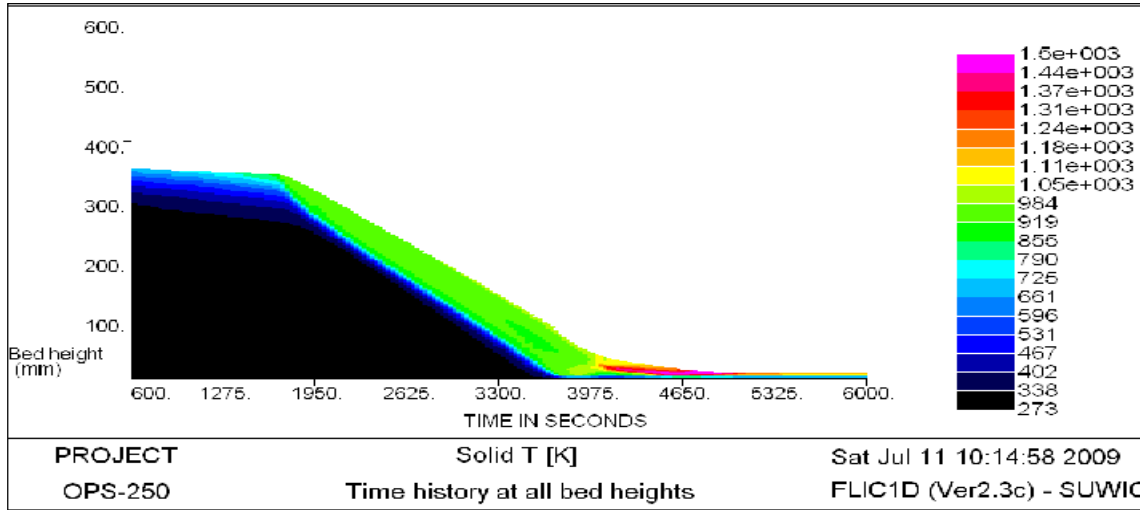
Figure 6-15: Predicted solid temperature distribution in the fixed bed combustion of the OPS at 250 l/min.

Figure 6-16 shows the predicted temperature profile in the fixed bed combustion of the OPS with an air flow rate of 450 l/min. The maximum temperature measured from this case was around 1,533 K. The combustion period for this case was around 2,700s, compared to about 4,000s in the case of an air flow rate 250 l/min. At higher air flow rate the combustion of volatiles and char occurred simultaneously, so that more heat was released within the combustion chamber. The fuel bed burnt vigorously within a short period of time.
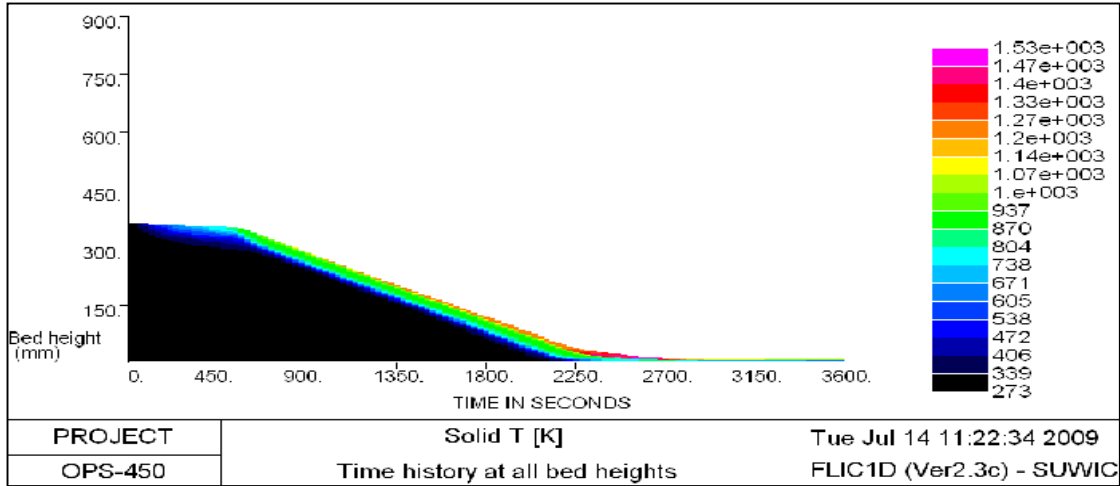
Figure 6-16: Predicted solid temperature distribution in fixed bed combustion of OPS at 450 l/min.

Figure 6-17 shows the temperature profiles obtained from modelling the fixed bed combustion of the OPS at the highest air flow rates of 600 l/min. The temperature profile obtained from the calculated values was higher compared to the case of the low air flow rate, at 250 l/min and 450 l/min. The maximum temperature measured for this case was around 1,720 K. As can be seen from Figure 6-17, the calculated combustion period was far shorter, at about 2,500 s compared to the previous two cases (250 l/min and 450 l/min).
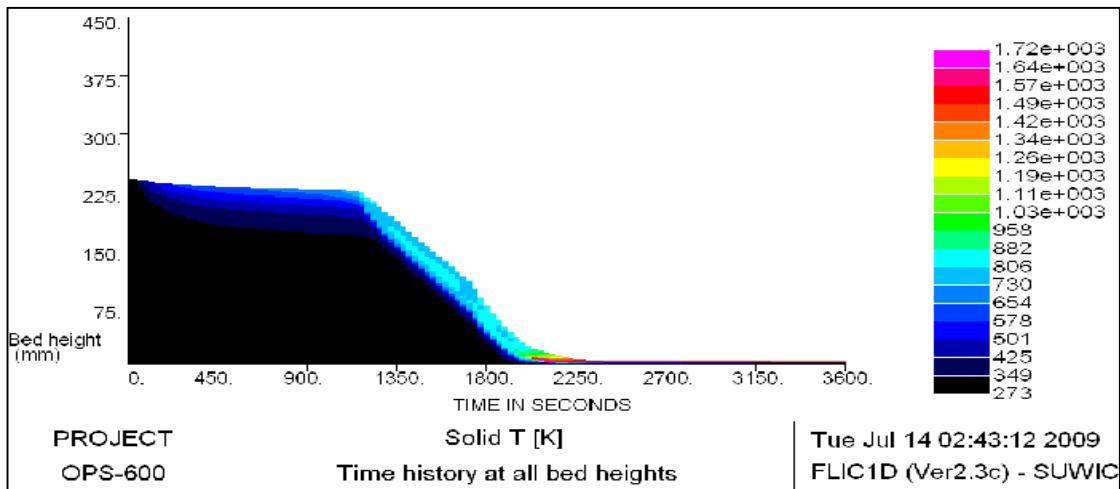
Figure 6-17: Predicted solid temperature distribution in the fixed bed combustion of the OPS at 600 l/min.

6.1.4.2 Comparison between the experimental and modelled results

A comparison of the gas emission distribution profiles between the modelled and experimental results are shown in Figure 6-18 to 6-20 for air flow rates of 250 l/min, 450 l/min and 600 l/min, respectively. In general, it can be seen that there is good agreement between the experimental and modelled results in terms of the distribution trends for all cases. However, there were some minor discrepancies observed between the predicted and measured results. All cases predicted a slightly lower concentration of CO and CO_2. This was due to un-burnt volatile compounds mostly C_mH_n, during the combustion process. These under-predicted results may also be due to char gasification. In the current modelling calculations, the char was assumed to be pure carbon; however, in fact, it consisted of a small amount of hydrogen and oxygen, as well as trace metals, such as potassium, calcium and iron. These trace elements can act as catalysts during char gasification, which leads to an increase in the concentration of CO during experimental study research. The combustion period for all the cases showed that the predicted results were shorter compared to the experimental results.
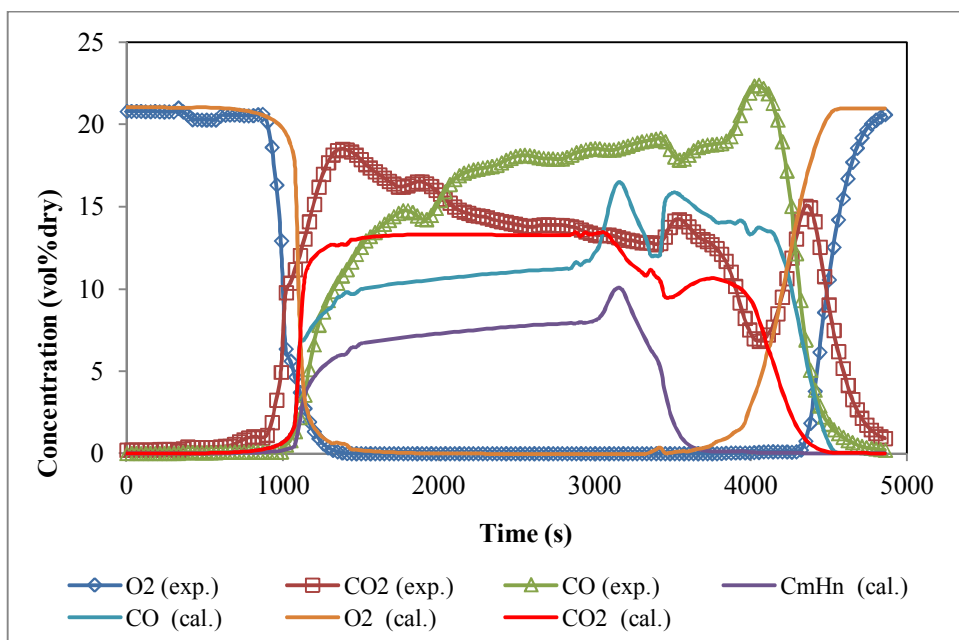
Figure 6-18: Measured and predicted gas emissions from the combustion of the OPS in a fixed bed reactor at an air flow rate of 250 l/min.
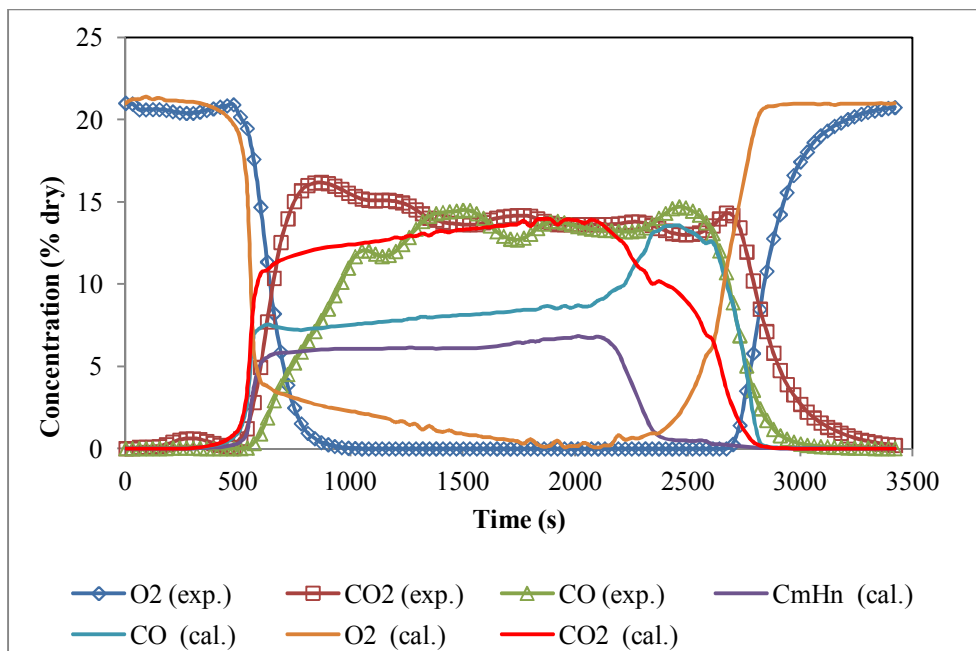
Figure 6-19: Measured and predicted gas emissions from the combustion of the OPS in a fixed bed reactor at an air flow rate of 450 l/min.
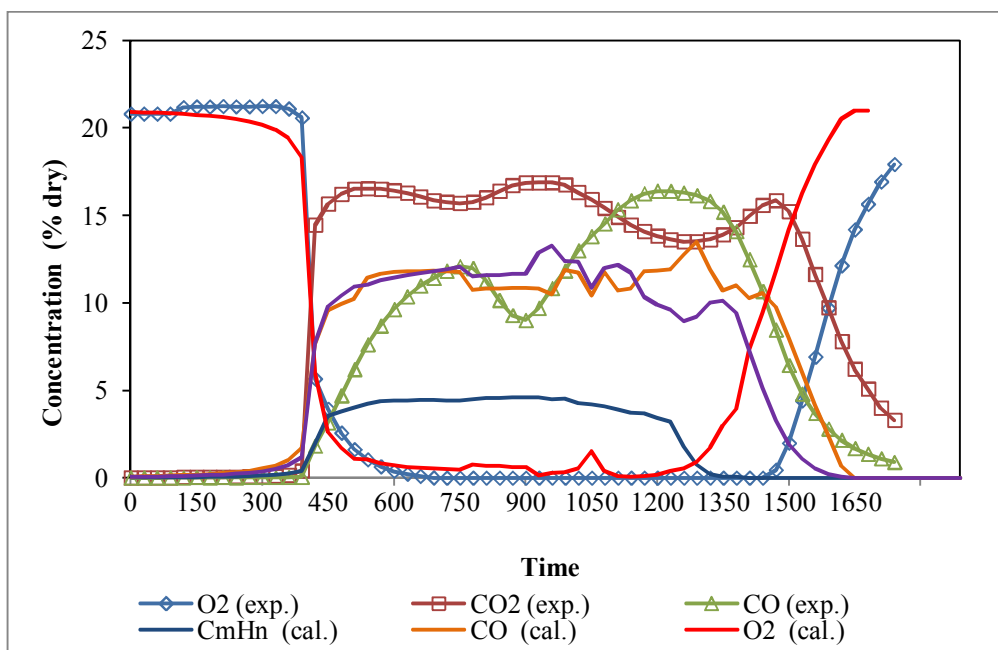
Figure 6-20: Measured and predicted gas emissions from the combustion of the OPS in a fixed bed reactor at an air flow rate of 600 l/min.

6.2   Pilot-scale fluidised bed reactor

This section discusses the results of the combustion tests carried out in the pilot-scale fluidised bed combustor. A series of combustion tests of oil palm stone (OPS) were carried out in the pilot-scale fluidised bed combustor. The tests were conducted to evaluate the effects of combustion air and bed temperatures on combustion characteristics in pilot-scale fluidised bed combustor. The operating conditions are summarised in Table 4-5 to Table 4-7.

6.2.1   Combustion characteristics

 A series of combustion tests were carried out on the OPS in the pilot-scale fluidised bed combustor. Two parameters, primary air and initial bed temperature were the main focus of this combustion study. The primary air was varied from 791 kg/m^2hr to 1,187 kg/m^2hr. Initial bed temperatures ranged from 850°C to 950°C.

The results and data from these tests are shown in Table 6-2 and Table 6-3. The temperature profiles from various primary air flows are shown in Figure 6-22, Figure 6-24 and Figure 6-26. Whereas Figure 6-23, Figure 6-25 and Figure 6-27 show the gas emission trends from the combustion process. Figure 6-29, Figure 6-31 and Figure 6-33 show the temperature profiles at different initial bed temperatures, whilst Figure 6-30, Figure 6-32 and Figure 6-34 show the concentration of combustion gases at different initial bed temperatures. Unstable patterns at the initial process were due to the combustion of propane during the pre-heat process. There were some delays (10-15 minutes) observed in the gas emission measurements. This may be due to several factors including; the long piping system between sampling probe and the gas analysers.

The secondary air, fuel feed rate and the bed depth were maintained at 356 kg/m^2hr, 1.2 kg/hr and 0.25 m respectively in all cases. Propane gas was used to pre-heat and stabilise the temperature of the reactor to around 800-850°C before the tests began.

6.2.2 Effect of manipulating the primary air flowrate on combustion characteristics

6.2.2.1 Temperature profile

Eight thermocouples were used to monitor the temperature throughout the test rig as described in section 4.2.2.2. However, only four thermocouples which represent the temperature of the bed (T7=0.20m), temperature at the surface of the bed (T5=0.42m) and freeboard temperatures (an average of T2=1.54m and T3=0.76m) were used to monitor the combustion temperature.   Figure 6-22, Figure 6-24 and Figure 6-26 shows the temperature profiles measured at different primary air flowrates, 791 kg/m^{2}hr, 989 kg/m^{2}hr and 1187 kg/m^{2}hr respectively. The trends revealed in all three cases were almost identical. The temperature of the bed (T7=0.2m) gradually dropped moments after introduction of sample into the reactor, however it was stabilised at around 750°C during the combustion period. A plateau was observed in the temperature above the bed (T5=0.42m). This indicates that the combustion occurred steadily during test periods. The intermittent pattern during the combustion period may be due to fuel feeding conditions. The freeboard temperature (an average of T2=1.54m and T3=0.76m) increased steadily over time. The highest temperature achieved at the freeboard was observed at 650-680°C.

Figure 6-21 shows the effect of varying primary air flowrate on temperatures at three different locations; bed (T7=0.2m), surface of the bed (T5=0.42m) and freeboard (an average of T2=1.54m and T3=0.76m). The bed (Tbed) and bed surface (Tbedsurface) temperatures were found to be quite uniform at around 750-850°C. However, freeboard temperature was slightly lower at around 600-620°C. In general, the bed and bed surface temperatures decreased as the primary air flowrate increased. The freeboard temperature was observed to be more uniform and almost independent of primary air.
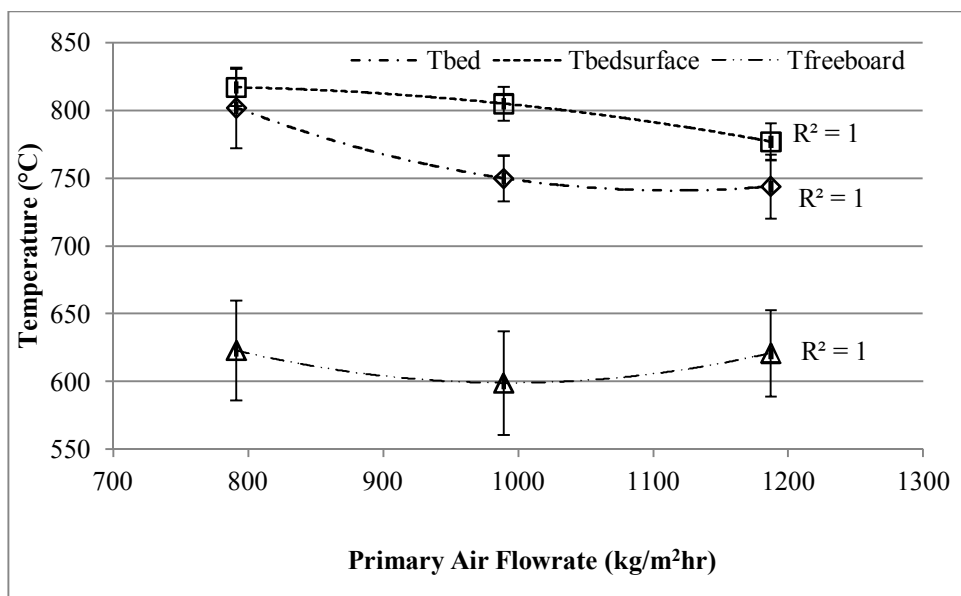
Figure 6-21: Trends for the temperatures across the rector at different primary air flowrate.

6.2.2.2 Acid gas emissions

The average NOx concentrations for all cases are shows in Table 6-2. The amount of NOx released during combustion process was relatively low from 162ppm to 238ppm. The potential nitrogen in the fuel converted to nitrogen oxides was 1.65%. Thermal-, prompt- and fuel-NO were considered the main sources of NOx formation during combustion process. Thermal-NO occurred at higher temperature (>1,300°C) during oxidation of molecular nitrogen with oxygen in the combustion air. Fuel-NO is formed during oxidation of nitrogen species bound in the fuel. Whereas, prompt-NO formed as a result of radical CH reacts with nitrogen from the combustion air to form HCN. At high temperatures HCN species reacts further to form NO (Werther *et al.*, 2000). NO is also formed via reactions of molecular nitrogen through intermediate compounds, for example nitrous oxide (N_2O) at low temperature. In fluidised bed combustion, NO and N_2O are mostly derived from nitrogen bound in fuel due to the low combustion temperature. However, N_2O species is a minor product of the combustion process. It is rapidly reacted with hydrogen to form the molecular nitrogen and hydroxyl by the reaction: $N_2O + H \rightarrow N_2 + OH$ (Winter *et al.*, 1999). According to Burling *et al.*, (2010) less than 1% of N_2O contributed to the nitrogen balance of the fuel nitrogen.

221

In this study, all pilot-scale fluidised bed combustion tests were conducted at the temperatures around 800-900°C, therefore the tendency of the NOx formation was low, hence the NOx formation depends only on fuel nitrogen (Hernandez-Atonal, 2007, Bis, 2010). Burling *et.al.*, (2010) studied gas emissions from biomass fired fuel. They concluded that the emission of the nitrogen-containing species were dependent on nitrogen content in the fuel. The directly proportional relationship between fuel-nitrogen content and the NOx emission was also established. The OPS contains low Nitrogen content (Table 7-1), thus the tendency of NOx formation is low.

Gas-phase hydrogen chloride (HCl) is an important species to analyse during combustion of biomass. This chemical species has a tendency to promote corrosion in the combustion systems. The main source of HCl formation is from chloride ions (Cl^-) contain in raw materials (Burling *et al.*, 2010). Chloride ions play an important role in plant growth through photosynthesis. The concentration of HCl present was calculated based on the assumption that all chloride ions in the gas phase were present in the form of HCl. The concentrations of HCl measured in all cases (Table 6-2 and Table 6-3) were below 0.05 ppm. This value falls below the minimum permitted level given by the waste incineration directive (WID) at 10 mg/m^3(6.70 ppm) (WID, 2009)

Sulphur dioxide (SO_2) was emitted with very low concentration during combustion of oil palm stone as shown in Table 6-2 and Table 6-3. SO_2 emissions depend on the sulphur content in the fuel and its burning behaviour (Burling *et al.*, 2010). The oil palm stone (fuel) used in this study contains very low sulphur content (< 0.01%). This is reflected in the lower concentration of SO_2 in flue gas captured during combustion process.

Table 6-2: The summary of test parameters and combustion characteristics of oil palm stone in pilot-scale fluidised bed reactor at various primary air flowrates.

Parameters		Case 1	Case 2	Case 3
Fuel feedrate (kg/hr)		1.2	1.2	1.2
Primary air (kg/m^{2}hr)		791	989	1187
Secondary air (kg/m^{2}hr)		356	356	356
λ(AFR/AFR$_{Stoic}$) based on primary air		1.20	1.50	1.80
λ(AFR/AFR$_{Stoic}$) actual		1.72	2.02	2.32
Average gas concentration	CO$_2$ (%)	15.11	13.32	9.15
	CO (%)	0.19	0.13	0.08
	O$_2$ (%)	8.72	9.86	13.16
	NOx (ppm)	232	238	162
	SO$_2$(ppm)	0.02	0.05	0.04
	HCl(ppm)	0.02	0.03	0.02
Average temperature (°C)	Bed	802	750	744
	Surface of the bed	871	805	777
	Freeboard	623	599	621
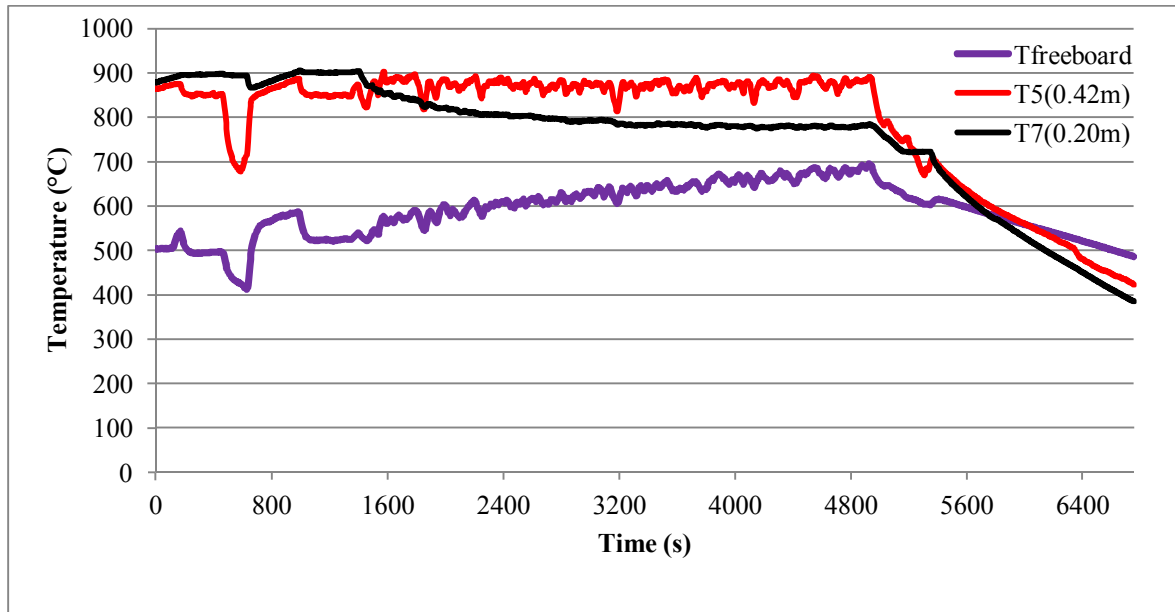
Figure 6-22: Temperature profiles for the combustion of oil palm stone in the pilot-scale fluidised bed reactor at a primary air flow of 791 kg/m^{2}hr.
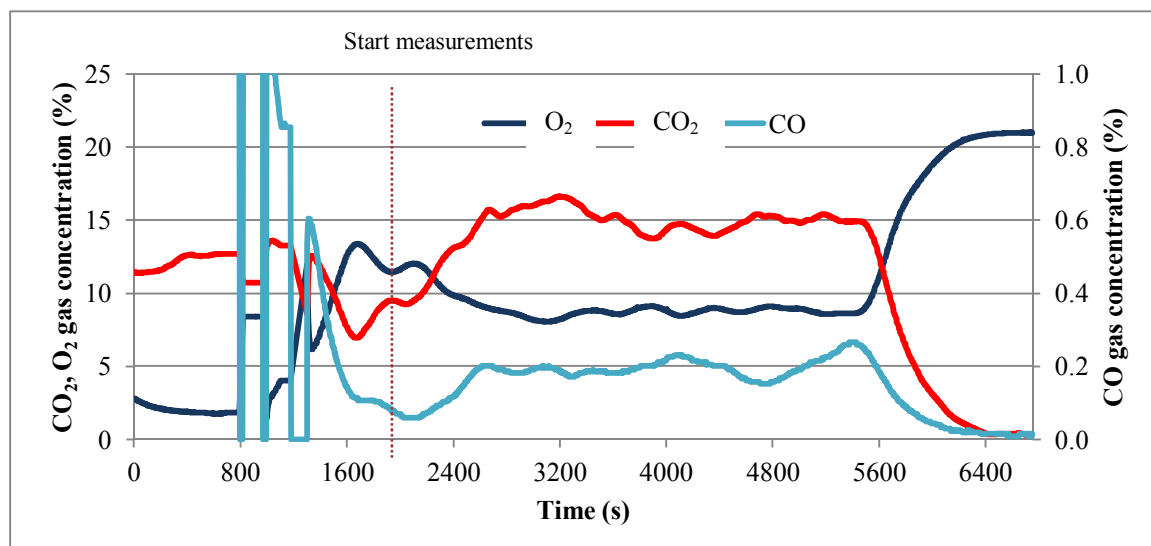
Figure 6-23: Gas emission from the combustion of oil palm stone in the pilot-scale fluidised bed reactor at a primary air flow of 791 kg/m^{2}hr.
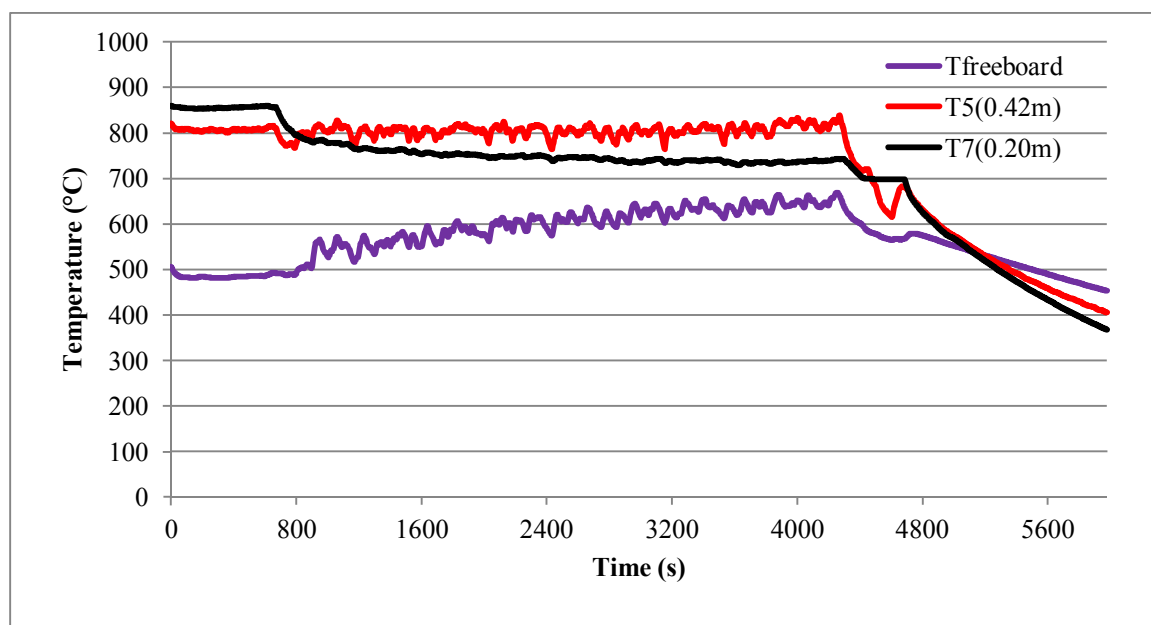
Figure 6-24: Temperature profiles for the combustion of oil palm stone in the pilot-scale fluidised bed reactor at a primary air flow of 989 kg/m^{2}hr.
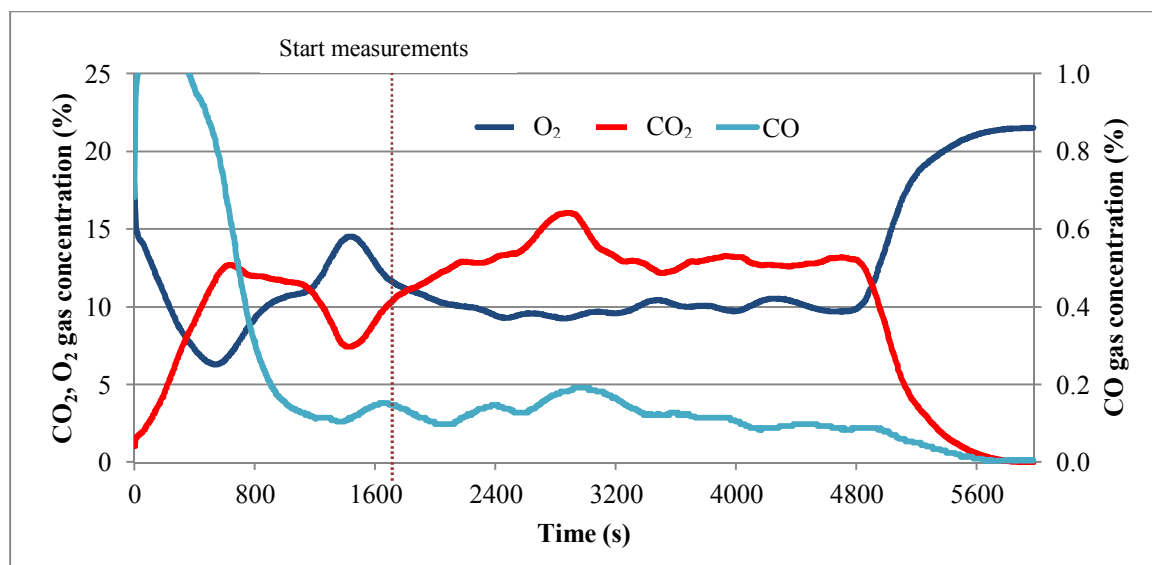
Figure 6-25: Gas emission from the combustion of oil palm stone in the pilot-scale fluidised bed reactor at a primary air flow of 989 kg/m^{2}hr.
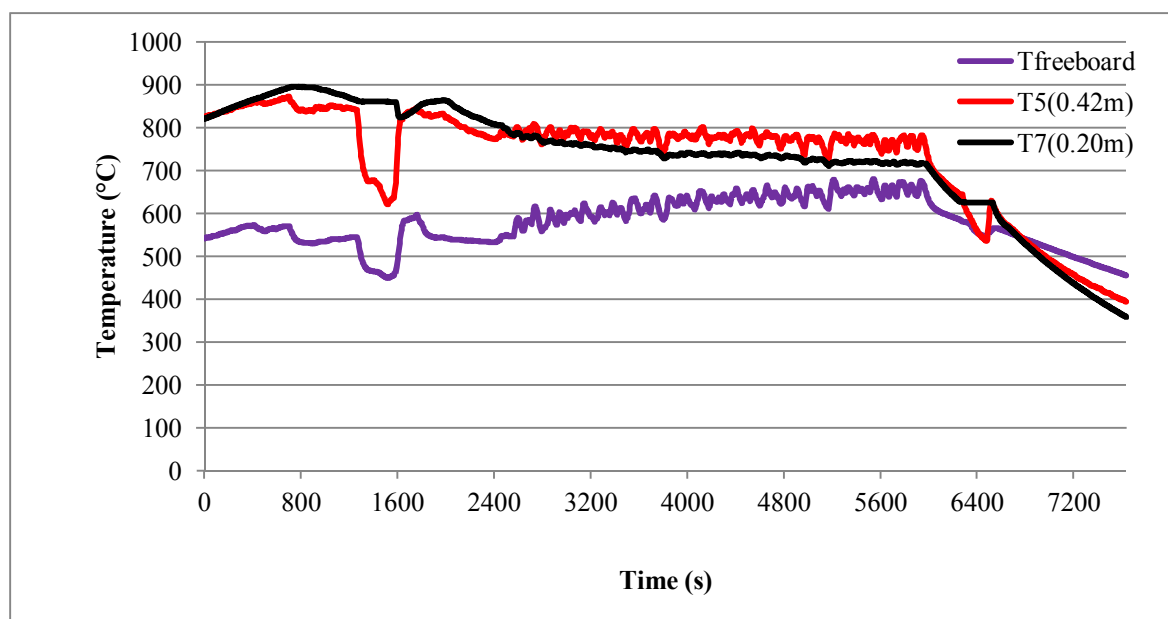
Figure 6-26: Temperature profiles for the combustion of oil palm stone in the pilot-scale fluidised bed reactor at a primary air flow of 1187 kg/m^{2}hr.
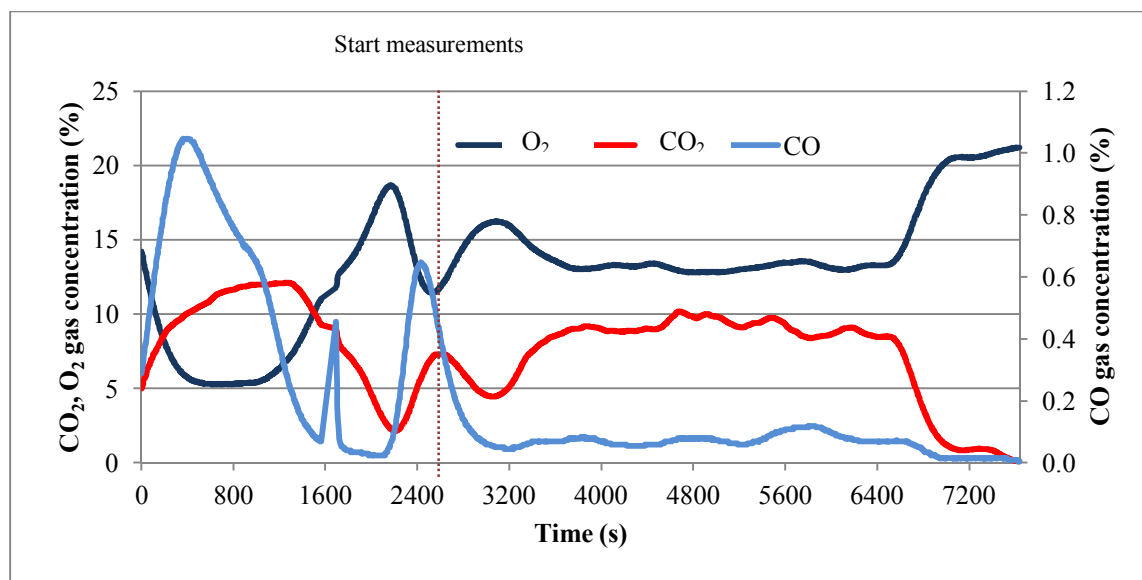
Figure 6-27: Gas emission from the combustion of oil palm stone in the pilot-scale fluidised bed reactor at a primary air flow of 1187 kg/m²hr.

6.2.3   Effect of primary air flowrate on gas emissions

Figure 6-23, Figure 6-25 and Figure 6-27 shows the gas emission for all three cases. In general, CO gas concentration decreased as primary air increased. Figure 6-28 shows the flue gas concentration O_2, CO_2 and CO at different primary air flowrate and thus the air ratio and stoichiometry of combustion. As discussed in the experimental operating condition in section 4.2.2.2 above, this combustion process was not aimed at the fuel-rich (sub-stoichiometric) region. All tests were conducted with 20-80% excess air. From this figure, it can be seen that CO_2 concentration decreased while O_2 increased as primary air increased. The CO concentration was significantly low giving an indication of complete combustion.
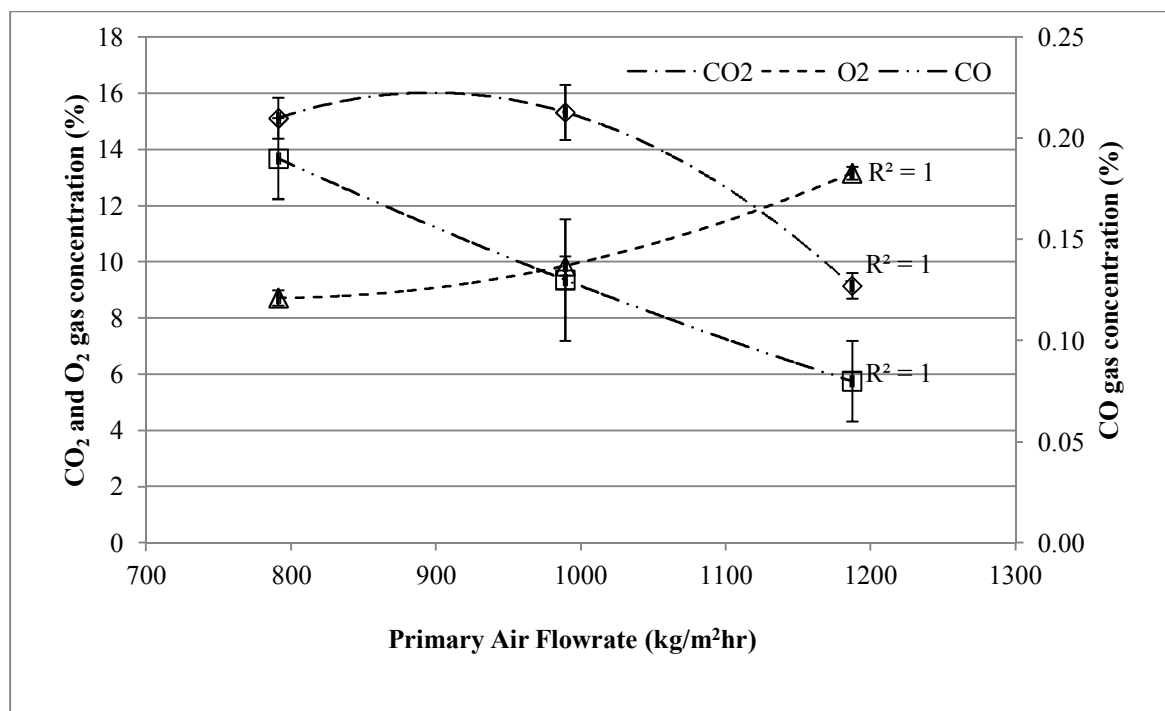
Figure 6-28: Effect of increasing primary air flowrate on the gas concentration.

6.2.4 Effect of changing initial bed temperature on combustion characteristics

Three initial temperatures were chosen in this study; 850°C, 900°C and 950°C. Summaries of some experimental conditions and the results are tabulated in Table 6-3. The tests were conducted to establish the effects of initial bed temperature on the stability of the combustion process. The influences of initial bed temperature in the combustion process begin with the introduction of the fuel until combustion temperature stabilised after about 30–40 min. After this period, the initial bed temperature no longer played a role and combustion stability depended on the combustion of volatiles and char within the combustion chamber. Figure 6-29, Figure 6-31 and Figure 6-33 show the temperature profiles for the initial bed temperatures of 850°C, 900°C and 950°C respectively. As can be seen from Figure 6-29, Figure 6-31 and Figure 6-33 the bed surface temperatures (T5=0.42m) for all cases were more stable than in other temperature regions throughout the combustion process. The bed temperatures (T7=0.20m) decreased immediately after the introduction of the sample, then stabilised at around 750-800°C towards the end of the combustion process. The temperature drops at the beginning of the combustion

process indicates that the net energy was negative due to the drying and devolatilasation of the fuel. The rate of consumption by these processes was greater than the rate of energy release in the bed. However, after the devolatilisation char residue started to burn and release energy (exothermic process), then the bed temperature stabilised as the rates of energy consumption and generation reached equilibrium. The freeboard temperatures (an average T2=1.54m and T3=0.76m) gradually increased over time. Energy released during volatile and char combustion caused the temperature to increase. The temperatures in all three regions were almost the same towards the end of the combustion process.

The surface bed temperature for case 4 and 5 (Figure 6-35) were unchanged. This is because the initial temperature gaps between case 4 and 5 were too small. However, the combustion of OPS at higher initial bed temperature (950°C) was found to be more stable as indicated by the plot of T5 (case 6), Figure 6-35.

Gas emissions from three different cases were plotted as shown Figure 6-30, Figure 6-32 and Figure 6-34. The effects of initial bed temperature on gas emissions were barely distinguishable due to the small temperature difference.

Table 6-3: The summary of tests parameters and combustion characteristics of oil palm stone in the pilot-scale fluidised bed reactor at a range of initial bed temperatures.

Parameters		Case 4	Case 5	Case 6
Fuel feedrate (kg/hr)		1.2	1.2	1.2
Primary air (kg/m^{2}hr)		791	791	791
Secondary air (kg/m^{2}hr)		356	356	356
Initial bed temperature (°C)		850	900	950
λ(AFR/AFR$_{Stoic}$) based on primary air		1.20	1.20	1.20
λ(AFR/AFR$_{Stoic}$) actual		1.72	1.72	1.72
Average gas concentration	CO$_2$ (%)	14.17	11.66	13.59
	CO (%)	0.16	0.16	0.20
	O$_2$ (%)	9.02	10.58	9.60
	NOx (ppm)	182	205	199
	SO$_2$ (ppm)	0.01	0.00	0.04
	HCl (ppm)	0.01	0.00	0.04
Average temperature (°C)	Bed	775	767	817
	Surface of the bed	847	856	877
	Freeboard	594	599	652
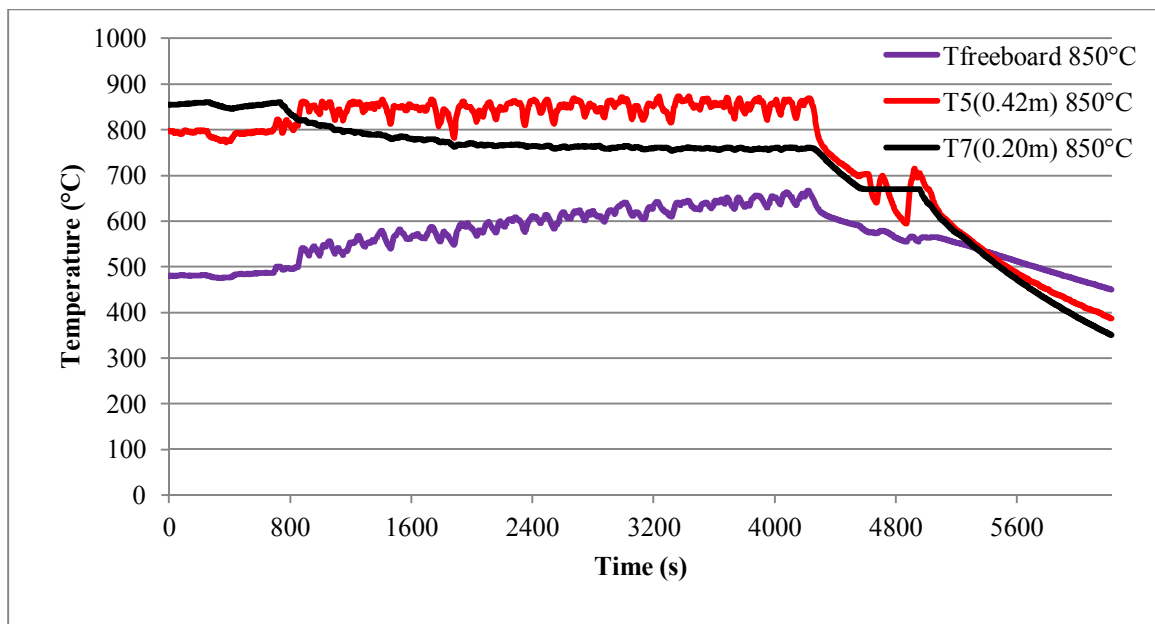
Figure 6-29: Temperature profiles for the combustion of oil palm stone in the pilot-scale fluidised bed reactor at an initial bed temperature of 850°C.
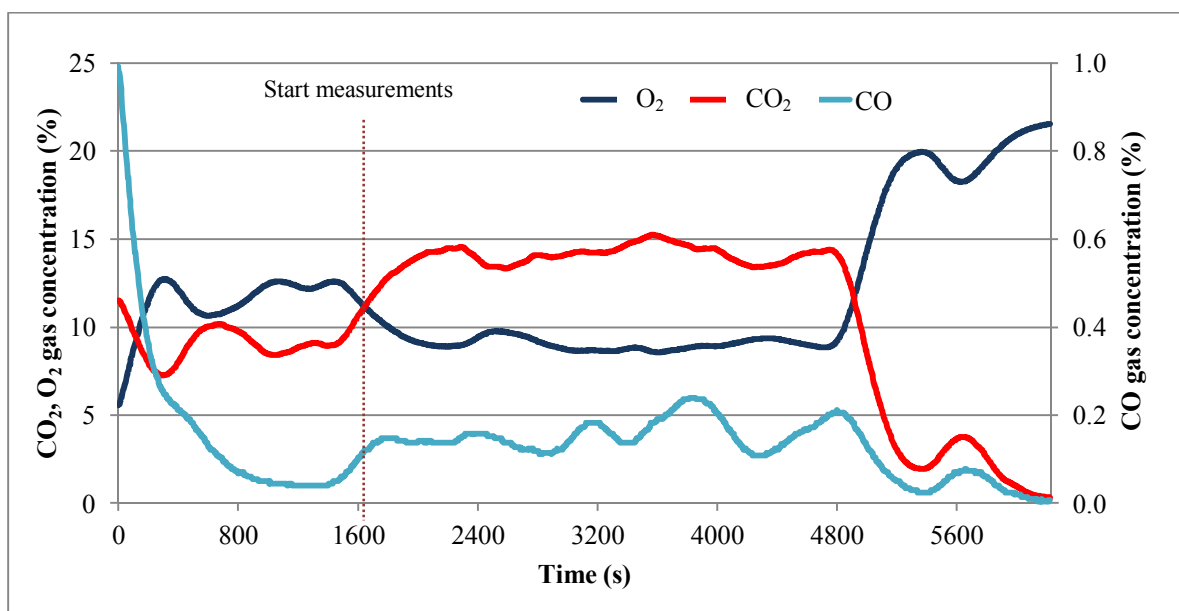
Figure 6-30: Gas emission from the combustion of oil palm stone in the pilot-scale fluidised bed reactor at an initial bed temperature of 850°C.
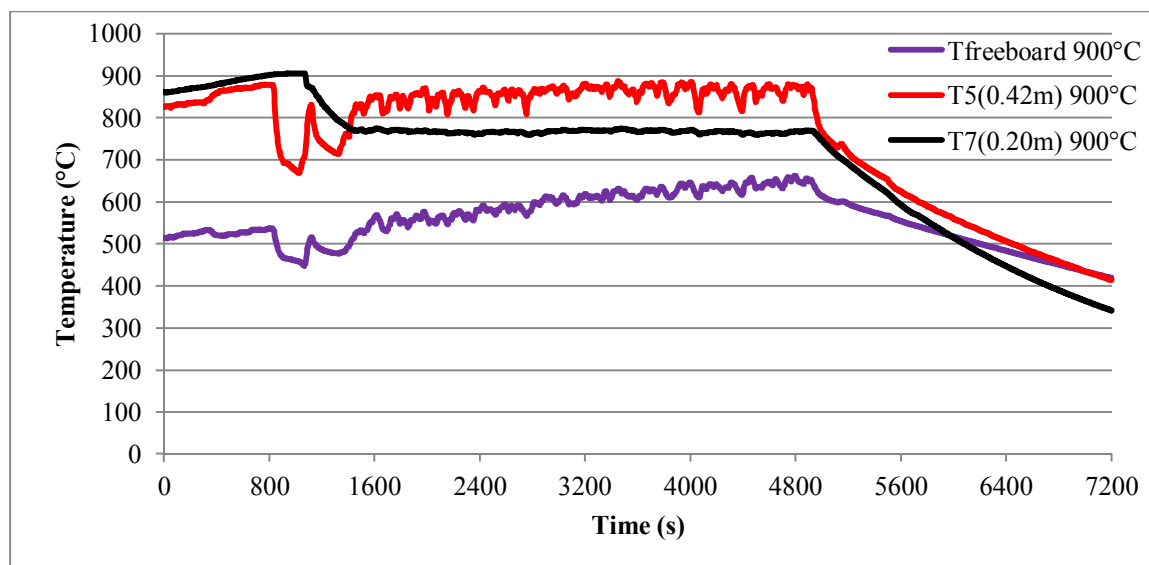
Figure 6-31: Temperature profiles for the combustion of oil palm stone in the pilot-scale fluidised bed reactor at an initial bed temperature of 900°C.
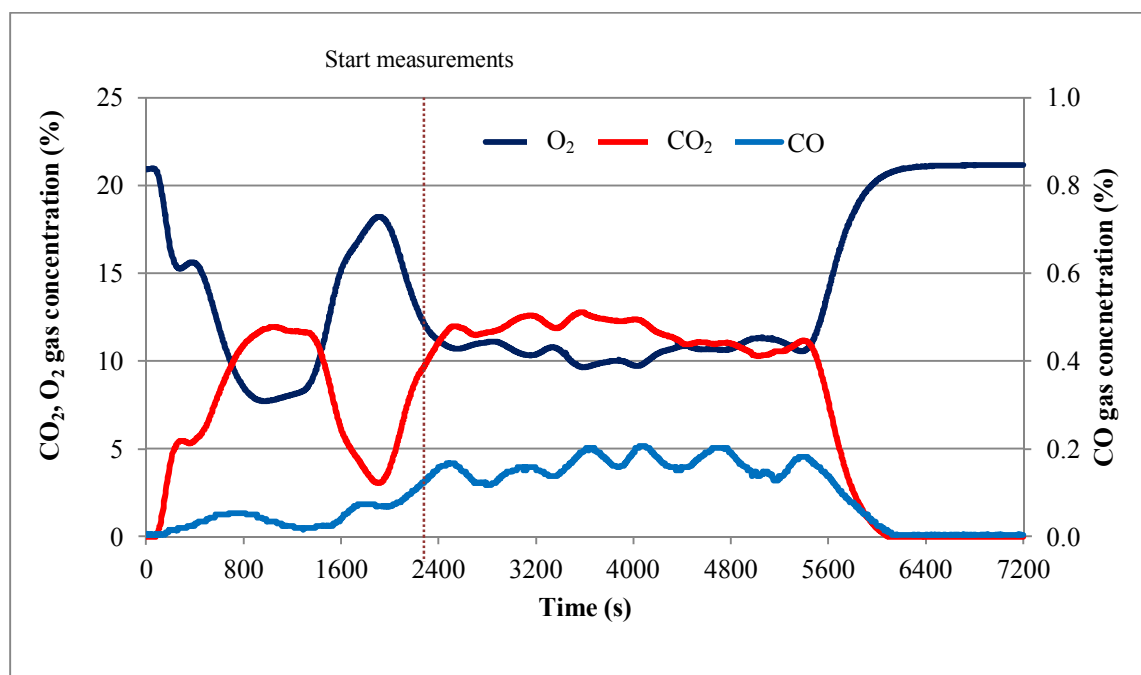
Figure 6-32: Gas emission from the combustion of oil palm stone in the pilot-scale fluidised bed reactor at an initial bed temperature of 900°C.
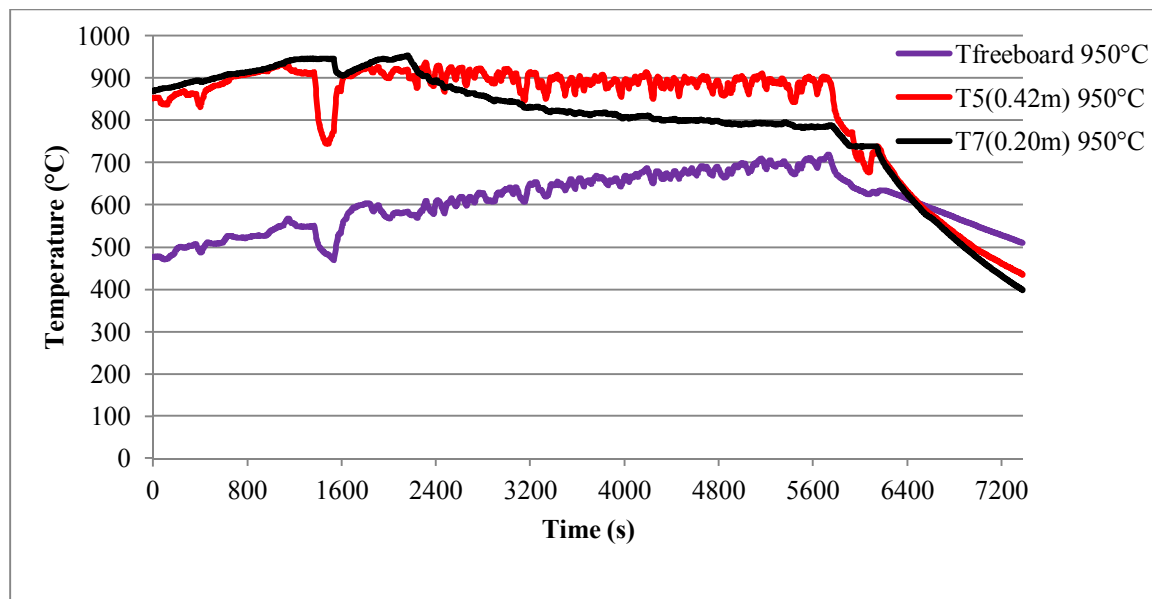
Figure 6-33: Temperature profiles for the combustion of oil palm stone in the pilot-scale fluidised bed reactor at an initial bed temperature of 950°C.
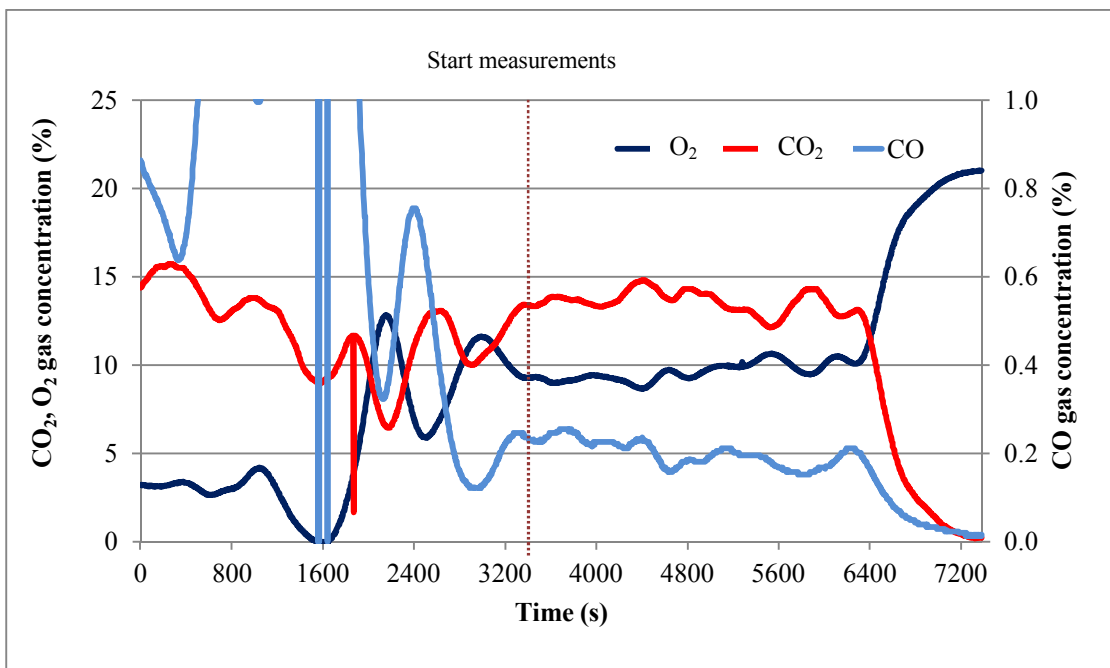
Figure 6-34: Gas emission from the combustion of oil palm stone in the pilot-scale fluidised bed reactor at an initial bed temperature of 950°C.
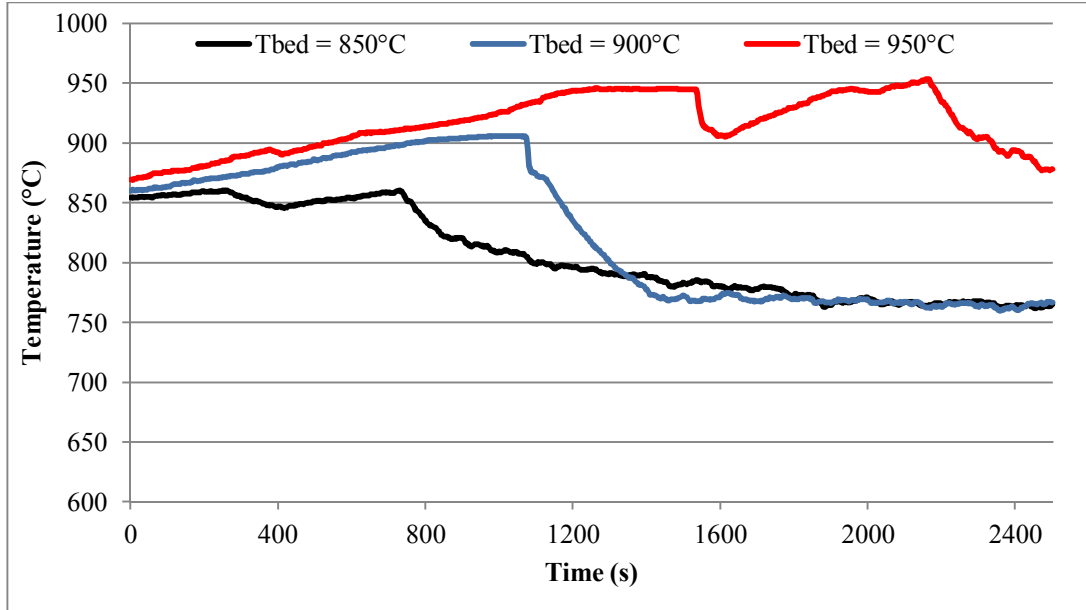
Figure 6-35: The bed surface temperature (T5) at different initial bed temperature.

6.2.5 Bottom and fly ash analysis

Fly ash was collected from the cyclone mounted at the top of the reactor. The fly ash residue was collected after each test. As shown in Table 6-4 less than 2% of the initial material was trapped as fly ash in the cyclone. Particles with particularly low densities may have been emitted with the exhaust gases (released to the atmosphere) if they were too small to be collected by particle inertia in the cyclone. The rest, particles with high densities, either mixed or agglomerated with the sand (quartz) particles at the bottom of the reactor. According to (Lind *et al.*, 2000) there are two mechanisms by which ash can become attached to sand particles: ash deposition on the sand surface; and diffusion of the ash compounds into the bed particles. Consequently these were quite difficult to separate and thus the proportion of ash in this mixture was calculated, along with the unburned carbon, using an ash tracer method (Li *et al.*, 2010, Munir *et al.*, 2010, Zhang *et al.*, 2010). For both case 1 and 2 around 1.7% of the mass of the mixture (sand + bottom ash) was determined to be bottom ash, of which 10% was calculated to be unburned carbon.

Analysis of trace elements showed that those present in high concentrations in the fly ash were also present in high concentrations in the bottom ash, Table 6-5. As expected, the most abundant elements were found to be Al, Ca, Fe, K, Mg, Mn, P, S and Si. The elements of concern for combustion systems are K, Na, Ca, Mg, Si, Cl and S (Vamvuka and Zografos, 2004) which can cause fouling. However, fouling is not likely to be of concern in the temperature regime used in this study.

Table 6-4: Fly ash, bottom ash fraction and unburned carbon from various combustion cases.

Case No.	OPS Feed (kg)	Fly Ash (%)	Sand + Bottom Ash (%)	Unburned Carbon (%)		Air Ratio
				Fly Ash	Sand + Bottom Ash	
1	1.2	1.25	1.7	15.76	10.00	1.20
2	1.2	1.58	1.7	15.73	10.00	1.50
3	1.2	1.67	-	18.09	-	1.80
4	1.2	1.08	-	16.88	-	1.20
5	1.2	1.25	-	16.56	-	1.20
6	1.2	1.33	-	16.05	-	1.20

Table 6-5: Full elemental analysis of fly and bottom ashes collected from the various tests of the OPS combustion in the pilot-scale fluidised bed.

Element (mg/kg)	Case 1 Fly ash	Case 1 Bottom ash	Case 2 Fly ash	Case 2 Bottom Ash	Case 3 Fly ash	Case 3 Bottom Ash	Case 4 Fly ash	Case 4 Bottom Ash	Case 5 Fly ash	Case 5 Bottom ash	Case 6 Fly ash	Case 6 Bottom Ash
Al	3620	4269	2820	5123	3100	4649	3840	5218	6120	-	3620	2087
As	17	<1	13.5	<0.1	12	<1	12.5	<1	30	-	17	<1
B	27.3	27	29.1	<1	24.1	<1	28.7	28	47.1	-	28.9	<1
Ba	67.9	50	53.8	65	56.4	56	64.4	59	170	-	61.5	46
Bi	0.68	<0.05	0.64	<0.05	0.62	<0.05	0.50	<0.05	1.9	-	0.86	<0.05
Ca	40400	2562	50000	1632	45600	2657	47400	1157	41700	-	40300	1404
Ce	5.6	17	3.6	23	4.6	21	5.6	27	8.4	-	5.2	23
Co	68	4	34	3	32	4	34	3	32	-	76	4
Cr	273	49	286	24	282	38	248	20	974	-	252	15
Cs	102	55	112	59	106	61	110	57	90	-	112	32
Cu	500	25	620	36	600	266	500	14	1160	-	480	21
Fe	97200	5218	71200	3700	63000	4934	58300	4032	134000	-	86000	4080
K	59000	5218	78800	5123	76400	6025	73000	3843	57200	-	61600	2467
La	2.8	9	1.9	12	2.6	10	3.0	14	4.4	-	2.8	11
Li	5.6	1	4.8	2	8.8	<0.1	6.4	<0.1	11.4	-	6.8	2
Mg	37400	2694	46200	2097	45400	2609	45600	1907	33800	-	39000	1528
Mn	3680	218	3990	155	3780	220	3850	135	3260	-	3910	143
Na	840	133	960	171	810	161	890	76	980	-	870	85
Nd	2.6	8	1.7	10	2.0	8	2.6	13	3.8	-	2.8	9
Ni	2710	97	1390	61	3120	82	1940	38	3570	-	3860	70
P	69500	4269	91200	3036	88500	4554	86200	2182	66400	-	72800	2372
Pb	36	5	56	7	52	23	38	6	128	-	40	3
S	2300	24	3500	52	3200	51	2700	67	4600	-	2000	29
Sb	2.4	<0.1	2.2	<0.1	1.8	<0.1	1.9	<0.1	5.0	-	2.0	<0.1
Sc	1.0	1	0.8	1	0.8	1	1.0	1	1.5	-	1.0	1
Si	2020	1755	2380	2106	2090	1983	2720	2116	2000	-	1900	1224
Sn	10.4	<0.2	9.4	<0.2	9.4	<0.2	7.0	<0.2	20	-	12.4	<0.2
V	28	14	22	11	19.4	10	22	11	42	-	28	9
W	9.4	<0.1	5.4	<0.1	6.2	<0.1	6.4	<0.1	32	-	9.2	<0.1
Y	1.5	2	0.9	2	1.1	2	1.5	2	1.8	-	1.4	1
Zn	800	49	840	53	900	218	1000	32	1880	-	710	30
Zr	1.5	<0.1	1.1	<0.1	1.2	<0.1	1.5	<0.1	2.4	-	1.5	<0.1

Based on this pilot-scale study OPS was found to be a good candidate for the clean fuel due to low sulphur content and low acid gas emission such as NOx, SOx and HCl. Furthermore, it shows signs of good combustion characteristics in a fluidised bed.

7 RESULTS AND DISCUSSION: SLOW PYROLYSIS OF OIL PALM STONE AND PALM KERNEL CAKE

Pyrolysis thermally decomposes biomass into char, liquid and gas products in an inert environment, each of which has potential use as a fuel. The char and liquid products are considered as the intermediate media of energy, being storable and high in energy content. According to Bridgwater, (2002) the fast pyrolysis of biomass has been demonstrated in reactors that are scaled up to several hundred kilograms per hour. Although current studies on pyrolysis liquids are focused more on the fast pyrolysis of biomass, slow pyrolysis can also produce oil with a mass yield of more than 40% (Zailani *et al.*, 1999). However, there has been limited research into pyrolysis in large scale reactors, particularly on oil palm wastes: oil palm stone (OPS) and palm kernel cake (PKC). Although the product distribution and properties have been thoroughly studied, most are based on simplified parameters using either a Thermogravimetric analyser (TGA) or small reactor size, using a few grams of samples. These indicates that there are gaps between the experimental results and industrial applications due to the differences in individual particle and bed sizes, which influence the temperature, heating rate and chemical reaction of the primary products inside and around the particles in the pyrolysis reactor. In this chapter, two materials, oil palm stone and palm kernel cake, were evaluated using a fixed bed pyrolysis reactor at two different final temperatures (500°C and 700°C) and three different heating rates (5°C/min, 10°C/min and 15°C/min) in a nitrogen flow environment.

7.1 The experimental approach

Pyrolysis involves the decomposition of the high molecular weight compound into smaller moieties. It breaks both the linkages and carbon bridges or opens non-aromatic rings at random. The primary products from pyrolysis are bio-oil, char and gas.

In this study, oil palm stones and palm kernel cake were investigated using a fixed bed pyrolyser with nitrogen pre-heater (Figure 4-1). The effect of heating rates on the yield of

the pyrolysis products were investigated for both samples at the final reactor temperatures of 700°C and 500°C. The elemental analysis and calorific value of both samples and products were determined. The gas and bio-oil composition were investigated using chromatographic and spectroscopic techniques.

7.2 Proximate and ultimate analysis of oil palm stone and palm kernel cake

The fuels were characterised according to proximate and ultimate analyses as described in section 4.4.2. The results for oil palm stone and palm kernel cake are shown in Table 7-1 and Table 7-2 respectively. Full elemental analysis of the as received samples was carried out by Inductively Coupled Plasma Spectroscopy (ICP). The results are given in Table 7-3.

Table 7-1: Proximate and ultimate analysis of oil palm stone.

Sample 1	Proximate (wt %) as received		±	Ultimate (wt %) daf		±
Oil palm stone	Volatiles	86.50	0.24	Carbon	72.54	4.77
	Fixed carbon	6.55	0.38	Hydrogen	9.11	0.24
	Moisture	4.71	0.12	Nitrogen	1.73	0.07
	Ash	2.24	0.13	Sulfur	0.37	0.33
	Calorific value (MJ/kg)	27.46	0.18	Oxygen	16.24	4.32

Based on 5 repeats

Table 7-2: Proximate and ultimate analyses of palm kernel cake.

Sample 2	Proximate (wt %) as received		±	Ultimate (wt %) daf		±
Palm kernel cake	Volatiles	71.84	0.62	Carbon	59.81	1.11
	Fixed carbon	16.00	0.72	Hydrogen	6.43	0.34
	Moisture	7.92	0.29	Nitrogen	3.26	0.11
	Ash	4.28	0.10	Sulfur	0.03	0.03
	Calorific value (MJ/kg)	18.67	0.27	Oxygen	30.48	0.92

Based on 5 repeats

Table 7-3: Full elemental analysis of oil palm stone and palm kernel cake.

Element	Oil palm stone	Palm kernel cake	Element	Oil palm stone	Palm kernel cake
Al	220	280	Na	11	23
As	1.6	1.0	Nd	0.01	0.12
B	2	4.8	Ni	1.4	1.4
Ba	0.7	1.6	P	3200	5900
Be	<0.01	<0.01	Pb	0.56	0.5
Ca	2250	4960	Pr	<0.01	0.03
Ce	0.03	0.29	S	1000	1800
Cl	300	550	Sb	0.09	0.07
Co	0.02	0.04	Sc	0.05	0.09
Cr	3.2	2.8	Si	290	450
Cu	12	21	Sm	<0.01	0.03
Fe	3900	1300	Sn	0.54	0.04
Ga	0.17	0.11	Th	0.06	0.1
K	3500	6500	V	4.9	1.7
La	0.02	0.13	Y	0.02	0.13
Li	0.02	0.06	Zn	27	40
Mg	1550	2700	Zr	0.11	0.06
Mn	130	240			

* All results in mg/kg as received

7.3 Thermogravimetric analysis (TGA)

Pyrolysis tests of OPS and PKC were also conducted in a thermogravimetric analyser (Perkin Elmer, model Pyris 1 TGA). A mass of 5.059 mg and 4.709 mg was used for OPS and PKC respectively. Purified nitrogen at a constant flow rate of 20 mL/min was used as a carrier gas to provide an inert atmosphere for pyrolysis and to remove the gaseous and condensable products, thus minimising any secondary vapour-phase interactions. The sample was heated to 50°C and held for 1 minute to ensure temperature homogenously distributed. It was then heated at a heating rate of 5°C/min to 800°C. This TGA analysis was to identify the kinetic data of OPS and PKC and to compare the results with the packed bed pyrolysis tests.

Figure 7-1 shows the residual weight fractions (TG) undergoing pyrolysis and the derivative thermograms (DTG) of OPS and PKC. There was an initial weight loss at a

temperature of approximately 100°C due to the evaporation of moisture in the raw materials. The second peak of weight loss occurred at temperature around 200°C. The onset temperature where the material started to decompose was around 250°C for OPS and PKC. The char yields at temperature of 400°C were 19 wt% and 29 wt% for OPS and PKC respectively, and then they decreased gradually to 10wt% and 22 wt% at 800°C. The main differences between the two samples are observed in their DTG plot. Both samples clearly showed that two separate steps of reactions that took place in distinct temperature regimes with two obvious maxima 2.5 and 3.8 wt%/°C for OPS and 3.0 and 1.9 wt%/°C for PKC. This was due to the different volatiles and fixed carbon content that exist in both wastes. According to (Yang *et al.*, 2004) the release of volatiles potentially cause an earlier degradation of carbon, resulting in one big peak. The two separate peaks represent, respectively, the release of volatiles and the degradation of carbon. These peaks were identified at 290°C and 350°C. These peaks are thought to be due to the decomposition of hemicelluloses and cellulose respectively.
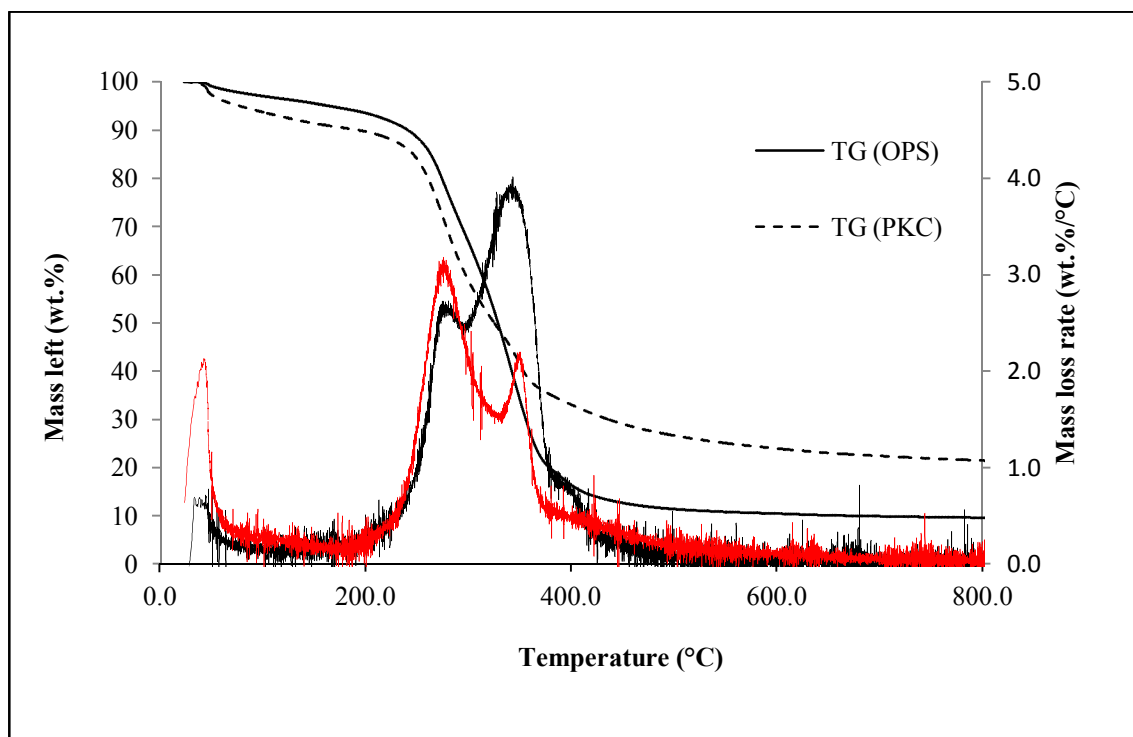
Figure 7-1: Thermogravimetric analysis (TGA) of OPS and PKC.

7.4 Product yield

The mass fraction of the primary pyrolysis products from the OPS and PKC at different heating rates is shown in Figure **7-2** and Figure **7-3** respectively. The mass yields of char and liquids were measured directly from the weight of the products collected. However, the gas product was determined by difference, which integrated the small fraction of fine droplets and dust or ash. Figure **7-4** and Figure **7-5** present the mass yields of the pyrolysis products from the OPS and PKC respectively, at the final temperature of 500°C, with the heating rate of 10°C/min. Ramlan Zailani *et.al.*, (1999) and Sukiran *et al.*, (2009) revealed that the liquid products from the pyrolysis of oil palm waste was optimum at temperature of 500°C.

The char yield obtained from the OPS was slightly lower compared to that produced from the PKC. The maximum char yield from the OPS was 16.95 wt% of feed-stock at a heating rate of 15°C/min, whilst the highest char product from PKC was 28.4 wt% of feed-stock at a heating rate of 5°C/min. Generally, the char yield was not significantly affected at low heating rates from 5°C/min to 15°C/min. This result was consistent with the previous study on the slow pyrolysis of oil palm empty fruit bunches, holm oak and pine-wood (Figueiredo *et al.*, 1989, Williams and Besler, 1996, Sukiran *et al.*, 2009). It shows that the wood type, small particle size and heating rate had very little influence on the char yield. However, at the final reactor temperature of 500°C, the char yield for both the OPS and PKC was slightly higher, at 17.13 wt% and 29.15 wt% respectively. This may be due to the slow decomposition process at a temperature of 500°C compared to 700°C.

At a temperature of 500°C, the liquid yields of the OPS and PKC were 54.48 wt% and 43.49 wt% respectively. Increasing the pyrolysis temperature to 700°C means that, the liquid yield of the OPS was increased to 57.92 wt%; however, the oil yield from the PKC fell to 42.84 wt%. The gas yields obtained from the OPS and PKC were in the ranges of 26.98-47.9 wt% and 29.55-33.17 wt%, respectively, at a pyrolysis temperature of 700°C.

However, at a pyrolysis temperature of 500°C, the gas yields were significantly lower at 28.40 wt% (OPS) and 27.37 wt% (PKC), respectively.
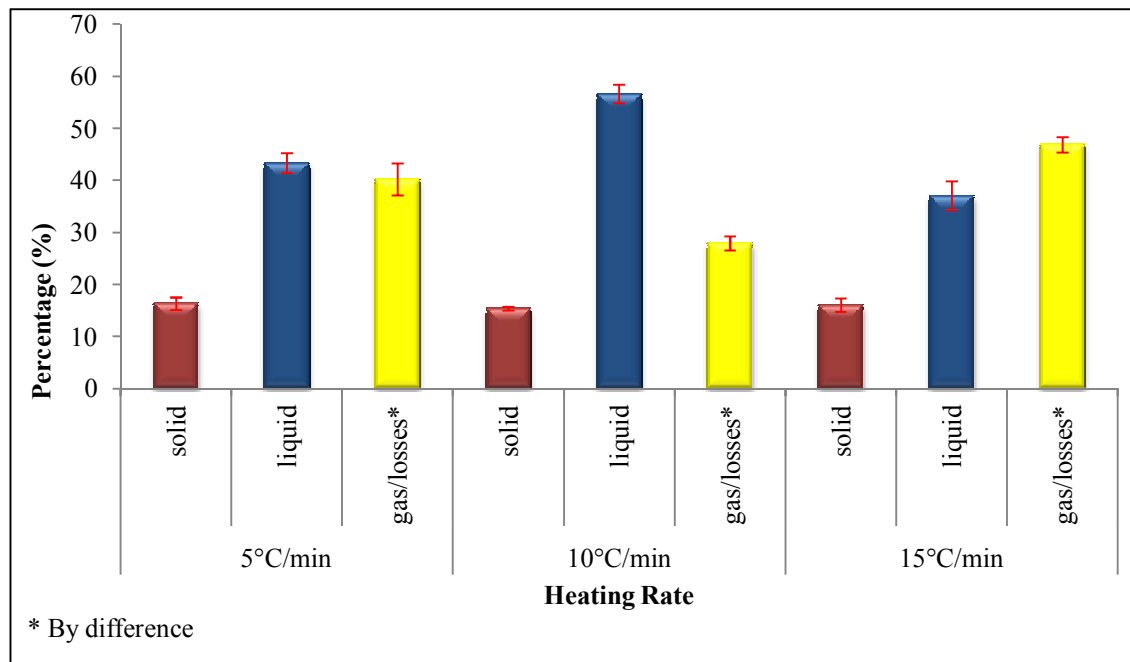
Figure 7-2: Yields of pyrolysis products (% wt of sample fed) from pyrolysis of oil palm stone at a Temperature of 700°C.
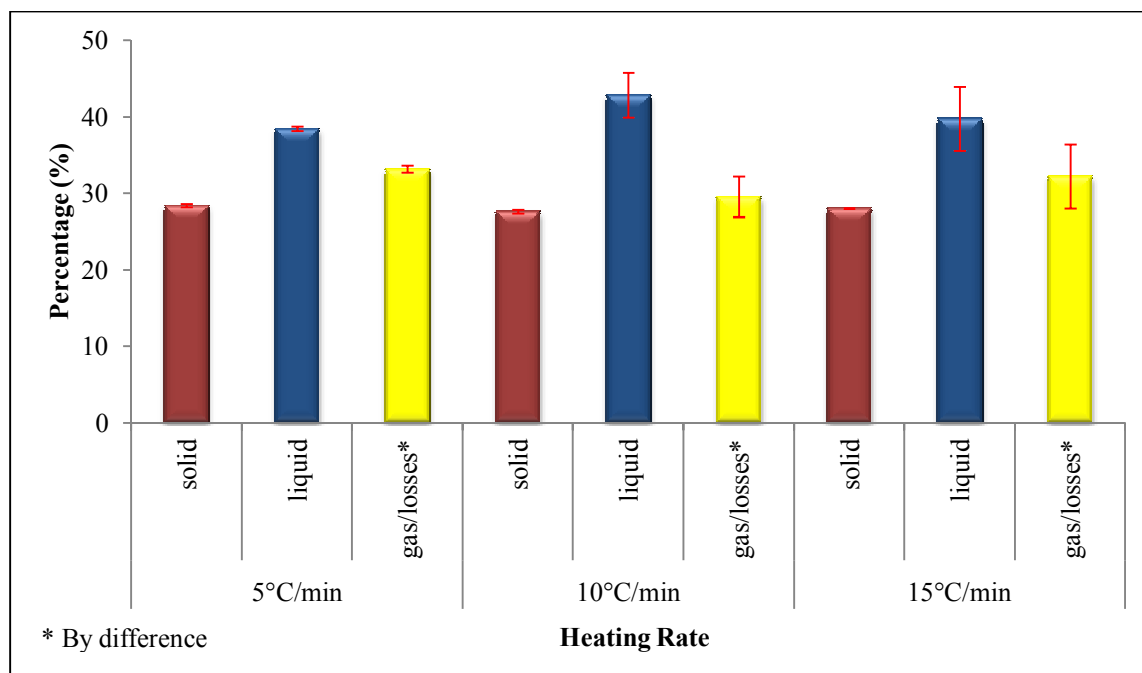
Figure 7-3: Yields of pyrolysis products (% wt of sample fed) from pyrolysis of palm kernel cake at a temperature of 700°C.
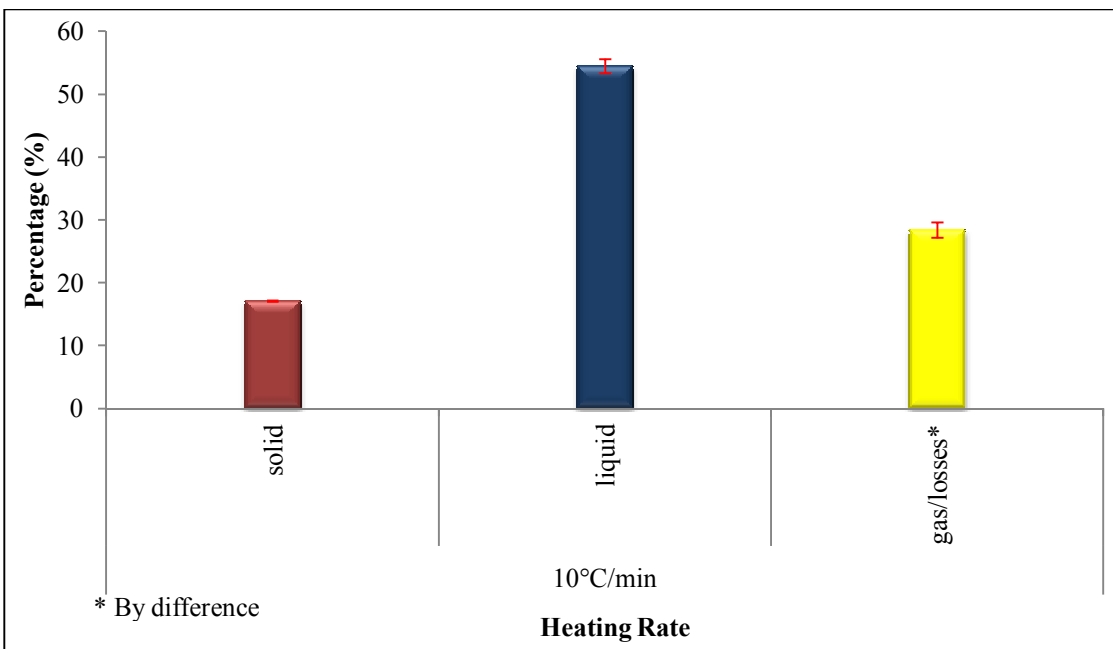
Figure 7-4: Yields of pyrolysis products (% wt of sample fed) from pyrolysis of oil palm stone at a temperature of 500°C.
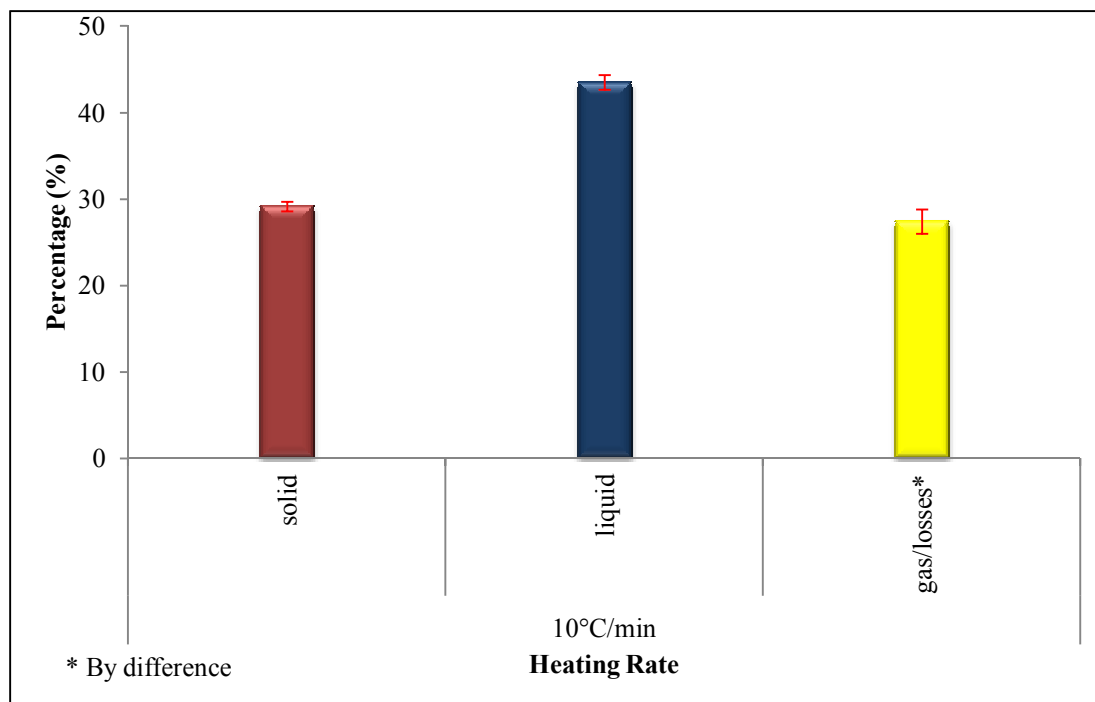
Figure 7-5: Yields of pyrolysis products (% wt of sample fed) from pyrolysis of palm kernel cake at a temperature of 500°C.

7.5   Characterisation of Pyrolysis Products

7.5.1   Char

Chars from pyrolysis of OPS (Figure 7-6 and Figure 7-7) and PCK (Figure 7-8 and Figure 7-9) were analysed based on a proximate and ultimate analysis in order to evaluate their quality. The volatiles, ash and fixed carbon were determined on a dry basis, because the moisture content of the char product was strongly dependent on the ambient conditions, as well as its characteristics. Table 7-4 to Table 7-7 show the properties of char obtained from the OPS and PKC at the different pyrolysis temperatures (500°C and 700°C), with the same heating rate of 10°C/min. The char mainly contained fixed carbon, with a small fraction of volatile matter. As seen in Table 7-4 to Table 7-7, the fixed carbon of char increases with the temperature. The fixed carbon of the char from the OPS is 68.48 wt% at a temperature of 500°C, but rose as high as 79.31 wt% at a temperature of 700°C. The high carbon content of char makes it suitable to utilise as a fuel, activated carbon or chemical feedstock. This finding is in agreement with that of Uzun *et al*. (2007), who studied the composition of products obtained via the fast pyrolysis of olive-oil residue. Their findings revealed that the fixed carbon obtained from olive-oil char reside was as high as 68.17 % at a temperature of 700°C.

It can be observed that the volatile matter content of the char decreased with the final temperature; for instance, in the case of the OPS, it decreased from about 14 wt% at 500°C to less than 7 wt% at 700°C or, in other words, the drop in volatile content was about 50% from the final pyrolysis temperature of 500°C to 700°C. This decrease in volatile content was due to the decomposition of cellulose and lignin, releasing a variety of volatile matters, both tar and non-tar forming compound. Increasing the reactor temperature, results in a further thermal degradation of these partially pyrolysed materials and converts less stable compounds in the char sample into more stable states.

At a temperature of 500°C, the char is dark brown in colour and there is very little change in the size of the materials (Figure 7-6 and Figure 7-8). However, physically, char

obtained at a temperature of 700°C manifested noticeable changes, being black in colour, brittle and sticky (Figure 7-7 and Figure 7-9).

Figure 7-6: Char obtained from pyrolysis of OPS at 500°C.
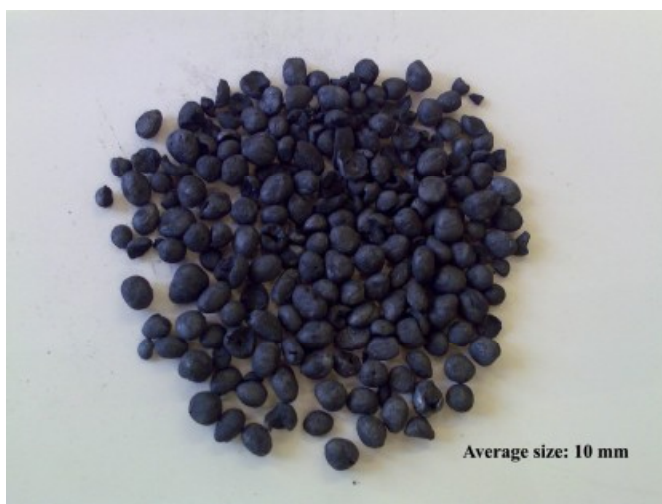
Figure 7-7: Char obtained from pyrolysis of OPS at 700°C.

Figure 7-8: Char obtained from pyrolysis of PKC at 500°C.
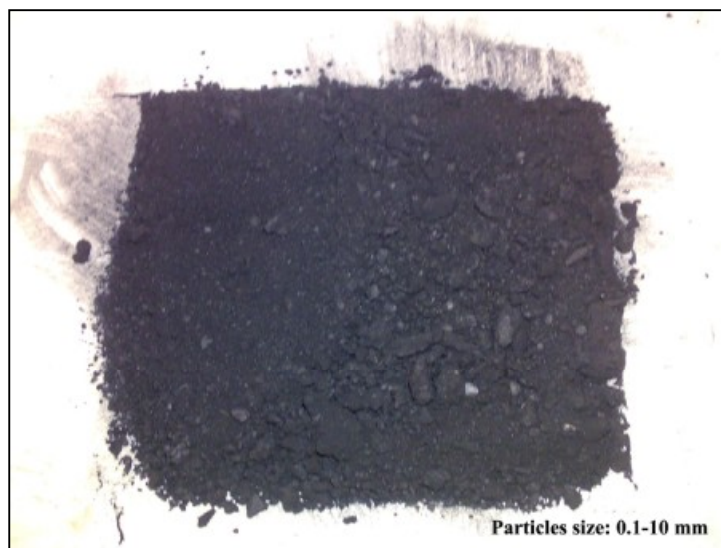
Figure 7-9: Char obtained from pyrolysis of PKC at 700°C.

Table 7-4: Properties of char from pyrolysis of OPS at a temperature of 500°C.

Sample 1	Proximate (wt %) as received		±	Ultimate (wt %) daf		±
	Volatiles	14.08	0.24	Carbon	80.27	2.73
Oil palm	Fixed carbon	68.48	2.08	Hydrogen	2.11	0.40
stone	Moisture	1.11	0.24	Nitrogen	4.42	0.20
500°C	Ash	16.33	1.68	Sulfur	0.04	0.01
	Calorific value (MJ/kg)	27.87	1.10	Oxygen	13.15	

Table 7-5: Properties of char from pyrolysis of OPS at a temperature of 700°C.

Sample 1	Proximate (wt %) as received		±	Ultimate (wt %) daf		±
	Volatiles	6.4	0.73	Carbon	84.56	2.29
Oil palm	Fixed carbon	79.31	0.99	Hydrogen	1.33	0.65
stone	Moisture	1.18	0.12	Nitrogen	3.79	0.40
700°C	Ash	13.10	0.25	Sulfur	0.14	0.15
	Calorific value (MJ/kg)	28.27	0.40	Oxygen	10.17	

Table 7-6: Properties of char from pyrolysis of PKC at a temperature of 500°C.

Sample 2	Proximate (wt %) as received		±	Ultimate (wt %) daf		±
	Volatiles	12.49	0.56	Carbon	62.78	1.67
Palm	Fixed carbon	73.46	0.41	Hydrogen	3.12	0.15
kernel	Moisture	0.0	0.13	Nitrogen	4.03	0.11
cake	Ash	14.42	0.18	Sulfur	0.02	0.02
500°C	Calorific value (MJ/kg)	28.12	0.15	Oxygen	30.05	

Table 7-7: Properties of char from pyrolysis of PKC at a temperature of 700°C.

Sample 2	Proximate (wt %) as received		±	Ultimate (wt %) daf		±
Palm kernel cake 700°C	Volatiles	6.69	1.20	Carbon	73.98	1.59
	Fixed carbon	78.18	1.43	Hydrogen	0.79	0.71
	Moisture	0.17	0.11	Nitrogen	3.49	0.59
	Ash	14.95	0.22	Sulfur	0.05	0.04
	Calorific value (MJ/kg)	28.06	0.10	Oxygen	21.70	

The empirical formula and calorific value of the raw materials and the char products at different temperatures are shown in Table 7-8. The C and H elements were determined using an elemental analyser on a dry weight basis. The oxygen content was determined by difference. The carbon content increased with the increase in temperature. In contrast, the hydrogen and oxygen contents decreased with an increase of temperature due to the release of volatiles and a further breaking of the weaker bonds within the char structure. The H/C ratio decreased with temperature, from 0.32 to 0.19 for the OPS and 0.6 to 0.13 for the PKC.

The calorific values of chars obtained from the OPS and PKC were approximately 28 MJ/kg. These chars had energy content as high as that of bituminous coal. The Hydrogen/Carbon (H/C) ratio decreases with temperature. The H/C ratios of solid char products change between 0.13 and 0.6. The highest H/C ratio obtained in this study is 0.6 at a reactor temperature of 500°C. The char product from the OPS and PKC obtained from this study were high carbon content compared to the empty fruit bunches (EFB) revealed in Sukiran *et al*., (2009); however, it was slightly lower compared to the oil palm shell (Yang *et al.*, 2006a).

Table 7-8: Empirical formula and calorific value of the solid char and raw material.

Pyrolysis temperature (°C)	Oil palm stone		Palm kernel cake	
	HHV (MJ/kg)	Empirical Formula	HHV (MJ/kg)	Empirical Formula
Raw material	27.46	$CH_{1.51}O_{0.17}$	18.67	$CH_{1.29}O_{0.38}$
500	28.77	$CH_{0.32}O_{0.12}$	28.12	$CH_{0.60}O_{0.36}$
700	28.27	$CH_{0.19}O_{0.09}$	28.06	$CH_{0.13}O_{0.22}$

*HHV: Higher Heating Value

The energy yield represents the total energy content of the products compared to that of raw material. It can be calculated by multiplying the product yield by the ratio of the calorific value of the product to the calorific value of the raw material (Phan, 2007, Ryu *et al.*, 2009). The energy yield for the char obtained from the pyrolysis of the OPS and PKC at temperatures of 500°C and 700°C, with a heating rate of 10°C/min, is shown in Table 7-9. The energy yield of the char produced from the pyrolysis of the PKC is higher than that of the char produced from the OPS at both final reactor temperatures.

Table 7-9: Energy yield from char product.

Temperature (°C)	OPS (%)	PKC (%)
500	17.95	43.90
700	15.55	41.50

7.5.2 Liquids

The liquids obtained at temperatures of 500°C and 700°C with a heating rate of 10°C/min were characterised based on the properties shown in Table 7-10. The liquid from the pyrolysis is a mixture of water and water-soluble organic compounds, as well as water-insoluble organic compounds. The proportions of these compounds depend on conditions such as feedstock, operating parameters and storage facilities. The typical water content in the liquid product from the fast pyrolysis of biomass (wood waste) was around 30% (Horne and Williams, 1996). The significant decrease in the oxygen content of the liquid (3.23-8.95% and 8.96-8.84%), compared to the original feedstock (16.24 and 30.48%)

implying that deoxygenation significantly proceeded during the pyrolysis (Cao *et al.*, 2011). This is important because the high oxygen content is not attractive for the production of transport fuels.

Table 7-10: Characteristics of liquid obtained from pyrolysis of OPS and PKC.

Properties	OPS		PKC		Palm Shell*
	Temperature (°C)				
	500	700	500	700	500
Calorific Value (MJ/kg)	38.27	37.81	27.74	20.79	22.1
Density @ 50°C (m²/s)		9.9×10^{-6}		1.5×10^{-6}	1.462×10^{-5}
Ultimate analysis (w/w%)					
Carbon	84.47	78.52	78.20	78.83	53.48
Hydrogen	10.53	10.64	8.97	8.13	6.69
Oxygen	3.23^{d}	8.95^{d}	8.96^{d}	8.84^{d}	39.27
Nitrogen	1.55	1.47	3.56	4.10	0.44
Sulphur	0.23	0.41	0.31	0.10	0.02
H/C molar ratio	1.51	1.63	1.38	1.24	1.50
O/C molar ratio	0.17	0.09	0.09	0.08	0.55
Empirical formula	$CH_{1.51}O_{0.17}$	$CH_{1.63}O_{0.09}$	$CH_{1.38}O_{0.09}$	$CH_{1.24}O_{0.08}$	$CH_{1.50}O_{0.55}$

* (Zailani *et al.*, 1999) ^{d} by difference

The pyrolysis liquid can either be homogeneous or heterogeneous. The liquid obtained from the pyrolysis of the OPS was observed to be homogeneous, as shown in Figure 7-10, whilst that, from the pyrolysis of the PKC was heterogeneous (Figure 7-11), about half of which was an aqueous fraction, which consisted mainly of water.

Figure 7-10: Liquid obtained from pyrolysis of oil palm stone at 500°C.
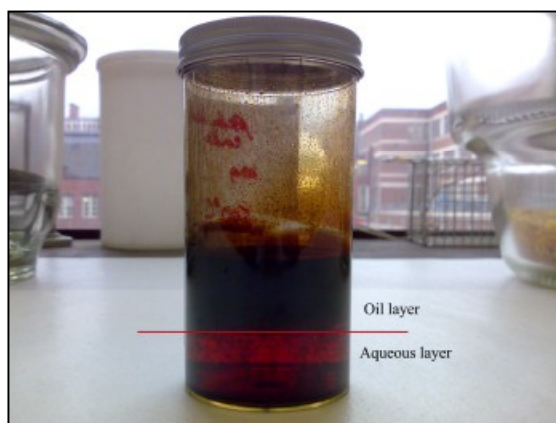
Figure 7-11: Liquid obtained from pyrolysis of palm kernel cake at 500°C.

The calorific values of the liquid obtained from the pyrolysis of the OPS and PKC range from 20.79 MJ/kg to 38.27 MJ/kg, which is about half that of gasoline (47 MJ/kg), diesel (45-46 MJ/kg) (Zailani *et al.*, 1999) and petroleum (42 MJ/kg) (Sensöz *et al.*, 2000). Typical fast pyrolysis liquid from biomass has a heating value of 16-19 MJ/kg, representing 60-80% of the energy content of the raw material (Phan, 2007). The liquid obtained from the OPS and PKC had a calorific value of 21-38 MJ/kg. This finding is in agreement with the results published in Sukiran *et al.*(2009) and Yang *et al.*(2006a). The energy yield of the liquid obtained from both samples is shown in Table 7-11. The liquid produced from the OPS has a high energy content compared to that obtained from the

PKC. This is because OPS contain higher volatile content compared to PKC material. Thus, increasing the CV of product liquid.

Table 7-11: Energy yield of liquid product.

Temperature (°C)	OPS (%)	PKC (%)
500	75.93	64.62
700	79.75	47.70

Fourier Transform Infrared (FTIR) was employed in this study to obtained information about the nature and type of organic compounds in the pyrolysis liquid products. The IR spectra of the dried samples are shown in Figure 7-12. Yang *et al*., (2006a) characterised oil palm biomass (fibre, empty fruit bunches and shell) using FTIR. They discovered that the functional group of chemical species are:

- ➢ O-H stretching vibration (3100-3600 cm^{-1}), O-H bending (1333 cm^{-1}) and O-H association (1108 cm^{-1}).
- ➢ C-H$_n$ (alkyl and aromatic) stretching and vibration (2860-2970 cm^{-1}), C-H bending vibration (1400-1460 cm^{-1}) and aromatic hydrogen (700-900 cm^{-1}).
- ➢ C=O stretching vibration (1700-1730 cm^{-1}) and (1510-1560 cm^{-1})
- ➢ C-O stretching vibration (1279-1060 cm^{-1}), and C-O-C aryl-alkyl ether linkage (1232cm^{-1}).
- ➢ Others, including aromatic skeletal mode (1606, 1516 and 1450 cm^{-1}), C-H deformation (1402 and 835 cm^{-1}) and CO deformation (1108 and 1060 cm^{-1}).

These functional groups are almost similar with the one obtained from OPS and PKC samples, Figure 7-12. This may be due to the similarity of plant species used in both studies. The IR absorbance of the liquids obtained from the pyrolysis of the OPS and PKC at temperatures of 500°C and 700°C are given in Figure 7-13 to Figure 7-16. The obvious functional groups of chemical compounds are phenol, alcohols, ketones, aldehydes and carboxylic acids. The functional group compositional analysis is shown in Table 7-12. Based on the IR spectra, it can be concluded that both samples had the same functional groups of chemical compound.
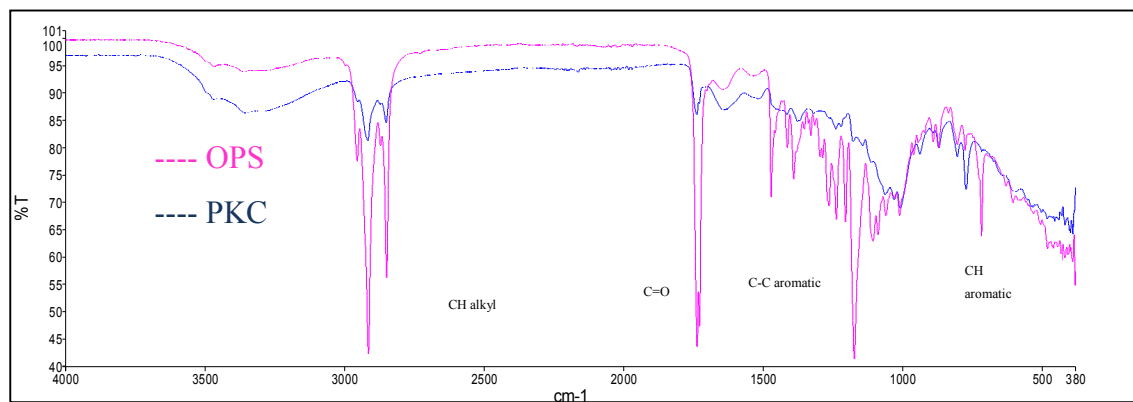
Figure 7-12: FTIR spectra of the OPS and PKC.
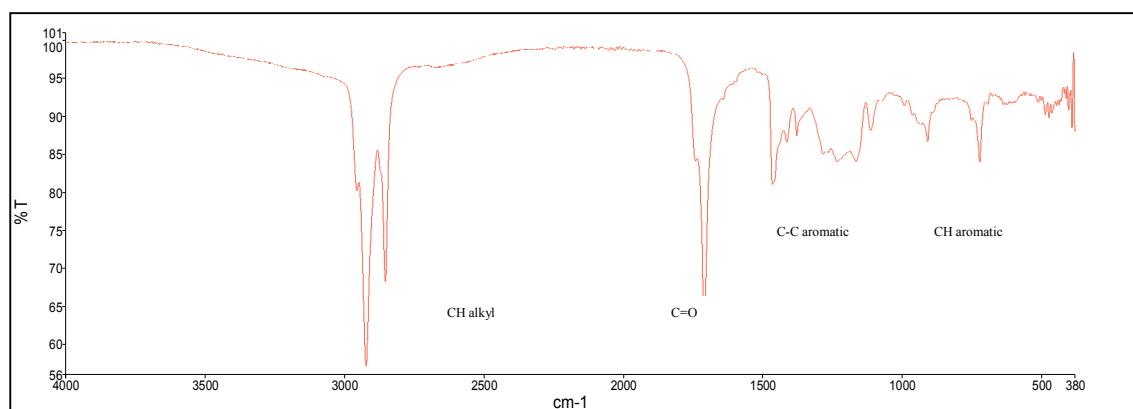
Figure 7-13: Infrared spectra of the liquid from the OPS at a temperature of 500°C.
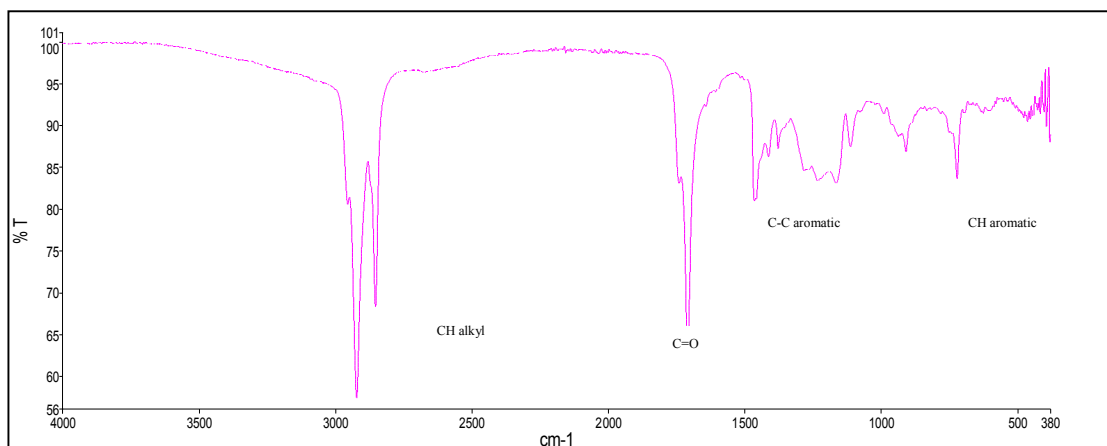
Figure 7-14: Infrared spectra of the liquid obtained from the OPS at a temperature of 700°C.
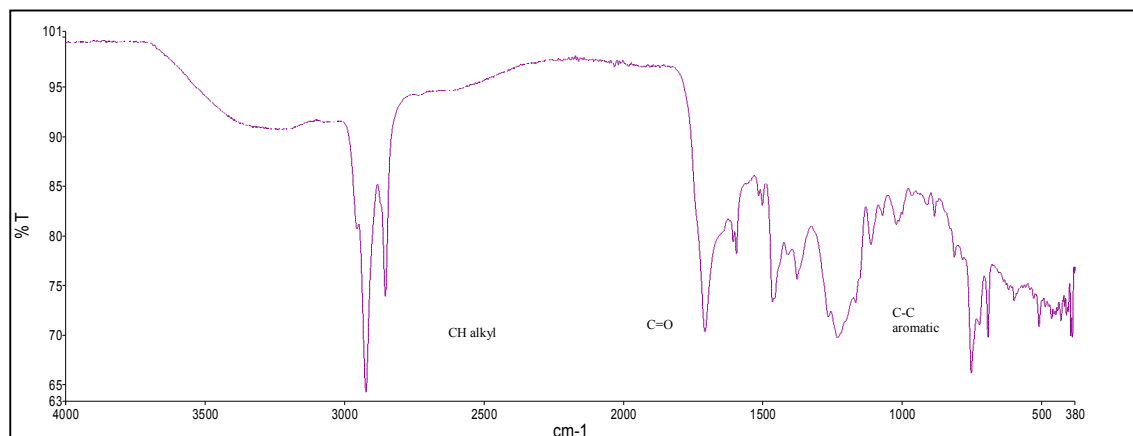
Figure 7-15: Infrared spectra of the liquid obtained from the PKC at a temperature of 500°C.
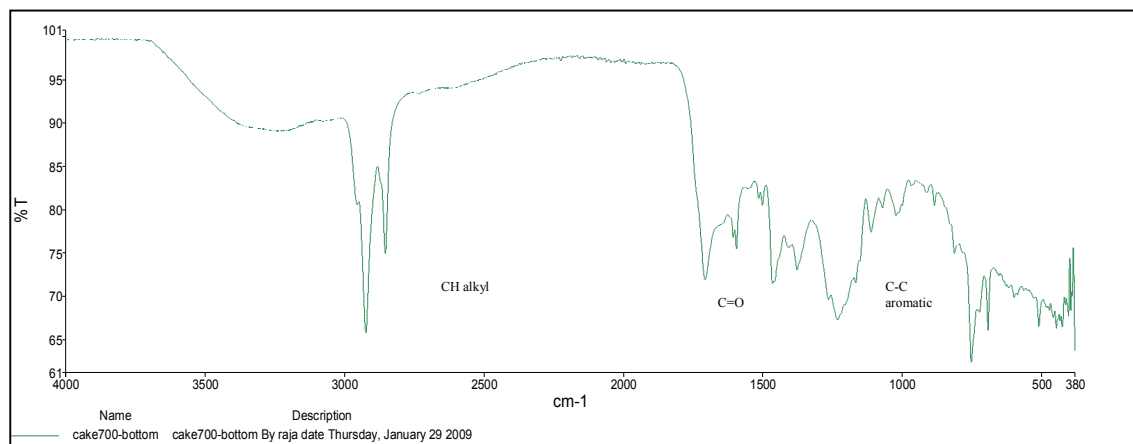
Figure 7-16: Infrared spectra of liquid obtained from the PKC at a temperature of 700°C.

Table 7-12: FTIR functional group compositions of pyrolysis liquid.

Frequency range(cm^{-1})	Group	Class of Compound
3200-3600	O-H stretching	Polymeric O-H, water impurities
3000-2800	C-H stretching	Alkanes
1780-1640	C=O stretching	Ketones, aldehydes, carboxylic acids
1680-1580	C=C stretching	Alkenes
1550-1490	-NO$_2$ stretching	Nitrogenous compounds
1465-1350	C-H bending	Alkanes
950-1300	C-O stretching	Primary, secondary and tertiary
	O-H bending	alcohol, phenol, esters and ethers
900-650		Aromatic compounds

7.5.3 Gases

The pyrolysis gases were collected at different final temperatures with different heating rate ranges, from 200°C to 700°C. The gas was analysed by a CP-3800 GC gas chromatograph. Figure 7-17 and Figure 7-18 show the composition of gases derived from the pyrolysis of the OPS, while Figure 7-19 and Figure 7-20 show the composition of gases obtained from the pyrolysis of the PKC at a final temperature of 700°C, with a heating rate of 5°C/min.

From Figure 7-18 and Figure 7-20, it can be observed that the CO_2 and CO derived from the pyrolysis of the OPS and PKC were mainly evolved at a lower temperature (< 500°C). This finding is in agreement with previous work on oil palm waste (Yang *et al.*, 2006a) and wood chip (Phan, 2007). As the temperature increases, the concentration of CO and CO_2 decreases gradually to about 15 vol% dry for both gases obtained from the OPS and approximately 20 vol% dry of CO_2 and no CO evolved from the PKC at a temperature of 700°C.

Two distinct regions of gas evolution were observed: at a lower temperature (< 500°C), CO and CO_2 were abundant, possibly be due to the breaking of C=O in raw material. On the other hand, at a high temperature (> 500°C), H_2 and other hydrocarbon gases (C1-C3) dominated the region, possibly due to the cracking and reforming of the aromatic rings which gives rise to H_2 release at high temperatures. As the temperature increased, the concentration of H_2 increased sharply and reached its maximum value (34.54 vol% dry) at 700°C. Most of the light hydrocarbon gases started to evolve at a temperature > 300°C, and then increased with increasing temperature to the highest percentage at a temperature of 600°C. A further increase in temperatures caused the concentration of hydrocarbon gases to decrease significantly. These gases were the result of alkyl breaking and diminishing. Both the OPS and PKC showed similar characteristics, but the gases that evolved from the PKC were of a slightly lower concentration, except for H_2 and CH_4.
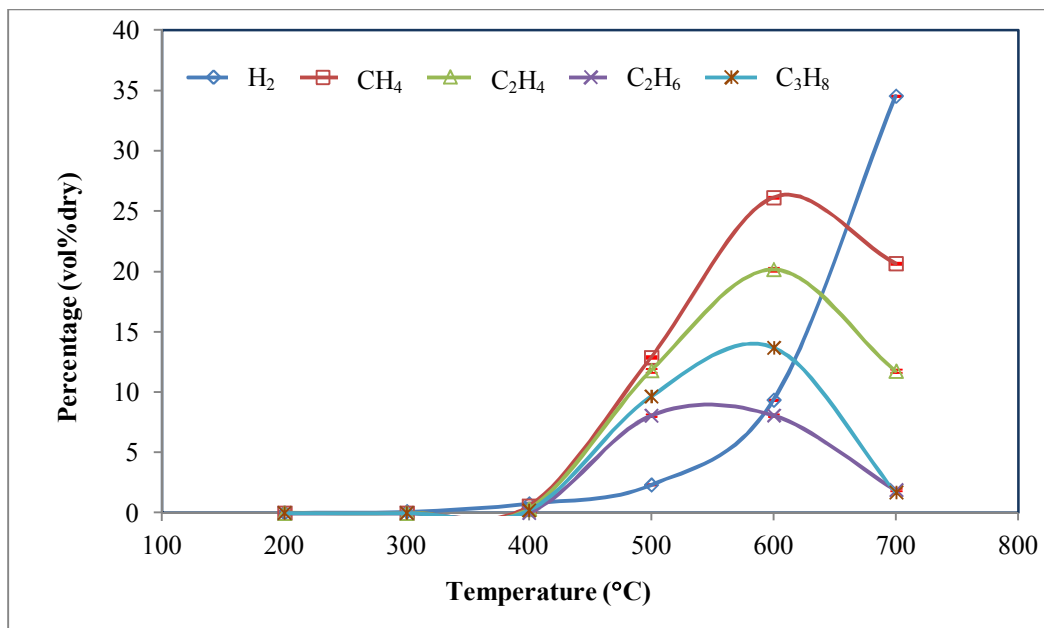
Figure 7-17: Gas compositions (H_2 and other hydrocarbon) from the pyrolysis of the OPS, with a heating rate of 5°C/min.
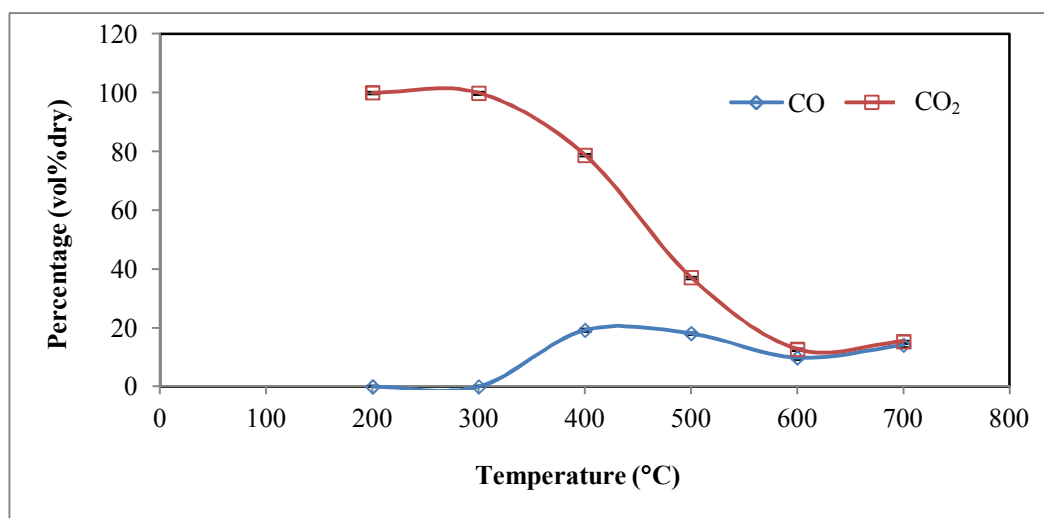
Figure 7-18: Gas compositions (CO and CO_2) from the pyrolysis of the OPS with a heating rate of 5°C/min.
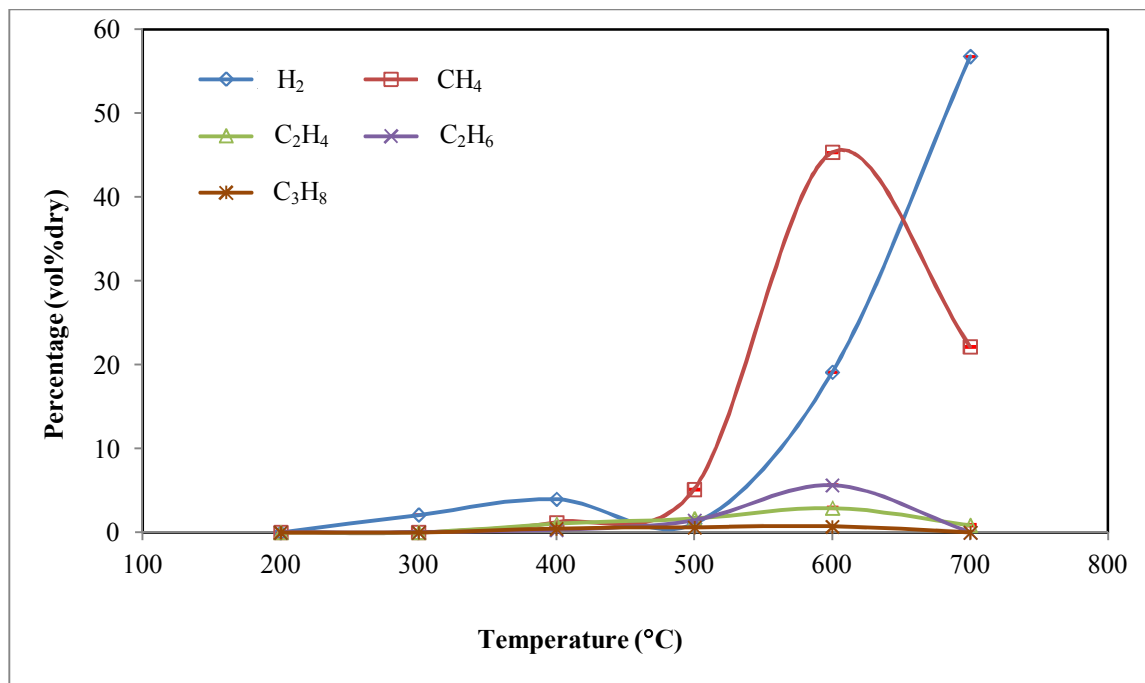
Figure 7-19: Gas compositions (H_2 and other hydrocarbon) from the pyrolysis of the PKC with a heating rate of 5°C/min.
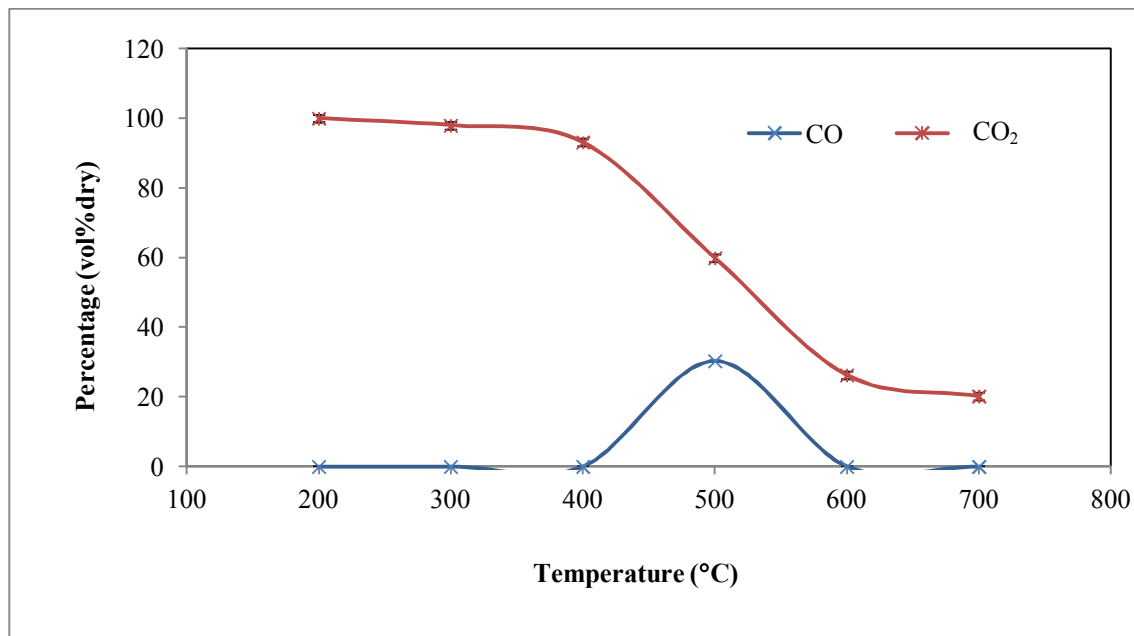
Figure 7-20: Gas compositions (CO and CO_2) from the pyrolysis of the PKC with a heating rate of 5°C/min.

Figure 7-21 and Figure 7-22 were obtained from the pyrolysis of the OPS with a heating rate of 15°C/min, whilst Figure 7-23 and Figure 7-24were from the pyrolysis of the PKC with a similar heating rate. Hydrogen and other hydrocarbon gases from the pyrolysis of the OPS evolved at a relatively lower temperature (300°C), compared to the case with a heating rate of 5°C/min. The slight drop in gas concentration at a temperature of 500°C (Figure 7-21) may be due to the evolution of the pyrolysis gases inside the reactor. However, the CO and CO_2 gases showed a similar trend as in the case of the heating rate of 5°C/min. A similar profile emerged for the gas distributions obtained from the pyrolysis of the PKC at different heating rates (5°C/min and 15°C/min). The light hydrocarbon (C2-C3) concentrations measured in both cases were less than 5 vol%.
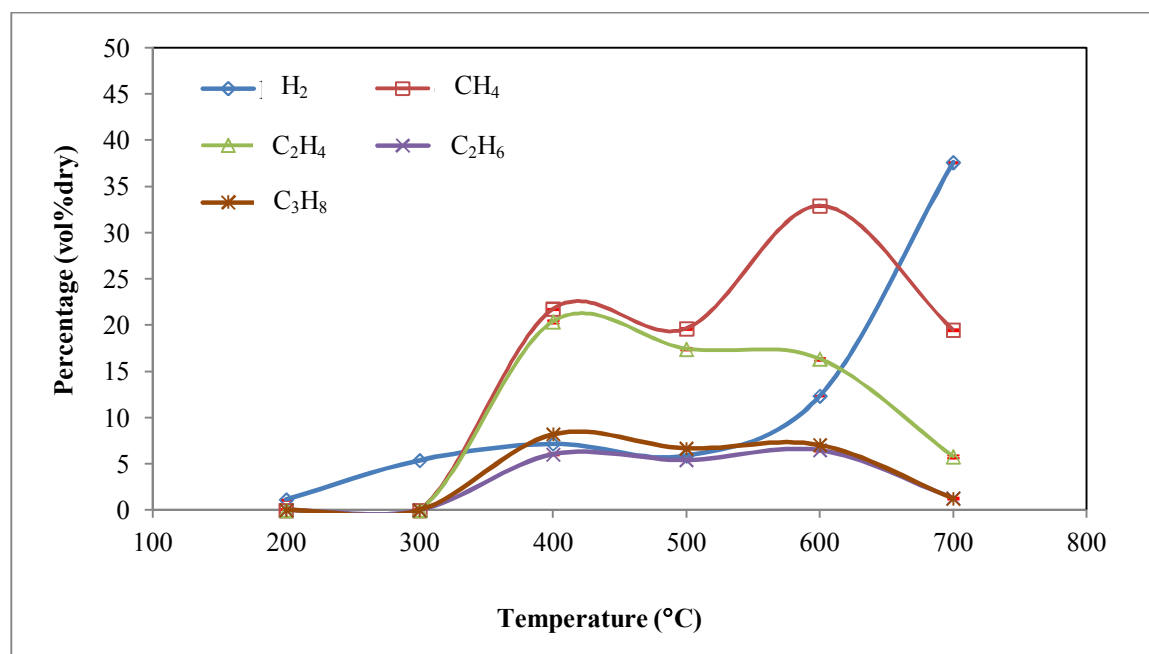
Figure 7-21: Gas compositions (H_2 and other hydrocarbon) from the pyrolysis of the OPS with a heating rate of 15°C/min.
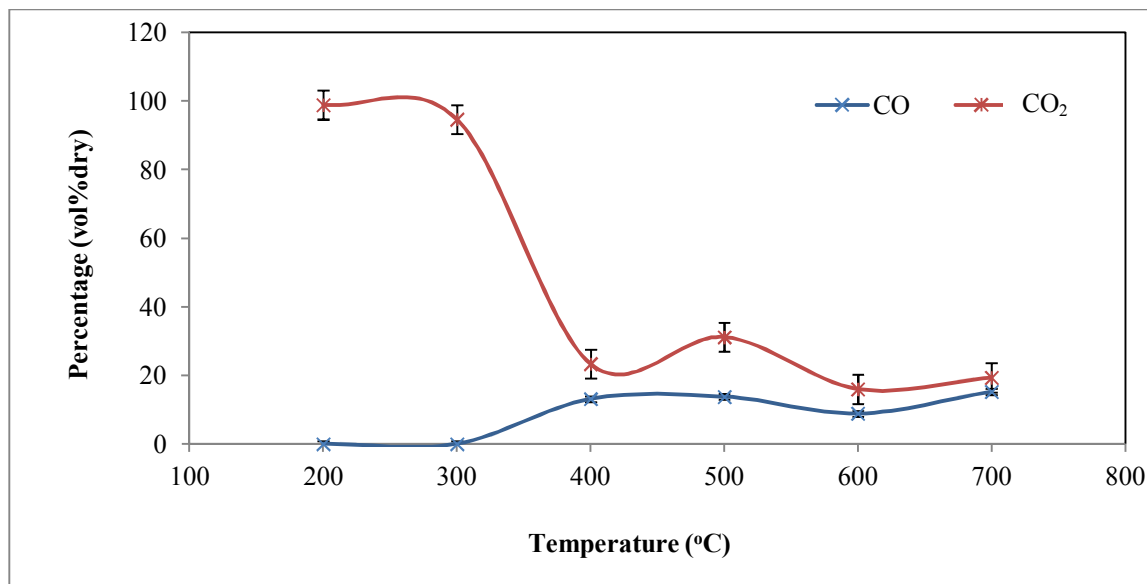
Figure 7-22: Gas compositions (CO and CO_2) from the pyrolysis of the OPS with a heating rate of 15°C/min.
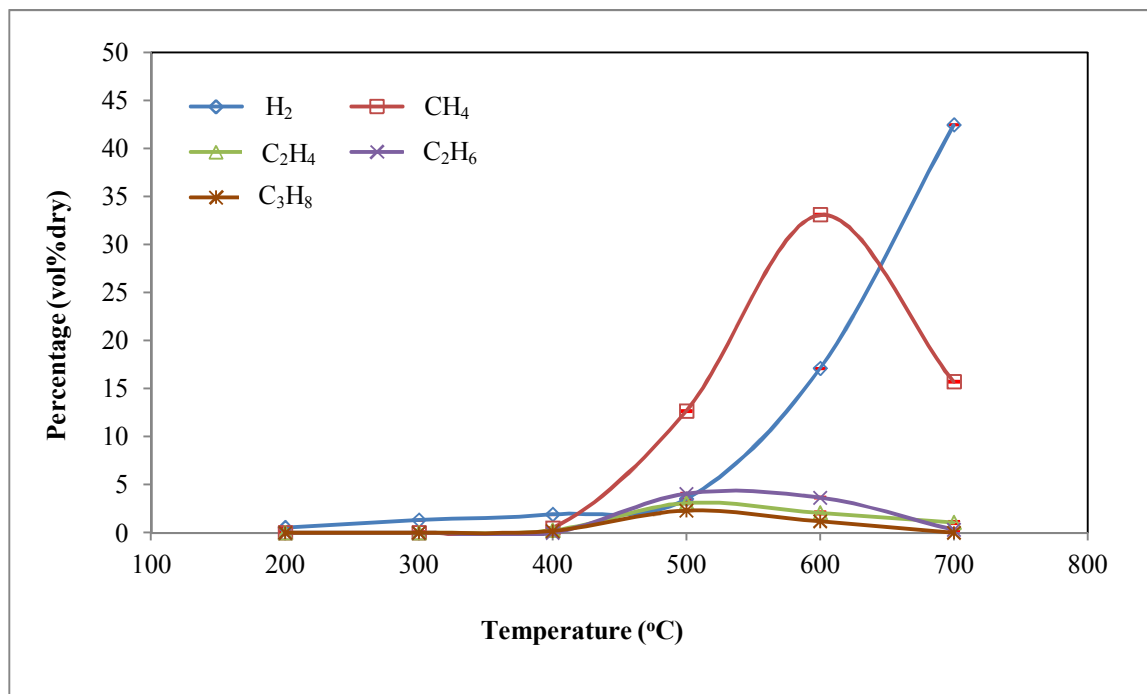
Figure 7-23: Gas compositions (H_2 and other hydrocarbon) from the pyrolysis of the PKC with a heating rate of 15°C/min.
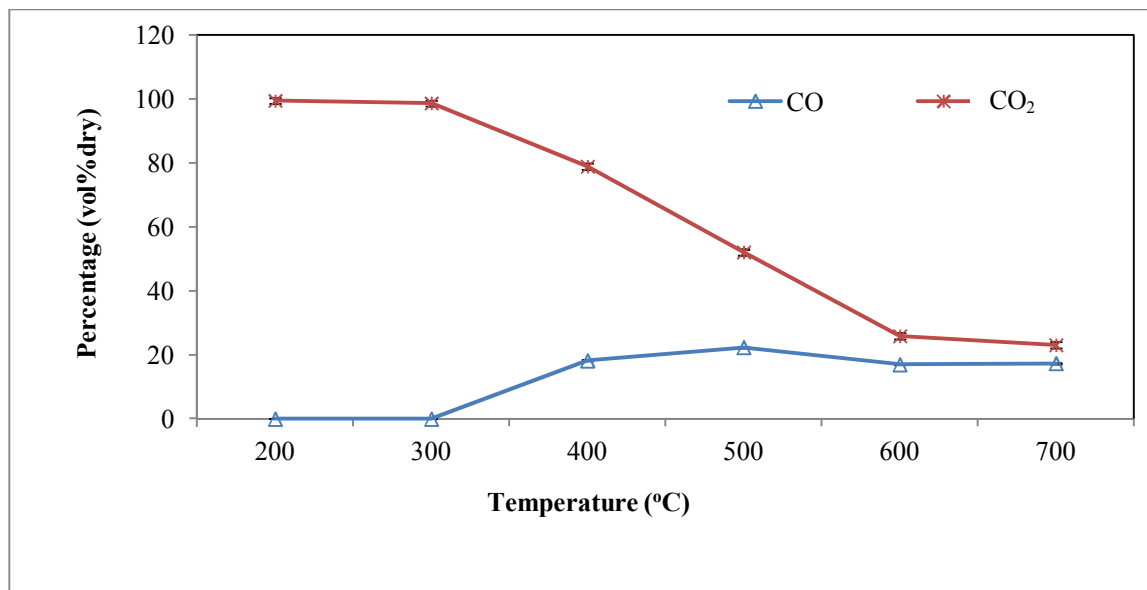
Figure 7-24: Gas compositions (CO and CO_2) from the pyrolysis of the PKC with a heating rate of 15°C/min.

8 OVERALL DISCUSSION ON COMBUSTION AND SLOW PYROLYSIS OF OIL PALM STONE AND PALM KERNEL CAKE

The demand for energy is increasing as world population increases year-by-year. It is obvious in developing countries as energy is important for an economic and social development. In recent years the world has relied heavily on fossil fuels such as coal, oil and gas to provide energy. Using fossil fuels to produce energy contributes to environmental problems such as the release of greenhouse gas emissions and toxic substances that lead to health problems. Therefore, it is important to find clean fuel as alternative sources for future energy generation that are more environmentally friendly.

Burning fossil fuels has become a major problem in terms of climate impact particularly on the emissions of CO_2. In Malaysia, CO_2 emission could reach 285 million tonnes by the year 2020 without any mitigation programmes, an increase of 67% since the year 2000. Electricity generation is the major contributor, approximately 43 %, along with other main sectors including transportation, industrial and residential (Safaai *et al.*, 2010).

It is therefore of paramount importance to speed up the process of finding alternative fuels (biomass or bioenergy) which are environmentally friendly, cost effective and above all renewable. Furthermore, improvements in technology, e.g., combustion or incineration may also help in reducing pollution. Although there are some improvements on toxic gases release from combustion achieved by optimising process parameters such as furnace, boiler and gas cleaning systems design, there is still a lot more that needs to be done for further improvements to accommodate very stringent regulations imposed by the regulatory bodies.

In this PhD study, the main characteristic of the thermo-chemical conversion of oil palm stone and palm kernel cake were investigated using fixed bed and pilot-scale fluidised bed reactors. A series of combustion and pyrolysis tests were carried out in two fixed-bed reactors. The effects of heating rate and pyrolysis temperature on the primary products

distributions and their properties were investigated. Theoretical modelling was also carried out in order to compare the results from fixed bed combustion experiments.

8.1 Potential utilisation of oil palm biomass

Many Southeast Asian countries such as Malaysia, Thailand and Indonesia are leading producers and/or exporters of agricultural products. Among major agricultural commodities exported are rice, palm oil, sugar cane and coconut. Cultivation of these crops generates biomass by-products such as rice straw, oil palm shell, palm kernel cake, oil palm stone, bagasse and coconut shell. However, only a small amount of these materials are being utilised as fuels in combustion plants or household cooking. Industries are therefore left with a significant amount of biomass materials generated year by year. There are approximately 120 million tonnes of biomass residues generated every year from this region (Carlos and Ba Khang, 2008). Some examples of the potential biomasses across the region are 34 million tonnes of bagasse produced annually from the sugar industry potentially generates more than 11,407 MW, 19 million tonnes of rice husks could potentially generate around 16,720 MW and residue from wood and wood based industry could generate around 30 million m^3 annually and could possibly produce about 1600 MW of power (Carlos and Ba Khang, 2008, Shuit *et al.*, 2009).

As the world's second largest palm oil producer and exporter, Malaysia produced more than 55.73 million tonnes of oil palm biomass annually or about 86 % of total 70 million tonnes of biomass generated across the country (Shuit *et al.*, 2009). As discussed in Section 2.2 oil palm biomasses have great potential as renewable fuels due to high energy (CV) content. One of the objectives of this PhD study was to characterise raw material, OPS and PKC. The composition of the OPS and PKC were characterised according to proximate, ultimate analyses. The results for OPS and PKC are shown in Table 7-1 and Table 7-2 respectively. The experimental data were analysed and compared with the literature (Lua and Guo, 1998, Zailani *et al.*, 1999, Sukiran *et al.*, 2009). Most of the components are comparable and show almost similar results. Both fuels contain high volatile and low fixed carbon contents. OPS had a calorific value (CV) of 27.46 MJ/kg in

the range of soft coal (bituminous, 24-35 MJ/kg). However, PKC had slightly lower heating value around 18.67 MJ/kg, in the range of brown coal (lignite, 10-20 MJ/kg). Based on data obtained from this study, OPS and PKC have great potential to be considered as green fuels for the future. However, concern may arise if a large plant is to be built particularly due to corrosion brought about by high concentrations of K, Ca and P in both fuels. Oxides of these metals could cause problems such as slagging and fouling and normally occur at high temperature (>1000°C) in the combustion systems. The presence of Cl in the raw material may cause severe damage to the environmental and combustion systems since KCl reduces the flash fusion temperature. Chlorine radicals and Cl_2 can react with organic compounds to form stable chlorinated by-products such as chlorinated benzenes and phenols. These compounds are known precursors for the formation of toxic substances such as polychlorinated dibenzofurans (PCDFs), polychlorinated dibenzodioxins (PCDDs) and biphenyls. These compounds can form at low temperatures around 250-400°C (Procaccini, 1999).

Malaysia's oil palm trees are mainly from *Elaeis* genus from the family of Palmae which originally come from West Africa. With the growth of palm oil production, the biomass generated also increases. It was estimated that one hectare of oil palm plantation could easily produce about 50-70 tonnes of biomass residues (Shuit *et al.*, 2009). Most of the residues come from activities such as plantation and milling which includes empty fruit bunches (EFBs), shell, fibre, palm kernel cake (PKC), oil palm stone (OPS), trunks and fronds.

OPS are the kernel that can be obtained by breaking the shell (endocarp) of the palm fruits. PKC is the residue of oil extraction from the kernels of palm fruits. Some of these materials are currently used as animal feed, fuel for boilers with low energy efficiency and soil conditioner. Only recently interest has started to arise on possible energetic use of these residues (Giuntoli *et al.*, 2011). However, knowledge of their thermo-chemical behaviour is still very limited. Thus this PhD study provides information needed for further investigation and utilisations of these materials. Data from characterisation of the

OPS and PKC based on proximate and ultimate analyses, pyrolysis and combustion tests provided valuable information for scale-up and operations of biomass plant.

Although there is great potential for biomass fuels in Southeast Asia region, lack of an enabling institutional, policy, political influence and regulatory environment to support the development and implementation of biomasses projects still remain the major barriers for this industry to growth. Attempt has been made to promote utilisation of untapped biomass from this region, but mostly by individual state members. At present there are no comprehensive programmes to promote biomass fuels in the wider region.

8.2   Technology assessment

Energy stored in OPS and PKC can be converted to valuable products such as electricity, heat and steam via various conversion methods. In general there are two groups of technologies available: thermo-chemical and bio-chemical methods that can be used to convert biomass to valuable products. The former includes conventional combustion; widely used for biomass to energy conversion purposes. However, new technology including gasification (partial oxidation) and pyrolysis (thermal degradation of biomass in absence or very limited of oxidising agent) are currently under development for industrial scale application (Henriksen *et al.*, 2006, Babu, 2008, Kirubakaran *et al.*, 2009). Combustion can be used directly for heating purposes or for power generation (via steam turbines or the like). In bio-chemical methods the most significant process in the stationary energy supply is anaerobic digestion. Fermentation belongs to this technology group, but the resulting fuel, ethanol, is rarely used as fuel for power generation as it has more value as a transportation fuel.

In this PhD study only thermo-chemical technology is assessed to convert OPS and PKC materials. Technologies based on the thermo-chemical methods are widely used in biomass conversion and include direct combustion boiler and steam turbines, co-firing, gasification and pyrolysis. Combustion technology is classified as mature and

commercially available on an industrial scale for biomass or fossil fuels. However, due to the more stringent regulations, further developments need to be carried out particularly on efficiency and gas emissions. The simplest method is the combustion of biomass in a furnace or pot burner. The group of technologies in use for conversion of biomass in larger scale (more than 10 MWe) include grate-fired (stationary, travelling and vibrating), suspension fired and fluidised-bed (bubbling and circulating). Descriptions, advantages and disadvantages of these technologies are presented in Table 8-1.

A commercial biomass steam boiler can achieve approximately 60-85 % efficiency using grate or fluidised bed combustors (Evald and Majidi, 2004). Among the thermal biomass conversion technologies that are commercially available, fluidised-bed combustion systems are found to be more efficient and flexible in terms of fuel properties (van den Broek *et al.*, 1996). However, in this study the combustion efficiency of the pilot-scale fluidised bed could not be calculated due to the difficulty to remove and separate the bottom ash at the bottom of the reactor. Thus, combustion performance of OPS in the pot burner and pilot-scale fluidised bed could not be established.

Table 8-1: Summary of biomass combustion technologies (van den Broek *et al.*, 1996).

Technology	Description	Advantages	Disadvantages
Pot burners	The biomass is dumped on pile in a furnace. Combustion air supply from bottom and above the pile to burn the biomass materials.	• Fuel flexibility • Simple design	➢ Low boiler efficiency ➢ Poor combustion control

Grate-fired
 	
Stationary
 	
Travelling
 	
Vibrating
	Fuel is spread evenly in thin layer on the grate. Primary and secondary air supply from the bottom and above the grate systems.
	
	Stationary sloping-grate: the grate does not move. Fuel burns as it slides down the slope.
	
	Travelling-grate: the fuel is fed in at one side of the grate. It has to be burnt before it reaches the ash dumping section of the furnace.
	
	Vibrating-grate: the fuel is fed evenly over the grate area by vibration mode.
		• Stationary grate:
		  o Easy to design
		
		• Travelling-grate:
		  o High maintenance costs due to the high moving parts.
		
		• Vibrating-grate
		  o Less maintenance costs compared to travelling-grate systems.
			➢ Stationary grate:
			  o Difficult to control the combustion process
			  o Risk of dumping the fuel.
			
			➢ Travelling grate:
			  o Improves combustion control due to the spreading of fuel layer. It become thinner and easy to burn.
			  o Improve carbon burnout efficiency as compared to sloping-grate system.
			
			➢ Vibrating-grate:
			  o Carbon burnout efficiency is further improved.
			  o In water-cooled grate systems it is possible to increase the amount of over fire air. Thus reduced the formation of thermal NOx.

Suspension fired	The fuel is fired as small particles which burn while it's being fed into the boiler. The system almost similar with pulverised coal-fired technology.	• High efficiency.	➢ Pre-treatment costs of the fuels are considerably high.

Fluidised bed
 	
Bubbling
 	
Circulating
	Fluidised bed combustion system use the speed of the combustion air from the bottom of the boiler to bubble-up the fuel. On the commercial scale either bubbling or circulating fluidised beds can be used.	• Fluidised bed:
		  o Flexibility in handling variety of fuels
		  o Very high in carbon burnout efficiency.
		  o Low combustion temperature-reduces the amount of NOx and SO_2 emissions.
		
		• Bubbling fluidised bed:
		  o Low capital investment compared to circulating fluidised bed system.
		
		• Circulating fluidised bed:
		  o Better carbon burnout efficiency compared to bubbling fluidised bed.
		  o Less acid gas releases to the environment with the addition of lime to the bed.
			➢ Fluidised bed:
			  o Required high capacity fan to provide high speed air required for the fuel to bubble-up.

8.2.1 Pyrolysis

Pyrolysis experiments were conducted using a fixed-bed reactor providing detailed information on the thermal behaviour of oil palm stone and palm kernel cake. The effect of parameters such as temperature and heating rates on the primary products (char, liquid and gas) compositions obtained from the pyrolysis tests provide an important input for the FLIC modelling study. Pyrolysis of the oil palm stone and palm kernel cake at 500°C with a heating rate of 10°C/min gave maximum liquid yields of 57.92 and 42.84 wt% respectively. Liquid obtained from pyrolysis of palm kernel cake was slightly lower compared to oil palm stone due to fact that the palm kernel cake contains low volatile content. The lower volatile content in PKC is due to several processing steps.

Increased pyrolysis temperature from 500 to 700 °C caused a decrease in the char yield due to further devolatilisation of the residual volatile matter in the char. Similarly, an increase in the final temperature resulted in the reduction of liquid yield and an increase in the gas yield. These trends were consistent with the results obtained by *Zailani et al*., (1999) and Sukiran *et al*., (2009). This observation is due to the breaking up of long carbon chains at higher temperatures, which produce lighter gases. The CO and CO_2 gases evolved at lower operating temperature (<500 °C), however hydrogen and hydrocarbon gases dominated at high temperature region (>500 °C). The chars obtained from the pyrolysis of oil palm stone and palm kernel cake possessed almost similar energy content of bituminous coal, approximately 28 MJ/kg. Proximate and ultimate analyses of the chars from both samples showed that fixed carbon had increased more 90% from the original samples after pyrolysed at 500-700°C. Chars from both samples mainly consisted of fixed carbon with small fraction of volatile matter. This finding is in good agreement with that of Uzun *et al*., (2007), who analysed char residue from pyrolysis of the olive-oil residues at the same temperature range.

8.2.2 Fixed-bed combustion

The combustion tests were successfully conducted in a fixed-bed combustor. Only the oil palm stone sample was used in the combustion tests due to the difficulty to convert loose palm kernel cake material into densified or pellet form. It is not suitable to conduct combustion tests using loose material as it easily elutriates through the primary air and escapes before being burned in the combustion chamber. Oil palm stone was room dried prior to the combustion tests. The processes start with the removal of chemically-bound moisture content and followed by devolatilisation process.

As discussed in Chapter 6, at around 1600 s after the combustion processes took place the fuel bed began to burn without assistance from the pilot burner. The combustion process of the fuel bed entered the ignition propagation period during which the devolatilisation and combustion of volatile matter in the upper layer of the bed resulted in the heating up and ignition of the next layer of the fuel bed. The local bed temperature increased to 800-1000°C as the ignition front propagated through the fuel bed. At the beginning of this period, O_2 concentration began to decrease whereas the concentrations of CO_2 and CO increased. At around 2150 s after the combustion process took place, all the oxygen supplied by the primary air was consumed. Meanwhile, CO_2 concentration began to decrease whereas CO concentration started to increase due to partial oxidation under lean oxygen condition. The CO is thermodynamically more stable than CO_2 at higher temperature (>700°C), thus the gas in equilibrium with carbon is predominantly CO (Gaskell, 2001). This phenomenon is explained by the Ellingham diagram outlined in Section 2.3.7.6.

As the burnout of the char material was more difficult than the volatile matter and there was insufficient amount of O_2, the char accumulated in the bed after the ignition front propagated in the region. The ignition propagation period ended at around 4400 s when the ignition front reached the grate. At the end of this stage, the residual fuel in the bed was about 20 %. Based on the temperature profiles, the ignition front propagation process was similar in all the cases. However, as the air flowrate increased, the heat transfer via

convection became more difficult. In addition, higher air flow rate also increased the local air-fuel ratio and consequently the combustion temperatures.

The NOx concentration remained constant at a level of about 5 ppm during the ignition propagation stage. During this stage, the top part of the fuel bed remained under reducing conditions. NOx formed during the volatile combustion stage can easily be reduced to N_2, as shown by Zakaria (2000). During the final char combustion stage, NOx concentration increased to a peak value of 46 ppm (Figure 6-6). As the oxygen concentration in the flue gas began to increase, the nitrogen in char was converted to NOx during the char combustion (Nussbaumer, 2003, Liang *et al.*, 2008).

8.2.3   FLIC modelling of fixed-bed combustion

The information obtained from pyrolysis and fixed bed combustion tests were used in the FLIC modelling study. This was used to validate the combustion temperature and gas emissions from fixed-bed experimental results. The predicted temperature profile in the fuel bed over reaction time was compared with the experimental results. It was found that the temperature during the ignition propagation period was similar to that from the experiments. FLIC modelling can also be used to predict the individual process rates of specific components such as moisture evaporation, devolatilasation and char combustion. However, in this study these parameters were not available for comparison due to the difficulty in measuring them during combustion experiments.

As discussed in Chapter 6, Section 6.1.4.2, the predicted gas composition was compared with that measured in the combustion tests. In general, the predicted gas composition was in good agreement with the measured data. However, some discrepancies were observed on the predicted concentrations of CO_2 and CO which were slightly lower than the measured data. This was due to under-prediction of char combustion or the combustion of volatile compounds, mostly hydrocarbons. In modelling calculations, it was assumed that char was pure carbon. Char, however, contains a small amount of hydrogen and

oxygen as well as trace metals such as potassium, calcium and iron. These metals could have a catalytic action to promote the release of CO and CO_2 during char combustion.

8.2.4   Pilot-scale fluidised bed combustion

A pilot-scale fluidised bed reactor was used to evaluate the combustion behaviour of oil palm stone. Currently, fluidised-bed systems (bubbling or circulating) are considered as the most efficient and flexible (in terms of fuel properties) technology available for high capacity (>10 MWe) biomass combustion power plant (van den Broek *et al.*, 1996). The key experimental results from combustion tests are very important in the design and operations of large scale power plants. The variables investigated in this study included the effects of primary air flowrate and initial temperature of the bed when feeding commenced on temperature profiles throughout the reactor as well as gas emissions. Ash residue and acid gases were also analysed in order to obtain a better understanding of OPS combustion in a pilot-scale fluidised bed reactor. A series of combustion tests were designed to investigate those effects on OPS material. Six cases were tested to investigate the influence of primary air flowrate and the initial bed temperature on the combustion properties in a pilot-scale fluidised bed reactor.

The bed temperature gradually decreased moments after the sample was introduced into the reactor. The temperature drop at the beginning of the combustion process indicates that the net energy was 'negative' due to the drying and devolatilasation process of the fuel. The rate of consumption by these processes was greater than the rate of energy release in the bed. However, after the devolatilised and residue char started to burn and release energy (exothermic process), then the bed temperature stabilised where the rates of energy consumption and generation were at equilibrium. The freeboard temperatures were gradually increased over time. Energy released during volatile and char combustion was dominant in this region and caused the temperature to increase. The temperature stabilised at around 750°C during the combustion period. A plateau was observed in the temperature above the bed. This suggested that the combustion occurred steadily during the test periods. In general, the bed and bed surface temperatures decreased as the

primary air flowrate increased. The freeboard temperature was observed to be uniform and almost independent of primary air flowrate.

Combustion gases (CO, CO_2 and O_2) were monitored by direct line measurements as discussed in detail in Chapter 4. The concentration of CO was observed to be less than 0.2% in all cases. The amount of O_2 was slightly higher compared to the concentration of CO_2 during the combustion period with higher excess air ($\lambda = 1.80$). This indicated that combustion occurred rapidly.

Acid gas emissions such as NOx, SOx and HCl were monitored in all combustion tests. The amount of NOx released during combustion process was relatively low from 162 ppm to 238 ppm. However, additional gas cleaning system should be considered if large plant is to be built. The permitted amount of NOx releases to the environment as stated in the waste incineration directive for England and Wales is 200-400 mg/m^3 (WID, 2009). The concentration of HCl presented was inferred using the Standard method (BS 1756 part 4) based on the assumption that all (Cl$^-$) ions in the gas phase were present in the form of HCl. The concentrations of HCl measured in all cases were below 0.05 ppm. This value is far below the permitted level given by WID at10 mg/m^3 (WID, 2009). Sulphur dioxide (SO_2) was emitted with very low concentration during combustion of oil palm stone.

Other important components analysed were fly and bottom ashes. The fly ash samples were taken from the cyclone mounted at the top of the reactor. Less than 2 % of the initial material was trapped as fly ash in the cyclone. This indicated good combustion characteristics in the pilot-scale fluidised bed reactor. According to Lind *et al*., (2000) there are two mechanisms by which ash can become attached to sand particles: ash deposition on the sand surface; and diffusion of the ash compounds into the bed particles. Consequently these were quite difficult to separate and thus the proportion of ash in this mixture was calculated, along with the unburned carbon, using an ash tracer method (Li *et al.*, 2010, Munir *et al.*, 2010, Zhang *et al.*, 2010). Only two tests (1 and 2) were used to calculated bottom ash using ash tracer method. Approximately 1.7% of the mass of the

mixture (sand + bottom ash) was determined to be bottom ash, of which 10% was estimated to be unburned carbon.

Chars contained in the cyclone and bottom part of the reactor were analysed using ICP-MS for full elemental analysis. Analysis of trace elements showed that those present in high concentrations in the fly ash were also present in high concentrations in the bottom ash. The most abundant elements were found to be Al, Ca, Fe, K, Mg, Mn, P, S and Si. The elements of concern for combustion systems are K, Na, Ca, Mg, Si, Cl and S (Vamvuka and Zografos, 2004) which can cause fouling. However, as this combustion system operated at relatively low temperature regime, fouling is not likely to be of concern.

8.2.5   Pelletisation

Palm kernel cake (PKC) is readily available in powder or loose form as described in Section 4.5. It is important to transform this material into densified (pellets) fuel prior any combustion tests. In this study, a manual pelletisation process based on a compression method was used as described in Chapter 4, Section 4.1.4. The main objective of this pelletisation study was to identify key parameters that affect the pelletisation process of PKC. Among others, the effect of fuel's moisture content, compression pressure, pelletisation temperature and several organic and inorganic binders were tested. Pellets produced at optimum conditions were then further analysed for their physical strength. The tensile strength, density and durability were analysed to determine the quality of the pellets produced.

It has been established that palm kernel cake can be pelletised to relatively high densies and tensile strengths at elevated temperature and pressure. The moisture content of the biomass strongly affected pellet quality; increasing the moisture from the 'as received' level of 7.9 % caused pellets to deteriorate, whereas reducing the moisture content resulted in the formation of weak pellets that were prone to cracking. The optimum

conditions for the production of these pellets were found to be a moisture content of 7.9%, a compaction pressure of 9338 psi (64.38 MPa) and a pelletisation temperature of 80-100°C. At these conditions, the pellets formed had a density of 1184-1226 kg/m^3 and a tensile strength of 930-1007 kPa.

Adding a small amount of inorganic binder improved the quality of the palm kernel cake pellets. Addition of caustic soda (<2 wt.%) increased the tensile strength to a maximum of 3055 kPa, where the density fluctuated between 1192 kg/m^3 and 1237 kg/m^3. Improvements were also seen with the addition of approximately 5 wt% calcium carbonate, where the tensile strength reached about 1500 kPa. Of the three organic binders (maize, tapioca and potato starches) tested, only small amounts of maize starch resulted in improved pellet quality, although this was not as effective as the inorganic binders. The addition of the other organic binders (tapioca starch and potato starch) did not result in any improvements in terms of tensile strength or density.

8.3 Economics of fuels feedstock: Costs analysis

The major concern of any investments in any biomass technologies are the costs and profits. Attempts have been made to estimate the costs of implementing pyrolysis technology on oil palm biomass. The cost of conversion of oil palm shell to liquid oil with the yield of 58 wt% of dry feed and 25 wt% of char products were determined. Biomass feed cost of RM40/t (£8/t), labour cost of RM3/ht (£0.60/ht), plant life span 10 years with capacity of 1.5t/y and total annual operating hours of 3000. It was found that the cost was higher than the conventional petroleum derived fuel price. However, it may be competitive with conventional fossil fuel for scale-up large units along with the other incentive policies for renewable sources of energy (Zailani *et al.*, 1999). Another economic feasibility study was reported in Evald and Majidi (2004) who examined four large scale industrial boilers and industrial processes (paper, cement, rubber and food) to utilise oil palm biomass fuels to replace fossil fuel. It was found that the feasibility in

terms of financial internal rate of return (FIRR) are in the following order cement, paper, food and rubber with the FIRR 263%, 67%, 50% and 16% respectively.

The costs of energy production via fast pyrolysis of biomass in the UK as outlined in Table 2-25 and Table 2-26 show the significant potential of utilising biomass as energy feedstock. At present production of energy from biomass via fast pyrolysis is not a good investment compared to established combustion and steam cycle system due to low system efficiency particularly at high capacities (Bridgwater *et al.*, 2002). However, as environmental regulations become more and more stringent, biomass fuels seem to be the best candidate for fuel and more competitive in the near future.

The drying and compaction processes consume a high amount of energy (Hirsmark, 2002). There are four main groups associate with the pelletisation of biomass: 1) Capital costs (capital and maintenance), 2) Usage-based costs, 3) Operational costs, and 4) Other costs. For example, the pelletisation of raw saw dust with a moisture content of 57 wt% and a bulk density of 350 kg/m^3. The overall production cost is £5 million corresponding to £70 per tonne of produced pellet at current prices. The most consuming energy in the process step is the drying, followed by the compaction process (Hirsmark, 2002). Mani (2005) analysed wood pellet production using the environmental systems assessment tool to evaluate energy, emissions and economics. It was found that the drying process consumed more than 80% of the energy supplied.

Data from literature were used to estimate the costs of pelletisation of PKC material. Similarity in terms of geographical region and waste source between the PKC material and those of Chaiyaomporn and Chavalparit (2010) and using the pelletisation process parameters in Thek and Obernberger (2004), it was estimated that the total production costs of PKC pellets would be between £24 and £43/tonne. This was based on the PKC material supplied in dry, powder form. The cost breakdown was based on the case study in Austria, as reported in Thek and Obernberger (2004). This included: (i) the cost of the dry raw material, which was £3.35/m^3; (ii) a plant capacity of 24,000 tonnes of pellets produced per annum; (iii) transportation costs of £1.25/km (based on an ordinary truck

272

with a capacity of 95 m^3); and (iv) a plant operating seven days a week, with three shifts per day. However, to maintain homogeneity of the raw material as well as the quality of the final product, a sieving machine is still to be considered. As discussed previously, adding small amounts of caustic soda could significantly improve pellet quality, although this may also increase the production costs of the pellets. Adding 2% of caustic soda may elevate the production costs around £28.20-47.20/tonne. This estimation is based on caustic soda price of £210/tonne (Wilson, 2010).

8.4   Energy policies evaluations

Most ASEAN countries including Malaysia have their own targets for the installation of renewable energy capacity. Countries such as Malaysia, Thailand, Indonesia and the Philippines have similar programmes to promote utilisation of biomass energy. The planning framework and implementation is normally reviewed every 5 to 10 years depending on the respective countries. Also, countries in the region are forging ahead with the Clean Development Mechanism (CDM) which was outlined by the Kyoto Protocol to promote energy efficiency and utilisation of renewable energy including biomass. Biomass power planning and programme including grid power capacity installation varies among member countries. Government regulations set, among others, the guidelines for the purchase and sale of power between independent power providers and electric utilities.

Malaysia has introduced many biomass related programmes and projects on utilisation of oil palm biomass to deal with issues on climate change and mitigation, to promote long-term solution on national energy needs. Among others, Small Renewable Energy Power Program (SREP) and Biomass-based power generation and cogeneration in the Malaysian palm oil industry (Biogen) were launched on May 2001 and October 2002 respectively (Sumathi *et al.*, 2008, Shuit *et al.*, 2009). These programmes were launched in line with the government's commitments to intensify utilisation of renewable energy as the fifth fuel in the national fuel energy mix. As discussed in Section 2.7 and 2.8, Malaysia

committed to promote the utilisation of unexploited biomass for energy purposes. The main objectives of these programmes are to establish small scale power producers that utilise biomass fuel to generate electricity and to mitigate greenhouse emissions via reducing dependency on the fossil fuels. Under both programs, the independent power producer (IPP) is allowed to sell electricity generated from biomass fuel to the national grid up to 10 MW at the price of RM 0.19/kWh (Shuit *et al.*, 2009). In addition, project developers are also entitled to incentives including income tax exemption up to 70% on statutory income for 5 years or investment tax allowance up to 60% of capital expenditures incurred within a period of 5 years. Import duty and sales tax exemption on imported machinery and equipment or sales tax exemption for domestically produced machinery and equipment are also available.

In Indonesia, the Small-Scale Renewable Energy Power Programme was launched in August 2002. Under this programme, the independent power providers are allowed to sell power of 1 MW and below to the national grid system at 80% selling price of electricity for medium voltage and 60% for low voltage (Balce *et al.*, 2003, Carlos and Ba Khang, 2008).

At present, The Philippines still do not have a comprehensive programme to accommodate electricity from renewable energy providers. However, the possibilities to implement minimum prices for electricity generated from renewable sources are quite promising with the aim to enhance the competiveness of renewable energy technology over a conventional one (Balce *et al.*, 2003).

Thailand implements almost the same programme as Malaysia to promote utilisation of biomass energy to mitigate environmental pollution particularly on greenhouse gases emissions. The small power producer (SPP) was launched in 1992. It mandated the national grid system to purchase electricity from renewable energy sources through a long-term power purchase agreement (PPA) (Carlos and Ba Khang, 2008).

In the European Union (EU), Waste Incineration Directive (2000/76/EC) was implemented with the aims to bring closer the requirements for incineration and co-incineration. The move is going in the right direction to address the concern of environmentalists that industrial plants co-incinerating waste derived fuels are not as strictly controlled as waste incinerators. The implementation of the EC Landfill Directive (1999/31/EC) has an indirect impact on energy production in EU. Strategies chosen by Member States to divert the biodegradable fraction of MSW and used tyres from landfill as required under this Directive are likely to encourage RDF production. In addition, several countries are implementing policies in respect of climate change and control of greenhouse gas emissions, which will also have an impact upon the use of RDF in co-incineration facilities.

The waste incineration directives (89/429/EEC and 89/369/EEC) were effective as of 1996. It aimed at reducing as far as possible the negative effects on the air, soil, surface and groundwater caused by emissions from waste-to-energy plants. To all thermal conversion plants it meant that either they install an efficient clean-up system for their flue gases or they close. Most closed, only the plants built after 1989 which were expecting the emission controls or those who could afford the expensive refit remained (WID, 2009).

8.5 Industrial applications

Significant applications can be drawn from the combustion and pyrolysis results of OPS and PKC materials. As stated in van den Broek *et al.*, (1996) the fluidised bed combustion system is the most effective system available for biomass thermal conversion in terms of efficiency and fuel flexibility in large scale power plant. OPS fuel can directly burn in the boiler without pre-treatment except drying. Air drying is more cost effective as it is not require special drying equipment to be installed. However, PKC materials as discussed in the earlier sections are available in loose powder form. Therefore, pelletisation is essential in order to utilise them as fuels and burn it in combustion plant. Based on the pelletisation tests, PKC produced good quality pellets at 'as received'

moisture content, therefore drying process is not a priority in the production of PKC pellets at large or commercial scale. However, due to uneven particle size, screening equipments still need to be considered. There are wide ranges of pelletisation equipments commercially available, some of them have been discussed in Chapter 2, Section 2.4. Among others, compression methods seem to be effectives for PKC material. In large scale productions, a continuous process could be a better option and cost-effective (Finney, 2009). Storage is another issue involving pelletisation of biomass fuels for power generation. To avoid large storage space, pelletisation plant should be built near or within biomass power plant complex.

Based on the combustion tests, it has been shown that OPS material can successfully be burnt for energy purposes. Pyrolysis of OPS and PKC produced highly valuable products, char, bio-oil and gas which could be utilised in large scale power plant. As discussed in previous section, OPS and PKC material contained considerable amount of alkali metals and ash. Therefore, if these fuels are going to be used in large scale power plant, the best technology options available is fluidised bed combustion. The fluidised bed technology can accommodate flexible fuels properties with high efficiencies and easy on gas emissions particularly on NOx and SOx (van den Broek *et al.*, 1996).

In summary, this PhD study evaluated the thermo-chemical behaviour of oil palm stone and palm kernel cake using thermal methods; pyrolysis, fixed bed and pilot-scale fluidised bed combustion. Loose palm kernel cake can be densified as a fuel using pelletisation process with caustic soda as a binder. Compaction methods are the most effective way to pelletise PKC material. Oil palm stone was successfully burnt in both fixed-bed and pilot-scale fluidised bed reactor. Pyrolysis results provided an important data for boundary conditions to be used in FLIC calculations and scale up process. Based on experimental data obtained from this study, oil palm stone and palm kernel cake should be considered as an important source of clean fuels for energy production in the near future.

9   CONCLUSIONS AND FUTURE WORK

The aims and objectives of this 3-year PhD programme have been achieved. The main conclusions and suggestions for future work are presented in this chapter.

9.1   Conclusions

9.1.1   Slow pyrolysis

Proximate and ultimate analyses on OPS and PKC showed that these fuels contain considerable amounts of ash content, high volatile matter and low fixed carbon content. Both materials also contain small amounts of sulphur and nitrogen with high calorific value. This indicates use as fuels for energy production. The experimental investigation into the fixed-bed pyrolysis reactor successfully produced detailed results on pyrolysis product compositions, and the characterisation of all primary products properties; char characterisation was based on proximate and ultimate analysis, properties of bio-oil were analysed using FTIR and the composition of gas products from pyrolysis was analysed using a gas chromatograph (GC).

Pyrolysis of the OPS and PKC at 500°C with a heating rate of 10°C/min gives maximum liquid yields of 57.92 wt. % and 42.84 wt. %, respectively. The char product obtained from the pyrolysis of the OPS and PKC contained approximately 18-44 % of the energy content of the raw materials at the temperature of 500°C, and 16-42 % at the higher temperature of 700°C. The liquid obtained from the pyrolysis of the PKC and OPS at 500°C contained approximately 65-76 % of the energy content of the raw materials, whilst the liquids derived from the pyrolysis of the PKC and OPS at a temperature of 700°C contained around 48-80 % energy yield of the original materials.

The pyrolysis char from both samples contained a gross calorific value of around 28 MJ/kg, whilst the liquid contained approximately 21 MJ/kg to 38 MJ/kg. Liquid derived from the pyrolysis of OPS formed a homogeneous mixture, whilst that obtained from the PKC consisted of an oil and aqueous layer. The liquids contained highly oxygenated compounds, with the obvious functional groups of the chemical compound being phenol,

alcohols, ketones, aldehydes and carboxylic acids. The pyrolysis gases consisted mainly of CO and CO_2, and evolved at a lower temperature, below 500°C. The main gases that evolved in the high temperature region (above 500°C) were hydrogen and other hydrocarbon gases (methane, ethane and propane).

9.1.2 Combustion

The experimental investigation of the combustion of the OPS in a fixed-bed reactor successfully produced detailed combustion characteristics of temperature profiles, burning rates, ignition front velocity and gas composition for OPS waste bed combustion. The air flow rate affected the ignition and burning rate of the fuel bed. An increase in air flow rate increased the ignition front speed and burning rate. At a lower air flow rate, two discrete regions were established; region I (Figure 6-1) was recognised as the combustion of volatiles, whilst region II (Figure 6-1) was the char gasification stage. The high concentration of NOx emission at the end of the combustion process was due to the char gasification reactions. In general, the FLIC modelling results showed satisfactory agreement with the fixed-bed tests results. The under-predicted CO and CO_2 concentrations were due to un-burnt volatile C_mH_n and the char was assumed to be pure carbon in the FLIC calculation. However, in the experiments the char contains substances such as K, Fe, and Ca that can act as a catalyst to promote the release CO and CO_2 during the combustion processes. A slightly shorter combustion period in all cases was predicted by FLIC modelling.

Thermochemical characteristics of OPS fuel was successfully evaluated using a pilot-scale fluidised bed combustor with various test parameters including the effects of primary air flowrate and initial bed temperature. The bed and bed's surface temperature decreased as the primary air flowrate increased. Acid gas (NOx, SOx and HCl) measured in this study showed all species well below the permitted level as regulated by the Waste Incineration Directive (WID). The combustion temperature was found to be more stable when OPS combustion was initiated at a higher initial bed temperature (950°C). About 10.54% to 14% ash was mixed with the sand bed, whilst around 1.08 to 1.67 % was

collected in the cyclone. The most abundant elements found in the ash sample were Al, Ca, Fe, K, Mg, Mn, P, S and Si.

9.1.3 Pelletisation

Pelletisation experiments were successfully conducted using manual pelletisation equipment based on the compression method to determine the optimum value for various process parameters for the formation of good quality palm kernel cake pellets. Palm kernel cake can be pelletised to relatively high densities and tensile strengths at elevated temperature and pressure. The optimum conditions for the production of these pellets were found to be a moisture content of 7.9%, a compaction pressure of 9338 psi (64.38 MPa) and a pelletisation temperature of 80-100°C. At these conditions, the pellets formed had a density of 1184-1226 kg/m^3 and a tensile strength of 930-1007 kPa.

Small additions of inorganic binders improved the quality of the palm kernel cake pellets. Additions of caustic soda (<2 wt.%) increased the tensile strength to a maximum of 3055 kPa, however, the density fluctuated between 1192 kg/m^3 and 1237 kg/m^3. Improvements were also seen with additions of about 5 wt.% of calcium carbonate, where the tensile strength reached approximately 1500 kPa. Three organic binders (maize, tapioca and potato starches) were tested. Small amounts of maize starch added to the PKC material resulted in improved pellet quality, although this was not as effective as the inorganic binders. The addition of the other organic binders (tapioca and potato starch) did not result in any improvements in terms of tensile strength or density.

279

9.2   Suggestions for future work

The results obtained from this research provide important data for energy production using oil palm stone or palm kernel cake. It provides valuable data for the design and operation of thermal biomass conversion methods such as combustion, gasification and pyrolysis. In this study, two different final pyrolysis temperatures and three heating rates were investigated. The combustion experiments were focused on oil palm stone samples in fixed-bed and pilot-scale fluidised bed reactors. Four different air flow rates were tested in fixed-bed experiments and two different parameters; primary air flow rate and initial bed temperatures were used to evaluate the combustion characteristics in the pilot-scale fluidised bed reactor.

Before these materials can be fully utilised as energy sources, further investigations should be carried-out on the following issues:

1. A through characterisation of the OPS and PKC materials should be carried-out particularly on properties of char, liquid and gas products. Characterisation techniques such as X-Ray and on-line GC/MS should be used in order to gain better understanding and more precise results.

2. Further experimental investigation should be undertaken into the combustion of the OPS and the PKC using a broad range of air flow rates at super-stoichiometric conditions.

3. The bottom section of the pilot-scale fluidised bed reactor should be re-designed to make it easier for the bottom ash to be collected and analysed after the combustion tests.

4. An experimental study should be carried out on the tar and char obtained from the pyrolysis at different temperatures, using the gasification test rig in order to gain a better understanding on the thermal behaviour of these materials.

5. The under predicted results obtained from FLIC modelling due to the assumption of char being pure carbon should be further investigated. Model improvements are

required. Furthermore, the FLUENT code or other combustion modelling techniques could be carried out to validate the fluidised bed experimental data.

6. Combustion tests should be carried out in larger combustion plants in order to gain better knowledge about the fuels' behaviour in thermally realistic conditions.

7. Actual cost analysis should be carried-out in order to evaluate the economic viability of OPS and PKC materials for energy purposes.

8. Even though caustic soda can work well and produce good quality pellets for PKC, excess of it could possibly affect combustion performance and equipment. Therefore, it is important to further investigate suitable binders that can provide better quality pellets as well as being healthy for the combustion equipment.

REFERENCES

Abdullah, I., Shamsuddin, A. H. and Sopian, K. (1999) "Combustion of palm oil solid waste in fluidized bed combustor". World Renewable Energy Congress 1999.

Abdullah, N. (2005) "An assesment of pyrolysis for processing empty fruit bunches". PhD Thesis. Chemical Engineering and Applied Chemistry, Aston University.

Abdullah, N. and Gerhauser, H. (2008) "Bio-oil derived from empty fruit bunches". Fuel, **87 (12)**, 2606-2613.

Acikgoz, C., Onay, O. and Kockar, O. M. (2004) "Fast pyrolysis of linseed: product yields and compositions". Journal of Analytical and Applied Pyrolysis, **71 (2)**, 417-429.

agricommodityprices.com "Palm oil". agricommodityprices.com http://www.agricommodityprices.com/palm_oil.php (13/8/2011).

Aguiar, L. and Garcia, L. M. (2006) "Influence of the temperature and air/biomass ratio in the air gasification of orange peel". in Bridgwater, A. V. and Boocock, D. G. B. (Eds.) Science in thermal and chemical biomass conversion.

André, R. N., Pinto, F., Franco, C., Dias, M., Gulyurtlu, I., Matos, M. A. A. and Cabrita, I. (2005) "Fluidised bed co-gasification of coal and olive oil industry wastes". Fuel, **84 (12-13)**, 1635-1644.

Andrei, M. A., Sarofim, A. F. and Beér, J. M. (1985) "Time-resolved burnout of coal particles in a fluidized bed". Combustion and Flame, **61 (1)**, 17-22.

Anis, M. (2007) "Current status of oil palm biomass supply". *Conference on Oil Palm Tree Utilization Committee (OPTUC 2007)*. Petaling Jaya, KL, MPOB.

Antal, M. J., Jr. and Varhegyi, G. (1995) "Cellulose pyrolysis kinetics: the current state of knowledge". Ind. Eng. Chem. Res., **34 (3)**, 703-717.

Antal, M. J., Mochidzuki, K. and Paredes, L. S. (2003) "Flash carbonization of biomass". Ind. Eng. Chem. Res., **42 (16)**, 3690-3699.

Armesto, L., Bahillo, A., Veijonen, K., Cabanillas, A. and Otero, J. (2002) "Combustion behaviour of rice husk in a bubbling fluidised bed". Biomass and Bioenergy, **23 (3)**, 171-179.

Babu, B. V. (2008) "Biomass pyrolysis: a state-of-the-art review". Biofuels, Bioproducts and Biorefining, **2 (5)**, 393-414.

Babu, B. V. and Chaurasia, A. S. (2003) "Modeling, simulation and estimation of optimum parameters in pyrolysis of biomass". Energy Conversion and Management, **44 (13)**, 2135-2158.

Balce, G. R., Tjaroko, T. S. and Zamora, C. G. (2003) "Overview of biomass for power generation in Southeast Asia" Asean Centre for Energy. http://www.aseanenergy.org/.

Barooah, J. N. and Long, V. D. (1976) "Rates of thermal decomposition of some carbonaceous materials in a fluidised bed". Fuel, **55 (2)**, 116.

Basiron, Y. (2007) "Palm oil production through sustainable plantations". European Journal of Lipid Science and Technology **109** 289-295.

Beychok, M. R. (1974a) "Coal gasification for clean energy". Energy Pipelines and Systems.

Beychok, M. R. (1974b) "Coal gasification and the Phenosolvan process". American Chemical Society 168th National Meeting, Atlantic City.

Beychok, M. R. (1975) "Process and environmental technology for producing SNG and liquid fuels". U.S. EPA report EPA-660/2-75-011.

Bhattacharya, S. C., Leon, M. A. and Rahman, M. M. (2002) "A study on improved biomass briquetting". Energy for Sustainable Development, **6 (2)**, 67-71.

Bhattacharya, S. C., Shah, N. and Alikhani, Z. (1984) "Some aspects of fluidized bed combustion of paddy husk". Applied Energy, **16 (4)**, 307-316.

Bis, Z. (Ed.) (2010) Fluidised beds, Weinheim, Wiley-VCH Verlag GmBH & Co. KGaA.

Bossong, K. (2011) "EIA report: Renewables surpass nuclear output" http://www.renewableenergyworld.com/rea/magazine.

Botterill, J. S. M., Teoman, Y. and Yüregir, K. R. (1982) "The effect of operating temperature on the velocity of minimum fluidization, bed voidage and general behaviour". Powder Technology, **31 (1)**, 101-110.

Boundy, B., Davis, S. C., Wright, L., Badger, P. C. and Perlack, B. (2010) "Biomass energy data book" U.S Department of Energy.

Bracmort, K. and Gorte, R. W. (2010) "Biomass: comparison of definitions in legislation". in Hemelt, K. C. (Ed.) Biomass: energy data, multi-year plan, and legislative definitions. New York, Nova Science Publishers, Inc.,

Brage, C., Yu, Q., Chen, G. and Sjöström, K. (1996a) "Use of amino phase adsorbent for biomass tar sampling and separation". Fuel, **76 (2)**, 137.

Brage, C., Yu, Q. and Sjöström, K. (1996b) "Characteristics of evolution of tar from wood pyrolysis in a fixed-bed reactor". Fuel, **75 (2)**, 213-219.

Bramer, E. A., Holthuis, M. R. and Brem, G. (Eds.) (2006) A novel thermogravimetric vortex reactor for the determination of the primary pyrolysis rate of biomass, Canada, CPL Press.

Bridgeman, T. G., Jones, J. M. and Williams, A. (Eds.) (2010) Overview of solid fuels, chracteristics and origin, Weinheim, Wiley-VCH Verlag GmBH & Co. KGaA.

Bridgwater, A. V. (1990) "Costs of biomass pyrolysis derived liquid fuels". First Canada/European Community R&D Contractors Meeting.

Bridgwater, A. V. (1999) "Principles and practice of biomass fast pyrolysis processes for liquids". Journal of Analytical and Applied Pyrolysis, **51 (1-2)**, 3-22.

Bridgwater, A. V. (2002) Fast pyrolysis biomass: A handbook volume 2, CPL Press.

Bridgwater, A. V. (2003) "Renewable fuels and chemicals by thermal processing of biomass". Chemical Engineering Journal, **91 (2-3)**, 87-102.

Bridgwater, A. V. and Boocock, D. G. B. (Eds.) (2006) Science in thermal and chemical biomass conversion, CPL Press.

Bridgwater, A. V. and Bridge, S. A. (1991) "A review of biomass pyrolysis technologies". in Bridgwater, A. V. and Grassi.G (Eds.) Biomass pyrolysis liquids, upgrading and utilisation. Elsevier Applied Science,

Bridgwater, A. V. and Grassi, G. (Eds.) (1991) Biomass pyrolysis liquids upgrading and utilisation, Elsevier Science

Bridgwater, A. V., Toft, A. J. and Brammer, J. G. (2002) "A techno-economic comparison of power production by biomass fast pyrolysis with gasification and combustion". Renewable and Sustainable Energy Reviews, **6 (3)**, 181-246.

Brown, T. R., Wright, M. M. and Brown, R. C. (2011) "Estimating profitability of two biochar production scenarios: slow pyrolysis vs fast pyrolysis". Biofuels, Bioproducts and Biorefining, **5 (1)**, 54-68.

Brunner, P. H. and Roberts, P. V. (1980) "The significance of heating rate on char yield and char properties in the pyrolysis of cellulose". Carbon, **18 (3)**, 217-224.

Burling, I. R., Yokelson, R. J., Griffith, D. W. T., Johnson, T. J., Veres, P., Roberts, J. M., Warneke, C., Urbanski, S. P., Reardon, J., Weise, D. R., Hao, W. M. and de Gouw, J. (2010) "Laboratory measurements of trace gas emissions from biomass burning of fuel types from the southeastern and southwestern United States". Atmospheric Chemistry and Physics, **10 (22)**, 11115-11129.

Cao, J.-P., Xiao, X.-B., Zhang, S.-Y., Zhao, X.-Y., Sato, K., Ogawa, Y., Wei, X.-Y. and Takarada, T. (2011) "Preparation and characterization of bio-oils from internally circulating fluidized-bed pyrolyses of municipal, livestock, and wood waste". Bioresource Technology, **102 (2)**, 2009-2015.

Carlos, R. M. and Ba Khang, D. (2008) "Characterization of biomass energy projects in Southeast Asia". Biomass and Bioenergy, **32 (6)**, 525-532.

Chaiyaomporn, K. and Chavalparit, O. (2010) "Fuel pellets production from biodiesel waste". EnvironmentalAsia, **3 (1)**, 103-110.

Charles (2011) "China's biomass energy potential". http://www.biomass-energy.org/author/agico/ (15/8/2011).

Chau, J., Sowlati, T., Sokhansanj, S., Preto, F., Melin, S. and Bi, X. (2009) "Techno-economic analysis of wood biomass boilers for the greenhouse industry". Applied Energy, **86 (3)**, 364-371.

Chen, L., Xing, L. and Han, L. (2009) "Renewable energy from agro-residues in China: Solid biofuels and biomass briquetting technology". Renewable and Sustainable Energy Reviews, **13 (9)**, 2689-2695.

Chuah, T. G., Azlina, A., Robiah, Y. and Omar, R. (2006) "Biomass as the renewable energy sources in Malaysia: An overview". International Journal of Green Energy, **3 (3)**, 323-346.

Darvell, L. I., Jones, J. M., Gudka, B., Baxter, X. C., Saddawi, A., Williams, A. and Malmgren, A. (2010) "Combustion properties of some power station biomass fuels". Fuel.

Daubert, D. D. (1973) "Compacting presses: how they work-what they do-where they are applied". in Messman, H. C. and Tibbetts, T. E. (Eds.) Elements of briquetting and agglomeration. Canada, Lehman Bookbinders Ltd., 83-93.

De Wiest, R. J. M. (1969) Flow Through Porous Media, London, Academic Press.

Deaubert, D. D. (Ed.) (1973) Compacting presses: how they work-what they do-wherethey are applied, Canada, Lehman Bookbinders Ltd.

Debdoubi, A., El amarti, A., Colacio, E., Blesa, M. J. and Hajjaj, L. H. (2006) "The effect of heating rate on yields and compositions of oil products from esparto pyrolysis". International Journal of Energy Research, **30 (15)**, 1243-1250.

DEFRA (2008) "Waste wood as a biomass fuel" Department for Environment, Food and Rural Affairs. Department for Environmental, F. a. R. A. www.defra.gov.uk.

Demiral, I. and Ayan, E. A. (2011) "Pyrolysis of grape bagasse: Effect of pyrolysis conditions on the product yields and characterization of the liquid product". Bioresource Technology, **102 (4)**, 3946-3951.

Demirbas, A. (2001) "Biomass resource facilities and biomass conversion processing for fuels and chemicals". Energy Conversion and Management, **42 (11)**, 1357-1378.

Demirbas, A. (2004) "Effects of temperature and particle size on bio-char yield from pyrolysis of agricultural residues". Journal of Analytical and Applied Pyrolysis, **72 (2)**, 243-248.

Di Blasi, C., Signorelli, G., Di Russo, C. and Rea, G. (1999a) "Product distribution from pyrolysis of wood and agricultural residues". Ind. & Eng. Chem. Res., **38 (6)**, 2216-2224.

Di Blasi, C., Signorelli, G. and Portoricco, G. (1999b) "Countercurrent fixed-bed gasification of biomass at laboratory scale". Ind. Eng. Chem. Res., **38 (7)**, 2571-2581.

Directive 2009/28/EC (2009) Directive 2009/28/EC of the European Parliment and of the Council http://eur-lex.europa.eu/LexUriServ/LexUriServ.do?uri=OJ:L:2009:140:0016:0062:EN:PDF (6/8/2011)

ERC (2011) "Renewable energy from waste". Energy Recovery Council: http://www.wte.org/ (5/8/2011).

Evald, A. and Majidi, M. I. B. (2004) "Biomass fuels for industrial use" Malaysian - Danish Environmental Cooperation Programme.

FAO (2011) "Bioenergy". Food and Agriculture Organisation of the United Nations http://www.fao.org/bioenergy/47280/en/ (6/8/2011).

Fassinou, W. F., Van de Steene, L., Toure, S., Volle, G. and Girard, P. (2009) "Pyrolysis of Pinus pinaster in a two-stage gasifier: influence of processing parameters and thermal cracking of tar". Fuel Processing Technology, **90 (1)**, 75-90.

Figueiredo, J. L., Valenzuela, C., Bernalte, A. and Encinar, J. M. (1989) "Pyrolysis of holm-oak wood: influence of temperature and particle size". Fuel, **68 (8)**, 1012-1016.

Finney, K. N. (2009) "Energy recovery from spent mushroom compost and coal tailings". PhD Thesis. Chemical and Process Engineering, The University of Sheffield.

Finney, K. N., Sharifi, V. N. and Swithenbank, J. (2009a) "Fuel pelletization with a binder: part I - identification of a suitable binder for spent mushroom compost - coal tailing pellets". <u>Energy & Fuels</u>, **23 (6)**, 3195-3202.

Finney, K. N., Sharifi, V. N. and Swithenbank, J. (2009b) "Fuel pelletization with a binder: Part II - the impacts of binders on the combustion of spent mushroom compost-coal tailing pellets". <u>Energy & Fuels</u>, **23 (6)**, 3203-3210.

Frey, H.-H., Peters, B., Hunsinger, H. and Vehlow, J. (2003) "Characterization of municipal solid waste combustion in a grate furnace". <u>Waste Management</u>, **23 (8)**, 689-701.

Friberg, R. and Blasiak, W. (2002) "Measurements of mass flux and stoichiometry of conversion gas from three different wood fuels as function of volume flux of primary air in packed-bed combustion". <u>Biomass and Bioenergy</u>, **23 (3)**, 189-208.

García-Ibañez, P., Cabanillas, A. and Sánchez, J. M. (2004) "Gasification of leached orujillo (olive oil waste) in a pilot plant circulating fluidised bed reactor. Preliminary results". <u>Biomass and Bioenergy</u>, **27 (2)**, 183-194.

Garcia-Perez, M., Wang, X. S., Shen, J., Rhodes, M. J., Tian, F., Lee, W.-J., Wu, H. and Li, C.-Z. (2008) "Fast pyrolysis of oil mallee woody biomass: effect of temperature on the yield and quality of pyrolysis products". <u>Ind. Eng. Chem. Res.</u>, **47 (6)**, 1846-1854.

Gaskell, D. R. (2001) "Metal production: Ellingham diagrams". in Buschow, K. H. J., Cahn, R. W., Flemings, M. C., Ilschner, B., Kramer , E. J. and Mahajan, S. (Eds.) <u>Encyclopedia of materials: Science and technology</u>. Amsterdam, London, New York, Oxford, Paris, Shahnon, Tokyo, Elsevier Science Ltd., 5481-5486.

Ghebre-Sellassie, I. (1989) "Mechanism of pellet formation and growth". in Ghebre-Sellassie, I. (Ed.) <u>Pharmaceutical Pelletisation Technology</u>. New York, Marcel Dekker, Inc., 123-143.

Gipe, P. (2011) "Malaysia's 2011 proposed solar, biomass, biogas and hydro tariffs "*:* http://www.renewableenergyworld.com/rea/news/article/2010/08/malaysias-2011-proposed-solar-biomass-biogas-hydro-tariffs (18/9/2011).

Giuntoli, J., Gout, J., Verkooijen, A. H. M. and de Jong, W. (2011) "Characterization of fast pyrolysis of dry distiller's grains (DDGS) and palm kernel cake using a

heated foil reactor: Nitrogen chemistry and basic reactor modeling". Industrial & Engineering Chemistry Research, **50 (8)**, 4286-4300.

Goh, Y. R., Siddall, R. G., Nasserzadeh, V., Zakaria, R., Swithenbank, J., Lawrence, D., Garrod, N. and Jones, B. (1998) "Mathematical modelling of the burning bed of a waste incinerator". Journal of the Energy Institute, **71,** 110.

Goh, Y. R., Yang, Y. B., Zakaria, R., Siddall, R. G., Nasserzadeh, V. and Swithenbank, J. (2001) "Development of an incinerator bed model for municipal solid waste incineration ". Combustion Science and Technology, **162,** 37-58.

Gomez-Barea, A. and Leckner, B. (Eds.) (2010) Gasification of biomass and waste, Weinheim, Wiley-VCH Verlag GmBH & Co. KGaA.

Gray, W. A. (1968) Compaction after deposition, in the packing of solid particles, New York, Barnes & Noble.

Green (2011) "Green assembly asia environment: Climate change": http://www.greenassembly.net/http:/greenassembly.net/2008/10/09/climate-change-news/malaysia-backpedalling-on-oil-palm-leadership-says-ngo/ (31/3/2011).

Grover, P. D. and Mishra, S. K. (1996) "Biomass briquetting: technology and practises" Food and Agriculture Organization of the United Nations. Asia, R. W. E. D. P. i. 43.

Gungor, A. and Eskin, N. (2008) "Effects of operational parameters on emission performance and combustion efficiency in small-scale CFBCs". Journal of the Chinese Institute of Chemical Engineers, **39 (6)**, 541-556.

Guo, J. and Lua, A. C. (1998) "Characterization of chars pyrolyzed from oil palm stones for the preparation of activated carbons ". Journal of Analytical and Applied Pyrolysis, **46,** 113-125.

Guo, J. and Lua, A. C. (2000) "Effect of heating temperature on the properties of chars and activated carbons prepared from oil palm stones". Journal of Thermal Analysis and Calorimetry, **60,** 417-425.

Guo, J. and Lua, A. C. (2002) "Characterization of adsorbent prepared from oil-palm shell by CO2 activation for removal of gaseous pollutants". Materials Letters, **55 (5)**, 334-339.

Hai, T. C. (2002) "The palm oil Industry in Malaysia: from seed to frying pan" World Wildlife Fund (WWF).

Hamid, K. H. K. (1999) "Production of activated carbon from Malaysian oil palm shell by chemical and physical methods". PhD Thesis. Chemical and Process Engineering, The University of Sheffield.

Hashim, H. and Ho, W. S. (2011) "Renewable energy policies and initiatives for a sustainable energy future in Malaysia". Renewable and Sustainable Energy Reviews, **15 (9)**, 4780-4787.

Hashim, M. and Ludin, N. A. (2008) "Present status and problems of biomass energy utilization in Malaysia" Malaysia Energy Centre.

Haw, L. C., Salleh, E. and Jones, P. (2006) "Renewable energy policy and initiatives in Malaysia". International journal on sustainable tropical design research and practise **1(1)**, 8.

He, R., Suda, T., Fujimori, T. and Sato, J. i. (2003) "Effects of particle sizes on transport phenomena in single char combustion". International Journal of Heat and Mass Transfer, **46 (19)**, 3619-3627.

Henriksen, U., Ahrenfeldt, J., Jensen, T. K., Gøbel, B., Bentzen, J. D., Hindsgaul, C. and Sørensen, L. H. (2006) "The design, construction and operation of a 75 kW two-stage gasifier". Energy, **31,** 1542-1553.

Hernandez-Atonal, F. D. (2007) "Combustion of refuse-derived fuel in a fluidised bed". PhD Thesis. Department of Chemical and Process Engineering, The University of Sheffield.

Heschel, W., Rweyemamu, L., Scheibner, T. and Meyer, B. (1999) "Abatement of emissions in small-scale combustors through utilisation of blended pellet fuels". Fuel Processing Technology, **61 (3)**, 223-242.

Hirsmark, S. (2002) "Densified biomass fuels in Sweden". <u>MSc. Dissertation</u>. Forest Management and Products, Swedish University of Agricultural Sciences.

Hogan, M., Otterstedt, J., Morin, R. and Wilde, J. (2010) "Biomass for heat and power - opportunity and economics" The European Climate Fundation, Sveaskog, Sodra and Vattenfall. .

Horne, P. A. and Williams, P. T. (1996) "Influence of temperature on the products from the flash pyrolysis of biomass". <u>Fuel</u>, **75 (9)**, 1051-1059.

Horttanainen, M., Saastamoinen, J. and Sarkomaa, P. (2002) "Operational limits of ignition front propagation against airflow in packed beds of different wood fuels.". <u>Energy & Fuels</u>, **16 (3)**, 676-686.

Hupa, M. (2007) "Current status and challenges within fluidized bed combustion". <u>Advanced Combustion and Aerothermal Technologies</u>. 87-101.

Husain, Z., Zainac, Z. and Abdullah, Z. (2002) "Briquetting of palm fibre and shell from the processing of palm nuts to palm oil". <u>Biomass and Bioenergy</u>, **22 (6)**, 505-509.

Idris, S. S., Rahman, N. A., Ismail, K., Alias, A. B., Rashid, Z. A. and Aris, M. J. (2010) "Investigation on thermochemical behaviour of low rank Malaysian coal, oil palm biomass and their blends during pyrolysis via thermogravimetric analysis (TGA)". <u>Bioresource Technology</u>, **101 (12)**, 4584-4592.

IPCC (2011) "Summary for policymakers". in Edenhofer, O., Pichs-Madruga, S., Sokona, Y., Seyboth, K., Matschoss, P., Kadner, S., Zwickel, T., Eickemeier, P., Hansen, G., Schlomer, S. and von Stechow, C. (Eds.) <u>IPCC special report on renewable energy sources and climate change mitigation</u>. Cambridge, UK and New York, USA, Cambridge University Press,

Johansson, L. S., Tullin, C., Leckner, B. and Sjövall, P. (2003) "Particle emissions from biomass combustion in small combustors". <u>Biomass and Bioenergy</u>, **25 (4)**, 435-446.

Kaliyan, N. and Morey, R. V. (2009) "Factors affecting strength and durability of densified biomass products". <u>Biomass and Bioenergy</u>, **33 (3)**, 337-359.

Khan, A. A., de Jong, W., Jansens, P. J. and Spliethoff, H. (2009) "Biomass combustion in fluidized bed boilers: Potential problems and remedies". Fuel Processing Technology, **90 (1)**, 21-50.

Kirubakaran, V., Sivaramakrishnan, V., Nalini, R., Sekar, T., Premalatha, M. and Subramanian, P. (2009) "A review on gasification of biomass". Renewable and Sustainable Energy Reviews, **13 (1)**, 179-186.

Klass and Donald, L. (1998) "Thermal conversion: combustion". Biomass for Renewable Energy, Fuels, and Chemicals. Elsevier,

Kobyashi, N., Itaya, Y., Piao, G., Mori, S., Kondo, M., Hamai, M. and Yamaguchi, M. (2005) "The behavior of flue gas from RDF combustion in a fluidized bed". Powder Technology, **151 (1-3)**, 87-95.

Koo, J. K., Kim, S. W. and Seo, Y. H. (1991) "Characterization of aromatic hydrocarbon formation from pyrolysis of polyethylene-polystyrene mixtures". Resources, Conservation and Recycling, **5 (4)**, 365-382.

Kuo, H. P., Zhang, H. Z. and Hsu, R. C. (2008) "CFD modelling of a countercurrent staged fluidised bed". Chemical Engineering Journal, **137 (3)**, 664-676.

Ladanai, S. and Vinterbäck, J. (2009) "Global potential of sustainable biomass for energy" SLU, Swedish University of Agricultural Sciences. http://www.globalbioenergy.org/uploads/media/0912_SLU_-_Global_potential_of_sustainable_biomass_for_energy.pdf.

Latif, A. (2000) "The biology of the genus *Eleais*". in Basiron, Y., Jailani, B. S. and Chan, K. W. (Eds.) Advances in Oil Research. Kuala Lumpur, Malaysian Palm Oil Board,

Li, J., Yan, R., Xiao, B., Liang, D. T. and Du, L. (2008) "Development of Nano-NiO/Al2O3 Catalyst to be Used for Tar Removal in Biomass Gasification". Environmental Science & Technology, **42 (16)**, 6224-6229.

Li, J., Yan, R., Xiao, B., Wang, X. and Yang, H. (2007) "Influence of temperature on the formation of oil from pyrolyzing palm oil wastes in a fixed bed reactor". Energy Fuels, **21 (4)**, 2398-2407.

Li, S., Wu, Y. and Whitty, K. J. (2010) "Ash deposition behavior during char−slag transition under simulated gasification conditions". Energy & Fuels, **24 (3)**, 1868-1876.

Li, Y. and Liu, H. (2000) "High-pressure densification of wood residues to form an upgraded fuel". Biomass and Bioenergy, **19 (3)**, 177-186.

Liang, L., Sun, R., Fei, J., Wu, S., Liu, X., Dai, K. and Yao, N. (2008) "Experimental study on effects of moisture content on combustion characteristics of simulated municipal solid wastes in a fixed bed". Bioresource Technology, **99 (15)**, 7238-7246.

Lin, C.-L., Wey, M.-Y. and You, S.-D. (2004) "Effect of concentration of bed materials on combustion efficiency during incineration". Energy, **29 (1)**, 125-136.

Lind, T., Vaimari, T., Kauppinen, E., Nilsson, K., Sfiris, G. and Maenhaut, W. (2000) "Ash formation mechanisms during combustion of wood in circulating fluidized beds". Proceedings of the Combustion Institute, **28 (2)**, 2287-2295.

Llorente, M. J. F. and Cuadrado, R. E. (2007) "Influence of the amount of bed material on the distribution of biomass inorganic elements in a bubbling fluidised bed combustion pilot plant". Fuel, **86 (5-6)**, 867-876.

Lua, A. C. and Guo, J. (1998) "Preparation and characterization of chars from oil palm waste". Carbon, **36 (11)**, 1663-1670.

Lyne, C. W. and Johnston, H. G. (1981) "The selection of pelletisers". Powder Technology, **29 (2)**, 211-216.

Mackay, D. M. and Roberts, P. V. (1982b) "The influence of pyrolysis condition on yield and microporosity of lignocellulosic chars". Carbon, **20 (2)**, 95.

Mani, S. (2005) "A system analysis of biomass densification process". PhD Thesis. Chemical and Biological Engineering, The University of British Columbia.

Mani, S., Tabil, L. G. and Sokhansanj, S. (2006) "Specific energy requirement for compacting corn stover". Bioresource Technology, **97 (12)**, 1420-1426.

May, C. Y. (2011) "Overview of the Malaysian oil palm industry 2010" Malaysian Palm Oil Board Economics and Industry Development Division http://econ.mpob.gov.my/economy/EID_web.htm.

McIlveen-Wright, D. R., Williams, B. C. and McMullan, J. T. (2001) "A re-appraisal of wood-fired combustion". Bioresource Technology, **76 (3)**, 183-190.

McKendry, P. (2002a) "Energy production from biomass (part 1): overview of biomass". Bioresource Technology, **83 (1)**, 37-46.

McKendry, P. (2002b) "Energy production from biomass (part 2): conversion technologies". Bioresource Technology, **83 (1)**, 47-54.

McKendry, P. (2002c) "Energy production from biomass (part 3): gasification technologies". Bioresource Technology, **83 (1)**, 55-63.

Mediavilla, I., Fernández, M. J. and Esteban, L. S. (2009) "Optimization of pelletisation and combustion in a boiler of 17.5 kWth for vine shoots and industrial cork residue". Fuel Processing Technology, **90 (4)**, 621-628.

Mengjie, W. and Suzhen, D. (2011) "A potential renewable energy resource development and utilization of biomass energy". FAO*: http://www.fao.org/docrep/T4470E/t4470e0n.htm (6/8/2011).

Messman, H. C. (1977) "Elements of briquetting and agglomeration". in Messman, H. C. and Tibbetts, T. E. (Eds.) Element of briquetting and agglomeration. Canada, Lehman Bookbinders Ltd., 1-7.

Mewes, E. (1959) "Berechung der druckverteilug an stroh-und heupressen (Calculation of the pressure distribution in straw and hay balers)". Landtechnische Forschung, **9 (6)**, 160-170.

Michaels, T. (2010) "The 2010 ERC directory of waste-to-energy plants" Energy Recovery Council, USA

Mohammed, M. A. A., Salmiaton, A., Wan Azlina, W. A. K. G., Mohammad Amran, M. S., Fakhru'l-Razi, A. and Taufiq-Yap, Y. H. (2011) "Hydrogen rich gas from oil palm biomass as a potential source of renewable energy in Malaysia". Renewable and Sustainable Energy Reviews, **15 (2)**, 1258-1270.

Mohan, D., Pittman, C. U., Jr and Steele, P. H. (2006) "Pyrolysis of wood/biomass for bio-oil: a critical review". Energy & Fuels, **20 (3)**, 848-889.

Mohd Noor, M. Y. (1995) "The production and performance of Malaysian oil palm shell activated carbon for flue gas treatment". PhD Thesis. Mechanical and Process Engineering, The University of Sheffield.

MPOB (2011) "Malaysian palm oil board". http://www.mpob.gov.my/ (13/8/2011).

Munir, S., Nimmo, W. and Gibbs, B. M. (2010) "Co-combustion of agricultural residues with coal: Turning waste into energy". Energy & Fuels, **24 (3)**, 2146-2153.

Na, J. I., Park, S. J., Kim, Y. K., Lee, J. G. and Kim, J. H. (2003) "Characteristics of oxygen-blown gasification for combustible waste in a fixed-bed gasifier". Applied Energy, **75 (3-4)**, 275-285.

Nasrin, A. B., Ma, A. N., Mohamad, S., Rohaya, M. H., Azali, A. and Zainal, Z. (2008) "Oil palm biomass as potential subtitution raw materials for commercial biomass briquettes production ". American Journal of Applied Sciences, **5 (3)**, 179-183.

Nussbaumer, T. (2003) "Combustion and Co-combustion of Biomass:Fundamentals, Technologies, and Primary Measures for Emission Reduction". Energy & Fuels, **17,** 1510-1521.

O'Dogherty, M. J. and Wheeler, J. A. (1984) "Compression of straw to high densities in closed cylindrical dies". Journal of Agricultural Engineering Research, **29 (1)**, 61-72.

OECD (2007) "Glossary of statistical terms". Organisation for Economic Co-operation and Development: http://stats.oecd.org/glossary/download.asp (24/8/2011).

ölz, S. and Beerepoot, M. (2010) "Deploying renewables in Southeast Asia: Trends and potentials" International Energy Agency (IEA). Publication, I. http://www.iea.org/papers/2010/Renew_SEAsia.pdf.

PalmOilWorld (2011) "Food use of palm oil" http://www.palmoilworld.org/Fooduses.htm.

Parikka, M. (2004) "Global biomass fuel resources". Biomass and Bioenergy, **27 (6)**, 613-620.

Patankar, S. V. (1980) Numerical Heat Transfer and Fluid Flow London, Hemisphere.

Perlack, R. D. and Stokes, B. J. (2011) "U.S. billion-ton update: biomass supply for a bioenergy and bioproducts industry" U.S. Department of Energy. ORNL/TM-2011/224. Oak Ridge National Laboratory, Oak Ridge, TN. 227p.: http://www.ascension-publishing.com/BIZ/Billion-Ton-2.pdf.

Phan, A. N. (2007) "Combustion/Pyrolysis/Gasification of Segregated Waste". PhD Thesis. Chemical and Process Engineering, The University of Sheffield.

Poersch, W. W. (Ed.) (1987) Fluidised Bed Combustor Design, Constraction and Operation, Elsevier Applied Science.

Procaccini, C. (1999) "The chemistry of chlorine in combustion systems and the gas-phase formation of chlorinated and oxygenated pollutants ". PhD Thesis. Civil and Environmental Engineering, Massachusettes Institute of Technology.

PTM (2007) "County report: Malaysia" Malaysia Energy Centre. www.ptm.org.my.

Putun, A. E., Apaydin, E. and Putun, E. (2004) "Rice straw as a bio-oil source via pyrolysis and steam pyrolysis". Energy, **29**.

Pütün, E. (2010) "Catalytic pyrolysis of biomass: Effects of pyrolysis temperature, sweeping gas flow rate and MgO catalyst". Energy, **35 (7)**, 2761-2766.

Quaak, P., Knoef, H. and Stassen, H. (1999) "Energy From Biomass: A Review of Combustion and Gasification Technologies" World Bank.

Razuan, R., Chen, Q., Finney, K. N., Russell, N. V., Sharifi, V. N. and Swithenbank, J. (2011) "Combustion of oil palm stone in a pilot-scale fluidised bed reactor". Fuel Processing Technology, **92 (12)**, 2219-2225.

Razuan, R., Chen, Q., Zhang, X., Sharifi, V. and Swithenbank, J. (2010) "Pyrolysis and combustion of oil palm stone and palm kernel cake in fixed-bed reactors". Bioresource Technology, **101 (12)**, 4622-4629.

Richard, S., Martin, J., Wilfried, P., Sandra, H. and André, P. C. F. (2010) "The international logistics of wood pellets for heating and power production in Europe: Costs, energy-input and greenhouse gas balances of pellet consumption in Italy, Sweden and the Netherlands". Biofuels, Bioproducts and Biorefining, **4 (2)**, 132-153.

Rieschel, I. H. (Ed.) (1963) Various types of briquetting presses and their application, Canada, Lehman Bookbinders Ltd.

RISI (2011) "European biomass demand to grow 44% between 2010 and 2050" Resource Information Systems Inc. http://www.woodbiomass.com/archive.html.

Roberts, P. V., Leckie, J. O. and Brunner, P. H. (1978) Pyrolysis for the production of activated carbon from cellulosic solid wastes.

Robinson, R. A. (1971) "The pelleting of animal feeds". in Messman, H. C. and Tibbetts, T. E. (Eds.) Elements of briquetting and agglomeration. Canada, Lehman bookbinders Ltd., 67-82.

Rogaume, T., Auzanneau, M., Jabouille, F., Goudeau, J. C. and Torero, J. L. (2002) "The effects of different airflows on the formation of pollutants during waste incineration". Fuel, **81 (17)**, 2277-2288.

Rogaume, T., Jabouille, F. and Torero, J. L. (2009) "Effect of excess air on grate combustion of solid wastes and on gaseous products". International Journal of Thermal Sciences, **48 (1)**, 165-173.

Rosilli-Calle, F., De Groot, P., Hemstock, S. L. and Woods, J. (2007) "Non-woody biomass and secondary fuels". in Rosilli-Calle, F., De Groot, P., Hemstock, S. L. and Woods, J. (Eds.) The biomass assessment handbook-bioenergy for a sustainable environment. London, Earthscan, 110-143.

Ross, D., Noda, R., Horio, M., Kosminski, A., Ashman, P. and Mullinger, P. (2007) "Axial gas profiles in a bubbling fluidised bed biomass gasifier". Fuel, **86 (10-11)**, 1417-1429.

Rovatti, M., Converti, A., Bisi, M. and Ferraiolo, G. (1994) "Pyrolysis of refuse derived fuel: Kinetic modelling from product composition". Journal of Hazardous Materials, **36 (1)**, 19-33.

Rozainee, M., Ngo, S. P., Salema, A. A., Tan, K. G., Ariffin, M. and Zainura, Z. N. (2008) "Effect of fluidising velocity on the combustion of rice husk in a bench-scale fluidised bed combustor for the production of amorphous rice husk ash". Bioresource Technology, **99 (4)**, 703-713.

Russell, N. V. (1998) "Thermal deactivation and reactivity of high temperature coal chars". PhD. The University of London.

Russell, N. V. and Jones, C. (2007) Dictionary of Energy and Fuels, Whittles Publishing.

Ryu, C., Finney, K., Sharifi, V. N. and Swithenbank, J. (2008) "Pelletised fuel production from coal tailings and spent mushroom compost -- Part I: Identification of pelletisation parameters". Fuel Processing Technology, **89 (3)**, 269-275.

Ryu, C., Sharifi, V. and Swithenbank, J. (2005) "Waste Pyrolysis and Generation of Storable Fuel" The ONYX Environmental Trust. RES/C/6019.

Ryu, C., Sharifi, V. N. and Swithenbank, J. (2007b) "Waste pyrolysis and generation of storable fuel ". International Journal of Energy Research, in press.

Ryu, C., Shin, D. and Choi, S. (1999) "Bed combustion and gas flow model for MSW incinerator". International Journal of Computer Application in Technology.

Ryu, C., Yang, Y. B., Gilbert, P., Chung, W., Phan, A. N., Le, A. K., Khor, A., Chen, Q., Sharifi, V. N. and Swithenbank, J. (2009) "Waste segregation presents thermal treatment opportunities". Proceedings of the Institution of Civil Engineers - Waste and Resource Management, **162 (WRI)**, 45-60.

Ryu, C., Yang, Y. B., Khor, A., Yates, N. E., Sharifi, V. N. and Swithenbank, J. (2006) "Effect of fuel properties on biomass combustion: Part I. Experiments--fuel type, equivalence ratio and particle size". Fuel, **85 (7-8)**, 1039-1046.

Saastamoinen, J., Kilpinen, P. T. and Norstrm, T. N. (2000a) "New Simplified Rate Equation for Gas-Phase CO Oxidation at Combustion". Energy & Fuels, **14**.

Saastamoinen, J. J., Taipale, R., Horttanainen, M. and Sarkomaa, P. (2000b) "Propagation of the ignition front in beds of wood particles". Combustion and Flame, **123 (1-2)**, 214-226.

Safaai, N. S. M., Noor, Z. Z., Hashim, H., Ujang, Z. and Talib, J. (2010) "Projection of CO_2 emissions in Malaysia". Environmental Progress & Sustainable Energy, **29 (3)**, 8.

Safi, M. J., Mishra, I. M. and Prasad, B. (2004) "Global degradation kinetics of pine needles in air". Thermochimica Acta, **412 (1-2)**, 155-162.

Salehi, E., Abedi, J. and Harding, T. (2009) "Bio-oil from Sawdust: Pyrolysis of Sawdust in a Fixed-Bed System". Energy & Fuels, **23 (7)**, 3767-3772.

Sancho, J. A., Aznar, M. P. and Toledo, J. M. (2008) "Catalytic Air Gasification of Plastic Waste (Polypropylene) in Fluidized Bed. Part I: Use of in-Gasifier Bed Additives". Industrial & Engineering Chemistry Research, **47 (4)**, 1005-1010.

Schweizer, W. P. (1963) "Extrusion as a menas of agglomeration". in Messman, H. C. and Tibbetts, T. E. (Eds.) Elements of briquetting and agglomeration. Canada, Lehman Bookbinders Ltd., 55-65.

Seifert, H. and Vehlow, J. (Eds.) (2010) Waste combustion, MSW, sewage sludge, hazardous, grate and rotory kiln, Weinheim, Wiley-VCH Verlag GmBH & Co. KGaA.

Senadeera, W. (2009) "Minimum fluidization velocity of food materials: effect of moisture and shape". Chemical Product and Process Modeling, **4 (4)**.

Sensöz, S. (2003) "Slow pyrolysis of wood barks from Pinus brutia Ten. and product compositions". Bioresource Technology, **89 (3)**, 307-311.

Sensoz, S. and Angin, D. (2008) "Pyrolysis of safflower (Charthamus tinctorius L.) seed press cake: Part 1. The effects of pyrolysis parameters on the product yields". Bioresource Technology, **99 (13)**, 5492-5497.

Sensöz, S., AngIn, D. and Yorgun, S. (2000) "Influence of particle size on the pyrolysis of rapeseed (Brassica napus L.): fuel properties of bio-oil". Biomass and Bioenergy, **19 (4)**, 271-279.

Sharma, A. K. (2009) "Experimental study on 75 kWth downdraft (biomass) gasifier system". Renewable Energy, **34 (7)**, 1726-1733.

Sheth, P. N. and Babu, B. V. (2009) "Experimental studies on producer gas generation from wood waste in a downdraft biomass gasifier". Bioresource Technology, **100 (12)**, 3127-3133.

Shin, D. and Choi, S. (2000) "The combustion of simulated waste particles in a fixed bed". Combustion and Flame, **121 (1-2)**, 167-180.

Shuit, S. H., Tan, K. T., Lee, K. T. and Kamaruddin, A. H. (2009) "Oil palm biomass as a sustainable energy source: A Malaysian case study". Energy, **34 (9)**, 1225-1235.

Smoot, L. D. and Pratt, D. T. (1976) Pulverized-Coal Combustion and Gasification, Plenum Press.

Smoot, L. D. and Smith, P. J. (Eds.) (1985) Coal Combustion and Gasification, New York and London, Plenum Press.

Snow, R. H., Allen, T., Ennis, B. J. and Litster, J. D. (1997) "Size reduction and size enlargement". in Perry, R. H. and Green, D. W. (Eds.) Perry's Chemical Engineers' Handbook. New York, McGraw-Hill, 20-1 - 20-89.

Sokhansanj, S. and Turhollow, A. F. (2004) "Biomass densification-cubing operations and costs for corn stover". American Society of Agricultural and Biological Engineers, **20 (4)**, 495-499.

Sukiran, M. A., Chin, C. M. and Abu Bakar, N. K. (2009) "Bio-oil from Pyrolysis of Oil Palm Empty Fruit Bunches". American Journal of Applied Sciences, **6 (5)**, 869-875.

Sultana, A., Kumar, A. and Harfield, D. (2010) "Development of agri-pellet production cost and optimum size". Bioresource Technology, **101 (14)**, 5609-5621.

Sumathi, S., Chai, S. P. and Mohamed, A. R. (2008) "Utilization of oil palm as a source of renewable energy in Malaysia". Renewable and Sustainable Energy Reviews, **12 (9)**, 2404-2421.

Sun, R., Lawther, J. M. and Banks, W. B. (1997) "A tentative chemical structure of wheat straw lignin". Industrial Crops and Products, **6 (1)**, 1-8.

Suri, A. and Horio, M. (2010) "Solid biomass combustion". in Lackner, M., Winter, M. and Agarwal, A. K. (Eds.) Handbook of combustion Wiley-VCH Verlag GmBH & Co. KGaA, Weinheim, 85-140.

Swithenbank, J., Nasserzadeh, V., Goh, Y. R. and Siddall, R. G. (1997) "Fundamental principles of incinerator design". 1st International Symposium on Incineration and Flue Gas Treatment Technology.

Temmerman, M., Rabier, F., Jensen, P. D., Hartmann, H. and Böhm, T. (2006) "Comparative study of durability test methods for pellets and briquettes". Biomass and Bioenergy, **30 (11)**, 964-972.

Thek, G. and Obernberger, I. (2004) "Wood pellet production costs under Austrian and in comparison to Swedish framework conditions". Biomass and Bioenergy, **27 (6)**, 671-693.

Thomas, M., van Vliet, T. and van der Poel, A. F. B. (1998) "Physical quality of pelleted animal feed. 3. Contribution of feedstuff components. ". Animal Feed Science and Technology, **76** 59-78.

Thunman, H. and Leckner, B. (2005) "Influence of size and density of fuel on combustion in a packed bed". Proceedings of the Combustion Institute, **30 (2)**, 2939-2946.

Thurner, F. and Mann, U. (1981) "Kinetic Investigation of Wood Pyrolysis". Industrial & Engineering Chemistry Process Design and Development, **20 (3)**, 482-488.

Tomeczek, J. (1994) Coal combustion, Krieger Pub Co.

Uslu, A., Faaij, A. P. C. and Bergman, P. C. A. (2008) "Pre-treatment technologies, and their effect on international bioenergy supply chain logistics. Techno-economic evaluation of torrefaction, fast pyrolysis and pelletisation". Energy, **33 (8)**, 1206-1223.

Uzun, B. B., Pütün, A. E. and Pütün, E. (2007) "Composition of products obtained via fast pyrolysis of olive-oil residue: Effect of pyrolysis temperature". Journal of Analytical and Applied Pyrolysis, **79 (1-2)**, 147-153.

Vamvuka, D. (2010) "Bio-oil, solid and gaseous biofuels from biomass pyrolysis processes—An overview". International Journal of Energy Research, n/a-n/a.

Vamvuka, D. and Zografos, D. (2004) "Predicting the behaviour of ash from agricultural wastes during combustion". Fuel, **83 (14-15)**, 2051-2057.

van den Broek, R., Faaij, A. and van Wijk, A. (1996) "Biomass combustion for power generation". Biomass and Bioenergy, **11 (4)**, 271-281.

van der Lans, R. P., Pedersen, L. T., Jensen, A., Glarborg, P. and Dam-Johansen, K. (2000) "Modelling and experiments of straw combustion in a grate furnace". Biomass and Bioenergy, **19 (3)**, 199-208.

Wan Mohd Asri, W. D. (1996) "Production and characterization of activated carbon from Malaysian oil palm shell". PhD Thesis. Mechanical and Process Engineering, The University of Sheffield.

Wereko-Brobby, C. Y. and Hagan, E. B. (1996) Biomass Conversion and Technology, New York, Wiley.

Werther, J., Saenger, M., Hartge, E. U., Ogada, T. and Siagi, Z. (2000) "Combustion of agricultural residues". Progress in Energy and Combustion Science, **26 (1)**, 1-27.

Department for Environment, Food and Rural Affairs (2009) Environmental permitting guidance, The directive on the incineration of waste for the environmental permitting (England and Wales) regulations 2007, Updated October 2009 Version 2 http://www.defra.gov.uk/environment/policy/permits/documents/wid-guidance.pdf (17/2/2011)

Williams, P. T. and Besler, S. (1993) "The pyrolysis of rice husks in a thermogravimetric analyser and static batch reactor". Fuel, **72 (2)**, 151-159.

Williams, P. T. and Besler, S. (1996) "The influence of temperature and heating rate on the slow pyrolysis of biomass". Renewable Energy, **7 (3)**, 233-250.

Williams, P. T. and Nazzal, J. M. (1998) "Polycyclic aromatic compounds in shale oils: Influence of process conditions". Environmental Technology, **19 (8)**, 775-787.

Williams, P. T. and Williams, E. A. (1998a) "Interaction of Plastics in Mixed-Plastics Pyrolysis". Energy & Fuels, **13 (1)**, 188-196.

Williams, P. T. and Williams, E. A. (1998b) "Recycling Plastic Waste by Pyrolysis". Journal of the Institute of Energy, **71,** 81.

Wilson, S. (2010) "Caustic soda prices and pricing information"*:* www.icis.com/v2/chemicals/9075188/caustic-soda/pricing.html (21/7/2010).

Winter, F., Wartha, C. and Hofbauer, H. (1999) "NO and N_2O formation during the combustion of wood, straw, malt waste and peat". Bioresource Technology, **70 (1)**, 39-49.

Wurzenberger, J. C., Wallner, S., Raupenstrauch, H. and Khinast, J. G. (2002) "Thermal conversion of biomass: Comprehensive reactor and particle modeling". AIChE Journal, **48 (10)**, 2398-2411.

Yan, R., Yang, H., Chin, T., Liang, D. T., Chen, H. and Zheng, C. (2005) "Influence of temperature on the distribution of gaseous products from pyrolyzing palm oil wastes". Combustion and Flame, **142 (1-2)**, 24-32.

Yang, H., Yan, R., Chen, H., Lee, D. H., Liang, D. T. and Zheng, C. (2006a) "Mechanism of palm oil waste pyrolysis in a packed bed". Energy Fuels, **20 (3)**, 1321-1328.

Yang, H., Yan, R., Chin, T., Liang, D. T., Chen, H. and Zheng, C. (2004) "Thermogravimetric analysis-fourier transform infrared analysis of palm oil waste pyrolysis". Energy Fuels, **18 (6)**, 1814-1821.

Yang, Y. B., Goh, Y. R., Swithenbank, J. and Sharifi, V. (1999) "The fluid dynamic incinerator code (FLIC) user's manual " Sheffield University Waste Incineration Centre (SUWIC), The University of Sheffield, UK.

Yang, Y. B., Goh, Y. R., Zakaria, R., Nasserzadeh, V. and Swithenbank, J. (2002) "Mathematical modelling of MSW incineration on a travelling bed". Waste Management, **22 (4)**, 369-380.

Yang, Y. B., Newman, R., Sharifi, V., Swithenbank, J. and Ariss, J. (2007) "Mathematical modelling of straw combustion in a 38 MWe power plant furnace and effect of operating conditions". <u>Fuel</u>, **86 (1-2)**, 129-142.

Yang, Y. B., Ryu, C., Khor, A., Yates, N. E., Sharifi, V. N. and Swithenbank, J. (2005) "Effect of fuel properties on biomass combustion. Part II. Modelling approach--identification of the controlling factors". <u>Fuel</u>, **84 (16)**, 2116-2130.

Yang, Y. B., Ryu, C., Sharifi, V. N. and Swithenbank, J. (2006b) "Effect of model and operating parameters on air gasification of char". <u>Energy & Fuels</u>, **20 (4)**, 1698-1708.

Yang, Y. B., Sharifi, V. N. and Swithenbank, J. (2006c) "Substoichiometric conversion of biomass and solid wastes to energy in packed beds". <u>AIChE Journal</u>, **52 (2)**, 809-817.

Yang, Y. B., Yamauchi, H., Nasserzadeh, V. and Swithenbank, J. (2003a) "Effects of fuel devolatilisation on the combustion of wood chips and incineration of simulated municipal solid wastes in a packed bed[small star, filled]". <u>Fuel</u>, **82 (18)**, 2205-2221.

Yang, Y. B., Yamauchi, H., Sharifi, V. N. and Swithenbank, J. (2003b) "Effect of moisture content of fuel on the combustion behaviour of biomass and municipal solid waste in a packed bed". <u>Journal of the Institute of Energy</u>, **76,** 105.

Yorgun, S., Sensöz, S. and Koçkar, Ö. M. (2001) "Characterization of the pyrolysis oil produced in the slow pyrolysis of sunflower-extracted bagasse". <u>Biomass and Bioenergy</u>, **20 (2)**, 141-148.

Youssef, M. A., Wahid, S. S., Mohamed, M. A. and Askalany, A. A. (2009) "Experimental study on Egyptian biomass combustion in circulating fluidized bed". <u>Applied Energy</u>, **86 (12)**, 2644-2650.

Yu, Q., Brage, C., Chen, G. and Sjöström, K. (1997) "Temperature impact on the formation of tar from biomass pyrolysis in a free-fall reactor". <u>Journal of Analytical and Applied Pyrolysis</u>, **40-41** 481-489.

Yusoff, S. (2006) "Renewable energy from palm oil - innovation on effective utilization of waste". <u>Journal of Cleaner Production</u>, **14** 87-93.

Zailani, R., Ani, F. N. and Islam, N. (1999) "Pyrolytic oil from fluidised bed pyrolysis of oil palm shell and its characterisation". <u>Renewable Energy</u>, **17 (1)**, 73-84.

Zakaria, R. (2000) "Static incinerator bed combustion". <u>PhD Thesis</u>. Department of Chemical and Process Engineering, The University of Sheffield.

Zanzi, R., Sjöström, K. and Björnbom, E. (2002) "Rapid pyrolysis of agricultural residues at high temperature". <u>Biomass and Bioenergy</u>, **23 (5)**, 357-366.

Zhang, L., Binner, E., Chen, L., Qiao, Y., Li, C.-Z., Bhattacharya, S. and Ninomiya, Y. (2010) "Experimental Investigation of the Combustion of Bituminous Coal in Air and O_2/CO_2 Mixtures: 1. Particle Imaging of the Combustion of Coal and Char". <u>Energy & Fuels</u>, **24 (9)**, 4803-4811.

Zhou, H., Jensen, A. D., Glarborg, P., Jensen, P. A. and Kavaliauskas, A. (2005) "Numerical modeling of straw combustion in a fixed bed". <u>Fuel</u>, **84 (4)**, 389-403.

APPENDIX I

Combustion Calculation

A.   Stoichiometry air calculation

The quantities and the products of combustion air involved per kg of fuel were determined as shown in table below. The amount of moisture in the combustion air is taken as 0.013 lb/lb of dry air corresponding to conditions of 26.6°C dry bulk temperature and 60 % relative humidity.

Ultimate analysis		%	Multipier: O_2 required to burnt the element	Air required to burnt the element	O_2 required for combustion	Dry air required for combustion (kg air/kg fuel)
Species	As received					
C	67.46	0.6746	2.66	11.46	1.7944	7.7309
H	7.96	0.0796	7.94	34.22	0.6320	2.7239
O	15.64	0.1564			0.0000	0.0000
N_2	1.61	0.0161			0.0000	0.0000
S	0.35	0.0035	1	4.31	0.0035	0.0151
H_2O	4.71	0.0471			0.0000	0.0000
Cl	0	0.0000			0.0000	0.0000
Ash	2.24	0.0224			0.0000	0.0000
SUM		0.9997			2.4300	10.4699
O_2 deduction from fuel					0.1564	0.7445
Total air required (100%)					2.2736	9.7254
	kg air /hr	No of Kmol of air	Volumetric Flow Rate (M^3/hr)	Volumetric Flow Rate (l/min)		
Thus for the combustion of 6 kg fuel (OPS) for one hour, the stoichiometric air required:	58.35	2.01	45.07	**751.21**		

Calculation of equivalence ratio (λ) for different cases:

Case 1: Air flow rate 250 l/min

Total air supplied: $250 \dfrac{l}{\min} \times 60 \min = 15000 l$

$\dfrac{15000 l}{22.4 l/mol} = 669.64 mol = 0.67 kmol \times 29 kg/kmol = 19.42 kg$

$Air\ Fuel\ Ratio\ (AFR) = 19.42 kg/hr$

$Air\ Fuel\ Ratio\ (AFR)_{stoich} = 58.35 kg/hr$

$(\lambda) = \dfrac{19.42}{58.35} = 0.33$

$Equivalence\ Ratio(\phi) = \dfrac{1}{\lambda} = \dfrac{1}{0.33} = 3.00$

Case 2: Air flow rate 450 l/min

Total air supplied: $450 \dfrac{l}{\min} \times 60 \min = 27000 l$

$\dfrac{27000 l}{22.4 l/mol} = 1205.34 mol = 1.205 kmol \times 29 kg/kmol = 34.96 kg$

$Air\ Fuel\ Ratio\ (AFR) = 34.96 kg/hr$

$Air\ Fuel\ Ratio\ (AFR)_{stoich} = 58.35 kg/hr$

$(\lambda) = \dfrac{34.96}{58.35} = 0.60$

$Equivalence\ Ratio(\phi) = \dfrac{1}{\lambda} = \dfrac{1}{0.60} = 1.67$

Case 3: Air flow rate 600 l/min

Total air supplied: $600 \dfrac{l}{\min} \times 60 \min = 36000 l$

$$\frac{36000l}{22.4l\,/\,mol} = 1607.143mol = 1.607kmol \times 29kg\,/\,kmol = 46.61kg$$

Air Fuel Ratio $(AFR) = 46.61kg\,/\,hr$

Air Fuel Ratio $(AFR)_{stoich} = 58.35kg\,/\,hr$

$$(\lambda) = \frac{46.61}{58.35} = 0.80$$

$$Equivalence\ Ratio(\phi) = \frac{1}{\lambda} = \frac{1}{0.80} = 1.25$$

Case 4: Air flow rate 650 l/min

Total air supplied: $650\dfrac{l}{\overset{.}{min}} \times 60\,min = 39000l$

$$\frac{39000l}{22.4l\,/\,mol} = 1741.07mol = 1.741kmol \times 29kg\,/\,kmol = 50.49kg$$

Air Fuel Ratio $(AFR) = 50.49kg\,/\,hr$

Air Fuel Ratio $(AFR)_{stoich} = 58.35kg\,/\,hr$

$$(\lambda) = \frac{50.49}{58.35} = 0.87$$

$$Equivalence\ Ratio(\phi) = \frac{1}{\lambda} = \frac{1}{0.87} = 1.16$$

B. Calculation for superficial mass velocity for minimum fluidisation

$$G_{mf} = \frac{0.005\, D_p^2 g_c \rho_f \left(\rho_s - \rho_f\right) \phi_s^2 \varepsilon_{mf}^3}{\mu\left(1 - \varepsilon_{mf}\right)}$$

Eq. A-1

$$G_{mf} = \frac{0.005(0.000036)\,(1)(1.2041)(1198.8)(0.64)(0.2746)}{0.00001827\,(1 - 0.65)}$$

$$G_{mf} = 0.874842\,\frac{\text{kg}}{\text{m}^2.s}$$

Where;

G_{mf} = fluid superficial mass velocity for minimum fluidisation

D_p = particulate diameter

g_c = dimensional constant

ρ_f = fluid density

ρ_s = solids density

ϕ = particle shape factor

ε_{mf} = voidage at minimum fluidisation

μ = fluid velocity

APPENDIX II

Experimental procedures

A.   Slow pyrolysis experiment

Start-up Procedures

1. Switch the GC on for two hours prior to the experiment.
2. Turn on the extract fan.
3. Weight the sample approximately 250 g and two glasses of bottle.
4. Transfer the sample into the furnace and place the reactor into the furnace.
5. Bolt the reactor tightly with the flange lid.
6. Insert three thermocouples into the reactor.
7. Cover the reactor with the insulating blocks.
8. Connect two glasses of bottle to the gas/liquid separator.
9. Connect the nitrogen line to the bottom of the second reactor.
10. Switch on the computer and run data acquisition software.
11. Turn on the nitrogen gas supply at a flow rate 1.5 l/min.
12. Turn on water supply to the condenser.
13. Switch on the temperature controller and set the final temperature and the heating rate.
14. Check all connections to avoid any leakages occurred during the experiment.
15. Start heating the furnace and record data.
16. Collect gas at 200, 300, 400, 500, 600, and 700°C for GC analysis.

Shut-down procedures

1. Turn off the temperature controller after pyrolysis is completed.
2. Stop data logger.
3. Turn off nitrogen gas and water supply when the reactor temperature reaches to approximately 200°C.
4. Leave the reactor until the next day for further cooling until it reaches at room temperature.

5. Weigh the glass bottle.

6. Disconnect the reactor from the rig.

7. Collect the remaining char and record the weight.

B. Fixed bed combustion experiment

The flow diagram of the experimental set-up is shown in Figure 0-1.
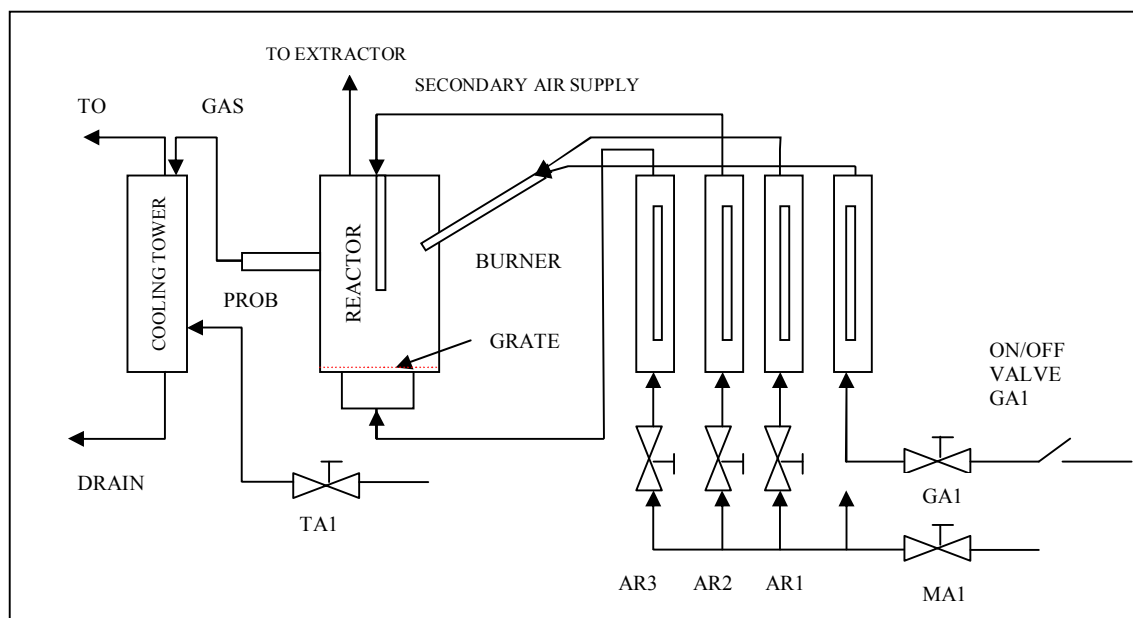
Figure 0-1: Flow diagram of the experimental set-up.

Start-up procedures

1. Switch on the gas analyser and pump for two hours before the test.

2. Turn on the extract fan.

3. Switch on the digital weighing balance and tare it to zero.

4. Weight sample and load it into the reactor through the fuel inlet hole at the top of the reactor.

5. Measure the bed height and screw the lid.

6. Open the water valve (valve T).

7. Check all connections and measuring ports.

8. Switch on the computer and run data acquisition software.

311

9. Calibrate the gas analyser.

10. Turn on the main compressed valve (MA).

11. Open the valve for air supply to the burner (A3) and adjust to 200 l/min.

12. Switch on the power supply for the burner and turn on the gas supply.

13. Ignite and observe the flame inside the bed.

14. Turn off the gas supply (GA) and the A3 valve as soon as the fuel is ignited.

15. Turn on A1 valve for primary air supply.

16. Record data using data logger.

Shut-down procedures

1. Stop data logger.

2. Turn off A1 and A2 valves.

3. Switch off the digital weighing balance.

4. Switch off the pump.

5. Disconnect the gas analyser from sampling port.

6. Switch off the gas analyser.

7. Turn off tap water valve (valve T).

8. Switch off the extract fan.

C.   Fluidised bed combustion experiment

The schematic diagram of the pilot-scale fluidised bed used in this study is shown in Figure 0-2.

Start-up procedures

1. Disconnect the feeder from the feeding tube and blank off the end of the feeding tube at the rig.

2. Place the feed material into the hopper, after the feedrate has been calibrated.

3. Turn on water valve (V_C), main air supply (V_A), Propane (V_B) and the room extractor fan.

4. Test the pilot burner and then place it in the bed at the correct depth.

5. Switch on the fluidising air (V1) to a high flowrate (e.g. 420l/min or 10 cm of rotameter reading) to unblock the bed (approx. 5 mins), and the gradually turn it down within stoichiometric.

6. Light the natural gas-fired pilot burner and then gradually open the valve (V4) to allow propane in to ignite and heat the bed; increase propane until with minimum fluidising air the correct air/propane ratio is reached (Stoichiometric).

7. Monitor the thermocouples in the bed whilst the air and propane remain the same, until they all give the same reading; then reduce the air and propane flowrates, increasing again if necessary to increase the thermocouple readings, until the temperature is stable at around 800°C for around 20 minutes.

8. If the flame is extinguished, turn off the propane immediately, purge with air and repeat from step 5.

9. Once the temperature is stabilised at around 800°C for around 20 minutes, turn on secondary air (V2 and V3) then start feeding the fuel. Increase the feedrate and reducing the propane until the flame stabilised (by visual inspection via view point), then stopped the propane line by shut down valve (V_B).

Shut-down procedures

1. Stop feeding in the fuel by press stop bottom on the screw feeding system.

2. Wait until the bed temperature has started to drop below 600°C indicating that all fuel has been burned.

3. Turn off the air supply and then disconnect the feeder from the feeding tube. Blank off the feeding tube. Turn the air back on.

4. Increase the flowrate of the fluidising air.

5. When the bed is sufficiently cooled, below 200°C, turn off the cooling water and fluidising air by shut down valve (V_C) and valve (V_A).

6. Switch off logging devices and safety valves.
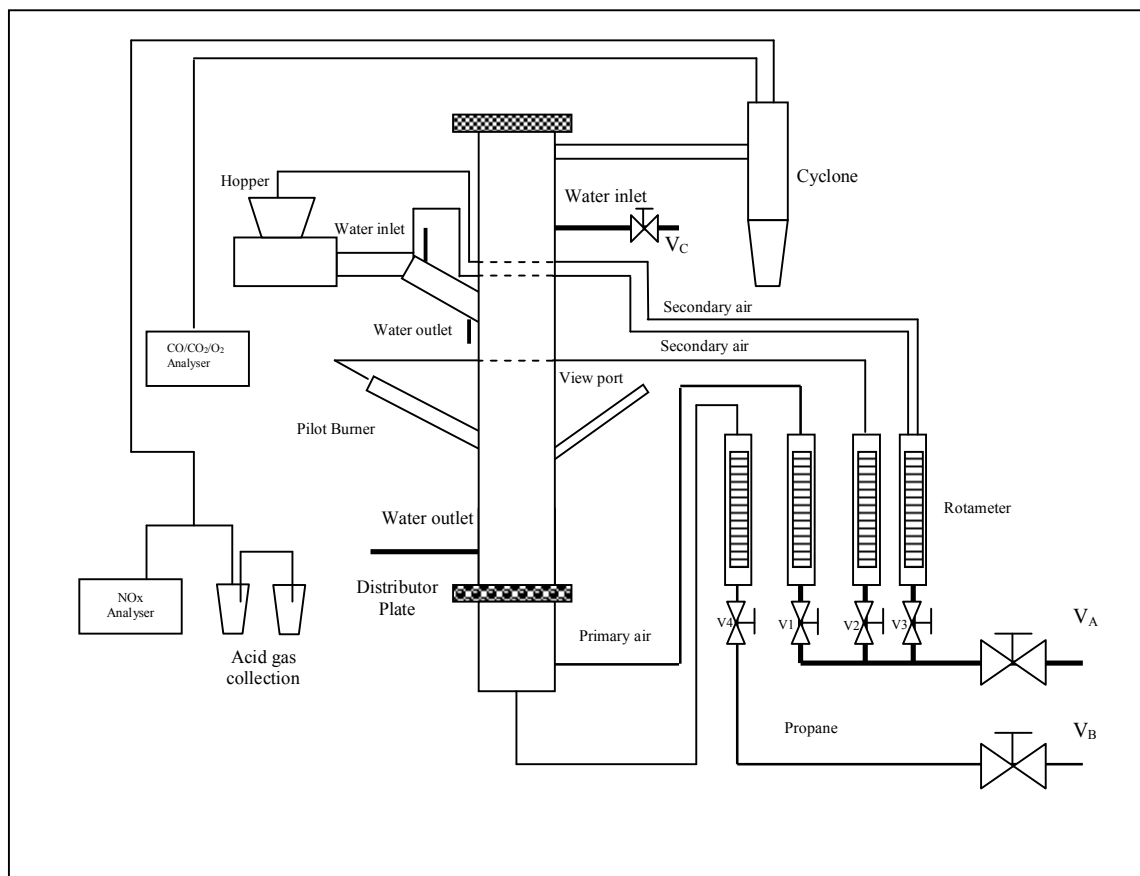
Figure 0-2: A Schematic diagram of pilot-scale fluidised bed used for thermal treatment.

D. Production of PKC pellets

Palm kernel cake (PKC) pellets were produced using a manual compression technique as shown in Figure 4-15. The process was based on the compaction series given in Figure 2-62.

Procedure

1. Approximately 20-25 g of PKC powder was weighed and placed into the opening hollow column at the centre of the pelletiser.

2. The stopper was then placed in the column on top of the material and the screw-on lid fastened.

3. Then, the handle or lever was used to increase the pressure inside the 26.8 mm diameter cavity by causing the horizontal plate to move up, until the required pressure was achieved, indicated on the gauge. The pelletiser was also equipped with rope heaters and thermocouple wires connected to the vertical shaft and a gauge to control the temperature at which the pellet was formed.

4. The pressure indicated on the this gauge is 4.06 times lower than the actual pressure experience by the material due to the differences in the areas of the piston and the ram, thus the pressure recorded were multiplied by this factor.

5. In the final stage (ejection), the pressure was released by twisting the pressure release grip and the plate moved down.

6. The screw-on lid was then removed and the lever was used to increase the height of the plate until the stopper emerged from the column.

7. The pellet was then emerged as the plate was pumped further.

8. Once the pellet had been removed, it was weighed and measured.

APPENDIX III

A. List of journal publications

1. Razuan, R., Finney, K. N., Chen, Q., Sharifi, V. N. and Swithenbank, J. (2011) "Pelletised fuel production from palm kernel cake". <u>Fuel Processing Technology</u>, **92 (3)**, 609-615.

2. Razuan, R., Chen, Q., Finney, K. N., Russell, N. V., Sharifi, V. N. and Swithenbank, J. (2011) "Combustion of oil palm stone in a pilot-scale fluidised bed reactor". <u>Fuel Processing Technology</u>, **92 (12)**, 2219-2225.

3. Razuan, R., Chen, Q., Zhang, X., Sharifi, V. and Swithenbank, J. (2010) "Pyrolysis and combustion of oil palm stone and palm kernel cake in fixed-bed reactors". <u>Bioresource Technology</u>, **101 (12)**, 4622-4629.

B. Conferences

1. Coal: The Social, Economic, Regeneration and Climate Change Opportunities, the Edge Conference Centre, University of Sheffield, UK (28th October 2009).

2. Symposium on biofuels science, engineering and sustainability, Sir Robert Hadfield Building, Chemical & Biological Engineering, University of Sheffield (12th April 2011).

C. Departmental seminars

1. 24-month poster presentation, 'Combustion and slow pyrolysis of oil palm stones and palm kernel cake' Sir Robert Hadfield Building, Chemical & Biological Engineering, University of Sheffield (10th November 2010).

2. 30-month departmental presentation, 'Combustion and slow pyrolysis of oil palm stones and palm kernel cake' Sir Robert Hadfield Building, Chemical & Biological Engineering, University of Sheffield (23rd March 2011).

D. Publications

D1. Bioresource Technology

1. Pyrolysis and combustion of oil palm stone and palm kernel cake in fixed-bed reactors.

Pyrolysis and combustion of oil palm stone and palm kernel cake in fixed-bed reactors

R. Razuan, Q. Chen*, X. Zhang, V. Sharifi, J. Swithenbank

SUWIC, Department of Chemical and Process Engineering, Sheffield University, Sheffield, UK

ARTICLE INFO

ABSTRACT

The main objective of this research was to investigate the main characteristics of the thermo-chemical conversion of oil palm stone (OPS) and palm kernel cake (PKC). A series of combustion and pyrolysis tests were carried out in two fixed-bed reactors. The effects of heating rate at the temperature of 700 °C on the yields and properties of the pyrolysis products were investigated. The results from the combustion experiments showed that the burning rates increased with an increase in the airflow rate. In addition, the PKC char was used to simulate the combustion of the oil palm stone to investigate the effect of primary air flow on the combustion process. The CFD modelling results were in good agreement with the experimental data in terms of predicting the temperature profiles along the bed height and the composition of the flue gases.

© 2010 Elsevier Ltd. All rights reserved.

1. Introduction

Biomass energy sources include wood, residues from agriculture or forestry, and the organic component of municipal and industrial wastes. Each type of biomass has specific properties that determine its performance as a fuel. Therefore, a wide range of biomass has been studied by many researchers around the globe, from municipal solid waste to agricultural waste.

Oil palm solid wastes (including shell, fibre and its kernel) are abandoned materials produced during palm oil milling process. For every ton of oil palm fruit bunch being fed to the palm oil refining process, about 0.07 tons of palm shell, 0.103 tons of palm fibre and 0.012 tons of kernel are produced as the solid wastes (Pansamut et al., 2003). Malaysia's ability to produce and consistently export a large quantity of high quality palm oil has made it one of the major vegetable oil exporters in the world. By-products or waste from the palm oil mills are generated in significant amounts and mainly consist of empty fruit bunches (EFB), oil palm stones (OPS), Oil Palm Shell (OPSh), palm kernel cake (PKC) and Palm Oil Mill Effluent (POME). Some of this waste is currently used as fuel for boilers with low energy efficiency, soil conditioner or in furniture making. Currently, there is a significant interest in recovering energy from OPSh. Extensive research has already been carried out in this area (Zailani et al., 1999; Yang et al., 2006;

Sukiran et al., 2009). Waste from the oil palm industry, especially OPS and PKC, is abundant and can help to meet the energy demand, if properly managed. However, limited research has been carried out on the utilisation of OPS and PKC for energy production.

Pyrolysis is currently the most promising thermo-chemical conversion technology for the production of pyrolysis liquid oil (Bridgwater and Bridge, 1991). According to Jakab et al. (2000), pyrolysis processes may be classified as conventional or slow pyrolysis and fast pyrolysis, depending on the operating conditions that are used. Some researchers (Williams and Besler, 1996; Zailani et al., 1999; Yan et al., 2005; Yang et al., 2006) have studied the mechanism and kinetics of oil palm waste pyrolysis in packed-bed reactors or with thermogravimetry. The yields and compositions of pyrolysis products are highly dependent on biomass species, chemical and structural composition of biomass material, process temperatures and heating rates (Mackay and Roberts, 1982a,b; Di Blasi et al., 1999a,b; Guo and Lua, 2000; Demirbas, 2001; Yang et al., 2006).

Combustion of biomass and related materials is widely practiced worldwide to produce heat and power (McKendry, 2002). This technology is commercially available and presents minimum risk to investors (Bridgwater, 2003). In general, there are two types of combustion systems commercially available: fixed-bed and fluidized-bed. Optimal operation is important in the combustion process in order to avoid any toxic gas releases into the environment. Horttanainen et al. (2002), studied the effect of the flow rate of air, moisture content, particle size and density of wood against the velocity of the ignition front and the maximum temperature in the bed. Zakaria (2000) studied combustion of simulated municipal

* Corresponding author. Address: Department of Chemical and Process Engineering, Sheffield University, Mappin Street, Sheffield, S1 3JD, UK. Tel.: +44 (0) 114 222 7563; fax: +44 (0) 114 222 7501.
E-mail address: q.chen@sheffield.ac.uk (Q. Chen).

solid waste and found that the ignition front speed was directly proportional to the primary air flow rate. Particle size strongly influences the bed temperature during biomass combustion. The ignition speed was directly proportional to the ratio of the surface area of particles over volume and inversely proportional to the density of fuel (Saastamoinen et al., 2000). Shin and Choi (2000) revealed that when the particle size increases, the maximum air supply rate for stable combustion increases due to the fact that larger particles have a smaller surface area per unit mass.

Although combustion tests for oil palm wastes can provide invaluable practical data, it is practically very difficult to conduct detailed study on fuel combustion behaviour under all possible operating conditions because of the physical limitations. Mathematical modelling, however, provides a powerful approach to evaluate the effects of fuel properties and operating conditions on the combustion process. Several models have been developed for simulating packed-bed combustion (Cooper and Hallet, 2000; Shin and Choi, 2000; Yang et al., 2003; Ryu et al., 2007).

In order to investigate the characteristics of the thermo-chemical conversion of OPS and PKC, a series of pyrolysis and combustion tests were carried using OPS and PKC as the raw materials. OPS and PKC samples were pyrolysed under different final temperatures and heating rates in a fixed-bed reactor. Fixed-bed combustion of OPS samples were investigated under different air flow rates. In addition, the FLIC code was used to simulate and predict the OPS combustion process using a wide range of primary air flow rates.

2. Methods

2.1. Materials

Oil palm stones (OPS) and palm kernel cake (PKC) were supplied by A.M.E Teras Marin Services Ltd. The oil palm stones were removed from shell and dried at room temperature for about 1 week prior to the experiments. The stones were about 6–10 mm in diameter and the PKC samples were crushed into fine and dusty material (most particles were less than 2 mm in diameter). The results of the proximate and ultimate analyses are shown in Table 1.

2.2. Pyrolysis experiments

The pyrolysis tests were conducted in a fixed-bed pyrolyser, as shown in Fig. 1a. The pyrolyser consisted of a stainless steel reactor with 125 mm in diameter and 500 mm in height. It was seated in

Table 1
Proximate and ultimate analyses of OPS and PKC samples.

		Palm stone	Palm kernel cake
Proximate analysis (%, as received)	Moisture	4.71	7.92
	Ash	2.24	4.28
	Volatiles	86.50	71.84
	Fixed carbon	6.55	16.00
Ultimate analysis (%daf)	C	67.49	52.53
	H	8.48	5.65
	O	22.07	38.93
	N	1.61	2.86
	S	0.35	0.03
Gross calorific value (MJ/kg)		27.46	18.67

an electrically heated furnace. The reactor was connected to two water-cooled condensers with liquid traps through an insulated stainless steel pipe. At the bottom of the reactor, another furnace was attached to preheat nitrogen stream.

Both OPS and PKC samples were used in pyrolysis tests. In each test, 150–200 g of sample was put into the reactor and heated from room temperature to a final temperature of 500 or 700 °C in a 2 L/min preheated nitrogen stream. The furnace heating rate was set at 10 °C/min for the final temperature of 500 °C and was set at 5 and 10 °C/min for the final temperature of 700 °C. The sample was then kept at the final temperature in order to allow the completion of pyrolysis process. The temperature of the sample within the reactor was measured using three thermocouples (T1, T2 and T3 in Fig. 1a).

The char and liquid products were collected after the reactor was cooled down. The mass yields of char and liquids were measured directly from the weight of the products collected. The mass yield of gas product was determined by difference, which included the small fraction of fine droplets and dust or ash. The ultimate analyses (C, H, N, S and O) of char and liquids were performed using the Carlo Erba EA1108 Elemental Analyser. The calorific values of char and liquids were determined using a Parr 1261 bomb calorimeter. Pyrolysis gas was collected after the condensers at process temperatures of 300, 400, 500, 600, and 700 °C. The gas composition was analysed using the Varian CP-3800 Gas Chromatograph with a CP-SIL cross-linked capillary column for hydrocarbons and a molecular sieve for H_2, O_2, N_2, CO and CO_2. The molecular sieve consisted of packed columns of 1.5 m long with an internal diameter of about 3.2 mm. The capillary column was
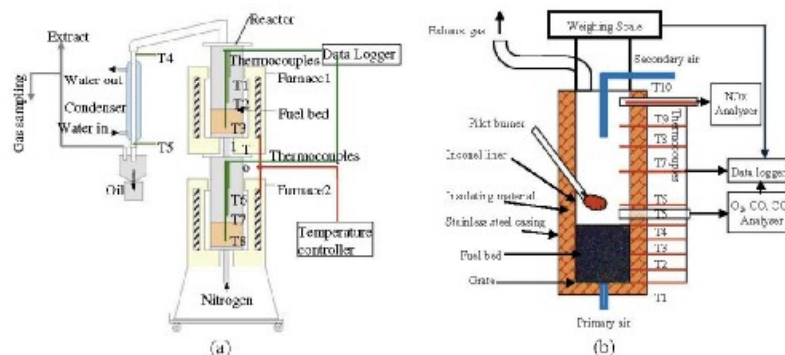
Fig. 1. Schematic diagrams of (a) the fixed-bed pyrolyser and (b) the fixed-bed combustor.

60 m long and 0.32 mm in inner diameter. The carrier gases used for molecular sieve and the capillary column were argon and helium, respectively.

2.3. Combustion experiments

The combustion tests were conducted in a counter-current fixed-bed combustor. The experimental reactor consisted of a vertical cylindrical chamber, pilot burner, grate, air supply system and weighing scale as shown in Fig. 1b. The height of the reactor was 1.5 m. It was suspended from two beams having four load cells (resolution: 20 g) in order to monitor the weight of the bed. The details of the experimental setup are presented in the authors' previous paper (Khor et al., 2007).

The grate for the fixed-bed reactor was a stainless steel perforated plate with approximately 700 holes of 2 mm in diameter. The primary air was supplied from below through the perforated plate. The secondary air was supplied from the top of the reactor through a stainless steel pipe. The flow rate of the secondary air was kept at 0.15 Nm^3/min in the study. Once the test sample (OPS) was fed into the reactor, the pilot burner was used to ignite the sample on top of the bed. The temperatures inside and above the bed were measured using 10 K-type thermocouples aligned at the centre of the reactor. The flue gas was sampled near the top of the bed (at the height above the grate $y = 43$ cm). CO/CO$_2$/O$_2$ gas analyser (ADC MGA3000, error ±1.0% due to calibration gas) was used to measure the gas concentrations. The time lag in the analyser readings was approximately 60 s due to the retention time of the flue gas in the sampling line. DAQ Factory Lite Release 5.11 (Azeo Tech, Inc.) data acquisition software was used to record the data automatically from the gas analyser and thermocouples. The data logger recorded the measured temperatures, gas concentrations and mass loss every 30 s.

Flue gas samples from the free board region (1.4 m above the grate) were also analysed for NO$_x$. The gas sample passed through a heated line followed by a heated filter to prevent moisture from condensing and to remove the dust before entering the Signal 4000VM NO$_x$ Analyser. The retention time of gas in the sampling system was about 3 min. The flue gas exited the combustor through an upward stainless steel pipe to a ventilation system.

Due to its small particle size, PKC is not suitable for fixed-bed combustion. Thus, only the combustion of OPS in the fixed-bed reactor was studied. The operating conditions are listed in Table 2. As the superficial mass velocity for minimum fluidisation was approximately 3100 kg/m^{2}h, three test cases were performed with air flow rate ranging from 618 to 1484 kg/m^{2}h.

2.4. Mathematical modelling

FLIC mathematical model (Yang et al., 2002; Goddard et al., 2005) was used to predict the in-bed combustion of the oil palm stones. In the model, the fuel bed was assumed to be one-dimensional and consist of uniform spherical particles with gas voids. The sub-processes of the solid phase combustion were taken into account by sub-models along with various modes of heat transfer.

The details of the model development, governing equations, various sub-models are reported in the authors' previous papers (Yang et al., 2002, 2005; Ryu et al., 2007).

In the FLIC modelling work, the initial bulk density of the material was assumed to be 545 kg/m^3, given the bed porosity of 0.5. The initial bed height was set at 350 mm. The particle size was assumed to be 8 mm. The computation domain of the fixed bed was discretised into 200 cells along the bed height. Oil palm stones were assumed to be ignited by over-bed radiation at temperatures of 1273 K. Details of the solving schemes, other general boundary conditions and parameters are reported in authors' previous paper (Yang et al., 2005).

3. Results and discussion

3.1. Pyrolysis of oil palm stone and palm kernel cake

The mass fractions of the primary pyrolysis products from the OPS and PKC under different heating conditions are shown in Fig. 2. As shown, the char yields obtained from the OPS were lower compared to those produced from the PKC however the gas yields from the OPS were higher. When the final temperature of the pyrolysis process increased from 500 to 700 °C, the char yield decreased slightly due to further devolatilisation of the residual volatile matter in char. Similarly, an increase in the final temperature resulted in the reduction of liquid yield and an increase in the gas yield. This tendency was consistent with the results obtained by Zailani et al. (1999) and Sukiran et al. (2009), which revealed that a liquid product from the pyrolysis of oil palm waste was maximal at a final temperature of 500 °C. This implies that long carbon chains are more easily broken to produce gas under higher temperatures.

When the heating rate increased from 5 to 10 °C/min with the final temperature of pyrolysis at 700 °C, the liquid yield from the OPS decreased whereas the gas yield increased. The results were different in the case of PKC. There was an increase in the liquid yield and a slight decrease in gas yield. The char yields from both waste samples, however, were not significantly affected by the changes in the heating rates. This result was consistent with the previous studies on the slow pyrolysis of oil palm empty fruit bunches, holm oak and pine-wood (Figueiredo et al., 1989; Williams and Besler, 1996; Sukiran et al., 2009), which showed that the wood type, particle size and heating rate had very little influence on the char yield.

Table 3 shows the properties of char obtained from pyrolysis of the OPS and PKC at a heating rate of 10 °C/min and different final temperatures. All the char samples mainly consisted of fixed carbon with a small fraction of volatile matter. This is in agreement with that of Uzun et al. (2007), who studied the composition of

Table 2
Conditions for the OPS combustion tests in the fixed-bed reactor.

Case	Sample weight (kg)	Bed height (mm)	Bulk density (kg/ m^3)	Air flow rate	
				l/ min	kg/ m^{2}h
1	6	320	597	250	618
2	6	350	546	450	1113
3	4.12	220	596	600	1484
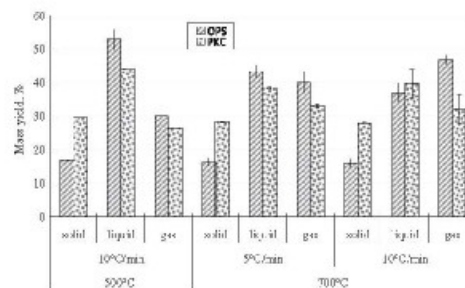
Fig. 2. Mass yields from the pyrolysis of OPS and PKC under different conditions.

R. Bazzar et al./Bioresource Technology 101 (2010) 4622–4625   4625

Table 3
Properties of the char samples from pyrolysis of the OPS and PKC.

		OPS char		PKC char	
		500 °C	700 °C	500 °C	700 °C
Proximate analysis (% as received)	Moisture	1.11 ± 0.04	1.18 ± 0.12	–	0.17 ± 0.11
	Ash	16.33 ± 1.68	13.16 ± 0.25	14.42 ± 0.18	14.95 ± 0.22
	Volatiles	14.08 ± 0.24	6.41 ± 0.73	12.48 ± 0.55	6.69 ± 1.20
	FC	68.48	79.31	73.08	78.19
Ultimate analysis (%daf)	C	80.27 ± 2.73	84.56 ± 2.29	62.78 ± 1.67	73.98 ± 1.59
	H	2.11 ± 0.40	1.33 ± 0.05	3.13 ± 0.11	0.29 ± 0.01
	O	13.15	10.17	30.05	21.7
	N	4.42 ± 0.20	3.79 ± 0.40	4.03 ± 0.11	3.49 ± 0.59
	S	0.04 ± 0.01	0.14 ± 0.15	0.03 ± 0.02	0.05 ± 0.04
Gross calorific value (MJ/kg)		27.6 ± 1.1	28.3 ± 0.4	26.1 ± 0.2	28.1 ± 0.1

Table 4
Properties of the liquid products from pyrolysis of the OPS and PKC.

	OPS oil		PKC oil (light fraction)		Palm Shell[a]
	500 °C	700 °C	500 °C	700 °C	500 °C
CV (MJ/kg)	38.27	37.81	27.74	20.79	22.1
Viscosity @ 50 °C (cSt)	–	9.9	–	1.5	–
Carbon	84.47	78.52	78.2	78.83	53.48
Hydrogen	10.53	10.64	8.97	8.13	6.68
Oxygen	3.23	8.95	8.96	8.84	39.27
Nitrogen	1.55	1.47	3.58	4.1	0.44
Sulfur	0.23	0.41	0.31	0.1	0.02
Empirical formula	$CH_{1.51}O_{0.17}$	$CH_{1.63}O_{0.09}$	$CH_{1.38}O_{0.09}$	$CH_{1.24}O_{0.08}$	$CH_{1.50}O_{0.55}$

[a] Data obtained by Zailani et al. (1999).

products obtained via the fast pyrolysis of olive-oil residue. With an increase in the final temperature of pyrolysis process, there was a decrease in the volatile matter content. The calorific values (HHV) of char samples obtained from the OPS and PKC tests were approximately 28 MJ/kg. These chars had an energy content as high as that of bituminous coal.

It was observed that liquid derived from the pyrolysis of OPS formed a homogeneous mixture. The liquid product from the KPC pyrolysis appeared to consist of two distinct layers. The light fraction was darker in colour than the heavy fraction. The heavy fraction was translucent and could not be ignited in the bomb calorimeter. This indicated that the calorific value of the heavy fraction was very low. Table 4 presents the properties of the light fraction of the liquid obtained from pyrolysis of PKC and the liquid products from pyrolysis of OPS at a heating rate of 10 °C/min and different final temperatures. The calorific values of the liquid obtained from the slow pyrolysis of the OPS and PKC ranged from approximately 21 to 38 MJ/kg. These values were higher than the values obtained from fast pyrolysis, i.e. 16–19 MJ/kg (Phan, 2007). These results are in good agreement with the results published by Sukiran et al. (2009) and Yang et al. (2006).

Fig. 3 shows the composition of gases obtained from the pyrolysis of the OPS and PKC at a final temperature of 700 °C. The gas consisted mainly of CO_2, CO, H_2, CH_4 and other hydrocarbons. It was assumed that the total sum of the fractions was one.

It can be seen that the CO_2 and CO were mainly evolved at low temperatures (<500 °C) during the pyrolysis of the OPS and PKC, this could possibly be due to the breaking of C=O in raw material (Yang et al., 2006). As the temperature increased to 600 °C, the concentrations of CO and CO_2 were reduced to about 15% for OPS and approximately 20% for PKC. At the final temperature of 700 °C, however, the concentrations of CO and CO_2 remained relatively constant. At high temperatures (>500 °C) H_2 and other hydrocarbons (C_1–C_3) were the dominant components in the gas products, possibly due to the cracking and reforming of the aromatic rings

(Yang et al., 2006). Most of the light hydrocarbon gases started to evolve at temperature >300 °C. There was an increase in the concentration of hydrocarbon gases as the temperature increased to 600 °C. However, a further increase in the temperature (up to 700 °C) resulted in a significant reduction in the concentration of gaseous hydrocarbons. This decrease was due to the breakage of alkyl compounds (Yang et al., 2006), as well as the possible steam reforming reactions that led to a slight increase in CO and CO_2 concentrations. Thus, as expected, the concentration of H_2 increased sharply when the temperature increased and reached its maximum value (35–45%) at 700 °C. Changes in the gas composition generated from pyrolysis of OPS and PKC showed similar trends.

The heating rate significantly affected the gas composition in the pyrolysis of the OPS and the PKC. For both the OPC and the PKC, when the heating rate was increased from 5 to 10 °C/min, the concentrations of CH_4 increased whereas C_mH_n ($m = 2$ and 3) decreased significantly at high temperature. Meanwhile, the concentrations of H_2 also increased with an increase in heating rate. This implies that it is easier to break alkyl and other carbon bonds at higher heating rates.

As shown in Fig. 3a, unusual high fractions of CH_4 and C_mH_n were released at 400 °C when OPS was pyrolysed at 10 K/min to 700 °C. This may be due to the extremely uneven temperature distribution in the fuel bed. The OPS sample had a wide particle size distribution (ranging from 6 to 10 mm) compared to the PKC sample. At high heating rate of 10 K/min, higher temperature difference between the centre of the bed and the bed outer layer was observed. Previous modeling work by the authors (Yang et al., 2007) has shown that this temperature difference could rise to above 100 °C at the process temperature of 400 °C.

3.2. Oil palm stone combustion

Fig. 4a presents the measured temperature profile in the fuel bed against the reaction time at the primary air flow rate of

320
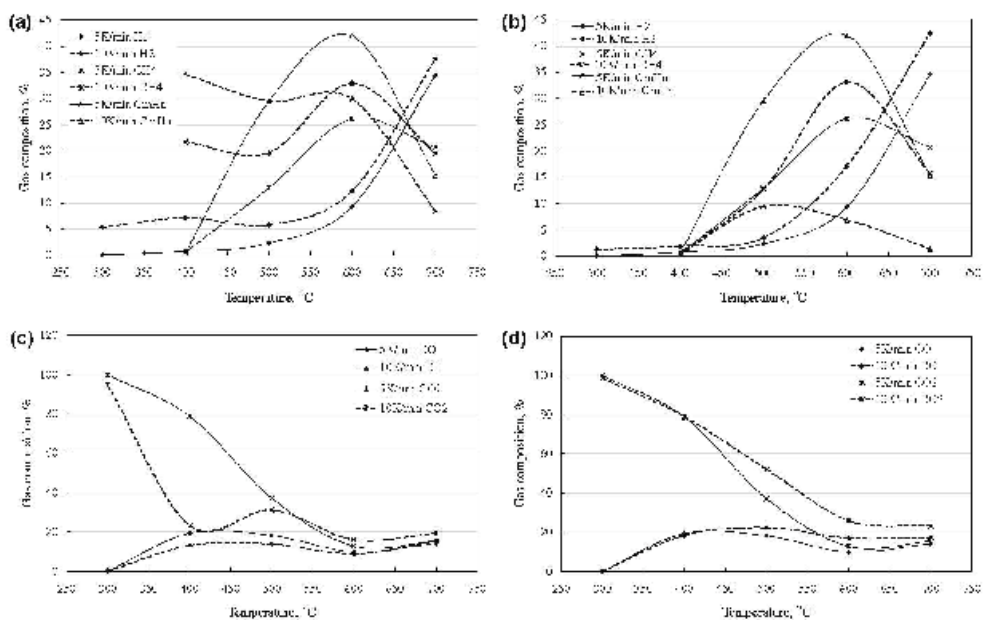
Fig. 3. H₂ and other hydrocarbons contents in the pyrolysis gases of (a) OPS, (b) PKC and the contents of CO and CO₂ in the pyrolysis gases of (c) OPS, (d) PKC at the final temperature, 700 °C.
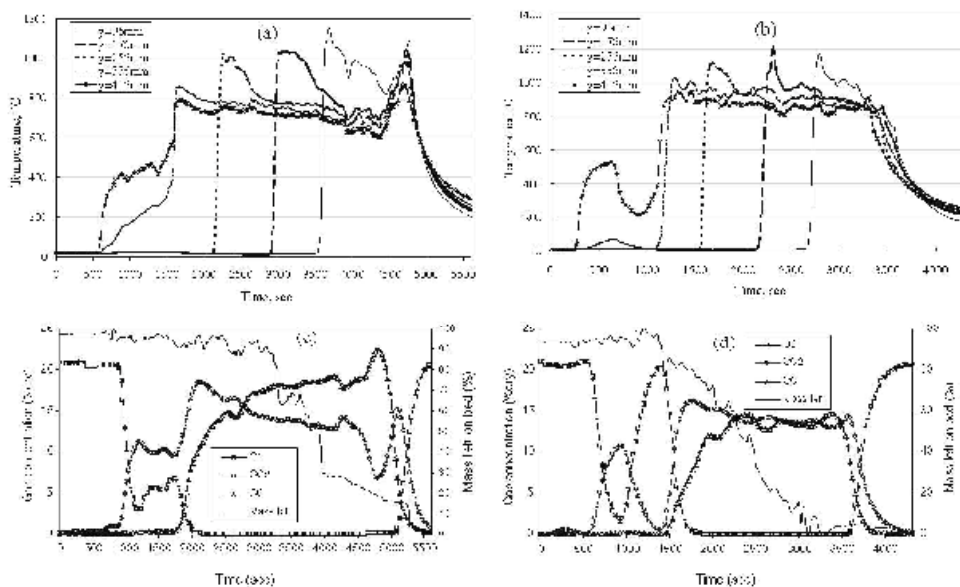
Fig. 4. Temperature profile of the combustion of OPS at the air flow rate of (a) 618 kg/m²h, (b) 1113 kg/m²h, at the height above the grate; and gas composition and residual mass for the OPS combustion at the air flow rate of (c) 618 kg/m²h, (d) 1113 kg/m²h.

321
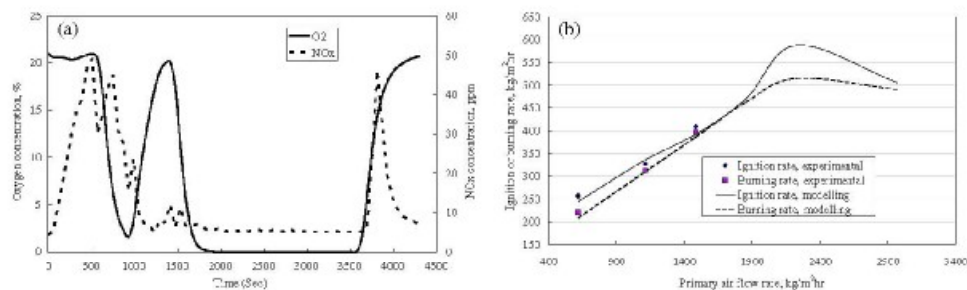
Fig. 5. (a) Oxides of nitrogen concentration from the combustion of the OPS at an air flow rate of 1113 kg/m²h. and (b) comparison of measured and predicted ignition rates and burning rates of the combustion of OPS at different air flow rates.

618 kg/m²h. Fig. 4c shows the gas composition above the bed as a function of reaction time. The whole combustion process can be divided into three stages.

Initially, the fuel had to be heated and ignited by the pilot burner which was located at the top of the bed. As shown in Fig. 4a ($t < 1600$ s), the temperature over the fuel bed quickly increased to 500 °C. The decrease in O_2 concentration and the increase in CO_2 concentration as shown in Fig. 4c (at $t < 1600$ s) could also be attributed to the combustion of propane in the pilot burner.

Once the surface of the OPS (fuel) bed was heated up, the moisture and volatile matter were released. At approximately 1600 s, the fuel bed began to burn without the pilot burner. The temperature at the bed surface increased swiftly to over 800 °C and the combustion process of the fuel bed entered the ignition propagation period. During this period, the devolatilisation and combustion of volatile matter in the upper layer of bed resulted in the heating up and ignition of the next layer of the fuel bed. Thus the local bed temperature increased instantly to 800–1000 °C as the ignition front propagated through the fuel bed. As shown in Fig. 4c, at the beginning of this period, O_2 concentration began to decrease whereas the concentrations of CO_2 and CO increased rapidly. At around 2150 s, all the oxygen supplied by the primary air was consumed. Meanwhile, CO_2 concentration began to decrease whereas CO concentration started to increase due to partial oxidation under lean oxygen condition. As the burnout of the char material was more difficult than the volatile matter and there was insufficient amount of O_2, the char accumulated in the bed after the ignition front propagated in the region. The ignition propagation period ended at around 4400 s when the ignition front reached the grate. At the end of this stage, the residual fuel in the bed was about 20%.

In the final stage, the char residual began to burn out. Due to its higher calorific value, char combustion increased the bed temperature to over 1000 °C. However, with the primary air flow rate of 618 kg/m²h, there was not enough oxygen (lean condition) in the system to completely burn the char and convert it to CO_2. As shown in Fig. 4c, the partial oxidation of char resulted in a small peak in CO concentration.

Fig. 4b presents the bed temperature profile against the reaction time at the primary air flow rate of 1113 kg/m²h. In this case, the ignition front propagation process was similar to that with air flow rate of 618 kg/m²h. However, as the air flow rate increased, the heat transfer via convection from the top layer to the lower part became difficult. On the other hand, higher air flow rate increased the local air–fuel ratio and consequently the combustion temperatures. As shown in Fig. 4a and b, the peak temperatures at the ignition front increased as the air flow rate increased from 618 to

1113 kg/m²h. Higher temperature at the ignition front increased the amount of heat transferred via radiation and conduction from the top fuel layer to the lower part of the bed. Consequently, the overall ignition rate was increased. Moreover, sufficient air supply made it possible for large amount of the char to be oxidised simultaneously with the volatile matter. Hence, during the final combustion stage, no significant increase in-bed temperature was observed. Fig. 4d shows the gas concentrations during the OPS combustion at the primary air flow rate of 1113 kg/m²h. During the ignition propagation period, the concentrations of CO_2 and CO remained constant for a long period of time, as shown in Fig. 4c. This also implied that some of char material was burnt locally together with the volatiles.

Fig. 5a shows NO_x concentrations during the combustion test. The NO_x concentration sharply increased to a maximum value of about 47 ppm at the initial stage ($t < 1000$ s). This was due to the firing of the pilot burner. The NO_x concentration stayed constant at a low level (only 5 ppm) during the ignition propagation stage. During this stage, the top part of the fuel bed remained under reducing conditions. NO_x formed during the volatile combustion stage can easily be reduced to N_2, as shown by Zakaria (2000). During the final char combustion stage, NO_x increased sharply to a peak value of 46 ppm at $t = 3800$ s. This result was also observed at the tests with other air flow rates. As the oxygen concentration in the flue gas began to increase, the nitrogen in char was converted to NO_x during the char combustion (Nussbaumer, 2003; Liang et al., 2008).

For the primary air flow rate of 1484 kg/m²h, the profiles of the bed temperature and the gas concentration against the reaction time were very similar to the profiles shown in Fig. 4b and d. During the ignition propagation period, CO_2 concentrations in the flue gas (15–16%) were higher than the CO concentrations (12–13%).

The average ignition and burning rates, as defined by Ryu et al. (2007), for the combustion of the OPS at various air flow rates obtained from the experiments (plotted in symbols) were shown in Fig. 5b. Both the ignition and the burning rates during the ignition propagation stage increased when the primary air flow rate was increased. This is expected because the combustion of OPS in the fixed bed was controlled by the low flow rate of the primary air (Shin and Choi, 2000), as shown in Fig. 4c and d. The burning rate at the primary air flow rate of 618 kg/m²h was lower than the ignition rate. When the air flow rate was increased, the burning rates also increased.

3.3. FLIC modelling of fixed-bed combustion

Fig. 6 presents the modelling results for the fixed-bed combustion of OPS at the primary air flow rate of 1113 kg/m²h. Fig. 6a

Fig. 6. FLIC simulation results for OPS at the primary air flow rate of 1113 kg/m³h: (a) temperature profile, (b) individual process rates, (c) gas composition in the flue gas.

bustion rate remained at a relatively low level. In the final stage, the devolatilisation rate decreased whereas the char combustion rate dominated the total mass loss rate.

In the experiments, it was difficult to measure the rates of moisture evaporation, volatile release, and fixed carbon burning. Therefore, no experimental data were available for comparison with these predicted individual process rates. It should be noted that the total mass loss is the sum of the individual process rates. It is thus feasible to compare the measured residual mass on the bed with the value obtained from the modelling work. As shown in Fig. 6b, the predicted value for mass loss is in good agreement with the value obtained from the experiment. However, there was a slight under-estimation at $t = 1800–2500$ s.

Fig. 6c compares the predicted gas composition (plotted in lines) with that measured in the experiments (plotted in symbols). When comparing the experimental and modelling results, the time co-ordinate of the experimental data was adjusted to fit in with the onset point of the combustion in the modelling. As shown, the predicted gas composition was in good agreement with the measured data. There were, however, some minor discrepancies between the modelling and measured results. During the ignition propagation period, the predicted concentrations of CO_2 and CO were slightly lower than the measured data. This may be due to the under-prediction of char combustion or the combustion of volatile compounds mostly C_mH_n, which was also shown in Fig. 6c. In modelling calculations, it was assumed that char was pure carbon. However, the char actually consisted of a small amount of hydrogen and oxygen, as well as trace metals, such as potassium, calcium and iron. These trace elements can act as catalysts during char combustion, which leads to an increase in the concentrations of CO and CO_2 in the combustion tests.

Fig. 5b compares the predicted and measured ignition and burning rates under different primary air flow rates. As shown, the predicted ignition rates were in good agreement with those obtained from the experiments. It should be noted that the predicted burning rates were approximately 5% lower than the measured values. As the primary air flow rate further increased, the ignition and burning rates reached their maximum values and then were decreased.

4. Conclusions

The main conclusions are as follows:

- Pyrolysis of the OPS and PKC at 700 °C with a heating rate of 10 °C/min gave maximum liquid yield of 57.92 and 42.84 wt.%, respectively.
- The pyrolysis gases consisted mainly of CO and CO_2, and evolved at a lower temperature, below 500 °C. The main gases that evolved in the high temperature region (above 500 °C) were hydrogen and other hydrocarbon gases (C_1–C_3).
- The results of the combustion tests showed that an increase in air flow rate increased the ignition front speed and burning rate. The FLIC modelling results were in good agreement with the experimental results.

Acknowledgements

shows the predicted temperature profile in the fuel bed versus the reaction time. As shown, the predicted temperature profile during the ignition propagation period was similar to that from the experiments (Fig. 4b). After around $t = 870$ s, the temperature at the top of the bed ($y \geqslant 336$ mm) increased to over 1100 K. During the ignition propagation period, the temperature increased to 1300–1400 K at the ignition front. At approximately $t = 2400–2500$ s, the ignition front reached the bottom of the bed. Then the residual char was burned out completely, which caused the temperature to increase to 1200 °C.

Fig. 6b presents the individual process rates of moisture evaporation, devolatilisation and char combustion during the OPS combustion in the fixed bed. In accordance with the temperature profile in Fig. 6a, three distinct staged can be identified. During the heating and ignition period, moisture in the OPS at the top layer was evaporated and a minor portion of volatile matter was also released. Once the bed was ignited, the devolatilisation rate increased sharply and the total mass loss of the bed was mainly attributed to the devolatilisation. During this period, the char com-

323

References

Bridgwater, A.V., 2003. Renewable fuels and chemicals by thermal processing of biomass. Chem. Eng. J. 91, 87–102.

Bridgwater, A.V., Bridge, S.A. 1991. A review of biomass pyrolysis technologies. In: Bridgwater, A.V., Grassi, G. (Eds.), Biomass Pyrolysis Liquids, Upgrading and Utilisation. Elsevier Applied Science, London.

Cooper, J., Hallet, W.L.H., 2000. A numerical model for packed-bed combustion of char particles. Chem. Eng. Sci. 55, 4451–4460.

Demirbas, A., 2001. Biomass resource facilities and biomass conversion processing for fuels and chemicals. Energy Conv. Manage. 42, 1357–1378.

Di Blasi, C., Signorelli, G., Di Russo, C., Rea, G., 1999a. Product distribution from pyrolysis of wood and agricultural residues. Ind. Eng. Chem. Res. 38, 2216–2224.

Di Blasi, C., Signorelli, G., Portoricco, G., 1999b. Counter current fixed-bed gasification of biomass at laboratory scale. Ind. Eng. Chem. Res. 38, 2571–2581.

Figueiredo, J.L., Valenzuela, C., Bernalte, A., Encinar, J.M., 1989. Pyrolysis of holm oak wood: influence of temperature and particle size. Fuel 68, 1012–1016.

Goddard, C.D., Yang, Y.B., Goodfellow, J., Sharifi, V.N., Swithenbank, J., Chartier, J., Mouquet, D., Kirkman, R., Barlow, D., Moseley, S., 2005. Optimisation study of a large waste-to-energy plant using computational modelling and experimental measurements. J. Energy Inst. 78, 106–116.

Guo, J., Lua, A.C., 2000. Effect of heating temperature on the properties of chars and activated carbons prepared from oil palm stones. J. Thermal Anal. Calorimetry 60, 417–425.

Horttanainen, M., Saastamoinen, J., Sarkomaa, P., 2002. Operational limits of ignition front propagation against airflow in packed beds of different wood fuels. Energy Fuels 16, 676–686.

Jakab, E., Várhegyi, G., Faix, O., 2000. Thermal decomposition of polypropylene in the presence of wood-derived materials. J. Anal. Appl. Pyrolysis 56, 273–285.

Khor, A., Ryu, C., Yang, Y.B., Sharif, V.N., Swithenbank, J., 2007. Straw combustion in a fixed bed combustor. Fuel 86, 152–160.

Liang, L., Sun, R., Fei, J., Wu, S., Liu, X., Dai, K., Yao, N., 2008. Experimental study on effects of moisture content on combustion characteristics of simulated municipal solid wastes in a fixed bed. Bioresource Technol. 99, 7238–7246.

Mackay, D.M., Roberts, P.V., 1982a. The dependence of char and carbon yield and lignocellulosic precursor composition. Carbon 20, 87–94.

Mackay, D.M., Roberts, P.V., 1982b. The influence of pyrolysis condition on yield and microporosity of lignocellulosic chars. Carbon 20, 95–104.

McKendry, P., 2002. Energy production from biomass (part 1): overview of biomass. Bioresource Technol. 83, 37–46.

Nussbaumer, T., 2003. Combustion and co-combustion of biomass: fundamentals, technologies, and primary measures for emission reduction. Energy Fuels 17, 1510–1521.

Pansamut, V., Pongrit, V., Intarangsi, C., 2003. The Oil Palm Efficiency. Department of Alternative Energy Development and Efficiency, Ministry of Energy, Thailand.

Phan, A.N., 2007. Combustion/Pyrolysis/Gasification of Segregated Waste. PhD Thesis. Chemical and Process Engineering, The University of Sheffield.

Ryu, C., Phan, A.N., Yang, Y.B., Sharifi, V.N., Swithenbank, J., 2007. Ignition and burning rates of segregated waste combustion in packed beds. Waste Manage. 27, 802–810.

Saastamoinen, J.J., Taipale, R., Horttanainen, M., Sarkomaa, P., 2000. Propagation of the ignition front in beds of wood particles. Combust. Flame 123, 214–226.

Shin, D., Choi, S., 2000. The combustion of simulated waste particles in a fixed bed. Combust. Flame 121, 167–180.

Sukiran, M.A., Chin, C.M., Abu Bakar, N.K., 2009. Bio-oil from pyrolysis of oil palm empty fruit bunches. Am. J. Appl. Sci. 6, 869–875.

Uzun, B.B., Pütün, A.E., Pütün, E., 2007. Composition of products obtained via fast pyrolysis of olive-oil residue: effect of pyrolysis temperature. J. Anal. Appl. Pyrolysis 79, 147–153.

Williams, P.T., Besler, S., 1996. The influence of temperature and heating rate on the slow pyrolysis of biomass. Renewable Energy 7, 233–250.

Yan, R., Yang, H., Chin, T., Liang, D.T., Chen, H., Zheng, C., 2005. Influence of temperature on the distribution of gaseous products from pyrolyzing palm oil wastes. Combust. Flame 142, 24–32.

Yang, Y.B., Goh, Y.R., Zakaria, R., Nasserzadeh, V., Swithenbank, J., 2002. Mathematical modelling of MSW incineration on a travelling bed. Waste Manage. 22, 369–380.

Yang, Y.B., Nasserzadeh, V., Goodfellow, J., Swithenbank, J., 2003. Simulation of channel growth in a burning bed of solids. Chem. Eng. Res. Des. 81, 221–232.

Yang, Y.B., Lim, C.N., Goodfellow, J., Sharifi, V.N., Swithenbank, J., 2005. A diffusion model for particle mixing in a packed bed of burning solids. Fuel 84, 213–226.

Yang, H., Yan, R., Chen, H., Lee, D.H., Liang, D.T., Zheng, C., 2006. Mechanism of palm oil waste pyrolysis in a packed bed. Energy Fuels 20, 1321–1328.

Yang, Y.B., Phan, A.N., Ryu, C., Sharifi, V., Swithenbank, J., 2007. Mathematical modelling of slow pyrolysis of segregated solid wastes in a packed-bed pyrolyser. Fuel 86, 169–180.

Zailani, R., Ani, F.N., Islam, N., 1999. Pyrolytic oil from fluidised bed pyrolysis of oil palm shell and its characterisation. Renewable Energy 17, 73–84.

Zakaria, R. 2000. Static Incinerator Bed Combustion. PhD Thesis. Department of Chemical and Process Engineering, The University of Sheffield.

D2. Fuel Processing Technology

1. Combustion of oil palm stone in a pilot-scale fluidised bed reactor.

Combustion of oil palm stone in a pilot-scale fluidised bed reactor

Raja Razuan, Qun Chen, Karen N. Finney, Nigel V. Russell *, Vida N. Sharifi, Jim Swithenbank

SUWIC, Department of Chemical and Biological Engineering, The University of Sheffield, Mappin Street, Sheffield S1 3JD, UK

ARTICLE INFO

ABSTRACT

Biomass is being generated in vast amounts from oil palm plantations particularly in developing countries such as Malaysia, Thailand and Indonesia. Oil palm stone (OPS) is currently considered a waste material and has not previously been considered for energy purposes. The main objective of this study was to investigate the thermochemical conversion of OPS in a pilot-scale fluidised bed combustor. The net heating value of OPS was 24.93 MJ/kg. The effect of primary air flowrate and initial bed temperature were the main parameters investigated. The bed and bed's surface temperature were found to decrease as the primary air flowrate increased. In all tests CO emissions were less than 0.2%. The emissions of SO_2 and HCl ranged from 0.02 ppm to 0.05 ppm, significantly below the permitted levels set by legislation. Stable combustion was observed at a bed temperature of 950 °C. The most abundant elements found in the ash were Al, Ca, Fe, K, Mg, Mn, P, S and Si. However, due to the temperature regime used in the study fouling would not be an issue.

© 2011 Elsevier B.V. All rights reserved.

1. Introduction

Biomass is a promising source of fuel for energy generation, contributing over 14% or 1250 million TOE of the global energy demand annually [1]. Most of the biomass production and utilisation are concentrated in developing countries. It is estimated that around 75% of biomass energy is used in developing countries and approximately 25% is consumed by industrialised nations [2]. Some biomass fuels such as woody biomass and energy crops are already important energy carriers in meeting the world's energy demand [2].

Utilisation of biomass fuel could help to mitigate climate destabilising emissions, particularly on issues related to global warming or greenhouse gases (GHG). Carbon dioxide (CO_2) emissions from burning fossil fuels is one of the major sources of GHG emissions and have rapidly increased in the last few decades particularly due to the burning of fossil fuels in power plants [3,4]. Global CO_2 emission will increase at a rate of 1.7% annually if present production and consumption trends continue [5]. According to Safaai et al. [3] by the year 2020 Malaysia could produce almost 260 million tonnes of CO_2 if there are no regulations imposed by the government to mitigate release. As the world's second largest palm oil producer and exporter Malaysia has potential to produce significant amounts of sustainable biomass for clean energy generation. Following environmental pressure, the Malaysian government has recognised this by making biomass the fifth fuel in the nation's energy mix from the year 2000 [6,7]. This has helped reduce the demand for fossil fuels and started the mitigation process against GHG emissions, particularly CO_2 gas.

Shells, fibres and palm kernel, among others, are the most abundant solid wastes produced during palm milling processes [8]. Shuit et al. [7] revealed that as much as 50–70 tonnes of biomass waste can easily be produced in 1 ha of oil palm plantation. With this capacity, Malaysia could potentially generate about 56 million tonnes of biomass, which is equivalent to about 16 Mtoe per annum [7]. Much of this waste is left to decay in plantation areas or used as soil conditioner [9]. Utilising waste from the oil palm industry, particularly the oil palm stone (OPS), for energy purposes could help Malaysia further mitigate CO_2 emissions [10].

The design of the combustion vessel or reactor and properties of the fuel are important considerations in achieving a high thermal efficiency. Therefore, understanding what happens to particles of solid fuel during the combustion process is of key importance. Biomass particles undergo a process of heating up, drying, and devolatilisation before combustion of volatile matter and the char [1]. Werther et al. [1] showed that volatile and moisture contents of biomass fuels have a significant effect on combustion and thus on the design and operation of the reactor. Thermochemical biomass conversions based specifically on combustion efficiency using different combustion systems such as grate-fired, fluidised bed and suspension fired have been thoroughly reviewed in literature [1,10–18]. The authors generally agreed that fluidised bed technology is the most efficient and suitable for converting fuels with low calorific value due to its flexibility, high efficiency and low impact on environmental problems. The release of gases from biomass combustion is affected by several factors including fuel chemistry, moisture content, particle size, particle shape and the combustion processes [19]. The principal gases released during combustion of biomass are CO_2 and water, the products of complete combustion. CO_2 emitted from biomass combustion is considered to be CO_2-neutral as a GHG where sustainable crops are used. Other

---

* Corresponding author. Tel.: +44 1142270736; fax: +44 1142270501.
E-mail address: n.russell@sheffield.ac.uk (N.V. Russell).

gases and residues may be released during combustion processes including CO, char, tar, polycyclic aromatic hydrocarbons, and other organic compounds as well as NOx, SOx, HCl and ash particles. These environmental pollutants can be treated by manipulating the combustion parameters or adopting gas or particulate cleaning systems.

The main objective of this research was to characterise the properties of oil palm stone (OPS) for use as fuel based on proximate and ultimate analyses and to examine the effects of combustion parameters on the thermochemical behaviour of OPS in a pilot-scale fluidised bed reactor. The variables investigated included the effects of primary air flowrate and initial temperature of the bed when feeding commenced on temperature profiles throughout the reactor as well as gas emissions. Ash residue and acid gases were also analysed in order to obtain a better understanding of OPS combustion in a pilot-scale fluidised bed reactor.

2. Materials and methods

2.1. OPS characterisation

The OPS used for these experiments was supplied by A.M.E. Teras Marin Services Ltd., Malaysia. The sample, Fig. 1, was air dried at room temperature following receipt. Standard analytical tests were then carried out on this material. Table 1 shows the calorific value and the results of the proximate and ultimate analyses for the OPS. The material had a very high volatiles content (88.21 wt.%), with a small amount of fixed carbon (7.24 wt.%). The net calorific value (LHV) of the OPS was measured around 24.93 MJ/kg. The LHV was found to be similar to that of lignite (26.80 MJ/kg) [20]. Ultimate analysis indicated that OPS has a very low sulphur content which would reduce the requirement for costly post-combustion SOx reduction technologies.

The thermal characteristics of dry OPS sample were analysed with a computerised Perkin-Elmer Pyris 1 thermogravimetric analyser (TGA). The experiments were carried out with the following conditions; about 5 mg of sample was heated at a rate of 5 °C/min from 50 to 800 °C. Oxygen-free nitrogen gas was used as the carrier. Fig. 2 shows the results for two TGA tests for the thermal degradation of OPS. Two main decomposition peaks were identified at 290 °C and 350 °C. These peaks are thought to be due to the decomposition of hemicelluloses and cellulose respectively [21]. Low weight loss was observed at temperatures up to 250 °C due to the release of the moisture content. A rapid loss in weight was achieved between 250 °C and 380 °C due to the release of volatile matter and decomposition of water. At elevated temperatures, >380 °C, the loss in weight decreased steadily mainly associated to liberation of hydrogen gas. The total weight loss between 28 °C and 380 °C was observed to be 88 wt.%. About 10 wt.% remained as char residue.

Table 1
Experimentally determined gross calorific value and proximate and ultimate analyses of oil palm stone.

Analysis		Oil palm stone
Proximate (%, as received)	Moisture	2.85 (±0.15)
	Ash	1.70 (±0.05)
	Volatiles	88.21 (±0.80)
	Fixed carbon	7.24 (±0.09)
Ultimate (%dry, ash free)	C	66.06 (±2.44)
	H	10.86 (±0.25)
	O	21.06 (±2.16)
	N	1.65 (±0.08)
	S	0.36 (±0.33)
Net calorific value (MJ/kg)		24.93 (±0.21)
Density (kg/m³)		630 (±10)
Average diameter (m)		0.01 (±0.05)

Table 2 shows the main elements obtained from OPS sample analysed using inductively coupled plasma-optical emission spectroscopy (ICP-OES). High concentrations of potassium (K) and phosphorus (P) were found and thought to be due to the presence of potassium nitrate (KNO_3) and phosphoric acid (H_3PO_4) that have been used in fertilisers [22]. High alkali metal contents in fuels can be problematic during combustion as they lower oxide melting/fusion temperature which leads to an increase in boiler fouling deposits [8,23]. OPS was found to contain significantly low concentrations of toxic and heavy metals such as antimony (Sb), arsenic (As), and lead (Pb).

2.2. Experimental facilities and conditions

2.2.1. Experimental set-up

The combustion tests were carried out in pilot-scale fluidised bed reactor. The combustor was made of 306 stainless steel 2.3 m × 0.15 m, 10 mm thick. A 10 mm thick stainless steel perforated distributor plate was used to distribute the primary air, located 200 mm from the base of the reactor as shown in Fig. 3. Nineteen 6 cm high with 45° angle capped standpipes covered the surface of the plate. Each pipe consisted of twenty-seven 1.5 mm diameter holes to evenly distribute the primary air, which acted as both the fluidising and combustion air. An average of 850 μm diameter medium sphericity sand was used as the inert bed material. The depth of the sand bed on the distributor plate was 250 mm. A propane-fired pilot burner was used to preheat and stabilise the sand bed temperatures during the reactor's start-up mode. In order to provide isothermal conditions the reactor was insulated using Kaowool blanket material

Fig. 1. Oil palm stone (OPS).
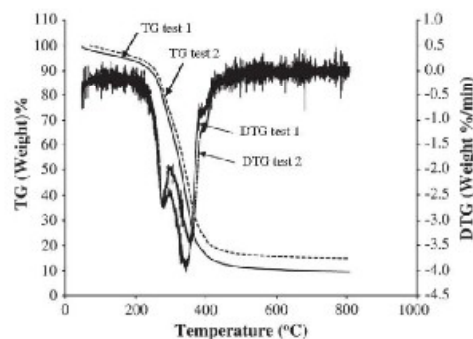
Fig. 2. Thermal degradation behaviour by TGA of OPS sample.

Table 2
Elemental analysis of oil palm stone carried out by ICP-OES.

Element	Concentration (mg/kg)[a]
Arsenic	1.6
Calcium	2250
Chromium	3.2
Copper	12
Iron	3900
Potassium	3500
Magnesium	1560
Manganese	130
Molybdenum	0.42
Sodium	11
Phosphorus	3200
Lead	0.56
Sulphur	1000
Antimony	0.09
Zinc	27

[a] Air dried.

Table 3
Operating conditions used to evaluate the effects of primary air and initial bed temperature on combustion behaviour of oil palm stone.

Test	Primary air ($kg/m^2/h$)	Secondary air ($kg/m^2/h$)	Fuel feedrate (kg/h)	Excess air (%)	Initial bed temperature (°C)	Depth of sand bed (m)
1	791	356	1.2	120	800–850	0.25
2	989	356	1.2	150	800–500	0.25
3	1187	356	1.2	188	800–850	0.25
4	791	356	1.2	120	850	0.25
5	791	356	1.2	120	900	0.25
6	791	356	1.2	120	950	0.25

to prevent heat loss. The fuel was fed at a rate of 1.2 kg/h from the sealed hopper by calibrated pneumatic screw feeder directly to the combustion chamber. Secondary air was used to assist the fuel feed process and to avoid any back-pressure from the reaction chamber. After a period of 1 h the feed was discontinued; the air flow was continued for a further 15 min or until the flame had extinguished to allow the fuel to completely burn. Once the temperature of the bed had decreased to 200 °C the reactor was shut down.

2.2.2. Experimental conditions

The experiments were designed to investigate the effect of primary air and initial temperature of the bed when feeding commenced (referred to as 'initial bed temperature') on the thermochemical behaviour of the OPS biomass for use as a fuel. The temperature profile, combustion gas, fly ash and acid gas were the main combustion characteristics examined. A series of primary air flowrates and initial temperatures of the sand bed were used to investigate combustion behaviour, Table 3. The sand bed depth was constant, at 250 mm, for all tests. The minimum fluidisation for the sand bed was calculated to be 115 l/min (0.002 m^3/s).

The temperatures of the sand bed and freeboard were monitored using eight K-type thermocouples, measuring temperatures from 0 °C

Fig. 3. Schematic of the Sheffield pilot-scale fluidised bed reactor.

to 1350 °C. These thermocouples were positioned at different heights in the centre of the combustion chamber, Fig. 3. Heights above the distributor plate for thermocouples T1, T2, T3, T4, T5, T6, T7 and T8 were 1.74 m, 1.54 m, 0.76 m, 0.56 m, 0.42 m, 0.31 m, 0.20 m and 0.11 m respectively. The accuracy of thermocouples used in this study was ±0.75% of the measured temperature.

3. Results

This study focused on the combustion characteristics of OPS in a pilot-scale fluidised bed combustor. Two parameters, primary air and initial bed temperature, were the main focus of the combustion study. The primary air varied from 791 kg/m^2/h to 1187 kg/m^2/h. Initial bed temperatures ranged from 850 °C to 950 °C. A summary of test parameters and the results for different primary air flowrates and initial bed temperatures are presented in Tables 4 and 5 respectively. Tests 1 and 5 were carried out at almost identical experimental conditions, Table 3. The differences between these tests related to the introduction of the sample into the combustion chamber. The sample in Test 5 was introduced immediately to the initial bed temperature that had reached 900 °C, whereas in Test 1 the introduction of the sample was between 800 °C and 900 °C and not subjected to the initial bed temperature control.

3.1. Effect of manipulating the primary air flowrate on combustion characteristics

3.1.1. Temperature profile

Although eight thermocouples were used to monitor the temperature throughout the tests, only four locations were found necessary to represent the temperature in the combustor: the temperature of the bed (T7 = 0.20 m); the bed surface temperature (T5 = 0.42 m); and the freeboard temperatures (an average of T2 = 1.54 m and T3 = 0.76 m).

Fig. 4(a)–(c) shows the temperature profiles measured at different primary air flowrates, (a) 791 kg/m^2/h, (b) 989 kg/m^2/h and (c) 1187 kg/m^2/h. Similar patterns were observed in all three cases. The temperature of the bed (T7 = 0.2 m) gradually decreased moments after the sample was introduced into the reactor. However, the temperature stabilised at around 750 °C during combustion period. A plateau was observed at the temperature above the bed (T5 = 0.42 m). This suggested that the combustion occurred steadily during the test periods. The freeboard temperatures (an average of T2 = 1.54 m and T3 = 0.76 m) increased steadily over time. The highest temperatures achieved at the freeboard were between 650 and 680 °C.

Fig. 5 shows the effect of manipulating primary air flowrate on temperatures at three different locations; bed (T7 = 0.2 m), surface of the bed (T5 = 0.42 m) and freeboard (an average of T2 = 1.54 m and T3 = 0.76 m). The bed (Tbed) and bed surface (Tbedsurface) temperatures were found to be between around 750 and 830 °C. The freeboard temperature was slightly lower at around 600–620 °C due to the effect of secondary air and heat loss through the combustor wall. In general, the bed and bed surface temperatures decreased as the primary air

Table 4
Summary of flue gas parameters and combustion characteristics at various primary air flowrates.
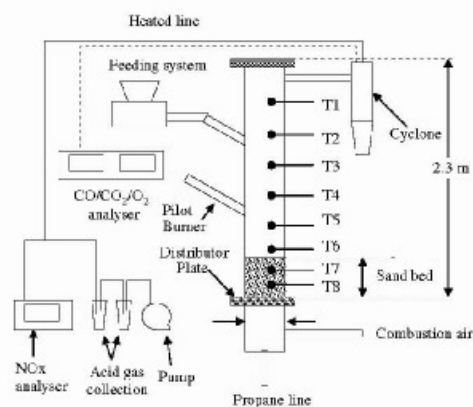
Parameters		Test 1	Test 2	Test 3
Fuel feedrate (kg/h)		1.3	1.3	1.2
Primary air (kg/m²/h)		791	881	187
Secondary air (kg/m²/h)		356	355	356
λ(AFR/AFRₛₜₒᵢ) based on primary air		1.20	1.50	2.09
λ(AFR/AFRₛₜₒᵢ) actual		1.66	2.03	3.52
Gas concentration	CO₂ (%)	15.11 (+0.73)	13.32 (−0.98)	9.15 (+0.45)
	CO (%)	0.19 (−0.02)	0.19 (±0.02)	0.08 (±0.00)
	O₂ (%)	6.72 (−0.27)	9.86 (+0.35)	13.16 (−0.23)
	NOx (ppm)	232 (±30)	238 (−43)	162 (−31)
	SO₂ (ppm)	0.03 (−0.002)	0.03 (±0.01)	0.04 (±0.00)
	HCl (ppm)	0.02 (−0.006)	0.03 (+0.01)	0.02 (+0.01)
Ash collected	Fly ash (%)	21	58	67
	Bottom ash (%)	10.54	14.00	NC
Temperature (°C)	Bed	802 (±30)	750 (±17)	744 (±24)
	Surface of the bed	871 (±14)	805 (±13)	777 (±14)
	Freeboard	623 (±42)	599 (±43)	621 (±35)

NC — not collected.

flowrate increased. The freeboard temperature was observed to be uniform and almost independent of primary air flowrate.

3.1.2. Gas emissions

Fig. 6(a)–(c) shows the gas emissions evolved for three different air flowrates: (a) 791 kg/m²/h, (b) 989 kg/m²/h and (c) 1187 kg/m²/h. The secondary air, fuel feedrate and the bed depth were maintained at 356 kg/m²/h, 1.2 kg/h and 0.25 m respectively. Propane gas was used to pre-heat and stabilise the temperature of the sand bed to around 800–850 °C before gases were collected and analysed.

It was found that CO gas concentration decreased as primary air increased, Fig. 7. The concentration of CO was observed to be < 0.2% in all cases. As expected, the concentration of O₂ was lower than CO₂ in Tests 1 and 2. However, in Test 3, the amount of O₂ was slightly higher compared to the concentration of CO₂ during the combustion period. This indicated that combustion occurred rapidly in excess air (λ = 1.80).

3.1.3. Acid gas emissions

Tables 4 and 5 show an average acid gas concentration including NOx, SOx and HCl. The amount of NOx released during combustion process was relatively low from 162 ppm to 238 ppm. The concentration of HCl presented was inferred using the Standard method (BS 1756 part 4) based on the assumption that all (Cl⁻) ions in the gas phase were present in the form of HCl. The concentrations of HCl measured in all cases were below 0.05 ppm. This value is far below the permitted level given by the waste incineration directive (WID) at

10 mg/m³ [24]. Sulphur dioxide (SO₂) was emitted with very low concentration during combustion of oil palm stone.

3.2. Effect of changing initial bed temperature on combustion characteristics

Three sets of initial bed temperature were chosen in this study; 850 °C, 900 °C and 950 °C. Summaries of the experimental conditions and the results are shown in Table 5. The temperature profiles obtained at three different locations; in the bed (T7), at the bed surface (T5) and freeboard (an average of T2 and T3) with respect to the initial bed temperatures of 850 °C, 900 °C and 950 °C over time are shown in Fig. 8. The influences of initial bed temperature in the combustion process begin with the introduction of the fuel until combustion temperature stabilised after about 30–40 min. After this period, the initial bed temperature no longer played a role and combustion stability depended on the combustion of volatiles and char within the combustion chamber.

In all cases, the combustion temperature decreased sharply following the introduction of the fuel. The temperature drop at the beginning of the combustion process indicated that the net energy was 'negative' due to the fuel drying and devolatilisation. Once the char residue started to burn and release energy, an exothermic process, the bed reached a stable temperature where the rates of energy consumption and generation were at equilibrium.

The combustion of OPS at higher initial bed temperature (950 °C) was found to be more stable as indicated by the plot of T7 (Test 6),

Table 5
Summary of test parameters and combustion characteristics at a range of initial bed temperatures.

Parameters		Test 4	Test 5	Test 6
Fuel feedrate (kg/h)		1.2	1.2	1.2
Primary air (kg/m²/h)		791	791	791
Secondary air (kg/m²/h)		356	355	356
Initial bed temperature (°C)		850	900	950
λ(AFR/AFRₛₜₒᵢ) based on primary air		1.30	1.30	1.30
λ(AFR/AFRₛₜₒᵢ) actual		1.66	1.66	1.73
Gas concentration	CO₂ (%)	4.17 (±0.46)	4.6 (−0.71)	4.50 (−0.46)
	CO (%)	0.16 (−0.03)	0.16 (+0.03)	0.20 (+0.03)
	O₂ (%)	1.03 (−0.46)	0.58 (−0.46)	0.06 (±0.03)
	NOx (ppm)	182 (+36)	205 (−12)	199 (−37)
	SO₂ (ppm)	0.01 (±0.04)	0.03 (±0.01)	0.04 (±0.04)
	HCl (ppm)	0.01 (±0.04)	0.03 (±0.01)	0.04 (±0.01)
Ash collected	Fly ash (%)	0.08	0.35	0.33
Temperature (°C)	Bed	806 (±30)	841 (−31)	910 (−24)
	Surface of the bed	821 (+60)	854 (−16)	805 (−32)
	Freeboard	557 (±30)	543 (−40)	630 (−48)
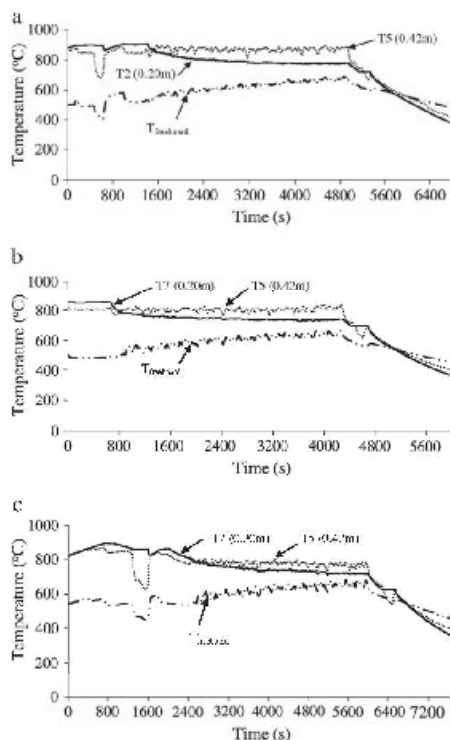
Fig. 4. Temperature profiles for the combustion of oil palm stone in the pilot-scale fluidised bed reactor at a primary air of (a) 791 kg/m³/h, (b) 989 kg/m³/h and (c) 1187 kg/m³/h.

Fig. 8. The surface bed temperature and rate of temperature change were increased as the initial bed temperature increased, Fig. 9. However, it was difficult to recognise the small changes in combustion temperature between Test 4 at 800 °C and Test 5 at 850 °C due to very close gap between these two initial bed temperature ranges. The freeboard temperatures (an average T2 = 1.54 m and T3 = 0.76 m)

Fig. 6. Gas emissions at primary air flowrates of (a) 791 kg/m²/h, (b) 989 kg/m²/h and (c) 1187 kg/m²/h.

were observed to gradually increase over time, Fig. 8. The energy released during combustion of the volatile matter and the char dominated in this region which caused the temperature to increase.
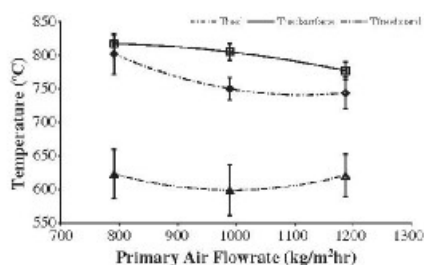
Fig. 5. Trends for the temperatures across the reactor at different primary air flowrates.
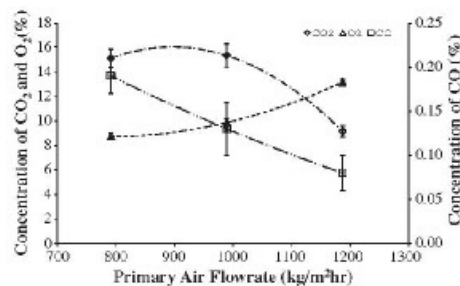
Fig. 7. Effect of increasing primary air flowrate on gas concentration.

2224   B. Abaah et al. / Fuel Processing Technology 92 (2011) 2215–2225
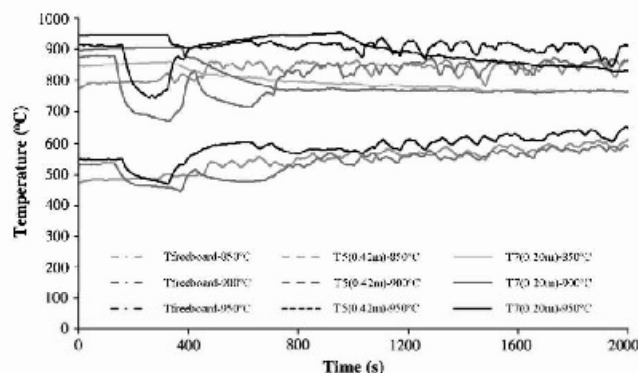
Fig. 8. Temperature profiles for the combustion of oil palm stone at different initial bed temperatures.

3.3. Bottom and fly ash analysis

Fly ash was collected from the cyclone mounted at the top of the reactor. The fly ash residue was collected after each test. As shown in Tables 4 and 5 less than 2% of the initial material was trapped as fly ash in the cyclone. Particles with particularly low densities may have been emitted with the exhaust gases (released to the atmosphere) if they were too small to be collected by particle inertia in the cyclone. The rest, particles with high densities, either mixed or agglomerated with the sand (quartz) particles that formed the fluidised bed at the bottom of the reactor. According to Lind et al. [25] there are two mechanisms by which ash can become attached to sand particles: ash deposition on the sand surface; and diffusion of the ash compounds into the bed particles. Consequently these were quite difficult to separate and thus the proportion of ash in this mixture was calculated, along with the unburned carbon, using an ash tracer method [27–29]. For both Tests 1 and 2 around 1.7% of the mass of the mixture (sand + bottom ash) was determined to be bottom ash, of which 10% was calculated to be unburned carbon.

Analysis of trace elements showed that those present in high concentrations in the fly ash were also present in high concentrations in the bottom ash. As expected, the most abundant elements were found to be Al, Ca, Fe, K, Mg, Mn, P, S and Si. The elements of concern for combustion systems are K, Na, Ca, Mg, Si, Cl and S [26] which can cause fouling. However, fouling is not likely to be of concern in the temperature regime used in this study.
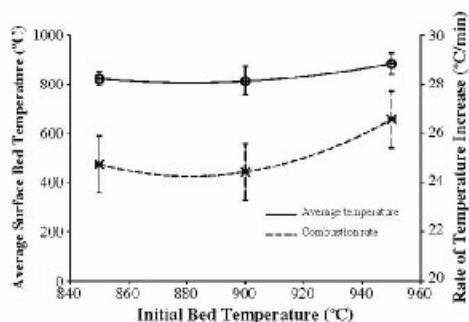
Fig. 9. Effect of initial bed temperature on the surface bed temperature and rate of temperature increase.

Based on this pilot-scale study OPS was found to be a good candidate for the future clean fuel due to low sulphur content and low acid gas emission such as NOx, SOx and HCl. Furthermore, it shows signs of good combustion characteristics in a fluidised bed.

4. Conclusions

Thermochemical characteristics of OPS fuel were evaluated using pilot-scale fluidised bed combustor with the various test parameters including the effects of primary air flowrate and initial bed temperature. The main results from this study are:

- The combustion of OPS in various primary air flowrates and initial bed temperatures was successfully conducted in a pilot-scale fluidised bed combustor.
- The bed and bed's surface temperatures decreased as the primary air flowrate increased.
- Acid gas (NOx, SOx and HCl) measured in this study showed that all species were well below permitted level as regulated by waste incineration directive.
- The combustion temperature was found to be more stable when the OPS combustion was initiated at higher initial bed temperature (950 °C).
- About 10.54% to 14% ash was mixed with the sand bed, whilst around 1.08–1.67% was collected in the cyclone.
- The most abundant elements found in the ash sample were Al, Ca, Fe, K, Mg, Mn, P, S and Si.

Acknowledgements

References

[1] J. Werther, M. Saenger, E.U. Hartge, T. Ogada, Z. Siagi, Combustion of agricultural residues, Progress in Energy and Combustion Science 26 (2000) 1–27.
[2] M. Parikka, Global biomass fuel resources, Biomass and Bioenergy 27 (2004) 613–620.
[3] N.S.M. Safaai, Z.Z. Noor, H. Hashim, Z. Ujang, J. Talib, Projection of CO₂ emissions in Malaysia, Environmental Progress & Sustainable Energy 29 (2010) 8.
[4] National Greenhouse Gas Inventory Data for the Period 1990 2006, FCCC/SBI/2008/12, United Nation, 2008 [Online], http://unfccc.int/resource/docs/2008/sbi/eng/12.pdf (18/1/2011).

[5] R. Leete, Malaysia Generating Renewable Energy from Palm Oil Wastes, United Nations Development Programme (UNDP), Malaysia, 2007 [Online]. http://www.undp.org.my/uploads/Renewable_Energy_Palm_Oil_Wastes.pdf (19/1/2011).

[6] A.B. Nasrin, A.N. Ma, S. Mohamad, M.H. Rohaya, A. Azali, Z. Zainal, Oil palm biomass as potential substitution raw materials for commercial biomass briquettes production, American Journal of Applied Sciences 5 (2008) 179–183.

[7] S.H. Shuit, K.T. Tan, K.T. Lee, A.H. Kamaruddin, Oil palm biomass as a sustainable energy source: a Malaysian case study, Energy 34 (2009) 1225–1235.

[8] R. Razuan, K.N. Finney, Q. Chen, V.N. Sharifi, J. Swithenbank, Pelletised fuel production from palm kernel cake, Fuel Processing Technology 92 (2011) 609–615.

[9] O.A. Hassan, M. Ishida, I.M. Shukri, Z.A. Tajuddin, Oil-palm Fronds as a Roughage Feed Source for Ruminants in Malaysia, Malaysia Agriculture Research and Development Institute, 1994.

[10] R. Razuan, Q. Chen, X. Zhang, V. Sharifi, J. Swithenbank, Pyrolysis and combustion of oil palm stone and palm kernel cake in fixed-bed reactors, Bioresource Technology 101 (2010) 4622–4629.

[11] M.A. Leon, A. Dutta, Fluidization characteristics of rice husk in a bubbling fluidized bed, The Canadian Journal of Chemical Engineering 88 (2010) 18–22.

[12] V.I. Kouprianov, W. Permchart, Emissions from a conical FBC fired with a biomass fuel, Applied Energy 74 (2003) 383–392.

[13] V.I. Kouprianov, W. Permchart, K. Janvijitsakul, Fluidized bed combustion of pre-dried Thai bagasse, Fuel Processing Technology 86 (2005) 849–860.

[14] T. Murakami, Y. Suzuki, H. Nagasawa, T. Yamamoto, T. Koseki, H. Hirose, S. Okamoto, Combustion characteristics of sewage sludge in an incineration plant for energy recovery, Fuel Processing Technology 90 (2009) 778–783.

[15] T. Rogaume, F. Jabouille, J.L. Torero, Effect of excess air on grate combustion of solid wastes and on gaseous products, International Journal of Thermal Sciences 48 (2009) 165–173.

[16] T. Rogaume, M. Auzanneau, F. Jabouille, J.C. Goudeau, J.L. Torero, The effects of different airflows on the formation of pollutants during waste incineration, Fuel 81 (2002) 2277–2288.

[17] Y.B. Yang, V.N. Sharifi, J. Swithenbank, L. Ma, L.I. Darvell, J.M. Jones, M. Pourkashanian, A. Williams, Combustion of a single particle of biomass, Energy & Fuels 22 (2008) 306–316.

[18] S.C. Bhattacharya, N. Shah, Z. Alikhani, Some aspects of fluidized bed combustion of paddy husk, Applied Energy 16 (1984) 307–316.

[19] M.O. Andreae, P. Merlet, Emission of trace gases and aerosols from biomass burning, Global Biogeochemical Cycles 15 (2001) 955–966.

[20] P. McKendry, Energy production from biomass (part 1): overview of biomass, Bioresource Technology 83 (2002) 37–46.

[21] T.G. Bridgeman, L.I. Darvell, J.M. Jones, P.T. Williams, R. Fahmi, A.V. Bridgwater, T. Barraclough, I. Shield, N. Yates, S.C. Thain, I.S. Donnison, Influence of particle size on the analytical and chemical properties of two energy crops, Fuel 86 (2007) 60–72.

[22] C.O. Plank, Plant Analysis Handbook for Georgia [Online]. http://aesl.ces.uga.edu/publications/plant/index.htm (28/1/2011).

[23] K.N. Finney, V.N. Sharifi, J. Swithenbank, Fuel pelletization with a binder: part II—the impacts of binders on the combustion of spent mushroom compost-coal tailing pellets, Energy & Fuels 23 (2009) 3203–3210.

[24] Environmental Permitting Guidance, The Directive on the Incineration of Waste, Department for Environment, Food and Rural Affairs, 2009 Version 2, [Online], http://www.defra.gov.uk/environment/policy/permits/documents/wid-guidance.pdf (17/2/2011).

[25] T. Lind, T. Valmari, E. Kauppinen, K. Nilsson, G. Sfiris, W. Maenhaut, Ash formation mechanisms during combustion of wood in circulating fluidized beds, Proceedings of the Combustion Institute 28 (2000) 2287–2295.

[26] D. Vamvuka, D. Zografos, Predicting the behaviour of ash from agricultural wastes during combustion, Fuel 83 (2004) 2051–2057.

[27] S. Munir, W. Nimmo, B.M. Gibbs, Co combustion of agricultural residues with coal: turning waste into energy, Energy & Fuels 24 (2010) 2146–2153.

[28] L. Zhang, E. Binner, L. Chen, Y. Qiao, C.-Z. Li, S. Bhattacharya, Y. Ninomiya, Experimental investigation of the combustion of bituminous coal in air and O_2/CO_2 mixtures: 1. Particle imaging of the combustion of coal and char, Energy & Fuels 24 (2010) 4803–4811.

[29] S. Li, Y. Wu, K.J. Whitty, Ash deposition behavior during char-slag transition under simulated gasification conditions, Energy & Fuels 24 (2010) 1868–1876.

2. Pelletised fuel production from palm kernel cake.

Pelletised fuel production from palm kernel cake

R. Razuan, K.N. Finney [*], Q. Chen, V.N. Sharifi, J. Swithenbank

SUWIC, Department of Chemical and Process Engineering, The University of Sheffield, Mappin Street, Sheffield, S1 3JD, UK

ARTICLE INFO

ABSTRACT

Biomass is an important source of renewable energy. Worldwide, the palm oil industry generates large amounts of waste materials, such as shells, fibres and palm kernel cake, which can be used for power generation. Processing the palm kernel cake into a uniform fuel through pelletisation will be an attractive option — assessing the suitability of this process was the main objective of this research. Extensive analytical and pelletisation tests were performed to evaluate the physical properties of pellets produced from this material. The variables explored included the pelletisation pressure, temperature, fuel moisture and the effect of binders, which all had significant effects on density and tensile strength. The most favourable conditions for pellet production were a pressure of 9038 psi/64.38 MPa, a temperature of 80–100 °C and a fuel moisture content of 7.9%. These pellets had densities of 1184–1226 kg/m^3 and tensile strengths of 930–1007 kPa. Adding small amounts of caustic soda (1.5–2.0wt%) to the palm kernel cake under these conditions increased the tensile strength to 3055 kPa, whereas starch additives were not found to be effective binders. It is estimated that the production of palm kernel cake pellets with 2 wt.% of the caustic soda binder would cost approximately €28–47/tonne.

© 2010 Elsevier B.V. All rights reserved.

1. Introduction

To overcome the issues associated with global warming, promoting biomass as a source of renewable fuel is vital, since the use of these energy resources is important in protecting the environment. Wood, energy crops, agricultural/forestry residues and the organic components of municipal and industrial wastes are major sources of biomass fuel. Each of them has specific properties that determine their performance and characteristics as a fuel.

The Malaysian palm oil industry has grown tremendously over the last four decades and is currently the world's second largest palm oil producer and exporter [1]. Malaysia has declared that biomass is the fifth fuel in its energy mix, which reduces the demand for fossil fuels [2,3]. Solid oil-palm waste materials (including the shells, fibres and its kernel) are produced during the palm oil milling process. Currently, most of the wastes generated are left to decompose in the plantation areas and are used as soil conditioners [4]. For every ton of oil-palm fruit being fed to the refining process, about 0.07 tons of palm shell, 0.103 tons of palm fibre and 0.012 tons of kernels are produced as solid wastes [5]. Waste from the palm oil industry, particularly the palm kernel cake (PKC) is abundant and can help meet the energy demand, if managed properly [6]. However, the research that has been carried out on the utilisation of PKC for energy production is very limited.

1.1. Fuel pelletisation

Pelletisation is a process of compacting loose material to form a densified, homogeneous product. Pellets are often favoured for fuel applications because of their enhanced physical properties, as well as being easy to feed and handle. According to Grover and Mishra [7], the most influential parameters in the selection of raw materials are the moisture content, ash content, flow characteristics and particle size. Most pelletisation processes involve either compression of extrusion techniques.

Nasrin, et al. [2] investigated the physical and chemical properties of pellets made from palm oil biomass. It was found that the conversion of a mixture of empty fruit bunches and PKC into a uniform fuel, such as pellets, can improve their properties and value, including the energy content, by reducing the moisture levels by 5% and 38% respectively.

Other studies have investigated the pelletisation of a range of other biomass fuels. Bhattacharya, et al. [8–10], for example, studied several biomass wastes and found that there were marked improvements in the combustion characteristics of pelletised biomass compared to the loose, raw material. Ryu, et al. [11] evaluated the quality (density, swelling, tensile strength and durability) of spent mushroom compost-coal tailing pellets. It was found that both materials were significantly influenced by the moisture content, where the optimum to produce good quality pellets was 10% for the coal tailings and 20% for the spent mushroom compost. Pelletisation at pressures exceeding 6000 psi (>41.37 MPa) did not show any significant improvements in density or strength from those made at 6000 psi (41.37 MPa). Finney,

* Corresponding author. Tel.: +44 1142227572; fax: +44 1142227501.
E-mail address: k.finney@sheffield.ac.uk (K.N. Finney).

et al. [12] later evaluated caustic soda and maize starch binders for these materials, in addition to inherent binders. They found that pellet tensile strength increased significantly by adding small amounts of either binder (up to 1 wt.%). The overall quality of the pellet could be further improved by pelletisation at elevated temperatures (45–75 °C), which softened the lignin components of the biomass, acting as a natural binder.

O'Dogherty, et al. [13] studied the energy required to form a pellet made from straw. They found that the specific energy increased linearly from 11 to 24 MJ/t for a pellet density range of 300–600 kg/m³. Trezek, et al. [14] studied the specific energy required to produce pellets from the light fraction of municipal solid waste. They found that most of the energy consumed was for material deformation; to overcome die friction required about 51.84 MJ/t of energy at a moisture content of 15%. Mani, et al. [15] determined the energy requirements for briquetting corn stover at different pressures and moisture contents. It was discovered that the specific energy consumption (12–30 MJ/t) was dependent on briquette density. Almost half of the total energy required in the compaction of the corn stover was used to overcome the surface friction.

1.2. Costs of pelletised fuel production

The costs involved with biomass fuel pelletisation have been studied extensively and there are guidelines on how to evaluate the costs of manufacturing biomass pellets [16–20]. Thek and Obernberger [19] outline the four main costs to consider for the production of fuel pellets: (i) the total capital costs, (ii) consumption costs, (iii) operating costs and (iv) any other costs. Thek and Obernberger [19] and Mani, et al. [21] stated that about one third of the total production costs for wood pellets are for the raw material and personnel. The drying (particularly involving very wet raw materials) and manufacturing processes were also considered as major contributions to the production costs.

A typical cost analysis for the production of fuel pellets includes plant capacity (t/h), hours of operation (h/day), total number of production days per year (days), electricity costs (currency/kWh), interest rate (%), average equipment utilisation period (year), labour wage (currency/h) and number of shifts [16]. Sultana, et al. [18] reported that the field and transportation costs contributed the most to the total pelletisation costs of wheat, barley and oat residues. The costs of producing one tonne of pellets from these residues were $170.89 (£116.34), $129.42 (£88.11) and $122.17 (£83.17) respectively. The typical costs for loading and unloading biomass in North America are reported as $5.45/tonne (£3.71/tonne) [18]. Transportation costs for moving corn stover bales about 64 km (40 miles) was estimated to be $54.57/dry tonne (£37.12/dry tonne) [22].

Mani, et al. [21] reported that the cost of producing sawdust pellets could be economically viable, about $51/tonne (£34.70/tonne) for a plant with a capacity of 45,000 tonnes/year. Chaiyaomporn and Chavalparit [23] evaluated the production costs of pellets made from a mixture of palm fibre and palm shell (80:20) with 10% moisture content. The analyses were based on three main factors, namely the cost of the raw materials, transportation and manufacturing. They found that the total production costs were around 1140 baht/tonne (£24/tonne).

1.3. Project objectives

The main objective of this research was to examine the effects of process parameters on the physical properties of palm kernel cake pellets, such as tensile strength, density and durability. The variables investigated included the pelletisation pressure, temperature, fuel moisture content and the effect of binders. An attempt was made to determine the optimum values of these parameters, which would result in the best pellet quality. This could help promote PKC as a source of renewable fuel in the future.

2. Materials and experimental methods

2.1. Materials

The palm kernel cake used for these tests was supplied by A.M.E Teras Marin Services Ltd. The sample was finely crushed, until the average particle size was 2 mm in diameter. The PKC has a bulk density of 623 kg/m³ prior to pelletisation. Standard analytical tests were performed on this material. Table 1 shows the calorific value and the results of the proximate and ultimate analyses for the PKC. The material had a very high volatiles content (71.84 wt.%), with a small amount of fixed carbon (16 wt.%). The calorific value (18.67 MJ/kg) was lower than that of lignite (~28 MJ/kg), possibly due to the low fixed carbon content. The oxygen content was high, and although this was calculated by difference and may therefore contain some errors, this may also negatively impact the calorific value of the fuel [24]. The ultimate analysis indicates that PKC could be an environmentally friendly fuel, as it has a low sulphur content.

Elemental analysis was also performed on the PKC. Table 2 lists the main elements. High concentrations of potassium (K) and phosphorus (P) were found and are thought to be due to the presence of potassium nitrate (KNO_3) and phosphoric acid (H_3PO_4) that are used in fertilisers [24–26]. High alkali metal (potassium and sodium) contents in fuels can be problematic during combustion; this increases the alkali metal oxide content in the ash residues, lowering their melting/fusion temperatures and potentially leading to slagging and fouling [27]. PKC was found to contain only low levels of toxic and heavy metals, such as antimony (Sb), arsenic (As) and lead (Pb). Based on the material specifications provided by the supplier, the PKC also contained about 21% of protein and fat from the palm oil residue.

2.2. Pelletisation experiments

2.2.1. Experimental set-up

PKC pellets were manufactured using the compression pelletiser shown schematically in Fig. 1. This consisted of a stainless steel cylindrical pelletisation chamber (150 mm high, with an internal diameter of 26.8 mm) and a ram. The mould was fixed below the top plate and the ram was attached to the movable platform (hydraulic press). About 20 g of material was loaded through the top of the mould to the centre of the pelletiser. This pelletiser could compress the material up to a maximum pressure of 10,000 psi (68.95 MPa). Two rope heaters (OMEGA FGR-060, 250 W each) were used to heat the mould and a K-type mineral insulated thermocouple was connected to a temperature controller to manipulate the temperature, which had an operating range of −20–300 °C.

2.2.2. Experimental conditions

The experiments were designed to investigate the effect of a range of parameters on PKC pellet properties. Firstly, the effect of the fuel moisture content was assessed, comparing three moisture contents.

Table 1
Experimentally determined gross calorific value and proximate and ultimate analyses of palm kernel cake.

	Analysis	Palm kernel cake
Proximate	Moisture	7.92
(% as received)	Ash	4.28
	Volatiles	71.84
	Fixed carbon	16.08
Ultimate	C	52.53
(% dry, ash free)	H	5.65
	O	38.53
	N	2.66
	S	1.03
Gross calorific value (MJ/kg)		18.67

611

Table 2
Elemental analysis of palm kernel cake.

Element	Concentration (mg/kg)
Arsenic	1.0
Calcium	4950
Chromium	2.8
Copper	21
Iron	1300
Potassium	6500
Magnesium	2700
Manganese	240
Molybdenum	0.35
Sodium	23
Phosphorous	5900
Lead	0.5
Antimony	0.07
Zinc	40

To increase the moisture content from the 'as received' level of 7.9%, the sample was wetted, mixed thoroughly and left it in an air-tight container for a period of 48 h; this increased the moisture content to 15%. The PKC was also oven dried at 60 °C overnight to reduce the moisture content to 5%.

Secondly, the impact of pelletisation pressure was evaluated. The pressures tested varied from 4060 to 9338 psi (28.0 to 64.4 MPa); a holding time of 5 s at the maximum pressure was used for all pellets. The optimum pressure was then used to examine the effect of temperature, comparing room temperature (~20 °C) to elevated temperatures of 40, 60, 80, 100 and 120 °C.

Once the optimum pressure (9338 psi/64.4 MPa) and temperature (80 °C) had been both established, these conditions were subsequently used to study the effect of the binders and how they influence agglomeration. Two different types were used: organic and inorganic binders. The organic binders were different types of starch — maize, tapioca and potato starch, and the inorganic binders were caustic soda (NaOH) and calcium carbonate (CaCO$_3$). The PKC was mixed with various amounts of each starch (up to 20 wt.%) in powder form prior to pelletisation. Various amounts of caustic soda (up to 2.5 wt.%) and calcium carbonate (up to 5 wt.%) were also tested.

2.2.3. Evaluation of pellet quality

Pellet quality was determined by examining pellet density (ρ), tensile strength (TS) and durability. Student's t-tests were carried out to evaluate the statistical significance between results for density and tensile strength.
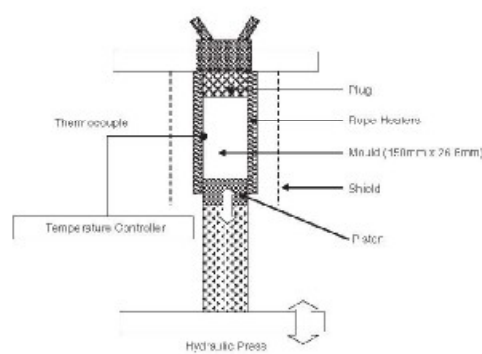
Fig. 1. Schematic of the compression pelletiser.

The pellet density (ρ, kg/m^3) was calculated using the following formula:

$$\rho = W / \pi L d \qquad (1)$$

where W is the pellet weight (kg), L is the pellet length (m) and d is the pellet diameter (0.0268 m).

The pellet tensile strength (TS, in kPa) was calculated based on its compressive strength (CS, in N) and the pellet dimensions; this relates pellet size and shape to its cohesion [12]. The compressive strength was analysed using the Brazilian test, where the sample was placed between the two plates of a Monsanto tensometer and pressure applied. The maximum radial force before fracturing was recorded. The tensile strength was then calculated using the following equation:

$$TS = 2CS / \pi L d \qquad (2)$$

Durability testing was based on the procedure described by Ryu, et al. [11]. Five pellets (limited by drum capacity) were placed in a 100 mm × 200 mm Perspex cylinder with a small baffle and mounted onto a lathe, which rotated at 40 rpm. The drum was rotated for a total of 10 min and was stopped at 5 min intervals. Durability (%), the ratio of the initial weight (W_1) and the final weight (W_2), both in kg, was calculated using the following equation:

$$Durability = W_1/W_2 \times 100 \qquad (3)$$

The process was repeated three times for each case and an average was taken. There are other similar methods available for assessing durability, such as ASAE S269.4 (ASAE 1996) [28,29]. This method requires a 300 mm × 300 mm × 125 mm tumbling device with a 230 mm long baffle to create a tumbling effect. Due to the time and cost constraints and readily available data for comparisons, the alternative procedure described above was used in this study.

3. Results and discussion

3.1. Effect of fuel moisture content

The effect of the moisture content on biomass pellet qualities, such as density, strength and durability has been examined by various researchers [11,13,15,30]. In this study, however, a relationship between moisture and pellet quality could not be established, as viable pellets could not be produced at high or low moisture contents and could thus not be tested. In the case of high moisture levels (15%), the pellets collapsed immediately upon ejection from the mould (Fig. 2a). At low moisture contents (5%), the pellets cracked instantly after being removed from the mould, as shown in Fig. 2b. Fig. 2c shows a good quality pellet produced at the 'as received' moisture content of 7.9%. As this was the only moisture level to produce coherent pellets, all subsequent tests were conducted at this moisture content.
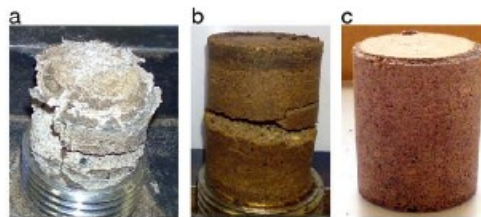
Fig. 2. Palm kernel cake pellets produced at different moisture contents: (a) at a high moisture content of 15%, (b) at a low moisture content of 5% and (c) at an 'as received' moisture content of 7.9%.

334

612   R. Razuan et at. / Fuel Processing Technology 92 (2011) 609–615

Fig. 3. Effect of pressure on palm kernel cake pellet density and tensile strength.
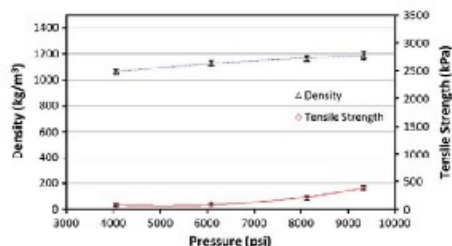
Fig. 5. Effect of temperature on palm kernel cake pellet density and tensile strength.

3.2. Effect of pressure

Fig. 3 shows the effect of pelletisation pressure on the tensile strength and density of PKC pellets. Pellets formed at higher pressures were found to be stronger and more uniform in shape over time. As the pressure increased from 4060 to 9338 psi (28.0 to 64.38 MPa), the densities of the PKC pellets, calculated using Eq. (1), increased steadily from 1060 to 1187 kg/m³. This is due to the low compression energy required to fill the inter-particle spaces during the compression process [11]. The density of the PKC pellets was almost comparable with the pellets made from palm fibres and shells, which ranged between 1100 kg/m³ and 1200 kg/m³ [31].

The pellet tensile strengths, calculated using Eq. (2), increased from 72 to 387 kPa as the pressure increased from 4060 to 9338 psi (28.0 to 64.38 MPa). Although a slight increase in density was observed between pelletisation pressures of 8120 and 9338 psi (55.99 to 64.38 MPa), the tensile strength of the pellets was found to increase quite significantly. The highest tensile strength (387 kPa) and the greatest pellet density (1187 kg/m³) were both obtained at a maximum pelletisation pressure of 9338 psi (64.38 MPa).

3.3. Pressure–density relationships

The association between pressure and density has been established by many researchers. O'Dogherty, et al. [13] suggested that the association between the density and pressure of high-density straw pellets was a simple power-law. Husain, et al. [31] established the relationship between the pressure and density of palm fibre and shell briquettes; they found an exponential increase in density with the increase in pressure. Fig. 4 shows the plot of pressure and density for the PKC pellets. There is also an exponential increase in density with the increase in PKC pelletisation pressure. The relationship is in the form of:

$$P = 3.689 e^{0.0056\rho} \qquad (4)$$

where P is mould pressure in psi.
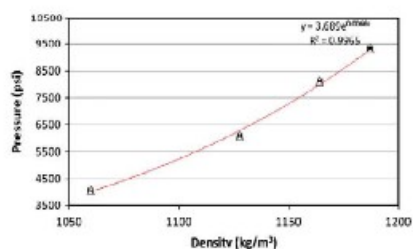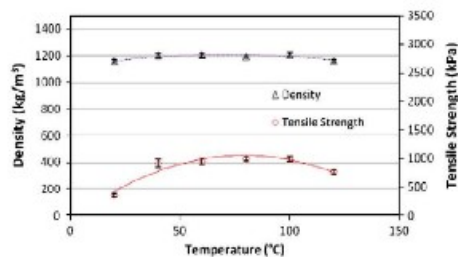
3.4. Effect of pelletisation temperature

The tensile strength of the PKC pellets was found to improve significantly at elevated temperatures, as shown in Fig. 5. As the pelletisation temperature increased from 20 to 40 °C, the tensile strength increased from 358 kPa to 914 kPa. The density, however, showed only a slight increase, from 1157 kg/m³ to 1200 kg/m³. For the pellets formed at temperatures above 40 °C, the tensile strength increased steadily from 914 kPa at 40 °C to 989 kPa at 100 °C. This may be due to a natural binding effect, where the lignin content of the material was softened and bound the pellets upon compression [32]. Beker, et al. [33] suggested that the protein and the long cellulose fibre content of biomass are responsible for the bonding and stabilisation of pellets. The optimum pelletisation temperature was found to be in the region of 80–100 °C. Temperatures above 100 °C had negative effects on the pellet tensile strength, which may be due to the evaporation of water, which resulted in lower moisture contents.

3.5. Effect of binders

3.5.1. Inorganic binders

Two inorganic binders were used in this study: caustic soda (NaOH) and calcium carbonate (CaCO₃). Figs. 6 and 7 show the effects of these binders on PKC pellets, in terms of density and tensile strength. As the concentration of caustic soda increased from 0.5 wt.% to 2.0 wt.%, the tensile strength increased from 1441 kPa to 3055 kPa (Fig. 6). However, further additions reduced the tensile strength to 1968 kPa. Caustic soda has the ability to bind loose particles together, thus improving pellet quality. However, it is important to note that, caustic soda may cause problems to the combustion system. As reported in Finney et al. [27], the combustion efficiency of spent mushroom compost-coal tailing pellets was reduced from 95% to 88.7% when a caustic soda binder was used to aid pellet agglomeration. Furthermore, higher concentrations of alkali metals were found in the ash, which could induce slagging/fouling, as reported above

Fig. 4. Relationship between pelletisation pressure and palm kernel cake pellet density.
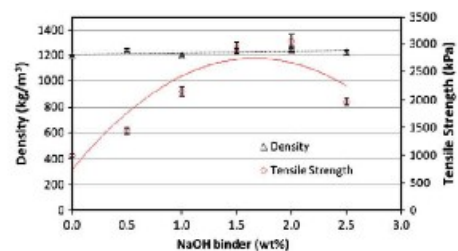
Fig. 6. Effect of caustic soda on the tensile strength and density of palm kernel cake pellets.

613

Fig. 7. Effect of the calcium carbonate binder on the tensile strength and density of palm kernel cake pellets.

Table 4
Student's t-test (two-sample assuming unequal variances) for the palm kernel cake pellets with 5 wt.% calcium carbonate binder.

	Variable 1	Variable 2
Mean	991.94	1460.52
Variance	1201.25	5169.96
Observations	5	5
Hypothesized mean difference	0	
DF	6	
t Stat	−13.13	
P(T<=t) one-tail	6.03E−06	
t Critical one-tail	1.94	
P(T<=t) two-tail	1.21E−05	
t Critical two-tail	2.45	

Variable 1: Tensile strength of PKC pellet without binder (control).
Variable 2: Tensile strength of PKC pellet with 5 wt.% calcium carbonate.

(Section 2.1). It is therefore important to keep the amount of caustic soda as low as possible, but not to compromise pellet quality. On the other hand, Yang et al. [34] studied the effect of sodium compounds on NO reduction at high temperatures in NOx control technologies. They found that the NO reduction efficiency was increased from 50% to 82.7% when the weight ratio of sodium hydroxide to the reburning coal was 3% and the supplied air to theoretical air ratio was 0.6.

As seen in Fig. 7, the tensile strength of the PKC pellets increased gradually with the increase in calcium carbonate from 0.5 wt.% to 2.0 wt.%. Further increases in calcium carbonate resulted in a steep increase in tensile strength, over 1450 kPa for 5 wt.%, although the strengths attained were not as high as for the caustic soda binder. The effect on the density was less clear. In both cases, the density fluctuated between 1192 kg/m^3 and 1237 kg/m^3.

Student's t-tests were conducted for both inorganic binders to assess the differences between these and the control, where no binder was included. The results for the tensile strength of PKC pellets with these binders are given in Tables 3 and 4; these show that the effects of both binders on pellet tensile strength were highly significant using a 95% confidence interval (P<0.05).

3.5.2. Organic binders

Three organic binders were chosen for this study: maize starch, tapioca starch and potato starch. Maize starch was the most effective of the starch binders, but was not as successful in aiding binding as either of the inorganic binders considered above (Section 3.5.1). As shown in Fig. 8, adding up to 10 wt.% of maize starch improved the tensile strength of PKC pellets, increasing it to 1057 kPa. The tapioca starch and potato starch had very little effect at low concentrations (5–10 wt.%); further additions of up to 20 wt.% deteriorated the pellets in terms of tensile strength, even though density increased

slightly in both cases with increasing proportions of these binders (Figs. 9 and 10).

3.6. Pellet durability

Table 5 shows the comparison between the durability of PKC pellets and pellets made from wood, straw and spent mushroom compost. The durability of the compressed PKC pellets, calculated using Eq. (3), was almost 50% lower than the other pellets. These low durability results may be due to the fact that PKC contains fat from the palm oil residue. Briggs, et al. [35] stated that increased oil contents produce poorer quality pellets. Since most particle binding incorporates water or, when involved, solubilised starches, proteins and fibres, fat with its
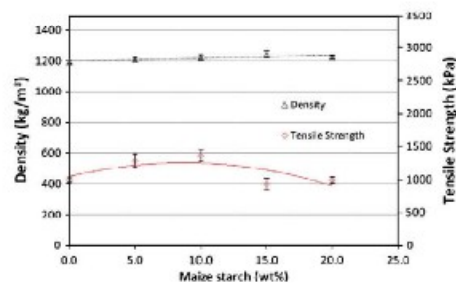
Fig. 8. Effect of maize starch on the tensile strength and density of palm kernel cake pellets.

Table 3
Student's t-test (two-sample assuming unequal variances) for the palm kernel cake pellets with 2 wt.% caustic soda binder.

	Variable 1	Variable 2
Mean	991.94	3054.57
Variance	1201.25	17,027.45
Observations	5	5
Hypothesized mean difference	0	
DF	5	
t Stat	−34.16	
P(T<=t) one-tail	2.02E−07	
t Critical one-tail	2.02	
P(T<=t) two-tail	4.04E−07	
t Critical two-tail	2.57	

Variable 1: Tensile strength of PKC pellet without binder (control).
Variable 2: Tensile strength of PKC pellet with 2 wt.% caustic soda.

Fig. 9. Effect of tapioca starch on the tensile strength and density of palm kernel cake pellets.

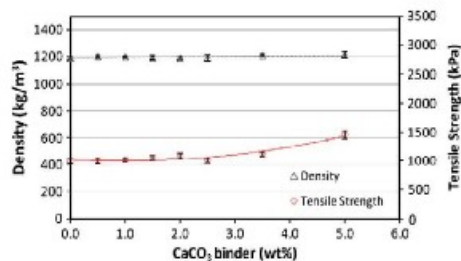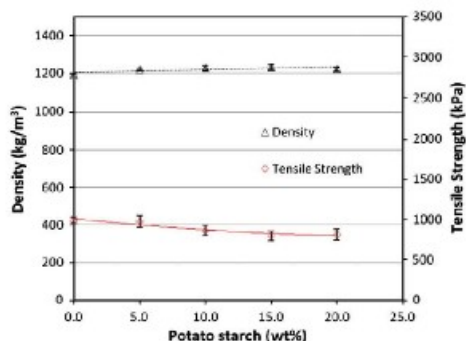614   *R. Razuan et al. / Fuel Processing Technology 92 (2011) 609–615*

Fig. 10. Effect of potato starch on the tensile strength and density of palm kernel cake pellets.

hydrophobic nature may interfere with the binding properties of the water-soluble components in the mixture. Furthermore, fat acts as a lubricant between the particles and the wall of the mould, which may result in a lower compacting pressure [36]. According to Ryu, et al. [11], the high durability of wood pellets is due to their lignin content that aids binding at elevated temperatures. Further investigations into a specific binder are needed to enhance the durability of PKC pellets.

3.7. Cost of PKC pelletisation

Due to the similarity in terms of geographical region and waste source between the material investigated here and those of Chaiyaomporn and Chavalparit [23] and using the pelletisation process parameters in Thek and Obernberger [19], it is estimated that the total production costs of PKC pellets would be between £24 and £43/tonne. This is based on the PKC material supplied in dry, powder form. The cost breakdown was based on the case study in Austria, as reported in Thek and Obernberger [19]. This included: (i) the cost of the dry raw material, which was £3.35/m³; (ii) a plant capacity of 24,000 t of pellets produced per annum; (iii) transportation costs of £1.25/km (based on an ordinary truck with a capacity of 95 m³); and (iv) a plant operating seven days a week, with three shifts per day. However, to maintain homogeneity of the raw material as well as the quality of the final product, a sieving machine is still to be considered.

As discussed in Section 3.5.1 above, adding small amounts of caustic soda could significantly improve pellet quality, although this may also increase the production costs of the pellets. Adding 2% of caustic soda may elevate the production costs from £24–43/tonne to £28.20–47.20/tonne (considering a price of £210/tonne for the caustic soda) [37].

Table 5
Durability of palm kernel cake pellets tested using a rotating drum compared to other biomass fuel pellets.

Pellet type	Pelletisation conditions	Durability (%) after 10 min
Wood pellet[a]	extruded	98.8
Straw[a]	2436 psi	98.8
Coal tailings[a]	2436 psi, air-dried	79.7
Spent mushroom compost[a]	2436 psi, air-dried	93.0
PKC pellet	9338 psi, 80 °C, 1.5 wt.% NaOH binder	48.9
	9338 psi, 80 °C, 10 wt.% maize binder	47.0

[a] Data obtained from [12].

4. Conclusions

Pelletisation experiments were conducted to determine the optimum value for various process parameters for the formation of good quality biomass fuel pellets from palm kernel cake — a waste material from the palm oil industry. It has been established that palm kernel cake can be pelletised to relatively high densities and tensile strengths at elevated temperature and pressure. The moisture content of the biomass strongly affected pellet quality; increasing the moisture from the 'as received' level of 7.9% caused pellets to deteriorate, whereas reducing the moisture content resulted in the formation of weak pellets that were prone to cracking. The optimum conditions for the production of these pellets were found to be a moisture content of 7.9%, a compaction pressure of 9338 psi (64.38 MPa) and a pelletisation temperature of 80–100 °C. At these conditions, the pellets formed had a density of 1184–1226 kg/m³ and a tensile strength of 930–1007 kPa.

Small additions of inorganic binders improved the quality of the palm kernel cake pellets. Caustic soda (<2 wt.%) increased the tensile strength to a maximum of 3055 kPa, where the density fluctuated between 1192 kg/m³ and 1237 kg/m³. Improvements were also seen with ~5 wt.% of calcium carbonate, where the tensile strength reached ~1500 kPa. Of the three organic binders tested, only small amounts of maize starch resulted in improved pellet quality, although this was not as effective as the inorganic binders. The addition of the other organic binders (tapioca starch and potato starch) did not result in any improvements in terms of tensile strength or density.

Acknowledgements

References

[1] J. Crutchfield, Indonesia: Palm oil production prospects continue to grow, United States Department of Agriculture, 2007, [Online]. Available: www.pecad.fas.usda.gov/highlights/2007/12/Indonesia_palmoil/, (31/12/2007).
[2] A.B. Nasrin, A.N. Ma, S. Mohamad, M.H. Rohaya, A. Azali, Z. Zainal, Oil palm biomass as potential substitution raw materials for commercial biomass briquettes production, American Journal of Applied Sciences 5 (2008) 179–183.
[3] S.H. Shuit, K.T. Tan, K.T. Lee, A.H. Kamaruddin, Oil palm biomass as a sustainable energy source: a Malaysian case study, Energy 34 (2009) 1225–1235.
[4] O. Abu Hassan, M. Ishida, I. Mohd Shukri, Z. Ahmad Tajuddin, Oil-palm fronds as a roughage feed source for ruminants in Malaysia, Malaysia Agriculture Research and Development Institute, Kuala Lumpur, Malaysia, 1994.
[5] P. Luangkiattikhun, C. Tangsathitkulchai, M. Tangsathitkulchai, Non-isothermal thermogravimetric analysis of oil-palm solid wastes, Bioresource Technology 99 (2008) 986–997.
[6] R. Razuan, Q. Chen, X. Zhang, V. Sharifi, J. Swithenbank, Pyrolysis and combustion of oil palm stone and palm kernel cake in fixed-bed reactors, Bioresource Technology 101 (2010) 4622–4629.
[7] P.D. Grover, S.K. Mishra, Biomass briquetting: technology and practices, Regional Wood Energy Development Programme in Asia, field document no. 46, Food and Agriculture Organization of the United Nations, Bangkok, Thailand, 1996.
[8] S.C. Bhattacharya, M.A. Leon, M.M. Rahman, A study on improved biomass briquetting, Energy for Sustainable Development 6 (2002) 67–71.
[9] S.C. Bhattacharya, R. Bhatia, M.N. Islam, N. Shah, Densified biomass in Thailand: potential status and problems, Biomass 8 (1985) 255–266.
[10] S.C. Bhattacharya, N. Shah, Z. Alikhani, Some aspects of fluidized bed combustion of paddy husk, Applied Energy 16 (1984) 307–316.
[11] C. Ryu, K. Finney, V.N. Sharifi, J. Swithenbank, Pelletised fuel production from coal tailings and spent mushroom compost — Part I: Identification of pelletisation parameters, Fuel Processing Technology 89 (2008) 269–275.
[12] K.N. Finney, V.N. Sharifi, J. Swithenbank, Fuel pelletisation with a binder: Part I — Identification of a suitable binder for spent mushroom compost–coal tailing pellets, Energy & Fuels 23 (2009) 3195–3202.
[13] M.J. O'Dogherty, J.A. Wheeler, Compression of straw to high densities in closed cylindrical moulds, Journal of Agricultural Engineering Research 29 (1984) 61–72.

[4] G.J. Trezek, G.M. Savage, D.B. Jones, Fundamental considerations for preparing densified refuse derived fuel, report no. EPA-600/2-81-180, Municipal Environmental Research Laboratory, Solid and Hazardous Waste Research Division, U.S. Environmental Protection Agency, Cincinnati, Ohio, 1981.

[5] S. Mani, L.G. Tabil, S. Sokhansanj, Specific energy requirement for compacting corn stover, Bioresource Technology 97 (2006) 1420–1426.

[6] S. Mani, A system analysis of biomass densification process, Ph.D. Thesis, The University of British Columbia, 2005.

[7] C. Ryu, A. Khor, V.N. Sharifi, J. Swithenbank, Pellet sed fuel production from coal tailings and spent mushroom compost — Part 1: economic feasibility based on cost analysis, Fuel Processing Technology 89 (2008) 273–283.

[8] A. Sultana, A. Kumar, D. Harfield, Development of agri-pellet production cost and optimum size, Bioresource Technology 101 (2010) 5609–5621.

[9] G. Thek, I. Obernberger, Wood pellet production costs under Austrian and in comparison to Swedish framework conditions, Biomass and Bioenergy 27 (2004) 671–693.

[20] A.K. Tripathi, P.V.R. Iyer, T.C. Kandpal, K.K. Singh, Assessment of availability and costs of some agricultural residues used as feedstocks for biomass gasification and briquetting in India, Energy Conversion and Management 39 (1998) 1611–1618.

[21] S. Mani, S. Sokhansanj, X. Bi, A. Thurhollow, Economics of producing fuel pellets from biomass, American Society of Agricultural and Biological Engineers 22 (2006) 421–426.

[22] S. Sokhansanj, A.F. Turhollow, Biomass densification—cubing operations and costs for corn stover, American Society of Agricultural and Biological Engineers 20 (2004) 495–499.

[23] K. Chaiyaomporn, O. Chavalparit, Fuel pellets production from biodiesel waste, EnvironmentAsia 3 (2010) 103–110.

[24] P. McKendry, Energy production from biomass (part 1): overview of biomass, Bioresource Technology 83 (2002) 37–46.

[25] C.O. Plank, Extension agronomist — soil testing and plant analysis, 2010, [Online]. Available:, aesl.ces.uga.edu/publications/plant/Nutrient.htm, (1/7/2010).

[26] C.P. Vance, C. Uhde-Stone, D.L. Allan, Phosphorus acquisition and use: critical adaptations by plants for securing a nonrenewable resource, New Phytologist 157 (2003) 423–447.

[27] K.N. Finney, V.N. Sharifi, J. Swithenbank, Fuel pelletization with a binder: Part II — The impacts of binders on the combustion of spent mushroom compost-coal tailing pellets, Energy & Fuels 23 (2009) 3203–3210.

[28] M.I.St. Josephs (Ed.), ASAE S269.4 Cubes, pellets and crumbles — definitions and methods for determining density, durability, and moisture content, ASAE Standards, 1996, pp. 477–479.

[29] M. Temmerman, F. Rabier, P.D. Jensen, H. Hartmann, T. Böhm, Comparative study of durability test methods for pellets and briquettes, biomass and Bioenergy 30 (2006) 964–972.

[30] M.L. Al-Widyan, H.F. Al-Jalil, M.M. Abu-Zreig, N.H. Abu-Hamdeh, Physical durability and stability of olive cake briquettes, Canadian Biosystems Engineering 44 (2002) 3–41.

[31] A. Hussain, A. Asance, A. Abdullah, Briquetting of palm fibre and shell from the processing of palm nuts to palm oil, Biomass and Bioenergy 22 (2002) 505–509.

[32] A. Uslu, A.P.C. Faaij, P.C.A. Bergman, Pre-treatment technologies and their effect on international bioenergy supply chain logistics. Techno-economic evaluation of torrefaction, fast pyrolysis and pelletisation, Energy 33 (2008) 1206–1223.

[33] O.C. Baker, Briquetting of Aslin Elbistan lignite of Turkey using different waste materials, Fuel Processing Technology 51 (1997) 137–144.

[34] W. Yang, J. Zhou, Z. Zhou, Z. Liu, Z. Wang, J. Liu, C. Reis, Characteristics of sodium compounds on NO reduction at high temperature in NOx control technologies, Fuel Processing Technology 89 (2008) 1316–1323.

[35] J.L. Briggs, D.E. Maier, B.A. Watkins, K.C. Behnke, Effect of ingredients and processing parameters on pellet quality, Poultry Science 78 (1999) 1464–1471.

[36] M. Thomas, T. van Vliet, A.F.B. van der Poel, Physical quality of pelleted animal feed 3. Contribution of feedstuff components, Animal Feed Science and Technology 70 (1998) 59–78.

[37] S. Wilson, Caustic soda prices and pricing information, European market review, 2010. Available:, www.icis.com/v2/chemicals/9075188/caustic-soda/pricing. html, (21/7/2010).

Abbreviations and Nomenclature

CS: Compressive strength (N)
d: Pellet diameter (m)
L: Pellet length (m)
P: Pelletisation pressure in the mould (psi)
PKC: Palm kernel cake
TS: Tensile strength (kPa)
W: Pellet weight (kg)
W_i: Weight of the initial pellet (g)
W_f: Weight of the final pellet (g)
ρ: Pellet density (kg/m^3)